frontiers | Research Topics

Stars and rising stars in neuroendocrinology

Edited by
Alexandre Benani

Published in
Frontiers in Endocrinology
Frontiers in Neuroscience

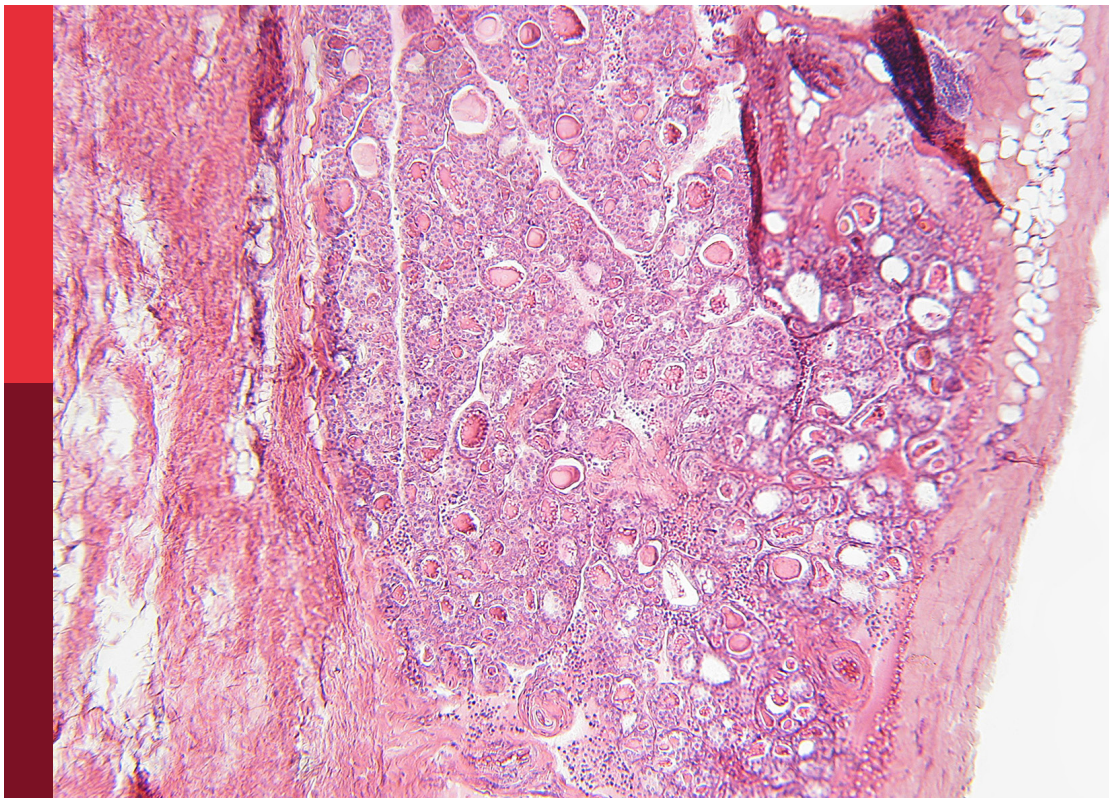

ISSN 1664-8714
ISBN 978-2-8325-5385-5
DOI 10.3389/978-2-8325-5385-5

About Frontiers

Frontiers is more than just an open access publisher of scholarly articles: it is a pioneering approach to the world of academia, radically improving the way scholarly research is managed. The grand vision of Frontiers is a world where all people have an equal opportunity to seek, share and generate knowledge. Frontiers provides immediate and permanent online open access to all its publications, but this alone is not enough to realize our grand goals.

Frontiers journal series

The Frontiers journal series is a multi-tier and interdisciplinary set of open-access, online journals, promising a paradigm shift from the current review, selection and dissemination processes in academic publishing. All Frontiers journals are driven by researchers for researchers; therefore, they constitute a service to the scholarly community. At the same time, the *Frontiers journal series* operates on a revolutionary invention, the tiered publishing system, initially addressing specific communities of scholars, and gradually climbing up to broader public understanding, thus serving the interests of the lay society, too.

Dedication to quality

Each Frontiers article is a landmark of the highest quality, thanks to genuinely collaborative interactions between authors and review editors, who include some of the world's best academicians. Research must be certified by peers before entering a stream of knowledge that may eventually reach the public - and shape society; therefore, Frontiers only applies the most rigorous and unbiased reviews. Frontiers revolutionizes research publishing by freely delivering the most outstanding research, evaluated with no bias from both the academic and social point of view. By applying the most advanced information technologies, Frontiers is catapulting scholarly publishing into a new generation.

What are Frontiers Research Topics?

Frontiers Research Topics are very popular trademarks of the *Frontiers journals series*: they are collections of at least ten articles, all centered on a particular subject. With their unique mix of varied contributions from Original Research to Review Articles, Frontiers Research Topics unify the most influential researchers, the latest key findings and historical advances in a hot research area.

Find out more on how to host your own Frontiers Research Topic or contribute to one as an author by contacting the Frontiers editorial office: frontiersin.org/about/contact

Stars and rising stars in neuroendocrinology

Topic editor
Alexandre Benani — Centre National de la Recherche Scientifique (CNRS), France

Citation
Benani, A., ed. (2024). *Stars and rising stars in neuroendocrinology*. Lausanne: Frontiers Media SA. doi: 10.3389/978-2-8325-5385-5

Table of contents

05 MRI Assessment of Cardiac Function and Morphology in Adult Patients With Growth Hormone Deficiency: A Systematic Review and Meta-Analysis
Fabio Bioletto, Nunzia Prencipe, Alessandro Maria Berton, Chiara Bona, Mirko Parasiliti-Caprino, Riccardo Faletti, Ezio Ghigo, Silvia Grottoli and Valentina Gasco

14 Positioning-dependent bidirectional NELL2 signaling in the brain
Byung Ju Lee and Jin Kwon Jeong

18 Mechanisms mediating the impact of maternal obesity on offspring hypothalamic development and later function
Isadora C. Furigo and Laura Dearden

30 Ontogeny of ependymoglial cells lining the third ventricle in mice
David Lopez-Rodriguez, Antoine Rohrbach, Marc Lanzillo, Manon Gervais, Sophie Croizier and Fanny Langlet

46 Water deprivation induces hypoactivity in rats independently of oxytocin receptor signaling at the central amygdala
Viviane Felintro, Verónica Trujillo, Raoni C. dos-Santos, Claudio da Silva-Almeida, Luís C. Reis, Fábio F. Rocha and André S. Mecawi

58 Maternal androgen excess significantly impairs sexual behavior in male and female mouse offspring: Perspective for a biological origin of sexual dysfunction in PCOS
Nina M. Donaldson, Melanie Prescott, Amy Ruddenklau, Rebecca E. Campbell and Elodie Desroziers

75 Isolated anterior pituitary dysfunction in adulthood
Nunzia Prencipe, Lorenzo Marinelli, Emanuele Varaldo, Daniela Cuboni, Alessandro Maria Berton, Fabio Bioletto, Chiara Bona, Valentina Gasco and Silvia Grottoli

96 Copeptin adaptive response to SGLT2 inhibitors in patients with type 2 diabetes mellitus: The GliRACo study
Alessandro Maria Berton, Mirko Parasiliti-Caprino, Nunzia Prencipe, Fabio Bioletto, Chiara Lopez, Chiara Bona, Marina Caputo, Francesca Rumbolo, Federico Ponzetto, Fabio Settanni, Valentina Gasco, Giulio Mengozzi, Ezio Ghigo, Silvia Grottoli, Mauro Maccario and Andrea Silvio Benso

108 Perinatal exposure to the fungicide ketoconazole alters hypothalamic control of puberty in female rats
Delphine Franssen, Hanna K. L. Johansson, David Lopez-Rodriguez, Arnaud Lavergne, Quentin Terwagne, Julie Boberg, Sofie Christiansen, Terje Svingen and Anne-Simone Parent

126 Histaminergic regulation of food intake
Axelle Khouma, Moein Minbashi Moeini, Julie Plamondon, Denis Richard, Alexandre Caron and Natalie Jane Michael

139 Hormonal contraceptive exposure relates to changes in resting state functional connectivity of anterior cingulate cortex and amygdala
Esmeralda Hidalgo-Lopez, Isabel Noachtar and Belinda Pletzer

150 ACTH-producing small cell neuroendocrine carcinoma from the gallbladder: a case report and literature review
Xiaofang Zhang, Dihua Huang, Xiaojie Pan, Qiya Si and Qiaoying You

156 Association between high serum blood glucose lymphocyte ratio and all-cause mortality in non-traumatic cerebral hemorrhage: a retrospective analysis of the MIMIC-IV database
Shiqiang Yang, Yanwei Liu, Shiqiang Wang, Zhonghai Cai, Anqiang Yang and Xuhui Hui

168 Brain and serum metabolomic studies reveal therapeutic effects of san hua decoction in rats with ischemic stroke
Ruisi Liu, Shengxuan Cao, Yufeng Cai, Mingmei Zhou, Xiaojun Gou and Ying Huang

182 Risk factors of acute ischemic stroke and the role of angiotensin I in predicting prognosis of patients undergoing endovascular thrombectomy
Shengkai Yang, Kemian Li, Zhengqian Huang, Yingda Xu, Jingshan Liang, Yong Sun and Aimin Li

196 Reproductive function and behaviors: an update on the role of neural estrogen receptors alpha and beta
Thomas Torres, Nolwenn Adam, Sakina Mhaouty-Kodja and Lydie Naulé

frontiers | Frontiers in Endocrinology

SYSTEMATIC REVIEW
published: 10 June 2022
doi: 10.3389/fendo.2022.910575

MRI Assessment of Cardiac Function and Morphology in Adult Patients With Growth Hormone Deficiency: A Systematic Review and Meta-Analysis

Fabio Bioletto[1]*, *Nunzia Prencipe*[1], *Alessandro Maria Berton*[1], *Chiara Bona*[1], *Mirko Parasiliti-Caprino*[1], *Riccardo Faletti*[2], *Ezio Ghigo*[1], *Silvia Grottoli*[1] *and Valentina Gasco*[1]

[1] Endocrinology, Diabetology and Metabolism, Department of Medical Sciences, University of Turin, Turin, Italy, [2] Radiology Unit, Department of Surgical Sciences, University of Turin, Turin, Italy

Background: Adult GH deficiency (GHD) has been described as a heterogeneous condition characterized by many clinical modifications, such as metabolic alterations, impaired quality of life, and increased mortality. The clinical relevance of cardiac involvement remains, however, only partially elucidated.

Methods: PubMed/Medline, EMBASE, Cochrane library, OVID and CINAHL databases were systematically searched until February 2022 for studies evaluating cardiac function and morphology by magnetic resonance imaging in adult patients with GHD. Effect sizes were pooled through a random-effect model.

Results: Four studies were considered in the meta-analysis. With respect to the left ventricle, GHD patients were characterized by a lower stroke-volume-index (-3.6 ml/m^2, standardized mean difference (SMD) -0.60, 95%CI [-1.15,-0.05], p=0.03), lower end-diastolic-volume-index (-6.2 ml/m^2, SMD -0.54, 95%CI [-0.97,-0.10], p=0.02) and, after accounting for possible biases, lower mass-index (-15.0 g/m^2, SMD -1.03, 95%CI [-1.89,-0.16], p=0.02). With respect to the right ventricle, a lower end-diastolic-volume-index (-16.6 ml/m^2, SMD -1.04, 95%CI [-2.04,-0.03], p=0.04) and a borderline-significant lower stroke-volume-index (-5.0 ml/m^2, SMD -0.84, 95%CI [-1.77,0.08], p=0.07) could be observed. Data about the effect of GH replacement therapy highlighted a significant increase in left ventricular mass-index after treatment initiation (+3.7 g/m^2, 95%CI [1.6,5.7], p<0.01).

OPEN ACCESS

Edited by:
Alexandre Benani, Centre National de la Recherche Scientifique (CNRS), France

Reviewed by:
Jörgen Isgaard, University of Gothenburg, Sweden
Daniele Gianfrilli, Sapienza University of Rome, Italy

***Correspondence:**
Fabio Bioletto
fabio.bioletto@unito.it
orcid.org/0000-0001-7550-7023

Specialty section:
This article was submitted to Neuroendocrine Science, a section of the journal Frontiers in Endocrinology

Received: *01 April 2022*
Accepted: *09 May 2022*
Published: *10 June 2022*

Citation:
Bioletto F, Prencipe N, Berton AM, Bona C, Parasiliti-Caprino M, Faletti R, Ghigo E, Grottoli S and Gasco V (2022) MRI Assessment of Cardiac Function and Morphology in Adult Patients With Growth Hormone Deficiency: A Systematic Review and Meta-Analysis. Front. Endocrinol. 13:910575. doi: 10.3389/fendo.2022.910575

Conclusion: With respect to the left ventricle, our results confirmed those retrieved by echocardiographic studies. In addition, significant alterations were demonstrated also for the right ventricle, for which echocardiographic data are nearly absent. This supports the thesis of a biventricular cardiac involvement in patients with GHD, with a similar pattern of morphological and functional alterations in both ventricles.

Keywords: cardiovascular system, cardiac magnetic resonance imaging, growth hormone deficiency, growth hormone replacement therapy, meta-analysis

INTRODUCTION

Adult GH deficiency (GHD) is a heterogeneous disorder that may result from a variety of causes, including structural lesions, traumas, infiltrative diseases, surgery or irradiation to the pituitary gland and/or hypothalamus, or idiopathic dysfunction (1–5). Its diagnosis depends on the demonstration of a subnormal rise in peak serum GH level in response to one or more GH stimulation tests (1, 6–9). From a clinical point of view, this condition is characterized by many alterations, such as impaired quality of life, decreased lean mass, increased fat mass, abnormal lipid profile, osteoporosis, and increased all-cause mortality (10–13). The clinical relevance of cardiac involvement in patients with adult GHD remains, however, only partially elucidated.

Physiologically, the GH/IGF-I axis interacts with the cardiovascular system, both indirectly by acting on various metabolic cardiovascular risk factors, and directly by actively maintaining the structure and function of the normal adult heart, through the stimulation of cardiac growth and myocardial contractility (14–17). An impairment of the GH/IGF-I axis contributes to determine cardiovascular alterations, as suggested by clinical studies reporting an increase in cardiovascular morbidity and mortality in hypopituitary adults with untreated GHD (18–22). With respect to cardiac structure, adult patients with untreated GHD show a reduced left ventricular (LV) mass (LVM) and diameter, coherently accompanied by a reduction in LV wall thickness at the interventricular septum (IVS) and posterior wall (PW) (23–28). Data about the LV systolic and diastolic function are less clear; a reduction of LV systolic performance has been consistently observed mostly during peak exercise (23, 29–31); recently, a subclinical systolic disfunction by speckle-tracking echocardiography has been suggested (32), but further studies are needed to confirm this result; with respect to diastolic filling, an impairment has been suggested by some authors (24, 29), but not clearly confirmed throughout the literature (33, 34).

Concerning the cardiac effects of recombinant human GH (rhGH) replacement therapy in patients with adult GHD, a previous meta-analysis (33), based on 16 echocardiographic studies, found that rhGH therapy determined a significant increase in LVM (+10.8 g), IVS thickness (+0.28 mm), PW thickness (+0.98 mm), LV end-diastolic diameter (LVEDD, +1.34 mm) and LV stroke volume (LVSV, +10.3 ml). On the contrary, no significant effects were found on LV end-systolic diameter (LVESD) and fractional shortening (FS), which was used as a proxy for systolic function and ejection fraction (EF).

As the authors themselves acknowledge, a limitation of this analysis, as well as of most studies evaluating cardiac structure and function in adult patients with GHD, is represented by the use of echocardiography, which suffers from a relatively low reproducibility with respect to other imaging techniques and, in particular, compared to magnetic resonance imaging (MRI). Moreover, the included studies were characterized by a significant heterogeneity in patient populations, with remarkable age-differences, and commonly with the enrollment of both childhood-onset and adult-onset GHD patients. These limitations may account at least in part for the sometimes-discrepant results obtained by different studies; moreover, they may have impaired the potential to correctly characterize subtler cardiac abnormalities in patients with GHD. This is particularly relevant when dealing with the structure and function of the right ventricle (RV) (35, 36), whose echocardiographic assessment suffers from significant challenges and limitations (37); within the specific context of adult GHD, echocardiographic studies provide almost no data about possible alterations in RV morphology and function. As a consequence, whether or not adult GHD is characterized by a biventricular cardiac involvement still remains, *de facto*, unclear.

Compared to echocardiography, cardiac MRI represents a more reliable and reproducible technique for measuring cardiac volumes, mass, and function; its use in clinical research, given its enhanced precision and reproducibility, has been estimated to allow for a reduction in sample size of 80–95% to obtain equal statistical power compared to investigations based on conventional echocardiography (38). In fact, it avoids most of the geometrical assumption required by echocardiographic estimates, and is currently considered the gold standard for the assessment of cardiac morphology and functionality (38–40); notably, this is particularly true when evaluating the structure and function of the RV, as cardiac MRI is considered the most accurate and reproducible method for the assessment of RV parameters (35, 36, 41).

Given these premises, cardiac MRI might provide finer information about cardiac alterations in patients with adult GHD, as well as their possible changes after the initiation of rhGH replacement therapy; in particular, it might answer to the question about if and how RV is involved. Some studies have been published in this regard (42–45), with interesting results. However, the strength of their conclusions is hampered by their limited sample size, and a quantitative synthesis of their results is still lacking. The aim of this systematic review and meta-analysis was, thus, to specifically summarize and quantitatively combine

the available evidence about the MRI assessment of cardiac function and morphology in patients with adult GHD.

METHODS

Search Strategy and Study Selection

This study was conducted according to the Preferred Reporting Items for Systematic Reviews and Meta-Analysis (PRISMA) guidelines (46). The process of literature search and study selection was made by two independent reviewers (F.B., V.G.); all disparities were resolved through consensus.

The following electronic databases were queried until the February 1st 2022: PubMed/Medline, EMBASE, Cochrane library, OVID, and CINAHL. The search strategy was performed using a combination of relevant database-specific search terms to identify pertinent studies about the evaluation of cardiac morphology and function by MRI in patients with adult GHD. The full search strategy is presented in Supplementary Material (**Appendix 1**). No filters were applied for study design, language, and publication date.

After duplicate removal, all studies found with the aforementioned search were evaluated for inclusion in the meta-analysis, first by title/abstract screening and then by full-text review. We excluded from our analysis studies according to the following exclusion criteria: (a) unavailability of any of the outcomes of interest, as defined in the following subsection; (b) case reports or case series; (c) conference abstracts. In case of patient overlap between studies, the one with the largest sample size was considered.

Outcomes

The following outcomes were assessed: (a) comparison of left and right ventricular morphology and function, as assessed by cardiac MRI, between patients with GHD and controls; (b) comparison of left and right ventricular morphology and function, as assessed by cardiac MRI, before and after treatment with rhGH in patients with GHD.

More in detail, the MRI parameters that were evaluated were: (i) left ventricular ejection fraction (LVEF); (ii) left ventricular stroke volume index (LVSVi); (iii) left ventricular end-diastolic volume index (LVEDVi); (iv) left ventricular end-systolic volume index (LVESVi); (v) left ventricular mass index (LVMi); (vi) right ventricular ejection fraction (RVEF); (vii) right ventricular stroke volume index (RVSVi); (viii) right ventricular end-diastolic volume index (RVEDVi); (ix) right ventricular end-systolic volume index (RVESVi).

Data Extraction

Two authors (F.B., V.G.) independently examined and extracted data from papers which met the inclusion criteria using pre-specified data extraction templates. For each eligible study, the following information were collected: (a) first author and publication year; (b) study design; (c) major selection criteria for each group; (d) matching criteria between GHD patients and controls; (e) number of subjects enrolled; (f) patients' characteristics in terms of demographic data; (g) cardiac MRI data in GHD patients and controls, according to the parameters specified in the previous section; (h) cardiac MRI data in GHD patients before and after treatment with rhGH, according to the parameters specified in the previous section.

Risk of Bias Assessment

The risk of bias was independently assessed for each included study by two authors (F.B., V.G.). The twenty components of the AXIS tool (Appraisal tool for Cross-Sectional Studies) (47) were used for the evaluation of cross-sectional studies comparing cardiac MRI parameters between patients with adult GHD and controls. The seven domains of the ROBINS-I tool (Risk Of Bias In Non-randomized Studies of Intervention) (48) were used for the evaluation of longitudinal studies evaluating the changes in cardiac MRI parameters before and after the initiation of rhGH therapy.

Statistical Analysis

Continuous variables and categorical variables were reported as numbers and percentages, respectively. Comparisons between patients with GHD and controls were reported as mean difference and as standardized mean difference (SMD), expressed as Hedges' g. Variations before and after rhGH treatment in patients with GHD were reported as mean paired differences. A random-effect restricted maximum likelihood model was adopted for statistical pooling of data. Higgins I^2 statistics and Cochran Q test were used to assess heterogeneity between studies. Statistical analysis was performed using STATA 17 (StataCorp, College Station, Texas, USA).

RESULTS

Search Results

A total of 165 records were identified in the initial literature search. Removal of duplicates led to an overall pool of 147 studies. An accurate title or abstract revision was sufficient to exclude 139 articles as not pertinent or not fulfilling our prespecified inclusion or exclusion criteria. The remaining 8 studies were assessed in full-text for eligibility (42–45, 49–52), and 4 of them were excluded due to patient overlap (49–52); thus, 4 studies finally met all criteria for being included in the final analysis (42–45) (**Figure 1**).

Characteristics of the Included Studies

Table 1 summarizes the basic studies characteristics. Almost all included patients had an adult-onset GHD, with the only exception of two adult patients with a childhood-onset GHD enrolled in the study by Andreassen et al. (42). All studies provided data comparing GHD patients with controls, in a cross-sectional design (42–45). The matching criteria adopted for the selection of the control group included age and sex in all studies (42–45); body surface area (BSA) was considered as an adjunctive matching criterion in two studies (42, 43), and body mass index (BMI) in one (43). Moreover, three out of four studies also provided a longitudinal evaluation of the

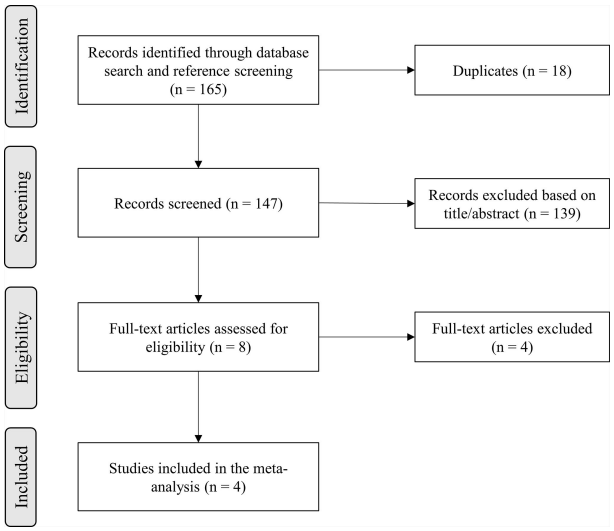

FIGURE 1 | Flow-chart of study inclusion.

effect of rhGH treatment on cardiac MRI parameters in the GHD group (42, 44, 45). Two of them had an observational design (42, 45), while one was designed as a randomized controlled trial with an open-label extension (44).

Of note, in the study by Thomas et al. (45), all parameters were declared to be summarized using standard deviation (SD) as the index of dispersion, but the reported p-values and interpretation of the results were internally consistent with the data only if the reported index of dispersion was actually the standard error (SE); thus, in our analysis, this erratum was taken into account, and SE were transformed into SD before our quantitative analyses.

Comparison of Cardiac MRI Parameters Between Patients With GHD and Controls

Data about LVEF (42–45) and LVMi (42–45) were reported in all studies; data about LVEDVi (42, 43, 45) and LVESVi (42, 43, 45) were reported in three studies; data about LVSVi (42, 45), RVEF (43, 45), RVEDVi (43, 45) and RVESVi (43, 45) were reported in two studies; data about RVSVi (45) were reported in one study.

With respect to LV function and morphology, LVSVi (-3.6 ml/m^2, SMD -0.60, 95%CI [-1.15,-0.05], p=0.03) and LVEDVi (-6.2 ml/m^2, SMD -0.54, 95%CI [-0.97,-0.10], p=0.02) were significantly lower in GHD patients compared to controls. On the other hand, no significant differences between GHD patients and controls could be found in terms of LVEF (+2.2%, SMD 0.39, 95%CI [-0.11,0.89], p=0.13) or LVESVi (-1.6 ml/m^2, SMD -0.24, 95%CI [-0.80,0.33], p=0.41). When assessing LVMi, no overall differences could be found when pooling data from all studies (-8.8 g/m^2, SMD -0.55, 95%CI [-1.67,0.58], p=0.34); this result, however, was remarkably influenced by the findings by Gonzalez et al. (44), as GHD patients presented a high rate of poorly controlled hypertension, which – as the author themselves recognize – could have significantly biased the assessment of LVMi in this cohort; excluding this paper from the analysis, the pooled effect sizes would yield significantly lower LVMi values in GHD patients compared to controls (-15.0 g/m^2, SMD -1.03, 95%CI [-1.89,-0.16], p=0.02) (**Figure 2** and **Supplementary Figure 1**).

With respect to RV function and morphology, RVEDVi (-16.6 ml/m^2, SMD -1.04, 95%CI [-2.04,-0.03], p=0.04) was significantly lower in GHD patients compared to controls, and a borderline-significant trend towards a lower RVSVi (-5.0 ml/m^2, SMD -0.84,

TABLE 1 | Study characteristics.

First author, year	Study design	Matching criteria between patients with GHD and controls	N of subjects[a]	Gender distribution[a](% male)	Mean age[a] (years)	Tests and cut-offs used for the definition of GHD	Duration of rhGH treatment (months)
Andreassen et al., 2011 (42)	Cross-sectional + Observational	Age, sex, BSA	16[b]/16	50.0/50.0	49.0/49.0	GHRH + PD GH cut-off: < 6.5 ng/ml	12
De Cobelli et al., 2019 (43)	Cross-sectional	Age, sex, BSA, BMI	15/15	53.3/53.3	52.0/49.0	GHRH + ARG GH cut-off: BMI-dependent[c]	NA
Gonzalez et al., 2017 (44)	Cross-sectional + RCT + OLE	Age, sex	17[d]/16	58.8/56.3	48.4/NA	ITT GH cut-off: < 3 ng/ml	12[e]
Thomas et al., 2016 (45)	Cross-sectional + Observational	Age, sex	10[f]/10	80.0/80.0	55.0/54.0	ITT or GST GH cut-off: < 3 ng/ml	12

[a]*Data regarding the GHD patient group and the control group are reported in this order, separated by a slash.*
[b]*Two patients were excluded from longitudinal analyses because they were lost at follow-up.*
[c]*< 11.5 ng/ml for lean subjects, < 8.0 ng/ml for overweight subjects, < 4.2 ng/ml for obese subjects.*
[d]*One patient was excluded because he had an intracranial clip and could not undergo cardiac MRI; one patient was excluded because he developed GHD after being cured for acromegaly.*
[e]*6-month cross-over RCT, followed by a 6-month OLE.*
[f]*One patient was excluded because he was discovered to have hypertension and diabetes; his age- and sex-matched control subjects was excluded as well; two more patients were excluded from longitudinal analyses because they were lost at follow-up.*
ARG, arginine; BMI, body mass index; BSA, body surface area; GH, growth hormone; GHD, growth hormone deficiency; GHRH, growth hormone releasing hormone; GST, glucagon stimulation test; ITT, insulin tolerance test; N, number; NA, not applicable/not available; OLE, open-label extension; PD, pyridostigmine; RCT, randomized controlled trial; rhGH, recombinant human growth hormone.

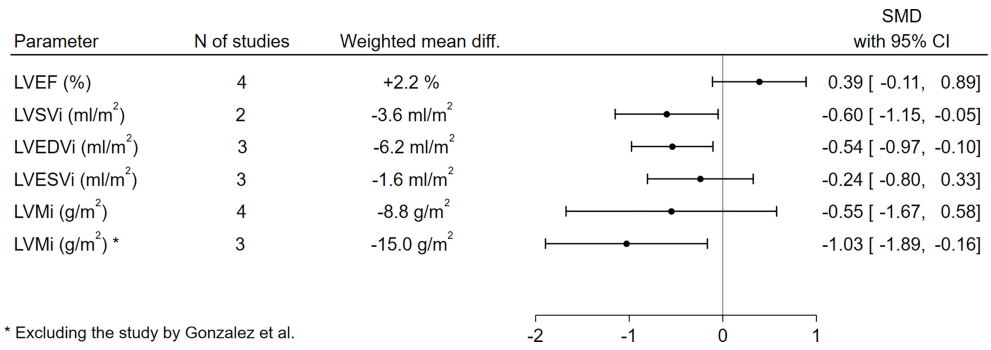

FIGURE 2 | Comparison of LV functional and morphological parameters between patients with GHD and controls. CI, confidence interval; GHD, growth hormone deficiency; LV, left ventricle; LVEDVi, left ventricular end-diastolic volume index; LVEF, left ventricular ejection fraction; LVESVi, left ventricular end-systolic volume index; LVMi, left ventricular mass index; LVSVi, left ventricular stroke volume index; N, number; SMD, standardized mean difference.

95%CI [-1.77,0.08], p=0.07) could also be observed. On the other hand, no significant differences between GHD patients and controls could be found in terms of RVEF (+2.9%, SMD 0.42, 95%CI [-0.38,1.23], p=0.30) or RVESVi (-7.1 ml/m^2, SMD -0.72, 95%CI [-1.65,0.20], p=0.13) (**Figure 3** and **Supplementary Figure 2**).

Variation of Cardiac MRI Parameters Before and After rhGH Treatment in Patients With GHD

Data concerning the variation of cardiac MRI parameters after rhGH treatment initiation in patients with GHD were sparser. Moreover, to the scope of the present meta-analysis, this evaluation was further limited by the unavailability, in most cases, of the exact data summarizing the paired differences of the parameters between baseline and follow-up, which would have been necessary for a correct quantitative synthesis of the results given the paired design of the research question.

Overall, the only parameter for which exact data about the variation between baseline and follow-up were available was LVMi, which was reported in one study (42) and obtainable by the supplementary material in another one (45). The statistical pooling of these results suggested a statistically significant increase in LVMi after the initiation of rhGH therapy (+3.7 g/m^2, 95%CI [1.6,5.7], p<0.01) (**Figure 4**). For all other parameters, the considered manuscripts only reported the pooled means at baseline and at the study end, without providing the mean paired differences and thus preventing a quantitative synthesis of these results. Nevertheless, as a qualitative appraisal, no significant variation in any parameter was found.

Quality Assessment

The results of the quality assessment of the studies are reported in **Supplementary Tables 1, 2**. Altogether, the risk of bias appeared to be moderate-to-low in most studies, with the exception of a significant concern related to the likely presence of confounding and selection bias in the study by Gonzalez et al. (44), as more specifically discussed in other sections of our paper. Publication bias was not formally assessed due to the low number of available studies.

DISCUSSION

This is the first systematic review and meta-analysis specifically evaluating the available evidence about the assessment by MRI of cardiac function and morphology in adult patients with GHD.

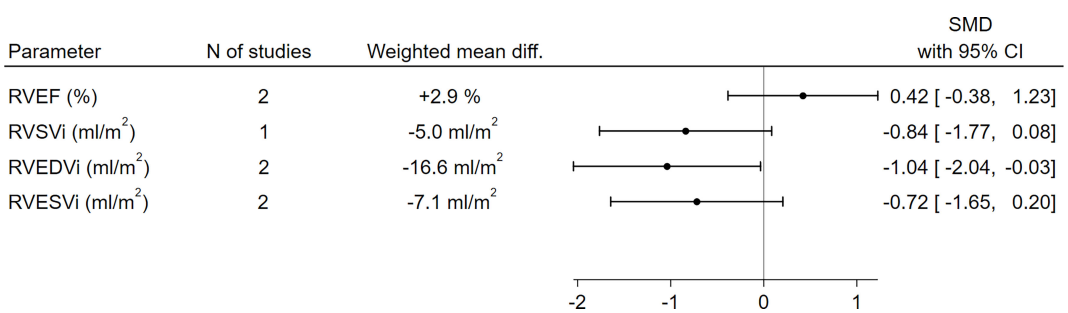

FIGURE 3 | Comparison of RV functional and morphological parameters between patients with GHD and controls. CI, confidence interval; GHD, growth hormone deficiency; RV, right ventricle; RVEDVi, right ventricular end-diastolic volume index; RVEF, right ventricular ejection fraction; RVESVi, right ventricular end-systolic volume index; RVSVi, right ventricular stroke volume index; N, number; SMD, standardized mean difference.

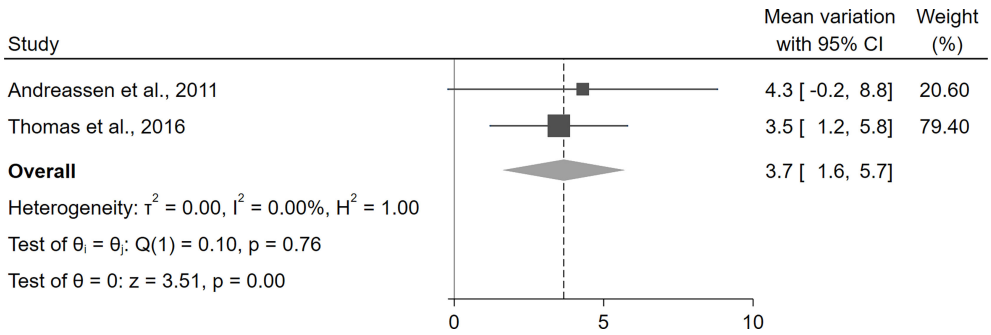

FIGURE 4 | Variation of LVMi before and after treatment with rhGH in patients with GHD. CI, confidence interval; GHD, growth hormone deficiency; LVMi, left ventricular mass index; rhGH, recombinant human growth hormone.

With respect to cardiac morphology, the available evidence pointed out a relevant impact of adult GHD on ventricular volumes. The LVEDVi and RVEDVi were significantly lower in GHD patients compared to controls; on the other hand, the impact of GHD on end-systolic volumes seemed to be less evident, as no significant differences between patients with GHD and controls could be found neither for the left nor for the right ventricle. Coherently with these data, the stroke volume, which can be calculated as the difference between the end-diastolic volume and the end-systolic volume, was found to be significantly lower in patients with GHD for the left ventricle, with a borderline-significance also for the right ventricle.

When considering systolic function, no significant differences could be found in terms of EF between GHD patients and controls, neither for the left nor for the right ventricle. Overall, these findings were in line with those already discussed about the left and right ventricular volumes; in fact, the EF can be computed as the ratio between the stroke volume and the end-diastolic volume, which were found to be both decreased (either significantly or with a borderline-significant trend) in GHD patients compared to control. Overall, thus, the data about the EF demonstrate that, in each ventricle, the reduction in stroke volume and end-diastolic volume was roughly proportional, with an overall maintenance of the fraction of ventricular blood that is pumped into the pulmonary or systemic arterial system at each stroke.

With respect to cardiac mass, the available data were contrasting. Physiologically, the somatotroph axis is known to exert a direct anabolic function on the cardiac muscle, as widely demonstrated, for example, in experimental models (53–55) and in patients with acromegaly (23, 24, 56–58); moreover, especially in males, an indirect anabolic effect *via* the hypothalamic-pituitary-gonadal axis is also possible, given the known cross-talk between the two axes (59) and the recognized anabolic effects of testosterone on cardiomyocytes (60). Previous data based on echocardiographic studies suggested that GHD patients were characterized by a reduced LV diameter and mass, accompanied by a reduction in LV wall thickness at the IVS and PW (23–28). Moreover, a meta-analysis, also based on echocardiographic studies, showed that the initiation of rhGH replacement therapy was associated with an increase in LV mass, IVS wall thickness, and PW thickness (33). In the present meta-analysis, when pooling the retrieved data on LV mass, a significant heterogeneity was found, mostly driven by a study by Gonzalez et al. (44), in which – contrarily to the common knowledge about the pathophysiological effect of GHD on cardiac structure – patients with GHD were found to have an increased LV mass compared to controls. However, as we already pointed out in the Results section of the present manuscript, this finding suffered from a remarkable bias given by the high rate of GHD patients with a poorly controlled hypertension; these patients, in fact, showed significantly higher systolic blood pressure values with respect to the control group (143 mmHg vs. 131 mmHg), with a reported mean systolic value above what is considered appropriate as an adequate target for blood pressure control. This could result in a significant bias on the retrieved results, as arterial hypertension, especially if poorly controlled, is a widely known stimulus for an increase in LV mass and, ultimately, a risk factor for the development of LV hypertrophy (61–63). When excluding this study from the analysis, the statistical pooling of the results retrieved by the other three studies unequivocally showed a significantly lower LV mass in GHD patients, which was consistent with previous findings by echocardiographic studies and, more broadly, with the well-established pathophysiology of the disease. When shifting the focus on the effect of rhGH replacement therapy on cardiac mass, the available data, as previously stated, are sparse; nevertheless, our findings were in line with those previously found by echocardiographic studies (33), showing an increase in LVMi after rhGH treatment initiation.

The main strength of this meta-analysis is the selection of studies assessing cardiac morphology and function by MRI, which is currently considered the gold-standard imaging technique to this scope. In fact, with respect to echocardiography, it is endowed with a higher accuracy and reproducibility, reducing the risk of biases, and possibly improving the potential to correctly characterize subtler cardiac abnormalities in patients with GHD. This is of utmost relevance when examining RV parameters; in fact, the echocardiographic assessment of the RV suffers from significant challenges and limitations and, within the specific

context of adult GHD, available echocardiographic studies provided almost no data about possible alterations in RV morphology and function.

Our meta-analysis had also some limitations. First, the strength of the conclusions was limited by the small number of available studies; this limitation could reasonably be expected, in light of the low frequency of GHD together with the relatively limited availability of cardiac MRI; on the other hand, as already pointed out, cardiac MRI has the significant advantage of a better precision and reproducibility of estimates compared to echocardiography, and it has been estimated that a sample size reduced by 80–95% is still sufficient to obtain equal statistical power compared to echocardiographic studies (38). Second, the quality of the results was limited by that of the included studies; however, the risk of bias was generally moderate-to-low, except for the study by Gonzalez et al. (44), whose potential biases have been already discussed and taken into account in the quantitative analyses. Third, patients' characteristics and inclusion criteria could differ between studies in some aspects, such as the underlying pituitary disease, the severity and presumed duration of GHD, and the diagnostic tests adopted for its definition, among others; this could be responsible for a certain degree of heterogeneity in the considered outcomes; nevertheless, heterogeneity is a common limitation of all meta-analyses, and appropriate statistical methods – such as the use of a random-effect model – were adopted to account for it. Fourth, the comparisons of cardiac MRI parameters between groups were all based on crude differences, as derived by univariate analyses; thus, the possible interplay with other predictors could not be evaluated. Fifth, no data were available about the effects of rhGH replacement therapy on cardiac function and morphology beyond the first year; therefore, the long-term course of cardiac MRI parameters during prolonged treatment with rhGH still remains to be elucidated.

CONCLUSIONS

In conclusion, the available evidence provided by cardiac MRI studies highlights significant left ventricular changes in patients with adult GHD, which are resumable as a reduction in end-diastolic volume, stroke volume, and ventricular mass; moreover, a significant increase in left ventricular mass can be seen after the initiation of rhGH replacement therapy. In addition, this is the first meta-analysis to provide a quantitative evaluation of the right ventricular involvement in GHD patients, for which echocardiographic data are nearly absent. Our results suggest a pattern of right ventricular alterations which is similar to left ventricular ones, with an almost significant reduction in end-diastolic volume and a statistical trend towards a lower stroke volume. This provides relevant information supporting a biventricular cardiac involvement in GHD, overall characterized by similar changes in left and right ventricular volumes and function.

DATA AVAILABILITY STATEMENT

The original contributions presented in the study are included in the article/**Supplementary Material**. Further inquiries can be directed to the corresponding author.

AUTHOR CONTRIBUTIONS

FB contributed to work conceptualization, data collection, data analysis and manuscript writing. NP, AB, CB, and MP-C contributed to data interpretation and manuscript writing. RF, SG, and EG supervised the manuscript drafting. VG contributed to work conceptualization, data collection, data analysis, manuscript writing and final draft supervision. All authors approved the manuscript in its final form.

SUPPLEMENTARY MATERIAL

The Supplementary Material for this article can be found online at: https://www.frontiersin.org/articles/10.3389/fendo.2022.910575/full#supplementary-material

REFERENCES

1. Molitch ME, Clemmons DR, Malozowski S, Merriam GR, Vance ML. Evaluation and Treatment of Adult Growth Hormone Deficiency: An Endocrine Society Clinical Practice Guideline. *J Clin Endocrinol Metab* (2011) 96:1587–609. doi: 10.1210/jc.2011-0179
2. Prodam F, Pagano L, Corneli G, Golisano G, Belcastro S, Busti A, et al. Update on Epidemiology, Etiology, and Diagnosis of Adult Growth Hormone Deficiency. *J Endocrinol Invest* (2008) 31(9 Suppl):6–11.
3. Appelman-Dijkstra NM, Kokshoorn NE, Dekkers OM, Neelis KJ, Biermasz NR, Romijn JA, et al. Pituitary Dysfunction in Adult Patients After Cranial Radiotherapy: Systematic Review and Meta-Analysis. *J Clin Endocrinol Metab* (2011) 96:2330–40. doi: 10.1210/jc.2011-0306
4. Gasco V, Cambria V, Bioletto F, Ghigo E, Grottoli S. Traumatic Brain Injury as Frequent Cause of Hypopituitarism and Growth Hormone Deficiency: Epidemiology, Diagnosis, and Treatment. *Front Endocrinol (Lausanne)* (2021) 12:634415. doi: 10.3389/fendo.2021.634415
5. Prodam F, Caputo M, Mele C, Marzullo P, Aimaretti G. Insights Into Non-Classic and Emerging Causes of Hypopituitarism. *Nat Rev Endocrinol* (2021) 17:114–29. doi: 10.1038/s41574-020-00437-2
6. Cook DM, Yuen KCJ, Biller BMK, Kemp SF, Vance ML. American Association of Clinical Endocrinologists Medical Guidelines for Clinical Practice for Growth Hormone Use in Growth Hormone-Deficient Adults and Transition Patients - 2009 Update. *Endocr Pract* (2009) 15:1–29. doi: 10.4158/EP.15.S2.1
7. Bioletto F, Parasiliti-Caprino M, Berton AM, Prencipe N, Cambria V, Ghigo E, et al. Development and Internal Validation of a Predictive Model for Adult GH Deficiency Prior to Stimulation Tests. *Front Endocrinol (Lausanne)* (2021) 12:737947. doi: 10.3389/fendo.2021.737947
8. Corneli G, Di Somma C, Baldelli R, Rovere S, Gasco V, Croce CG, et al. The Cut-Off Limits of the GH Response to GH-Releasing Hormone-Arginine Test Related to Body Mass Index. *Eur J Endocrinol* (2005) 153:257–64. doi: 10.1530/eje.1.01967
9. Gasco V, Ferrero A, Bisceglia A, Prencipe N, Cambria V, Bioletto F, et al. The Cut-Off Limits of GH Response to Insulin Tolerance Test Related to Body

Mass Index for the Diagnosis of Adult GH Deficiency. *Neuroendocrinology* (2020) 111:442–50. doi: 10.1159/000508103
10. Cuneo RC, Salomon F, McGauley GA, Sonksen PH. The Growth Hormone Deficiency Syndrome in Adults. *Clin Endocrinol (Oxf)* (1992) 37:387–97. doi: 10.1111/j.1365-2265.1992.tb02347.x
11. Svensson J, Bengtsson BÅVerifytat, Rosén T, Odén A, Johannsson G. Malignant Disease and Cardiovascular Morbidity in Hypopituitary Adults With or Without Growth Hormone Replacement Therapy. *J Clin Endocrinol Metab* (2004) 89:3306–12. doi: 10.1210/jc.2003-031601
12. Simpson H, Savine R, Sönksen P, Bengtsson BÅ, Carlsson L, Christiansen JS, et al. Growth Hormone Replacement Therapy for Adults: Into the New Millennium. *Growth Horm IGF Res* (2002) 12:1–33. doi: 10.1054/ghir.2001.0263
13. Carroll PV, Christ ER, Bengtsson BÅ, Carlsson L, Christiansen JS, Clemmons D, et al. Growth Hormone Deficiency in Adulthood and the Effects of Growth Hormone Replacement: A Review. *J Clin Endocrinol Metab* (1998) 83:382–95. doi: 10.1210/JCEM.83.2.4594
14. Di Somma C, Scarano E, Savastano S, Savanelli MC, Pivonello R, Colao A. Cardiovascular Alterations in Adult GH Deficiency. *Best Pract Res Clin Endocrinol Metab* (2017) 31:25–34. doi: 10.1016/j.beem.2017.03.005
15. Isgaard J, Arcopinto M, Karason K, Cittadini A. GH and the Cardiovascular System: An Update on a Topic at Heart. *Endocrine* (2015) 48:25–35. doi: 10.1007/s12020-014-0327-6
16. Colao A. The GH-IGF-I Axis and the Cardiovascular System: Clinical Implications. *Clin Endocrinol (Oxf)* (2008) 69:347–58. doi: 10.1111/j.1365-2265.2008.03292.x
17. Colao A, Di Somma C, Savanelli MC, De Leo M, Lombardi G. Beginning to End: Cardiovascular Implications of Growth Hormone (GH) Deficiency and GH Therapy. *Growth Horm IGF Res* (2006) 16:41–8. doi: 10.1016/j.ghir.2006.03.006
18. Rosén T, Bengtsson BÅ. Premature Mortality Due to Cardiovascular Disease in Hypopituitarism. *Lancet* (1990) 336:285–8. doi: 10.1016/0140-6736(90)91812-O
19. Bates AS, Van't Hoff W, Jones PJ, Clayton RN. The Effect of Hypopituitarism on Life Expectancy. *J Clin Endocrinol Metab* (1996) 81:1169–72. doi: 10.1210/jc.81.3.1169
20. Bülow B, Hagmar L, Mikoczy Z, Nordström CH, Erfurth EM. Increased Cerebrovascular Mortality in Patients With Hypopituitarism. *Clin Endocrinol (Oxf)* (1997) 46:75–81. doi: 10.1046/j.1365-2265.1997.d01-1749.x
21. Tomlinson JW, Holden N, Hills RK, Wheatley K, Clayton RN, Bates AS, et al. Association Between Premature Mortality and Hypopituitarism. *Lancet* (2001) 357:425–31. doi: 10.1016/S0140-6736(00)04006-X
22. Svensson J, Bengtsson BÅ, Rosén T, Odén A, Johannsson G. Malignant Disease and Cardiovascular Morbidity in Hypopituitary Adults With or Without Growth Hormone Replacement Therapy. *J Clin Endocrinol Metab* (2004) 89:3306–12. doi: 10.1210/jc.2003-031601
23. Lombardi G, Di Somma C, Grasso LFS, Savanelli MC, Colao A, Pivonello R. The Cardiovascular System in Growth Hormone Excess and Growth Hormone Deficiency. *J Endocrinol Invest* (2012) 35:1021–9. doi: 10.3275/8717
24. Colao A, Vitale G, Pivonello R, Ciccarelli A, Di Somma C, Lombardi G. The Heart: An End-Organ of GH Action. *Eur J Endocrinol* (2004) 151:93–101. doi: 10.1530/eje.0.151S093
25. Amato G, Carella C, Fazio S, La Montagna G, Cittadini A, Sabatini D, et al. Body Composition, Bone Metabolism, and Heart Structure and Function in Growth Hormone (GH)-Deficient Adults Before and After GH Replacement Therapy at Low Doses. *J Clin Endocrinol Metab* (1993) 77:1671–6. doi: 10.1210/JCEM.77.6.8263158
26. Colao A, Di Somma C, Cuocolo A, Spinelli L, Acampa W, Spiezia S, et al. Does a Gender-Related Effect of Growth Hormone (GH) Replacement Exist on Cardiovascular Risk Factors, Cardiac Morphology, and Performance and Atherosclerosis? Results of a Two-Year Open, Prospective Study in Young Adult Men and Women With Severe GH Defici. *J Clin Endocrinol Metab* (2005) 90:5146–55. doi: 10.1210/JC.2005-0597
27. Merola B, Cittadini A, Colao A, Longobardi S, Fazio S, Sabatini D, et al. Cardiac Structural and Functional Abnormalities in Adult Patients With Growth Hormone Deficiency. *J Clin Endocrinol Metab* (1993) 77:1658–61. doi: 10.1210/JCEM.77.6.8263155
28. Sartorio A, Ferrero S, Conti A, Bragato R, Malfatto G, Leonetti G, et al. Adults With Childhood-Onset Growth Hormone Deficiency: Effects of Growth Hormone Treatment on Cardiac Structure. *J Intern Med* (1997) 241:515–20. doi: 10.1111/J.1365-2796.1997.TB00010.X
29. Colao A, Di Somma C, Cuocolo A, Filippella M, Rota F, Acampa W, et al. The Severity of Growth Hormone Deficiency Correlates With the Severity of Cardiac Impairment in 100 Adult Patients With Hypopituitarism: An Observational, Case-Control Study. *J Clin Endocrinol Metab* (2004) 89:5998–6004. doi: 10.1210/jc.2004-1042
30. Chanson P. The Heart in Growth Hormone (GH) Deficiency and the Cardiovascular Effects of GH. *Ann Endocrinol (Paris)* (2021) 82:210–3. doi: 10.1016/j.ando.2020.03.005
31. Colao A, Cuocolo A, Di Somma C, Cerbone G, Della Morte AM, Pivonello R, et al. Does the Age of Onset of Growth Hormone Deficiency Affect Cardiac Performance? A Radionuclide Angiography Study. *Clin Endocrinol (Oxf)* (2000) 52:447–55. doi: 10.1046/J.1365-2265.2000.00972.X
32. Mihaila S, Mincu RI, Rimbas RC, Dulgheru RE, Dobrescu R, Magda SL, et al. Growth Hormone Deficiency in Adults Impacts Left Ventricular Mechanics: A Two-Dimensional Speckle-Tracking Study. *Can J Cardiol* (2015) 31:752–9. doi: 10.1016/j.cjca.2015.01.008
33. Maison P, Chanson P. Cardiac Effects of Growth Hormone in Adults With Growth Hormone Deficiency: A Meta-Analysis. *Circulation* (2003) 108:2648–52. doi: 10.1161/01.CIR.0000100720.01867.1D
34. Zhang S, Li Z, Lv Y, Sun L, Xiao X, Gang X, et al. Cardiovascular Effects of Growth Hormone (GH) Treatment on GH-Deficient Adults: A Meta-Analysis Update. *Pituitary* (2020) 23:467–75. doi: 10.1007/s11102-020-01036-0
35. Grothues F, Moon JC, Bellenger NG, Smith GS, Klein HU, Pennell DJ. Interstudy Reproducibility of Right Ventricular Volumes, Function, and Mass With Cardiovascular Magnetic Resonance. *Am Heart J* (2004) 147:218–23. doi: 10.1016/j.ahj.2003.10.005
36. Mooij CF, De Wit CJ, Graham DA, Powell AJ, Geva T. Reproducibility of MRI Measurements of Right Ventricular Size and Function in Patients With Normal and Dilated Ventricles. *J Magn Reson Imaging* (2008) 28:67–73. doi: 10.1002/jmri.21407
37. Dandel M, Hetzer R. Evaluation of the Right Ventricle by Echocardiography: Particularities and Major Challenges. *Expert Rev Cardiovasc Ther* (2018) 16:259–75. doi: 10.1080/14779072.2018.1449646
38. Bellenger NG, Davies LC, Francis JM, Coats AJS, Pennell DJ. Reduction in Sample Size for Studies of Remodeling in Heart Failure by the Use of Cardiovascular Magnetic Resonance. *J Cardiovasc Magn Reson* (2000) 2:271–8. doi: 10.3109/10976640009148691
39. Bellenger NG, Burgess MI, Ray SG, Lahiri A, Coats AJS, Cleland JGF, et al. Comparison of Left Ventricular Ejection Fraction and Volumes in Heart Failure by Echocardiography, Radionuclide Ventriculography and Cardiovascular Magnetic Resonance. Are They Interchangeable? *Eur Heart J* (2000) 21:1387–96. doi: 10.1053/euhj.2000.2011
40. Pennell DJ, Sechtem UP, Higgins CB, Manning WJ, Pohost GM, Rademakers FE, et al. Clinical Indications for Cardiovascular Magnetic Resonance (CMR): Consensus Panel Report. *Eur Heart J* (2004) 25:1940–65. doi: 10.1016/j.ehj.2004.06.040
41. Alfakih K, Reid S, Jones T, Sivananthan M. Assessment of Ventricular Function and Mass by Cardiac Magnetic Resonance Imaging. *Eur Radiol* (2004) 14:1813–22. doi: 10.1007/S00330-004-2387-0
42. Andreassen M, Faber J, Kjær A, Petersen CL, Kristensen LØ. Cardiac Function in Growth Hormone Deficient Patients Before and After 1 Year With Replacement Therapy: A Magnetic Resonance Imaging Study. *Pituitary* (2011) 14:1–10. doi: 10.1007/s11102-010-0250-7
43. De Cobelli F, Rossini A, Esposito A, Canu T, Manzoni G, Del Maschio A, et al. Short-Term Evaluation of Cardiac Morphology, Function, Metabolism and Structure Following Diagnosis of Adult-Onset Growth Hormone Deficiency. *Growth Horm IGF Res* (2019) 46–47:50–4. doi: 10.1016/j.ghir.2019.06.003
44. Gonzalez S, Windram JD, Sathyapalan T, Javed Z, Clark AL, Atkin SL. Effects of Human Recombinant Growth Hormone on Exercise Capacity, Cardiac Structure, and Cardiac Function in Patients With Adult-Onset Growth Hormone Deficiency. *J Int Med Res* (2017) 45:1708–19. doi: 10.1177/0300060517723798
45. Thomas JDJ, Dattani A, Zemrak F, Burchell T, Akker SA, Gurnell M, et al. Characterisation of Myocardial Structure and Function in Adult-Onset

Growth Hormone Deficiency Using Cardiac Magnetic Resonance. *Endocrine* (2016) 54:778–87. doi: 10.1007/s12020-016-1067-6
46. Moher D, Liberati A, Tetzlaff J, Altman DG, Altman D, Antes G, et al. Preferred Reporting Items for Systematic Reviews and Meta-Analyses: The PRISMA Statement. *PloS Med* (2009) 6:e1000097. doi: 10.1371/journal.pmed.1000097
47. Downes MJ, Brennan ML, Williams HC, Dean RS. Development of a Critical Appraisal Tool to Assess the Quality of Cross-Sectional Studies (AXIS). *BMJ Open* (2016) 6:1–7. doi: 10.1136/bmjopen-2016-011458
48. Sterne JA, Hernán MA, Reeves BC, Savović J, Berkman ND, Viswanathan M, et al. ROBINS-I: A Tool for Assessing Risk of Bias in non-Randomised Studies of Interventions. *BMJ* (2016) 355:i4919. doi: 10.1136/bmj.i4919
49. Andreassen M. The Growth Hormone System and Cardiac Function in Patients With Growth Hormone Disturbances and in the Normal Population. *Dan Med Bull* (2010) 57:1–21.
50. Javaid MR, Stone IS, Grossman AB, Korbonits M, Thomas JD, Petersen SE, et al. Cardiac Magnetic Resonance Myocardial Feature-Tracking: The Effect of Treatment in Patients With Adult-Onset Growth Hormone Deficiency and Acromegaly. *J Cardiovasc Magn Reson* (2013) 15:45–6. doi: 10.1186/1532-429X-15-S1-E55
51. Javaid MR, Stone I, Grossman A, Korbonits M, Thomas J, Petersen S, et al. Cardiac Magnetic Resonance Myocardial Feature Tracking: The Effect of Treatment in Patients With Adult-Onset Growth Hormone Deficiency and Acromegaly. *Int J Cardiol* (2013) 163:S60. doi: 10.1186/1532-429X-15-S1-E55
52. Dattani A, Thomas J, Zemrak F, Burchell TR, Petersen SE, Grossman A, et al. Cardiovascular Changes in Patients With Adult-Onset Growth Hormone Deficiency Assessed by CMR. *J Cardiovasc Magn Reson* (2012) 14:P192. doi: 10.1186/1532-429X-14-S1-P192
53. Hunter JJ, Chien KR. Signaling Pathways for Cardiac Hypertrophy and Failure. *N Engl J Med* (1999) 341:1276–83. doi: 10.1093/cvr/25.2.176
54. Cittadini A, Strömer H, Katz SE, Clark R, Moses AC, Morgan JP, et al. Differential Cardiac Effects of Growth Hormone and Insulin-Like Growth Factor-1 in the Rat. A Combined *In Vivo* and *In Vitro* Evaluation. *Circulation* (1996) 93:800–9. doi: 10.1161/01.CIR.93.4.800
55. Timsit J, Riou B, Bertherat J, Wisnewsky C, Kato NS, Weisberg AS, et al. Effects of Chronic Growth Hormone Hypersecretion on Intrinsic Contractility, Energetics, Isomyosin Pattern, and Myosin Adenosine Triphosphatase Activity of Rat Left Ventricle. *J Clin Invest* (1990) 86:507–15. doi: 10.1172/JCI114737
56. Colao A, Ferone D, Marzullo P, Lombardi G. Systemic Complications of Acromegaly: Epidemiology, Pathogenesis, and Management. *Endocr Rev* (2004) 25:102–52. doi: 10.1210/er.2002-0022
57. Clayton RN. Cardiovascular Function in Acromegaly. *Endocr Rev* (2003) 24:272–7. doi: 10.1210/ER.2003-0009
58. Colao A, Pivonello R, Grasso LFS, Auriemma RS, Galdiero M, Savastano S, et al. Determinants of Cardiac Disease in Newly Diagnosed Patients With Acromegaly: Results of a 10 Year Survey Study. *Eur J Endocrinol* (2011) 165:713–21. doi: 10.1530/EJE-11-0408
59. Tenuta M, Carlomagno F, Cangiano B, Kanakis G, Pozza C, Sbardella E, et al. Somatotropic-Testicular Axis: A Crosstalk Between GH/IGF-I and Gonadal Hormones During Development, Transition, and Adult Age. *Andrology* (2021) 9:168–84. doi: 10.1111/ANDR.12918
60. Altamirano F, Oyarce C, Silva P, Toyos M, Wilson C, Lavandero S, et al. Testosterone Induces Cardiomyocyte Hypertrophy Through Mammalian Target of Rapamycin Complex 1 Pathway. *J Endocrinol* (2009) 202:299–307. doi: 10.1677/JOE-09-0044
61. Nicholls MG. Hypertension, Hypertrophy, Heart Failure. *Heart* (1996) 76:92–7. doi: 10.1136/HRT.76.3_SUPPL_3.92
62. Yildiz M, Oktay AA, Stewart MH, Milani RV, Ventura HO, Lavie CJ. Left Ventricular Hypertrophy and Hypertension. *Prog Cardiovasc Dis* (2020) 63:10–21. doi: 10.1016/j.pcad.2019.11.009
63. Shenasa M, Shenasa H. Hypertension, Left Ventricular Hypertrophy, and Sudden Cardiac Death. *Int J Cardiol* (2017) 237:60–3. doi: 10.1016/j.ijcard.2017.03.002

Conflict of Interest: The authors declare that the research was conducted in the absence of any commercial or financial relationships that could be construed as a potential conflict of interest.

Publisher's Note: All claims expressed in this article are solely those of the authors and do not necessarily represent those of their affiliated organizations, or those of the publisher, the editors and the reviewers. Any product that may be evaluated in this article, or claim that may be made by its manufacturer, is not guaranteed or endorsed by the publisher.

frontiers | Frontiers in Endocrinology

TYPE Opinion
PUBLISHED 18 October 2022
DOI 10.3389/fendo.2022.1049595

OPEN ACCESS

EDITED BY
Alexandre Benani,
Centre National de la Recherche Scientifique (CNRS), France

REVIEWED BY
Shunji Yamada,
Kyoto Prefectural University of Medicine, Japan

*CORRESPONDENCE
Byung Ju Lee
bjlee@ulsan.ac.kr
Jin Kwon Jeong
jinkwon0911@gwu.edu

SPECIALTY SECTION
This article was submitted to Neuroendocrine Science, a section of the journal Frontiers in Endocrinology

RECEIVED 20 September 2022
ACCEPTED 06 October 2022
PUBLISHED 18 October 2022

CITATION
Lee BJ and Jeong JK (2022) Positioning-dependent bidirectional NELL2 signaling in the brain. *Front. Endocrinol.* 13:1049595. doi: 10.3389/fendo.2022.1049595

Positioning-dependent bidirectional NELL2 signaling in the brain

Byung Ju Lee[1*] and Jin Kwon Jeong[2*]

[1]Department of Biological Sciences, College of Natural Sciences, University of Ulsan, Ulsan, South Korea, [2]Department of Pharmacology and Physiology, School of Medicine & Health Sciences, The George Washington University, Washington, DC, United States

KEYWORDS

NELL2, neurotrophic peptide, endoplasmic reticulum, protein kinase C (PKC), cardiometabolism

Introduction

A network with appropriate quality and quantity of intercellular and intracellular communication is fundamental for healthy brain function. In other words, molecular, cellular, and structural impairments of brain cells are associated with a broad range of pathophysiological conditions, including aging and age-associated diseases, motor and behavioral symptoms, and metabolic syndromes. A neural tissue-specific epidermal growth factor (EGF)-like protein was first identified in 1995 in chick embryos and named NEL (1). Subsequently, two mammalian homologs of chicken NEL were identified in rodents and humans and named NELL1 and NELL2 (2, 3). Among them, NELL2 is more closely related to NEL and is highly conserved among species including humans. An expression profile of NELL2 in rodent brains revealed the broad distribution of NELL2 throughout the entire brain (4). Interestingly, accumulating evidence has demonstrated that NELL2 is a secreting neuropeptide (2, 3, 5) and, at the same time, is an intracellular neuromodulator through a direct interaction with protein kinase C (PKC) within neurons (6, 7). Importantly, these investigations have further indicated a positioning-dependent conflicting outcome of NELL2-triggered signaling in downstream target gene activation within neurons (7) as well as in competitive synaptic remodeling between neurons (8, 9). Therefore, this review will discuss a site-specific multifactorial nature of NELL2 action in brain, and further a possible involvement of NELL2 in central cardiometabolism regulation.

A site of NELL2 action: Intracellular vs. extracellular

In the beginning, investigations have mainly focused to characterize the biochemical and structural signature of NELL2 protein (2, 3), and revealed that NELL2 peptide consists of multiple functional domains, including the von Willebrand factor C, a thrombospondin-1-like structure, and several EGF-like repeats. In particular, some of the EGF-repeat domains possessed Ca^{2+}-binding ability. The physiological function of these domains remains largely unidentified; however, accumulated investigations have recognized that these domains share common characteristics with extracellular matrix proteins known to be critical in neural growth and development (2, 3, 10). Indeed, NELL2 is a glycosylated protein and possesses a signal peptide domain that is necessary for secreting proteins (3), and is able to bind to the roundabout (Robo) family of membrane receptors (9, 11, 12), or an orphan receptor tyrosine kinase, c-ros oncogene 1 (ROS1) (13). Within the cytoplasm, localization of NELL2 was highly limited to the endoplasmic reticulum (ER), Golgi apparatus, and moving vesicles between soma and axons (5). These investigations together clearly indicate the nature of NELL2 as a secreting neuropeptide.

On the other hand, other studies have recognized an intracellular NELL2 action through the PKC–ERK pathway. In these studies, NELL2 was identified as a PKC-binding intracellular molecule through the EGF-like motifs (6), and an ablation of endogenous NELL2 synthesis reduced the survival of neurons under cell death conditions (14), and resulted in the shortening axonal projections of cells (8), both of which through the downregulation of ERK signaling. Based on these studies, it is reasonable to mention that NELL2 is a novel and unique molecule that can trigger both intracellular and extracellular signaling pathways simultaneously. Additionally, the EGF-like motifs on NELL2 might be the key to induce NELL2-dependent signaling cascades, regardless of the area of NELL2 action.

Positioning-dependent contrasting NELL2 signaling

Our recent findings newly recognized a NELL2 function on gene expression of preproenkephalin (PPE) (7), a precursor peptide for multiple endogenous opioids that have been known to be involved in diverse brain functions including pain, stress, and cardiovascular and metabolic regulation (15–19). In this study, we first observed a negative regulatory role of intracellular NELL2 on PPE gene expression. Before being released, endogenously biosynthesized NELL2 would be processed through the ER as mentioned above (5), and therefore, an expression vector carrying a NELL2-coding region conjugated with an ER retention motif has been utilized to confine NELL2 in the ER. Importantly, accumulated NELL2 in the ER resulted in a reduced PPE gene expression through the Ca^{2+}-binding EGF motifs, by downregulating a series of intracellular signaling pathways including PKC, ERK, and c-Fos. Surprisingly, the overall outcomes were opposite from the extracellular NELL2: a level of PKC, ERK, and c-Fos signaling is upregulated following extracellular NELL2 treatment, and thus, gene expression of PPE is enhanced. Additionally, the intracellular NELL2 action seemed to be dominant to extracellular NELL2 signaling in terms of PPE gene expression as an *in vivo* disruption of NELL2 synthesis resulted in an enhanced PPE gene expression in the rat brains. These observations clearly indicate a positioning-dependent bidirectional NELL2 function on PPE gene expression.

Interestingly, recent studies have also demonstrated a role for NELL2 in competitive synaptic remodeling in neurons (8, 9). Both extracellular and intracellular NELL2 induced overall axonal elongation of neurons (8), and therefore, NELL2 is suggested to be an activator of axonal projections regardless of the site of action. However, another investigation has further demonstrated that cells that received extracellular NELL2 from a certain direction withhold their fibers from the cell surface facing the NELL2, but elongate their fibers to the opposing direction (9). Therefore, the nature of extracellular NELL2 on axonal growth is likely inhibitory. Together, these results indicate a positioning-dependent opposing effect of NELL2 on PPE gene expression as well as synaptic remodeling.

A possible role of NELL2 in central cardiometabolism regulation

As mentioned above, qualitative and quantitative information on NELL2-dependent molecular and cellular mechanisms is now available. However, a physiological NELL2 function has not been well determined in adult mammalian brains. Interestingly, our anatomical approaches to determining brain distribution of NELL2 revealed a relatively high expression of NELL2 in terms of both mRNA and protein levels in multiple cardiometabolic nuclei, including the subfornical organ (SFO), paraventricular and ventromedial hypothalamic nucleus (PVN and VMH, respectively), and the arcuate nucleus (ARC) in adult rodent brains (4, 20). Especially in the ARC, NELL2 expression is detected on proopiomelanocortin (POMC) cells as well as cells expressing neuropeptide Y (NPY) (20). In the context of central cardiometabolism regulation, the SFO and ARC are believed to be the forebrain gates for circulating cardiometabolic signaling molecules, and transform the information into the deep brain regions, such as the PVN, to regulate neuroendocrine and

autonomic outcomes for the preservation of cardiometabolic homeostasis (21, 22). Following these anatomical observations, studies utilizing the loss-of-function approach further demonstrated an involvement of NELL2 in metabolism regulation (20). Hypothalamus-targeted ablation of NELL2 biosynthesis in adult rats resulted in a reduction in daily food intake and body weight gain. In addition, mRNA levels of hypothalamic NELL2 were increased under fasting conditions compared to those in a fed state. These molecular and behavioral results clearly indicate an involvement of hypothalamic NELL2 in metabolic homeostasis as an orexigenic molecule. Unlike PPE, NELL2 did not affect the gene expression of both POMC and NPY in the ARC. Therefore, an investigation aimed at understanding the detailed underlying mechanism through which NELL2 affects metabolism regulation is necessary.

Conclusion

NELL2 is a secreting neuropeptide and thus believed to be an extracellular signaling molecule with an autocrine, paracrine, and/or endocrine nature. At the same time, NELL2 also possesses the ability to modify ER-initiated intracellular signaling pathways. A striking finding from us and other groups is that the outcome of NELL2 signaling is dependent on the site of NELL2 action: the effects of intracellular NELL2 signaling in terms of downstream gene expression and/or synaptic reorganization could be reversed by the NELL2 signaling initiated extracellularly.

In spite of recent efforts, NELL2-mediated cellular signaling and physiological functions are still largely unknown. For example, NELL2 is able to bind to certain receptors as described above; however, specific receptor-dependent NELL2 signaling has not been elucidated. Additionally, there is a possibility that some cells utilize NELL2 only as an intracellular modulator while the other cells use it exclusively as an extracellular molecule. Therefore, in-depth and targeted investigations to address these questions are clearly necessary.

NELL2 is a newly identified rising molecule in the field of brain physiology, and the site of NELL2 action should be considered in future studies.

Author contributions

BL and JJ equally contributed to the design and development of the draft, and approved the final manuscript.

Funding

This research was supported by the Priority Research Centers Program (2014R1A6A1030318) through the National Research Foundation of Korea (to BL).

Conflict of interest

The authors declare that the research was conducted in the absence of any commercial or financial relationships that could be construed as a potential conflict of interest.

Publisher's note

All claims expressed in this article are solely those of the authors and do not necessarily represent those of their affiliated organizations, or those of the publisher, the editors and the reviewers. Any product that may be evaluated in this article, or claim that may be made by its manufacturer, is not guaranteed or endorsed by the publisher.

References

1. Matsuhashi S, Noji S, Koyama E, Myokai F, Ohuchi H, Taniguchi S, et al. New gene, nel, encoding a m(r) 93 K protein with EGF-like repeats is strongly expressed in neural tissues of early stage chick embryos. *Dev Dyn* (1995) 203 (2):212–22. doi: 10.1002/aja.1002030209

2. Watanabe TK, Katagiri T, Suzuki M, Shimizu F, Fujiwara T, Kanemoto N, et al. Cloning and characterization of two novel human cDNAs (NELL1 and NELL2) encoding proteins with six EGF-like repeats. *Genomics* (1996) 38(3):273–6. doi: 10.1006/geno.1996.0628

3. Kuroda S, Oyasu M, Kawakami M, Kanayama N, Tanizawa K, Saito N, et al. Biochemical characterization and expression analysis of neural thrombospondin-1-like proteins NELL1 and NELL2. *Biochem Biophys Res Commun* (1999) 265(1):79–86. doi: 10.1006/bbrc.1999.1638

4. Jeong JK, Kim HR, Hwang SM, Park JW, Lee BJ. Region- and neuronal phenotype-specific expression of NELL2 in the adult rat brain. *Mol Cells* (2008) 26 (2):186–92.

5. Ha CM, Hwang EM, Kim E, Lee DY, Chang S, Lee BJ, et al. The molecular mechanism of NELL2 movement and secretion in hippocampal progenitor HiB5 cells. *Mol Cells* (2013) 36(6):527–33. doi: 10.1007/s10059-013-0216-5

6. Kuroda S, Tanizawa K. Involvement of epidermal growth factor-like domain of NELL proteins in the novel protein-protein interaction with protein kinase c. *Biochem Biophys Res Commun* (1999) 265(3):752–7. doi: 10.1006/bbrc.1999.1753

7. Ha CM, Kim DH, Lee TH, Kim HR, Choi J, Kim Y, et al. Transcriptional regulatory role of NELL2 in preproenkephalin gene expression. *Mol Cells* (2022) 45 (8):537–49. doi: 10.14348/molcells.2022.2051

8. Kim HR, Kim DH, An JY, Kang D, Park JW, Hwang EM, et al. NELL2 function in axon development of hippocampal neurons. *Mol Cells* (2020) 43 (6):581–9.

9. Jaworski A, Tom I, Tong RK, Gildea HK, Koch AW, Gonzalez LC, et al. Operational redundancy in axon guidance through the multifunctional receptor

Robo3 and its ligand NELL2. *Science* (2015) 350(6263):961–5. doi: 10.1126/science.aad2615

10. Nakamura R, Nakamoto C, Obama H, Durward E, Nakamoto M. Structure-function analysis of nel, a thrombospondin-1-like glycoprotein involved in neural development and functions. *J Biol Chem* (2012) 287(5):3282–91. doi: 10.1074/jbc.M111.281485

11. Pak JS, DeLoughery ZJ, Wang J, Acharya N, Park Y, Jaworski A, et al. NELL2-Robo3 complex structure reveals mechanisms of receptor activation for axon guidance. *Nat Commun* (2020) 11(1):1489. doi: 10.1038/s41467-020-15211-1

12. Yamamoto N, Kashiwagi M, Ishihara M, Kojima T, Maturana AD, Kuroda S, et al. Robo2 contains a cryptic binding site for neural EGFL-like (NELL) protein 1/2. *J Biol Chem* (2019) 294(12):4693–703. doi: 10.1074/jbc.RA118.005819

13. Kiyozumi D, Noda T, Yamaguchi R, Tobita T, Matsumura T, Shimada K, et al. NELL2-mediated lumicrine signaling through OVCH2 is required for male fertility. *Science* (2020) 368(6495):1132–5. doi: 10.1126/science.aay5134

14. Choi EJ, Kim DH, Kim JG, Kim DY, Kim JD, Seol OJ, et al. Estrogen-dependent transcription of the NEL-like 2 (NELL2) gene and its role in protection from cell death. *J Biol Chem* (2010) 285(32):25074–84. doi: 10.1074/jbc.M110.100545

15. Bowman BR, Goodchild AK. GABA and enkephalin tonically alter sympathetic outflows in the rat spinal cord. *Auton Neurosci* (2015) 193:84–91. doi: 10.1016/j.autneu.2015.08.006

16. Ikeda H, Ardianto C, Yonemochi N, Yang L, Ohashi T, Ikegami M, et al. Inhibition of opioid systems in the hypothalamus as well as the mesolimbic area suppresses feeding behavior of mice. *Neuroscience* (2015) 311:9–21. doi: 10.1016/j.neuroscience.2015.10.002

17. Will MJ, Vanderheyden WM, Kelley AE. Striatal opioid peptide gene expression differentially tracks short-term satiety but does not vary with negative energy balance in a manner opposite to hypothalamic NPY. *Am J Physiol Regul Integr Comp Physiol* (2007) 292(1):R217–26. doi: 10.1152/ajpregu.00852.2005

18. Yang J, Zhang L, Xie P, Pan M, Ma G. Transplantation of mesenchymal stromal cells expressing the human preproenkephalin gene can relieve pain in a rat model of neuropathic pain. *Neurochem Res* (2020) 45(9):2065–71. doi: 10.1007/s11064-020-03068-1

19. Melo I, Drews E, Zimmer A, Bilkei-Gorzo A. Enkephalin knockout male mice are resistant to chronic mild stress. *Genes Brain Behav* (2014) 13(6):550–8. doi: 10.1111/gbb.12139

20. Jeong JK, Kim JG, Kim HR, Lee TH, Park JW, Lee BJ. A role of central NELL2 in the regulation of feeding behavior in rats. *Mol Cells* (2017) 40(3):186–94.

21. Jeong JK, Dow SA, Young CN. Sensory circumventricular organs, neuroendocrine control, and metabolic regulation. *Metabolites* (2021) 11(8):494. doi: 10.3390/metabo11080494

22. Jeong JK, Kim JG, Lee BJ. Participation of the central melanocortin system in metabolic regulation and energy homeostasis. *Cell Mol Life Sci* (2014) 71 (19):3799–809. doi: 10.1007/s00018-014-1650-z

frontiers | Frontiers in Endocrinology

TYPE Review
PUBLISHED 22 December 2022
DOI 10.3389/fendo.2022.1078955

OPEN ACCESS

EDITED BY
Alexandre Benani,
Centre National de la Recherche Scientifique (CNRS), France

REVIEWED BY
Zhi Yi Ong,
University of New South Wales, Australia
Jin Kwon Jeong,
George Washington University, United States

*CORRESPONDENCE
Laura Dearden
ld454@medschl.cam.ac.uk

SPECIALTY SECTION
This article was submitted to Neuroendocrine Science, a section of the journal Frontiers in Endocrinology

RECEIVED 24 October 2022
ACCEPTED 06 December 2022
PUBLISHED 22 December 2022

CITATION
Furigo IC and Dearden L (2022) Mechanisms mediating the impact of maternal obesity on offspring hypothalamic development and later function. *Front. Endocrinol.* 13:1078955. doi: 10.3389/fendo.2022.1078955

Mechanisms mediating the impact of maternal obesity on offspring hypothalamic development and later function

Isadora C. Furigo[1] and Laura Dearden[2]*

[1]Centre for Sport, Exercise and Life Sciences, School of Life Sciences, Coventry University, Coventry, United Kingdom, [2]Metabolic Research Laboratories, Wellcome MRC Institute of Metabolic Science, University of Cambridge, Cambridge, United Kingdom

As obesity rates have risen around the world, so to have pregnancies complicated by maternal obesity. Obesity during pregnancy is not only associated with negative health outcomes for the mother and the baby during pregnancy and birth, there is also strong evidence that exposure to maternal obesity causes an increased risk to develop obesity, diabetes and cardiovascular disease later in life. Animal models have demonstrated that increased weight gain in offspring exposed to maternal obesity is usually preceded by increased food intake, implicating altered neuronal control of food intake as a likely area of change. The hypothalamus is the primary site in the brain for maintaining energy homeostasis, which it coordinates by sensing whole body nutrient status and appropriately adjusting parameters including food intake. The development of the hypothalamus is plastic and regulated by metabolic hormones such as leptin, ghrelin and insulin, making it vulnerable to disruption in an obese *in utero* environment. This review will summarise how the hypothalamus develops, how maternal obesity impacts on structure and function of the hypothalamus in the offspring, and the factors that are altered in an obese *in utero* environment that may mediate the permanent changes to hypothalamic function in exposed individuals.

KEYWORDS

Obesity, hypothalamus, pregnancy, developmental programming, food intake

1 Introduction

There can be no doubt that the world is in the midst of an obesity crisis. The rise in obesity has occurred in both sexes and across all ages, meaning that there has inevitably been an increase in the number of pregnancies complicated by obesity. The most recent figures from the UK collected in 2019 show that 27.4% of women were overweight and 21.6% were living with obesity or severe obesity at the time of their first antenatal appointment (usually around 8-10 weeks gestation) (1). In the USA, figures from 2019 show that 29% of women were living with obesity when they became pregnant (2). This data is from before the Covid-

19 pandemic, during which we know that obesity rates have risen globally. Post- pandemic figures from Scotland collected in 2021 show that 25.9% of women entered pregnancy whilst living with obesity or severe obesity (3).

Obesity during pregnancy is associated with negative health outcomes for the mother and the baby both during pregnancy and birth. For the mother, obesity is associated with greater odds of developing gestational diabetes (GDM), hypertension and the life-threatening condition pre-eclampsia. For the fetus, maternal obesity is associated with an increased risk of stillbirth, being born both small or large for gestational age, and an increased incidence of emergency caesarean birth. As well as these immediate effects on the health of the mother and the baby, exposure to maternal obesity during pregnancy is also associated with more long-term health problems in offspring. There is now strong evidence that exposure to maternal obesity causes an increased risk to develop obesity, diabetes, and cardiovascular disease later in life.

It is extremely concerning that the most recent report from the National Child Measurement Programme in the UK reported that nearly 30% of children in Reception (age 4 and 5 years old) are overweight or living with obesity (4). The children of today are the parents of tomorrow- meaning that pregnancies complicated by parental obesity are likely to become even more common. It is clear there is a pressing need for more interventions- be they lifestyle based or pharmacological- to stop the inter-generational transmission of obesity risk. There is also a lack of sound advice for expectant parents- in many cultures the old missive of "eating for two" during pregnancy still prevails. However, in order for researchers and health care professionals to deliver sound clinical advice and interventions, we first need to understand the mechanisms by which changes in the *in utero* environment of an obese pregnancy are translated into an increased cardio- metabolic disease risk in offspring. Animal models have consistently demonstrated that increased weight gain in offspring exposed to maternal obesity is preceded by increase food intake, implicating altered neuronal control of food intake as a likely area of change. The hypothalamus is the primary site in the brain for maintaining energy homeostasis, which it does by appropriately adjusting parameters including food intake. This review will summarise how the hypothalamus develops, how maternal obesity impacts on structure and function of the hypothalamus, and the factors that are altered in an obese *in utero* environment that may program these changes.

2 Development of hypothalamic energy balance circuits

Neurons and regions within the neuroendocrine portion of the hypothalamus are largely characterized by the neuropeptides and neurotransmitters that have been defined over the last half-century. As researchers continue to uncover the complexity of hypothalamic circuitry it is becoming clear that it may not be sufficient to classify a neuronal sub-type based on its expression of a specific, well-known neuropeptide. Indeed, recent studies have demonstrated the heterogeneity of neurons not only within a defined region of the hypothalamus, such as the arcuate nucleus (ARC) (5) but also within what was previously thought of as being one sub-type of neuron, for example proopiomelanocortin (POMC) neurons (6). Continued efforts to define the genetic make-up of all neurons within the hypothalamus and collate this into large datasets (7) will undoubtedly further our understanding of how the hypothalamus develops, as well as functions.

The data described in this section is essentially limited to rodents, as- for obvious reasons- there is a paucity of data on hypothalamic development in non-human primates (NHP) and humans. Although the highly conserved functions of hypothalamic regions between rodents and higher organisms suggest that many developmental mechanisms may be shared, our knowledge of NHP and human hypothalamic development is far from complete. The hypothalamus is a region of the brain where neurons are added for an extended prenatal period and are even born postnatally (8). There is also considerable remodelling of hypothalamic connections during the early post-natal period. Therefore, both the fetal and neonatal period represent critical periods of vulnerability in the hypothalamus.

2.1 Neurogenesis and cell fate determination

Over the past fifty years, numerous models have been proposed as to how the forebrain, including the hypothalamus, develops. Although many early models have now been disproved by the advent of data showing the temporal expression of specific transcription factors, there remains a dispute as to whether the hypothalamus and telencephalon should be classed as a single unit, termed the secondary prosencephalon (9), or whether the hypothalamus is part of the diencephalon (10). The cells that will form the hypothalamus are primarily derived from precursor cells located in a proliferative zone in the neuroepithelium of the third ventricle. In rodents, by embryonic day (E) 10, the presumptive hypothalamus has acquired regional identity by the combined action of morphogens such as Shh (extensively reviewed in (11)) and a well-characterised transcriptional network (e.g., *Nkx2.1, Six3, Otp*). For an excellent comprehensive review of early hypothalamic regional patterning and progenitor cell determination see Burbridge et al. (12). The early hypothalamus can be roughly divided into three regions along it's rostral to caudal axis- the anterior,

tuberal and posterior regions. Once these hypothalamic regions are established, the progenitors within begin to acquire their subtype-specific identities.

The neuroendocrine portion of the hypothalamus- which is the primary site of feeding regulatory pathways- comprises the anterior and tuberal hypothalamus. In the tuberal hypothalamus, all neurons are produced during a period of only a few days (13). The majority of neurons in the paraventricular nucleus (PVH) and dorsomedial nucleus (DMH) are generated between E12-E14, whereas the ARC and ventromedial nucleus (VMH) have longer periods of neuronal generation from E12-E16 (14, 15). Following this initial wave of neurogenesis in the hypothalamus, there is a gradual shift to gliogenesis that generates hypothalamic astrocytes (13).

The Notch signalling pathway is a key regulator of neurogenesis in the central nervous system (CNS). As Notch signalling inhibits pro-neural genes, models lacking Notch signalling exhibit an increase in neurons throughout the embryo (16). Conditional loss of function mice using *Nkx2.1*-Cre to specifically knock out Notch signalling in the hypothalamus show that Notch signalling is essential for the differentiation of late ARC neurons in the mouse from E13.5 (17). The pro-neural transcription factor Mash1 is inhibited by Notch signalling, and loss of Mash1 in a mouse model is associated with a reduction of POMC and NPY neurons in the ARC (18). Consistent with this study, mice lacking Notch signalling in hypothalamic cells show an increased number of POMC and NPY neurons (17).

2.2 Neurite extension

Neuronal axons grow by extending a growth cone, which travels toward a target and trails behind it the growing neurite. The path of a growing axon is determined by cell-cell interactions and diffusible chemorepulsive and chemoattractive cues. Axon guidance molecules such as netrins (19), ephrins (20) and semaphorins have been show to regulate axon growth in the hypothalamus. Semaphorins are one of the largest family of guidance molecules. The semaphorin 3 family members are required for correct development of hypothalamic reproductive pathways (21), and the melanocortin system; if the semaphorin receptor Neuropillin is disrupted then neurite projections from the ARC innervate the VMH rather than their correct target, the PVH (22).

Dii tracing studies demonstrate that hypothalamic connections develop with a high degree of spatial and temporal specificity, innervating each target with a unique developmental schedule which in many cases can be correlated with the functional maturity of the projection (23). The development of axonal projections from the ARC begins prenatally. As early as E14, there are long descending projections from POMC neurons that follow a longitudinal route towards the upper thoracic spinal cord (24). Intra-hypothalamic connections from the ARC to other hypothalamic areas such as the PVH form post-natally. Studies by Bouret et al. have elegantly demonstrated that projections from the ARC do not represent an adult distribution until post-natal day (PND) 18 in mice, with connections specifically between the ARC and PVH forming between PND8-10 (25). Further studies in rodents have demonstrated that orexigenic NPY positive neurons from the ARC innervate the PVH at PND10-11, but brainstem NPY positive neuronal fibers arrive at the PVH much earlier and are present from PND2 (26). In comparison, in the NHP the development of NPY positive projections from the ARC occurs during the third trimester of gestation, and offspring are born with an abundance of NPY positive fibers originating from the ARC. However, the pattern of ARC projections seen in the NHP in late gestation is less dense than in adults, suggesting additional refinement of the connectivity occurs in the post-natal period (27), as in rodents.

2.3 Epigenetic regulation of neural maturation

It is becoming increasingly apparent that epigenetic processes play an important role in maturation of the hypothalamus. Extensive changes in DNA methylation that differentiate between neurons and non-neuronal sub types in the ARC and PVH occur in the early post-natal period in rodents (28). The activity of both methylating and de-methylating enzymes in the hypothalamus is developmentally regulated and shows different activity patterns between male and female brains (29). Most recently, MacKay et al. have shown that post-natal epigenetic maturation in the ARC is cell type and sex specific and occurs particularly in genomic regions enriched for heritability of BMI in humans (30).

There is accumulating evidence that miRNAs, which are small non- coding RNAs that regulate gene function through degradation of mRNAs and/or inhibition of protein translation (31), may reflect an important mechanism by which maternal environment can alter long-term phenotypes in the offspring (32, 33). Although hypothalamic miRNAs are still not well characterised- either in adult life or during development- a recent paper has shown that 30% of the miRNAs present in the ARC show altered expression throughout the post-natal period (34). Furthermore, Croizier and colleagues have shown that miR103/107 are required for the process when POMC expressing precursors switch to become mature NPY expressing neurons (35).

3 Impact of maternal obesity on the offspring hypothalamus

The hypothalamus is a highly dynamic region of the brain that is continually sensing and responding to changes in the nutrition status of the body. It has been extensively shown that the hypothalamus retains plasticity throughout life, and indeed this is required for hypothalamic function. In addition to the high plasticity in the adult hypothalamus, development of the hypothalamus is closely coupled to the external environment (via the involvement of metabolic hormones in neurodevelopmental processes) and is therefore extremely vulnerable to disruption in both the *in utero* and neonatal period. In this section we describe how exposure to maternal obesity alters hypothalamic structure and function in the offspring (summarised in Figure 1). Interestingly, many of the routes through which maternal obesity impacts on the offspring hypothalamus are similar to disruptions observed in human adults with obesity (for e.g.: reduced hypothalamic proliferation (36), disrupted wiring of melanocortin pathways (22), altered nutrient sensing (37)), although in the context of adult obesity it is hard to separate cause and effect.

It is important to note that due to the inherent differences between the sexes in both brain structure and control of metabolism, the consequences of exposure to maternal obesity in the offspring hypothalamus may vary between the sexes. Unfortunately, to date not enough studies have been conducted in both sexes to draw clear conclusions on sex differences in this brain region. However, there is some evidence that the maternal obesity related programming of hypertension and altered heart rate *via* the melanocortin system in the hypothalamus may be sex- specific (38), as may be programming of hypothalamic- pituitary- adrenal axis (39) and glucose-sensitive gene transcription regulation in the PVH (40). For a general review of sex differences in the offspring phenotype following exposure to maternal obesity, see (41).

3.1 Cell guidance signals

As discussed above, axon guidance cues such as netrins and semaphorins are essential for correct hypothalamic development. Unfortunately, how these signals may be pathogenically altered is understudied in animal models of maternal obesity. However, a mouse study has shown that the offspring of obese mothers have altered levels of the Netrin receptors Dcc and Unc5d in the fetal ARC, and this is associated with significantly reduced NPY fibre innervation of the PVH compared with that in offspring from lean mothers (42). A recent study by van der Klaauw et al. (22) provides direct evidence that disrupting semaphorin systems in the hypothalamus leads to early-onset obesity in zebrafish, mice, and humans. This research identified 40 rare variants in semaphorin 3 signalling in people living with severe obesity which caused disruption of signalling in melanocortin circuits. This is the first evidence that disruption to the machinery required for axonal guidance in the hypothalamus can cause obesity and highlights the need for more research investigating how this process is altered in the context of maternal obesity.

3.2 Neurogenesis

Neurogenesis occurs throughout life in the hypothalamus. The impact of maternal obesity on hypothalamic neurogenesis appears to vary depending on age of the offspring. Maternal

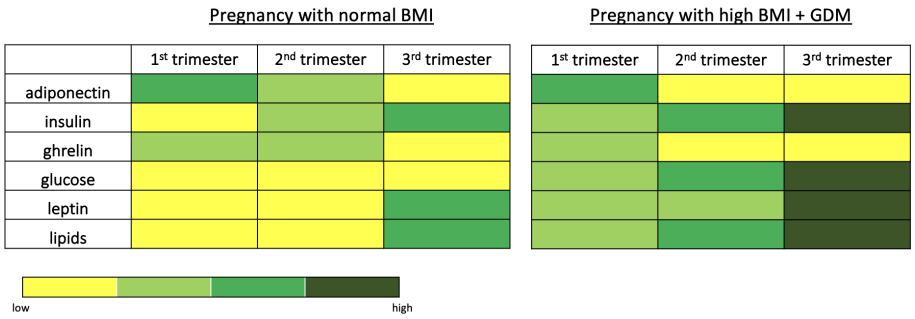

FIGURE 1
Main routes by which maternal obesity impacts on hypothalamic development and function in the offspring. Animal models have shown that exposure to maternal obesity impacts on hypothalamic development throughout fetal development. Maternal obesity is associated with reduced proliferation of hypothalamic progenitor cells in the fetal and neonatal hypothalamus, whether this is a permanent reduction or a delay in the normal neurogenic process is unknown. The formation of intra- hypothalamic projections- particularly in the melanocortin system- is also disrupted in offspring exposed to maternal obesity. This may be due to altered signalling of neurotrophic factors such as leptin, resulting in a reduction in neurite projections, or altered expression of axon guidance cues, resulting in incorrect targets of growing neurites. The offspring of obese mothers also show reduced nutrient sensing, which is one of the primary functions of the hypothalamus and required for the correct regulation of energy homeostasis.

obesity results in a reduction in the proliferative potential of hypothalamic neural progenitor cells generated from the fetal hypothalamus on E13 (43) and neurogenic markers in newborn mice (44), whereas an increase in proliferative markers has been reported in the hypothalamus of mice born from an obese pregnancy at PND 21 (45). Whether the early reductions in neurogenesis reflect a permanent reduction, or simply a delay in the peak of proliferation in the embryonic hypothalamus is currently unclear. The Notch signalling pathway is key for the regulation of neurogenesis within the hypothalamus. Exposure to maternal obesity results in an up-regulation of Notch signalling in the neonatal period (43), and a concomitant decrease in expression of the pro-neural transcription factor Mash (44) which may underlie some of the reports of reduced neurogenesis.

3.3 Alterations to the melanocortin system

The central melanocortin system is a collection of circuits capable of sensing signals from a wide array of hormones, nutrients and neural inputs. Long-term energy signals from leptin and insulin received by the hypothalamus are integrated with acute signals regulating hunger and satiety, primarily received by the brainstem. Exposure to maternal obesity has been shown to alter frequently studied components of this system are the NPY/AgRP and POMC positive fibres projecting from the ARC to the PVH. These projections are reduced in numerous animal models of maternal obesity and/or diabetes, ranging from rodents to NHP (46–49). Reduction in the number of projections of POMC expressing neurons is also observed in offspring exposed to maternal over-nutrition exclusively during the post-natal period, reflecting the fact that these projections form post-natally in rodents and are vulnerable to disruption during this developmental time window (50). Previous studies have also shown increased gene expression of the target of ARC POMC containing projections- the melanocortin 4 receptor (MC4R) in the PVH- in offspring exposed to maternal obesity, which is also modulated by pup nutrition in the post-natal period (51). A recent study of the translatomic signatures of POMC neurons in offspring after exposure to maternal obesity revealed an altered translatome consistent with other reports of aberrant neuronal development and axonal growth (52).

3.4 Nutrient sensing

One of the primary roles of the hypothalamus is to sense changes in nutrient status in the rest of the body, *via* information received from circulating hormones and nutrients. Exposure to maternal obesity is associated with signs of hypothalamic insulin resistance in offspring in both during the *in utero* and post-natal period (43, 53). Many rodent models have utilised post-natal small litter rearing as a way to cause neonatal over-nutrition, and show outcomes similar to the over-nutrition that is experienced in the post-natal period in models of maternal obesity and/or maternal over-nutrition. Neonatal overnutrition is associated with resistance to a host of metabolic hormones including ghrelin (54), leptin (55) and insulin in ARC neurons (56). Studies across a range of species have shown that exposure to over-nutrition- whether *via* maternal HFD consumption or direct induction of hyperglycemia during development- reduces the sensitivity of neurons to glucose in areas of the hypothalamus including the PVH and VMH (40, 57, 58), as well as altering expression of the leptin receptor in the VMH (59). Perhaps due to the inherent sex differences in nutrient sensitivity in the hypothalamus, these programmed effects in offspring are reported to be sex specific (40). Although less studied, there are reports that exposure to maternal obesity also results in altered hypothalamic sensing of fatty acids and their downstream metabolism in the ARC and PVH (Furigo and Dearden, unpublished observation) (57, 60). Furthermore, hypothalamic transcriptome regulation in response to whole body nutrient status (in this example: response to fasting) are altered in offspring of obese mothers in a rat model (61).

Many of the studies mentioned here suggest that the reduced nutrient and hormonal sensitivity is due to altered signalling either at the level of receptor activation, or in downstream pathways (for e.g. in gene expression). However, it should also be noted that disruptions in nutrient sensing may be in part due to altered permeability of the blood brain barrier to circulating peripheral signals, as has been reported in mouse offspring exposed to maternal obesity (62).

3.5 Studies of the human hypothalamus in pregnancies complicated by maternal obesity and/or GDM

Due to the lack of tissue for experimental studies, the preceding section is based on observations primarily in rodent models. However, some notable brain imaging studies in the fetuses of women living obesity or GDM have been undertaken in recent years. During pregnancies complicated by maternal obesity, both maternal and fetal insulin levels are high in response to maternal hyperglycemia, and the fetuses of obese mothers develop insulin resistance whilst *in utero* (63). The effects of persistent hyperinsulinemia on brain development are not well characterised, however a recent study in humans has shown that fetal brain activity is altered in response to a maternal oral glucose challenge, and that the magnitude of fetal brain response is correlated with maternal insulin sensitivity (64). Furthermore, fetal postprandial brain responses are slower in the offspring of women with GDM, indicating that GDM directly affects fetal brain

activity and may lead to central insulin resistance in the fetus (65). This apparent change in fetal brain glucose and insulin sensitivity is not rescued by late pregnancy lifestyle interventions, suggesting that changes are programmed early in gestation (66). Similarly, a recent MRI imaging study in fetuses from pregnancies complicated by GDM has shown evidence of gliosis in the fetal mediobasal hypothalamus (containing the ARC and other closely surrounding hypothalamic nuclei) that is present early in pregnancy, occurring pre-28 weeks of gestation (67). Due to the observational nature of these imaging studies, it is not possible to draw any conclusions on whether the reported changes in the hypothalamus are causative or indicative of later dysfunction in hypothalamic regulation of energy homeostasis. They do however prove that in human pregnancies, the nutritional state of the mother has a direct impact on the fetal hypothalamus.

4 Mechanisms underlying the effects of maternal obesity on offspring hypothalamus

There is clearly a strong impact of the peri-natal environment on hypothalamic development, and this is likely to contribute to the increased obesity risk in offspring exposed to maternal obesity. However, the precise mechanisms by which maternal obesity impacts on long-term hypothalamic control of energy homeostasis remain largely undefined. In this section we will discuss the molecular mechanisms with the strongest evidence to date. Pregnancy is a time of high energy demand for the mother, and as such during pregnancy the body makes a series of metabolic adjustments to support the growing fetus. Many metabolic hormones or nutrients are also altered in obesity, and thus remain altered- or are further dysregulated- in a pregnancy complicated by obesity or GDM. As maternal obesity is a major risk factor for GDM, disentangling the effect of maternal obesity *per se* from that of maternal GDM on pregnancy outcomes in women with obesity and diabetes in pregnancy is almost impossible without very large cohorts with refined metabolic measures. Therefore, this section refers to many studies that are complicated by both obesity and GDM, but we have attempted to differentiate between the two where possible. These metabolic changes across pregnancy and in lean or mothers with obesity are summarised in Figure 2. Although discussed separately in this section, there is likely considerable overlap between these pathways.

4.1 Leptin

The adipokine leptin is released from adipose tissue in proportion to adipose tissue mass. In humans, leptin levels rise throughout pregnancy, reaching a peak in the third trimester. In mothers with overweight or obesity, pre-pregnancy serum leptin levels are already raised, so although they rise less during

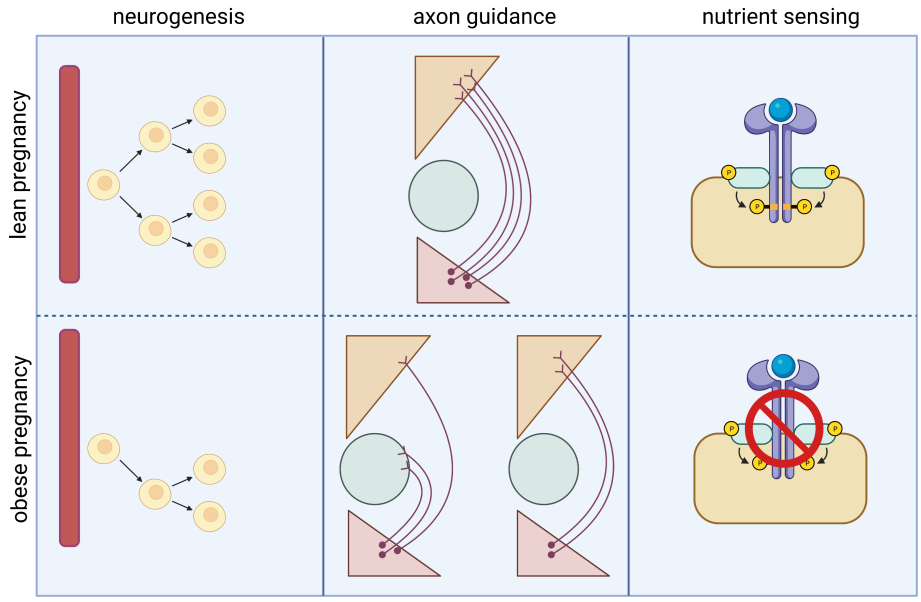

FIGURE 2
Heat map depicting changes in hormone/nutrient levels across the course of pregnancy in lean and obese mothers. The change in circulating levels of metabolic hormones and nutrients such as glucose and lipids throughout the course of a normal, lean pregnancy are shown in the left panel. Many of these factors are altered in women living with obesity and are thus altered also in pregnancies complicated by obesity with GDM as depicted in the right panel.

gestation than in a normal weight pregnancy, they remain higher at term in the mother (68) and fetus (69). The higher leptin levels in an obese pregnancy may contribute to some of the well-known maternal adverse health outcomes: leptin is known to contribute to obesity- related hypertension (70) and leptin concentrations are higher in women with preeclampsia compared with normotensive controls (71, 72) and thus may mediate some of the relationship between higher maternal BMI and preeclampsia risk.

In addition to playing an important role in controlling energy homeostasis, leptin has a significant role in neurodevelopment, particularly in development of the hypothalamic feeding circuitry (73). The formation of POMC and NPY/AgRP positive projections from the ARC to the neuroendocrine and autonomic regions of the PVH in rodents coincides with the timing of the post-natal leptin surge, from around PND 4 to PND 14, in neonatal mice and rats (74). Experiments in rodents manipulating the post-natal leptin surge have shown that not only is the surge necessary for the establishment of these ARC to PVH projections (75), but manipulation of leptin levels in the post-natal period have long-term effects on body weight control. Experimental blockage of the neonatal leptin surge affects gene expression of growth factors, glial proteins, and neuropeptides involved in the control of metabolism and reproduction in peripubertal male and female rats and is associated with increased susceptibility to develop diet-induced obesity (76). Conversely, in a separate mouse model which allowed manipulation of circulating leptin levels during discrete time windows, mice who experienced transient hyperleptinemia from PND0 to PND22 showed a greater susceptibility to develop obesity as adults (77). There studies suggest that the relationship between post-natal leptin and later body weight is a U- shaped curve, and that deviation from normal leptin levels in either direction can increase obesity risk.

Several studies examining hypothalamic architecture in leptin deficient Ob/Ob mice have defined the critical time window when leptin exerts neurotrophic effects within the hypothalamus, but shown that not all projections from the ARC to the PVH are rescued by post-natal leptin replacement in leptin deficient mice (75, 78). A more recent study that analysed the effect of leptin receptor rescue in young (4 weeks) and adult (10 weeks) mice formerly null for the leptin receptor suggests that the development of ARC neural projections can be rescued further into adulthood than previously thought (79). However, a reduction in hypothalamic Pomc, Cartpt and Prlh mRNA expression are persistent in adulthood in this rescue model, which may explain the permanent metabolic alterations caused by early defects in leptin signalling.

The post-natal leptin surge can be altered by the perinatal nutritional environment. Rodent pups reared by obese, or HFD-fed dams have an augmented and prolonged leptin surge magnitude (46, 80). Conversely, the leptin surge is reduced in models of intra- uterine growth restriction (81, 82). Furthermore, mice reared in small litters to induce post-natal over-nutrition display an augmented plasma leptin surge, whereas large litter size- a model of under-nutrition- is associated with a delayed surge of reduced magnitude (80). Manipulation of leptin levels may be a route to overcome programmed effects due to nutrition in the perinatal period. Collden et al. have recently shown that neonatal administration of a leptin antagonist normalises adiposity and hypothalamic leptin sensitivity in postnatally over-nourished mice (55). Taken together, these studies have shown that leptin is an important trophic factor for the development of hypothalamic feeding circuits critical for the control of energy balance, and that altered leptin levels are a likely route by which the nutritional environment in the peri-natal period alters energy homeostasis control.

4.2 Insulin

At the start of pregnancy, there is an initial rise in insulin secretin and sensitivity in the mother which stimulates lipogenesis and reduces fatty acid oxidation, causing maternal fat storage. Around mid-gestation, insulin resistance develops to direct all available fuel towards the growing fetus. This natural state of insulin resistance during pregnancy is worsened in pregnancies complicated by GDM or obesity (83–85). Interestingly, the augmented insulin resistance seen in GDM pregnancies seems to be caused by enhanced activity of the same mechanisms present in an uncomplicated pregnancy, rather than *via* novel pathogenic routes (86). Enhanced maternal insulin resistance in obese and GDM pregnancies contributes to high maternal glucose levels, leading to a state of hyperglycemia in the mother and fetus, since glucose freely crosses the placenta. This then leads to a compensatory rise in fetal insulin levels (63). Women living with obesity even without GDM have higher glucose profiles on continuous glucose monitoring performed during pregnancy than normal weight women (87). Maternal glycemia is a strong determinant of fetal growth, as demonstrated by the strong, continuous associations of maternal glucose levels with increasing birth weight (88).

It has long been established that insulin plays a neurotrophic role in numerous brain regions and across a range of species (89–93). Insulin also has an important function in both embryonic and adult stem cell homeostasis *via* a role in maintaining neural stem cell self-renewal, neurogenesis and, in some instances, promoting differentiation (94, 95). Insulin also acts to inhibit neuronal apoptosis *via* activation of protein kinase B and protein kinase C (96, 97) resulting in increased neuronal survival. Artificial manipulation of insulin in the brain during the perinatal period

via the implantation of insulin containing agar implants results in an altered ratio of neuronal to glial cells in the VMH (98).

There is also evidence from rodent studies that insulin signalling is required both in the pre- and post- natal periods for correct development of hypothalamic projections. Although the genetic deletion of InsR from POMC neurons does alter their development under normal conditions, it prevents the reduction of ARC POMC projections to the pre-autonomic compartment of the PVH that occurs in offspring exposed to maternal over-nutrition, suggesting this particular disrupted circuit development in response to maternal nutrition is mediated through insulin signalling (50). It has recently been shown that the impact of insulin on growth of primary neuronal cultures originating from the ARC is dependent on the nutrient availability in the postnatal period, further demonstrating an important interaction between insulin signalling and nutritional state in determining neuronal growth and circuit formation (99).

High insulin levels and fetal brain insulin signalling are essential for appropriate brain maturation. However, chronic hyperinsulinemia, which is present in insulin resistant mothers and corresponds to high insulin levels in the fetus, can induce insulin resistance in the fetus (63). We have previously reported that the fetuses of obese, hyperinsulinemic mice display reduced expression of proliferative genes in the hypothalamus and disrupted neural stem cell growth in primary culture, and that these two markers of neuronal proliferation were correlated with maternal insulin levels (43). Due to the essential role for insulin signalling in neural stem cell self-renewal and neurogenesis, insulin resistance in the developing hypothalamus could explain the reduced proliferative response of hypothalamic neurons in offspring exposed to an environment of energy excess (43, 56) that results in long term morphological changes in the hypothalamus and ultimately a lack of energy balance regulation.

4.3 Ghrelin

Ghrelin is a gut hormone with a strong orexigenic signal. Following release into the circulation, ghrelin circulates as two major forms: acyl- ghrelin and desacyl- ghrelin. Maternal total ghrelin concentrations decrease slightly throughout pregnancy, and there is a positive correlation between the ratio of acylated to total circulating ghrelin in the mother during the third trimester of gestation and infant birth weight (100). Circulating maternal desacyl- ghrelin is increased in pregnancies with GDM, possibly reflecting resistance to the inhibitory effect of insulin on ghrelin secretion (100). Cord blood total ghrelin levels are inversely correlated with birth weight and are decreased in women with GDM (101) concomitant with the increased birth weight seen in babies from GDM pregnancies.

Rodent and human studies have suggested that maternal ghrelin regulates fetal development during the late stages of pregnancy. Administration of ghrelin to mice during the last week of gestation causes a 10–20% increase in offspring birth weight (102). This effect is persistent even when maternal food intake after ghrelin treatment is restricted through paired feeding, suggesting a direct action of ghrelin on the fetus trough a transplacental transfer. Importantly, studies performed in mice to block ghrelin action during early post-natal development have shown an enhancement of ARC neural projections that are associated with long-term metabolic effects (103). It appears that ghrelin plays an inhibitory role in the development of hypothalamic neural circuits- acting as the "break" in balance to the neurotrophic action of leptin- and therefore correct expression of ghrelin, similar to leptin, during neonatal life could be important for later hypothalamic regulation of energy homeostasis.

4.4 Fatty acids and links to endoplasmic reticulum stress/inflammation

During pregnancy there is an accumulation of lipids in the first and second trimester in the mother and later increased lipolysis of maternal adipose tissue stores. The catabolic state of maternal adipose tissue during late gestation is associated with hyperlipidemia, mainly corresponding to plasma rises in triglycerides, with smaller rises in phospholipids and cholesterol (104). There are conflicting reports as to whether maternal cholesterol levels are altered in a pregnancy complicated by GDM (104). Maternal obesity is however associated with an increase in maternal lipid levels, higher triglycerides and VLDL, and lower HDL-C than observed in lean women (105). GDM in women with obesity is associated with elevated plasma concentrations of a specific series of triglycerides consistent with increased *de novo* lipogenesis (106). Several recent studies indicate that maternal post-prandial triglycerides and free fatty acids are a stronger predictor of newborn adiposity and birth weight than maternal glucose in an obese pregnancy (106, 107).

The quantity and specification of fatty acids ingested by the mother during pregnancy is of importance for brain development and hypothalamic function in the offspring. Hypothalamic dysfunction is observed in mice and rat offspring born to mothers that ingested increased amounts of saturated or trans fatty acids (108, 109). Park et al. (47) have demonstrated that exposure to high concentrations of a specific combination of fatty acids (designed to mimic the commonly used high- fat diets in diet- induced obesity studies) causes reduced neurite outgrowth from the ARC, suggesting that this may be a cause of the widely reported phenotype of reduced ARC to PVH projections in the offspring of obese mothers.

Endoplasmic reticulum (ER) stress and inflammation are important mechanisms that link changes in fatty acid levels to hypothalamic impairment. Over-nutrition typically activates

hypothalamic inflammatory signalling at least in part through elevated ER stress in the hypothalamus and this might be a general neural mechanism for energy imbalance underlying obesity (110, 111). In the context of an obese pregnancy, ER stress and inflammation are increased in the offspring hypothalamus (53) and the former is reported to be a consequence of elevated circulating fatty acids in obese dams and their offspring (47). Furthermore, neonatal treatment with tauroursodeoxycholic acid, an ER stress-relieving drug, ameliorates the metabolic and neurodevelopmental deficits observed in these animals, suggesting the increase in ER stress is causative of later metabolic dysfunction (47). Therefore, it is suggested that fatty acids play an important role in the hypothalamic dysfunction observed in offspring born to mothers that ingest increased amounts of saturated or trans fatty acids, and the mechanisms underlying these alterations may be through ER stress and hypothalamic inflammation.

4.5 Growth hormone

Growth hormone (GH) is well known for its function to stimulate growth, cell reproduction, and cell regeneration, and as such is hugely important for development. A growing body of evidence has shown the brain is an important target of GH for the regulation of food intake, energy expenditure, and glycemia, particularly in response to different forms of metabolic stress such as glucoprivation, food restriction, and exercise (112–114). During pregnancy, central GH action is related to the regulation of food intake, fat retention, and sensitivity to insulin and leptin in the mother, suggesting that GH acts in concert with other gestational hormones to prepare the maternal organism for the metabolic demands of the offspring (115). Interestingly offspring born to mothers with a genetic knockout of the GH receptor in cells that co-express leptin receptor exhibit a significantly lower growth rate from the second week of life, compared to offspring born to mothers with a loss of GH receptor in the entire brain or wild type mothers (115).

Despite the importance of GH in fetal development, little is known about the programming effects of maternal and/or fetal GH on offspring hypothalamic development. There is some evidence that GH regulates hypothalamic neurocircuits controlling energy homeostasis from experiments demonstrating a direct trophic role of GH on the formation of POMC and AgRP axonal projections (116). Mice with deletions of GH receptor in neurons that co-express leptin receptor have decreased density of POMC positive neuronal innervation in the PVH and DMH. Conversely, AgRP-specific ablation of GH receptor led to a significant reduction in AgRP projections to the PVH, LHA and DMH, without affecting POMC innervation (116). Further studies are needed to define whether altered maternal or fetal GH levels have other impacts on the developing hypothalamus, and whether changes are causative of later obesity.

5 Conclusions and future perspectives

Due to the increasing number of women who are overweight or living with obesity before entering pregnancy, it is essential that we investigate the long-term consequences of this exposure for their offspring. A greater understanding of the mechanisms by which the maternal environment acts on the offspring hypothalamus to disrupt energy homeostasis control is essential to reduce the inter-generational transmission of obesity risk. It is becoming increasingly understood that people living with obesity are fighting against their biology to maintain a healthy body weight, and the developmental programming of obesity risk is an underappreciated factor in this issue that determines our lifelong health before we are born. Whilst there are undoubtedly many contributing factors to the growing obesity epidemic, interventions in pregnancies complicated by obesity give us a unique opportunity to improve the health of two generations at the same time, and at a time when an individual is in frequent contact with health professionals. Future research in this field should aim to fill the gaps in our knowledge that will allow us to provide detailed information to enable mothers to make informed choices for their unborn offspring.

Author contributions

IF wrote the manuscript, LD conceived ideas, made figures and wrote the manuscript. All authors contributed to the article and approved the submitted version.

Funding

LD is a Royal Society Dorothy Hodgkin Fellow (DHF\R1 \221051). Figures were created with Biorender.com.

Conflict of interest

The authors declare that the research was conducted in the absence of any commercial or financial relationships that could be construed as a potential conflict of interest.

Publisher's note

References

1. England PH. *Health of women before and during pregnancy: health behaviours, risk factors and inequalities* (2019). Available at: https://assets.publishing.service.gov.uk/government/uploads/system/uploads/attahment_data/file/844210/Health_of_women_before_and_during_pregnancy_2019.pdf.

2. Driscoll AK, Gregory ECW. Increases in prepregnancy obesity: United states, 2016-2019. *NCHS Data Brief* (2020) 2020(392):1–8.

3. Scotland PH. *Births in Scotland year ending 31 march 2021* . Available at: https://publichealthscotland.scot/publications/births-in-scottish-hospitals/births-in-scottish-hospitals-year-ending-31-march-2021/2021.

4. Digital N. *National child measurement programme, England 2020/21 school year* . Available at: https://digital.nhs.uk/data-and-information/publications/statistical/national-child-measurement-programme/2020-21-school-year#2021.

5. Campbell JN, Macosko EZ, Fenselau H, Pers TH, Lyubetskaya A, Tenen D, et al. A molecular census of arcuate hypothalamus and median eminence cell types. *Nat Neurosci* (2017) 20(3):484–96. doi: 10.1038/nn.4495

6. Lam BYH, Cimino I, Polex-Wolf J, Nicole Kohnke S, Rimmington D, Iyemere V, et al. Heterogeneity of hypothalamic pro-opiomelanocortin-expressing neurons revealed by single-cell RNA sequencing. *Mol Metab* (2017) 6 (5):383–92. doi: 10.1016/j.molmet.2017.02.007

7. Steuernagel L, Lam BYH, Klemm P, Dowsett GKC, Bauder CA, Tadross JA, et al. HypoMap-a unified single-cell gene expression atlas of the murine hypothalamus. *Nat Metab* (2022) 4(10):1402–19. doi: 10.1038/s42255-022-00657-y

8. Djogo T, Robins SC, Schneider S, Kryzskaya D, Liu X, Mingay A, et al. Adult NG2-glia are required for median eminence-mediated leptin sensing and body weight control. *Cell Metab* (2016) 23(5):797–810. doi: 10.1016/j.cmet.2016.04.013

9. Puelles L. Recollections on the origins and development of the prosomeric model. *Front Neuroanat.* (2021) 15:787913. doi: 10.3389/fnana.2021.787913

10. Bedont JL, Newman EA, Blackshaw S. Patterning, specification, and differentiation in the developing hypothalamus. *Wiley Interdiscip Rev Dev Biol* (2015) 4(5):445–68. doi: 10.1002/wdev.187

11. Blaess S, Szabó N, Haddad-Tóvolli R, Zhou X, Álvarez-Bolado G. Sonic hedgehog signaling in the development of the mouse hypothalamus. *Front Neuroanat.* (2014) 8:156. doi: 10.3389/fnana.2014.00156

12. Burbridge S, Stewart I, Placzek M. Development of the neuroendocrine hypothalamus. *Compr Physiol* (2016) 6(2):623–43. doi: 10.1002/cphy.c150023

13. Alvarez-Bolado G, Paul FA, Blaess S. Sonic hedgehog lineage in the mouse hypothalamus: from progenitor domains to hypothalamic regions. *Neural Dev* (2012) 7:4. doi: 10.1186/1749-8104-7-4

14. Ishii Y, Bouret SG. Embryonic birthdate of hypothalamic leptin-activated neurons in mice. *Endocrinology* (2012) 153(8):3657–67. doi: 10.1210/en.2012-1328

15. Padilla SL, Carmody JS, Zeltser LM. Pomc-expressing progenitors give rise to antagonistic neuronal populations in hypothalamic feeding circuits. *Nat Med* (2010) 16(4):403–5. doi: 10.1038/nm.2126

16. de la Pompa JL, Wakeham A, Correia KM, Samper E, Brown S, Aguilera RJ, et al. Conservation of the notch signalling pathway in mammalian neurogenesis. *Development* (1997) 124(6):1139–48. doi: 10.1242/dev.124.6.1139

17. Aujla PK, Naratadam GT, Xu L, Raetzman LT. Notch/Rbpjκ signaling regulates progenitor maintenance and differentiation of hypothalamic arcuate neurons. *Development* (2013) 140(17):3511–21. doi: 10.1242/dev.098681

18. McNay DE, Pelling M, Claxton S, Guillemot F, Ang SL. Mash1 is required for generic and subtype differentiation of hypothalamic neuroendocrine cells. *Mol Endocrinol* (2006) 20(7):1623–32. doi: 10.1210/me.2005-0518

19. Low VF, Fiorini Z, Fisher L, Jasoni CL. Netrin-1 stimulates developing GnRH neurons to extend neurites to the median eminence in a calcium- dependent manner. *PloS One* (2012) 7(10):e46999. doi: 10.1371/journal.pone.0046999

20. Gervais M, Labouèbe G, Picard A, Thorens B, Croizier S. EphrinB1 modulates glutamatergic inputs into POMC-expressing progenitors and controls glucose homeostasis. *PloS Biol* (2020) 18(11):e3000680. doi: 10.1371/journal.pbio.3000680

21. Oleari R, Lettieri A, Paganoni A, Zanieri L, Cariboni A. Semaphorin signaling in GnRH neurons: From development to disease. *Neuroendocrinology* (2019) 109(3):193–9. doi: 10.1159/000495916

22. van der Klaauw AA, Croizier S, Mendes de Oliveira E, Stadler LKJ, Park S, Kong Y, et al. Human semaphorin 3 variants link melanocortin circuit development and energy balance. *Cell* (2019) 176(4):729–42.e18. doi: 10.1016/j.cell.2018.12.009

23. Makarenko IG. DiI tracing of the hypothalamic projection systems during perinatal development. *Front Neuroanat.* (2014) 8:144. doi: 10.3389/fnana.2014.00144

24. Croizier S, Bouret SG. Molecular control of the development of hypothalamic neurons involved in metabolic regulation. *J Chem Neuroanat.* (2022) 123:102117. doi: 10.1016/j.jchemneu.2022.102117

25. Bouret SG, Draper SJ, Simerly RB. Formation of projection pathways from the arcuate nucleus of the hypothalamus to hypothalamic regions implicated in the neural control of feeding behavior in mice. *J Neurosci* (2004) 24(11):2797–805. doi: 10.1523/JNEUROSCI.5369-03.2004

26. Singer LK, Kuper J, Brogan RS, Smith MS, Grove KL. Novel expression of hypothalamic neuropeptide y during postnatal development in the rat. *Neuroreport* (2000) 11(5):1075–80. doi: 10.1097/00001756-200004070-00034

27. Grayson BE, Allen SE, Billes SK, Williams SM, Smith MS, Grove KL. Prenatal development of hypothalamic neuropeptide systems in the nonhuman primate. *Neuroscience* (2006) 143(4):975–86. doi: 10.1016/j.neuroscience.2006.08.055

28. Li G, Zhang W, Baker MS, Laritsky E, Mattan-Hung N, Yu D, et al. Major epigenetic development distinguishing neuronal and non-neuronal cells occurs postnatally in the murine hypothalamus. *Hum Mol Genet* (2014) 23(6):1579–90. doi: 10.1093/hmg/ddt548

29. Cisternas CD, Cortes LR, Bruggeman EC, Yao B, Forger NG. Developmental changes and sex differences in DNA methylation and demethylation in hypothalamic regions of the mouse brain. *Epigenetics* (2020) 15(1-2):72–84. doi: 10.1080/15592294.2019.1649528

30. MacKay H, Gunasekara CJ, Yam KY, Srisai D, Yalamanchili HK, Li Y, et al. Sex-specific epigenetic development in the mouse hypothalamic arcuate nucleus pinpoints human genomic regions associated with body mass index. *Sci Adv* (2022) 8(39):eabo3991. doi: 10.1126/sciadv.abo3991

31. Zamore PD, Haley B. Ribo-gnome: the big world of small RNAs. *Science* (2005) 309(5740):1519–24. doi: 10.1126/science.1111444

32. Fernandez-Twinn DS, Hjort L, Novakovic B, Ozanne SE, Saffery R. Intrauterine programming of obesity and type 2 diabetes. *Diabetologia* (2019) 62 (10):1789–801. doi: 10.1007/s00125-019-4951-9

33. Heerwagen MJ, Miller MR, Barbour LA, Friedman JE. Maternal obesity and fetal metabolic programming: a fertile epigenetic soil. *Am J Physiol Regul Integr Comp Physiol* (2010) 299(3):R711–22. doi: 10.1152/ajpregu.00310.2010

34. Doubi-Kadmiri S, Benoit C, Benigni X, Beaumont G, Vacher CM, Taouis M, et al. Substantial and robust changes in microRNA transcriptome support postnatal development of the hypothalamus in rat. *Sci Rep* (2016) 6:24896. doi: 10.1038/srep24896

35. Croizier S, Park S, Maillard J, Bouret SG. Central dicer-miR-103/107 controls developmental switch of POMC progenitors into NPY neurons and impacts glucose homeostasis. *Elife* (2018) 7. doi: 10.7554/eLife.40429

36. McNay DE, Briançon N, Kokoeva MV, Maratos-Flier E, Flier JS. Remodeling of the arcuate nucleus energy-balance circuit is inhibited in obese mice. *J Clin Invest.* (2012) 122(1):142–52. doi: 10.1172/JCI43134

37. Hallschmid M, Benedict C, Schultes B, Born J, Kern W. Obese men respond to cognitive but not to catabolic brain insulin signaling. *Int J Obes (Lond).* (2008) 32 (2):275–82. doi: 10.1038/sj.ijo.0803722

38. Samuelsson AS, Mullier A, Maicas N, Oosterhuis NR, Eun Bae S, Novoselova TV, et al. Central role for melanocortin-4 receptors in offspring hypertension arising from maternal obesity. *Proc Natl Acad Sci U S A.* (2016) 113(43):12298–303. doi: 10.1073/pnas.1607464113

39. Sullivan EL, Grayson B, Takahashi D, Robertson N, Maier A, Bethea CL, et al. Chronic consumption of a high-fat diet during pregnancy causes perturbations in the serotonergic system and increased anxiety-like behavior in nonhuman primate offspring. *J Neurosci* (2010) 30(10):3826–30. doi: 10.1523/JNEUROSCI.5560-09.2010

40. Dearden L, Balthasar N. Sexual dimorphism in offspring glucose-sensitive hypothalamic gene expression and physiological responses to maternal high-fat diet feeding. *Endocrinology* (2014) 155(6):2144–54. doi: 10.1210/en.2014-1131

41. Dearden L, Bouret SG, Ozanne SE. Sex and gender differences in developmental programming of metabolism. *Mol Metab* (2018) 15:8–19. doi: 10.1016/j.molmet.2018.04.007

42. Sanders TR, Kim DW, Glendining KA, Jasoni CL. Maternal obesity and IL-6 lead to aberrant developmental gene expression and deregulated neurite growth in the fetal arcuate nucleus. *Endocrinology* (2014) 155(7):2566–77. doi: 10.1210/en.2013-1968

43. Dearden L, Buller S, Furigo IC, Fernandez-Twinn DS, Ozanne SE. Maternal obesity causes fetal hypothalamic insulin resistance and disrupts development of hypothalamic feeding pathways. *Mol Metab* (2020) 42:101079. doi: 10.1016/j.molmet.2020.101079

44. Lemes SF, de Souza ACP, Payolla TB, Versutti MD, de Fátima da Silva Ramalho A, Mendes-da-Silva C, et al. Maternal consumption of high-fat diet in mice alters hypothalamic notch pathway, NPY cell population and food intake in offspring. *Neuroscience* (2018) 371:1–15. doi: 10.1016/j.neuroscience.2017.11.043

45. Bae-Gartz I, Janoschek R, Breuer S, Schmitz L, Hoffmann T, Ferrari N, et al. Maternal obesity alters neurotrophin-associated MAPK signaling in the hypothalamus of Male mouse offspring. *Front Neurosci* (2019) 13:962. doi: 10.3389/fnins.2019.00962

46. Kirk SL, Samuelsson AM, Argenton M, Dhonye H, Kalamatianos T, Poston L, et al. Maternal obesity induced by diet in rats permanently influences central processes regulating food intake in offspring. *PloS One* (2009) 4(6):e5870. doi: 10.1371/journal.pone.0005870

47. Park S, Jang A, Bouret SG. Maternal obesity-induced endoplasmic reticulum stress causes metabolic alterations and abnormal hypothalamic development in the offspring. *PloS Biol* (2020) 18(3):e3000296. doi: 10.1371/journal.pbio.3000296

48. Steculorum SM, Bouret SG. Maternal diabetes compromises the organization of hypothalamic feeding circuits and impairs leptin sensitivity in offspring. *Endocrinology* (2011) 152(11):4171–9. doi: 10.1210/en.2011-1279

49. Sullivan EL, Rivera HM, True CA, Franco JG, Baquero K, Dean TA, et al. Maternal and postnatal high-fat diet consumption programs energy balance and hypothalamic melanocortin signaling in nonhuman primate offspring. *Am J Physiol Regul Integr Comp Physiol* (2017) 313(2):R169–R79. doi: 10.1152/ajpregu.00309.2016

50. Vogt MC, Paeger L, Hess S, Steculorum SM, Awazawa M, Hampel B, et al. Neonatal insulin action impairs hypothalamic neurocircuit formation in response to maternal high-fat feeding. *Cell* (2014) 156(3):495–509. doi: 10.1016/j.cell.2014.01.008

51. Chen H, Simar D, Morris MJ. Hypothalamic neuroendocrine circuitry is programmed by maternal obesity: interaction with postnatal nutritional environment. *PloS One* (2009) 4(7):e6259. doi: 10.1371/journal.pone.0006259

52. Haddad-Tóvolli R, Altirriba J, Obri A, Sánchez EE, Chivite I, Milà-Guasch M, et al. Pro-opiomelanocortin (POMC) neuron translatome signatures underlying obesogenic gestational malprogramming in mice. *Mol Metab* (2020) 36:100963. doi: 10.1016/j.molmet.2020.02.006

53. Melo AM, Benatti RO, Ignacio-Souza LM, Okino C, Torsoni AS, Milanski M, et al. Hypothalamic endoplasmic reticulum stress and insulin resistance in offspring of mice dams fed high-fat diet during pregnancy and lactation. *Metabolism* (2014) 63(5):682–92. doi: 10.1016/j.metabol.2014.02.002

54. Collden G, Balland E, Parkash J, Caron E, Langlet F, Prevot V, et al. Neonatal overnutrition causes early alterations in the central response to peripheral ghrelin. *Mol Metab* (2015) 4(1):15–24. doi: 10.1016/j.molmet.2014.10.003

55. Colldén G, Caron E, Bouret SG. Neonatal leptin antagonism improves metabolic programming of postnatally overnourished mice. *Int J Obes (Lond).* (2022) 46(6):1138–44. doi: 10.1038/s41366-022-01093-4

56. Davidowa H, Plagemann A. Insulin resistance of hypothalamic arcuate neurons in neonatally overfed rats. *Neuroreport* (2007) 18(5):521–4. doi: 10.1097/WNR.0b013e32805dfb93

57. Le Foll C, Irani BG, Magnan C, Dunn-Meynell A, Levin BE. Effects of maternal genotype and diet on offspring glucose and fatty acid-sensing ventromedial hypothalamic nucleus neurons. *Am J Physiol Regul Integr Comp Physiol* (2009) 297(5):R1351–7. doi: 10.1152/ajpregu.00370.2009

58. Tzschentke B, Bogatyrev S, Schellong K, Rancourt RC, Plagemann A. Temporary prenatal hyperglycemia leads to postnatal neuronal 'glucose-resistance' in the chicken hypothalamus. *Brain Res* (2015) 1618:231–40. doi: 10.1016/j.brainres.2015.05.037

59. Mühlhäusler BS, Adam CL, Marrocco EM, Findlay PA, Roberts CT, McFarlane JR, et al. Impact of glucose infusion on the structural and functional characteristics of adipose tissue and on hypothalamic gene expression for appetite regulatory neuropeptides in the sheep fetus during late gestation. *J Physiol* (2005) 565(Pt 1):185–95. doi: 10.1113/jphysiol.2004.079079

60. Rivera P, Guerra-Cantera S, Vargas A, Díaz F, García-Úbeda R, Tovar R, et al. Maternal hypercaloric diet affects factors involved in lipid metabolism and the endogenous cannabinoid systems in the hypothalamus of adult offspring: sex-specific response of astrocytes to palmitic acid and anandamide. *Nutr Neurosci* (2022) 25(5):931–44. doi: 10.1080/1028415X.2020.1821519

61. Chen H, Morris MJ. Differential responses of orexigenic neuropeptides to fasting in offspring of obese mothers. *Obes (Silver Spring).* (2009) 17(7):1356–62. doi: 10.1038/oby.2009.56

62. Kim DW, Glendining KA, Grattan DR, Jasoni CL. Maternal obesity in the mouse compromises the blood-brain barrier in the arcuate nucleus of offspring. *Endocrinology* (2016) 157(6):2229–42. doi: 10.1210/en.2016-1014

63. Catalano PM, Presley L, Minium J, Hauguel-de Mouzon S. Fetuses of obese mothers develop insulin resistance in utero. *Diabetes Care* (2009) 32(6):1076–80. doi: 10.2337/dc08-2077

64. Linder K, Schleger F, Ketterer C, Fritsche L, Kiefer-Schmidt I, Hennige A, et al. Maternal insulin sensitivity is associated with oral glucose-induced changes in fetal brain activity. *Diabetologia* (2014) 57(6):1192–8. doi: 10.1007/s00125-014-3217-9

65. Linder K, Schleger F, Kiefer-Schmidt I, Fritsche L, Kümmel S, Böcker M, et al. Gestational diabetes impairs human fetal postprandial brain activity. *J Clin Endocrinol Metab* (2015) 100(11):4029–36. doi: 10.1210/jc.2015-2692

66. Schleger F, Linder K, Fritsche L, Pauluschke-Fröhlich J, Heni M, Weiss M, et al. No effect of lifestyle intervention during third trimester on brain programming in fetuses of mothers with gestational diabetes. *Nutrients* (2021) 13(2):556. doi: 10.3390/nu13020556

67. Chandrasekaran S, Melhorn S, Olerich KL, Angelo B, Chow T, Xiang A, et al. Exposure to gestational diabetes mellitus prior to 26 weeks is related to the presence of mediobasal hypothalamic gliosis in children. *Diabetes* (2022) 71 (12):2552–6. doi: 10.2337/figshare.21066211

68. Misra VK, Straughen JK, Trudeau S. Maternal serum leptin during pregnancy and infant birth weight: the influence of maternal overweight and obesity. *Obes (Silver Spring).* (2013) 21(5):1064–9. doi: 10.1002/oby.20128

69. Patro-Małysza J, Trojnar M, Skórzyńska-Dziduszko KE, Kimber-Trojnar ŻChecktae, Darmochwał-Kolarz D, Czuba M, et al. Leptin and ghrelin in excessive gestational weight gain-association between mothers and offspring. *Int J Mol Sci* (2019) 20(10):2398. doi: 10.3390/ijms20102398

70. Simonds SE, Pryor JT, Ravussin E, Greenway FL, Dileone R, Allen AM, et al. Leptin mediates the increase in blood pressure associated with obesity. *Cell* (2014) 159(6):1404–16. doi: 10.1016/j.cell.2014.10.058

71. Taylor BD, Ness RB, Olsen J, Hougaard DM, Skogstrand K, Roberts JM, et al. Serum leptin measured in early pregnancy is higher in women with preeclampsia compared with normotensive pregnant women. *Hypertension* (2015) 65(3):594–9. doi: 10.1161/HYPERTENSIONAHA.114.03979

72. Hendler I, Blackwell SC, Mehta SH, Whitty JE, Russell E, Sorokin Y, et al. The levels of leptin, adiponectin, and resistin in normal weight, overweight, and obese pregnant women with and without preeclampsia. *Am J Obstet Gynecol* (2005) 193(3 Pt 2):979–83. doi: 10.1016/j.ajog.2005.06.041

73. Bouret SG, Draper SJ, Simerly RB. Trophic action of leptin on hypothalamic neurons that regulate feeding. *Science* (2004) 304(5667):108–10. doi: 10.1126/science.1095004

74. Ahima RS, Prabakaran D, Flier JS. Postnatal leptin surge and regulation of circadian rhythm of leptin by feeding. implications for energy homeostasis and neuroendocrine function. *J Clin Invest.* (1998) 101(5):1020–7. doi: 10.1172/JCI1176

75. Bouyer K, Simerly RB. Neonatal leptin exposure specifies innervation of presympathetic hypothalamic neurons and improves the metabolic status of leptin-deficient mice. *J Neurosci* (2013) 33(2):840–51. doi: 10.1523/JNEUROSCI.3215-12.2013

76. Mela V, Díaz F, Lopez-Rodriguez AB, Vázquez MJ, Gertler A, Argente J, et al. Blockage of the neonatal leptin surge affects the gene expression of growth factors, glial proteins, and neuropeptides involved in the control of metabolism and reproduction in peripubertal Male and female rats. *Endocrinology* (2015) 156 (7):2571–81. doi: 10.1210/en.2014-1981

77. Skowronski AA, LeDuc CA, Foo KS, Goffer Y, Burnett LC, Egli D, et al. Physiological consequences of transient hyperleptinemia during discrete developmental periods on body weight in mice. *Sci Transl Med* (2020) 12 (524):6629. doi: 10.1126/scitranslmed.aax6629

78. Kamitakahara A, Bouyer K, Wang CH, Simerly R. A critical period for the trophic actions of leptin on AgRP neurons in the arcuate nucleus of the hypothalamus. *J Comp Neurol* (2018) 526(1):133–45. doi: 10.1002/cne.24327

79. Ramos-Lobo AM, Teixeira PD, Furigo IC, Melo HM, de M Lyra E Silva N, De Felice FG, et al. Long-term consequences of the absence of leptin signaling in early life. *Elife* (2019) 8. doi: 10.7554/eLife.40970

80. Skowronski AA, Shaulson ED, Leibel RL, LeDuc CA. The postnatal leptin surge in mice is variable in both time and intensity and reflects nutritional status. *Int J Obes (Lond).* (2022) 46(1):39–49. doi: 10.1038/s41366-021-00957-5

81. Coupe B, Amarger V, Grit I, Benani A, Parnet P. Nutritional programming affects hypothalamic organization and early response to leptin. *Endocrinology* (2010) 151(2):702–13. doi: 10.1210/en.2009-0893

82. Delahaye F, Breton C, Risold PY, Enache M, Dutriez-Casteloot I, Laborie C, et al. Maternal perinatal undernutrition drastically reduces postnatal leptin surge and affects the development of arcuate nucleus proopiomelanocortin neurons in neonatal male rat pups. *Endocrinology* (2008) 149(2):470–5. doi: 10.1210/en.2007-1263

83. Xiang AH, Peters RK, Trigo E, Kjos SL, Lee WP, Buchanan TA. Multiple metabolic defects during late pregnancy in women at high risk for type 2 diabetes. *Diabetes* (1999) 48(4):848–54. doi: 10.2337/diabetes.48.4.848

84. Friedman JE, Ishizuka T, Shao J, Huston L, Highman T, Catalano P. Impaired glucose transport and insulin receptor tyrosine phosphorylation in

skeletal muscle from obese women with gestational diabetes. *Diabetes* (1999) 48 (9):1807–14. doi: 10.2337/diabetes.48.9.1807

85. Catalano PM, Ehrenberg HM. The short- and long-term implications of maternal obesity on the mother and her offspring. *BJOG* (2006) 113(10):1126–33. doi: 10.1111/j.1471-0528.2006.00989.x

86. Kirwan JP, Hauguel-De Mouzon S, Lepercq J, Challier JC, Huston-Presley L, Friedman JE, et al. TNF-alpha is a predictor of insulin resistance in human pregnancy. *Diabetes* (2002) 51(7):2207–13. doi: 10.2337/diabetes.51.7.2207

87. Harmon KA, Gerard L, Jensen DR, Kealey EH, Hernandez TL, Reece MS, et al. Continuous glucose profiles in obese and normal-weight pregnant women on a controlled diet: metabolic determinants of fetal growth. *Diabetes Care* (2011) 34 (10):2198–204. doi: 10.2337/dc11-0723

88. Metzger BE, Lowe LP, Dyer AR, Trimble ER, Chaovarindr U, Coustan DR, et al. Hyperglycemia and adverse pregnancy outcomes. *N Engl J Med* (2008) 358 (19):1991–2002. doi: 10.1056/NEJMoa0707943

89. Toran-Allerand CD, Ellis L, Pfenninger KH. Estrogen and insulin synergism in neurite growth enhancement *in vitro*: mediation of steroid effects by interactions with growth factors? *Brain Res* (1988) 469(1-2):87–100. doi: 10.1016/0165-3806 (88)90172-1

90. Recio-Pinto E, Ishii DN. Effects of insulin, insulin-like growth factor-II and nerve growth factor on neurite outgrowth in cultured human neuroblastoma cells. *Brain Res* (1984) 302(2):323–34. doi: 10.1016/0006-8993(84)90246-4

91. Lázár BA, Jancsó G, Pálvölgyi L, Dobos I, Nagy I, Sántha P. Insulin confers differing effects on neurite outgrowth in separate populations of cultured dorsal root ganglion neurons: The role of the insulin receptor. *Front Neurosci* (2018) 12:732. doi: 10.3389/fnins.2018.00732

92. Song J, Wu L, Chen Z, Kohanski RA, Pick L. Axons guided by insulin receptor in drosophila visual system. *Science* (2003) 300(5618):502–5. doi: 10.1126/science.1081203

93. Fex Svenningsen A, Kanje M. Insulin and the insulin-like growth factors I and II are mitogenic to cultured rat sciatic nerve segments and stimulate [3H] thymidine incorporation through their respective receptors. *Glia* (1996) 18 (1):68–72. doi: 10.1002/(SICI)1098-1136(199609)18:1<68::AID-GLIA7>3.0.CO;2-#

94. Ziegler AN, Levison SW, Wood TL. Insulin and IGF receptor signalling in neural-stem-cell homeostasis. *Nat Rev Endocrinol* (2015) 11(3):161–70. doi: 10.1038/nrendo.2014.208

95. Vento R, Giuliano M, Lauricella M, Carabillò M, Main H, Gerbino E, et al. Differentiation of Y79 cells induced by prolonged exposure to insulin. *Mol Cell Biochem* (1997) 170(1-2):163–70. doi: 10.1023/A:1006813705101

96. Dudek H, Datta SR, Franke TF, Birnbaum MJ, Yao R, Cooper GM, et al. Regulation of neuronal survival by the serine-threonine protein kinase akt. *Science* (1997) 275(5300):661–5. doi: 10.1126/science.275.5300.661

97. Apostolatos A, Song S, Acosta S, Peart M, Watson JE, Bickford P, et al. Insulin promotes neuronal survival *via* the alternatively spliced protein kinase CδII isoform. *J Biol Chem* (2012) 287(12):9299–310. doi: 10.1074/jbc.M111.313080

98. Plagemann A, Harder T, Rake A, Janert U, Melchior K, Rohde W, et al. Morphological alterations of hypothalamic nuclei due to intrahypothalamic hyperinsulinism in newborn rats. *Int J Dev Neurosci* (1999) 17(1):37–44. doi: 10.1016/S0736-5748(98)00064-1

99. Decourtye L, Clemessy M, Mire E, Ledent T, Périn L, Robinson IC, et al. Impact of insulin on primary arcuate neurons culture is dependent on early-postnatal nutritional status and neuronal subpopulation. *PloS One* (2018) 13(2): e0193196. doi: 10.1371/journal.pone.0193196

100. Tham E, Liu J, Innis S, Thompson D, Gaylinn BD, Bogarin R, et al. Acylated ghrelin concentrations are markedly decreased during pregnancy in mothers with and without gestational diabetes: relationship with cholinesterase. *Am J Physiol Endocrinol Metab* (2009) 296(5):E1093–100. doi: 10.1152/ajpendo.90866.2008

101. Karakulak M, Saygili U, Temur M, Yilmaz Ö, Özün Özbay P, Calan M, et al. Comparison of umbilical cord ghrelin concentrations in full-term pregnant women with or without gestational diabetes. *Endocr Res* (2017) 42(2):79–85. doi: 10.1080/07435800.2016.1194855

102. Nakahara K, Nakagawa M, Baba Y, Sato M, Toshinai K, Date Y, et al. Maternal ghrelin plays an important role in rat fetal development during pregnancy. *Endocrinology* (2006) 147(3):1333–42. doi: 10.1210/en.2005-0708

103. Steculorum SM, Collden G, Coupe B, Croizier S, Lockie S, Andrews ZB, et al. Neonatal ghrelin programs development of hypothalamic feeding circuits. *J Clin Invest.* (2015) 125(2):846–58. doi: 10.1172/JCI73688

104. Herrera E, Ortega-Senovilla H. Implications of lipids in neonatal body weight and fat mass in gestational diabetic mothers and non-diabetic controls. *Curr Diabetes Rep* (2018) 18(2):7. doi: 10.1007/s11892-018-0978-4

105. Merzouk H, Meghelli-Bouchenak M, Loukidi B, Prost J, Belleville J. Impaired serum lipids and lipoproteins in fetal macrosomia related to maternal obesity. *Biol Neonate.* (2000) 77(1):17–24. doi: 10.1159/000014190

106. Furse S, Koulman A, Ozanne SE, Poston L, White SL, Meek CL. Altered lipid metabolism in obese women with gestational diabetes and associations with offspring adiposity. *J Clin Endocrinol Metab* (2022) 107(7):e2825–e32. doi: 10.1210/clinem/dgac206

107. Barbour LA, Farabi SS, Friedman JE, Hirsch NM, Reece MS, Van Pelt RE, et al. Postprandial triglycerides predict newborn fat more strongly than glucose in women with obesity in early pregnancy. *Obes (Silver Spring).* (2018) 26(8):1347–56. doi: 10.1002/oby.22246

108. Pimentel GD, Lira FS, Rosa JC, Oliveira JL, Losinskas-Hachul AC, Souza GI, et al. Intake of trans fatty acids during gestation and lactation leads to hypothalamic inflammation *via* TLR4/NFκBp65 signaling in adult offspring. *J Nutr Biochem* (2012) 23(3):265–71. doi: 10.1016/j.jnutbio.2010.12.003

109. Rother E, Kuschewski R, Alcazar MA, Oberthuer A, Bae-Gartz I, Vohlen C, et al. Hypothalamic JNK1 and IKKβ activation and impaired early postnatal glucose metabolism after maternal perinatal high-fat feeding. *Endocrinology* (2012) 153(2):770–81. doi: 10.1210/en.2011-1589

110. Zhang X, Zhang G, Zhang H, Karin M, Bai H, Cai D. Hypothalamic IKKbeta/NF-kappaB and ER stress link overnutrition to energy imbalance and obesity. *Cell* (2008) 135(1):61–73. doi: 10.1016/j.cell.2008.07.043

111. Sadagurski M, Debarba LK, Werneck-de-Castro JP, Ali Awada A, Baker TA, Bernal-Mizrachi E. Sexual dimorphism in hypothalamic inflammation in the offspring of dams exposed to a diet rich in high fat and branched-chain amino acids. *Am J Physiol Endocrinol Metab* (2019) 317(3):E526–E34. doi: 10.1152/ajpendo.00183.2019

112. Furigo IC, Teixeira PDS, de Souza GO, Couto GCL, Romero GG, Perelló M, et al. Growth hormone regulates neuroendocrine responses to weight loss *via* AgRP neurons. *Nat Commun* (2019) 10(1):662. doi: 10.1038/s41467-019-08607-1

113. Furigo IC, de Souza GO, Teixeira PDS, Guadagnini D, Frazão R, List EO, et al. Growth hormone enhances the recovery of hypoglycemia. *FASEB J* (2019) 33 (11):11909–24. doi: 10.1096/fj.201901315R

114. Donato J, Wasinski F, Furigo IC, Metzger M, Frazão R. Central regulation of metabolism by growth hormone. *Cells* (2021) 10(1):129. doi: 10.3390/cells10010129

115. Teixeira PDS, Couto GC, Furigo IC, List EO, Kopchick JJ, Donato J. Central growth hormone action regulates metabolism during pregnancy. *Am J Physiol Endocrinol Metab* (2019) 317(5):E925–E40. doi: 10.1152/ajpendo.00229.2019

116. Wasinski F, Furigo IC, Teixeira PDS, Ramos-Lobo AM, Peroni CN, Bartolini P, et al. Growth hormone receptor deletion reduces the density of axonal projections from hypothalamic arcuate nucleus neurons. *Neuroscience* (2020) 434:136–47. doi: 10.1016/j.neuroscience.2020.03.037

frontiers | Frontiers in Endocrinology

TYPE Original Research
PUBLISHED 05 January 2023
DOI 10.3389/fendo.2022.1073759

OPEN ACCESS

EDITED BY
Alexandre Benani,
Centre National de la Recherche Scientifique (CNRS), France

REVIEWED BY
Karine Rizzoti,
Francis Crick Institute, United Kingdom
Shannon William Davis,
University of South Carolina, United States

*CORRESPONDENCE
Fanny Langlet
fanny.langlet@unil.ch

†These authors share second authorship

‡These authors share last authorship

SPECIALTY SECTION
This article was submitted to Neuroendocrine Science, a section of the journal Frontiers in Endocrinology

RECEIVED 18 October 2022
ACCEPTED 02 December 2022
PUBLISHED 05 January 2023

CITATION
Lopez-Rodriguez D, Rohrbach A, Lanzillo M, Gervais M, Croizier S and Langlet F (2023) Ontogeny of ependymoglial cells lining the third ventricle in mice. *Front. Endocrinol.* 13:1073759. doi: 10.3389/fendo.2022.1073759

Ontogeny of ependymoglial cells lining the third ventricle in mice

David Lopez-Rodriguez[1], Antoine Rohrbach[1†], Marc Lanzillo[2†], Manon Gervais[2], Sophie Croizier[2‡] and Fanny Langlet[1*‡]

[1]Department of Biomedical Sciences, Faculty of Biology and Medicine, University of Lausanne, Lausanne, Switzerland, [2]Center for Integrative Genomics, Faculty of Biology and Medicine, University of Lausanne, Lausanne, Switzerland

Introduction: During hypothalamic development, the germinative neuroepithelium gives birth to diverse neural cells that regulate numerous physiological functions in adulthood.

Methods: Here, we studied the ontogeny of ependymal cells in the mouse mediobasal hypothalamus using the BrdU approach and publicly available single-cell RNAseq datasets.

Results: We observed that while typical ependymal cells are mainly produced at E13, tanycyte birth depends on time and subtypes and lasts up to P8. Typical ependymocytes and β tanycytes are the first to arise at the top and bottom of the dorsoventral axis around E13, whereas α tanycytes emerge later in development, generating an outside-in dorsoventral gradient along the third ventricle. Additionally, α tanycyte generation displayed a rostral-to-caudal pattern. Finally, tanycytes mature progressively until they reach transcriptional maturity between P4 and P14.

Discussion: Altogether, this data shows that ependyma generation differs in time and distribution, highlighting the heterogeneity of the third ventricle.

KEYWORDS

third ventricle, tanycytes, ependymal cells, hypothalamic development, scRNAseq, BrdU

Introduction

The mediobasal hypothalamus controls different physiological processes and behaviors essential for life, ranging from feeding (1) to reproduction (2, 3).

Organized around the third ventricle (3V), the mediobasal hypothalamus developed from the germinative neuroepithelium during embryonic development (4). The

embryonic ventricular zone is mainly composed of radial glial cells. These neural stem cells are bipolar progenitors producing neurons and glia and serving as scaffolds for newborn neural cells to reach their final destination within the brain parenchyma (5, 6). Classically, the mantle layer forms upon three consecutive waves of neurogenesis, leading first to lateral, then medial, and finally periventricular zones, as illustrated by the genesis of melanin-concentrating hormone (MCH) neurons in the lateral hypothalamus (LHA) (7, 8) or other neurons in the ventromedial nucleus (VMH) (9, 10). Later, the ventricular zone evolves to give the ependymal layer (11).

Along the 3V in the mediobasal hypothalamus, the ependymal layer is characterized by the presence of heterogeneous ependymal cells. First, ciliated and cuboidal cells –typical in diverse brain regions– line the upper part of the 3V and participate in circulating cerebrospinal fluid (12). A second cell type, characterized by a long process and the presence of only one or two cilia, lines the lateral wall and the bottom of the 3V. These peculiar ependymal cells called tanycytes are considered reminiscent radial glial cells within the brain and are currently subdivided into four different subtypes, α1, α2, β1, and β2 (13, 14). Restricted to circumventricular organs in mammals (15), tanycytes play a role in numerous neuroendocrine functions such as glucose homeostasis, energy balance, and reproduction (16–18).

While hypothalamic neurogenesis from the mantle layer is well documented in rodents (19, 20), the ontogeny of the ependyma within the mediobasal hypothalamus is still limited (13, 19, 21–23). Here, we used BrdU incorporation to provide a spatiotemporal characterization of the mouse gliogenesis along the ependymal layer. In addition, neuron birthdate was analyzed in the arcuate (ARH), the ventromedial (VMH), and the dorsomedial (DMH) nuclei of the hypothalamus for a comparative perspective. We first confirmed that the ependyma is mainly generated once the neighboring neurons are produced. However, this generation is highly heterogeneous regarding the cell subtypes. Indeed, we determined different spatiotemporal gradients for the generation of the ependyma on the rostrocaudal and dorsoventral axis. Using publicly available scRNAseq datasets, we finally highlighted the transcriptional pseudotime developmental trajectories giving rise to mature tanycyte and typical ependymal cell populations.

Materials and methods

Animals

C57Bl/6J mice (initially obtained from Charles River) were used in this study. Male and female mice were put together around 5 pm, and the presence of a vaginal plug was checked on the following day (before 9 am). In this case, the time of conception was documented and considered as embryonic day 0 (E0). The day of birth was regarded as postnatal day 0 (P0). All animal procedures were performed at the University of Lausanne and were reviewed and approved by the Veterinary Office of Canton de Vaud.

Bromodeoxyuridine injections

BrdU crystals (5-Bromo-2-deoxyuridine, BrdU, Roche Applied Science, # 10280879001) were dissolved in 0.07 M NaOH solution warmed to 65°C. Pregnant mice (from gestational day 9 to 18) and male pups (from P0 to P8) were given a single i.p. injection around 10 a.m. (50mg/kg).

Tissue preparation. 21 to 23 days after birth (P21-P23), BrdU-injected male mice were anesthetized with isoflurane and perfused transcardially with a 0.9% NaCl solution, followed by an ice-cold solution of 4% paraformaldehyde in 0.1 M phosphate buffer, pH 7.4. Brains were quickly removed, postfixed in the same fixative for two hours at 4°C, and immersed in 20% sucrose in 0.1M phosphate-buffered saline (PBS) at 4°C overnight. Brains were finally either embedded in ice-cold OCT medium (optimal cutting temperature embedding medium, Tissue Tek, Sakura) and frozen in liquid nitrogen-cooled isopentane (most of the postnatally injected animals) or directly frozen in crushed dry ice without OCT (all prenatally injected animals). The different groups (n=3 to 7 per group) were then called "E9", "E10", "P1", …: these developmental time points correspond to the day of the single i.p. BrdU injection.

Immunohistochemistry

Brains were cut using a cryostat into 25-µm-thick coronal sections and processed for immunohistochemistry as described previously (24). Briefly, the slide-mounted sections were 1) incubated in a boiling 10 mM Citrate Buffer solution, pH 6.0, for 12 minutes; 2) blocked for 1 hour using a solution containing 2% normal goat serum and 0.3% Triton X-100; 3) incubated overnight at 4°C with primary antibodies (Table S1) followed by two hours at room temperature with a cocktail of secondary Alexa Fluor-conjugated antibodies (1:500, Molecular Probes, Invitrogen, San Diego, CA) (Table S2); 4) mounted with DAPI Fluoromount-G (Southern Biotech; REF: 0100-20).

Antibody characterization

All primary and secondary antibodies used are listed in Supplementary Tables S1, S2. The rabbit polyclonal antibody to BrdU (Bio-rad Cat#AHP2405, RRID: AB_2922993) recognizes the synthetic thymidine analog bromodeoxyuridine (BrdU). The chicken polyclonal antibody to VIM (Vimentin) (Millipore Cat# AB5733, RRID: AB_11212377) produced a pattern of staining

associated with tanycytes, ependymal cells, and endothelial cells, similar to that described elsewhere in the literature (25). The mouse monoclonal antibody to NeuN (Neuron-specific nuclear protein) (Millipore Cat# MAB377, RRID: AB_2298772) produced a pattern of staining associated with neuronal cells, similar to that described elsewhere in the literature (26).

Microscopic imaging

Pictures were acquired using a ZEISS Axio Imager.M2 microscope, equipped with ApoTome.2 and a Camera Axiocam 702 mono (Zeiss, Germany). Specific filter cubes were used for the visualization of green (Filter set 38 HE eGFP shift free (E) EX BP 470/40, BS FT 495, EM BP 525/50), red (Filter set 43 HE Cy 3 shift free (E) EX BP 550/25, BS FT 570, EM BP 605/70), and blue (Filter set 49 DAPI (E) EX G 365, BS FT 395, EM BP 445/50) fluorescence. Different magnifications were selected using a Zeiss x20 objective (Objective Plan-Apochromat 20x/0.8 M27 (FWD=0.55mm)) and a 63× oil immersion objective (Objective C Plan-Apochromat 63x/1.4 Oil DIC M27 (FWD=0.14mm)). To create photomontages, images were acquired using ZEN 2.3 pro software using Z-Stack and Tiles/Positions ZEN modules for each fluorophore sequentially. Quintuple-ApoTome frames were collected stepwise over a defined z-focus range corresponding to all visible fluorescence within the section. Multiple-plane frames were collected at a step of 0.3 µm while using the x63 objective (between 43 and 60 frames per image) and 1 µm while using the x20 objective (between 11 and 18 frames per image). Weak deconvolution was finally applied to images following the acquisition. All images were saved in.czi, processed to get maximal intensity projections, and finally exported in.tiff. for the processing steps (*i.e.*, adjust brightness and contrast and merge channels) using Adobe Photoshop (Adobe Systems, San Jose, CA)).

Data analysis

BrdU quantifications were performed using the AxioImager D1 microscope. Two investigators determined ependymocyte birthdate by counting the number of BrdU-positive and vimentin-positive cells. Tanycytes were differentiated from typical ependymal cells by their vimentin-positive basal process. One investigator quantified the neurogenesis by counting the number of BrdU-positive and NeuN-positive cells. The regions of interest (*i.e.*, the ventricular layer, the ARH, the VMH, and the DMH) were identified based on DAPI staining. For the ventrodorsal analysis, the ventricle was divided into seven subregions corresponding to the area where tanycyte processes are sent (*i.e.*, the medial median eminence, the lateral median eminence, the ventromedial ARH, the dorsomedial ARH, the VMH, and the DMH) and the layer composed of typical ependymal cells (Figure 1). For the rostrocaudal axes, the region was divided into four subregions, corresponding to zone 1 (from bregma -1.2 to -1.5mm), zone 2 (from bregma -1.6 to -1.75 mm), zone 3 (from bregma -1.8 to -2.1 mm), and zone 4 (from bregma -2.15 to -2.5 mm) (Figure 1). From a neuroanatomical point of view, these subdivisions were defined based on the shape of the ventricle and the presence/absence of hypothalamic nuclei along the 3V. These subdivisions were already described and used in former studies (27, 28).

Quantifications were performed on 3 to 7 animals per time point, on 5 to 12 sections per brain (1 to 3 sections per zone on average), and on both hemispheres. The total number of BrdU-positive cells was then calculated per zone and normalized by the number of analyzed sections (Table S3). The BrdU labeling pattern displayed low variability between animals injected at the same age.

Single-cell RNAseq data analysis

Publicly available scRNAseq datasets were analyzed as described in their original papers with few modifications (26, 29). Developmental time points (E10-E16, E18, P4, P14, and P45) scRNAseq datasets from Kim et al. (26) (GSE132355) were independently analyzed using *Seurat 4.1.1* to identify the developmental age at which tanycyte-like cells can be found as an independent cluster. After generating a *SeuratObject* from raw data and splitting the matrix by developmental time points ("*orig.ident*"), we filtered cells to contain at least 200 features, and all datasets were normalized and scaled using *scTransform* (30). Following UMAP dimensional reduction (maintaining the first 50 PCA variables), we clustered cells using a resolution of 1.7 to maximize cluster separation. Furthermore, we used differential gene expression (DGE) analysis between clusters to identify major hypothalamic cell types using known cell marker genes from the original publication. Gene ontology analysis was performed using ShinyGO (v0.76) to obtain enriched GO terms using features expressed in tanycyte clusters at every developmental time point analyzed. ShinyGO was set to get the biological processes ordered by the false discovery rate (FDR) with a threshold of 0.05.

To identify the ependyma developmental trajectory, hypothalamic datasets from E11 to P45 (except P8) from Kim et al. (26) were integrated using *Harmony* (31). Normalization, dimensional reduction, and clustering were performed as described above. Following cell type identification, clusters containing progenitor cells (NPCs), ependyma, and tanycytes were subset in Seurat. The resulting Seurat object was then converted to *CellDataSet* to calculate the pseudotime trajectory from NPCs to the ependyma and tanycyte populations using Monocle3. A differentially expressed gene analysis across a single-cell trajectory from NPCs to ependyma and tanycyte populations was performed using the *graph_test* function.

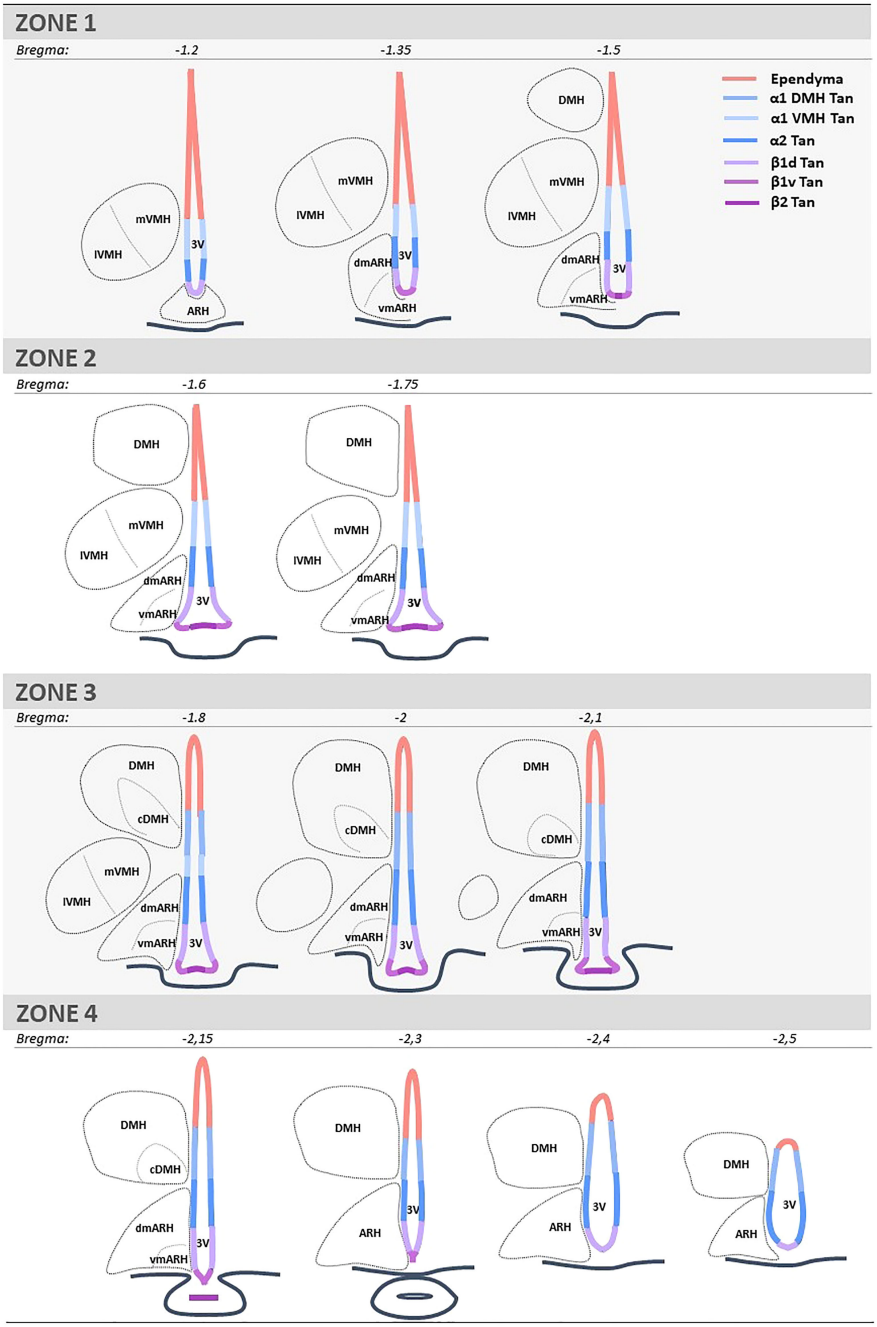

FIGURE 1
Schematic representation and coordinates of the four consecutive rostrocaudal zones used to analyze the mediobasal hypothalamus. Zone 1 corresponds to the anterior part of the ARH and the ME, where tanycyte processes are mainly found in the ARH and a few in the VMH. Zone 2 corresponds to the medial part of ME, where the bottom of the ventricle is more considerable, and tanycyte processes are found in both the ARH and VMH. Zone 3 corresponds to the medial-posterior part of the ME, where the VMH is lateral, and tanycyte processes are now observed in the DMH. Zone 4 corresponds to the posterior part of the ME and the presence of the infundibular stalk, where tanycyte processes are sent in the ARH and DMH. ARH is subdivided into vmARH and dmARH. VMH is subdivided into mVMH and lVMH. DMH is subdivided into cDMH. The ependyma is subdivided into 7 subregions: the ependymal layer facing the medial ME for beta-2 tanycytes (β2 Tan), the lateral ME for ventral beta-1 tanycytes (β1v Tan), the vmARH for dorsal beta-1 tanycytes (β1d Tan), the dmARH for alpha-2 tanycytes (α2 Tan), the VMH for rostral alpha-1 tanycytes (α1 VMH Tan), the cDMH for caudal alpha-1 tanycytes (α1 DMH Tan), and the dorsal part of the DMH for typical ependymal cells. 3V, third ventricle; ARH, arcuate nucleus of the hypothalamus; cDMH, compact dorsomedial nucleus of the hypothalamus; dmARH, dorsomedial arcuate nucleus of the hypothalamus; DMH, dorsomedial nucleus of the hypothalamus; lVMH, lateral ventromedial nucleus of the hypothalamus; ME, median eminence; mVMH, medial ventromedial nucleus of the hypothalamus; vmARH, ventromedial arcuate nucleus of the hypothalamus.

To identify tanycyte subtypes across developmental time points, we analyzed the Yoo et al. (29) (GSE160378) scRNAseq dataset using Seurat. The original dataset was subset to contain the developmental time points P8 from wild-type mice exclusively. Data normalization, dimensional reduction, and cell-type identification were performed as described above. All analyses were performed in RStudio (v1.4.1103) using 4.1.1. version.

Results

To analyze the birth of ependymal cells and neurons within the periventricular zone in the mediobasal hypothalamus, pregnant dams (from E9 to E18) and male pups (from P0 to P8) were given a single i.p. injection of BrdU, and its labeling was then performed on coronal brain sections from 21- to 23-day-old male mice. Vimentin (Figures 2A–C) and NeuN (Figures 2D–F) were co-stained to visualize ependymal cells and neurons, respectively. We first observed a differential pattern of BrdU labeling along the ventricle (Figures 2A, C). Indeed, at a younger age, BrdU is incorporated along the ventricle, but its labeling does not fill out the entire nucleus of the cell (Figure 2C, double arrowhead), suggesting additional cell divisions afterward and highlighting a high generative capacity. Alternatively, BrdU staining filled out the entire cell nucleus (Figure 2C, arrowheads), indicating no additional cell divisions and, consequently, the birth of the cell. For the analysis, we focused on full BrdU-staining in ependymal cells (Figures 2A–C) and neuronal cells (Figures 2D–F). The ependymal cells were

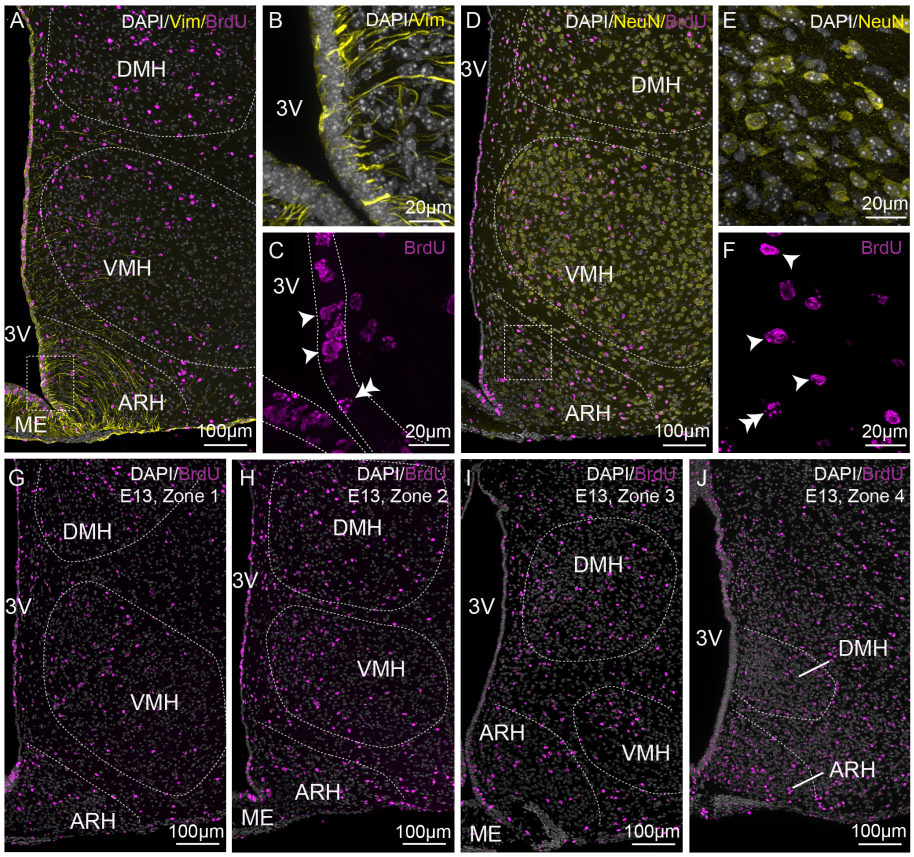

FIGURE 2
Characterization of BrdU-positive cells on the rostrocaudal axis. **(A–C)** Low- (x20, A) and high- (x63, B-C) magnification z-stack images showing the colocalization of vimentin immunoreactivity (yellow) and BrdU (pink) in zone 2 with Dapi counterstaining (white) in a coronal section from P21 male pups after BrdU injection to pregnant dams at E13. **(D–F)** Low- (x20, D) and high- (x63, E-F) magnification z-stack images showing the colocalization of NeuN immunoreactivity (yellow) and BrdU (pink) with Dapi counterstaining (white) in a coronal section at E13 in zone 2. **(G–J)** Low-magnification z-stack images (20x) showing the distribution of BrdU immunoreactivity (pink) with Dapi counterstaining (white) in coronal sections at E13 in zone 1 **(G)**, zone 2 **(H)**, zone 3 **(I)**, and zone 4 **(J)**. "E13" indicates the BrdU injection time point. Single arrowheads point out a BrdU labeling filling out the entire cell nucleus, whereas the double arrowheads point out a labeling that does not. ARH, arcuate nucleus of the hypothalamus; DMH, dorsomedial nucleus of the hypothalamus; ME, median eminence; VMH, ventromedial nucleus of the hypothalamus; 3V, third ventricle.

further subdivided into typical cuboid ependymal cells *versus* tanycytes based on the presence of a basal vimentin-positive process (Figures 2A, B).

To adequately evaluate the heterogeneity of ependymoglial cell and neuronal birthdate along the 3V, a methodical analysis was performed on the ventrodorsal and rostrocaudal axes (Figures 1, 2G–J). The 3V was first divided into seven subregions on the ventrodorsal axis: the ependymal layer facing the medial median eminence for β2 tanycytes, the lateral median eminence for ventral β1 tanycytes, the ventromedial ARH (vmARH) for dorsal β1 tanycytes, the dorsomedial ARH (dmARH) for α2 tanycytes, the VMH for rostral α1 tanycytes, the compact part of the DMH (cDMH) for caudal α1 tanycytes, and the dorsal part of the DMH for typical ependymal cells (Figure 1). Additionally, the region was divided into four subregions along the rostrocaudal axis, corresponding to zone 1 (from bregma -1.2 to -1.5 mm), zone 2 (from bregma -1.6 to -1.75 mm), zone 3 (from bregma -1.8 to -2.1 mm) and zone 4 (from bregma -2.15 to -2.5 mm) (Figures 1, 2G–J). Finally, the analysis of newborn neural cells was based on a single BrdU injection performed at different time points from E9 to P8 to infer temporal gradients in BrdU labeling patterns (Figure 3 and File S1). Thus, "E12" brains (*i.e.*, brains harvested from P21-22 male pups whose mothers received a single BrdU injection during pregnancy at E12) revealed a high generation of neurons and a low rate for ependymal cells at this time point (Figure 3A). In contrast, the ependyma mainly arises from E13 (Figures 3B–D) at different generation rhythms according to the ependymal subpopulations (File S1). Indeed, typical ependymal cells, α2 and α1 tanycytes display a higher generation at E13, E14 and E15, respectively (Figures 3B–D, brackets).

Neuron birthdate in the mediobasal zone mostly occurs between E11 and E13 in mice

In the periventricular (*i.e.*, ARH and DMH) and medial nuclei (*i.e.*, VMH), BrdU/NeuN-positive neurons were found in animals injected between E9 and E18 (Figure 4A and Table S3). No postnatal neurogenesis was observed. Thus, the neurogenic generative peak mainly occurs between E11 and E13, concentrating 75.6% of the total number of cells generated over the entire period (Figure 4A). However, BrdU/NeuN labeling patterns revealed regional differences (Figures 4A, B). First, most BrdU/NeuN cells were found in the dmARH, the DMH, the mVMH, and the lVMH with 24.0%, 22.7%, 20.9%, and 15.9% of generated cells over the entire developmental window (i.e., from E9 to P8), respectively (Figures 4A, B and Table S3). Lower generation levels were observed in the vmARH (8.2%) and the cDMH (8.3%) (Figures 4A, B and Table S3). Secondly, BrdU/NeuN labeling patterns confirmed a lateral-to-medial gradient in the generation of the VMH (9, 10). Indeed, most of the observed newborn neurons in the lateral VMH were generated at E11, whereas those within the medial VMH arose a day later at E12 (Figure 4B and Figure S1). Then, the neuronal generative peak in the periventricular nuclei (*i.e.*, ARH and DMH regions) was concentrated within a few days between E12 and E13 without a lateral-to-medial gradient (Figures 4B, S1). Third, some nuclei additionally display a rostrocaudal gradient in their neuronal generation (Figures 4C–H). Specifically, the generation of newborn neurons in the vmARH, which mainly arises between E11 and E13 (Figures 4B, S1), actually starts in the rostral zone 1 at E10 and ends in the caudal region zone 4 by E13 (Figure 4C). In the dmARH, most neurons were born from E11 to E14 (Figure 4B), starting in the rostral zone 1 at E10 and

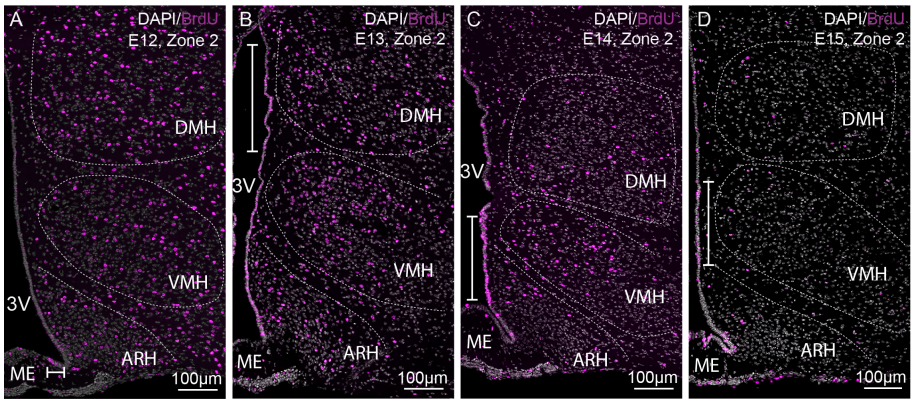

FIGURE 3
Characterization of BrdU-positive cells in time. **(A–D)** Low-magnification z-stack images (20x) showing the distribution of BrdU immunoreactivity (pink) in zone 2 (bregma -1.8) with Dapi counterstaining (white) in coronal sections from P21 male pups after BrdU injection to pregnant dams at E12 **(A)**, E13 **(B)**, E14 **(C)**, and E15 **(D)** (labeled "E12", "E13", "E14", and "E15" on the pictures, respectively). The white bars point out the peaks of genesis along the third ventricle. ARH, arcuate nucleus of the hypothalamus; DMH, dorsomedial nucleus of the hypothalamus; ME, median eminence; VMH, ventromedial nucleus of the hypothalamus; 3V, third ventricle.

ending in the caudal region zone 4 by E16 (Figure 4D). In contrast, VMH neurons were generated between E11 and E12 (Figure 4B) without a rostrocaudal gradient (Figures 4E, F). DMH neurons were generated between E11 and E14, with the first peak of genesis in zones 2 and 3 and a second in caudal zone 4 (Figure 4G). However, neuronal generation starts first and lasts longer in zone 3 and 4 (Figure 4G). In the cDMH, most neurons were generated in zone 3 at E13 (Figure 4H). To summarize, these different patterns of neurogenesis revealed a lateral-to-medial gradient for the VMH and a slight rostral-to-caudal direction for the periventricular ARH and DMH nuclei.

The typical ependymal cell generation peaks at E13, whereas tanycytes are generated over an extended time window

Ependymal cell generation (*i.e.*, typical ependymal cells and tanycytes) occurred over an extended time window and appeared highly heterogeneous (Figures 5, 6 and Table S3). The distribution of full BrdU-positive cells along the 3V displayed different temporal, dorsoventral, and rostrocaudal gradients (Figure 5 and File S1).

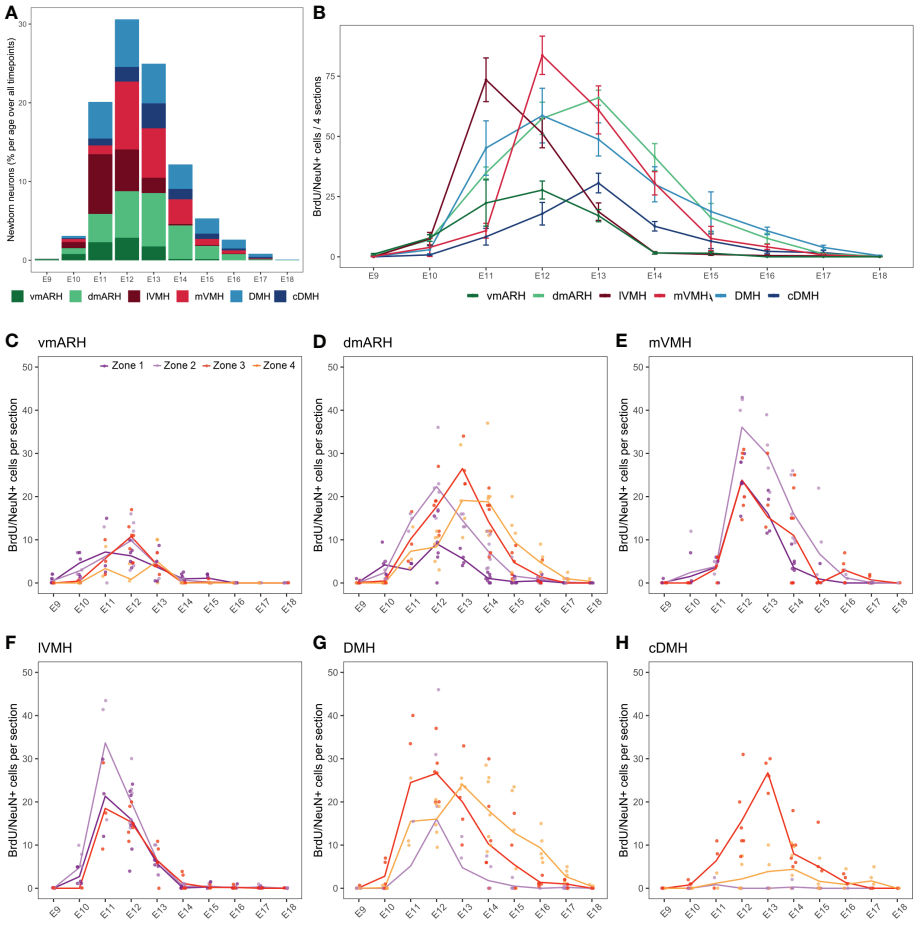

FIGURE 4
Developmental hypothalamic BrdU incorporation in NeuN-positive cells. **(A)** Stacked graph displaying the proportion of newborn BrdU/NeuN-positive cells in the hypothalamic regions vmARH, dmARH, lVMH, mVMH, cDMH, and DMH per age over all analyzed brains from P21-22 animals having received a single BrdU injection from E9 to P8 (*e.g.*, "E9" brains were harvested from P21-22 male pups whose mothers received a single BrdU injection during pregnancy at E9; "E10" brains were harvested from P21-22 male pups whose mothers received a single BrdU injection during pregnancy at E10...). The bars represent the percentage of cells per age over the whole analyzed period. Within a single age, the colors represent the percentage of cells per nucleus over the entire analyzed region. **(B)** Number (mean ± SEM) of BrdU/NeuN-positive cells per nucleus and per age over 4 hypothalamic sections (one in each rostrocaudal zone). **(C–H)** Number (average -line- and individual values -dots-) of BrdU/NeuN-positive cells per rostrocaudal zones (1 to 4) and per age in each hypothalamic region. n=3 to 7 animals per group. vmARH, ventromedial arcuate nucleus of the hypothalamus; dmARH, dorsomedial arcuate nucleus of the hypothalamus; lVMH, lateral ventromedial nucleus of the hypothalamus; mVMH, medial ventromedial nucleus of the hypothalamus; cDMH, compact dorsomedial nucleus of the hypothalamus; DMH, dorsomedial nucleus of the hypothalamus. See Figure S1.

First, as observed for neurons (Figure 4), BrdU incorporation differed along the 3V (Figure 6A). While α tanycytes displayed high levels of generation, representing 62.0% (α1 = 33.0%, α2 = 29.0%) of newborn ependymal cells within the whole period (i.e., from E9 to P8), typical ependymal cells, β1, and especially β2 tanycytes, had low levels of generation, representing 9.5%, 26% (β1ventral = 7.3%, β1dorsal = 18.7%), and 2.5% of generated ependymal cells, respectively (Figures 6A, B and Table S3). Consequently, no clear generation peak was observed for β2 tanycytes, instead displaying a low generation between E11 and E18 (Figure 6B).

Across development, typical ependymal cells were generated in a short time window between E12 and E16, peaking at E13 with 38.5% of cell generation over the whole period (i.e., from E9 to P8) (Figures 6A, B and Table S3). In contrast, tanycytes were generated over an extended time window from E10 to P8 (Figures 6A, B). Specifically, we first found BrdU incorporation in β1 tanycytes occurring mostly between E11 and E18, with a peak at E12-13 for ventral β1 tanycytes and E14 for dorsal β1 tanycytes (Figure 6B). Next, α1 and α2 tanycytes arose with a more extended distribution throughout development, mainly between E12 and P3 (Figure 6A), with two generation peaks at E14-15 and E17 (Figure 6B). α2 tanycytes start to be generated one day before α1 tanycytes (Figure 6B). Therefore, these results show an "outside-in" generation pattern along the dorsoventral axis of the 3V. Indeed, cells were first generated in typical ependymal cells and β tanycytes in the dorsal and ventral regions between E12 and E14 and then in α tanycytes located in the central region between E14 and P3 (Figure 6B).

To further understand the extended time windows and the multiple peaks for the ependyma generation, we next analyzed BrdU incorporation along the rostrocaudal axis (Figures 6C–H; S2), revealing additional differences according to ependymal subpopulations. Ependymal cells were generated mainly at E13 in every zone without a rostrocaudal gradient (Figure 6C). Regarding α tanycytes, we observed a strong developmental rostral-to-caudal gradient in their generation. Indeed, α1 and α2 tanycytes are first generated in the rostral zones 1 and 2, followed by 3 and 4 later in development in a more prominent way

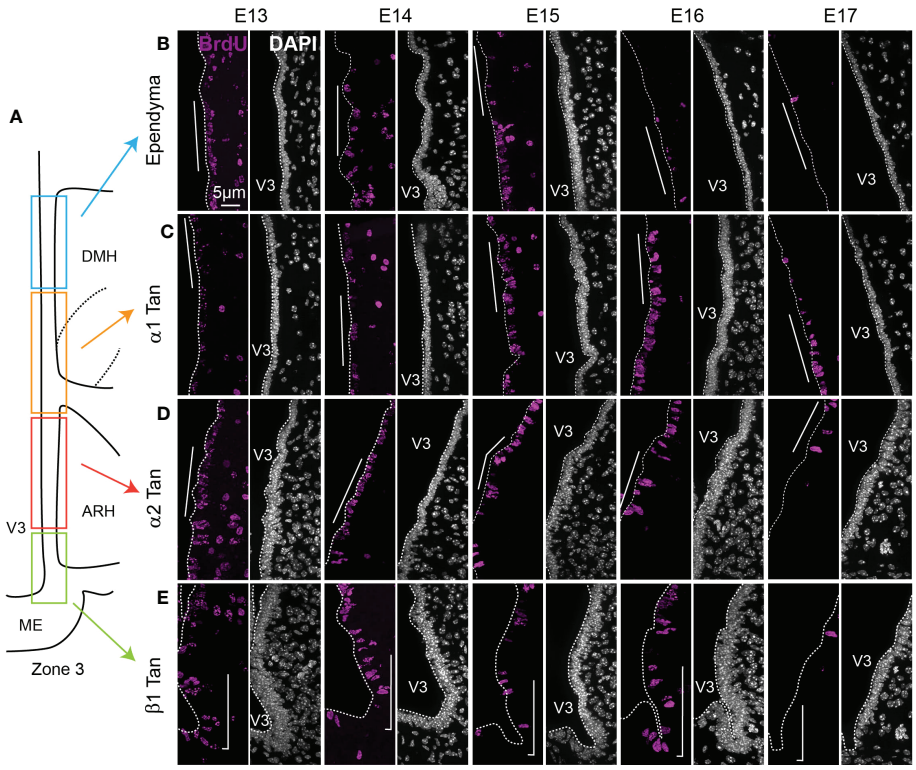

FIGURE 5
Characterization of BrdU-positive ependymoglial cells along the ventricular wall. **(A)** Schematic representation of zone 3 in the mediobasal hypothalamus. Rectangles display the different ependymal regions used for the analysis: beta-1 tanycytes facing the lateral ME and the vmARH (β1 Tan), alpha-2 tanycytes facing the dmARH (α2 Tan), alpha-1 tanycytes facing the cDMH (α1 Tan), and typical ependymal cells facing the dorsal part of the DMH. **(B–E)** High-magnification z-stack (63x) illustrative coronal images showing the distribution of BrdU immunoreactivity (pink) in the typical ependymal cells **(B)**, α1 **(C)**, α2 **(D)**, and β1 **(E)** from the developmental timepoint E13 to E17. DAPI counterstaining is represented in white. The white bars point out the respective cells of interest along the third ventricle. ARH, arcuate nucleus of the hypothalamus; DMH, dorsomedial nucleus of the hypothalamus; ME, median eminence; V3, third ventricle. The scale bar is shown in the figure. See File S1.

(Figures 6D, E). This strong gradient explains the two peaks of generation observed at E14 and E17 when the rostrocaudal axis is not considered (Figure 6B). In contrast, β1 tanycytes facing the vmARH (β1d) did not display a clear rostrocaudal gradient of generation (Figure 6F). Interestingly, the generation of ventral β1 tanycytes (β1v) was more extended in zones 1 and 2 –from E11 to E18–, whereas it peaks at E12-13 in zones 3 and 4 (Figure 6G), suggesting a slight caudal-to-rostral gradient. Similarly, for β2 tanycytes, although we observed low BrdU incorporation in this cell subtype, the generation pattern suggests a slight caudal-to-rostral gradient with an extended generation up to P1 in zone 2 *versus* an earlier and shorter window in zone 3 (Figure 6H).

To summarize, our results demonstrated that typical ependymal cells (E13) and β tanycytes (E12-14) are the first generated shortly after the peak of neuron birthdate (E11-13) (Figure 7A). However, this time difference is less clear when considering the rostrocaudal gradient observed for neuronal generation (Figure 7B). Indeed, neurons are born before ependymal cells and β tanycytes in the rostral zone, but they arise concomitantly in the caudal region (Figure 7B). In contrast, there is little or no overlap between neuron and α tanycyte birthdate. Specifically, at the timing of the peak of neuron birth between E11 and E13, only a small proportion of α2 tanycytes is generated. α tanycytes arise later with a robust rostral-to-caudal gradient (Figure 7B).

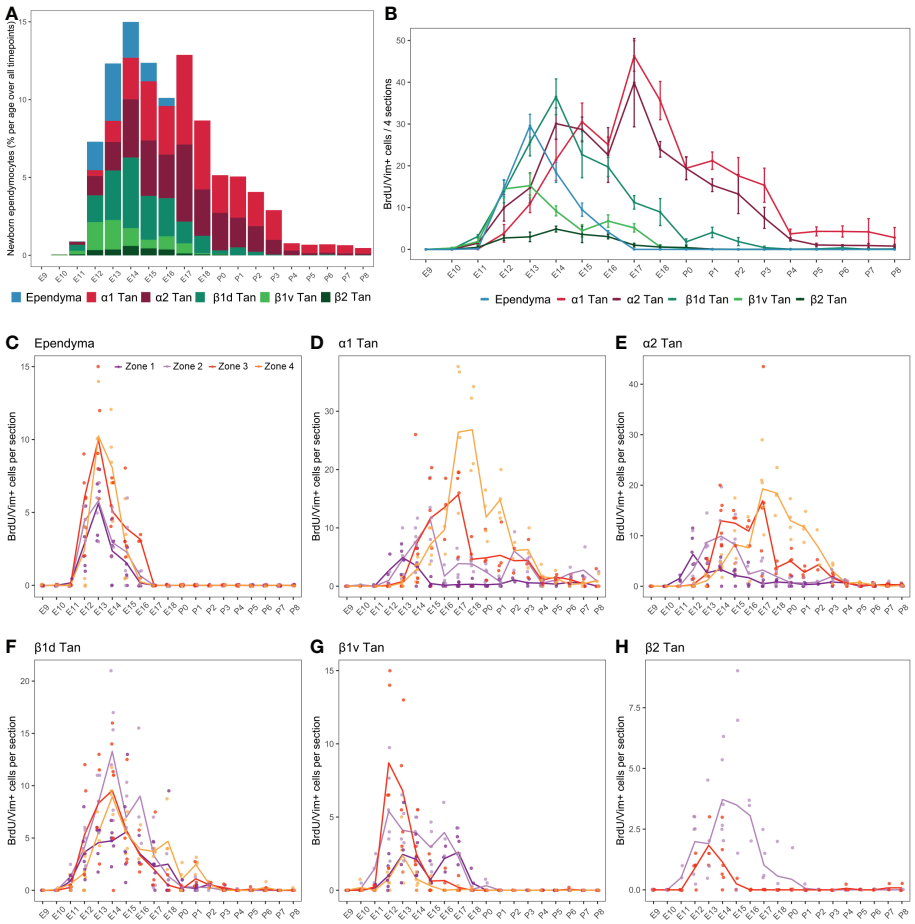

FIGURE 6
Developmental hypothalamic BrdU incorporation in vimentin (Vim)-positive cells. **(A)** Stacked graph displaying the proportion of newborn BrdU/Vim-positive cells in typical ependymal and tanycyte populations per age over all analyzed brains from P21-22 animals having received a single BrdU injection from E9 to P8 (*e.g.*, "E9" brains were harvested from P21-22 male pups whose mothers received a single BrdU injection during pregnancy at E9; "E10" brains were harvested from P21-22 male pups whose mothers received a single BrdU injection during pregnancy at E10…). The bars represent the percentage of cells per age over the whole analyzed period. Within a single age, the colors represent the percentage of cells per ependymal subpopulation over the whole analyzed region. **(B)** Number (mean ± SEM) of BrdU/Vim-positive cells per ependymal subpopulations and per age over 4 hypothalamic sections (one in each rostrocaudal zone). **(C–H)** Number (average -line- and individual values -dots-) of BrdU/Vim-positive cells per rostrocaudal zones (1 to 4) and per age in each ependymal subpopulation. n=3 to 7 animals per group. α1 Tan, alpha-1 tanycytes; α2 Tan, alpha-2 tanycytes; β1v Tan, ventral beta-1 tanycytes; β1d Tan, dorsal beta-1 tanycytes; β2 Tan, beta-2 tanycytes. See Figure S2.

10.3389/fendo.2022.1073759

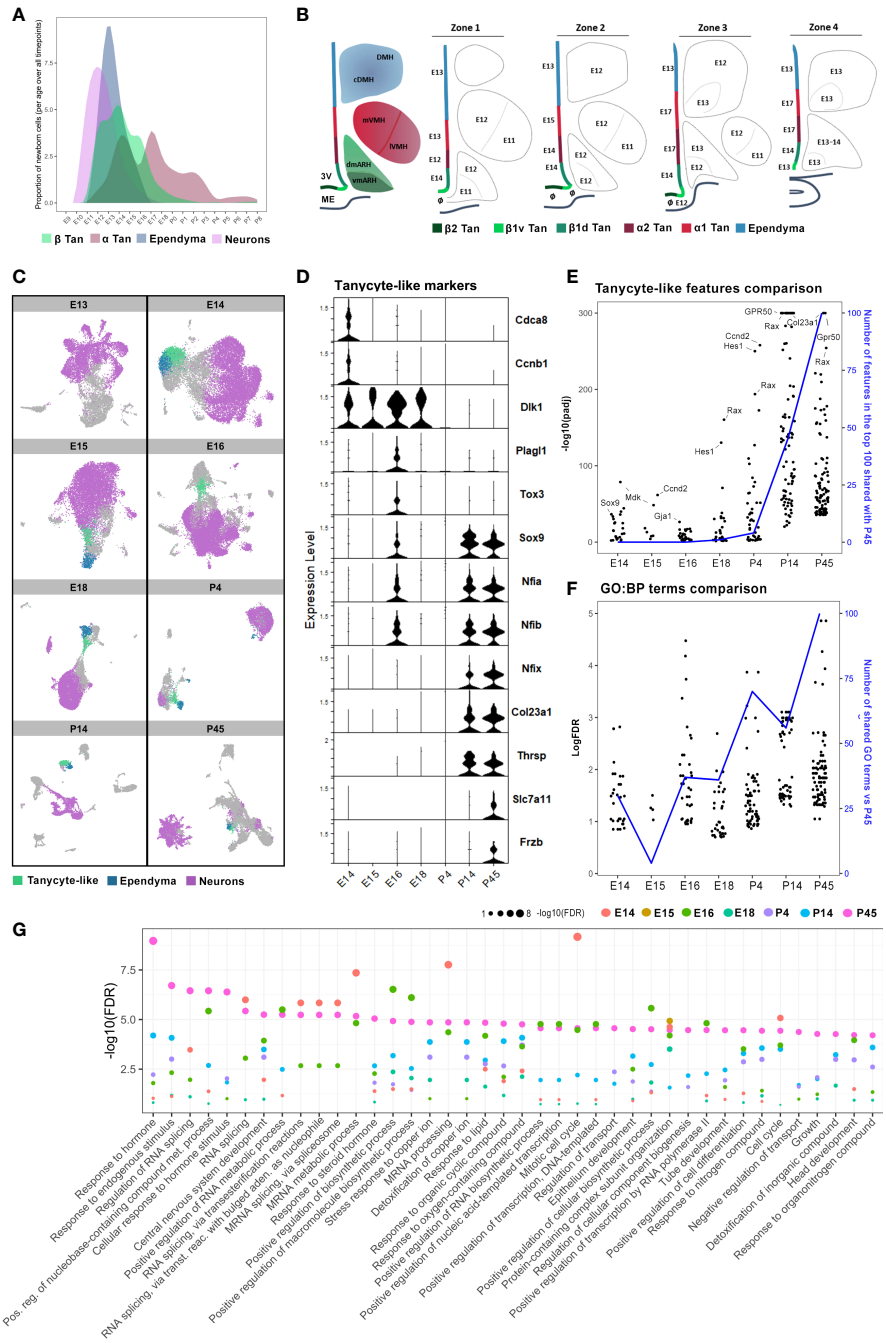

FIGURE 7
Cellular and molecular hypothalamic generation of mature tanycytes. **(A)** Representative plot illustrating the patterns of neuron, ependymal, and tanycyte generation across embryonic and early postnatal development extrapolated from our quantifications. **(B)** Rostrocaudal neuroanatomical representations of the developmental peaks of BrdU integration along the ventricular wall and hypothalamic nuclei. The ages indicate the peaks of genesis. The symbol ø indicates no clear peak of genesis (*i.e.*, either multiple peaks or a continuous generation). **(C)** UMAP plots showing neuron (pink), ependymal (blue), and tanycyte-like (green) clusters in diencephalic and hypothalamic scRNAseq datasets (26), from E13 to P45, per developmental time point. **(D)** Violin plot showing specific features in tanycyte-like clusters across developmental time points from E14 to P45. **(E)** Comparison between the expression of the top 100 features of tanycyte-like cells at P45 *versus* those of tanycyte-like cells from every other developmental time point. The black dots represent features regarding their -log10(pAdj) significance. The blue line displays the number of features in the top 100 at each timepoint shared with the top 100 at P45. **(F)** Plot showing the comparison between the 100 more enriched GO terms from tanycyte-like cells at P45 (based on FDR) *versus* GO terms found in tanycyte-like cells from every other developmental time point. The black dots represent GO terms regarding their -log(FDR) significance. The blue line represents the number of GO terms shared in tanycyte-like clusters compared to P45. **(G)** Plot showing the -log10(FDR) of the top 40 more enriched GO terms in tanycyte-like cells at P45 compared to all time points. See Figure S3.

Tanycyte-like cells emerge as an independent cell population at E14 but are considered mature between P4 and P14

Our analysis revealed that neuron birthdate mainly peaks at E11-E13, ependymal cells at E13, and β and α tanycytes have a more widely distributed generation with multiple generative peaks between E12 and E18 (Figure 7A). To explore the developmental differences in the pattern of ependymal cell birthdate, we analyzed publicly available developmental hypothalamic scRNAseq datasets (26, 29). By using whole diencephalic or hypothalamic explants across embryonic and postnatal time points, Kim et al. (26) identified tanycytes to form an independent cluster starting at P4. Furthermore, they demonstrated that tanycytes diverge in trajectory from ependymal cells at E13 when they begin to express tanycyte and ependymal cell-specific markers, such as *Rax* and *Foxj1*, respectively (Figure S3A).

In agreement with their results, the analysis of the developmental scRNAseq datasets at each time point separately demonstrated that a population of tanycyte-like (*Rax*-positive) cells can be identified as an independent cluster starting from E14 (Figure 7C). Still, tanycyte-like cells do not share the same transcriptional profile across the different developmental time points. Indeed, DGE analysis of tanycyte-like cells at each developmental time point first showed that features commonly found in mature tanycytes, such as *Col23a1*, *Frzb, Slc7a11*, and *Thrsp*, are only observed in the P14 and P45 datasets (Figure 7D and Table S4). In contrast, genes involved in cell division, such as *Cdca8* and *Ccnb1*, are expressed specifically at E14 (Figure 7D). Similarly, tanycyte-like cells from embryonic time points express *Dlk1* and *Cdk4* up to E18 (Figure 7D and Table S4), consistent with their proliferative capacity during early development (6, 32). The cyclin-dependent kinase *Cdk4* is a master regulator of mitosis involved in cell proliferation (32), suggesting that these generating cells are likely radial glia. Interestingly, the genes *Sox9*, *Tox3*, *Plag1*, and several features from the NFI family of transcription factors (*Nfia, Nifb*), known to be involved in the negative regulation of neurogenesis (29) and the control of the onset of gliogenesis (33–35), are expressed at E16 (Figure 7D), corresponding to the end of neurogenesis peak and the burst in α tanycyte generation (Figures 4, 6). Consistently, *Sox9* appears to be involved in the neurogenic-to-gliogenic fate switch (36). Secondly, we performed a comparative analysis of differentially expressed features in tanycyte-like clusters across development. Specifically, the 100 more significantly expressed genes in tanycyte-like cells at P45 were compared to tanycyte-like cell markers from the other developmental time points: most P14 and partially P4 tanycyte-like cells shared the same features compared to mature tanycytes at P45 (Figure 7E), highlighting the beginning of tanycyte maturation around P4. Indeed, we observed high levels of expression of the mature tanycyte markers *Col23a1*, *Gpr50*, and *Ccnd2*. Additionally, *Hes1*, a gene associated with the GO terms radial glia and neuroendocrine cell differentiation, shows an increase in expression levels starting from E18 (Figure 7E). Third, to further explore the immature *versus* mature state of tanycyte-like cells across developmental time points, we performed a gene ontology analysis focusing on biological process terms in tanycyte-like cells at P45 (Figure 7F) and compared the first 50 more significant GO terms to the other developmental time points (Figures 7F, G). Consistent with the known tanycyte functions (16–18), P45 GO terms comprise the response to hormones, endogenous stimulus, or lipids, and transport regulation (Figure 7G). As reported above, P4 and P14 tanycyte-like clusters shared the most GO terms compared to the older postnatal dataset (Figure 7F, blue line). Interestingly, many GO terms related to RNA processing and splicing are shared between E14 and P45 tanycyte-like clusters (Figure 7G). To summarize, these results suggest that while tanycytes-like cells are identified starting E14, these cells are not fully mature until early postnatal development, likely between P4 and P14.

Finally, to confirm the tanycyte maturity during postnatal development, we explored the occurrence of the different subtype specialization (*i.e.*, α1, α2, β1, and β2 tanycytes) (Figures S3B, C). Due to the high heterogeneity of cell types found in the hypothalamic dataset of Kim et al. (26) and the relatively low number of tanycytes identified per age, tanycyte subtypes are not distinguishable at any time point. To overcome this issue, we analyzed a scRNAseq dataset of *Rax*+ hypothalamic cells in wild-type mice at P8 (29). In agreement with the original article, our analysis allowed the identification of the tanycyte α1, α2, β1, and β2 cell populations (Figures S3B, C), suggesting that tanycyte subtypes are already present during early postnatal development.

Transcriptional switch from gliogenesis to tanycyte maturation

To explore the tanycyte maturation process, we finally performed an integrative analysis of the hypothalamic developmental dataset of Kim et al. (26), focusing on the developmental trajectory of tanycytes from undifferentiated cells. Following cell type identification, we subset the progenitor (NPCs), tanycytes, and ependymal cell populations (Figures 8A, B) and perform pseudotime trajectory analysis (Figure 8C). The pseudotime analysis allowed us to visualize the transitional state and the timing of the developing trajectory from NPCs to tanycytes *versus* typical ependymal cells, respectively (Figure 8C). Developmental trajectories for the tanycyte population identified an age around E16 at which there is a first switch in cell fate towards glia differentiation (Figures 8D–F). From E11 to E16, the genes *Tubb2b* and *Rlp10*

10.3389/fendo.2022.1073759

involved in neurogenesis are highly expressed in the NPC clusters and rapidly decrease afterward (Figure 8F). At this time point (E16), the expression of genes involved in glial cell proliferation and differentiation (*i.e.*, *Dbi, Ptn, Nfix*) and the negative regulation of neurogenesis (*i.e.*, *Mt3*) increases (Figure 8F). Furthermore, we observed starting at E16 but more clearly around P4-P14 that a second switch towards tanycyte maturation characterized by an increased expression tanycyte specific markers (*i.e.*, *Col23a1*) and genes involved in the negative regulation of astrocyte differentiation (*i.e.*, *Gpr37l1,*

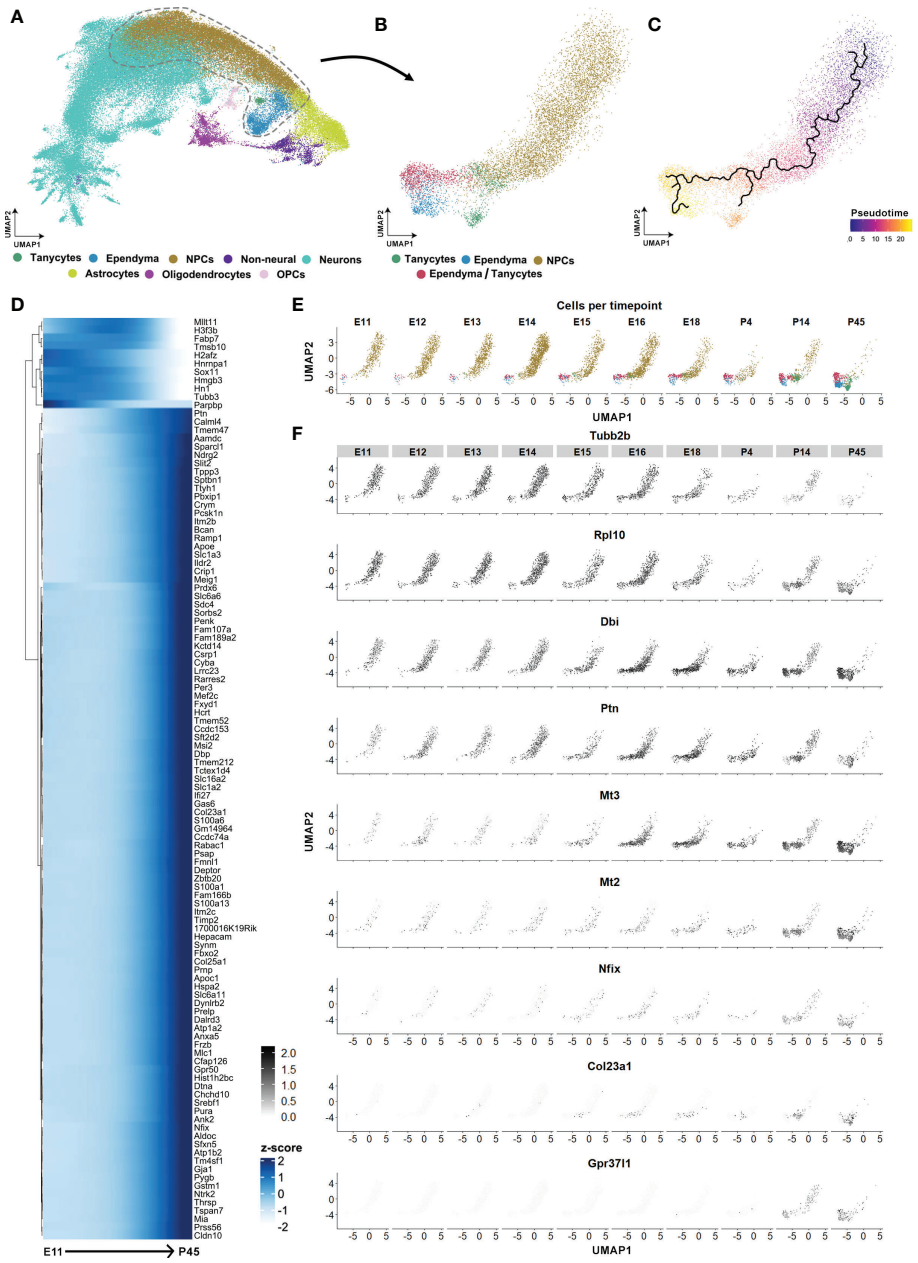

FIGURE 8
Tanycyte and ependyma developmental trajectories. **(A)** UMAP showing the integrated developmental scRNAseq datasets from hypothalamic and diencephalic explants between E11 and P45 (excluding E10 and P8 datasets) from Kim et al. (26). **(B)** UMAP showing the subclustering of progenitor cells (NPCs), tanycytes, ependyma, and tanycyte/ependymal cell populations. **(C)** UMAP plot displaying the pseudotime ependymal and tanycyte trajectories originating from NPCs. **(D)** Heatmap displaying the first 100 genes expressed in the pseudotime NPC to tanycyte trajectory. **(E)** UMAP displaying the development of tanycytes and ependymal cells split by age from E11 to P45. **(F)** UMAP showing features expressed across the developmental trajectory from NPCs to the tanycyte population. See Figure S4.

Mt2) (Figure 8F and Table S5). Finally, similar maturation patterns were found in the ependyma trajectory (Figure S4 and Table S5). Specifically, starting from E16-18 and more clearly during the postnatal time points, ependyma begins to express specific markers such as *Foxj1, Cdhr4, Pltp, Tm4sf1, Pcp4l1, Tmem212, Stoml3 and Hdc* (Figure S4 and Table S5). These markers were associated with the GO terms glycolipid transport, positive regulation of cholesterol efflux, cilium, and negative regulation of mitotic cell cycle. In contrast, before E16 and along the trajectory from NPCs, we observed the expression of the immature markers *Taf10*, *Kldhc2*, *Tead2*, *Nusap1*, and *Gap43*, associated with cell division, radial glial cell differentiation, and embryonic development. Altogether, these results demonstrate that tanycyte-like cells originate from NPCs early during development and mature starting E16.

Discussion

This study shows that neurons, typical ependymal cells, and tanycytes arise at different generation rhythms during embryonic development. Neurons mainly arise at E11-13, typical ependymal cells at E13, and tanycytes display a wider developmental generation from E12-P3 without a clear peak when the different subtypes are not considered. Neuron birthdates differ in time and space in the mediobasal hypothalamus, defining a lateral-to-medial gradient for the VMH and a slight rostral-to-caudal gradient for the ARH and DMH. Furthermore, the ependyma arises with an outside-in dorsoventral gradient (*i.e.*, typical ependymal cells and β tanycytes are generated before α tanycytes), as well as a marked rostral-to-caudal gradient for α1 et α2 tanycyte populations.

During embryonic development, neural cells originate from radial glial cells (37, 38), which display numerous cell functions such as (1) neurogenic (13, 37, 39) and gliogenic (40–42) competences, (2) helping migration of newborn neurons, and (3) monitoring gyrification of the cerebral cortex (43). First, in agreement with our results, it has been largely described that neurogenesis occurs from E10 to E16 in rodents, peaking between E12 and E14 in the mediobasal hypothalamic regions (8, 19, 24, 44, 45). Basically, it is usually established that hypothalamic neurogenesis peaks at E12-14 in mice and E13-15 in rats (46). Additionally, numerous studies –using the BrdU approach or others– observed a lateral-to-medial gradient in neuron generation that first occurs in the lateral hypothalamus around E11 and finish in the medial hypothalamic nucleus at E13 (8, 44, 45), although some did not find any variations in the timing and the neuroanatomical distribution (47). Here, we confirmed a lateral-to-medial gradient in the generation of the VMH. Additionally, our results showed a slight rostral-to-caudal gradient for neuronal generation in the ARH and DMH. In agreement with these results, such a gradient has already been described (19, 45). Notably, a study demonstrated that neuron birthdate first occurs at E11 in mid-rostral and ventral regions, followed by caudal regions at E14 (20). The authors found that mid-rostral neurons were mainly growth-releasing hormone (GRH)-neurons in the ARH region in rats. Such neuroanatomical generative gradients participate in hypothalamic regionalization and functions (26). Finally, our study does not reveal postnatal neurogenesis while it was already reported in the mediobasal hypothalamus (4). The difference is likely due to the approach we used (*i.e.*, single BrdU injection) that does not allow the visualization of low-rate neurogenesis.

In mice and rats, typical ependymal cells and tanycytes also originate from radial glial cells (13, 43). In the rat, typical ependymal cells are mainly generated from E16 to E18, whereas tanycytes are generated from the last two days of gestation and during the first postnatal week (19). Besides, ependymal cell birthdate precedes tanycyte generation (19, 21, 22), and α2 tanycytes precede α1 tanycyte development (13). Similar developmental birthdates were found in primates where tanycyte differentiation occurs mid-gestation (23). Our results demonstrate a similar chronology with the generation of ependymal cells, followed by β tanycytes and α tanycytes. However, the ependyma generation appears early in mice, starting at E12. Additionally, our data reveal a robust rostral-to-caudal developmental gradient for α tanycytes, with more prominent activity in the caudal region. Altman and Bayer also defined the latest tanycyte generation in the caudal region, extending up to P8 in rats (19). These developmental gradients are also consistent with the fact that, among tanycyte subpopulations, the most dorsal α tanycytes are the last to reach maturity (48). Alternatively, it is worth noticing that a slight caudal-to-rostral gradient is present in the generation of β2 and ventral β1 tanycytes, suggesting a different developmental pattern in the median eminence, but without additional clues in the literature. Finally, comparing tanycyte subtype generative activity over the whole period revealed that α tanycyte generation is more prominent than β subpopulations. Interestingly, α tanycytes are the main subtype maintaining neurogenic competence in the postnatal brain (4, 29) and adulthood (49, 50). Therefore, BrdU incorporation in this subpopulation up to P8 may indirectly be linked to their stem cell properties in postnatal brains. Finally, we propose here the existence of a developmental "outside-in" dorsoventral gradient of generation, by which cells situated in the top (*i.e.*, typical ependymal cells) and bottom of the ventricle (*i.e.*, β tanycytes) generate the first together, followed by cells in the central regions (*i.e.*, α tanycytes). Nothing to our knowledge was previously described in the literature regarding such an unusual dorsoventral gradient along the third ventricle. However, it may also rely on the limited area we analyzed (*i.e.*, the mediobasal hypothalamus) and the way we cut the brain tissue (*i.e.*, 2d coronal sections). Further studies are needed to reconstruct the genesis of the whole third ventricle and obtain a tridimensional picture of ependymal generation gradients.

To understand the temporal and spatial heterogeneity in the generation of the mediobasal 3V ependyma, we used a publicly available molecular atlas of the developing mouse hypothalamus, generated using diencephalic and hypothalamic explants across embryonic and postnatal time points (26). In this study, the authors identified the transcriptional divergence between tanycytes and typical ependymal cells at E13, with the differential expression of cell-type-specific markers such as *Rax* and *Foxj1*, respectively. Consistently, our BrdU analysis highlighted the peak of typical ependymal cell generation at E13. Using the same scRNAseq dataset, we also identified the appearance of tanycyte-like (*Rax*-positive) clusters starting at E14: however, a mature transcriptional profile is more clearly observed during the postnatal developmental time points P4-14, as reported by others (4). Indeed, between P4 and P14, tanycytes increase the expression of numerous markers described in adult cells, such as glucose (*i.e.*, *Slc2a1*, *Slc2a2*) and glutamatergic transporters (*i.e.*, *Slc1a2*, *Slc1a3*) (51–53) and growth factor receptors (*i.e.*, *Fgfr1*, *Igf1*) (54–59). These observations suggest that tanycytes are mature enough between P4 and P14 to respond to variations in energy availability. Using a different approach, Mirzadeh et al. (60) estimated the maturation of tanycytes later by examining the postnatal expression of Nestin, a marker for radial glia (61), and GFAP. Over the first ten days postnatally, the authors observed a decrease in nestin expression and an increase in GFAP expression (60), suggesting that tanycyte maturation continues up to P10. Consistently, morphological and histological studies in the rat and mice have demonstrated that tanycytes begin to fully mature during the first month of life (19, 48, 62). Further studies integrating additional time points during postnatal development would be helpful to expand our knowledge about tanycytes maturation.

The molecular atlas of the developing mouse hypothalamus generated by Kim et al. also allowed us to infer the transcriptional trajectory of ependymal cells during development. Within the tanycyte developmental pseudotime trajectory, we identified E16 as another critical time point for the differentiation of tanycytes. At this point, the expression of specific genes increases, particularly *Nfia*, *Nfib*, and *Nfix*, known as negative regulators of neurogenesis in tanycyte populations (4). Indeed, a study showed recently that tanycyte-specific disruption of the NFI family of transcription factors robustly stimulates tanycyte dedifferentiation, proliferation, and neurogenesis (29). Interestingly, regarding our BrdU analysis, this increased expression of negative regulators of neurogenesis at E16 is concomitant with the end of the neuronal birth and the burst of α tanycytes generation in the mediobasal hypothalamus. Other transcription factors (*i.e.*, *Hes1, Notch2, Egr1, Id4*) and genes (*i.e.*, *Apoe, Cd63, Cnih2, Arxes2*) have also been identified during tanycyte differentiation (starting E16) and maturation (starting P4), and constitute excellent candidates for controlling the specification of these peculiar hypothalamic cell types. Interestingly, the helix-loop-helix gene *Hes1*, together with *Notch1*, responds to *Rax* to promote Muller glia cell differentiation (63). Further exploration of these candidates is needed to understand their role in tanycyte development better.

In conclusion, the ontogeny of ependymoglial cells diverges according to cell type, time, and neuroanatomical distribution. Our original cellular and molecular approach allowed us to demonstrate that tanycytes originate around E13, start to differentiate as early as E16, and reach full maturation during early postnatal development (P4-14). Globally, our data allowed us to generate a comprehensive spatiotemporal atlas of tanycyte birth and development and identify molecular candidates involved in the development of tanycytes.

Data availability statement

The datasets presented in this study can be found in online repositories. The names of the repository/repositories and accession number(s) can be found in the article/Supplementary Material.

Ethics statement

The animal study was reviewed and approved by Veterinary Office of Canton de Vaud & University of Lausanne.

Author contributions

DL-R contributed to data analysis, performed the bioinformatic analysis and wrote the manuscript. AR, ML and MG performed the experiments and participated in data analysis. SC and FL contributed to conception and design of the study, performed experiments, participated in data analysis and wrote the manuscript. All authors contributed to the article and approved the submitted version.

Funding

SC was supported by the Swiss National Science Foundation (PZ00P3_167934/1), the Professor Dr Max Cloëtta Foundation, and the Novartis Foundation for Medical-Biological Research (19B145). FL was supported by the Swiss National Science Foundation (PZ00P3_174120, PCEFP3_194551), the European Research Council Starting Grant (TANGO, No. 948196), Novartis Foundation for medical-biological research, the Department of Biomedical Sciences and the Faculty of Biology and Medicine at University of Lausanne. DL-R was supported by the Wallonie-Bruxelles Federation and the Leon Fredericq Foundation.

Conflict of interest

The authors declare that the research was conducted in the absence of any commercial or financial relationships that could be construed as a potential conflict of interest.

Publisher's note

All claims expressed in this article are solely those of the authors and do not necessarily represent those of their affiliated organizations, or those of the publisher, the editors and the reviewers. Any product that may be evaluated in this article, or claim that may be made by its manufacturer, is not guaranteed or endorsed by the publisher.

Supplementary material

The Supplementary Material for this article can be found online at: https://www.frontiersin.org/articles/10.3389/fendo.2022.1073759/full#supplementary-material

References

1. García-Cáceres C, Balland E, Prevot V, Luquet S, Woods SC, Koch M, et al. Role of astrocytes, microglia, and tanycytes in brain control of systemic metabolism. *Nat Neurosci* (2019) 22(1):7–14. doi: 10.1038/s41593-018-0286-y

2. George JT, Seminara SB. Kisspeptin and the hypothalamic control of reproduction: Lessons from the human. *Endocrinology* (2012) 153(11):5130–6. doi: 10.1210/en.2012-1429

3. Lechan RM, Toni R. "Functional anatomy of the hypothalamus and pituitary.," In: Feingold KR, Anawalt B, Boyce A, Chrousos G, de Herder WW, Dhatariya K, Dungan K, Hershman JM, Hofland J, Kalra S, et al., editors. *Endotext*. South Dartmouth (MA): MDText.com, Inc. (2000). Available at: http://www.ncbi.nlm.nih.gov/books/NBK279126/.

4. Yoo S, Blackshaw S. Regulation and function of neurogenesis in the adult mammalian hypothalamus. *Prog Neurobiol* (2018) 170:53–66. doi: 10.1016/j.pneurobio.2018.04.001

5. Kriegstein A, Alvarez-Buylla A. The glial nature of embryonic and adult neural stem cells. *Annu Rev Neurosci* (2009) 32:149–84. doi: 10.1146/annurev.neuro.051508.135600

6. Noctor SC, Flint AC, Weissman TA, Wong WS, Clinton BK, Kriegstein AR. Dividing precursor cells of the embryonic cortical ventricular zone have morphological and molecular characteristics of radial glia. *J Neurosci* (2002) 22 (8):3161–73. doi: 10.1523/JNEUROSCI.22-08-03161.2002

7. Brischoux F, Fellmann D, Risold PY. Ontogenetic development of the diencephalic MCH neurons: A hypothalamic "MCH area" hypothesis. *Eur J Neurosci* (2001) 13(9):1733–44. doi: 10.1046/j.0953-816x.2001.01552.x

8. Croizier S, Franchi-Bernard G, Colard C, Poncet F, La Roche A, Risold P-Y. A comparative analysis shows morphofunctional differences between the rat and mouse melanin-concentrating hormone systems. *PLoS One* (2010) 5(11):e15471. doi: 10.1371/journal.pone.0015471

9. Díaz C, Morales-Delgado N, Puelles L. Ontogenesis of peptidergic neurons within the genoarchitectonic map of the mouse hypothalamus. *Front Neuroanat* (2014) 8:162. doi: 10.3389/fnana.2014.00162

10. McClellan KM, Parker KL, Tobet S. Development of the ventromedial nucleus of the hypothalamus. *Front Neuroendocrinol* (2006) 27(2):193–209. doi: 10.1016/j.yfrne.2006.02.002

11. Redmond SA, Figueres-Oñate M, Obernier K, Nascimento MA, Parraguez JI, López-Mascaraque L, et al. Development of ependymal and postnatal neural stem cells and their origin from a common embryonic progenitor. *Cell Rep* (2019) 27(2):429–41.e3. doi: 10.1016/j.celrep.2019.01.088

12. Jiménez AJ, Domínguez-Pinos M-D, Guerra MM, Fernández-Llebrez P, Pérez-Fígares J-M. Structure and function of the ependymal barrier and diseases associated with ependyma disruption. *Tissue Barriers* (2014) 2:e28426–6. doi: 10.4161/tisb.28426

13. Rodríguez EM, Blázquez JL, Pastor FE, Peláez B, Peña P, Peruzzo B, et al. Hypothalamic tanycytes: a key component of brain-endocrine interaction. *Int Rev Cytology* (2005) 247:89–164. doi: 10.1016/S0074-7696(05)47003-5

14. Rodríguez E, Guerra M, Peruzzo B, Blázquez JL. Tanycytes: A rich morphological history to underpin future molecular and physiological investigations. *J Neuroendocrinol* (2019) 31(3):e12690. doi: 10.1111/jne.12690

15. Langlet F, Mullier A, Bouret SG, Prevot V, Dehouck B. Tanycyte-like cells form a blood-cerebrospinal fluid barrier in the circumventricular organs of the mouse brain. *J Comp Neurol* (2013) 521(15):3389–405. doi: 10.1002/cne.23355

16. Bolborea M, Langlet F. What is the physiological role of hypothalamic tanycytes in metabolism? *Am J Physiol Regulatory Integr Comp Physiol* (2021) 320 (6):R994–R1003. doi: 10.1152/ajpregu.00296.2020

17. Clasadonte J, Prevot V. The special relationship: glia-neuron interactions in the neuroendocrine hypothalamus. *Nat Rev Endocrinol* (2018) 14(1):25–44. doi: 10.1038/nrendo.2017.124

18. Langlet F. Tanycyte gene expression dynamics in the regulation of energy homeostasis. *Front Endocrinol* (2019) 10:286. doi: 10.3389/fendo.2019.00286

19. Altman J, Bayer SA. Development of the diencephalon in the rat. III. ontogeny of the specialized ventricular linings of the hypothalamic third ventricle. *J Comp Neurol* (1978) 182(4 Pt 2):995–1015. doi: 10.1002/cne.901820513

20. Markakis EA, Swanson LW. Spatiotemporal patterns of secretomotor neuron generation in the parvicellular neuroendocrine system. *Brain Res Brain Res Rev* (1997) 24(2–3):255–91. doi: 10.1016/s0165-0173(97)00006-4

21. Das GD. Gliogenesis and ependymogenesis during embryonic development of the rat: An autoradiographic study. *J Neurological Sci* (1979) 43(2):193–204. doi: 10.1016/0022-510X(79)90115-1

22. Korr H. Proliferation of different cell types in the brain. *Advances in anatomy. Embryology Cell Biol* (1980) 61:1–72. doi: 10.1007/978-3-642-67577-5

23. Scott DE, Pepe GJ. The fetal baboon median eminence as a circumventricular organ: I. transmission electron microscopy. *Brain Res Bull* (1987) 19(1):87–94. doi: 10.1016/0361-9230(87)90170-5

24. Ishii Y, Bouret SG. Embryonic birthdate of hypothalamic leptin-activated neurons in mice. *Endocrinology* (2012) 153(8):3657–67. doi: 10.1210/en.2012-1328

25. Chauvet N, Prieto M, Alonso G. Tanycytes present in the adult rat mediobasal hypothalamus support the regeneration of monoaminergic axons. *Exp Neurol* (1998) 151(1):1–13. doi: 10.1006/exnr.1998.6784

26. Kim DW, Washington PW, Wang ZQ, Lin SH, Sun C, Ismail BT, et al. The cellular and molecular landscape of hypothalamic patterning and differentiation from embryonic to late postnatal development. *Nat Commun* (2020) 11(1):4360. doi: 10.1038/s41467-020-18231-z

27. Pasquettaz R, Kolotuev I, Rohrbach A, Gouelle C, Pellerin L, Langlet F. Peculiar protrusions along tanycyte processes face diverse neural and nonneural cell types in the hypothalamic parenchyma. *J Comp Neurol* (2021) 529(3):553–75. doi: 10.1002/cne.24965

28. Rohrbach A, Caron E, Dali R, Brunner M, Pasquettaz R, Kolotuev I, et al. Ablation of glucokinase-expressing tanycytes impacts energy balance and increases adiposity in mice. *Mol Metab* (2021) 53:101311. doi: 10.1016/j.molmet.2021.101311

29. Yoo S, Kim J, Lyu P, Hoang T, Ma A, Trinh V, et al. Control of neurogenic competence in mammalian hypothalamic tanycytes. *Sci Adv* (2021) 7(22): eabg3777. doi: 10.1126/sciadv.abg3777

30. Choudhary S, Satija R. Comparison and evaluation of statistical error models for scRNA-seq. *Genome Biol* (2022) 23(1):27. doi: 10.1186/s13059-021-02584-9

31. Korsunsky I, Millard N, Fan J, Slowikowski K, Zhang F, Wei K, et al. Fast, sensitive and accurate integration of single-cell data with harmony. *Nat Methods* (2019) 16(12):1289–96. doi: 10.1038/s41592-019-0619-0

32. Malumbres M, Barbacid M. Mammalian cyclin-dependent kinases. *Trends Biochem Sci* (2005) 30(11):630–41. doi: 10.1016/j.tibs.2005.09.005

33. Clark BS, Stein-O'Brien GL, Shiau F, Cannon GH, Davis-Marcisak E, Sherman T, et al. Single-cell RNA-seq analysis of retinal development identifies

NFI factors as regulating mitotic exit and late-born cell specification. *Neuron* (2019) 102(6):1111–26.e5. doi: 10.1016/j.neuron.2019.04.010

34. Glasgow SM, Zhu W, Stolt CC, Huang T-W, Chen F, LoTurco JJ, et al. Mutual antagonism between Sox10 and NFIA regulates diversification of glial lineages and glioma subtypes. *Nat Neurosci* (2014) 17(10):1322–9. doi: 10.1038/nn.3790

35. Matuzelski E, Bunt J, Harkins D, Lim JWC, Gronostajski RM, Richards LJ, et al. Transcriptional regulation of nfix by NFIB drives astrocytic maturation within the developing spinal cord. *Dev Biol* (2017) 432(2):286–97. doi: 10.1016/j.ydbio.2017.10.019

36. Kang P, Lee HK, Glasgow SM, Finley M, Donti T, Gaber ZB, et al. Sox9 and NFIA coordinate a transcriptional regulatory cascade during the initiation of gliogenesis. *Neuron* (2012) 74(1):79–94. doi: 10.1016/j.neuron.2012.01.024

37. Malatesta P, Hartfuss E, Götz M. Isolation of radial glial cells by fluorescent-activated cell sorting reveals a neuronal lineage. *Dev (Cambridge England)* (2000) 127(24):5253–63. doi: 10.1242/dev.127.24.5253

38. Malatesta P, Hack MA, Hartfuss E, Kettenmann H, Klinkert W, Kirchhoff F, et al. Neuronal or glial progeny: regional differences in radial glia fate. *Neuron* (2003) 37(5):751–64. doi: 10.1016/s0896-6273(03)00116-8

39. Alvarez-Buylla A, García-Verdugo JM, Tramontin AD. A unified hypothesis on the lineage of neural stem cells. *Nat Rev Neurosci* (2001) 2, Issue 4:287–93. doi: 10.1038/35067582

40. Levitt P, Cooper ML, Rakic P. Early divergence and changing proportions of neuronal and glial precursor cells in the primate cerebral ventricular zone. *Dev Biol* (1983) 96(2):472–84. doi: 10.1016/0012-1606(83)90184-7

41. Merkle D, Manuel G-VJ, Arturo A-B. Radial glia give rise to adult neural stem cells in the subventricular zone. *Proc Natl Acad Sci* (2004) 101(50):17528–32. doi: 10.1073/pnas.0407893101

42. Tramontin AD, García-Verdugo JM, Lim DA, Alvarez-Buylla A. Postnatal development of radial glia and the ventricular zone (VZ): a continuum of the neural stem cell compartment. *Cereb Cortex (New York N.Y: 1991)* (2003) 13(6):580–7. doi: 10.1093/cercor/13.6.580

43. Goodman T, Hajihosseini MK. Hypothalamic tanycytes–masters and servants of metabolic, neuroendocrine, and neurogenic functions. *Front Neurosci* (2015) 9:387. doi: 10.3389/fnins.2015.00387

44. Byerly MS, Blackshaw S. Vertebrate retina and hypothalamus development. *Wiley Interdiscip Rev Syst Biol Med* (2009) 1(3):380–9. doi: 10.1002/wsbm.22

45. Shimada M, Nakamura T. Time of neuron origin in mouse hypothalamic nuclei. *Exp Neurol* (1973) 41(1):163–73. doi: 10.1016/0014-4886(73)90187-8

46. Zhou X, Zhong S, Peng H, Liu J, Ding W, Sun L, et al. Cellular and molecular properties of neural progenitors in the developing mammalian hypothalamus. *Nat Commun* (2020) 11(1):4063. doi: 10.1038/s41467-020-17890-2

47. Bedont JL, Newman EA, Blackshaw S. Patterning, specification, and differentiation in the developing hypothalamus. *Wiley Interdiscip Rev Dev Biol* (2015) 4(5):445–68. doi: 10.1002/wdev.187

48. Walsh RJ, Brawer JR, Lin PL. Early postnatal development of ependyma in the third ventricle of male and female rats. *Am J Anat* (1978) 151(3):377–407. doi: 10.1002/aja.1001510305

49. Robins SC, Stewart I, McNay DE, Taylor V, Giachino C, Goetz M, et al. α-tanycytes of the adult hypothalamic third ventricle include distinct populations of FGF-responsive neural progenitors. *Nat Commun* (2013) 4:2049. doi: 10.1038/ncomms3049

50. Chaker Z, George C, Petrovska M, Caron JB, Lacube P, Caillé I, et al. Hypothalamic neurogenesis persists in the aging brain and is controlled by energy-sensing IGF-I pathway. *Neurobiol Aging* (2016) 41:64–72. doi: 10.1016/j.neurobiolaging.2016.02.008

51. Berger UV, Hediger MA. Differential distribution of the glutamate transporters GLT-1 and GLAST in tanycytes of the third ventricle. *J Comp Neurol* (2001) 433(1):101–14. doi: 10.1002/cne.1128

52. García MA, Millán C, Balmaceda-Aguilera C, Castro T, Pastor P, Montecinos H, et al. Hypothalamic ependymal-glial cells express the glucose transporter GLUT2, a protein involved in glucose sensing. *J Neurochem* (2003) 86(3):709–24. doi: 10.1046/j.1471-4159.2003.01892.x

53. Peruzzo B, Pastor FE, Blázquez JL, Amat P, Rodríguez EM. Polarized endocytosis and transcytosis in the hypothalamic tanycytes of the rat. *Cell Tissue Res* (2004) 317(2):147–64. doi: 10.1007/s00441-004-0899-1

54. Cardona-Gómez GP, DonCarlos L, Garcia-Segura LM. Insulin-like growth factor I receptors and estrogen receptors colocalize in female rat brain. *Neuroscience* (2000) 99(4):751–60. doi: 10.1016/s0306-4522(00)00228-1

55. De Seranno S, d'Anglemont de Tassigny X, Estrella C, Loyens A, Kasparov S, Leroy D, et al. Role of estradiol in the dynamic control of tanycyte plasticity mediated by vascular endothelial cells in the median eminence. *Endocrinology* (2010) 151(4):1760–72. doi: 10.1210/en.2009-0870

56. Everitt BJ, Meister B, Hökfelt T, Melander T, Terenius L, Rökaeus A, et al. The hypothalamic arcuate nucleus-median eminence complex: Immunohistochemistry of transmitters, peptides and DARPP-32 with special reference to coexistence in dopamine neurons. *Brain Res* (1986) 396(2):97–155. doi: 10.1016/s0006-8993(86)80192-5

57. Fekete C, Mihály E, Herscovici S, Salas J, Tu H, Larsen PR, et al. DARPP-32 and CREB are present in type 2 iodothyronine deiodinase-producing tanycytes: implications for the regulation of type 2 deiodinase activity. *Brain Res* (2000) 862(1–2):154–61. doi: 10.1016/s0006-8993(00)02105-3

58. Lerant A, Freeman ME. Ovarian steroids differentially regulate the expression of PRL-r in neuroendocrine dopaminergic neuron populations: a double label confocal microscopic study. *Brain Res* (1998) 802(1–2):141–54. doi: 10.1016/s0006-8993(98)00583-6

59. Matsuo A, Tooyama I, Isobe S, Oomura Y, Akiguchi I, Hanai K, et al. Immunohistochemical localization in the rat brain of an epitope corresponding to the fibroblast growth factor receptor-1. *Neuroscience* (1994) 60(1):49–66. doi: 10.1016/0306-4522(94)90203-8

60. Mirzadeh Z, Kusne Y, Duran-Moreno M, Cabrales E, Gil-Perotin S, Ortiz C, et al. Bi- and uniciliated ependymal cells define continuous floor-plate-derived tanycytic territories. *Nat Commun* (2017) 8(1):13759. doi: 10.1038/ncomms13759

61. Park D, Xiang AP, Zhang L, Mao FF, Walton NM, Choi SS, et al. The radial glia antibody RC2 recognizes a protein encoded by nestin. *Biochem Biophys Res Commun* (2009) 382(3):588–92. doi: 10.1016/j.bbrc.2009.03.074

62. Monroe BG, Paull WK. Ultrastructural changes in the hypothalamus during development and hypothalamic activity: the median eminence. In: Swaab DF, Schadé BR, editors. *Integrative hypothalamic activity*, (Amsterdam: The Netherlands) vol. 41 . Elsevier (1974). p. 185–208. J. P. B. T.-P. doi: 10.1016/S0079-6123(08)61907-X

63. Furukawa T, Mukherjee S, Bao Z-Z, Morrow EM, Cepko CL. Rax, Hes1, and notch1 promote the formation of müller glia by postnatal retinal progenitor cells. *Neuron* (2000) 26(2):383–94. doi: 10.1016/S0896-6273(00)81171-X

frontiers | Frontiers in Endocrinology

TYPE Original Research
PUBLISHED 31 January 2023
DOI 10.3389/fendo.2023.1062211

OPEN ACCESS

EDITED BY
Alexandre Benani,
Centre National de la Recherche Scientifique (CNRS), France

REVIEWED BY
Vito Salvador Hernandez,
National Autonomous University of Mexico, Mexico
Yu-Feng Wang,
Harbin Medical University, China
Soledad Bárez-López,
Spanish National Research Council, CSIC, Spain
Aicha Dekar,
University of Sciences and Technology Houari Boumediene, Algeria

*CORRESPONDENCE
André S. Mecawi
mecawi@unifesp.br

†These authors have contributed equally to this work and share first authorship

SPECIALTY SECTION
This article was submitted to Neuroendocrine Science, a section of the journal Frontiers in Endocrinology

RECEIVED 05 October 2022
ACCEPTED 19 January 2023
PUBLISHED 31 January 2023

CITATION
Felintro V, Trujillo V, dos-Santos RC, da Silva-Almeida C, Reis LC, Rocha FF and Mecawi AS (2023) Water deprivation induces hypoactivity in rats independently of oxytocin receptor signaling at the central amygdala.
Front. Endocrinol. 14:1062211.
doi: 10.3389/fendo.2023.1062211

Water deprivation induces hypoactivity in rats independently of oxytocin receptor signaling at the central amygdala

Viviane Felintro[1†], Verónica Trujillo[2,3†], Raoni C. dos-Santos[1], Claudio da Silva-Almeida[1], Luís C. Reis[1], Fábio F. Rocha[1] and André S. Mecawi[3*]

[1]Department of Physiological Sciences, Instituto de Ciências Biológicas e da Saúde, Universidade Federal Rural do Rio de Janeiro, Seropédica, Brazil, [2]Department of Physiology, Facultad de Ciencias Exactas, Físicas y Naturales, Universidad Nacional de Córdoba, Córdoba, Argentina, [3]Department of Biophysics, Escola Paulista de Medicina, Universidade Federal de São Paulo, São Paulo, Brazil

Introduction: Vasopressin (AVP) and oxytocin (OXT) are neuropeptides produced by magnocellular neurons (MCNs) of the hypothalamus and secreted through neurohypophysis to defend mammals against dehydration. It was recently demonstrated that MCNs also project to limbic structures, modulating several behavioral responses.

Methods and Results: We found that 24 h of water deprivation (WD) or salt loading (SL) did not change exploration or anxiety-like behaviors in the elevated plus maze (EPM) test. However, rats deprived of water for 48 h showed reduced exploration of open field and the closed arms of EPM, indicating hypoactivity during night time. We evaluated mRNA expression of glutamate decarboxylase 1 (Gad1), vesicular glutamate transporter 2 (Slc17a6), AVP (Avpr1a) and OXT (Oxtr) receptors in the lateral habenula (LHb), basolateral (BLA) and central (CeA) amygdala after 48 h of WD or SL. WD, but not SL, increased Oxtr mRNA expression in the CeA. Bilateral pharmacological inhibition of OXTR function in the CeA with the OXTR antagonist L-371,257 was performed to evaluate its possible role in regulating the EPM exploration or water intake induced by WD. The blockade of OXTR in the CeA did not reverse the hypoactivity response in the EPM, nor did it change water intake induced in 48-h water-deprived rats.

Discussion: We found that WD modulates exploratory activity in rats, but this response is not mediated by oxytocin receptor signaling to the CeA, despite the upregulated Oxtr mRNA expression in that structure after WD for 48 h.

KEYWORDS

central amygdala, oxytocin receptor, dehydration, exploratory behavior, elevated plus maze test

1 Introduction

Water and sodium balance in vertebrates involves several neuroendocrine systems that are finely orchestrated to maintain the extracellular fluid (ECF) osmolality and volume within a narrow range of variation. One of the essential responses to this regulation is the development of thirst, which motivates animals to seek and drink water (1). The

hypothalamic-neurohypophysial system (HNS) is key to the plasma osmolality control. It is composed of osmosensory magnocellular neurons (MCNs) located at the paraventricular (PVN) and supraoptic (SON) hypothalamic nuclei, and is responsible for producing and secreting the neuropeptides arginine vasopressin (AVP) and oxytocin (OXT) to the blood through neurohypophysis to control kidney function (1). Recent neuroanatomical studies have consistently demonstrated that AVP and OXT MCNs from both PVN and SON send their main axonal projection to the neurohypophysis and also send dense collateral axons to extra-neurohypophyseal brain regions that control anxiety-like behavior, including, among others, the amygdala and lateral habenula (2–5).

Challenges to nutritional homeostasis, such as water deprivation (WD), motivate behaviors related to thirst sensation. Moreover, recent studies of rodents have demonstrated the relationship between body water and sodium balance on the one hand and exploratory behaviors, anxiety and fear response on the other (6–9). Those findings strongly suggest that mechanisms controlling body fluid homeostasis may modulate neuronal circuitries, including the limbic system, related to anxiety and other behavioral responses during dehydration (6). In addition, it has been demonstrated that AVP and OXT MCNs send collateral projections to the basolateral and central amygdala (BLA and CeA, respectively) (4, 5). Furthermore, MCNs AVPergic projections to the lateral habenula (LHb) have also been observed (6). BLA, CeA and LHb have distinct populations of glutamatergic and GABAergic neurons. The balance of their activity is crucial to the final modulation response of those limbic structures at the behavioral level (10, 11). Furthermore, the activation of AVP and OXT receptors produces different physiological responses, with *Avpr1a* inducing an anxiogenic response and *Oxtr* inducing an anxiolytic one (5, 12–14). Hence, it is possible that the imbalance between AVP and OXT contributes to the underlying mechanism of motivated exploratory behaviors in dehydration conditions.

Hyperosmolality is the main stimulus that activates the hypothalamic MCNs, and it can be experimentally induced by WD, inducing both extra- and intracellular dehydration associated with peripheral renin-angiotensin system (RAS) activation, or by salt loading (SL), which induces intra- but not extracellular dehydration, associated with peripheral RAS inhibition (1, 15). Since the RAS has also been found to play an important role in controlling anxiety levels (16), it is possible that the behavioral responses are differentially expressed in WD and SL animals. Therefore, recruitment of RAS, AVPergic and OXTergic systems is an efficient homeostasis regulatory mechanism for coupling hydromineral balance and anxiety-like behaviors.

This study aimed to investigate whether dehydration modulates the exploratory or anxiety-like behaviors at night, the regular activity period of rats. Therefore, we investigated the behavioral responses of rats submitted WD or SL when exposed to the elevated plus maze (EPM) or the open field (OF). We also analyzed *Avpr1a*, *Oxtr*, glutamate decarboxylase 1 (*Gad1*), and vesicular glutamate transporter 2 (*Slc17a6)* mRNA expression in the BLA, CeA and LHb in both hyperosmolality models to elucidate possible plastic molecular responses. Finally, bilateral pharmacological inhibition of OXTR signaling in the CeA was applied to evaluate its potential role in regulating nocturnal exploratory behaviors in rats submitted to WD.

2 Materials and methods

2.1 Animals

Male Wistar rats (~290g) were obtained from the Animal Facility of the Department of Physiological Sciences, Institute of Biological and Health Sciences, Federal Rural University of Rio de Janeiro (UFRRJ), or from the Center for the Development of Experimental Models for Biology and Medicine (CEDEME) Federal University of São Paulo (UNIFESP). The rats were housed under controlled conditions of temperature (22 ± 2 °C) and 12/12 hours light-dark cycle (lights on at 6 a.m.). All procedures performed were in accordance with current Brazilian legislation and the "Guide for the Care and Use of Laboratory Animals" (17) and were evaluated and approved by the ethical committees for animal use of Federal Rural University of Rio de Janeiro (CEUA-ICBS, protocol number 001/2017) and Federal University of São Paulo (CEUA-UNIFESP, protocol number 7236281119, ID 009443, 2019).

2.2 Experimental protocols

Figure 1 illustrates the experimental procedures performed in this work. A first set of rats was randomly separated into the following groups: control (CT) which had free access to filtered water and standard chow (1% w/v NaCl, Rhoster, São Paulo, Brazil); WD group, in which water was removed for 24 or 48 hours with free access to standard chow; and SL group, in which the only fluid available was 1.8% NaCl solution for 24 or 48 hours, also with free access to standard chow. The exploratory and anxiety-like behaviors were evaluated *via* 5 minutes of exposure to the elevated plus maze (EPM) test. A different set of animals of control, 48h WD and 48 SL groups were tested for 10 min in the open field test. The behavioral tests were performed at night (7:00 to 11:00 p.m.) because the dark period is the normal activity period of rats (18) and also because Martelli et al., 2012 (9) observed that changes in the locomotor behaviors occur during the dark but not during the light period in water deprived rats. Immediately after the EPM test, the animals were euthanized and blood was collected to determine the hematocrit and plasma osmolality.

A third set of rats was submitted to the control procedure, 48h WD or 48h SL and euthanized at night (7:00 to 11:00 p.m.) for gene expression evaluation by qPCR. The brains were rapidly removed from the skull, frozen with dry ice, and stored at −80°C.

Additionally, to investigate the contribution of OXTR signaling to the WD induced hypoactivity, a fourth set of rats was used to test whether the microinjection of OXTR antagonist in the CeA would be able to alter the dehydration-induced hypoactivity observed in the 48-h WD rats when tested in the EPM. So, 7 days after CeA cannulation, the rats were submitted to a control procedure or 48 h of WD and on day 9 received the OXTR antagonist or vehicle microinjection 30 min before EPM testing. At the end of the test, the rats were returned to their home cages and were allowed to drink water freely. The water consumption, measured in grams, was recorded at 30 and 120 minutes.

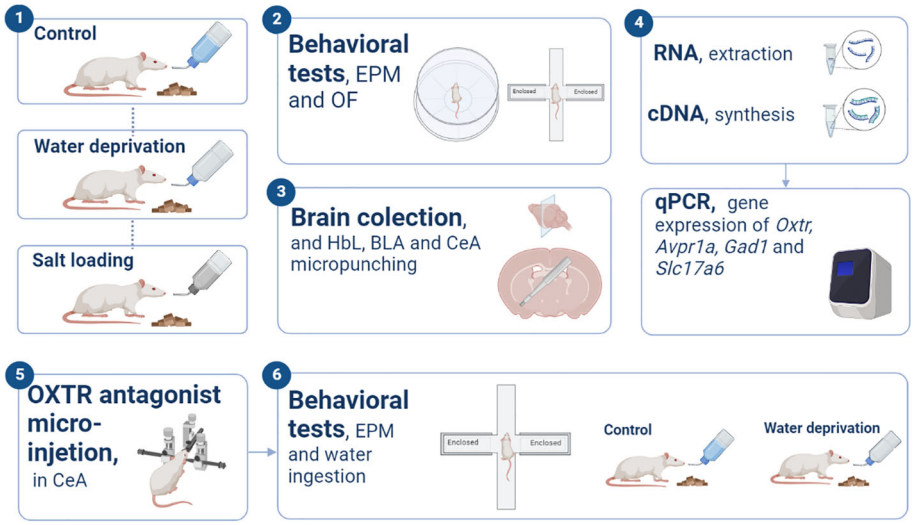

FIGURE 1
Experimental procedures. Schematic illustration representing the experimental designs and basic procedures employed in the present study. "EPM", elevated plus maze; "OF", open field; "LHb", Lateral habenula; "BLA", basolateral amygdala; "CeA", Central amygdala; "OXTR", oxytocin receptor.

2.3 Elevated plus maze test

The EPM was employed to analyze the exploratory and anxiety-like behavior in rats (19). This apparatus consists of two opposed open arms (50 × 10 cm each), and two opposed closed arms of the same size with 40 cm high sidewalls, connected by a central area (10 × 10 cm) and raised 50 cm from the ground. Rats were placed into the center area of the apparatus facing a closed arm. Each animal was tested in the EPM for 5 minutes and the apparatus was cleaned between one rat and another with a 10% ethanol solution. The EPM is used to evaluate anxiety-like behavior in rodents. The number of arm entries reflects the locomotion of the animal and the open arm exploration reflects the anxiety-like behaviors. Thus, increased exploration of open arms is associated with decreases in anxiety levels. In addition, the ethological parameter head dipping was evaluated to support the assessment of emotional reactivity. The entries in closed arms and rearing indicate horizontal and vertical exploratory activity, respectively. The time in the center area and the episodes of stretch-attend posture are associated with decision making (19, 20).

2.4 Open field test

The open field test was carried out as previously described (21) to confirm that 48 h of WD induced changes in exploratory activity. Each rat was placed individually in the periphery area at the beginning of the test and allowed to explore it freely for 10 min. The arena was cleaned between one rat and another with a 10% ethanol solution. Total, peripheric and central distance travelled and percentage of time spent in the central area were subsequently analyzed using the video-tracking software EthoVision 8.5 (Noldus Information Technology, Leesburg, VA, USA).

2.5 Hydromineral parameters

Trunk blood was collected in heparinized tubes and centrifuged (20 min, 3000 rpm at 4 °C), after which plasma osmolality was measured in 10 µl aliquots by using a benchtop osmometer (model 5005, Precision Systems, Natick, MA, USA), based on the freezing-point method. For hematocrit determination, the blood was placed into heparinized capillaries and centrifuged at 2000 rpm for five minutes. Next, a microhematocrit scale was used to determine the percentage of blood composed of erythrocytes.

2.6 Microdissection, RNA extraction and cDNA synthesis

Immediately after the EPM test, rats were decapitated and their brains were frozen on dry ice and stored at −80°C. The brains were cut into 60 µm coronal sections using a cryostat (Leica Biosystems, CM 1860, Wetzlar, Germany), and the brain nuclei were identified and delimited according to the rat brain atlas (22). A 1 mm diameter micropunch needle (Fine Science Tools) was used to bilaterally collect LHb (coordinates from Bregma −2.30 to −4.70 mm), BLA (coordinated from Bregma −1.80 to −3.80 mm) and CeA (coordinated from Bregma -1.80 to -3.30 mm). The micropunch material was immediately placed in microtubes containing TRIzol® reagent (Life Technologies, Waltham, MA, USA) and stored at −80°C. Sections were mounted on glass slides and stained with 0.1% toluidine blue to confirm the location of the punches using a light microscope. Micropunches from incorrect dissection were not used. Total RNA was extracted from punch samples using TRIzol® reagent as recommended by the manufacturer, and was quantified in a nanospectrophotometer (DS-11® Denovix Inc. Wilmington, DE,

USA). Samples presenting a ratio of optical density (OD) 260/280 in the 1.8-2.1 range were used for reverse transcription. The synthesis of cDNA was performed using the QuantiTect Reverse Transcription Kit (Qiagen) with 500 ng of total RNA. The cDNA obtained was diluted in a proportion of 1:3 and stored at −20°C.

2.7 Quantitative real-time polymerase chain reaction

The qPCR was performed in duplicate or triplicate using SYBR green (Applied Biosystems) or Taqman Universal PCR Master Mix kit (Carlsbad, CA, USA). The qPCR was performed with the QuantStudio 3® system (ThermoFisher Scientific). With the SYBR green, the following primers (Applied Biosystems) were used: *Avpr1a* (5′-ATCTGCTACCACATCTGGCG-3′ and 5′-TTATGAAA GGGACCCACGGC-3′), *Oxtr* (5′-CTTCATCCAACCCTGGGGAC-3′ and 5′-CTTGAAGCTGATGAGGCCG–3′), and *Rpl19* (5′-GCGTCTGCAGCCATGAGTA-3′ and 5′-TGGCATTGGCG ATTTCGTTG-3′) as the endogenous control gene. With the Taqman Gene Expression Assays (Applied Biosystems), the following probes were used: *Gad1* (Rn00690300_m1), *Slc17a6* (Rn00584780_m1), and *Actb* (Rn00667869_m1) as endogenous control. The reactions were performed using an ABI 7500 Sequence Detection System (ABI, Warrington, UK), with universal cycling conditions carried out according to the manufacturer's instructions. The genes RPL19 and β-Actin give highly reproducible and stable expression measurements between different physiological challenges within the CeA, BLA and LHb. For relative quantification of gene expression, the $2^{-\Delta\Delta CT}$ method was employed (23).

2.8 The OXTR antagonist microinjection in the CeA

Rats were anesthetized with ketamine (100 mg/Kg; i.p.) and xylazine (10 mg/Kg; i.p.). After the onset of anesthesia, animals received ketoprofen (3 mg/kg; s.c.) as analgesic, pentobiotic (30000 I.U./Kg; i.m.) as antibiotic, polyacrylic acid as eye lubricant and lidocaine 0.5% as local anesthetic in ears and at the incision site. A 23 G and 14 mm length cannula was implanted bilaterally using the following stereotaxic coordinates relative to the bregma: posterior −2.2 mm, lateral ± 4.3 mm and ventral −7.6 mm. A stylet was inserted into the guide cannula for obturation. The cannula guide and the stylet were fixed with dental cement. Twenty-four hours after surgery, the ketoprofen injection was repeated. Rats were allowed to recover for one week after the surgical procedure. Two hours before the EPM test, rats were individually placed in standard polyethylene cages and the stylet was removed from the guide cannula. Thirty minutes before the EPM test, a 32 G needle connected to a polyethylene tube (PE 10), which in turn was connected to a 1 µL syringe (Hamilton) was inserted and extended 0.2 mm from the end of the cannula guide. Then, 0.4 µl of the OXTR antagonist L-371,257 (Santa Cruz Biotechnology, Inc., Dallas, TX, 1; sc-204038; 4 µM in 0.9% saline-10% DMSO) or vehicle (0.9% saline-10% DMSO) was manually infused during 1 min. The needle was left for 1 additional minute to allow the complete diffusion of the drug and then it was removed. The antagonist dose was chosen based on the literature (4, 24).

In order to verify the right infusion site at the CeA (Supplementary Figures 1 and 2), at the end of the experiment the rats were administrated identically as described above with 0.4 µl of 0.2% Evans blue, anesthetized with isoflurane and decapitated. Then the brains were removed and fixed by placing them into a solution of 4% paraformaldehyde in 0.1 M phosphate buffer for two days. Fixed brains were sliced into 60 µm coronal sections with a cryostat (Leica Microsystems CM1850 Cryostat; Wetzlar, Germany) and light microscopy was used to confirm the infusion site according to the Paxinos atlas (22). Data from rats with one or two misplaced cannulas were not included in the analyses.

2.9 Statistical analysis

All values are presented as means ± SD. Data from hematocrit, plasma osmolarity, EPM, OF and qPCR with normal distribution (depending on the Shapiro–Wilk test) were subjected to 1-way analysis of variance (ANOVA; the value of the F-statistic is reported) with 3 levels: control, WD and SL. Significant differences between groups were further analyzed through the Tukey *post hoc* test. When these variables were not normally distributed, data were subjected to the Kruskal-Wallis test (the value of the H-statistic is reported) with three levels: control, WD and SL. Significant differences between groups were further analyzed through Dunn's multiple comparisons test. Data from OXTR antagonist were submitted to 2-way ANOVA with the hydration status factor having two levels (control and WD) and the drug administration factor also with two levels (vehicle or OXTR antagonist). The values of stretch-attend posture and rearing in EPM did not have normal distribution and were rank transformed before statistical analysis according to Hora and Conover, 1984 (25). All statistical analyses were conducted with the GraphPad Prism software (version 8, San Diego, USA). In all cases, p-values smaller than 0.05 were considered to indicate a significant effect.

3 Results

3.1 Effects of dehydration on the plasma osmolality and hematocrit

In order to validate our dehydration models (WD and SL), we evaluated the plasma osmolality and the hematocrit (Figure 2 and Supplementary Table 1). As expected, osmolality was significantly affected by dehydration protocols after 24 [H=6.051; df=2; p=0.0485; Figure 2B] and 48 hours [H=10.94; df=2; p=0.0042; Figure 2D]. The hematocrit was affected by 48 h of WD [$F_{(2,25)}$=12.86; p=0.0001] since rats submitted to 48 h of WD showed higher hematocrit values than the control and the SL groups (p=0.0003 and p=0.0019; respectively; Figure 2C). These results demonstrated that after 48 h, both WD and SL increased the plasma osmolality, thus validating our dehydration models.

10.3389/fendo.2023.1062211

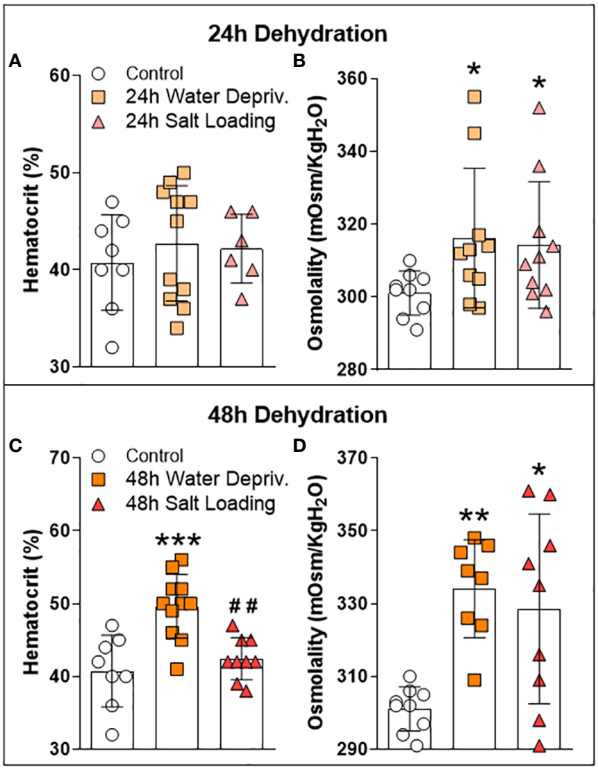

FIGURE 2
Effects of **(A, B)** 24 h or **(C, D)** 48 h of dehydration in male adult rats on **(A, C)** hematocrit and **(B, D)** plasma osmolality. Values are mean ± SD. The number of animals used per group was: Control = 9; 24 h WD = 11; 24 h SL = 10; 48 h WD = 11; 48 h SL = 9. Hematocrit data were submitted to one-way ANOVA followed by the Tukey post hoc test. Osmolality data were analyzed by the Kruskal-Wallis test followed by Dunn's post hoc test. *p<0.05, **p<0.01 and ***p<0.001 compared to control groups; ##p<0.01 compared to the WD group.

3.2 Effects of WD and SL on the anxiety-like and locomotory behaviors

We carried out the EPM test to assess whether dehydration triggered by WD and SL influences anxiety-like behavior and/or locomotion (Figure 3 and Supplementary Table 2). Figure 3A–F shows that 24 h of WD or SL did not alter rats' behavior in the EPM test. However, after 48 h of dehydration (Figure 3G), we found a significant effect on closed arm entries [$F_{(2,33)}$=6.192; p=0.0052], with WD rats entering less in the closed arms than the control (p=0.0085) and SL rats (p=0.0185). The other parameters assessed were not altered by 48 h of WD or SL (Figures 3G–L). These results suggest that 48 h of WD induces hypolocomotion in EPM without affecting anxiety-like behavior.

Additionally, the open field test (Figure 4 and Supplementary Table 3) showed a decrease in total (Figure 4A) and peripheral (Figure 4B) exploration of 48 h WD group [$F_{(2,12)}$=5.05; p=0.0256 and H=8.42; p=0.0068; d.f. = 12; respectively]. On the other hand, the distance traveled and time spent in the central area were not affected by WD or SL, confirming that 48 h reduced nocturnal exploratory behavior without significantly affecting the anxiety-like behaviors.

3.3 Effects of WD and SL on the gene expression in LHb, BLA, and CeA

Dehydration activates the MCNs, increasing AVP and OXT synthesis and secretion (1). In addition to their classical osmoregulation function, these neuropeptides have key roles in modulating anxiety-like and locomotory behaviors (6, 9). For this reason, we investigated the gene expression of AVP and OXT receptors in the CeA, BLA and LHb, limbic structures known to regulate anxiety-like and locomotory behaviors and to receive projections from MCNs (2, 5, 6). Additionally, we measured the mRNA expression of gene markers of GABAergic (Gad1) or glutamatergic (Slc17a6) neurons to infer whether the dehydration could modulate the level of excitation or inhibition of the neurons of the structures mentioned above (Figure 5 and Supplementary Table 4).

While dehydration did not change the expression of these genes in the LHb (Figures 5A–D) and BLA (Figures 5E–H), it altered *Oxtr* gene expression in CeA [$F_{(2,15)}$=5.994; p=0.0122]. Our data showed that rats submitted to 48 h of WD had higher *Oxtr* gene expression levels in CeA compared to controls (p=0.0103; Figure 5L). The gene expression values of *Slc17a6*, *Gad1* and *Avpr1a* in CeA were not altered by the dehydration model (Figures 5I–K). Thus, we investigated whether OXTR in CeA can modulate the locomotor response of rats.

3.4 Effect of OXTR antagonist microinjection in CeA

To further investigate whether OXTR signaling in the CeA mediates the behavioral alteration observed in WD rats, we injected the OXTR antagonist L-371,257 into the CeA of rats after 48 h of WD.

10.3389/fendo.2023.1062211

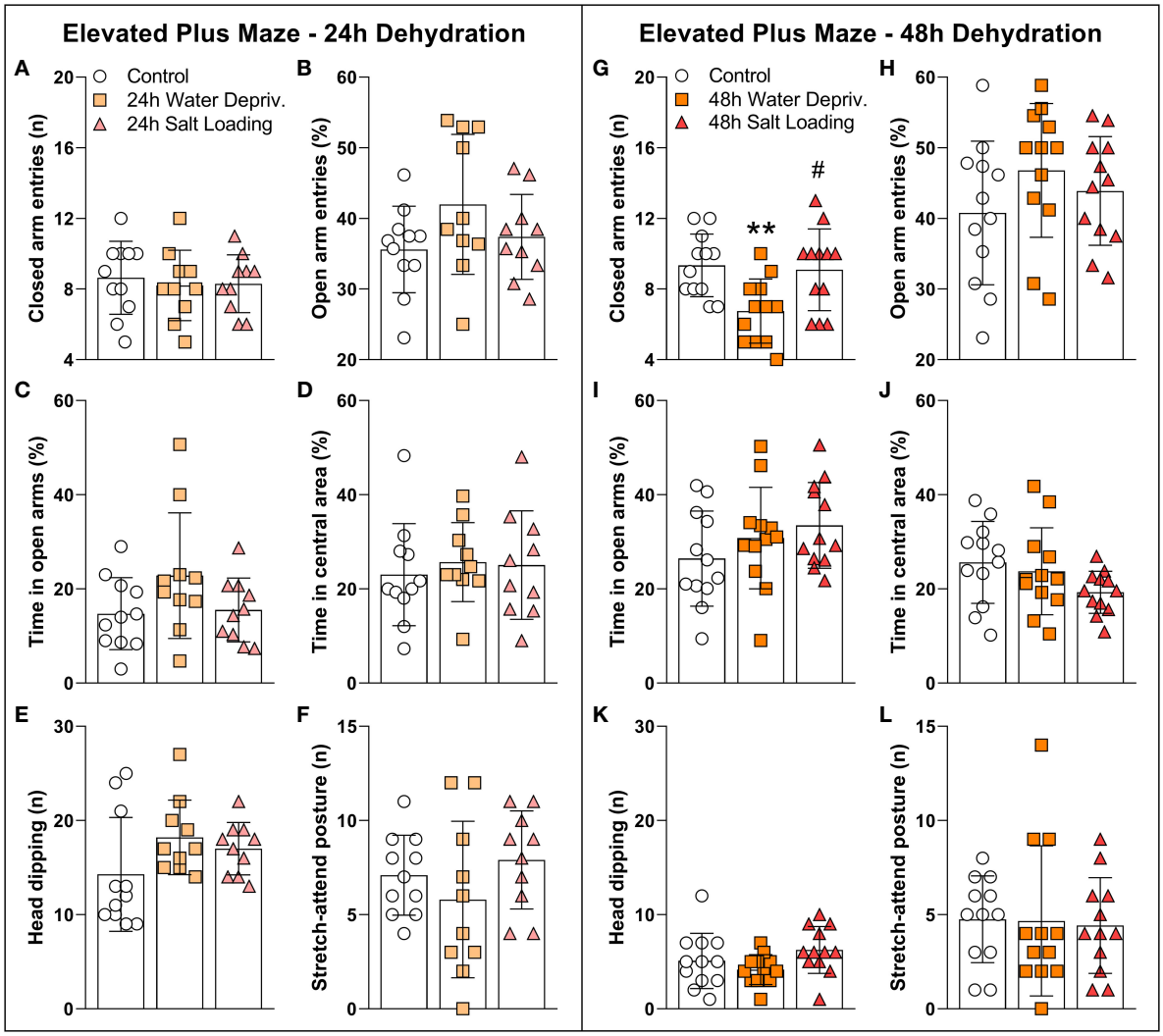

FIGURE 3
Effects of **(A–F)** 24 h or **(G–L)** 48 h of dehydration in male adult rats on **(A, G)** number of entries into closed arms, **(B, H)** percentage of entries into open arms, **(C, I)** percentage of time spent in open arms, **(D, J)** percentage of time spent in the central area, **(E, K)** number of head dipping episodes, and **(F, L)** number of stretch-attend postures during 5 min of evaluation in the elevated plus maze apparatus. Values are mean ± SD. The number of animals used per group was: 24 h Control = 11; 24 h WD = 10; 24 h SL = 10; 48 h Control = 12; 48 h WD = 12; 48 h SL = 12. Data were submitted to one-way ANOVA followed by the Tukey *post hoc* test, except for the percentage of time spent in the open arms after 24 h of dehydration and the number of stretch-attend postures after 48 h of dehydration, in which the Kruskal-Wallis test was used. **p<0.01 compared to control group; #p<0.05 compared to the WD group.

Twenty minutes later, the animals were submitted to the EPM test (Figure 6 and Supplementary Table 5). Figure 6A shows that rats submitted to 48 h of WD entered the closed arms less than the control rats (not water deprived) [$F_{(1,32)}$=8.154; p=0.0075]. However, the OXTR antagonist used failed to reverse the reduction of closed arm exploration in water-deprived rats. Open arm entries and time in the center area, head dipping and stretch-attend posture episodes (Figures 6B–F) were not affected by the OXTR antagonist or by WD. Note that these data match those presented in Figure 3. There was a significant effect of antagonist administration on reduction of rearing episodes [$F_{(1,32)}$=5.670; p=0.0234], demonstrating the efficiency of the oxytocin receptor antagonist used (Supplementary Figure 3 and Supplementary table 5).

At the end of the plus maze test, animals were allowed to drink water freely, and the respective intakes at 30 and 120 minutes (Figures 7A, B and Supplementary Table 6) were recorded. As expected, water-deprived rats drank more water than the control animals at 30 and at 120 minutes [$F_{(1,33)}$=504.8; p<0.0001 and $F_{(1,33)}$=521.4; p<0.0001; respectively]. However, the oxytocin receptor antagonist had no effect on the water drank by the rats (Figures 7A, B).

4 Discussion

It has been suggested that homeostatic signals, such as thirst, can modulate emotion, motivation, and motor functions (6). Here we used two dehydration models to induce thirst and activate the MCNs of PVN and SON: WD and SL (1). As we expected, both protocols increased plasma osmolarity, agreeing with previous results using mice (26) and rats (27), and validating our models. Additionally, WD

10.3389/fendo.2023.1062211

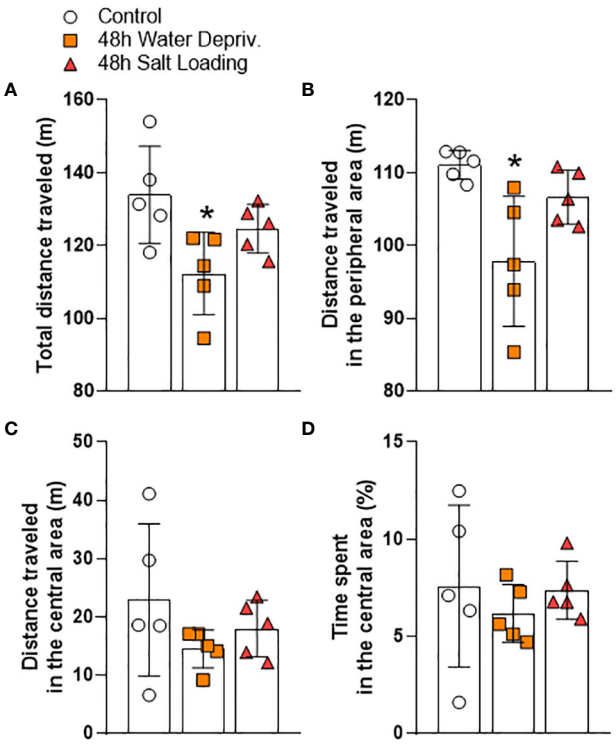

FIGURE 4
Effects of 48 h of dehydration in male adult rats on **(A)** total locomotion, **(B)** locomotion in the peripheral area, **(C)** locomotion in the central area, and **(D)** percentage the time spent in the central area during 10 min of evaluation in the open field test. Values are mean ± SD of 5 animals per group. Data were submitted to one-way ANOVA followed by the Tukey *post hoc* test, except for the distance traveled in the peripheral area, in which the Kruskal-Wallis test was used, followed by Dunn's *post hoc* test. *p<0.05 compared to the control group.

increased the hematocrit, as was also expected, coinciding with the previously mentioned results of Fujio et al., 2006 (27).

Our results support the notion that locomotor alterations occur in response to WD. A previous study (9) showed a decrease in locomotion of water-deprived rats within their home cage only during the dark period. Our results corroborate and extend those of Martelli et al., 2012 (9), since we demonstrated that locomotion is also impaired in novel environments. Interestingly, hyperosmotic thirst induced by SL does not produce alterations in locomotion even though both kinds of thirst activate hypothalamic MCNs (1, 28, 29). Although both models induce dehydration, they have several differences (29). While plasma osmolality is progressively increased following WD and SL, urinary osmolality only increases with WD. In addition, WD reduces food intake by approximately 50% compared to SL. AVP and OXT levels are increased in both models compared to controls. However, the AVP level is lower, but the OXT level is higher in the WD compared to SL. It is likely that the physiological and behavioral discrepancies in response to WD and SL result from different central activation of several brain nuclei in each model. Indeed, transcriptome analysis of SON after SL or WD revealed 7060 genes are regulated by WD but not by SL (29). On the other hand, the anxiety-like behavior evaluated in the EPM was not affected by any of the thirst models used. In contrast, Zhang et al. (2016) found a decrease in the open arm exploration after 24 h of WD (6). In that work, rats were evaluated during the light period of the light/dark cycle. Probably evaluating animals during the normally non-active period and under an aversive stimulus such as light affected their behavior, explaining the differences with our results.

In the cited work of Zhang et al. (2016), increased activation (assessed by Fos-immunoreactivity) of GABAergic neurons of the LHb was found (6). The authors suggested that the habenula may link the forebrain with midbrain structures that regulate emotional behavior, since habenula lesions resulted in stress, anxiety, reward and motor dysfunctions (30). For example, habenular lesions prompted animals to increase anxiety-like behavior in the EPM test and increased locomotion in the open field test (31, 32). The amygdala participates in the fluid intake regulation (33). Additionally, it has already been shown that WD increases Fos expression in the CeA (34) and it is well established that BLA (35, 36) and CeA (37, 38) mediate anxiety-like behavior. However, our data show that *Gad1*, *Slc17a6, Avpr1a* and *Oxtr* mRNA expression are not changed in LHb or BLA after 48 h of WD or SL. Therefore, the observed changes found in the locomotion of rats submitted to 48 h of WD were not mediated by expression levels of these genes in the LHb or BLA. However, we cannot discard that the protein expression and/or post-transcriptional modifications may result in functional alterations of oxytocin and/or vasopressin type 1a receptors, as well as glutamatergic and/or GABAergic signaling in those brain areas.

Regarding the CeA, we found an increase in the *Oxtr* mRNA expression. This brain structure has a large number of oxytocin receptors involved, among others, in fear behavior inhibition (2, 39) and stress-coping behavior (40). Moreover, subcutaneous (41) and intracerebroventricular (42) oxytocin administration reduces anxiety-

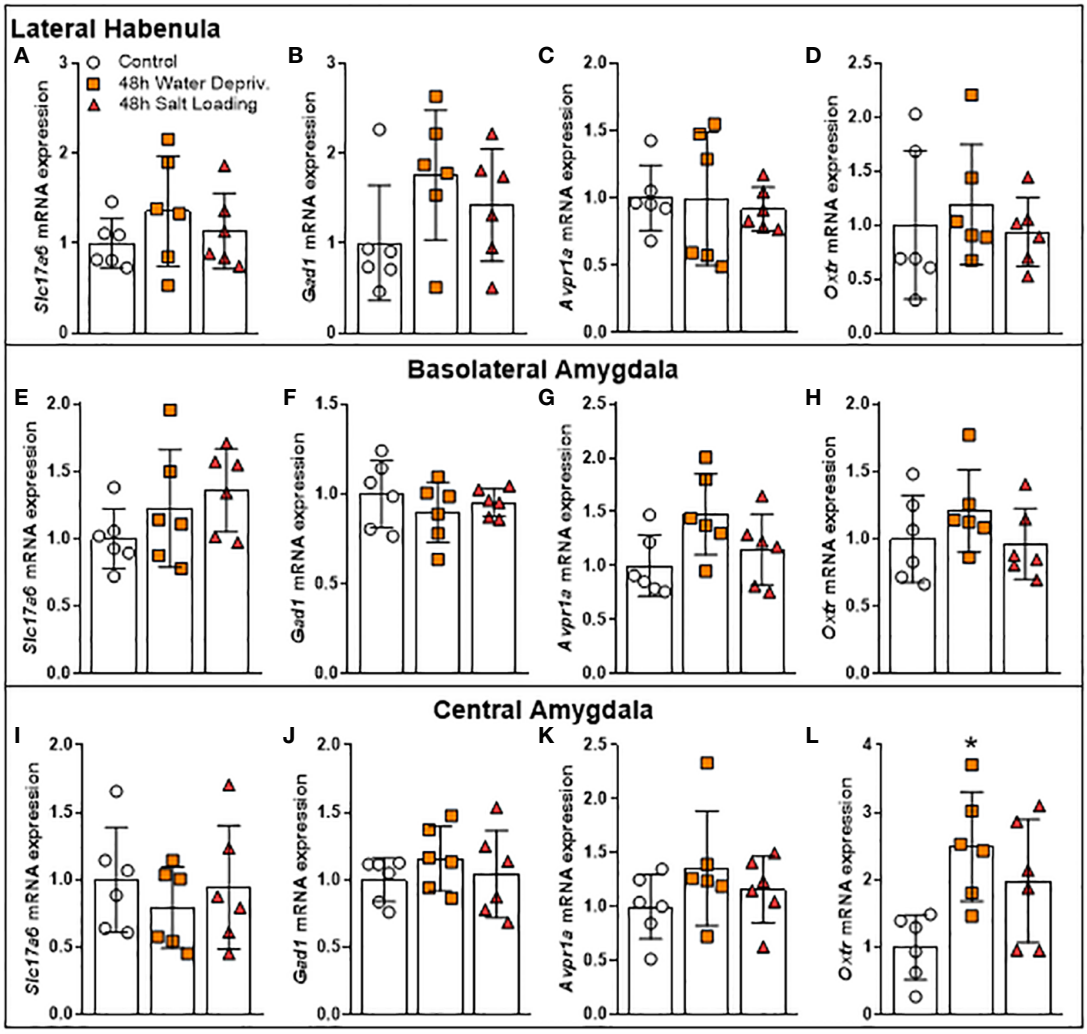

FIGURE 5
Effects of 48 h of dehydration in male adult rats on relative mRNA expression of **(A, E, I)** the Vesicular Glutamate Transporter 2 (*Slc17a6*), **(B, F, J)** the Glutamate Decarboxylase 1 (*Gad1*), **(C, G, K)** the Arginine Vasopressin Receptor 1A (*Avpr1a*), and **(D, H, L)** the Oxytocin Receptor (*Oxtr*) in the **(A–D)** lateral habenula, **(E–H)** the basolateral amygdala (BLA), and **(I-L)** the central amygdala (CeA). Values are mean ± SD of 6 animals per group. Data of gene expression in BLA as well as *Oxtr* mRNA expression in CeA were analyzed by one-way ANOVA followed by the Tukey *post hoc* test. The other data were submitted to the Kruskal-Wallis test. *p<0.05 compared to the control group.

like behavior in rats. Also, Windle et al., 1997 (42) reported a reduction of rearing by i.c.v. administration of oxytocin. Since the CeA has oxytocin receptors, whose activation regulates several behaviors, we investigated the possibility that OXT acting on the CeA could regulate locomotion in rats. To determine whether oxytocin receptors were involved in the locomotor alteration of water-deprived rats observed in the EPM, we administrated an oxytocin receptor antagonist in the CeA. The results showed that the OXTR antagonist did not reverse the exploratory reduction of 48-h water-deprived rats or change water intake of those rats. On the other hand, the OXTR antagonist decreased vertical exploration (assessed as rearing episodes in the EPM test) independently of the hydration state of the animal. In addition to demonstrating that oxytocin receptor blockade was efficient, this result indicates that although the general action of oxytocin on the central nervous system can decrease exploration (41, 43), the activation of CeA oxytocin receptors seems to stimulate exploration, since their blocked reduced rearing. On the other hand, the WD-induced alteration in locomotory activity may involve other brain nuclei. In the present work, we focus on limbic structures involved in anxiety-like and exploratory behaviors. In future works, it would be interesting to study gene expression in brain nuclei that control voluntary motricity. Of particular interest may be the caudate-putamen, a mesolimbic structure involved in motor activity and motivation behaviors (44), which also participates in thirst regulation (45) and expresses oxytocin receptors (46).

The present study provides evidence that WD modulates the exploratory activity and upregulates *Oxtr* expression in the CeA. However, our work has some limitations to consider. First, to dissolve the OXT antagonist, we had to use 10% DMSO. This compound can affect the excitability of neurons, having a considerable inhibitory effect (47). Although the antagonist-treated groups were compared to vehicle-treated groups that also received 10% DMSO, future works using other antagonists or solvents are needed. Secondly, this work would benefit from others that confirm the changes observed here in

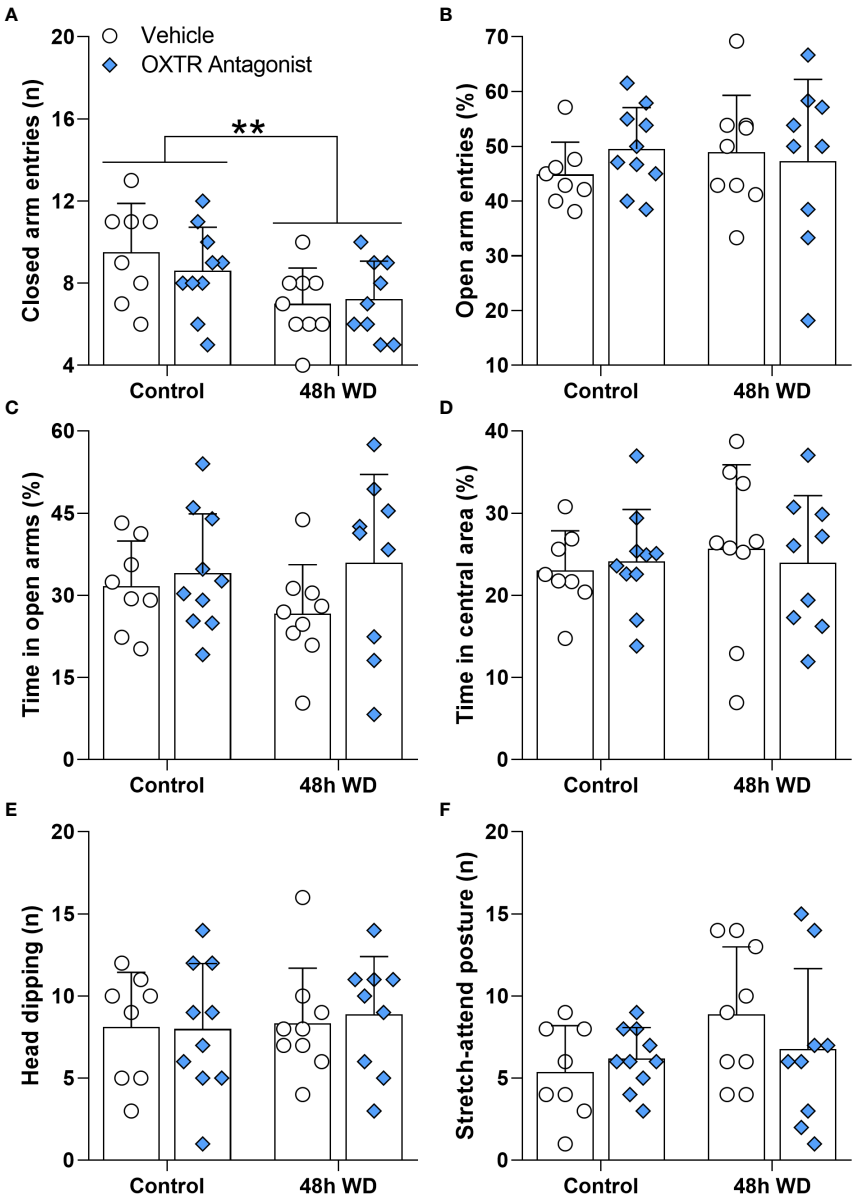

FIGURE 6
Effects of oxytocin receptor antagonist microinjection in the central amygdala of 48-h water-deprived male adult rats on **(A)** number of entries into closed arms, **(B)** percentage of entries into open arms, **(C)** percentage of time spent in open arms, **(D)** percentage of time spent in the central area, **(E)** number of head dipping episodes, and **(F)** number of stretch-attend postures during 5 min of evaluation in the elevated plus maze apparatus. Values are mean ± SD. The number of animals used per group was: Control + vehicle = 8; Control + antagonist = 10; 48 h WD + vehicle = 9; 48 h WD + antagonist = 9. Data were submitted to two-way ANOVA. The values of the number of stretch-attend postures were transformed to ranks before ANOVA. **p<0.01 comparing Water Deprived *vs*. Control groups.

the *Oxtr* expression through different techniques, such as RNAscope, to add information on the cellular location of the *Oxtr* whose expression was altered. Finally, considering that plasma levels of angiotensin II are increased by WD and decreased by SL (29), it might be interesting to study the gene expression of the RAS components in the brain areas regulating exploratory behavior, such as the amygdaloid complex. It has been found that the microinjection of a selective AT1 antagonist into the amygdala induces an anxiolytic-like effect in rats, increasing the time spent in the EPM open arms and the total of entries (48). On the other hand, the microinjection of PD123319, a selective AT_2 antagonist, into the medial amygdala of rats increased anxiety-like behavior assessed in EPM (49). These data indicate that the differential levels of angiotensin II at the circulation or in the brain, or even changes in its signaling mechanisms, might contribute to locomotor activity changes observed in rats submitted to WD but not to SL. Thus, future studies might address the role of the RAS in the nocturnal hypoactivity induced by WD in rats.

In summary, we found dehydration-induced hypoactivity and increased levels of *Oxtr* mRNA expression in the CeA after 48 h of WD. However, after blockade of the OXTR signaling to the CeA of WD rats, we found no significant changes on the nocturnal

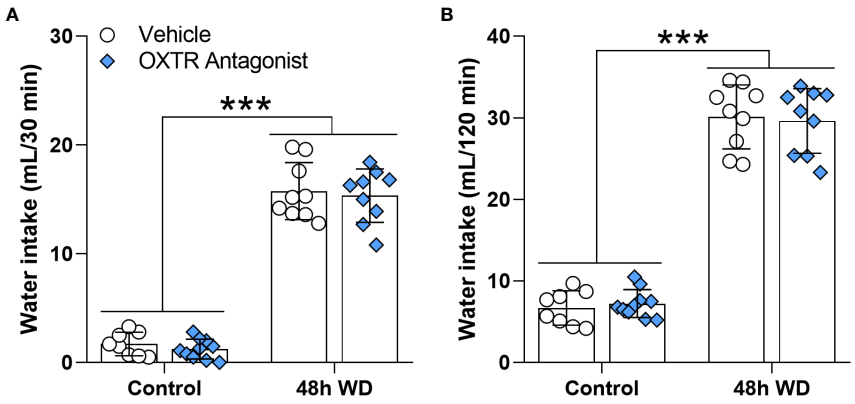

FIGURE 7
Effects of oxytocin receptor antagonist microinjection in the central amygdala of 48 h water-deprived male adult rats on water intake during **(A)** 30 and **(B)** 120 minutes. Values are mean ± SD. The number of animals used per group was: Control + vehicle = 8; Control + antagonist = 10; 48 h WD + vehicle = 9; 48 h WD + antagonist = 9. Data were submitted to two-way ANOVA.

exploration in the EPM, indicating that OXTR signaling to the CeA does not mediate dehydration-induced hypoactivity in male rats.

Data availability statement

The raw data supporting the conclusions of this article will be made available by the authors, without undue reservation.

Ethics statement

The animal study was reviewed and approved by ethical committees for animal use of Federal Rural University of Rio de Janeiro (CEUA-ICBS, protocol number 001/2017) and Federal University of São Paulo (CEUA-UNIFESP, protocol number 7236281119, ID 009443, 2019).

Author contributions

AM, LR, and FR contributed to the conception and design of the study. AM supervised the project and acquired financial support. VF, VT, RD-S, CA, and AM performed the experiments. VF, VT, and AM analyzed the data. VF and VT wrote the first draft of the manuscript. All authors contributed to manuscript revision, read, and approved the submitted version.

Funding

This study was financed in part by grants from the Fundação de Amparo è Pesquisa do Estado de São Paulo (FAPESP, 2019/27581-0), Conselho Nacional de Desenvolvimento Científico e Tecnológico (CNPq, 309882/2020-6) and Coordenação de Aperfeiçoamento de Pessoal de Nível Superior - Brasil (CAPES, Finance Code 001 and 88887.568866/2020-00).

Conflict of interest

The authors declare that the research was conducted in the absence of any commercial or financial relationships that could be construed as a potential conflict of interest.

Publisher's note

All claims expressed in this article are solely those of the authors and do not necessarily represent those of their affiliated organizations, or those of the publisher, the editors and the reviewers. Any product that may be evaluated in this article, or claim that may be made by its manufacturer, is not guaranteed or endorsed by the publisher.

Supplementary material

The Supplementary Material for this article can be found online at: https://www.frontiersin.org/articles/10.3389/fendo.2023.1062211/full#supplementary-material

SUPPLEMENTARY FIGURE 1
Histological location at −2.16 mm posterior to bregma of the cannulas implanted in CeA are shown for control rats administered with vehicle (blue circles) or OXTR antagonist (green circles) and 48-h water-deprived rats administered with vehicle (pink circles) or OXTR antagonist (violet circles).

SUPPLEMENTARY FIGURE 2
Drawing of a coronal section of rat brain at bregma -2.16 mm, and representative microphotograph at 4x showing the microinjection site in the central amygdala. "CeA", central amygdala; "opt", optic tract; "ec", external capsule; and "I.S.", injection site.

SUPPLEMENTARY FIGURE 3
Effects of oxytocin receptor antagonist microinjection in the central amygdala of 48-h water-deprived male adult rats on rearing episodes during 5 min of evaluation in the elevated plus maze apparatus. Values are mean ± SD. The number of animals used per group was: Control + vehicle = 8; Control + antagonist = 10; 48 h WD + vehicle = 9; 48 h WD + antagonist = 9. Data were submitted to two-way ANOVA. The values were transformed to ranks before submission to two-way ANOVA. *p<0.05 comparing rats receiving OXTR antagonist *vs.* rats receiving vehicle.

References

1. Mecawi AS, Ruginsk SG, Elias LL, Varanda WA, Antunes-Rodrigues J. Neuroendocrine regulation of hydromineral homeostasis. *Compr Physiol* (2015) 5 (3):1465–516. doi: 10.1002/cphy.c140031

2. Knobloch HS, Charlet A, Hoffmann LC, Eliava M, Khrulev S, Cetin AH, et al. Evoked axonal oxytocin release in the central amygdala attenuates fear response. *Neuron* (2012) 73(3):553–66. doi: 10.1016/j.neuron.2011.11.030

3. Hernandez VS, Vazquez-Juarez E, Marquez MM, Jauregui-Huerta F, Barrio RA, Zhang L. Extra-neurohypophyseal axonal projections from individual vasopressin-containing magnocellular neurons in rat hypothalamus. *Front Neuroanat* (2015) 9:130. doi: 10.3389/fnana.2015.00130

4. Zhang B, Qiu L, Xiao W, Ni H, Chen L, Wang F, et al. Reconstruction of the hypothalamo-neurohypophysial system and functional dissection of magnocellular oxytocin neurons in the brain. *Neuron* (2021) 109(2):331–46.e7. doi: 10.1016/j.neuron.2020.10.032

5. Hernandez VS, Hernandez OR, Perez de la Mora M, Gomora MJ, Fuxe K, Eiden LE, et al. Hypothalamic vasopressinergic projections innervate central amygdala gabaergic neurons: Implications for anxiety and stress coping. *Front Neural Circuits* (2016) 10:92. doi: 10.3389/fncir.2016.00092

6. Zhang L, Hernandez VS, Vazquez-Juarez E, Chay FK, Barrio RA. Thirst is associated with suppression of habenula output and active stress coping: Is there a role for a non-canonical vasopressin-glutamate pathway? *Front Neural Circuits* (2016) 10:13. doi: 10.3389/fncir.2016.00013

7. Smith JA, Pati D, Wang L, de Kloet AD, Frazier CJ, Krause EG. Hydration and beyond: Neuropeptides as mediators of hydromineral balance, anxiety and stress-responsiveness. *Front Syst Neurosci* (2015) 9:46. doi: 10.3389/fnsys.2015.00046

8. Krause EG, de Kloet AD, Flak JN, Smeltzer MD, Solomon MB, Evanson NK, et al. Hydration state controls stress responsiveness and social behavior. *J Neurosci Off J Soc Neurosci* (2011) 31(14):5470–6. doi: 10.1523/JNEUROSCI.6078-10.2011

9. Martelli D, Luppi M, Cerri M, Tupone D, Perez E, Zamboni G, et al. Waking and sleeping following water deprivation in the rat. *PloS One* (2012) 7(9):e46116. doi: 10.1371/journal.pone.0046116

10. Meye FJ, Lecca S, Valentinova K, Mameli M. Synaptic and cellular profile of neurons in the lateral habenula. *Front Hum Neurosci* (2013) 7:860. doi: 10.3389/fnhum.2013.00860

11. Zhang X, Ge TT, Yin G, Cui R, Zhao G, Yang W. Stress-induced functional alterations in amygdala: Implications for neuropsychiatric diseases. *Front Neurosci* (2018) 12:367. doi: 10.3389/fnins.2018.00367

12. Blume A, Bosch OJ, Miklos S, Torner L, Wales L, Waldherr M, et al. Oxytocin reduces anxiety *Via* Erk1/2 activation: Local effect within the rat hypothalamic paraventricular nucleus. *Eur J Neurosci* (2008) 27(8):1947–56. doi: 10.1111/j.1460-9568.2008.06184.x

13. Mak P, Broussard C, Vacy K, Broadbear JH. Modulation of anxiety behavior in the elevated plus maze using peptidic oxytocin and vasopressin receptor ligands in the rat. *J Psychopharmacol* (2012) 26(4):532–42. doi: 10.1177/0269881111416687

14. van den Burg EH, Stindl J, Grund T, Neumann ID, Strauss O. Oxytocin stimulates extracellular Ca2+ influx through Trpv2 channels in hypothalamic neurons to exert its anxiolytic effects. *Neuropsychopharmacol Off Publ Am Coll Neuropsychopharmacol* (2015) 40(13):2938–47. doi: 10.1038/npp.2015.147

15. Greenwood MP, Greenwood M, Paton JF, Murphy D. Control of polyamine biosynthesis by antizyme inhibitor 1 is important for transcriptional regulation of arginine vasopressin in the Male rat hypothalamus. *Endocrinology* (2015) 156(8):2905–17. doi: 10.1210/en.2015-1074

16. Balthazar L, Lages YVM, Romano VC, Landeira-Fernandez J, Krahe TE. The association between the renin-angiotensin system and the hypothalamic-Pituitary-Adrenal axis in anxiety disorders: A systematic review of animal studies. *Psychoneuroendocrinology* (2021) 132:105354. doi: 10.1016/j.psyneuen.2021.105354

17. NIH. *Guide for the care and use of laboratory animals*. Washington, DC: National Institute of Health (2011).

18. Andrade MM, Tome MF, Santiago ES, Lucia-Santos A, de Andrade TG. Longitudinal study of daily variation of rats' behavior in the elevated plus-maze. *Physiol Behav* (2003) 78(1):125–33. doi: 10.1016/s0031-9384(02)00941-1

19. Pellow S, Chopin P, File SE, Briley M. Validation of Open:Closed arm entries in an elevated plus-maze as a measure of anxiety in the rat. *J Neurosci Methods* (1985) 14 (3):149–67. doi: 10.1016/0165-0270(85)90031-7

20. Cruz AP, Frei F, Graeff FG. Ethopharmacological analysis of rat behavior on the elevated plus-maze. *Pharmacol Biochem Behav* (1994) 49(1):171–6. doi: 10.1016/0091-3057(94)90472-3

21. Prut L, Belzung C. The open field as a paradigm to measure the effects of drugs on anxiety-like behaviors: A review. *Eur J Pharmacol* (2003) 463(1-3):3–33. doi: 10.1016/s0014-2999(03)01272-x

22. Paxinos G, Watson C. *The rat brain in stereotaxic coordinates*. San Diego: Elsevier Academic Pess (2007). 6ta ed.

23. Livak KJ, Schmittgen TD. Analysis of relative gene expression data using real-time quantitative pcr and the 2(-delta delta C(T)) method. *Methods* (2001) 25(4):402–8. doi: 10.1006/meth.2001.1262

24. Cragg B, Ji G, Neugebauer V. Differential contributions of vasopressin V1a and oxytocin receptors in the amygdala to pain-related behaviors in rats. *Mol Pain* (2016) 12. doi: 10.1177/1744806916676491

25. Hora SC, Conover WJ. The f statistic in the two-way layout with rank–score transformed data. *J Am Stat Assoc* (1984) 79(387):6. doi: 10.1080/01621459.1984.10478095

26. Faraco G, Wijasa TS, Park L, Moore J, Anrather J, Iadecola C. Water deprivation induces neurovascular and cognitive dysfunction through vasopressin-induced oxidative stress. *J Cereb Blood Flow Metab* (2014) 34(5):852–60. doi: 10.1038/jcbfm.2014.24

27. Fujio T, Fujihara H, Shibata M, Yamada S, Onaka T, Tanaka K, et al. Exaggerated response of arginine vasopressin-enhanced green fluorescent protein fusion gene to salt loading without disturbance of body fluid homeostasis in rats. *J Neuroendocrinol* (2006) 18(10):776–85. doi: 10.1111/j.1365-2826.2006.01476.x

28. Pool AH, Wang T, Stafford DA, Chance RK, Lee S, Ngai J, et al. The cellular basis of distinct thirst modalities. *Nature* (2020) 588(7836):112–7. doi: 10.1038/s41586-020-2821-8

29. Greenwood MP, Mecawi AS, Hoe SZ, Mustafa MR, Johnson KR, Al-Mahmoud GA, et al. A comparison of physiological and transcriptome responses to water deprivation and salt loading in the rat supraoptic nucleus. *Am J Physiol Regulatory Integr Comp Physiol* (2015) 308(7):R559–68. doi: 10.1152/ajpregu.00444.2014

30. Hikosaka O. The habenula: From stress evasion to value-based decision-making. *Nat Rev Neurosci* (2010) 11(7):503–13. doi: 10.1038/nrn2866

31. Murphy CA, DiCamillo AM, Haun F, Murray M. Lesion of the habenular efferent pathway produces anxiety and locomotor hyperactivity in rats: A comparison of the effects of neonatal and adult lesions. *Behav Brain Res* (1996) 81(1-2):43–52. doi: 10.1016/s0166-4328(96)00041-1

32. Lee EH, Huang SL. Role of lateral habenula in the regulation of exploratory behavior and its relationship to stress in rats. *Behav Brain Res* (1988) 30(3):265–71. doi: 10.1016/0166-4328(88)90169-6

33. Yao ST, Antunes VR, Paton JF, Murphy D. Osmotic regulation of neuronal nitric oxide synthase expression in the rat amygdala: Functional role for nitric oxide in adaptive responses? *J Neurosci Res* (2007) 85(2):410–22. doi: 10.1002/jnr.21114

34. Dalmasso C, Antunes-Rodrigues J, Vivas L, De Luca LAJr. Mapping brain fos immunoreactivity in response to water deprivation and partial rehydration: Influence of sodium intake. *Physiol Behav* (2015) 151:494–501. doi: 10.1016/j.physbeh.2015.08.020

35. Wang DV, Wang F, Liu J, Zhang L, Wang Z, Lin L. Neurons in the amygdala with response-selectivity for anxiety in two ethologically based tests. *PloS One* (2011) 6(4): e18739. doi: 10.1371/journal.pone.0018739

36. Prager EM, Bergstrom HC, Wynn GH, Braga MF. The basolateral amygdala gamma-aminobutyric acidergic system in health and disease. *J Neurosci Res* (2016) 94 (6):548–67. doi: 10.1002/jnr.23690

37. Fox AS, Shackman AJ. The central extended amygdala in fear and anxiety: Closing the gap between mechanistic and neuroimaging research. *Neurosci Lett* (2019) 693:58–67. doi: 10.1016/j.neulet.2017.11.056

38. Babaev O, Piletti Chatain C, Krueger-Burg D. Inhibition in the amygdala anxiety circuitry. *Exp Mol Med* (2018) 50(4):1–16. doi: 10.1038/s12276-018-0063-8

39. Viviani D, Charlet A, van den Burg E, Robinet C, Hurni N, Abatis M, et al. Oxytocin selectively gates fear responses through distinct outputs from the central amygdala. *Science* (2011) 333(6038):104–7. doi: 10.1126/science.1201043

40. Ebner K, Bosch OJ, Kromer SA, Singewald N, Neumann ID. Release of oxytocin in the rat central amygdala modulates stress-coping behavior and the release of excitatory amino acids. *Neuropsychopharmacol Off Publ Am Coll Neuropsychopharmacol* (2005) 30 (2):223–30. doi: 10.1038/sj.npp.1300607

41. Uvnas-Moberg K, Ahlenius S, Hillegaart V, Alster P. High doses of oxytocin cause sedation and low doses cause an anxiolytic-like effect in Male rats. *Pharmacol Biochem Behav* (1994) 49(1):101–6. doi: 10.1016/0091-3057(94)90462-6

42. Windle RJ, Shanks N, Lightman SL, Ingram CD. Central oxytocin administration reduces stress-induced corticosterone release and anxiety behavior in rats. *Endocrinology* (1997) 138(7):2829–34. doi: 10.1210/endo.138.7.5255

43. Uvnas-Moberg K, Alster P, Hillegaart V, Ahlenius S. Oxytocin reduces exploratory motor behaviour and shifts the activity towards the centre of the arena in Male rats. *Acta Physiol Scand* (1992) 145(4):429–30. doi: 10.1111/j.1748-1716.1992.tb09385.x

44. Aher CV, Duwaerts CC, Akama KT, Lucas LR. Effects of acute diuresis stress on egr-1 (Zif268) mrna levels in brain regions associated with motivated behavior. *Brain Res Bull* (2010) 81(1):114–9. doi: 10.1016/j.brainresbull.2009.10.004

45. Pal GK, Bharathi B, Thombre DP. Modulation of daily water intake by dopamine in caudate and accumbens nuclei in rats. *Physiol Behav* (1992) 51(4):851–6. doi: 10.1016/0031-9384(92)90126-m

46. Rogers FD, Freeman SM, Anderson M, Palumbo MC, Bales KL. Compositional variation in early-life parenting structures alters oxytocin and vasopressin 1a receptor

development in prairie voles (Microtus ochrogaster). *J Neuroendocrinol* (2021) 33(8): e13001. doi: 10.1111/jne.13001

47. Tamagnini F, Scullion S, Brown JT, Randall AD. Low concentrations of the solvent dimethyl sulphoxide alter intrinsic excitability properties of cortical and hippocampal pyramidal cells. *PloS One* (2014) 9(3):e92557. doi: 10.1371/journal.pone.0092557

48. Llano Lopez LH, Caif F, Garcia S, Fraile M, Landa AI, Baiardi G, et al. Anxiolytic-like effect of losartan injected into amygdala of the acutely stressed rats. *Pharmacol Rep PR* (2012) 64(1):54–63. doi: 10.1016/s1734-1140(12)70730-2

49. Moreno-Santos B, Marchi-Coelho C, Costa-Ferreira W, Crestani CC. Angiotensinergic receptors in the medial amygdaloid nucleus differently modulate behavioral responses in the elevated plus-maze and forced swimming test in rats. *Behav Brain Res* (2021) 397:112947. doi: 10.1016/j.bbr.2020.112947

frontiers | Frontiers in Endocrinology

TYPE Original Research
PUBLISHED 15 February 2023
DOI 10.3389/fendo.2023.1116482

OPEN ACCESS

EDITED BY
Alexandre Benani,
Centre National de la Recherche Scientifique (CNRS), France

REVIEWED BY
Linus R. Shao,
University of Gothenburg, Sweden
Arnab Banerjee,
Birla Institute of Technology and Science, India

*CORRESPONDENCE
Elodie Desroziers
elodie.crossard_desroziers@sorbonne-universite.fr
Rebecca E. Campbell
rebecca.campbell@otago.ac.nz

†PRESENT ADDRESS
Elodie Desroziers,
Sorbonne Université - Faculté de Sciences et Ingénierie, Neuroplasticité des Comportements de la Reproduction, Neurosciences Paris Seine, UM119 - CNRS UMR 8246 - INSERM UMRS 1130, Paris, France

‡These authors have contributed equally to this work and share last authorship

SPECIALTY SECTION
This article was submitted to Neuroendocrine Science, a section of the journal Frontiers in Endocrinology

RECEIVED 05 December 2022
ACCEPTED 31 January 2023
PUBLISHED 15 February 2023

CITATION
Donaldson NM, Prescott M, Ruddenklau A, Campbell RE and Desroziers E (2023) Maternal androgen excess significantly impairs sexual behavior in male and female mouse offspring: Perspective for a biological origin of sexual dysfunction in PCOS.
Front. Endocrinol. 14:1116482.
doi: 10.3389/fendo.2023.1116482

Maternal androgen excess significantly impairs sexual behavior in male and female mouse offspring: Perspective for a biological origin of sexual dysfunction in PCOS

Nina M. Donaldson, Melanie Prescott, Amy Ruddenklau, Rebecca E. Campbell*‡ and Elodie Desroziers*†‡

Centre for Neuroendocrinology and Department of Physiology, School of Biomedical Sciences, University of Otago, Dunedin, New Zealand

Introduction: Polycystic ovary syndrome (PCOS) is the most common infertility disorder worldwide, typically characterised by high circulating androgen levels, oligo- or anovulation, and polycystic ovarian morphology. Sexual dysfunction, including decreased sexual desire and increased sexual dissatisfaction, is also reported by women with PCOS. The origins of these sexual difficulties remain largely unidentified. To investigate potential biological origins of sexual dysfunction in PCOS patients, we asked whether the well-characterized, prenatally androgenized (PNA) mouse model of PCOS exhibits modified sex behaviours and whether central brain circuits associated with female sex behaviour are differentially regulated. As a male equivalent of PCOS is reported in the brothers of women with PCOS, we also investigated the impact of maternal androgen excess on the sex behaviour of male siblings.

Methods: Adult male and female offspring of dams exposed to dihydrotestosterone (PNAM/PNAF) or an oil vehicle (VEH) from gestational days 16 to 18 were tested for a suite of sex-specific behaviours.

Results: PNAM showed a reduction in their mounting capabilities, however, most of PNAM where able to reach ejaculation by the end of the test similar to the VEH control males. In contrast, PNAF exhibited a significant impairment in the female-typical sexual behaviour, lordosis. Interestingly, while neuronal activation was largely similar between PNAF and VEH females, impaired lordosis behaviour in PNAF was unexpectedly associated with decreased neuronal activation in the dorsomedial hypothalamic nucleus (DMH).

Conclusion: Taken together, these data link prenatal androgen exposure that drives a PCOS-like phenotype with altered sexual behaviours in both sexes.

KEYWORDS

androgen, PCOS (polycystic ovary syndrome), sexual behavior, DHT (5α-dihydrotestosterone), sexual dysfunction (biological)

Introduction

Fertility and sexuality are controlled by the brain and dependent upon complex neuronal circuits that are organized early in life and then activated by sex steroid hormones in adulthood. Prenatal exposure to testosterone, aromatized into oestradiol in the brain, is required for the development of male-typical brain circuitry and behaviors in rodents (1). Over the last 10 years, the dogma that the female brain develops by default in the absence of sex steroids has been challenged with the discovery that peri-pubertal oestradiol and progesterone are also required for feminization of the brain and sexual behaviors (2–5). Noteworthy, the role of androgen signaling through androgen receptor (AR) on the development of the brain and behavior has been recently highlighted in the male through the study of the neural deletion of AR in male mice showing a central role for AR in the development of proper male copulatory behaviors (6, 7). However, the role of AR-mediated signaling remains poorly investigated in the female despite AR being present in the developing female brain and behavior (8). In addition, very little is currently understood about male- and female-typical sexual behaviors that are programmed by *in utero* androgen excess states such as in PCOS (9, 10), congenital adrenal hyperplasia (CAH) (11, 12) and in the case of environmental exposure to androgenic compounds (13–15).

Polycystic ovary syndrome (PCOS) is a common endocrine disorder characterized by androgen excess. PCOS affects roughly 1 in 8 women of reproductive age and is the most common form of anovulatory infertility (16). In addition to hyperandrogenism, PCOS is characterized by menstrual irregularities and polycystic ovarian morphology (16–18) and is associated with a wide range of comorbidities, including obesity, diabetes and cardiovascular disease (16). The hypothalamo-pituitary-gonadal (HPG) axis, that controls fertility and reproductive behavior, is disrupted in many women with PCOS. In particular, luteinizing hormone (LH) pulse frequency, which mirrors gonadotropin-releasing hormone (GnRH) neuron activity and secretion, is significantly elevated. An elevated LH to follicle stimulating hormone (FSH) ratio contributes downstream to polycystic ovarian morphology, elevated androgen production and infertility (19, 20). Steroid hormone feedback to the HPG axis, that would ordinarily slow GnRH/LH secretion is diminished in PCOS patients, suggesting that PCOS originates from a miscommunication between the brain and the ovaries (20–22).

The etiopathogenesis of PCOS is most likely multifactorial with genetic susceptibility and environmental exposure playing predominant roles (9). In line with this, recent studies in men suggest the existence of a male PCOS equivalent in the brothers of women with PCOS (23–26). These men share common endocrine, metabolic and cardiovascular comorbidities with their sisters such as an elevated free androgen index, a low level of FSH leading to an elevated LH/FSH ratio, insulin resistance, type II diabetes and hypertension (23, 25, 26). Among the current hypotheses of PCOS origins, *in utero* androgen excess has been highlighted by human and animal-based study as a substantial contributor (9, 27). Indeed, pregnant women with PCOS show high levels of circulating androgens during gestation, and this is correlated with an increased likelihood of having a daughter diagnosed with PCOS (28). Maternal androgen excess has also been linked to the development of PCOS-like features in a wide range of female mammalian species (27). For example, exposure of female mice to elevated levels of the non-aromatisable androgen dihydrotestosterone (DHT) during late gestation programs the development of hyperandrogenism, irregular oestrous cycles and theca cell hyperplasia (29). These prenatally-androgenized (PNA) female mice exhibit impaired steroid hormone feedback associated with reduced progesterone receptor (PR) expression, elevated LH pulse frequency (29, 30) and elevated GnRH neuronal activity (31), associated with programmed changes in the GnRH neuronal network (29–33). There is some evidence indicating that prenatal androgen excess also alters reproductive function in males. Rams born to mothers exposed to testosterone propionate or dihydrotestosterone exhibit altered testicular function and disrupted neuroendocrine axis function in adulthood (34–38). However, similar disruptions do not appear to be evident in the male siblings of PNA mice modeling PCOS (39).

Epidemiological studies indicate that women with PCOS are more likely to experience sexual dysfunction, including low sex drive and sexual dissatisfaction, that can negatively impact their quality of life (40–48). Interestingly, men diagnosed with early onset androgenetic alopecia (AGA), now considered as a clinical sign of male PCOS equivalent (23, 24, 26), also indicate experiencing sexual dysfunction (49, 50). In women, the cause of PCOS-related sexual dysfunction is frequently attributed to psychological factors, including reduced self-esteem related to hirsutism and/or obesity, a higher prevalence of anxiety, depression and mood disorders and decreased interest in sexual activities due to infertility issues (40–42, 44–46, 48, 51–56). Similarly, in men with AGA, the early onset of baldness is also often discussed in epidemiological studies as a potential factor for sexual dysfunction (49, 50). However, it is not unreasonable to imagine that prenatal androgen exposure that is associated with the programming of PCOS-like reproductive features also might impact the development of male and female sexual behaviors. Obviously, human sexual behavior is incredibly complex and difficult to model, however, the PNA mouse model of PCOS, exposed to the non-aromatisable androgen dihydrotestosterone, provides a powerful reductionist approach to tease apart whether prenatal androgen exposure is associated with changes in sex behavior in male and female mice. To investigate how prenatal androgen excess impacts adult sexual behaviors in female and male mice, we performed a series of sexual behavior tests in PNA male (PNAM) and female (PNAF) mice. Finding a significant impairment in PNAF mice, we then further investigated the potential neural substrates involved in the PNA-related female sexual dysfunction.

Materials and methods

Animals

Male and female C57BL/6J mice were generated and housed in the Otago Biomedical Research Facility at the University of Otago until adulthood. Mice were kept under a 12 h light/dark cycle with food and water ad libitum. All mice were kept in same-sex housing from weaning and hence were not exposed to the opposite sex before

sexual behavior testing. Adult mice were moved to the Otago Behavioural Phenotyping Unit (BPU) for subsequent behavioral testing. In the BPU, mice were kept under a 12 h reverse light/dark cycle with food and water ad libitum. Sodium lamps permitted observation of the mice during the dark phase. All protocols were approved by the University of Otago Animal Ethics Committee.

Generation of prenatally-androgenized mice modeling PCOS

Control (VEH) and prenatally-androgenized (PNA) male and female mice were generated using the well-characterized prenatally androgenized (PNA) mouse model protocol (29–33, 57). Adult male and female C57BL/6J mice were paired overnight on the day of proestrus. Gestational day 1 was recorded as the following day after overnight mating and the male was removed from the cage. Females were then monitored for signs of pregnancy such as increased body weight and increased belly circumference. From gestational day 16-19, pregnant dams received a daily subcutaneous (s.c.) injection in the nape of the neck of either 100 µL dihydrotestosterone (DHT, 250 µg/100µL) in sesame oil as the PNA treatment or 100 µL of sesame oil only as the vehicle control. This window of prenatal androgen exposure has been shown to lead to PCOS-like features in mice and largely avoid the critical period for the differentiation of external genitalia (29–33, 57).The male (M) and female (F) offspring of dams injected with DHT (PNAM or PNAF) and vehicle control (VEH) mice were studied from adulthood (postnatal day (PND) 60 onward) in the following experimental protocols. Oestrous cyclicity of VEH and PNA female mice was assessed to establish the expected loss of oestrous cyclicity in PNA mice by collecting daily vaginal smears over a 20-day period (PND 60–80) (Figure S1) as previously described (29–31, 33, 58).

Experiment 1: Phenotyping male and female-typical sexual behaviors in prenatally-androgenized mice

A cohort of C57Bl6 male (n=9-12/group) and female (n=6-11/group) control and prenatally-androgenized (PNA) mice underwent the following behavioral tests as previously described (3–5) (Figure 1).

Anxiety and locomotion tests

Male and female-typical sexual behavior in mice are highly impacted by anxiety and dependant upon locomotor activity. Since previous studies in the PNA mouse model highlighted anxiety-like behaviors during the diurnal/inactive phase (59–61), we decided to test the basal level of anxiety and locomotion in PNA mice under the same conditions used for testing sexual behavior: during the nocturnal/active phase and under a sodium light imperceptible by mice. Mice were tested in Open-field tests and Elevated-plus maze tests to determine basal locomotor activity and anxiety as detailed below.

Open-field test: Mice were placed in the center of a plexiglass aquarium (40 x 40 x 30 cm) under sodium lamps and their movements were recorded for 10 min. Between each animal, the aquarium was cleaned using 10% ethanol. Video recordings were analyzed using TopScan® software. Two virtual zones of the aquarium floor were demarcated: the center zone (60% of the total floor area) and the periphery zone (surrounding area). TopScan® recorded the distance travelled by the mice and the amount of time mice spent in each zone over 10 min (600 s). Locomotion was measured as the distance travelled (mm). Anxiety behavior was determined by comparing the time (s) spent in the center versus peripheral zone, with less time in the center reflecting heightened anxiety.

Elevated-plus maze: The maze apparatus was comprised of four arms (30 cm long, 5 cm wide) elevated 40 cm above the ground by metal legs and arranged in a plus shape. Two arms were open without walls and two arms were enclosed by high walls (15 cm). Mice were placed at the junction of the four arms (center) and their movements were recorded for 10 min. Between each animal, the maze was cleaned using 10% ethanol. Video recordings were analyzed using TopScan®. Each of the four arms and the center zone were virtually demarcated. The distance travelled by the mice and the amount of time spent in each arm and center over the 10 min (600 s) period was traced and recorded. Locomotion was measured as the distance travelled (mm) and anxiety behavior was measured by the time (s) spent in the center, the open arms and the closed arms, with less time in the open arms reflecting heightened anxiety.

Ovariectomies and hormones replacement for induction of female receptivity

All female mice in this study were ovariectomized and implanted with a silastic capsule of oestradiol as previously described (3–5). This ensures uniform hormone concentrations across females and mimics an oestrus hormonal level of estradiol in order to artificially trigger receptivity (3–5). Briefly, all females were bilaterally ovariectomized under general anaesthesia with isofluorane. At the same time, a 5-mm-long Silastic capsule (inner diameter: 1.57 mm; outer diameter: 2.41 mm) containing crystalline 17β-oestradiol (E2758, Sigma-Aldrich, USA) (diluted 1:1 with cholesterol (C8667, Sigma-Aldrich, USA)) was inserted under the skin at the nape of the neck to induce oestrous levels of oestradiol. Mice received Carprofen (5 mg/kg) and were allowed to recover for two weeks before the onset of behavioral tests. On the day of testing, the females (either tests or stimuli) were administered progesterone (P) (P0130, Sigma-Aldrich, USA) (500 µg/mL, s.c.) 3 hours prior to test commencement.

Male and female partner discrimination test

Three-Chambers Box Partner preference: A partner preference test was carried out in virgin animals prior to sexual behavior experiments. Partner preference testing was conducted in a plexiglass box divided into three compartments (60 x 13 x 30 cm) by opaque partitions with fenestrations that allow for odours to

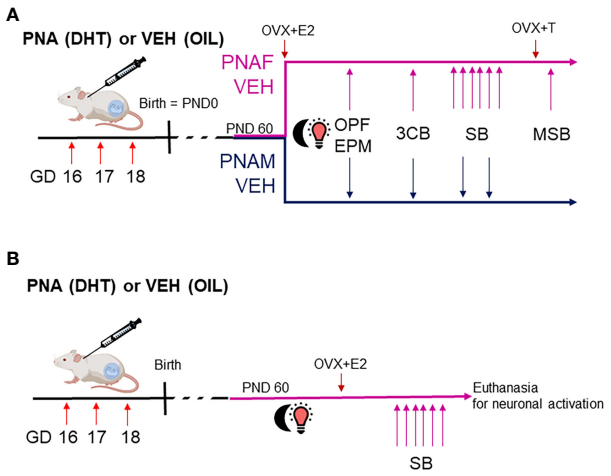

FIGURE 1
Experimental design to study the effect of prenatal DHT exposure on sexual behaviors in male and female mice. In this study, we used two batches of mice. **(A)** The first batch of mice was used to determine if male and female-typical sexual behaviors could be affected by prenatal androgen exposure (experiment 1 and 2). Dams were treated with either dihydrotestosterone (DHT) or oil vehicle (VEH) at gestational day (GD) 16, 17 and 18. After birth, the male and female offspring entered the experimental protocol at adulthood around postnatal day 60 (PND60). PNAF and VEH females (magenta line) were ovariectomized and implanted with a silastic capsule containing estradiol in order to normalize hormonal status and artificially induced receptivity (OVX+E2). PNAM and VEH male mice (blue line) were left intact. Then, the animals entered a series of behavioral procedures to test their anxiety-like behavior and locomotion within an open-field (OPF) and an elevated-plus maze (EPM) tests, their abilities to discriminate a sexual partner within a three-compartments box partner preference test (3CB) and their typical sexual behavior (SB, i.e. lordosis behavior for female over 6 consecutive weeks and male copulatory behavior within 2 consecutive weeks). Finally, the PNAF and VEH female mice had their estradiol implant replaced by an implant containing testosterone (OVX+T) in order to activate and therefore test male-like sexual behavior (MSB) and verify if prenatal DHT exposure could have led to masculinization of the brain. **(B)** The second batch of mice was used to identify the neural target of prenatal androgen in female mice associated with impaired lordosis behavior. Only the female offsprings were used in this experiment 3. The PNAF and VEH female mice underwent ovariectomies and implantation of a silastic capsule of estradiol followed by 6 consecutive weeks of lordosis behavior testing. At the last test, PNAF and VEH female mice were euthanized 90 min after the beginning of the test in order to study neural activation induced by lordosis behavior. VEH, control male; PNAF, prenatally androgenized female; PNAM, prenatally androgenized male; PND, postnatal day; OPF, open-field test; EPM, elevated plus-maze; 3CB, three-chamber test; SB, sexual behavior test; MSB, male-like sexual behavior.

diffuse throughout the arena. The day before testing, test females were allowed to habituate in the central compartment for 10 min. On the day of testing, females were administered P (500 µg/mL s.c.) 3 h prior to test commencement. For the test, two other mice, an intact sexually experienced stimulus male and an oestrous stimulus female (OVX + E2 female injected with P 3 h prior to the experiment, OVX+E+P) were placed in the two lateral compartments with their own bedding in order to make their respective compartments as odorous as possible. The test animal (PNAM/PNAF or VEH counterpart), was then placed in the middle compartment containing no bedding and observed for 10 min (the experimenter was blinded to group at the time of experiment). The time (s) that the test female spent actively sniffing each partition was recorded with a stopwatch. Between each test, the middle compartment was cleaned using 10% ethanol to eliminate the previous test subject's odours. A preference score was calculated by dividing the time spent investigating the male compartment minus the time spent investigating the female compartment by the total time spent investigating both compartments. A positive value of the preference score indicates a partner preference toward the stimulus male, whereas a negative value of the preference score indicates a partner preference toward the stimulus female.

Male sexual behaviors

All male mice were gonadally intact and sexual behavior tests were conducted in a transparent plexiglass aquarium (35 x 25 x 19 cm) filled with a layer of fresh sawdust as previously described (3–5). At the beginning of each test, the male was placed alone in the cage and allowed to adapt for 15 min. A receptive female (OVX+E+P) was then introduced into the cage and the latencies to the first mount and intromission, the latency to ejaculate, as well as the number of mounts, intromissions, and pelvic thrusts, were recorded. The test lasted until ejaculation occurred or 30 min if no ejaculation was achieved. If a male never displayed a certain behavior within the 30 min test, the latency was scored as 1800 s.

Female sexual behaviors

Female typical lordosis behavior: The lordosis behavior test was carried out over six consecutive weeks allowing seven days of rest between each test. Lordosis behavior testing was conducted in the same Plexiglas aquarium as described above. For the test, a sexually experienced male was placed in the aquarium and allowed to habituate for 15 min. Subsequently, a test female was introduced to the aquarium and the pair was observed. The number of mounts exhibited by the male and the number of lordosis behavior displays exhibited by the female was recorded for 15 min. The lordosis quotient corresponds to the number of lordosis postures recorded following a trial mount by the male, divided by the number of mounts attempted by the male throughout the duration of the test, and multiplied by 100 (i.e. (number of lordosis/numbers of male mount trials) * 100).

Anogenital sniffing/aggressive behaviors: During all lordosis behavior tests, bouts of anogenital investigation and aggressive behavior toward the male were counted. Bouts of anogenital sniffing was recorded every time the female nose was in contact with the male genitalia. Bouts of aggressive behaviors were recorded every time the female attempted to kick or to bite the male.

Experiment 2: Determining if prenatal androgen excess drives masculinized sex behavior

Following the female typical sexual behavior tests, a random subset of VEH female (n = 6) and PNAF (n = 5) mice were

anesthetized again with isofluorane in order to remove the oestradiol implant, and replaced it with a testosterone implant as previously described (4). The testosterone implant was made of a 5-mm-long Silastic capsule (inner diameter: 1.57 mm; outer diameter: 2.41 mm) filled with crystalline testosterone (T1875, Sigma-Aldrich, USA) diluted 1:1 with cholesterol (C8667, Sigma-Aldrich, USA). This procedure mimics typical testosterone levels of adult male mice by 2 weeks and can induce male-like sexual behavior in female mouse (4). Mice received Carprofen (5mg/kg) and were allowed to recover for 10 days before additional behavior testing. Following recovery, male-like sexual behavior (i.e. mounting, intromission and pelvic thrust) was tested in a plexiglass aquarium (35 x 25 x 19 cm) filled with a layer of fresh sawdust as previously described (62). Briefly, a test female (PNAF or VEH) was placed alone in the aquarium to habituate for 15 min. Subsequently, an oestrous stimulus female (OVX + E + P) was introduced to the aquarium and the pair was observed. The initial latency to mount, number of mounts and number of pelvic thrusting movements shown by the test female (PNAF or VEH) were scored over 30 min.

Experiment 3: Mapping sex behavior-related neuronal activation in prenatally-androgenized mice

A second cohort of VEH female (n=5) and PNAF (n=5) mice were tested for lordosis behavior as described above over 6 consecutive weeks. After the last lordosis test, i.e. week 6, female mice were euthanized 90 minutes after the beginning of the lordosis test in order to study neuronal activation following lordosis behavior. In addition, we also euthanized a group of adult females C57Bl6 mice (Basal n=3-4) who went through the same procedure as the VEH and PNAF mice except that no male stimulus was introduced into the aquarium for the last lordosis behavior test. This basal group allowed us to determine the basal neural activation without lordosis behavior.

Tissue processing for immunostaining

Upon completion of all behavioral tests, female mice were anesthetized with a lethal i.p. injection of pentobarbital (150 mg/kg/mice) and perfused transcardially with 4% cold paraformaldehyde. Brains were removed and post-fixed in 4% paraformaldehyde overnight. Brains were then cryoprotected in 30% sucrose/tris-buffered saline (TBS) solution over 72 h. Free-floating brain sections were cut at 30µm-thickness on a freezing microtome and collected in cryoprotectant. Forebrains were cut coronally from the rostral telencephalon to the posterior hypothalamus. Sections were collected in four different series and stored at -20°C until immunostaining.

Immunohistochemistry procedures

All the following immunohistochemistry procedures were performed on brain sections from the second cohort of female VEH (n=5) and PNAF (n=5) mice after lordosis behavioral testing. One set of sections (i.e every fourth section) was rinsed for 10 minutes in TBS six times to remove cryoprotectant. Sections were then treated with 3%H_2O_2 and 40% methanol in TBS for 10 minutes to quench endogenous peroxidases, and then washed a further three times in TBS. Sections were incubated in blocking solution with 2% normal donkey/goat serum and 1% bovine serum albumin in TBST (TBS + 0.3% Triton-X) for 1 hour. Sections were then incubated with primary antibodies against Kisspeptin, Progesterone Receptor and cFOS (Table 1) for 96 hours at 4 degrees. Then, the sections were washed again three times 10 minutes before incubation with IgG biotinylated secondary antibodies (donkey anti-sheep IgG biotinylated/goat anti-rabbit IgG biotinylated) diluted in blocking solution for 90 minutes at room temperature. Sections were then washed before being incubated with the avidin-biotin complex diluted in TBST (1/200, ABC, Vector Laboratory, Burlingham, CA). To finish, after rinsing, sections were reacted with 3,3'diaminobenzidine tetrahydrochloride in TBS with nickel ammonium sulfate and glucose oxidase. After a last wash, the sections were mounted onto gelatin-coated slides, dried for 48h, dehydrated in ethanol followed by xylene and then coverslipped with DPX.

Image analysis

Photomicrographs of cFOS and PR immunohistochemistry in different brain regions were captured using a 20x objective on a bright field microscope (Olympus BX51). The representative images of each brain region analyzed were identified using the mouse brain atlas from Paxinos and Franklin, 3rd Edition. An experimenter blinded to treatment counted the number of cFOS- and PR-immunoreactive nuclei using Image J software®.

For the kisspeptin immunohistochemistry, photomicrographs of the anteroventral periventricular nucleus (AVPV) were captured using a Nikon Eclipse TiE2 inverted microscope at x20 magnification. Z-stacks of 1um focal thickness were captured across three representative sections of the AVPV. The images were then analyzed by a blinded experimenter using the NIS-element software (RRID : SCR_014329). The experimenter counted the number of kisspeptin immunoreactive cells on three representative sections of the AVPV.

Statistical analysis

Statistical analysis was performed with PRISM® software 9.0 (Graph Pad Prism, RRID:scr_002798). Normal distribution and homogeneity of variance were determined using a Shapiro-Wilk test and Fisher's test, respectively. The percentage of animals performing either male sexual behaviors or female typical lordosis behavior were compared by a Fisher exact tests. All data are represented as the mean +/- SEM. Analysis of lordosis, investigative and aggressive behaviors was performed by a 2-way ANOVA mixed models for repeated measures. All other data were analyzed by an unpaired Students t-tests when the normal distribution and variance homogeneity parameters were met. Otherwise, a Mann-Whitney test was used. A p-value < 0.05 was considered statistically significant and a p-value <0.07 was considered a tendency.

TABLE 1 Primary antibodies used.

Proteins of interest	Primary antibodies	Dilutions
Kisspeptin	#Kp052, INRAe	1:10000
Progesterone	#63605, Abcam	1:800
cFOS	#sc-52, Santa Cruz	1:1000

Results

Experiment 1: Male and female-typical sexual behaviors are impaired in prenatally-androgenized mice

Male sexual behavior is slightly altered by prenatal androgen exposure

Locomotion was not affected by prenatal androgen excess in male, indicated by both the open-field test (10155 +/- 652.8 mm for VEH and 9318 +/- 554.4 mm for PNAM; t=0.98, df=19, p=0.34) and the elevated-plus maze test (6663 +/- 367.9 mm for VEH and 7004+/- 279.6 for PNAM; U=52, p=0.92). Basal anxiety was also not affected by prenatal DHT exposure, as indicated by the percentage of time spend in the center of the open-field (Figure 2A; t=0.697, df=19, p=0.49) and in the open-arm of the elevated plus maze (Figure 2B; U=52, p=0.92).

Two sexual behavior tests were performed because male sexual behavior is subject to learning with an increase in sexual behavior efficiency after a first experience (63, 64). In the first test, 55% of VEH males exhibited complete sexual behavior with mounting, intromission, pelvic thrust and ejaculation (Figure 2C). In contrast, only 25% of PNAM exhibited complete sexual behavior (Figure 2C). Significantly fewer PNAM performed mounting (p=0.02) or thrusts (p=0.03) compared to VEH males (Figure 2C), while the percentage of animals performing intromission (p=0.08) and ejaculating (p=0.20) by the end of the first test was not statistically different (Figure 2C). After sexual experience, in test 2, 55% of VEH males and 33% of PNAM exhibited complete sexual behavior (Figure 2D). While the percentage of PNAM performing mounting behavior remained significantly reduced compared to VEH males (p=0.0046, Figure 2D), the percentage of animals exhibiting intromission (p=0.08), thrusts (p=0.08) and ejaculation (p=0.39) were not different between PNAM and VEH during the second test.

To further investigate the effect of prenatal DHT exposure on male sexual behavior, we analyzed different components of male typical sexual behavior such as the latencies to perform (Figures 2E, F) and numbers (Table 2) of each behavior were also measured. In the first test, we observed that the latency to first intromission increased significantly for the PNAM compare to the VEH (Figure 2E; t=2.68, df=19, p=0.03). In addition, we observed a tendency to an increase latency to mount (t= 1.704, df=19, p=0.07) and to ejaculate (t=1.841, df=19, p=0.07) for the PNAM compared to their VEH counterparts (Figure 2E). These increased latencies are associated with significantly fewer mounts with intromission (U=27, p=0.0467) and fewer pelvic thrusts (U=25, p=0.0251) in PNAM compared to VEH males (Table 2). In addition, the intromission rate of the PNAM tended toward being decreased compare with VEH males (Figure 2G; U=28.5, p=0.057). During the second test, only the latency to first mount was significantly increased for the PNAM compared to the VEH males (Figure 2F; t=3.972, df=19, p=0.001). PNAM and VEH had the same latencies to first intromission (t=1.621, df=19, p=0.13) and ejaculation (t=0.08, df=19, p=0.65) during the second test. Interestingly, PNAM displayed significantly fewer mounts (U=13, p=0.0018), mounts with intromission (U=23, p=0.0185) and pelvic thrusts (U= 24, p=0.0233) compared to the VEH males (Table 2) which was also associated with a trend toward a lower intromission rate (Figure 2H; U=28, P=0.052) during the second test.

Male partner discrimination is not affected by prenatal androgen exposure

Male sexual behavior is dependent upon the odor recognition of a partner. Therefore, the ability of male mice to recognize a female was assessed using the three compartments box partner preference tests. PNAM and VEH male mice spent a similar percentage of time sniffing the male (p=0.4117) and the female (p=0.4116) compartments (Figure 2I). Noteworthy, the total time spent sniffing both compartments was also not different between PNAM and VEH male mice (413 +/- 10.45 s for VEH and 389.25+/- 10.91 s for PNAM; t=1,529, df=19, p=0.22).

Female sexual behavior is significantly impaired by prenatal androgen exposure

Before to test for the female typical sexual behavior, lordosis, we needed to verify that prenatal androgen exposure was not altering locomotion and anxiety in the PNAF compare to control female mice (VEH). Surprisingly, we observed a slight increase of the distance travelled by PNAF compare to VEH female mice in the open-field test (5336 +/- 438.7 mm for VEH and 6923 +/- 944.7 mm for PNAF; U=13, p=0.048) while no effect of prenatal DHT exposure on locomotion was observed in the elevated-plus maze test (2199 +/- 151.8 mm for VEH and 2436 +/- 330.4 for PNAF; t=0.75, df=15, p=0.46). Despite this discrepancy in the locomotion, basal anxiety, represented by the percentage of time spend in the center of the open-field (Figure 3A; t=0.44, df=15, p=0.67) and in the open-arm of the elevated plus maze (Figure 3B; U=32, p=0.96), was not affected by prenatal androgen exposure.

The female typical sexual behavior, lordosis, is a learned process. Therefore, we tested lordosis behavior over 6 consecutive weeks. As expected, during the first three weeks, the percentage of VEH female mice exhibiting lordosis behavior increased to reach 100% and then remained over 80% until the last week of testing. In contrast, the percentage of PNAF mice showing lordosis behavior remained lower throughout the 6 consecutive weeks of testing compared to VEH females: 16.67% at week 1 and 2, 66.67% at week 3, 50% at week 4 and only 40% at week 5 and 6. The percentage of PNAF displaying lordosis behavior was significantly reduced compare to VEH females at week 2 (p=0.03) and 4 (p=0.03) (Figure 3C). These results were associated with a significant reduction in the lordosis quotient in PNAF mice compared to VEH females (Figure 3D). Statistical analysis with repeated measures mixed model ANOVA revealed a significant effect of the prenatal androgen treatment (F (1,15) = 25.60, p=0.0001). Following *post hoc* comparisons, the lordosis quotient was significantly reduced in PNAF mice compared to VEH females in

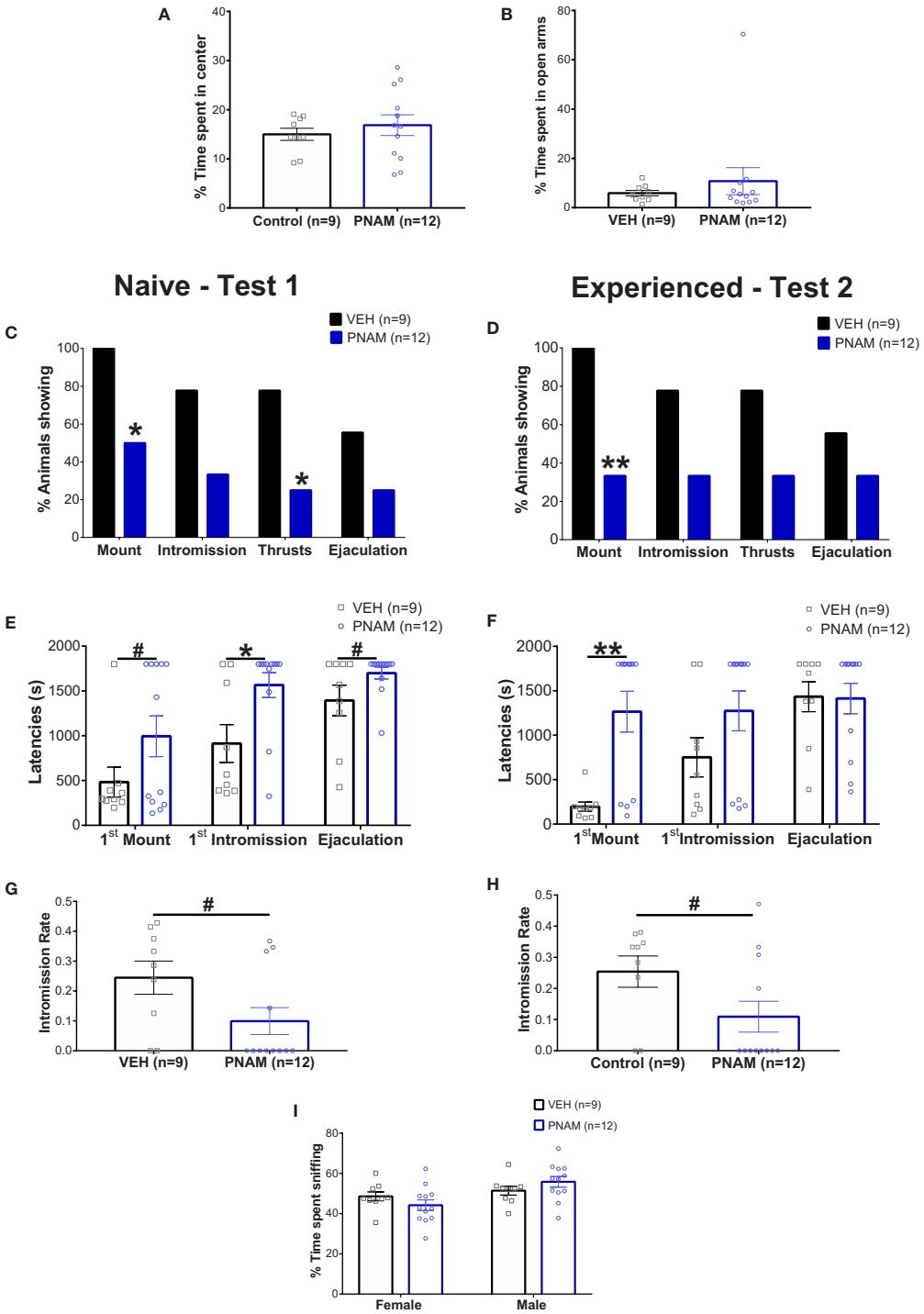

FIGURE 2
Prenatal DHT exposure modifies male-typical sexual behavior. **(A, B)** Histogram representing the percentage of time spent in the center zone of the Open-field test **(A)** and the percentage of time spent in the open arms of the Elevated-plus maze **(B)** for the VEH male (black bar) and PNAM (dark blue bar). **(C, D)** Histograms representing the percentage of animals performing each component of male copulatory behavior (mount, intromission, pelvic thrusts and ejaculation) while naive **(C)** (i.e. during the first test) or experienced **(D)** (i.e. during the second test) for the VEH male (black bars) and PNAM (dark blue bars). **(E, F)** Histograms representing the latencies to first mount, first intromission and ejaculation while naive **(E)** (i.e. during the first test) or experienced **(F)** (i.e. during the second test) for the VEH male (black bars) and PNAM (dark blue bars). **(G, H)** Histograms representing the intromission rate, corresponding to the number of mounts with intromission divided by the total number of mount trial, while naive **(C)** (i.e. during the first test) or experienced **(D)** (i.e. during the second test) for the VEH male (black bar) and PNAM (dark blue bar). **(I)** Histograms representing the percentage of time spent sniffing either the male of the female compartment in the three-compartment box partner preference test for the VEH male (black bars) and PNAM (dark blue bars). **p<0.01, *p<0.05, #p<0.07. VEH, control male; PNAM, prenatally androgenized male, s, seconds. Mean +/- SEM.

TABLE 2 Prenatal DHT exposure affect the number of different parameters of male copulatroy behvaiour in the adult male mice. PNAM, prenatally-androgenized male. Mean +/- SEM.

	Naive Male (Test 1)		Experienced Male (Test 2)	
Number of	*Control (n=9)*	*PNAM (n=12)*	*Control (n=9)*	*PNAM (n=12)*
Mounts	13.22 +/- 3.227	8.417 +/- 3.607	22.67 +/- 5.649	3.667 +/- 1.982**
Mounts with Intromission	6.889 +/- 2.664	2.417 +/- 1.598*	10.67 +/- 3.078	2.25 +/- 1.415*
Pelvic Thrusts	153.2 +/- 55.46	58.42 +/- 36.14*	211 +/- 65.71	54.58 +/- 26.08*

**p-<0.01, *p-<0.05.

week 2 (*p=0.0091*, t=3.988, df=13.14), week 3 (*p=0.002*, t=5.731, df=14.99) and week 4 (*p=0.0271*, t=3.383, df=13.75). For the last test in week 6, the *post-hoc* comparison detected a trend toward a decreased lordosis quotient in PNAF compared to VEH females (*p=0.0583*, t=3.016, df=12.95).

Investigative and rejection behaviors during lordosis

Sexual motivation was assessed by quantifying the number of times the female sniffed the anogenital region of the male: anogenital sniffing bouts (Table 3). Prenatal androgen treatment had no significant effect on the number of anogenital sniffing bouts (F (1,15) = 0.01529, *p=0.9032*).

Rejection behaviors toward the male were assessed by the number of times the female rejected male approaches by kicking or biting (Table 3). Prenatal androgen treatment was found to have no significant effect on the number of aggressive behavior bouts (F (1,15) = 3.296, *p=0.0895*).

Female partner discrimination is not affected by prenatal androgen exposure

The female-typical sexual behavior, lordosis behavior is also dependent upon the odor recognition of a male partner. Therefore, the ability of mice to recognize the male was assessed using the three compartments box partner preference tests. PNAF and VEH female mice spent a similar percentage of time sniffing the male (p=0.39) and the female (p=0.39) compartments (Figure 3E). The total time spent sniffing both compartments was not different between PNA and VEH female mice (332.81 +/- 18.16 s for VEH and 328.60 +/- 29.09 s for PNA; U=18, p=0.30).

Experiment 2: Prenatal androgen exposure with DHT, a non-aromatisable androgen, does not masculinize sexual behavior in female mice

To determine whether prenatally androgenized females exhibited masculinized sexual behaviors, adult PNAF and VEH female mice were subjected to elevated testosterone which is triggers male-like sexual behaviors in presence of a receptive stimulus female (Figure 4). The latency to first mount was not different between PNAF (991.4 +/- 346 s) and VEH (726.0 +/-342.4 s) female mice (U=10, *p=0.3853*) (Figure 4A). The number of mounts performed by the female over an oestrous stimulus female was also not statistically different between PNAF (11.40 +/- 4.95 mounts) and VEH (12.50 +/- 4.24 mounts) female mice (t=0.1699, df=9, *p=0.8688*) (Figure 4B). Finally, the number of pelvic thrust-like movements performed by the female during mount of the stimulus female was also not different between PNA (58.20 +/- 31.44 pelvic thrusts) and VEH (61.83 +/- 31.42 pelvic thrusts) female mice (t=0.810, df=9, *p=0.9372*) (Figure 4C).

Experiment 3: Identifying female sexual behavior-related neural changes in prenatally-androgenized mice

AVPV Kisspeptin neuron population size is not affected by PNA exposure

AVPV Kisspeptin neurons have been demonstrated to play a major role in the expression of lordosis behavior (65). In addition, AVPV kisspeptin neurons are sexually dimorphic (66) and sensitive to prenatal testosterone rise (67). Here, we found that the number of kisspeptin immunoreactive cells per section of the AVPV was not different between PNA (7.27 +/- 1.35 kisspeptin positive cells) and VEH (8.74 +/- 1.28 kisspeptin positive cells) female mice.

Progesterone receptor immunoreactivity is not different between VEH and PNA female mice after priming with ovarian hormones (OVX+E+P)

In adulthood, lordosis behavior is dependent upon oestradiol and progesterone signaling in the brain (68–70). As reduced PR immunostaining has been reported in intact PNA mice (30), we aimed to determine if reduced lordosis behavior observed in PNA females might correspond with reduced PR expression in brain regions regulating female sexual behavior. PR-positive cells were counted in the anteroventral periventricular nucleus (AVPV), the median arcuate nucleus (mARN) and the ventrolateral part of the vendromedial hypothalamus (VMHvl) (Figures 5A–D). Robust PR-immunoreactivity was observed in both groups throughout the regions analyzed and no differences were found in the number of PR-positive cells in any of the regions analyzed between PNA and VEH mice that had previously been OVX and steroid primed for sexual behavior analysis (Figures 5A–D).

Neural activation is reduced only in the dorsomedial hypothalamus after lordosis behavior in prenatally-androgenized female mice

In a second cohort of PNA and VEH female mice, that were tested for lordosis behavior again during 6 consecutive weeks, we detected

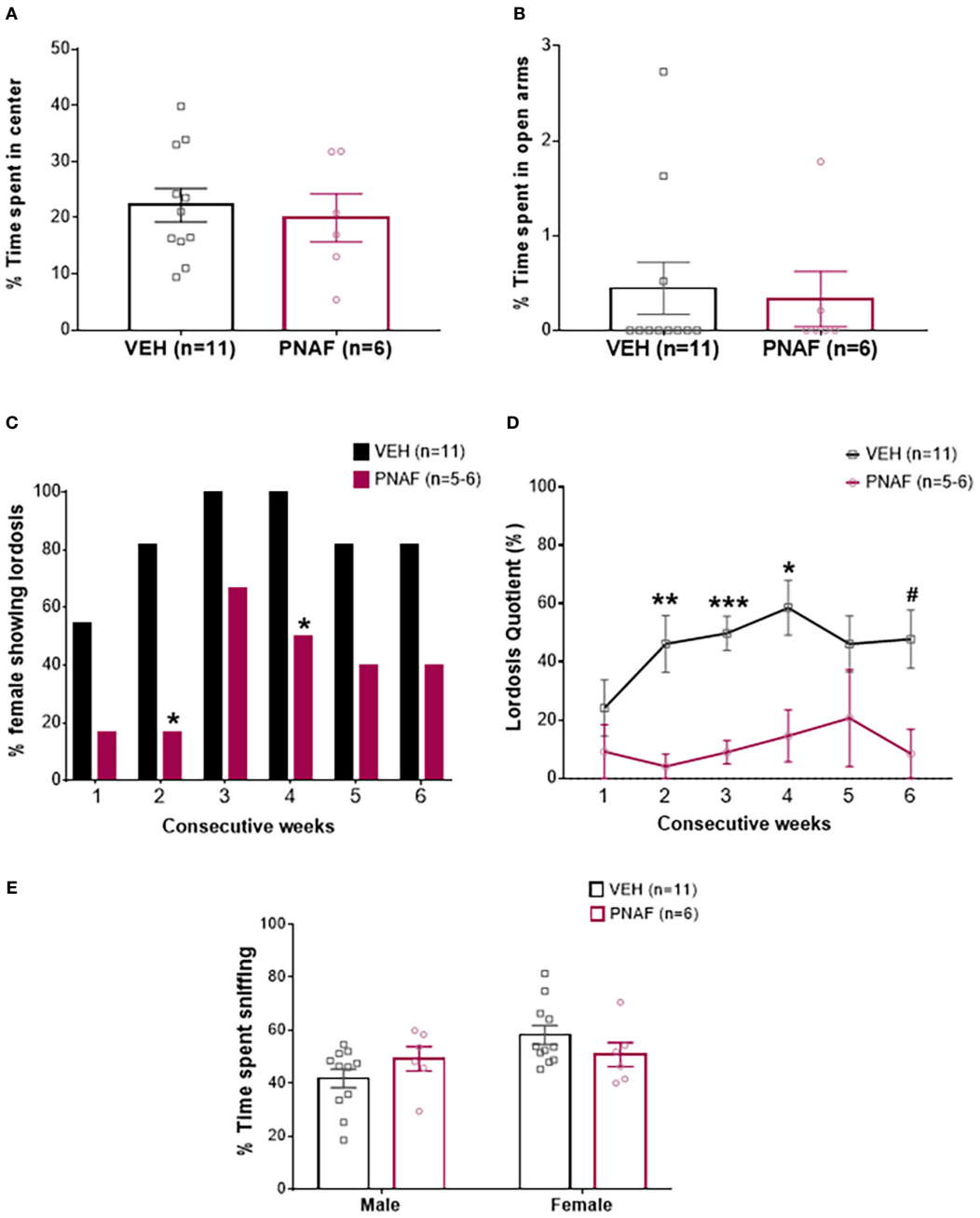

FIGURE 3
Prenatal DHT exposure significantly impairs female-typical sexual behavior in the prenatally-androgenized female mouse modeling PCOS. **(A, B)** Histograms representing the percentage of time spent in the center zone of the Open-field test **(A)** and the percentage of time spent in the open arm of the Elevated-plus maze **(B)** for the VEH female (black bars) and PNAF (magenta bars). **(C)** Histograms representing the percentage of animals showing lordosis behavior for the VEH female (black bars) and PNAF (magenta bars) over 6 consecutive weeks of testing. **(D)** Graphical curve representing the percentage of lordosis quotient, i.e. the number of lordosis behavior divided by the number of male mount trial, over the 6 consecutive weeks of testing for the VEH female (black line) and PNAF (magenta line). **(E)** Histograms representing the percentage of time spent sniffing either the male or the female compartment in the three-compartment box partner preference test for the VEH female (black bars) and PNAF (magenta bars). #p<0.06, *p<0.05, **p<0.01, ***p<0.001. VEH, control female; PNAF, prenatally androgenized female. Mean +/- SEM.

again a significant impairment of lordosis behavior in PNA female mice over the 6 consecutive tests (F (1,8) =13, $p=0.0069$). Ninety minutes following the last lordosis behavior test, animals were euthanized and neural activation was assessed by cFOS immunostaining in several brain regions known to be implicated in sexual behaviors and/or fertility regulation in female mice (Figures 6A–C). As expected, the number of cFOS-positive cells increased between control females that did not participate in lordosis behavior (Basal, n=3-4) and control females who underwent lordosis behavior tests (VEH, n=5) (Figure 6A). Indeed, a significant increase in the number of cFOS-ir positive cells was observed between the Basal and VEH female mice in the majority of the brain regions analyzed and known to be implicated in the regulation of lordosis behavior: the olfactory tuberal nucleus (TU; p=0.03), the median preoptic area (MnPOA; p=0.03), the posterior median part of the bed nucleus of the stria terminalis (BNSTpm;

TABLE 3 Prenatal DHT exposure does not affect investigative and aggressive behaviors in the adult female mice. Mean +/- SEM. W, week; PNAF, prenatally-androgenized female. Mean +/- SEM.

	Anogenital Sniffing bouts		Aggressive behaviors bouts	
	Control (n=11)	PNAF (n=5/6)	Control (n=11)	PNAF (n=5/6)
W1	0.30 +/- 0.20	1.17 +/- 0.65	3.0 +/- 0.75	5.17 +/- 1.51
W2	1.45 +/- 0.62	1.50 +/- 0.56	3.45 +/- 1.36	4.0 +/- 1.81
W3	1.91 +/-0.72	1.50 +/- 0.50	0.91 +/- 4.17	4.17 +/- 1.80
W4	0.73 +/- 0.36	1.00 +/- 0.63	2.36 +/- 0.89	1.67 +/- 0.84
W5	1.18 +/- 0.40	1.00 +/- 0.55	1.09 +/- 0.74	3.40 +/- 1.40
W6	2.55 +/- 0.79	2.20 +/- 0.86	2.64 +/- 0.86	7.20 +/- 2.69

p=0.0009), the paraventricular nucleus of the hypothalamus (PVN; p=0.01) and the dorsomedian part of the ventromedial hypothalamus (VMHdm; p=0.007) (Figure 6A). In addition, we found a trend toward an increase in cFOS-ir positive cells between Basal and VEH female mice in three other regions: the Piriform Cortex (PirCx; p=0.06), the anteroventral part of the periventricular nucleus of the third ventricle (AVPV; p=0.06) and the periaqueductal gray nucleus (PAG; p=0.067) (Figure 6A). In contrast, the numbers of cFOS-ir positive cells were not different between PNAF and VEH mice in the majority of brain regions analyzed except for the dorsomedial hypothalamus where we counted significantly lower cFOS-ir positive cells in PNAF mice (14.2 +/- 2.25) compared to VEH female mice (41 +/- 14.15) (U=1, *p=0.0159*) (Figures 6A, C).

Discussion

This study aimed to investigate how maternal androgen excess impacts adult sexual behavior in male and female offspring. We demonstrate here, that prenatally androgenized female mice that model several PCOS features (29–33, 57–61) and their male siblings exhibit altered adult sexual behaviors. We found that PNAM displayed reduced performance in some components of sexual behavior, mostly the mounting and intromission behavior parameters. However, PNAM were able to perform complete sexual behavior similarly to control males independently of their sexual experience. In contrast, PNAF exhibited impaired lordosis behavior throughout the 6 weeks of testing. In addition, female PNA mice displayed similar male-like sexual behaviors to VEH female mice after hormonal replacement with testosterone to induce male-like sexual behavior. This result demonstrates that the observed sexual dysfunction in PNAF is not likely due to masculinization of the brain. This finding is supported by the AVPV kisspeptin population size remaining unaffected in PNAF mice. These results suggest, instead, a specific impairment in the feminization of the brain in the PNA mouse model of PCOS. Noteworthy, in our study condition with PNA and VEH female mice being ovariectomized and supplemented with artificial high level of oestradiol, the PR expression is similar between the PNAF and VEH in three brain regions known to regulate lordosis behavior. This result suggests that the sexual dysfunction of the PNA female mice could have an organizational origin. Lordosis behavior-induced cFOS expression was largely unchanged, but apparently reduced activation of the DMH suggests potential avenues for future investigation. Interestingly, the sexual dysfunction experienced by women with PCOS and men with AGA has long been dismissed as an unfortunate symptom of impaired body image and self-esteem (42). Our findings suggest an alternative theory regarding the origins of PCOS-related sexual dysfunction. These data in an animal model indicate

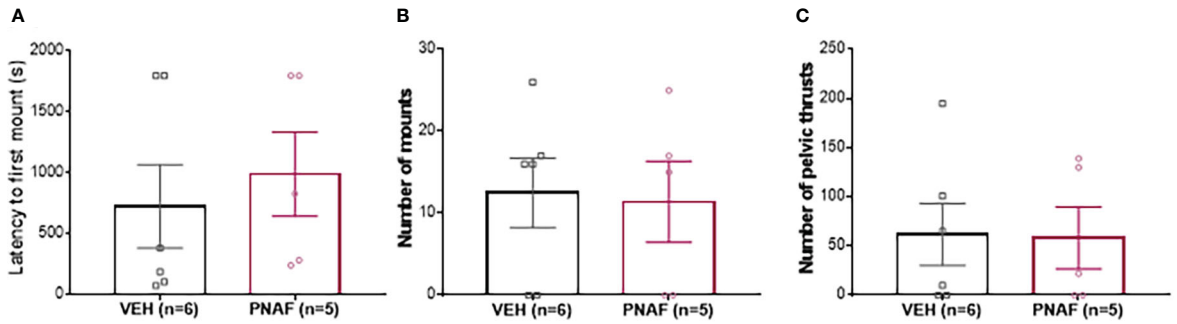

FIGURE 4
Prenatal DHT exposure does not masculinize behavior in the prenatally-androgenized female mouse modeling PCOS. **(A)** Histogram representing the latency to first mount for VEH female (black bar) and PNAF (magenta bar). **(B)** Histograms representing the number of mounts for VEH female (black bar) and PNAF (magenta bar). **(C)** Histograms representing the number of pelvic thrusts for VEH female (black bar) and PNAF (magenta bar). VEH, control female; PNAF, prenatally androgenized female. Mean +/- SEM.

10.3389/fendo.2023.1116482

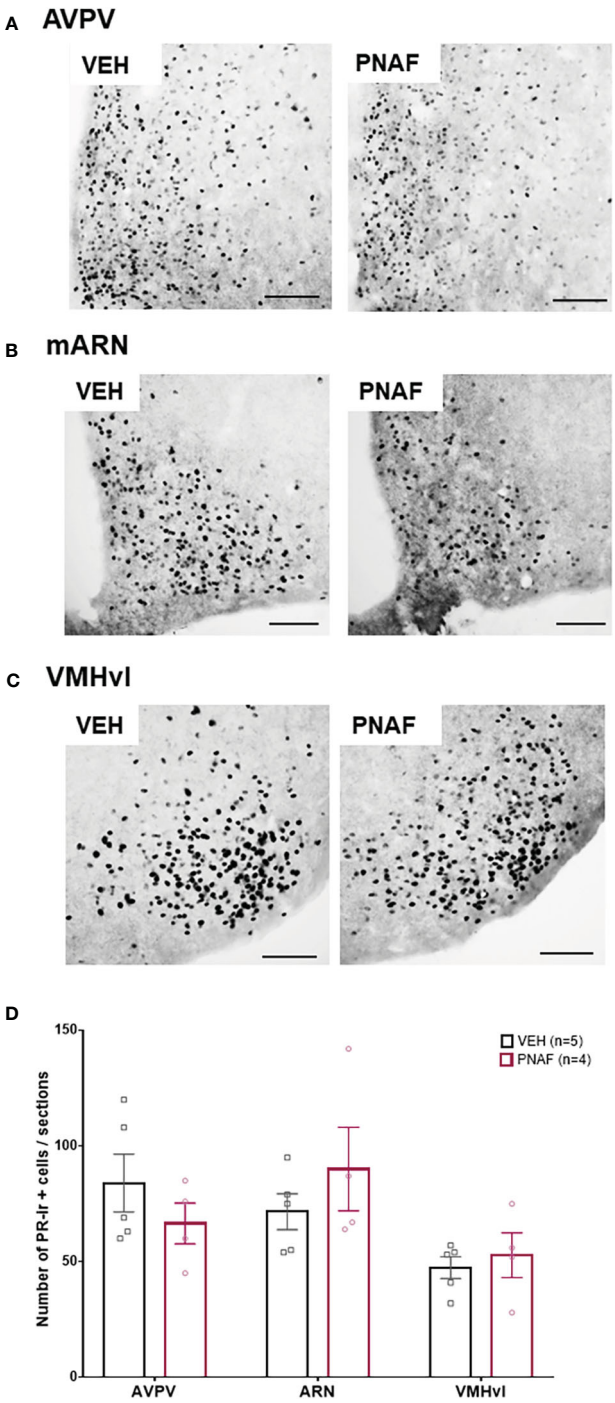

FIGURE 5
Prenatal DHT exposure does not alter adult progesterone receptor expression in after hormonal normalization. **(A–C)** Representative photomicrographs of PR immunoreactivity in the anteroventral part of the periventricular nucleus of the third ventricle **(A)**, the medial arcuate nucleus **(B)** and the ventrolateral part of the ventromedial hypothalamus **(C)** in VEH and PNA mice. **(D)** Histograms representing the number of Progesterone receptor (PR) immunoreactive cells per sections analyzed between ovariectomized and hormone replaced PNAF mice (magenta bars) and VEH female controls (black bars) within the three brain regions analyzed. AVPV, anteroventral part of the periventricular nucleus of the third ventricle; ARN, arcuate nucleus; VMHvl, ventrolateral part of the ventromedial hypothalamus. VEH, control female; PNAF, prenatally androgenized female modeling PCOS. Mean +/- SEM. Scale bar: 100µm.

programming effects of prenatal androgen excess on the regulation of adult sexual behavior. The effect of maternal androgen excess appears to vary from a pernicious effect for the male offspring to a detrimental effect for the female offspring, leading to an inability to copulate with a male. These findings may be applicable beyond PCOS, to other diseases where androgen signaling is enhanced from early life such as in congenital adrenal hyperplasia (CAH) (11, 12). Moreover, exposure to endocrine disrupting chemicals may lead to increased androgen production or androgen receptor activity at early stages of life (13–15).

10.3389/fendo.2023.1116482

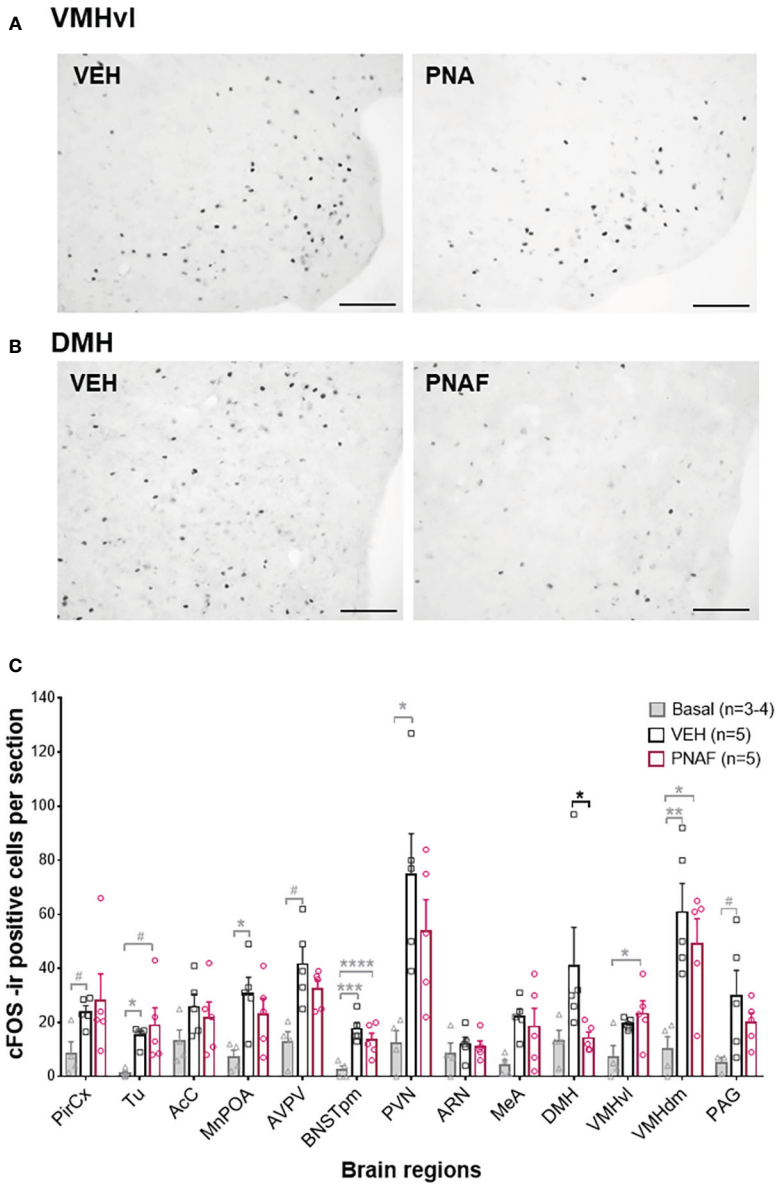

FIGURE 6
Prenatal DHT exposure decreases neural activation only in the dorsomedial hypothalamus of the PNAF modeling PCOS **(A, B)** Representative photomicrographs of cFOS immunoreactivity in the ventrolateral part of the ventromedial hypothalamus (VMHvl) **(A)** and the dorsomedial hypothalamus (DMH) in VEH and PNA mice. **(C)** Histograms representing the number of cFOS immunoreactive cells per section analyzed for each brain regions studied for Basal female who did not undergo lordosis behavior (grey bars), VEH control females (black bars) and PNAF (magenta bars) who were tested for lordosis behavior during the 6th test. Mean +/- SEM. *p<0.05, Mann-Whitney test. VEH, controls; PNA, prenatally androgenized; Pir Cx, piriform cortex nuclei; Tu, olfactory tuberal nucleus; AcC, Accumbens nucleus core; MnPOA, median preoptic area; AVPV, anteroventral part of the periventricular nucleus of the third ventricle; BNSTpm, posterior median part of the bed nucleus of the stria terminalis; PVN, parventricular nucleus of the hypothalamus; ARN, arcuate nucleus; DMH, dorsomedial hypothalamus; VMHvl, ventrolateral part of the ventromedial hypothalamus; VMHdm, dorsomedian part of the ventromedial hypothalamus, MeA, medial amygdala; VTA, ventral tegmental area; PAG, periaqueductal nucleus. # p<0.07, * p<0.05, **p<0.01, ***p<0.001, ****p<0.0001. The grey bars and grey statistical signs represent the differences between the Basal and VEH groups while the black bars and black statistical signs represent the differences between the PNAF and VEH groups. VEH = control female; PNAF= prenatally androgenized female modeling PCOS. Mean +/- SEM. Scale bar: 100µm.

Prenatal androgen exposure in male mice altered male copulatory behavior but does not alter their fertilization capabilities.

To date, most of the studies on the role of androgens on male copulatory behavior have focused on the role of testosterone, aromatized into estradiol and therefore acting on estradiol receptors for the development but also the activation of male sexual behavior (1). Studies on the role of androgens acting through the androgen receptor remains sparse (6). A set of recent studies using androgen receptor and estradiol receptors deletion within the central nervous system in mice highlighted that neural androgen receptor signaling throughout life is required for the full expression of male copulatory behavior (7, 71, 72). Studies in sheep injected with either testosterone propionate or DHT during gestation indicate that maternal androgen excess compromises the reproductive function of ram offspring (34–

38, 73) without altering sexual behavior (38). Here, we investigated for the first time, the effect of prenatal exposure to the non-aromatisable androgen, DHT. We observed an alteration only in certain sexual behaviors parameters. Indeed, naïve and experienced PNAM needed more time to perform their first attempt to mount and intromit the stimulus female. They also performed fewer mount with and without intromission as well as fewer pelvic thrusts. These results could suggest a lack of motivation for socio-sexual interaction which remains to be determined. Interestingly, at the end of both tests, a similar number of PNAM and control males were able to reach ejaculation, the endpoint of male copulatory behavior. In addition, the PNAM were more similar to VEH males after experience with only the mounting behavior remaining significantly reduced during the second test. These findings are aligned with previous work demonstrating no significant impairments in the neuroendocrine hypothalamo-pituitary-gonadal axis in PNAM mice (39). Altogether, these findings suggest that while prenatal DHT exposure disrupts some parameters of adult male copulatory behavior, mostly motivational components, the endpoint capability of the PNAM to fertilize a female mouse is unaffected. Similarly, sexual dysfunction in men with androgenic alopecia, a clinical sign of PCOS equivalent in men, has been also associated with motivation such as decreased desire and decreased sexual arousal without affecting erectile function (50).

Prenatal androgen exposure in mice specifically impairs lordosis behavior

In females, PNA resulted in a sustained impairment in lordosis behavior. In an attempt to decipher the cause of this sexual dysfunction, several behaviors related to sexual behavior that might explain the observed reduction of sexual receptivity in the PNA mouse were also examined. Anxiety and the physical ability to perform sexual behaviors are considered to be potential confounding factors that might influence an animal's ability to perform normal sexual behaviors. PCOS patients are more likely to develop anxiety and depression which have been shown to negatively impact their quality of life (41, 45, 51–54). It was therefore pertinent to determine changes in anxiety and locomotion evident in the PNAF mouse model. Previous studies have reported anxiety-like behaviors in the PNA mouse model of PCOS (59–61). However, here, no significant differences were detected in anxiety-like behaviors in PNAF mice. This discrepancy is likely to be experimental as the previous studies were performed during the light phase of the light-dark cycle i.e. the inactive phase of the animals. In the present experiment, tests were performed under a sodium lamp, which cannot be seen by mice, during the dark phase of the light-dark cycle i.e. the active phase of the animals. Those conditions are the same conditions that were used to test lordosis behavior, partner preference and male-like sexual behavior. Therefore, the decrease in lordosis behavior observed in the PNAF mice is unlikely to be due to basal anxiety or deficits in locomotion during their naturally active phase. However, we cannot rule out that the introduction of the male stimulus could have triggered an anxiety-like response similar to the one observed when the animals where tested during their inactive phase in the previous studies (59–61).

Like lordosis, male-oriented sexual partner preference is a female-typical. Behavioral tests found no overt difference in the partner preference of the PNAF mice compared to VEH females, suggesting that prenatal androgen does not impact preference for male or female scent. Ano-genital sniffing and defensive behaviors were also unchanged in PNAF, suggesting that reduced sexual motivation and/or an increase in aggression toward the male are unlikely to explain the PNA related sexual dysfunction.

In agreement with other studies, repeated testing of lordosis yielded a steady increase in the lordosis quotient over time in VEH females (3–5). PNAF mice, however, did not exhibit this same increase in lordosis quotient over time. Further investigation is needed to determine if prenatal androgen exposure modifies the neuroplasticity occurring in the brain to learn lordosis behaviors (74, 75) or other cognitive behavioral outcomes such as learning, memory, or social interactions.

Impaired sexual behaviors have also been reported in the female offspring of dams exposed to anti-mullerian hormone (prenatal AMH or PAMH mice) (76), a paradigm that also models PCOS features (77). In addition to impaired lordosis, PAMH females also demonstrated altered partner preference and increased rejection/aggression behaviors (76). Differences in partner preference and aggression behaviors between the two PCOS-like models may reflect the nature of the androgen exposure. PAMH likely drives elevated maternal testosterone, which when aromatized in the fetal brain will result in masculinization (1).

Prenatal DHT does not masculinize the female brain and behavior

How excess non-aromatisable androgens like DHT impact the development of the female brain and behavior remains poorly understood (78) despite androgen receptor being present in the female brain (6). Here, we determined that prenatal androgenization with DHT that models PCOS does not masculinize the female brain or sex behaviors. The levels of three domains of male-like sexual behaviors (latency to mount, mounting behavior and pelvic thrusting) were indistinguishable between PNAF mice and control females. These behavioral findings were supported by anatomical data demonstrating a feminized AVPV kisspeptin population as already described (79). AVPV kisspeptin neurons are a clearly sexually differentiated population in the brain, with the number of neurons decreased by the male-typical prenatal testosterone rise (67).

Organizational versus activational effects of sex steroid hormones?

Oestradiol and progesterone are crucial for the expression of female-typical rodent sexual behavior (69). In PCOS patients, progesterone and estradiol levels can be abnormal in association

with impaired folliculogenesis and ovulation. To overcome differences in circulating oestradiol and progesterone levels between PNA and VEH, animals were ovariectomized and the hormones required for lordosis behavior were replaced. This also effectively removed the adult hyperandrogenism observed in this model (29), and allowed us to investigate the potential organizational effects of prenatal exposure to DHT on sexual behaviors. Impaired lordosis in PNA mice following a normalization of circulating steroid hormones, therefore, suggests an earlier, organizational impact of sex steroids or other downstream signals on the neural substrates controlling lordosis behavior. The organizational effect of oestradiol and progesterone for feminization of the brain has been demonstrated to occur during the peripubertal period (3–5). As hormone replacement in the present study occurred in adults, after the expected rise in endogenous testosterone levels in the PNA model (at 40-50 days of age) (33), we cannot rule out an impact of this pubertal rise in androgens on the circuits mediating female-typical sexual behavior.

PCOS is associated with impaired estradiol and progesterone feedback to the reproductive axis to slow GnRH/LH secretion (21, 80, 81), suggesting a central insensitivity to steroid hormone signaling. Knowing that PNA mice also model this impaired steroid hormone feedback to the reproductive axis by exhibiting mainly a reduced number of PR expressing cells in several hypothalamic nuclei (29, 30), we investigated whether impaired lordosis may be the result of an impaired ability to respond to the artificially delivered hormones (implant of estradiol and injection of progesterone). PR was robustly expressed and not different between VEH and PNAF mice in any of the areas investigated, suggesting that exogenous hormone treatment together with the absence of hyperandrogenism can overcome the impaired progesterone feedback observed in the intact PNAF mice (29), and that this is not a likely explanation for impaired lordosis behavior.

Which neural target could explain the lordosis behavior impairment?

In an effort to identify the neural target of prenatal DHT exposure correlated with lordosis behavior impairment, cFos immunoreactivity, a proxy for neural activation, was measured after lordosis behavior in a wide range of brain regions known to be implicated in the neuronal circuitry controlling female sexual behaviors (68). Although cFos expression was significantly elevated in all of the expected regions in mice experiencing lordosis compared to a basal control group, cFos expression patterns were largely unaffected by PNA. In view of the recent evidences highlighting the role of RP3V Kisspeptin and VMHvl nNOS neurons in lordosis behavior in healthy female mice (65) as well as in the PAMH mouse model of PCOS (76), we would have expected some changes in cFOS in the RP3V and VMHvl region. As noted earlier RP3V Kisspeptin neurons remain unchanged in the PNA mice (data showed here and recently published (79). Similarly, a previous study from our group showed no changes in arcuate nucleus nNOS neurons in the PNA mice contrary to the PAMH mouse model (76). Finally, our data showed an absence of cFOS and PR changes in the VMHvl in the PNA mouse model compare to control therefore it is unlikely that VMHvl nNOS neurons could be involved in the sexual dysfunction observed in the PNA mouse model of PCOS. The changes in Kisspeptin and nNOS observed in the PAMH likely results from a masculinization of the brain circuit controlling sexual behavior since prenatal AMH treatment leads to increase testosterone level (77). Noteworthy, our cFOS data highlighted a change in the DMH, with PNAF showing reduced cFOS immunoreactivity compare to controls suggestive of reduced activation in this area. The role of the DMH in female sexual behaviors remains unclear, however, RF-amide related-peptide 3 (RFRP-3) neurons in the DMH have recently been identified as potential novel factors of female sexual motivation and behaviors in addition to their known roles in energy balance and GnRH neuron function (82). Interestingly, recent studies also showed that injection of RPRP-3 leads to suppression of either sexual motivation or receptivity in female hamsters, rats and eusocial mammals (83–85). Thus, further investigation on RFRP-3 in the PNAF mice would be of interest to decipher the potential role of RFRP-3 in the suppression of lordosis behavior.

Conclusion

These new data provide a significant step forward in our knowledge of how prenatal androgenization can influence adult sexual behaviors in male and female mice. These findings are aligned with the "Developmental Origins of Health and Diseases" (DOHaD) hypothesis in which early-life environment can increase sensitivity or risk toward developing adverse outcomes later in life. Combined with evidence that prenatal androgen exposure leads to reproductive disorders in both sexes, these findings suggest a critical sensitive period of development where both the neuroendocrine regulation of reproductive function and behavior are sensitive to androgen specifically through the androgen receptor. The underlying central mechanisms underpinning impaired sexual behavior in PCOS-like female mice and their male siblings remains to be elucidated.

Data availability statement

The raw data supporting the conclusions of this article will be made available by the authors, without undue reservation.

Ethics statement

The animal study was reviewed and approved by University of Otago Ethical committee.

Author contributions

ND, as the first author, was a honours student under the supervision of ED (co-last author). She performed most of the experiments under ED supervision. MP is an ARF within the

Campell Laboratory. She provided her technical assistance throughout the study as well as provided feedbacks on the manuscript. AR is a PhD student working on progesterone receptor changes in PCOS under supervision of ED and RC has funded ED salary throughout the duration of this study and provided feedbacks on the manuscript. ED and RC received joint funding to start the experiments in this study then ED received her own funding to complete the experimental work in this study. RC gave feedbacks on the manuscript before submission. ED has designed the experimental procedure, performed some experiments herself, supervised the first author undertaking most of the experiments, co-analyzed the results with the first author and wrote the manuscript. All authors contributed to the article and approved the submitted version.

Funding

We are grateful for support for this work from the University of Otago Department of Physiology Aim fund, awarded to RC (PI) and ED (AI), the British Society for Neuroendocrinology Support project grant awarded to ED (PI), and the New Zealand Health Research Council Program (HRC #18-671) awarded to RC and ED (HRC #21-033).

Acknowledgments

All the work presented here has been performed at the University of Otago, Dunedin, New Zealand. I would like to thank RC for her unconditional support as she helped me to start and pursue this independent project while in her laboratory. I am also grateful to Dr. Sakina Mahouty-Kodja and her team, that I recently joined, for our fruitful discussion on the male data in this paper.

Conflict of interest

The authors declare that the research was conducted in the absence of any commercial or financial relationships that could be construed as a potential conflict of interest.

Publisher's note

Supplementary material

The Supplementary Material for this article can be found online at: https://www.frontiersin.org/articles/10.3389/fendo.2023.1116482/full#supplementary-material

SUPPLEMENTARY FIGURE 1
Androgen excess disrupt oestrous cyclicity. **(A,B)** Representative examples of oestrous cyclicity of a VEH **(A)** and PNA **(B)** mice after 21 days of vaginal smears. **(C)** Histogram of the frequency of each oestrous cycle phase in VEH and PNAF mice. Mean +/- SEM. ***p<0.001, multiple t-test. VEH = control female, PNAF = prenatally androgenized female mice modeling PCOS.

SUPPLEMENTARY FIGURE 2
Characterization of the progesterone receptor antibody Abcam 63605 in the adult female mediobasal hypothalamus. To our knowledge, while this antibody has been used in mouse uterine and ovaries tissues as well as on *in vitro* GnRH neurons from embryonic mouse explants, it has not yet been characterized in the mouse brain. The specificity of this PR antibody for PR has been demonstrated in uterine tissue lacking PR. The optimal concentration was determined by a dilution series and the sensitivity to detect PR in the mouse brain was demonstrated in brain tissue from mice with increasing circulating levels of oestradiol (OVX, diestrous, OVX+E2, n=2/group), as PR expression in the female brain is dependent upon oestradiol. We observed a slight increase in PR-immunoreactivity between the female mice in diestrous and the female OVX+E2 in hypothalamic brain regions where PR expression is expected (Supplemental Figure). A complete lack of PR-immunoreactivity was observed in OVX mice, consistent with a very low circulating levels of oestradiol. These data together support the specificity and sensitivity of this PR antibody to detect physiological differences in PR expression in the mouse brain. **(A)** Representative photomicrographs of the PR immunoreactivity in the mediobasal hypothalamus of an adult female mouse on diestrous. **(B)** Representative photomicrographs of the PR immunoreactivity in the mediobasal hypothalamus of an adult female mouse after at least 2-months of ovariectomy and estradiol replacement. (OVX + E). **(C)** Representative photomicrographs of the PR immunoreactivity in the mediobasal hypothalamus of an adult female mouse after 2-months of ovariectomy (OVX). Scale bar: Top panels 200 µm; Bottom panels 100 µm.

References

1. McCarthy MM, Arnold AP. Reframing sexual differentiation of the brain. *Nat Neurosci* (2011) 14(6):677–83. doi: 10.1038/nn.2834

2. Bakker J, Brock O. Early oestrogens in shaping reproductive networks: evidence for a potential organisational role of oestradiol in female brain development. *J Neuroendocrinol* (2010) 22(7):728–35. doi: 10.1111/j.1365-2826.2010.02016.x

3. Bakker J, Honda S, Harada N, Balthazart J. The aromatase knock-out mouse provides new evidence that estradiol is required during development in the female for the expression of sociosexual behaviors in adulthood. *J Neurosci* (2002) 22(20):9104–12. doi: 10.1523/JNEUROSCI.22-20-09104.2002

4. Brock O, Baum MJ, Bakker J. The development of female sexual behavior requires prepubertal estradiol. *J Neurosci* (2011) 31(15):5574–8. doi: 10.1523/JNEUROSCI.0209-11.2011

5. Desroziers E, Brock O, Bakker J. Potential contribution of progesterone receptors to the development of sexual behavior in male and female mice. *Horm Behav* (2017) 90:31–8. doi: 10.1016/j.yhbeh.2016.05.008

6. Mhaouty-Kodja S. Role of the androgen receptor in the central nervous system. *Mol Cell Endocrinol* (2018) 465:103–12. doi: 10.1016/j.mce.2017.08.001

7. Raskin K, de Gendt K, Duittoz A, Liere P, Verhoeven G, Tronche F, et al. Conditional inactivation of androgen receptor gene in the nervous system: effects on male behavioral and neuroendocrine responses. *J Neurosci* (2009) 29(14):4461–70. doi: 10.1523/JNEUROSCI.0296-09.2009

8. Brock O, De Mees C, Bakker J. Hypothalamic expression of oestrogen receptor alpha and androgen receptor is sex-, age- and region-dependent in mice. *J Neuroendocrinol* (2015) 27(4):264–76. doi: 10.1111/jne.12258

9. Abbott DH, Dumesic DA, Levine JE. Hyperandrogenic origins of polycystic ovary syndrome - implications for pathophysiology and therapy. *Expert Rev Endocrinol Metab* (2019) 14(2):131–43. doi: 10.1080/17446651.2019.1576522

10. Lizneva D, Gavrilova-Jordan L, Walker W, Azziz R. Androgen excess: Investigations and management. *Best Pract Res Clin Obstet Gynaecol* (2016) 37:98–118. doi: 10.1016/j.bpobgyn.2016.05.003

11. Kepczynska-Nyk A, Kurylowicz A, Nowak A, Bednarczuk T, Ambroziak U. Sexual function in women with androgen excess disorders: Classic forms of congenital adrenal hyperplasia and polycystic ovary syndrome. *J Endocrinol Invest* (2021) 44(3):505–13. doi: 10.1007/s40618-020-01332-3

12. Schernthaner-Reiter MH, Baumgartner-Parzer S, Egarter HC, Krebs M, Kautzky-Willer A, Kirchheiner K, et al. Influence of genotype and hyperandrogenism on sexual function in women with congenital adrenal hyperplasia. *J Sex Med* (2019) 16(10):1529–40. doi: 10.1016/j.jsxm.2019.07.009

13. Gray LEJr., Wilson VS, Stoker T, Lambright C, Furr J, Noriega N, et al. Adverse effects of environmental antiandrogens and androgens on reproductive development in mammals. *Int J Androl* (2006) 29(1):96–104. doi: 10.1111/j.1365-2605.2005.00636.x

14. Ho SM, Cheong A, Adgent MA, Veevers J, Suen AA, Tam NNC, et al. Environmental factors, epigenetics, and developmental origin of reproductive disorders. *Reprod Toxicol* (2017) 68:85–104. doi: 10.1016/j.reprotox.2016.07.011

15. Mhaouty-Kodja S, Naule L, Capela D. Sexual behavior: From hormonal regulation to endocrine disruption. *Neuroendocrinol* (2018) 107(4):400–16. doi: 10.1159/000494558

16. Lizneva D, Suturina L, Walker W, Brakta S, Gavrilova-Jordan L, Azziz R. Criteria, prevalence, and phenotypes of polycystic ovary syndrome. *Fertil Steril* (2016) 106(1):6–15. doi: 10.1016/j.fertnstert.2016.05.003

17. Azziz R. PCOS: a diagnostic challenge. *Reprod BioMed Online* (2004) 8(6):644–8. doi: 10.1016/S1472-6483(10)61644-6

18. Farquhar CM, Birdsall M, Manning P, Mitchell JM, France JT. The prevalence of polycystic ovaries on ultrasound scanning in a population of randomly selected women. *Aust N Z J Obstet Gynaecol* (1994) 34(1):67–72. doi: 10.1111/j.1479-828X.1994.tb01041.x

19. Coyle C, Campbell RE. Pathological pulses in PCOS. *Mol Cell Endocrinol* (2019) 498:110561. doi: 10.1016/j.mce.2019.110561

20. Ruddenklau A, Campbell RE. Neuroendocrine impairments of polycystic ovary syndrome. *Endocrinol* (2019) 160(10):2230–42. doi: 10.1210/en.2019-00428

21. Eagleson CA, Gingrich MB, Pastor CL, Arora TK, Burt CM, Evans WS, et al. Polycystic ovarian syndrome: evidence that flutamide restores sensitivity of the gonadotropin-releasing hormone pulse generator to inhibition by estradiol and progesterone. *J Clin Endocrinol Metab* (2000) 85(11):4047–52 doi: 10.1210/jcem.85.11.6992.

22. Moore AM, Campbell RE. Polycystic ovary syndrome: Understanding the role of the brain. *Front Neuroendocrinol* (2017) 46:1–14. doi: 10.1016/j.yfrne.2017.05.002

23. Cannarella R, Condorelli RA, Mongioi LM, La Vignera S, Calogero AE. Does a male polycystic ovarian syndrome equivalent exist? *J Endocrinol Invest* (2018) 41(1):49–57. doi: 10.1007/s40618-017-0728-5

24. Di Guardo F, Ciotta L, Monteleone M, Palumbo M. Male Equivalent polycystic ovarian syndrome: Hormonal, metabolic, and clinical aspects. *Int J Fertil Steril* (2020) 14 (2):79–83 doi: 10.22074/ijfs.2020.6092.

25. Liu DM, Torchen LC, Sung Y, Paparodis R, Legro RS, Grebe SK, et al. Evidence for gonadotrophin secretory and steroidogenic abnormalities in brothers of women with polycystic ovary syndrome. *Hum Reprod* (2014) 29(12):2764–72. doi: 10.1093/humrep/deu282

26. Sanke S, Chander R, Jain A, Garg T, Yadav P. A comparison of the hormonal profile of early androgenetic alopecia in men with the phenotypic equivalent of polycystic ovarian syndrome in women. *JAMA Dermatol* (2016) 152(9):986–91. doi: 10.1001/jamadermatol.2016.1776

27. Stener-Victorin E, Padmanabhan V, Walters KA, Campbell RE, Benrick A, Giacobini P, et al. Animal models to understand the etiology and pathophysiology of polycystic ovary syndrome. *Endocr Rev* (2020) 41(4). doi: 10.1210/endrev/bnaa010

28. Cesta CE, Mansson M, Palm C, Lichtenstein P, Iliadou AN, Landen M. Polycystic ovary syndrome and psychiatric disorders: Co-morbidity and heritability in a nationwide Swedish cohort. *Psychoneuroendocrinol* (2016) 73:196–203. doi: 10.1016/j.psyneuen.2016.08.005

29. Moore AM, Prescott M, Campbell RE. Estradiol negative and positive feedback in a prenatal androgen-induced mouse model of polycystic ovarian syndrome. *Endocrinol* (2013) 154(2):796–806. doi: 10.1210/en.2012-1954

30. Moore AM, Prescott M, Marshall CJ, Yip SH, Campbell RE. Enhancement of a robust arcuate GABAergic input to gonadotropin-releasing hormone neurons in a model of polycystic ovarian syndrome. *Proc Natl Acad Sci U S A* (2015) 112(2):596–601. doi: 10.1073/pnas.1415038112

31. Sullivan SD, Moenter SM. Prenatal androgens alter GABAergic drive to gonadotropin-releasing hormone neurons: Implications for a common fertility disorder. *Proc Natl Acad Sci U S A* (2004) 101(18):7129–34. doi: 10.1073/pnas.0308058101

32. Marshall CJ, Desroziers E, McLennan T, Campbell RE. Defining subpopulations of arcuate nucleus GABA neurons in Male, female, and prenatally androgenized female mice. *Neuroendocrinol* (2017) 105(2):157–69. doi: 10.1159/000452105

33. Silva MS, Prescott M, Campbell RE. Ontogeny and reversal of brain circuit abnormalities in a preclinical model of PCOS. *JCI Insight* (2018) 3(7). doi: 10.1172/jci.insight.99405

34. Recabarren SE, Lobos A, Figueroa Y, Padmanabhan V, Foster DL, Sir-Petermann T. Prenatal testosterone treatment alters LH and testosterone responsiveness to GnRH agonist in male sheep. *Biol Res* (2007) 40(3):329–38. doi: 10.4067/S0716-97602007000400007

35. Recabarren SE, Recabarren M, Sandoval D, Carrasco A, Padmanabhan V, Rey R, et al. Puberty arises with testicular alterations and defective AMH expression in rams prenatally exposed to testosterone. *Domest Anim Endocrinol* (2017) 61:100–7. doi: 10.1016/j.domaniend.2017.06.004

36. Recabarren SE, Rojas-Garcia PP, Recabarren MP, Alfaro VH, Smith R, Padmanabhan V, et al. Prenatal testosterone excess reduces sperm count and motility. *Endocrinol* (2008) 149(12):6444–8. doi: 10.1210/en.2008-0785

37. Rojas-Garcia PP, Recabarren MP, Sarabia L, Schon J, Gabler C, Einspanier R, et al. Prenatal testosterone excess alters sertoli and germ cell number and testicular FSH receptor expression in rams. *Am J Physiol Endocrinol Metab* (2010) 299(6):E998–E1005. doi: 10.1152/ajpendo.00032.2010

38. Scully CM, Estill CT, Amodei R, McKune A, Gribbin KP, Meaker M, et al. Early prenatal androgen exposure reduces testes size and sperm concentration in sheep without altering neuroendocrine differentiation and masculine sexual behavior. *Domest Anim Endocrinol* (2018) 62:1–9. doi: 10.1016/j.domaniend.2017.07.001

39. Holland S, Prescott M, Pankhurst M, Campbell RE. The influence of maternal androgen excess on the male reproductive axis. *Sci Rep* (2019) 9(1):18908. doi: 10.1038/s41598-019-55436-9

40. Davis SR, Worsley R, Miller KK, Parish SJ, Santoro N. Androgens and female sexual function and dysfunction–findings from the fourth international consultation of sexual medicine. *J Sex Med* (2016) 13(2):168–78. doi: 10.1016/j.jsxm.2015.12.033

41. Elsenbruch S, Hahn S, Kowalsky D, Offner AH, Schedlowski M, Mann K, et al. Quality of life, psychosocial well-being, and sexual satisfaction in women with polycystic ovary syndrome. *J Clin Endocrinol Metab* (2003) 88(12):5801–7. doi: 10.1210/jc.2003-030562

42. Fliegner M, Richter-Appelt H, Krupp K, Brunner F. Sexual function and socio-sexual difficulties in women with polycystic ovary syndrome (PCOS). *Geburtshilfe Frauenheilkd* (2019) 79(5):498–509. doi: 10.1055/a-0828-7901

43. Hashemi S, Ramezani Tehrani F, Farahmand M, Bahri Khomami M. Association of PCOS and its clinical signs with sexual function among Iranian women affected by PCOS. *J Sex Med* (2014) 11(10):2508–14. doi: 10.1111/jsm.12627

44. Kowalczyk R, Skrzypulec V, Lew-Starowicz Z, Nowosielski K, Grabski B, Merk W. Psychological gender of patients with polycystic ovary syndrome. *Acta Obstet Gynecol Scand* (2012) 91(6):710–4. doi: 10.1111/j.1600-0412.2012.01408.x

45. Mansson M, Norstrom K, Holte J, Landin-Wilhelmsen K, Dahlgren E, Landen M. Sexuality and psychological wellbeing in women with polycystic ovary syndrome compared with healthy controls. *Eur J Obstet Gynecol Reprod Biol* (2011) 155(2):161–5. doi: 10.1016/j.ejogrb.2010.12.012

46. Nohr EA, Hansen AB, Andersen MS, Hjorth S. Sexual health in parous women with a history of polycystic ovary syndrome: A national cross-sectional study in Denmark. *Int J Gynaecol Obstet* (2021) 157(3):702-9 doi: 10.1002/ijgo.13911

47. Noroozzadeh M, Ramezani Tehrani F, Bahri Khomami M, Azizi F. A comparison of sexual function in women with polycystic ovary syndrome (PCOS) whose mothers had PCOS during their pregnancy period with those without PCOS. *Arch Sex Behav* (2017) 46 (7):2033–42. doi: 10.1007/s10508-016-0919-8

48. Thannickal A, Brutocao C, Alsawas M, Morrow A, Zaiem F, Murad MH, et al. Eating, sleeping and sexual function disorders in women with polycystic ovary syndrome (PCOS): A systematic review and meta-analysis. *Clin Endocrinol (Oxf)* (2020) 92(4):338–49. doi: 10.1111/cen.14153

49. Haber RS, Gupta AK, Epstein E, Carviel JL, Foley KA. Finasteride for androgenetic alopecia is not associated with sexual dysfunction: A survey-based, single-centre, controlled study. *J Eur Acad Dermatol Venereol* (2019) 33(7):1393–7. doi: 10.1111/jdv.15548

50. Molina-Leyva A, Caparros-Del Moral I, Gomez-Avivar P, Alcalde-Alonso M, Jimenez-Moleon JJ. Psychosocial impairment as a possible cause of sexual dysfunction among young men with mild androgenetic alopecia: A cross-sectional crowdsourcing web-based study. *Acta Dermatovenerol Croat* (2016) 24(1):42–8.

51. Chaudhari AP, Mazumdar K, Mehta PD. Anxiety, depression, and quality of life in women with polycystic ovarian syndrome. *Indian J Psychol Med* (2018) 40(3):239–46. doi: 10.4103/IJPSYM.IJPSYM_561_17

52. Cooney LG, Lee I, Sammel MD, Dokras A. High prevalence of moderate and severe depressive and anxiety symptoms in polycystic ovary syndrome: A systematic review and meta-analysis. *Hum Reprod* (2017) 32(5):1075–91. doi: 10.1093/humrep/dex044

53. Damone AL, Joham AE, Loxton D, Earnest A, Teede HJ, Moran LJ. Depression, anxiety and perceived stress in women with and without PCOS: A community-based study. *Psychol Med* (2019) 49(9):1510–20. doi: 10.1017/S0033291718002076

54. Dokras A, Stener-Victorin E, Yildiz BO, Li R, Ottey S, Shah D, et al. Androgen excess- polycystic ovary syndrome society: Position statement on depression, anxiety, quality of life, and eating disorders in polycystic ovary syndrome. *Fertil Steril* (2018) 109 (5):888–99. doi: 10.1016/j.fertnstert.2018.01.038

55. Liu M, Murthi S, Poretsky L. Polycystic ovary syndrome and gender identity. *Yale J Biol Med* (2020) 93(4):529–37.

56. Wahlin-Jacobsen S, Pedersen AT, Kristensen E, Laessoe NC, Lundqvist M, Cohen AS, et al. Is there a correlation between androgens and sexual desire in women? *J Sex Med* (2015) 12(2):358–73. doi: 10.1111/jsm.12774

57. Roland AV, Nunemaker CS, Keller SR, Moenter SM. Prenatal androgen exposure programs metabolic dysfunction in female mice. *J Endocrinol* (2010) 207(2):213–23. doi: 10.1677/JOE-10-0217

58. Sati A, Prescott M, Holland S, Jasoni CL, Desroziers E, Campbell RE. Morphological evidence indicates a role for microglia in shaping the PCOS-like brain. *J Neuroendocrinol* (2021) 33(8):e12999. doi: 10.1111/jne.12999

59. Manti M, Fornes R, Qi X, Folmerz E, Linden Hirschberg A, de Castro Barbosa T, et al. Maternal androgen excess and obesity induce sexually dimorphic anxiety-like behavior in the offspring. *FASEB J* (2018) 32(8):4158–71. doi: 10.1096/fj.201701263RR

60. Risal S, Manti M, Lu H, Fornes R, Larsson H, Benrick A, et al. Prenatal androgen exposure causes a sexually dimorphic transgenerational increase in offspring susceptibility to anxiety disorders. *Transl Psychiatry* (2021) 11(1):45. doi: 10.1038/s41398-020-01183-9

61. Risal S, Pei Y, Lu H, Manti M, Fornes R, Pui HP, et al. Prenatal androgen exposure and transgenerational susceptibility to polycystic ovary syndrome. *Nat Med* (2019) 25 (12):1894–904. doi: 10.1038/s41591-019-0666-1

62. Brock O, Bakker J. Potential contribution of prenatal estrogens to the sexual differentiation of mate preferences in mice. *Horm Behav* (2011) 59(1):83–9. doi: 10.1016/j.yhbeh.2010.10.012

63. Jean A, Bonnet P, Liere P, Mhaouty-Kodja S, Hardin-Pouzet H. Revisiting medial preoptic area plasticity induced in male mice by sexual experience. *Sci Rep* (2017) 7 (1):17846. doi: 10.1038/s41598-017-18248-3

64. Jean A, Mhaouty-Kodja S, Hardin-Pouzet H. Hypothalamic cellular and molecular plasticity linked to sexual experience in male rats and mice. *Front Neuroendocrinol* (2021) 63:100949. doi: 10.1016/j.yfrne.2021.100949

65. Hellier V, Brock O, Candlish M, Desroziers E, Aoki M, Mayer C, et al. Female sexual behavior in mice is controlled by kisspeptin neurons. *Nat Commun* (2018) 9 (1):400. doi: 10.1038/s41467-017-02797-2

66. Clarkson J, Herbison AE. Postnatal development of kisspeptin neurons in mouse hypothalamus; sexual dimorphism and projections to gonadotropin-releasing hormone neurons. *Endocrinol* (2006) 147(12):5817–25. doi: 10.1210/en.2006-0787

67. Clarkson J, Busby ER, Kirilov M, Schutz G, Sherwood NM, Herbison AE. Sexual differentiation of the brain requires perinatal kisspeptin-GnRH neuron signaling. *J Neurosci* (2014) 34(46):15297–305. doi: 10.1523/JNEUROSCI.3061-14.2014

68. Blaustein JD. Neuroendocrine regulation of feminine sexual behavior: lessons from rodent models and thoughts about humans. *Annu Rev Psychol* (2008) 59:93–118. doi: 10.1146/annurev.psych.59.103006.093556

69. Blaustein JD, Tetel MJ, Ricciardi KH, Delville Y, Turcotte JC. Hypothalamic ovarian steroid hormone-sensitive neurons involved in female sexual behavior. *Psychoneuroendocrinology* (1994) 19(5-7):505–16. doi: 10.1016/0306-4530(94)90036-1

70. Pfaff D, Frohlich J, Morgan M. Hormonal and genetic influences on arousal–sexual and otherwise. *Trends Neurosci* (2002) 25(1):45–50. doi: 10.1016/S0166-2236(00)02084-1

71. Naule L, Marie-Luce C, Parmentier C, Martini M, Albac C, Trouillet AC, et al. Revisiting the neural role of estrogen receptor beta in male sexual behavior by conditional mutagenesis. *Horm Behav* (2016) 80:1–9. doi: 10.1016/j.yhbeh.2016.01.014

72. Trouillet AC, Ducroq S, Naule L, Capela D, Parmentier C, Radovick S, et al. Deletion of neural estrogen receptor alpha induces sex differential effects on reproductive behavior in mice. *Commun Biol* (2022) 5(1):383. doi: 10.1038/s42003-022-03324-w

73. Bormann CL, Smith GD, Padmanabhan V, Lee TM. Prenatal testosterone and dihydrotestosterone exposure disrupts ovine testicular development. *Reproduction* (2011) 142(1):167–73. doi: 10.1530/REP-10-0210

74. Herrera-Morales WV, Herrera-Solis A, Nunez-Jaramillo L. Sexual behavior and synaptic plasticity. *Arch Sex Behav* (2019) 48(8):2617–31. doi: 10.1007/s10508-019-01483-2

75. Meisel RL, Mullins AJ. Sexual experience in female rodents: cellular mechanisms and functional consequences. *Brain Res* (2006) 1126(1):56–65. doi: 10.1016/j.brainres.2006.08.050

76. Silva MSB, Decoster L, Trova S, Mimouni NEH, Delli V, Chachlaki K, et al. Female sexual behavior is disrupted in a preclinical mouse model of PCOS via an attenuated hypothalamic nitric oxide pathway. *Proc Natl Acad Sci U S A* (2022) 119(30): e2203503119. doi: 10.1073/pnas.2203503119

77. Tata B, Mimouni NEH, Barbotin AL, Malone SA, Loyens A, Pigny P, et al. Elevated prenatal anti-mullerian hormone reprograms the fetus and induces polycystic ovary syndrome in adulthood. *Nat Med* (2018) 24(6):834–46. doi: 10.1038/s41591-018-0035-5

78. Handa RJ, Pak TR, Kudwa AE, Lund TD, Hinds L. An alternate pathway for androgen regulation of brain function: Activation of estrogen receptor beta by the metabolite of dihydrotestosterone, 5alpha-androstane-3beta,17beta-diol. *Horm Behav* (2008) 53(5):741–52. doi: 10.1016/j.yhbeh.2007.09.012

79. Jamieson BB, Moore AM, Lohr DB, Thomas SX, Coolen LM, Lehman MN, et al. Prenatal androgen treatment impairs the suprachiasmatic nucleus arginine-vasopressin to kisspeptin neuron circuit in female mice. *Front Endocrinol (Lausanne)* (2022) 13:951344. doi: 10.3389/fendo.2022.951344

80. Sir-Petermann T, Codner E, Perez V, Echiburu B, Maliqueo M, Ladron de Guevara A, et al. Metabolic and reproductive features before and during puberty in daughters of women with polycystic ovary syndrome. *J Clin Endocrinol Metab* (2009) 94(6):1923–30. doi: 10.1210/jc.2008-2836

81. Stener-Victorin E, Holm G, Labrie F, Nilsson L, Janson PO, Ohlsson C. Are there any sensitive and specific sex steroid markers for polycystic ovary syndrome? *J Clin Endocrinol Metab* (2010) 95(2):810–9. doi: 10.1210/jc.2009-1908

82. Anjum S, Khattak MNK, Tsutsui K, Krishna A. RF-amide related peptide-3 (RFRP-3): A novel neuroendocrine regulator of energy homeostasis, metabolism, and reproduction. *Mol Biol Rep* (2021) 48(2):1837–52. doi: 10.1007/s11033-021-06198-z

83. Peragine DE, Pokarowski M, Mendoza-Viveros L, Swift-Gallant A, Cheng HM, Bentley GE, et al. RFamide-related peptide-3 (RFRP-3) suppresses sexual maturation in a eusocial mammal. *Proc Natl Acad Sci U S A* (2017) 114(5):1207–12. doi: 10.1073/pnas.1616913114

84. Rahdar P, Khazali H. Rfamide-related peptide-3 suppresses the substance p-induced promotion of the reproductive performance in female rats modulating hypothalamic kisspeptin expression. *Exp Brain Res* (2020) 238(11):2457–67. doi: 10.1007/s00221-020-05860-5

85. Schneider JE, Benton NA, Russo KA, Klingerman CM, Williams WP3rd, Simberlund J, et al. RFamide-related peptide-3 and the trade-off between reproductive and ingestive behavior. *Integr Comp Biol* (2017) 57(6):1225–39. doi: 10.1093/icb/icx097

frontiers | Frontiers in Endocrinology

TYPE Review
PUBLISHED 08 March 2023
DOI 10.3389/fendo.2023.1100007

OPEN ACCESS

EDITED BY
Alexandre Benani,
Centre National de la Recherche Scientifique (CNRS), France

REVIEWED BY
Fahrettin Kelestimur,
Yeditepe University, Türkiye
Paolo Marzullo,
Università degli Studi del Piemonte Orientale, Italy
Mattia Barbot,
University Hospital of Padua, Italy

*CORRESPONDENCE
Nunzia Prencipe
nunzia.prencipe@gmail.com

SPECIALTY SECTION
This article was submitted to Neuroendocrine Science, a section of the journal Frontiers in Endocrinology

RECEIVED 16 November 2022
ACCEPTED 21 February 2023
PUBLISHED 08 March 2023

CITATION
Prencipe N, Marinelli L, Varaldo E, Cuboni D, Berton AM, Bioletto F, Bona C, Gasco V and Grottoli S (2023) Isolated anterior pituitary dysfunction in adulthood. *Front. Endocrinol.* 14:1100007. doi: 10.3389/fendo.2023.1100007

Isolated anterior pituitary dysfunction in adulthood

Nunzia Prencipe *, Lorenzo Marinelli, Emanuele Varaldo, Daniela Cuboni, Alessandro Maria Berton, Fabio Bioletto, Chiara Bona, Valentina Gasco and Silvia Grottoli

Department of Medical Science, Division of Endocrinology, Diabetes and Metabolism, University of Turin, Turin, Italy

Hypopituitarism is defined as a complete or partial deficiency in one or more pituitary hormones. Anterior hypopituitarism includes secondary adrenal insufficiency, central hypothyroidism, hypogonadotropic hypogonadism, growth hormone deficiency and prolactin deficiency. Patients with hypopituitarism suffer from an increased disability and sick days, resulting in lower health status, higher cost of care and an increased mortality. In particular during adulthood, isolated pituitary deficits are not an uncommon finding; their clinical picture is represented by vague symptoms and unclear signs, which can be difficult to properly diagnose. This often becomes a challenge for the physician. Aim of this narrative review is to analyse, for each anterior pituitary deficit, the main related etiologies, the characteristic signs and symptoms, how to properly diagnose them (suggesting an easy and reproducible step-based approach), and eventually the treatment. In adulthood, the vast majority of isolated pituitary deficits are due to pituitary tumours, head trauma, pituitary surgery and brain radiotherapy. Immune-related dysfunctions represent a growing cause of isolated pituitary deficiencies, above all secondary to use of oncological drugs such as immune checkpoint inhibitors. The diagnosis of isolated pituitary deficiencies should be based on baseline hormonal assessments and/or dynamic tests. Establishing a proper diagnosis can be quite challenging: in fact, even if the diagnostic methods are becoming increasingly refined, a considerable proportion of isolated pituitary deficits still remains without a certain cause. While isolated ACTH and TSH deficiencies always require a prompt replacement treatment, gonadal replacement therapy requires a benefit-risk evaluation based on the presence of comorbidities, age and gender of the patient; finally, the need of growth hormone replacement therapies is still a matter of debate. On the other side, prolactin replacement therapy is still not available. In conclusion, our purpose is to offer a broad evaluation from causes to therapies of isolated anterior pituitary deficits in adulthood. This review will also include the evaluation of uncommon symptoms and main etiologies, the elements of suspicion of a genetic cause and protocols for diagnosis, follow-up and treatment.

KEYWORDS

hypopituitarism, traumatic brain injury, radiotherapy, hypocortisolism, hypothyroidism, hypogonadism, hypoprolactinemia, growth hormone deficiency

10.3389/fendo.2023.1100007

1 Background

Hypopituitarism is defined as a complete or partial deficiency in one or more pituitary hormones. It can be a result of diseases that either reduce or abolish the pituitary function or which can interfere with pituitary stalk integrity or the hypothalamic secretion of pituitary-releasing hormones. The prevalence of hypopituitarism is approximately 45 cases per 100.000 and the incidence of about 4 cases per 100.000 per year (1). Anterior hypopituitarism can include central adrenal insufficiency (CAI), central hypothyroidism (CH), hypogonadotropic hypogonadism (HH), growth hormone deficiency (GHD) and seldom hypoprolactinemia. Patients with hypopituitarism suffer from an increased disability and sick days, resulting in lower health status, higher cost of care and an increased mortality (2).

Pituitary deficits usually present as combined; in adulthood, however, it is not uncommon to develop isolated pituitary deficits as well. This often becomes a diagnostic challenge for the physicians due to several reasons: the clinical picture may be vague and baseline and dynamic hormonal assessments may not be fully reliable. For these reasons, a considerable proportion of isolated pituitary deficits still remains without a defined cause and thus precise data on their prevalence and incidence are lacking.

The aim of this narrative review is to analyse the main etiopathogenetic processes that lead to isolated anterior pituitary deficits, focusing on their signs, symptoms, hormonal evaluations, and treatments. It is important to remark that there is a lack of guidelines for the specific management of isolated anterior pituitary deficits; as such, part of the evidence related to diagnosis and management of these conditions derives from current knowledge regarding hypopituitarism.

2 Common and shared causes of isolated pituitary deficiencies

Before discussing the specific causes linked to each anterior pituitary deficit, it is pivotal to describe the most common causes that can induce isolated deficits in adulthood (Table 1). Among them, pituitary region masses (tumors and infiltrative diseases), treatments as neurosurgery and radiotherapy, autoimmune diseases and traumatic brain injuries (TBI) are surely to be considered. Genetic causes generally determine isolated deficits with an onset early in childhood, but HH and CH can be linked to altered genes that can manifest even later in life (3, 4).

2.1 Pituitary tumors

Pituitary dysfunction, as a consequence of intrasellar tumor masses originating from the pituitary or Rathke's pouch, is a well-known problem. Sellar masses are often associated with combined pituitary deficits, and these are induced by the tumor itself or by further damage secondary to surgery, radiotherapy, or medical therapies. However, at diagnosis no hormonal deficits can be reported and they may develop only during the follow-up, generally as a consequence of the tumor growth (5).

TABLE 1 Main causes of isolated pituitary deficits.

CAUSES OF ISOLATED PITUITARY DEFICIENCIES
ACQUIRED CAUSES
Pituitary tumors: • Hormone-secreting adenoma • Non-functioning adenoma
Non pituitary tumors: • Rathke's cleft cyst, Craniopharyngioma, Meningioma, Chordoma, Astrocytoma, Ependymoma, Germinoma, Lymphoma, others • Metastases
Oncological treatments: • Neurosurgery • Irradiation • Chemotherapy
Infiltrative disorders: • Sarcoidosis, Wegener granulomatosis, Haemochromatosis, Langerhans cell Histiocytosis, Erdheim–Chester disease
Autoimmune diseases: • Primary hypophysitis (lymphocytic, granulomatous, xanthomatous, necrotizing) • Drug induced hypophysitis (Immune checkpoint inhibitors: PD1, PDL1, CTLA4 inhibitors)
Traumatic brain injuries and vascular damage: • Traumatic brain injury • Sub-arachnoid haemorrhage • Stroke • Pituitary apoplexy • Sheehan syndrome
Drugs
Idiopathic
GENETIC CAUSES

2.2 Irradiation

The potential damage induced by radiotherapy is usually confined to the anterior pituitary gland. The sensitivity to radiation is quite different for each hypothalamic-pituitary axis (Figure 1). The GH (growth hormone)-secreting cells are the most sensitive, followed by the FSH (Follicle-Stimulating Hormone)- and LH (Luteinizing Hormone)-secreting cells, while those secreting ACTH (Adrenocorticotropic Hormone) and TSH (Thyroid Stimulating Hormone) are the most resistant (6, 7). In agreement with these observations, a single dose of 3 Gray (Gy) has been reported to impair the *in vitro* secretion of GH (and prolactin) by pituitary cells, whereas TSH-secreting cells have proven to be resistant to doses higher than 10 Gy (8). Although lower than conventional radiotherapy, the risk of onset of hypopituitarism needs to be considered also in patients undergoing sellar/parasellar post-surgery gamma knife radiosurgery (GKRS), with an approximate incidence rate of hypopituitarism of 18–32% both for non-secreting and secreting adenomas (9, 10). The delayed onset of post-GKRS hypopituitarism has been reported in a few studies,

10.3389/fendo.2023.1100007

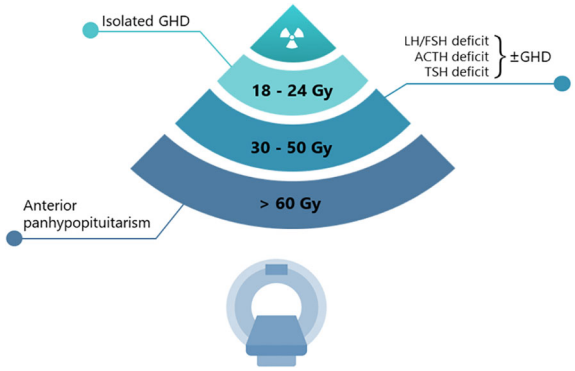

FIGURE 1
Radiation progressive damage of pituitary function.

approximately occurring 22–25 months after treatment and with an increased rate over time (11).

2.3 Other than pituitary tumors

Pituitary dysfunction can also be the result of brain damage due to extra-pituitary tumors (and their surgical treatment). For example, an emerging clinical entity is primary lymphoma, localized in the sellar region (12). However, after a long-term disease remission, patients who suffered from lymphoma can experience gradual reverse of hypopituitarism up to a residual isolated pituitary deficit (13). Moreover, chemotherapy (14) or irradiation might cause additional pituitary insufficiencies. In their study, Schneider et al. (15) recorded isolated pituitary hormone deficits in 16.2% of patients diagnosed and treated for an extra-sellar tumor. Endocrine deficiencies may become evident from 3 months to more than 10 years after irradiation (7).

2.4 Infiltrative diseases

Rare causes of hypopituitarism include infiltrative disorders such as neurosarcoidosis, Wegener granulomatosis, hemochromatosis, Langerhans cell histiocytosis and Erdheim–Chester disease. Diabetes insipidus usually represents the onset of these diseases; however, in all unknown cases of anterior hypopituitarism they need to be ruled out (16).

2.5 Autoimmune disease and drug induced autoimmune disorders

Based on histological features, primary hypophysitis is classified as lymphocytic, granulomatous, xanthomatous or necrotizing inflammation (17, 18). Lymphocytic hypophysitis is the most frequent (19) and it is caused by immune-mediated diffuse infiltration of lymphocytes and plasma cells. IgG4-related hypophysitis is a recently discovered subtype of autoimmune disorder associated with multiorgan IgG4-related systemic disease (IgG4-RD). Pituitary involvement of IgG4-RD had initially been considered rare, but more recent studies (20) suggested that its prevalence is underestimated. In these conditions, isolated anterior pituitary hormone deficiencies and/or central diabetes insipidus could be observed. Pituitary inflammation may also be secondary to several kinds of drugs. Although various forms of drug-induced hypophysitis have been reported, with the inclusion of immunotherapy for many types of cancer, immune checkpoint inhibitor (ICPi)-induced hypophysitis has recently emerged as a not uncommon immune-related adverse event. Interestingly, relatively specific hormone deficiency has been detected in these cases, as described in the following paragraphs (21).

2.6 Traumatic brain injuries, vascular damage and infective diseases

Pituitary hormone deficiency is frequent among TBI survivors; in fact, 40–50% of patients studied suffered from some degree of pituitary dysfunction (22–24). In particular Steven et al. (23) reported a prevalence of 51.4% of isolated deficits in TBI patients, while Kelly et al. (24) reported that somatotroph and gonadotroph deficiencies were the most common and that diffuse brain swelling, hypotensive or hypoxic insults, and a relatively low Glasgow Coma Scale (GCS) score were associated with pituitary insufficiency. Because the majority of TBI survivors are young adults with near-normal life expectancy, the implications of undiagnosed post-traumatic pituitary failure can be serious and may contribute to the significant morbidity associated to it.

Among the causes of vascular damage which can potentially lead to pituitary deficits are to be counted subarachnoid haemorrhage (SAH), aneurysms, pituitary apoplexy, Sheehan syndrome and rarer infective causes such as tuberculosis, neurosyphilis, and snake bite (25, 26). In particular, it must be considered that pituitary masses, in particular non-functioning adenomas, are susceptible to haemorrhages and infarction (pituitary apoplexy). This can occur if an imbalance between oxygen or metabolic demand and available supplies happens (27). Surgeries (in particular cardiac and orthopaedic), arterial pressure fluctuations, micro-embolism, cranial trauma, dynamic pituitary testing [in particular insulin tolerance test (ITT), TRH (thyrotropin releasing hormone) and GHRH (Growth Hormone Releasing Hormone) tests], anticoagulant and to a lesser extent dopamine-agonist therapy are the main factors which can predispose to pituitary apoplexy. Hypopituitarism can be an early result of these phenomena in 15 to 85% of patients (28). The Sheehan syndrome represents a particular subtype of pituitary apoplexy; this can occur in pregnant women who suffer from an extensive uterine bleeding during the peri- or post-partum periods. This results in a pituitary infarction that leads to progressive pituitary

function deficit up to a definitive hypopituitarism and a radiological "empty sella" (29, 30). It is notable to mention that an increased risk of cerebral and subsequent pituitary haemorrhage can be related to congenital conditions of increased spontaneous bleeding. This being said, hemophilic patients are considered at potential higher risk of pituitary dysfunction (31, 32) due to a significant prevalence of intracranial haemorrhage, particularly in children (33).

2.7 Drugs

Several drugs can lead to transient or permanent hypopituitarism. In some cases, the pituitary deficits can be isolated due to the involvement of a single axis. In fact, physiopathological mechanisms are different for each drug and for each involved pituitary hormone. A more detailed discussion is present in the dedicated paragraph of the isolated deficit.

2.8 Genetic causes

In embryonic life, pituitary gland development is a result of a specific sequence of genes that express certain transcription factors (34). Particular genetic mutations can lead to a certain degree of hypopituitarism. In particular, each of the isolated pituitary deficits analysed in this review can find in genetics a possible etiology. Considered to be congenital, the clinical picture usually manifests at birth or in early childhood. The clinical phenotype can include also somatic alterations (35). However, we are going to further discuss potentially involved genes in each of the following dedicated sections.

3 Isolated central adrenal insufficiency

3.1 Definition and epidemiology

Isolated central adrenal insufficiency (ICAI) is a rare disorder, first reported by Steinberg in 1954, characterized by low or absent cortisol production and normal secretion of other pituitary hormones (36). The prevalence of CAI, most commonly due to exogenous glucocorticoid administration, is much higher than that of primary adrenal insufficiency (PAI), with an estimate of 150–280 cases per million (37). Due to its rarity, however, epidemiology and etiology of ICAI still remain uncertain.

ICAI is classified into congenital and acquired forms. In neonatal or childhood ICAI a genetic origin may be suspected, while in adults the main cause is the prolonged use of synthetic glucocorticoids (sGC). In fact, sGC are widely used for their anti-inflammatory and immunosuppressive actions and an undesirable effect of sGC treatment is, indeed, suppression of the hypothalamic-pituitary-adrenal (HPA) axis, which can lead to ICAI. A systematic review and meta-analysis found that this is a frequent scenario which could happen in 48.7% of cases, with the highest risk in hematologic patients (60%), in kidney transplant (56.2%), inflammatory bowel disease (52.2%), and rheumatologic disorders (39.4%). Risk factors for sGC-induced ICAI include the duration of glucocorticoid therapy, the dose, potency, route of administration and individual susceptibility (38). Moreover, an emerging cause of ICAI is related to an autoimmune response, due to drugs administration, such as CTLA4 (Cytotoxic T-Lymphocyte Antigen 4) and PD1/PDL1 (Programmed Cell Death Protein 1/Programmed Death Ligand 1) inhibitors. Hypophysitis appears more often in men older than 60 years of age and it is 2–5 times more frequent than in women. The reported incidence is 4%–20% with ipilimumab, 0.6% with nivolumab, 0.7% with pembrolizumab and slightly more commonly (8-10%) with combination ipilimumab and nivolumab (21, 39). Of note, these drugs could also be responsible for PAI with an incidence of less than 1% with monotherapy and 4%–8% with combined immunotherapy (40). In this clinical setting ACTH measurement can be useful for a proper differential diagnosis.

CAI is common in ICPi-related hypophysitis and, while CH and HH may be transient and spontaneously recover, ICPi-related CAI appears to be permanent in most cases resulting as an isolated deficiency.

3.2 When to suspect an isolated central adrenal insufficiency

CAI has several clinical presentations and, if unrecognized, a potentially fatal course. Usually, clinical manifestations of ICAI are similar to those found in pan-hypopituitarism and PAI although, generally less severe (41).

Patients with ICAI usually feel relatively well during unstressed periods until certain events trigger an acute adrenal crisis. This serious condition is characterized by extreme fatigue, severe hypotension and hypoglycemia, fever, acute abdominal pain, nausea, vomiting and diarrhoea and, if not promptly recognized, it may be irreversible and lethal. Except for adrenal crisis, patients with ICAI usually present with non-specific symptoms, such as asthenia, anorexia, unintentional weight loss and tendency to hypoglycemia. Unlike PAI, both hyperpigmentation and symptoms and signs of mineralocorticoid deficiency (e.g., salt-craving, postural hypotension) are absent. Hyponatremia may occasionally occur as the result of the increased antidiuretic hormone secretion, due to higher levels of corticotropin releasing factor (CRF). Under normal circumstances, cortisol suppresses both production of CRF and vasopressin (AVP) in the hypothalamus. In ICAI, persistently low concentrations of cortisol fail to suppress AVP and hyponatremia results from impaired free-water excretion, as it happens in the syndrome of inappropriate antidiuresis (SIAD) (42).

Another interesting clinical scenario of isolated ACTH deficiency is the so-called "critical illness-related corticosteroid insufficiency (CIRCI)" which is a condition that may develop in prolonged critically ill patients. When patients remain dependent on vital organ support for weeks, they are at risk of acquiring ICAI. This situation is determined by the increase in the systemic availability of glucocorticoids, mainly due to the reduction of circulating cortisol-binding proteins; the resulting transient

elevation in serum free cortisol values exerts a negative feedback mechanism at the hypothalamus and pituitary level on the HPA axis. Additionally, elevated levels of other glucocorticoid receptor ligands (such as bile acids) and drugs (such as opioids) can further suppress ACTH secretion. The adrenal cortex, deprived for weeks of the trophic stimulus due to the ACTH signalling, can become structurally and functionally impaired, resulting in insufficient cortisol secretion. This HPA axis suppression can be maladaptive and contributes to the persistent need for vasopressors and to the development of encephalopathy, thus reducing the chances of recovery (43).

Besides typical symptoms of CAI, in Literature several cases of atypical ICAI presentation are reported as well, like flexion contractures of the legs (44), severe muscle atrophy (45) and rhabdomyolysis (46). Other unusual presentations are pericardial effusion (47), recurrent syncope (48), cholestatic jaundice (49) and petrified ear auricles (50). These clinical manifestations, though not typical of ICAI, seem to be closely related to the hypoadrenal condition because they disappear upon the start of steroid replacement therapy. Primary infertility (51), Crohn's disease (52), myasthenia gravis (53), polycystic kidney disease (54), spinocerebellar ataxia type 3 (55), benign endocranic hypertension (56), Down syndrome (57), cognitive impairment and mental health disorders (58, 59), chronic opiate use (60) and haemodialysis (61) have also been reported in conjunction with ICAI, as well as paraneoplastic syndrome (55).

Lastly, ICAI is not infrequent in chronic alcoholism (62) and, as in patients with the above-mentioned disorders, it should be considered if more typical hypoadrenal symptoms are present. Likewise, ICAI should also be kept in mind in patients with other autoimmune diseases: ICAI due to lymphocytic hypophysitis has often been described associated with autoimmune hypothyroidism (63, 64) and, occasionally, with Graves' disease (65), type 1 diabetes mellitus (66) and polyglandular autoimmune failure (67). Recently Morita et al. described a case of ICAI following immunization with the BNT162b2 SARS-CoV-2 vaccine (68).

3.3 Diagnosis

Guidelines addressing the specific management of ICAI, as of today, are lacking. Despite this, the diagnostic and therapeutic process can be ascribed to the non-isolated form. The diagnosis of CAI is mainly based on measurement of morning serum cortisol. In fact, cortisol level <3 μg/dL is indicative of adrenal insufficiency (AI) and a cortisol level >15 μg/dL likely excludes an AI diagnosis (69). In addition, guidelines suggest performing a corticotropin stimulation test when morning cortisol values are between 3 and 15 μg/dL to diagnose AI. Peak cortisol levels <18.1 μg/dL at 30 or 60 minutes indicates AI. Both 250 μg and 1 μg stimulation tests could be used (70). In fact, since after the injection of 250 μg supra-physiological concentration of corticotrophin is achieved, a stimulation with 1 μg dose was proposed (71). However, In CAI before adrenal atrophy has occurred, the sensitivity of both tests may be low (72). Some Centres propose metyrapone test to evaluate the response to drug-blocking 11 beta hydroxylase. In fact, the administration of metyrapone should cause a reduction in blood cortisol levels, further incrementing ACTH, and finally an increase of adrenal steroids synthesis of 11- deoxycortisol, measured during the test (73). Despite the interesting pathophysiological basis, the analysis of 11-deoxycortisol levels is not available in most laboratories. The Glucagon (GST) test is another alternative. Although it has been used more frequently in the evaluation of GH axis, GST offers an opportunity to assess both the HPA and GH axes, making it an interesting possibility (74). However, the proper establishment of cut-off levels of cortisol is needed to properly interpret the results. The insulin tolerance test (ITT) is another option for CAI diagnosis, although it is contraindicated in some clinical conditions, it is unpleasant for patients, and requires close medical supervision (75). To avoid performing ITT, Gasco et al. in their study aimed to detect the morning serum cortisol cut-off with a specificity or a sensitivity above 95% that could identify those patients who should not be tested with ITT, finding that the cut-off of morning serum cortisol concentration that best predicted a normal response to ITT was >16.11 μg/dL (76). Moreover, a multiparametric score has been recently proposed for the prediction of CAI when morning cortisol is in the grey zone; this score might be helpful for a finer tailoring of the diagnostic process, as it might avoid the execution of a stimulation test in approximately one-fourth of the patients in which morning cortisol values are 'per se' non-diagnostic (77). Although the medical history and some symptoms could help the clinician in discerning ICAI from PAI, in dubious cases, ACTH measurement is also recommended (78).

In patients without any pituitary deficit before surgery, it is necessary to assess the HPA axis as early as possible in the post-operative phase, while the evaluation of the other axes (thyroid, gonadal and growth hormone function) can be carried out later. The indications for the diagnosis of ICAI in the early post-pituitary surgery period are slightly different. In this setting, there are not clear recommendations (69); in spite of that it would be cautious to assess adrenal function on the second day after pituitary surgery, using cut-off values that international guidelines suggested for non-stressed conditions (69, 78). In fact, second-day cortisol levels ≤3.2 μg/dL and >14 μg/dL would be diagnostic of ICAI and normal HPA function, respectively (79).

For the diagnosis of sGC-induced ICAI (Figure 2), the indications are, again, different. Since the risk of developing it mainly depends on the molecule and the duration of therapy, the recovery of ICAI should be assessed only in patients taking a prednisolone dose equivalent or inferior to the replacement one (i.e., doses of prednisone no higher than 5 mg a day). Several approaches can be used, but all evaluations require at least a 24-hour wash-out of any sGC therapy in place: the most common strategies include measurement of morning cortisol concentration, synthetic ACTH stimulation tests, metyrapone test and ITT. Recently, Prete and Bancos proposed a risk guided algorithm for the recovery evaluation of HPA axes (80).

In general, once the diagnosis of ICAI has been established, a magnetic resonance imaging (MRI) of the hypothalamic-pituitary region is mandatory. In patients with autoimmune endocrine disorders pituitary antibodies should be assessed, especially in

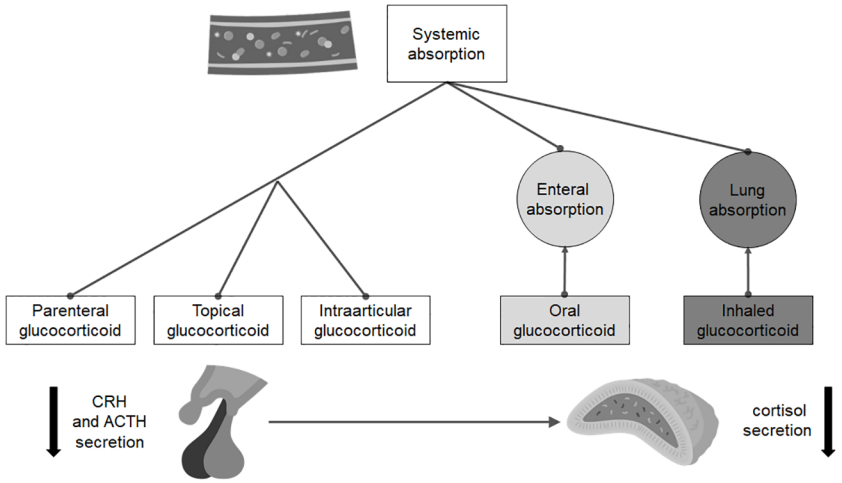

FIGURE 2
Routes of administration and absorption of the main steroid drugs that can induce isolated adrenal insufficiency.

case of consistent radiological findings. Genetic testing has so far proven to be of little use in adult ICAI.

3.4 Therapy and follow-up

Before starting a proper replacement therapy, clinicians should carefully assess the presence of ICAI (excluding combined pituitary deficiencies) in order to deliver the most adequate therapy (69). The latest hypopituitarism guidelines recommend using hydrocortisone, usually 15–20 mg total daily dose in single or divided doses as the proper replacement therapy.

It is possible that some patients are suffering from ICAI and epilepsy (or taking preventive anti-epileptic therapy) at the same time (e.g., TBI/SAH); in these patients it is necessary to take into account the possible need for higher doses of hydrocortisone replacement treatment (69).

Clinicians should appropriately warn patients about stress-dose and emergency sGC administration and suggest obtaining an AI emergency card and an emergency kit containing injectable high-dose sGC. Lastly it is advisable not to use fludrocortisone in patients with ICAI (69). As for PAI, guidelines recommend that clinicians treat patients with suspected adrenal crisis due to ICAI with an immediate parenteral injection of 50 –100 mg hydrocortisone.

Once ICAI is diagnosed and replacement treatment is started, the patient's follow-up includes periodic evaluation of AI symptoms and assessment of serum sodium, potassium and glucose. In the same way, follow-up of patients at risk of developing ICAI over time needs to be more standardized since, in this setting, there are different and not univocal recommendations.

For example, in all patients that previously underwent to brain/pituitary irradiations (cranial RT at doses > 30 Gy) or sellar or suprasellar region surgeries, who are at risk for developing ICAI, an annual evaluation of morning cortisol blood concentration should be performed (81).

In patients with a history of TBI, signs and symptoms possibly related to life-threatening adrenal deficiency must be immediately investigated whenever they become apparent. Alternatively, some authors suggest an endocrine evaluation performed routinely at a period between 6 and 12 months after TBI (82).

During treatment with some CTLA-4/PD-1 blockers, routine monitoring for adrenal dysfunction is controversial. Some authors suggest measuring morning cortisol ± ACTH in patients receiving ipilimumab-based treatment at every cycle (39), while others suggest performing a Synacthen (cosyntropin, 1–24 ACTH) stimulation test when basal cortisol measurements are inconclusive, considering that results may be falsely reassuring in the early phase of ICAI, when the adrenal glands may still respond normally to the stimulation (83).

Patients with sGC-induced ICAI require continuation of GC therapy until such treatment can be tapered to physiologic doses. At that point, testing for functional recovery of the HPA axis should be performed before attempting to stop the substitutive therapy. The optimal time to test for HPA axis recovery following prolonged sGC use remains controversial due to variability of data for timelines of when that occurs. Generally, the recovery of HPA axis has been documented as quick as about four weeks after the stop of a continuous sGCs use. It would be therefore reasonable to plan assessment of the HPA axis around that time and then every one-two months until complete recovery is documented (84). In the meantime, patients are recommended to continue adequate hydrocortisone replacement therapy (80).

Although there are no strong recommendations on how to perform an adequate follow-up, all authors agree on the importance of educating specialists other than endocrinologists and patients at risk of AI to recognize any suggesting symptom in order to obtain an early diagnosis and prompt treatment.

To conclude, it seems useful to periodically assess the presence of ICAI in particular for transient or ambiguous etiologies. In fact, improper replacement therapy leads to inappropriate GC exposure that may have a bearing on a patient's metabolism. However, nowadays no recommendation is available.

10.3389/fendo.2023.1100007

4 Isolated central hypothyroidism

4.1 Definition and epidemiology

CH is a disorder characterized by defective thyroid hormone production and/or secretion, secondary to the insufficient stimulation by TSH of a healthy thyroid gland (4). In most patients, CH occurs in combination with other pituitary hormone deficiencies but occasionally it may present as an isolated deficit (ICH). This condition is mainly the result of anatomic or functional disorders of the pituitary gland (secondary hypothyroidism) or the hypothalamus (tertiary hypothyroidism) (4), although this distinction is no longer in use.

CH is a rare cause of hypothyroidism (about 1 in 1,000 patients with hypothyroidism) with a global prevalence that ranges from 1 in 20,000 to 1 in 80,000 individuals in the general population. It is reported to affect individuals of all ages and both sexes equally (85), although the presence of some X-linked pattern may suggest a male predominance. It is also likely that these data may underestimate the real incidence and prevalence. In fact, most countries perform a TSH-reflex assessment, both for paediatric and adult individuals but this strategy may contribute to missing diagnoses. All this considered, precise data regarding epidemiology of ICH are missing.

Infants and young children are usually affected by genetic and hereditary conditions, while expansive processes in the pituitary/hypothalamic region represent the most common cause of acquired ICH; however, milder genetic mutations can be the underlying cause of ICH with a delayed onset during life (4).

In general, there are different pathological mechanisms accounting for CH: impaired TSH secretion due to reduced hormonal reserve (quantitative, typical of the congenital forms), poor intrinsic biological activity of secreted TSH molecules (qualitative), or both (more common in the acquired cases) (85–87).

4.2 When to suspect an isolated central hypothyroidism and possible confounding factors

Patients with ICH may have a very heterogeneous clinical presentation. Indeed, it is related to several factors such as the etiology of the disorder (congenital ICH is generally more severe than acquired), and the patient's age at the onset of the disease (85). Signs and symptoms, if any, may be due to the underlying hormonal disturbance and/or the possible mass effect in the case of space-occupying lesions. In the first scenario the clinical picture is usually similar to primary hypothyroidism but typically milder; this includes cold intolerance, asthenia and lethargy, constipation, bradycardia, weight gain, hoarseness of voice, thinning of hair and dry skin (85–88). Conversely, goitre is rarely present, since it is secondary to the trophic action of TSH on the thyrocytes, which in the presence of CH results, by definition, blunted. In the second case, headache, dizziness, or visual field defects are the most frequently encountered alterations (85).

Nonetheless, when a clear clinical picture is missing, people usually refer to an endocrinologist after performing routine biochemical evaluations with their general practitioner: they typically show a low-normal TSH and a low fT4 (free thyroxine); fT3 (free triiodothyronine), conversely, is usually normal in mild and moderate forms (85). Moreover, there may be several cases which go undetected since the general screening for thyroid disease is based on a cascade mechanism that starts from the detection of an altered TSH (the so-called TSH-reflex strategy). Diagnosis may be further complicated when fT4 concentration is around the lower limit of the reference range (by definition, a reference range usually comprises only 95% of a reference population and so 2.5% of healthy individuals have an fT4 below the reference interval) (89). Similarly, euthyroid patients can have up to 10% variation in fT4 levels, which is still considered normal (90). Consequently, in patients followed-up for hypothalamic-pituitary disease, a decrease in circulating fT4 levels of more than 20%, even if the values are still within the normal range, has been proposed as suggestive of CH (4, 85, 91).

Generally, it is always essential to confirm this biochemical finding on two occasions before proceeding with further analyses and with an MRI of the hypothalamic-pituitary region.

Dynamic tests using the TRH stimulation (92, 93) were more commonly used in the past but they have shown some utility even today especially in doubtful cases in which TSH values are not markedly reduced and fT4 is in the medium-low range of normality (94).

For the diagnosis of CH, it is important to exclude other confounding factors such as iodine deficiency (95) (iodine supplementation before retesting may be useful) and interfering drugs (96). Indeed, many drugs, such as bexarotene (97), mitotane (98) and immune checkpoint inhibitors (99) may alter the thyrotropic cell activity of TSH production or release determining, in general, permanent CH (96). Other drugs, like glucocorticoids, dopamine/dopamine-agonists, somatostatin analogues, metformin (100) as well as some antipsychotic and antidepressant medications (101), may exert a mild suppressive effect on TSH release without appreciably affecting circulating fT4 levels and hence without a real clinical significance (96). Finally, certain antiepileptic medications, including carbamazepine, oxcarbamazepine, valproic acid and phenytoin along with salsalate may determine falsely low levels of fT4 (secondary to pre-analytical variability due to sample dilution) and normal TSH levels in clinically euthyroid patients, mimicking the biochemical picture of ICH (96, 102, 103).

To conclude, during severe intercurrent events (organic as well as psychiatric), physiological adaptation mechanisms of the hypothalamus-pituitary-thyroid axis are involved, which can determine a biochemical picture comparable to that of ICH (this condition is called non-thyroidal illness syndrome or euthyroid sick syndrome) (104). In consideration of a reduced peripheral deiodinase activity (105), the latter condition differs from ICH because the values of fT3 are generally reduced, but a re-evaluation once the acute picture is overcome may be useful in dubious cases.

Once that CH has been diagnosed, other concomitant pituitary deficits must be assessed; in particular, it is always mandatory to

exclude possible concomitant CAI that, if present, must be treated in advance to avoid triggering an adrenal crisis.

4.2.1 Hereditary and congenital forms and role of genetic analysis

As of today, five genes related to ICH have been identified (89): *TRHR* (TRH receptor) and *TSHB* with an autosomal recessive inheritance and the more recently identified *IGSF1*, *TBL1X* and *IRS4* with an X-linked pathway transmission (Table 2).

Mutations in *TSHB*, which encodes for the β subunit of TSH (TSHβ), constitute the most frequent cause of inheritable ICH (85, 106–108). Typically, the genetic forms manifest at birth or in the first weeks of life but mutations in the TRHR gene for example, described so far only in a few families, can determine a completely asymptomatic phenotype with only growth retardation found during puberty. Congenital hypothyroidism is one of the pathologies for which there is a newborn screening (NBS) program in many countries of the world. Unfortunately, as the main objective of these programs is the detection of the much more common condition of primary hypothyroidism (approximately only 1 in 30-40 newborns with congenital hypothyroidism has CH) (109), the vast majority of NBS are TSH-based with a cascade mechanism of dosing fT4 that starts from the detection of an altered TSH. For this reason, as often TSH may not be frankly reduced, many cases of congenital CH may go undetected and recognized only later in life resulting in possible ICH of the adulthood (109).

According to the European Guidelines, it is recommended to perform a genetic analysis in congenital cases and in cases of CH onset at any age in childhood or when the etiology is otherwise unexplained (4). Furthermore, a genetic analysis is useful as a confirmation test for conditions where fT4 may be in the low quartile of normality range interval, such as rare cases of idiopathic mild CH.

The operative method to carry out such analysis is to directly sequence a panel of candidate genes, chosen on the basis of the patient's phenotype. In the case that this test is negative, the evaluation can be expanded to the whole genome. After the successful identification of a causative mutation related to the phenotype in the index case, the genetic analyses should be subsequently extended to all the first-degree relatives of the patient for the purposes of early diagnosis or to detect any healthy carrier of the mutation (4).

4.3 Therapy and follow-up

Treatment of ICH aims to restore and maintain euthyroidism and levothyroxine (LT4) is the mainstay of pharmacological therapy, since there is no evidence for the use of a combined treatment with liothyronine which is burdened, conversely, by a higher risk of overtreatment (4, 85, 88).

The replacement dose of LT4 in ICH is approximately 1.6 μg/kg of bodyweight/day, similar to primary hypothyroidism replacement therapy (110). Appropriate LT4 dose varies depending on sex (higher in women), age (lower after menopause) and concomitant treatment (such as oestrogens); similarly, younger people often require higher dosages (111). Children and young adults can generally start a full replacement dose of LT4 when commencing the treatment, while in the elderly it may be safer to start with low doses (e.g., 25-50 μg/day) to increase with caution (4).

As of today, the proper assessment of the adequacy of LT4 therapy in patients with CH and subsequently for ICH still remains an object of debate. Indeed, TSH serum levels are not fully reliable to monitor replacement therapy like in primary hypothyroidism, because they appear to be suppressed even during low-dose LT4 treatment. All this considered, it is safe to ascertain that TSH levels

TABLE 2 Genetic etiologies in Isolated Central Hypothyroidism.

GENETIC CONGENITAL HYPOTHYROIDISM		
Gene	Characteristics	Biochemical assessment
TRHR	- Autosomal recessive inheritance - Described in a few families both in males and females - Mild to moderate hypothyroidism usually asymptomatic until puberty (growth retardation)	↔ or rarely ↑ TSH levels in affected individuals ↑ TSH levels in carriers
TSHB	- Autosomal recessive inheritance - Most frequent cause of inheritable ICH that affects both males and females - Severe hypothyroidism with precocious onset	↔ or ↓ TSH levels in affected individuals ↑↑ α-subunit
IGSF1	- X-linked inheritance - Mild to moderate hypothyroidism associated to macroorchidism, GH deficiency in childhood and increased GH secretion in male adults with acromegaloid features - Delayed menarche and increased BMI in female carriers	↔ TSH levels in affected individuals ↔ or ↓ fT4 levels in female carriers
TBL1X	- X-linked inheritance with incomplete penetrance - Mild to moderate hypothyroidism in males associated to hearing loss - Mild hypothyroidism to euthyroidism in female carriers	↔ TSH levels in affected individuals ↔ or ↓ fT4 levels in female carriers
IRS4	- X-linked inheritance - Mild hypothyroidism	↔ or rarely ↑ TSH levels in affected individuals ↔ or ↓ fT4 levels in female carriers

↔ normal; ↑ increased; ↓ reduced; ICH, Isolated central hypothyroidism; TSH, Thyroid stimulating hormone; fT4, free thyroxine; GH, Growth hormone; BMI, Body Mass Index.

above 0.5-1.0 mU/L should be considered as a sign of insufficient replacement in such class of patients (4, 85). Over the last years, increasing evidence investigating the efficacy of LT4 replacement therapy shows that patients with CH have significantly lower levels of fT4 with respect to patients with primary hypothyroidism adequately treated; therefore, subjects with CH are often left untreated, thus increasing their long-life cardiovascular risk (90, 110). For these reasons, in the context of ICH, the best markers to properly set the adequate therapy are fT4 and fT3, aiming at bringing fT4 values in the upper range of normality and fT3 in the normal range of population (4, 109).

The first evaluation after starting the treatment should occur after 6-8 weeks and the measurement of fT4 should anticipate the assumption of LT4 therapy. Once reaching the aforementioned biochemical target and obtaining the concomitant resolution of the symptoms, if present, thyroid function can be checked periodically, at least annually (4, 90).

5 Isolated hypogonadotropic hypogonadism

5.1 Definition and epidemiology

Isolated hypogonadotropic hypogonadism (IHH) is defined as a condition of secondary hypogonadism not associated with other pituitary deficits. It can manifest as a congenital (CIHH) or acquired (AIHH) disruption of the hypothalamic-pituitary-gonadal (HPG) axis (112). Despite lack of definite data, IHH can be considered an infrequent condition as a whole: for CIHH, a male predominance is reported (2-5 males to 1 female) with an estimated prevalence between 1/10,000 and 1/86,000 in males, while no piece of information is available about CIHH in females (113). Furthermore, AIHH has still no clear evidence about incidence or prevalence, probably due to the wide number of involved etiologies and due to the variability of the definition of this condition between studies and over time.

CIHH is mostly related to a genetic alteration and among 50% to 60% of the patients have an associated olfactory dysfunction (anosmia or hyposmia), defining Kallmann syndrome (114).

AIHH presents when a disruption of the hypothalamus or the hypophysis alters the release of gonadotropin-releasing hormone (GnRH) or of LH and FSH, leaving untouched the release of the other pituitary hormones.

The clinical signs can be present early during life, from childhood and in particular puberty, when IHH can manifest with delayed or absent pubertal development until clinical pictures characterised by infertility and hypogonadism in adulthood. Therapies are available to accomplish an eugonadal state and, whether possible, fertility.

After this glimpse, we will further describe these sections hereafter.

5.1.1 Etiopathogenesis

The etiology of IHH is mostly related to the time of onset of the clinical picture. Talking about CIHH, this condition is mainly linked to genetic causes, thus familial history can insinuate the doubt. The primarily involved genes are associated with GnRH, which regulates the release of LH and FSH by the pituitary gland. The majority of hypothalamic GnRH neurons originates in the olfactory placode around the 5th gestational week and migrates alongside the olfactory, vomeronasal and terminal nerves until arrives at mediobasal hypothalamus, infundibulum and periventricular region (115). CIHH is a result of the failure of GnRH neurons to differentiate, develop or function properly or, in a subgroup of patients, there may be a GnRH resistance in pituitary gonadotropic cells (e.g., loss of function mutations in the GnRH receptor) (114). The olfactory defects can occur as a result of the close link between GnRH neurons and olfactory axons; in fact, an embryonal abnormal migration of GnRH neurons and olfactory fibres from their origin in the olfactory placode to the forebrain can result in a hypoplasia or aplasia of the olfactory tract/bulbs associated to GnRH deficiency, that is usually described in CIHH as Kallmann Syndrome (116).

Many genes have been pointed out in the pathogenesis, including X-linked recessive (such as *ANOS1*, formerly known as *KAL1*), autosomal dominant (e.g., *FGFR1*), and autosomal recessive genes (like *KISS1-KISS1R, GNRHR*); even oligogenic (caused by more than one gene defect) and sporadic forms have been described (114). Mutations in *ANOS1* occur in approximately 4.5% of all CIHH patients (117–122), with an important olfactory and reproductive phenotype. *FGFR1* mutations are the most commonly known molecular cause of CIHH that may cause isolated defects in GnRH neuronal proliferation and migration without necessarily affecting olfactory bulbs and function (123, 124). Kisspeptin produced by periventricular and arcuate nuclei, is a pivotal regulator of GnRH neurons. Mutations in Kisspeptin, encoded by the *KISS1* gene, or of its receptor encoded by *KISS1R* and expressed in the surface of the GnRH secreting neurons, are linked with patients with normosmic CIHH (125). Eventually, GnRH receptor (*GNRHR*) mutations have been shown to be responsible for a significant proportion of normosmic CIHH cases, associated with a broad phenotypic reproductive spectrum, varying from partial to complete GnRH resistance (126–128).

AIHH is related to defects of the hypothalamus or of the pituitary gland, such as trauma, inflammation, infiltrative diseases, and tumors (Table 1) (129). These conditions can manifest both in early and adult life. A certain percentage of AIHH may present with a genetic alteration, that seems to be associated with a mild pattern of pubertal delay, suggesting a possible underlying pre-existing slight impairment of HPG axis (117, 130, 131); moreover, a part of AIHH patients present characteristics of classical CIHH of pre-pubertal onset, including anomalous olfactory bulbs and sulci on MRI (132).

5.2 When to suspect an isolated hypogonadotropic hypogonadism

Clinical pictures can be heterogeneous, ranging from clear manifestations in newborn (such as cryptorchidism and

micropenis in males, while in females there are not clear signs) to nuanced manifestations in adults. Moreover, some genetic defects may manifest with alterations in other organs such as olfactory deficit, cleft lip or palate, dental agenesis, ear anomalies, congenital hearing loss, renal agenesis, mirror movements (bimanual synkinesis) or skeletal anomalies. Moreover, acquired conditions can be associated with other symptoms, related to the causing condition (132–134).

Puberty development: puberty is a pivotal phase where suspicions for IHH can arise, in particular for CIHH: there can be no puberty or just the first signs, with a partial development. Girls may have an initial breast development associated with primary amenorrhea (only a few shows a couple of menstrual bleedings) associated with a variable pubarche; boys usually present no (the majority, around ⅔) or only initial testicular development (testicular size > 4 mL, a milestone of male puberty) with no further increase. Eunuchoid proportions (arm spans exceeding by 5 cm the height) are a typical presentation, due to delayed epiphyseal closure (116).

Adult: in adult life, men with IHH can present with signs and symptoms of hypogonadism such as loss of libido, erectile dysfunction, loss of body hair growth, fatigue, reduced bone mass, muscles hypotrophy, low mood. Normal sized genitalia (penis and testicles with a normal or slightly reduced volume), a normal stature and a low-pitched voice should be present, due to the normal pubertal development and androgenization that occurred (112). Women can complain of secondary oligo-amenorrhea up to amenorrhea, flushing, fatigue, loss of libido, reduced bone mass, low mood. In these patients, the presence of hyperandrogenism (such as acne, alopecia, hirsutism, clitoromegaly) should be assessed, to exclude androgen-excess related amenorrhea (135).

When CIHH is suspected, clinicians should investigate the sense of smell in order to find hypo-anosmia (113). On the other hand, if an AIHH is suspected, it is useful to investigate conditions that may impair HPG axis, asking about e.g., headache, visual impairment, breast tenderness and discharge.

5.3 Diagnosis

In this section we are going to focus on the adolescent-adult diagnosis to remain faithful to the aim of this paper. For a more punctual reading about infant diagnosis, we suggest referring to dedicated articles. A proper anamnesis should be collected, in order to evaluate familial pattern of this condition and to collect information about general health status, including potential exposition to endocrine disrupting chemicals (136).

In puberty, a growth delay is challenging to distinguish between IHH and constitutional delay of growth (CDGP) and puberty. After a clinical evaluation, initial assessments should comprehend the evaluation of HPG axis: gonadotropins (LH, FSH) associated with total testosterone (TT), in boys and with estradiol (E2) in girls. IHH is characterised by low gonadotropins and low levels of TT or E2. When the suspicion between IHH and CDGP exists, no gold standard evaluation is recommended to dispel this uncertainty, thus a GnRH stimulation test is the one proposed, but it lacks reliability (137). Adjunctive assessments that may help in the diagnosis are inhibin B and Anti-Müllerian Hormone (AMH). Inhibin B is a glycoprotein produced by Sertoli cells and it correlates with spermatogonia function and status. Its serum levels rise with the onset of puberty and tend to be very low in patients with CIHH (138). The FSH-stimulated inhibin B has shown to correctly differentiate pubertal delay from HH; however further studies are needed to confirm this finding (139). In adults who went through puberty, the assessment of inhibin B may not be reliable to further point out IHH. In fact, these men are supposed to have developed a normal testicular volume (underlying a proper germ cell proliferation) and consequently potentially normal inhibin B levels. Moreover, AMH, a hormone released by Sertoli cells and granulosa cells, could be a useful tool in pre-pubertal boys. In fact, in CIHH boys serum AMH tends to remain elevated for age (due to lack of down regulation mediated by testosterone rising), but lower than expected for the patient's Tanner stage (due to the lack of FSH feedback that induces an elevation of AMH) (140). In adults, if the clinical picture is consistent with IHH, serum LH, FSH associated with TT, sex-hormone-binding globulin (SHBG), and albumin to evaluate calculated free testosterone (CFT) in men, and associated with E2 in women should be evaluated. CFT is a particularly useful assessment in those conditions that may raise SHBG (e.g., liver dysfunction, obesity, HIV) and in which the evaluation of lone TT may improperly diagnose hypogonadism. Sense of smell assessed by a formal smell test should be addressed to help in the diagnosis (141).

Through an extensive anamnesis, it is important to exclude functional hypogonadism in these men; this is a potentially reversible condition, with a hormonal pattern similar to IHH but with no link with a direct disruption of HPG axis. It is rather related to an impairment of general health condition (diabetes, metabolic syndrome, multiple comorbidities, acute disease, sleep apnoea, HIV, and energy imbalance that can result from a strenuous physical activity e.g., endurance sports) or drug induced (opioids, corticosteroids, androgenic/anabolic androgenic therapies, GnRH analogues, psychotropic treatments) (129, 142). Notably, the abuse of anabolic-androgenic steroids has been growing exponentially among elite and amateur athletes, of both genders (143). The use of aromatizable steroids, the imbalance between testosterone and estradiol serum levels, and their withdrawal after long-term use seem to represent the main reasons for men to incur an anabolic steroid-induced hypogonadism (ASIH) (144), which may not properly recover over time (129).

In women presenting with amenorrhea, pregnancy must be firstly excluded by evaluating serum β-hCG (human chorionic gonadotropin). Then, hormonal levels should be evaluated after a progesterone challenge test (e.g., using a medroxyprogesterone acetate for 10 days and after the withdrawal of the drug check for menstrual bleeding), within a week from the start of the bleeding, in order to proper interpret the assessment and to exclude other conditions that may mime a secondary hypogonadism. If signs of clinical hyperandrogenism are present, it is useful to assess serum androgens (mainly TT) and evaluation of free androgen index (FAI) using SHBG (145), but also 17-hydroxyprogesterone (17-OHP) and dehydroepiandrosterone sulphate (DHEA-s) could be useful to

exclude other conditions (such as polycystic ovary syndrome) that may elicit this menstrual pattern. Adjunctive evaluations should exclude hyperprolactinemia, severe hypothyroidism, and the presence of functional amenorrhea (a form of chronic anovulation that is not due to identifiable organic cause and usually related to excessive energy expenditure). A gynaecological evaluation should be performed especially in younger women (135). Adjunctive assessments, such as AMH, are unfortunately not useful to further address the diagnosis, yet. In fact, in females with IHH, AMH can be either low, normal, or high (146).

After assessing HH, a second blood test should be performed to confirm the results. Then, it is appropriate to evaluate the whole anterior pituitary function to exclude other associated abnormalities and to properly diagnose IHH. Eventually, an MRI should be performed to evaluate the hypothalamic-pituitary area, the olfactory bulbs, and to investigate the possible etiologies of AIHH above mentioned. A formal smell test can be ordered to find alterations (113). It is interesting to highlight that even some AIHH patients also show alterations of olfactory bulbs on MRI that are commonly associated with classical CIHH (132).

When the diagnosis has been made, a genetic counselling should be offered accordingly. The current increased use of next generation sequencing (targeted exome) in clinical practice allows the identification of causative genes without necessarily completing an exhaustive search for associated signs (147).

5.4 Therapy and follow-up

Once IHH has been diagnosed, a proper treatment, in accordance with the age of the person, should be offered. During childhood, an early diagnosis can provide better outcomes in terms of puberty development, to best benefit for sexual, bone and metabolic health, and help minimize some of the possible psychological effects (116). In general, in CIHH the proper age to start puberty treatments should be individualised and the aim is to obtain a final endocrine environment with gradual increase of doses to mimic physiological pubertal development (148). In boys there are two main therapeutic approaches: induction of virilization by testosterone injection (which has more efficacy and a more robust body of literature) or transdermal gel (it could be more physiological but scarce data are available) in order to reduce sexual infantilism and psychological distress (low doses if started at about 12 years of age and subsequently titrated or higher doses if started in later adolescence or early adulthood) (148). Another possible approach is the use of pulsatile GnRH or gonadotrophin therapy (hCG ± FSH) resulting in an endogenous increase of serum TT (even intratesticular) that results in improving testicular growth. This approach seems to grant better responses of sperm retrieval, in particular in men with cryptorchidism that have poorer fertility prognosis (116). A growing body of evidence suggests that the combination therapy with recombinant FSH, especially before adding hCG, is significantly more effective than hCG alone both for inducing spermatogenesis and increasing testicular volume (117, 149–151). After pubertal induction, boys can continue these treatments or switch to testosterone replacement therapy, which can be made of mild or long-term intramuscular injections, transdermal gel or patches, tablets, intranasal and subcutaneous implants (Table 3). When men desire fertility, they stop assuming testosterone and can start a treatment with gonadotropins (hCG + FSH) or pulsatile GnRH therapy in order to induce spermatogenesis (113).

Data about puberty induction in girls with IHH are scanty. An incremental dose, by 11-13 years of age, is recommended over a period of 2–3 years to reach a proper adult dose (148). This slow progression is pivotal to avoid a negative impact on breast development or growth (152). If the diagnosis is made in late adolescence, clinicians may start with higher doses. Bioidentical human estrogens (estradiol/17β-estradiol) are the preferred formulations that can be used orally or transdermally. The metabolic effects of transdermal and oral routes did not show differences in fibrinogen and antithrombin activity, glucose and insulin, liver enzymes activity, lipids concentration, plasma renin, as well as insulin growth factor 1 (IGF-I) levels (153). After at least 2 years of treatment with estradiol for puberty induction, progesterone should be started after breakthrough bleeding, to avoid the risk of endometrial hyperplasia (148). No preferred routes are currently known, and progesterone can be delivered orally, vaginally, transdermally, intranasally or intramuscularly, with a 10-day cycling treatment. After about 3 years of pubertal induction, girls should have reached adult doses of estrogen therapy (transdermal or oral routes are suggested) always associated with a cyclic therapy with progesterone (Table 4). Unlike boys, there is no specific data about the need of gonadotropin therapy during adolescence in girls. However, when the fertility desire comes, the available treatment is the use of exogenous gonadotropins, and clinicians should modulate hCG and FSH resembling the various phases of the menstrual cycle (Table 4). To induce fertility, gonadotropin therapy is effective, but is much more likely to be complicated by multiple pregnancy and ovarian hyperstimulation due to lack of the protective HPG feedback that normally would lead to selection of the dominant follicle (154). Women with secondary hypogonadism seem to have a very narrow gonadotropin therapeutic window between low and excessive response, with a potential high number of responsive follicles (146).

IHH, in particular CIHH, has been traditionally considered a permanent condition. Patients typically require lifelong treatment and monitoring in order to maintain sexual function, fertility and secondary sexual characteristics, although 5-20% of male patients (3, 149, 155–158) exhibit a spontaneous recovery (permanent or transient) of gonadal function. Moreover, some men seem to sustain reversal of the disease after discontinuation of hormonal therapy (no clear connection with genetic defects or clinical presentations are currently known). Reversal should be suspected if testicular volume increases during testosterone administration or in cases of spontaneous fertility in IHH patients (114). Conversely, there are no cases of documented reversal of IHH in women. It is reasonable to think that, in the case of AIHH, when the subsequent cause has been underlined and treated, hypothalamic-pituitary function may be restored. Progressively lowering hormone replacement therapy until withdrawing it for a certain period, could be a useful approach to evaluate symptoms and signs

TABLE 3 Summary of treatment options in male adult affected by Isolated Hypogonadotropic Hypogonadism.

ADULT MALE HYPOGONADISM			PROs	CONTRAs
Testosterone enanthate, cypionate or mixture of esters	150-250 mg IM every 2-4 weeks	Titrating dose based on clinical signs and symptoms, serum testosterone levels	Self-injection Easily available	Higher risk of erythrocytosis Frequent serum testosterone peaks Frequent injections
Testosterone undecanoate	750-1000 mg every 10-14 weeks		Longer interval injections Stable serum testosterone levels	injection by a health care provider risk of pulmonary oil microembolism
Testosterone gel	40 mg-80 mg/daily		Easy avoidable side effects Non invasive Mimics physiology	Daily administration Skin irritation Possible skin to skin transfer of therapy
Testosterone patch	2.5–5 mg/day		Mimics physiology	Skin irritation, Possible issues with frequent showering or certain lifestyle
Oral testosterone	Undecanoate testosterone 158–396 mg twice daily		Oral administration	Daily multiple doses; need lipid rich meals; gastrointestinal side effects; hypertension
Intranasal testosterone	11 mg twice/die		Easy to administer	Sense of taste alteration
Testosterone pellets	75 mg pellets, 3-4 every 4-6 months		Easier compliance	Risk of local side effects (extrusion, fibrosis, infection) Higher cost
ADULT SPERMATOGENESIS INDUCTION				
Gonadotropins	Starting dose: hCG 500 UI SC thrice/week + FSH 75-150 UI thrice/week	Titrating dose: - hCG increase based on serum testosterone - FSH increase based on serum FSH and sperm count	Self-injections	Require optimal compliance Need frequent injections
Pulsatile GnRH	SC pump: 25 ng/kg per pulse every 120 min	Dose e adapted based on serum testosterone levels	Most physiological	Not easily available Pituitary resistance (rare)

Adapted from Young et al., 2019 and Nordenstrom et al., 2022.
SC, subcutaneous; IM, intramuscular; hCG, Human chorionic gonadotropin; FSH, Follicle stimulating hormone.

reported by the patient and to perform hormonal assessment to definitively ascertain HPG recovery.

6 Isolated growth hormone deficiency

6.1 Definition and epidemiology

GHD results from a decrease in GH secretion by the pituitary gland, leading to a reduction of IGF-I. Although GHD usually represents the first pituitary deficit to appear in combination with others, rarely it may present as an isolated deficit (159).

Isolated GHD (IGHD) is widely studied in infants and childhood population as a result of genetic disorders and anatomical abnormalities. In these cases, GHD syndrome, clinically characterized by short length, recurrent hypoglycemia, and severe dwarfism, is easily suspected; in adulthood instead, the lack of pathognomonic signs and the overlap with other clinical conditions, makes the diagnosis more challenging. However, the interest on GHD diagnosis in adulthood has grown during the last decades thanks to the availability of different dynamic tests and positive data of rhGH (recombinant human growth hormone) treatment.

Incidence and prevalence of adult-onset GHD (AO-GHD) are difficult to estimate. Sassolas G et al. in 1999 conducted an epidemiological study to evaluate the frequency of this syndrome in the French population; they analyzed data from 1652 patients with a history of hypothalamic-pituitary damage and they found an incidence of 12 GHD per million of adults and a prevalence of 46 per million (160). Another nation-wide cohort study in Denmark reported an incidence of 1 per 100.000 people yearly and 2 per 100.000 when childhood onset GHD (CO-GHD) were included, with approximately 15-20% of cases being transition of CO-GHD into adulthood (161, 162). Combining both AO-GHD and CO-GHD yields an overall prevalence of 2 to 3 per 10.000 population (163). Specific epidemiological data of isolated GHD, however, are not available.

6.2 Etiopathogenesis

About 15-20% of cases of adult IGHD are transitions of CO-GHD (161). In this context, the most common cause is idiopathic deficit followed by genetic syndromes (Table 5).

Childhood idiopathic IGHD is a well-recognized form, characterized by growth failure due to the lack of GH action in

TABLE 4 Summary of treatment options in female adult affected by Isolated Hypogonadotropic Hypogonadism.

ADULT FEMALE HYPOGONADISM			PROS	CONTRAS
Estrogenic therapy (patch)	50-100 micrograms/24 h Applied twice/week	Titrating dose based on clinical signs and symptoms	No first passage effect	Skin irritation, Possible issues with frequent showering or certain lifestyle
Estrogenic therapy (gel)	Estradiol or estradiol hemihydrate 0,5 to 2 mg/die		No first passage effect	Skin irritation; need to be accurately dried
Estrogenic therapy (tablets)	Micronized or valerate estradiol 1-4 mg/die			First passage effect
Progesterone	e.g., Micronized progesterone (100-200 mg/die for last 10 days/month) vaginal route			
ADULT OVULATION INDUCTION				
Gonadotropins	*Follicular Phase:* FSH + LH) 75 to 150 IU SC daily, *Ovulation phase:* induced by hCG 6500 IU *Luteal phase:* hCG 1500 UI every 3 days, thrice or progesterone 200 mg intravaginally daily	Follicular phase: depending on follicular growth (serum estradiol and ultrasonography)	Self-injection	Higher risk of overstimulation and multiple pregnancies
Pulsatile GnRH	SC pump: 15 mg per pulse every 90 min	Dose adapted based on response, up to 30 mg per pulse	Less risk in multiple pregnancy; most physiological treatment	Pituitary resistance (rare)

Adapted from Young et al., 2019 (113) and Nordenstrom et al., 2022 (148).
SC, subcutaneous; hCG, Human chorionic gonadotropin; FSH, Follicle stimulating hormone; LH, luteinizing hormone.

absence of both organic lesions and genetic mutations (167). Still, the majority of these patients undergo subsequent recovery of the somatotropic axis during transitional age (168, 169), resulting in only a small fraction of them still having GHD in adulthood. The definition of idiopathic GHD in adulthood, therefore, remains controversial: Melmed described it as a rare condition in which rigorous criteria must be applied, excluding all known common organic causes (170).

Conversely, when there are specifically genetic mutations responsible for GHD, patients CO-GHD remain always adult IGHD. A mutation responsible for the condition has been identified in up to 11% of isolated CO-GHD; *GH1, GHRH, SOX3* are the most studied genes with four types of genetic forms recognized (IA autosomal recessive, IB autosomal recessive, II autosomal dominant, III X-linked) (159).

As previously pointed out, GH-axis is the most vulnerable axis to pathological insult to the pituitary gland; therefore, GHD can be the first detectable deficit (171, 172).

Apart from known genetic syndromes, identifying IGHD in adults is not easy because the majority of studies does not

TABLE 5 Genetic etiologies and their clinical and biochemical phenotype in Isolated Growth Hormone Deficiency (164).

GENETIC GROWTH HORMONE DEFICIENCIES			
Inheritance	Type	Gene	Phenotype
Autosomal recessive	IA	*GH1*	↓↓ stature ∅ serum GH + anti-GH antibodies on treatment*
Autosomal recessive	IB	*GH1* *GHRH*	↓ stature ↓↓ serum GH ∅ anti-GH antibodies on treatment
Autosomal dominant	II	*GH1*	↓↔ stature - normal or hypoplastic anterior pituitary on MRI scan - Other pituitary hormone deficiencies
X-linked	III	*SOX3* Other	↓ stature ↓ serum GH agammaglobulinemia ± intellectual disability and ectopic posterior pituitary on MRI scan

↔ normal; ↑ increased; ↓ reduced; ∅ undetectable; + detectable; ± possible; GH, growth hormone; MRI, Magnetic Resonance Imaging.
*The initial good response to exogenous GH is hampered by the development of anti-GH-antibodies (165) (166).

differentiate between GHD in combination with other pituitary deficits (multiple pituitary hormone deficiency, MPHD) from isolated forms. To our knowledge, only one study focused on the comparison between IGHD and MPHD in adults. In this study, a sub-analysis of KIMS database (Pfizer International Growth Study Database) conducted by Roger Abs et al. (166), no significant difference regarding causes was found, and hypothalamic-pituitary tumors and/or their treatment regimens constitute the most frequent causes for both groups IGHD and MPHD. Despite not being statistically significant, it was observed a higher rate of other sellar tumors (germ cell tumor, hamartoma, chordoma, glioma, meningioma, cyst) in IGHD (166). While macroadenomas are more likely associated with MPHD (165), small pituitary lesions, in particular non-functioning adenomas, may present with only IGHD (42).

Moreover, partial or complete hypopituitarism is often a consequence of pituitary surgery, but unlike other pituitary deficits that may recover over time, the somatotropic axis represents the one with the lowest probability to be reacquired (173).

Bearing in mind the consequences of the treatment of pituitary lesions, radiotherapy plays an important role in the onset of IGHD. As previously pointed out, GH-axis cells seem to be more radiosensitive, with damage tending to be irreversible even at very low doses (174). Specifically, in adults, the risk of GHD is dose and time related and continues to increase during time with a median onset latency of 27 months (175).

While doses of up to 18 Gy result in a rapid onset of IGHD, lower doses (≤ 10 Gy) could cause a late-onset damage, with a cumulative risk that increases with longer follow-up (176, 177), making therefore important investigating previous history of RT in childhood, both for sellar and non sellar tumors (178).

IGHD is also related to TBI (even mild) and SAH with a frequency at 3 months from the event that can be up to the 30% of the cases; anyway, in these situations IGHD is frequently transient, with a complete axis recovery by 12 months (22, 179, 180). An interesting review conducted by Gasco et al. has recently analyzed the literature data on hypopituitarism and GHD related to TBI. The pathophysiological mechanisms involved include neurotransmitter-mediated excitotoxicity, secondary ischemia and inflammatory response. Particularly, long hypophyseal portal vessels represent the only supply to the lateral portion of the gland and to the pars tuberalis, mostly populated by GH, PRL and FSH/LH secreting cells, subjected to a higher risk of damage. GHD is common both in the acute stage of TBI (first two weeks) and in the chronic phase (3 months after TBI) with a severe impact on the rehabilitation post-TBI (181).

A peculiar cause of TBI-induced pituitary dysfunction is represented by sport injuries. It was observed that amateur boxing and kickboxing, as a consequence of chronic and repetitive head trauma, may both cause IGHD (182, 183). Nervous system infections (25, 184, 185) and ischemic stroke (186–188) are other rarely reported causes of GHD. Anyway, these data are derived from broader studies on hypopituitarism and are not specific to IGHD.

Finally, GHD may be the possible consequence of ICPi but data on the isolated form are not available; as a matter of fact, in this clinical context somatotropic axis is surely less studied because potential substitutive therapy would be contraindicated from the oncological point of view (99).

6.3 When to suspect an isolated growth hormone deficiency

Nowadays, GHD is a well-recognized syndrome characterized by increased fat body mass and decreased lean one, osteoporosis and augmented fracture risk, hypertension, abdominal obesity, diabetes mellitus (DM), dyslipidemia and enhanced thrombotic factors with an increased global cardiovascular risk. Reduced vitality, muscle strength and early exhaustion are the most reported symptoms (189). Rogers et Arm (166) showed no statistically significant differences in clinical presentation between IGHD and MPHD, supporting the thesis that GHD alone is responsible for all metabolic aspects. Because of the high frequency of these signs and symptoms in the general population, clinicians are usually not able to clinically suspect IGHD. This aspect explains why GH-stimulation tests are generally performed only in patients with a suggestive clinical context and with a history of possible pituitary damage.

In the presence of documented genetic alteration, re-testing in transition age is unnecessary. In idiopathic CO-GHD, conversely, patients with low-normal (between 0 to -2DS) or low (< -2DS) serum IGF-I levels, re-testing after at least 1 month withdrawal of rhGH is mandatory (159).

Recent guidelines have focused on the need to test for GHD only patients who may actually be treated if the biochemical diagnosis is confirmed (159). The Food and Drug Administration approval of rhGH replacement therapy for adults lists active malignancy as a contraindication, considering the known growth-promoting effects of GH and IGF-I. Several studies demonstrated the safety of rhGH on tumor regrowth or recurrence after surgery in patients with pituitary tumors or craniopharingiomas making IGHD diagnosis still recommended in these cases (190–197).

IGHD should definitely be suspected in patients with previous history of TBI or SAH because of the high frequency of the condition in this setting, and considering the positive effect of therapy on the reduction of post-TBI sequelae and subsequent rehabilitation (181). Indications for testing are: moderate/severe TBI based on GCS score or mild complicated TBI (i.e., those who need hospitalisation, neurosurgical intervention, monitoring in Intensive Care Units or present anatomical changes on computed tomography scan, always on a risk/benefit ratio (181).

6.4 Diagnosis

GH secretion is pulsatile; thus, random GH levels have no diagnostic value in the evaluation of GHD. The measurement of serum IGF-I alone does not allow to properly identify GHD; indeed,

many physiological and pathological conditions, such as older age, DM, malnutrition, chronic liver disease and renal failure may lower serum IGF-I levels in adults, making the definition of a threshold challenging. Moreover, it is possible to assess normal IGF-I levels even in patients with GHD diagnosis. For example, an interesting study conducted by Yuen *at al* (159). has shown that patients with clinically non-functioning microadenomas may have normal serum IGF-I but biochemical evidence of incomplete response to GHRH-arginine test. For all these reasons, in case of strong suspicion of GHD, a stimulation test (ITT test, GHRH+arginine test, glucagon stimulation test, macimorelin stimulation test) is mandatory to confirm the diagnosis.

Furthermore, several studies have demonstrated that IGF-I levels are significantly higher in IGHD than in MPHD patients; similarly, these patients show a tendency for a higher GH response to stimulation tests than people with MPHD (166, 198). Again, a strong negative correlation between baseline IGF-I and the number of additional hormone deficiencies has been reported (199). Therefore, in patients with no other hormonal deficit, some authors suggest performing two tests in order to confirm the IGHD diagnosis (166, 200).

ITT still remains the gold standard. However, because of safety concerns, other tests are more widely performed in clinical practice, such as GHRH+arginine and GST. Furthermore, the identification of GH cut-offs is a widely debated issue because of the variability related to factors such as body mass index (BMI) and age. Diagnostic cut-offs for GHD generally recognized for the various possible tests are summarized in Table 6 (159, 201). As of today, regarding ITT, the diagnostic criteria do not correlate with BMI or age. A first attempt to integrate these data has been performed by Gasco et al, who have identified through ROC curves the best cut-off BMI-related to avoid false positive results (≤ 3.5 µg/L if BMI<25 Kg/m^2, ≤ 1.3 µg/L if BMI≥25 Kg/m^2) (202).

The best test and the correct timing to perform it has to be chosen taking into account the clinical history. Regarding this, no specific guidelines are available. Anyway, the evaluation of GH-axis with dynamic tests should be carried out after having properly corrected other concomitant pituitary hormone deficits.

As far as TBI is involved, it is recommended to test somatotropic axis at least six months after post-acute phase (203), even though other Authors proposed to postpone the evaluation until one year after TBI (204). Moreover, ITT is often considered unsafe in these patients because of the possible contraindications (i.e., seizure, cardiac disease). In the same way, in the post-surgery and SAH context, an early evaluation is not recommended because of the possibility of subsequent recovery over time. In patients with a previous history of radiotherapy, considering the possibility of late onset of IGHD and hypopituitarism, a longer follow-up should be scheduled, although no data regarding actual duration are available. Moreover, in previous cranial irradiation GHRH + Arginine is not recommended (190), because of the possibility of coexisting hypothalamic defect (cause of false negative outcomes).

TABLE 6 Growth Hormone Deficiency diagnostic cut-offs with different tests.

TEST	GH PEAK
ITT	≤ 3-5 µg/L
Macimorelin	≤ 2.8 µg/L
GST	≤ 3.0 µg/L in normal-weight patients ≤ 3.0 µg/L in overweight patients with a high pre-test probability ≤ 1.0 µg/L in overweight patients with a low pre-test probability ≤ 1.0 µg/L in obese patients
GHRH +arginine	≤ 11.5 µg/L in normal-weight patients ≤ 8.0 µg/L in overweight patients ≤ 4.2 µg/L in obese patients

GH, Growth hormone; ITT, Insulin tolerance test; GST, Glucagon stimulation test; GHRH, Growth Hormone Releasing Hormone.

6.5 Treatment and follow-up

GHD therapy is based on the hormone replacement with rhGH. Many commercial products are available and there is no evidence about the superiority of one on another. RhGH therapy has shown to be of benefit for body mass composition, skeletal integrity, lipid profile and muscle performance, although an improvement in overall cardiovascular mortality has not been demonstrated.

RhGH therapy is contraindicated in presence of an active malignancy, severe illness or advanced non-proliferative diabetic retinopathy. Individual patient characteristics should be taken into account when choosing the starting dose: 0.1 to 0.2 mg/day in patients with concurrent DM, obesity or age>60 years, 0.2-0.3 mg/day in 30-60 years, 0.4-0.5 mg/day in age < 30 years. Starting doses may be higher for patients transitioning from pediatric treatment (159). An evaluation every 1-2 months is suggested to properly titrate rhGH dose based on clinical response, side effects and individual consideration. Serum IGF-I levels and subjective perception of symptoms with validated quality of life questionnaires (QoL-AGHDA) (205) are the best markers to monitor the ongoing therapy. When maintenance rhGH doses are achieved, serum IGF-I, fasting glucose, glycosylated hemoglobin, lipidic profile, BMI, waist circumference and waist-to-hip ratio may be assessed at 6 to 12-months intervals and bone mineralization dual x-ray absorptiometry every 24 months (159).

It is important to remember that the initiation of replacement therapy can unmask the presence of other hormonal deficits but, at the same time, that GHD may simply be the first of several hormonal axes deficits to appear. It is therefore necessary to periodically monitor the remaining anterior-pituitary function. In particular, we need to consider that any clinical deterioration not otherwise explained may be related to the onset of other pituitary deficits, like CAI (69). For this reason, Guidelines suggest checking serum fT4 and the HPA axis annually, either by morning cortisol measurement or cosyntropin-stimulation test (159).

A review from Cerbone M. and Dattani M.T. focused on the risk factors for progression from IGHD to MPHD, identifying absent pituitary stalk, ectopic posterior pituitary, abnormal corpus callosum, empty sella, septo-optic dysplasia, longer duration of follow-up and genetic defects as risk factors for progression, with strong evidence (206).

No differences on therapy response were observed between MPHD and IGHD (166).

7 Isolated prolactin deficiency

7.1 Definition and epidemiology

Prolactin (PRL) deficiency is a condition characterized by low or undetectable PRL levels, as a potential consequence of the aforementioned causes of anterior pituitary dysfunction (Table 1). It usually presents in association with other hormonal insufficiencies and in this context, it has been reported as a marker for a more severe degree of hypopituitarism (207). Isolated PRL deficiency (IPRLD), conversely, is an extremely rare condition and up to now only few cases have been reported in literature (208–213). IPRLD is generally considered idiopathic; however, in some cases a potential genetic etiology can be speculated. In fact, in literature familial cases of hypoprolactinemia (e.g., mother and daughter) associated with puerperal alactogenesis are reported (210) and an autosomal recessive inheritance has been hypothesized (212). However, no genetic investigations were performed in the described cases and, to date, a specific gene for IPRLD has never been discovered. Finally, in one patient an autoimmune disorder selectively affecting the lactotroph cells has been outlined (212).

The most frequent cause of IPRLD is iatrogenic. Dopamine agonists (DA) are commonly used in clinical practice to treat PRL-secreting tumors and the chronic administration of these molecules (cabergoline, bromocriptine, quinagolide or pergolide) can sometimes lead to an inhibition of circulating PRL levels (214). In fact, lower PRL levels during DA are associated with long-term recovery in patients with prolactinomas (215). Even aripiprazole, an atypical antipsychotic agent with a partial agonist activity on dopamine receptors (D2), could determine a reduction and suppression of PRL levels when administered at higher doses than 5 mg/day (216).

Moreover, hypoprolactinemia has been described in patients with hemochromatosis (217) and in patients with pseudohypoparathyroidism, a rare genetic disorder characterized by a resistance to parathyroid hormone (PTH) caused by GNAS (guanine nucleotide binding protein, alpha stimulating) mutations. In pseudohypoparathyroidism lactotroph cells has shown a lack of responsivity to PTH, that normally increases plasma PRL in adults (218).

7.2 When to suspect an isolated prolactin deficiency and diagnosis

All reported cases of IPRLD described in literature concerned women, and the condition was revealed by a lactation failure occurring after delivery (puerperal alactogenesis). To date, in men and in non-lactating and non-pregnant women, PRL deficiency has no clinical implications, even if recent data have demonstrated an apparent impaired sexual functioning, reduced wellbeing and increased cardiometabolic risk in patients with iatrogenic IPRLD (219).

In IPRLD women, usually no alteration of menses was reported. However, some women suffered from oligomenorrhea (209, 211) while some others reported a delayed ovulation (209) and a woman reported the necessity to be treated with clomiphene citrate in order to conceive (209). Due to the paucity of data, no cause-and-effect correlation can be determined between these conditions and hypoprolactinemia.

The diagnosis of IPRLD is established in the context of a normal pituitary function with the evidence of low or undetectable PRL levels and failure to increase after administration of TRH or antidopaminergic medications (e.g., metoclopramide or chlorpromazine) (212, 220).

7.3 Therapy and follow up

As of today, it is still not clear how to treat women with hypoprolactinemia and with the consequent inability to breastfeed. Lactation has been shown to be positively affected by human recombinant prolactin (R-hPRL), which is able to increase serum PRL levels and milk volume in PRL-deficient women (221). Nevertheless, no further studies were published after 2011 about this topic, and R-hPRL is not commercially available nor routinely used in clinical practice.

It has been suggested to use a dopamine antagonist (such as domperidone or metoclopramide) in order to increase PRL levels and favour lactation. These drugs, however, are considered off-label and no recommendation regarding their routine use is available yet (222).

In general, given the low impact of this condition on the general health status, there are no further indications about the follow up.

8 Conclusions

As emerged from this review, the knowledge regarding isolated hormonal deficits of anterior pituitary gland is still lacking a full and wide characterization, from an epidemiological, etiological and therapeutical point of view. Although some deficits present a characteristic clinical picture that allows the clinicians to raise a prompt diagnostic suspicion (e.g., ICAI and IHH), other deficits present non-specific signs and symptoms leading to potential underdiagnosed conditions. This can result in a lower detection rate and underestimated incidence and prevalence. Furthermore, little is known about the possible causes of the alterations (e.g., genetic or environmental) that may be responsible for a late onset disease. Eventually, considering that some deficits can be life threatening or at least can lead to a worse quality of life, more awareness is needed to make a diagnosis and to start a proper treatment as early as possible.

Author contributions

NP and SG conceived and designed the review. NP, LM, EV and DC conducted the literature search and wrote the first draft of the manuscript. MB, FB, CB, VG helped in writing the last version of the manuscript and supervised the whole work. All authors contributed to the article and approved the submitted version.

Acknowledgments

The Authors would thank Prof. Ezio Ghigo which gave the needed encouragement and support to investigate and supervised the findings of this work and Chiara Prencipe for her contribution in the design and graphic realization of the images of the manuscript.

Conflict of interest

The authors declare that the research was conducted in the absence of any commercial or financial relationships that could be construed as a potential conflict of interest.

Publisher's note

References

1. Regal M, Páramo C, Sierra JM, García-Mayor RV. Prevalence and incidence of hypopituitarism in an adult Caucasian population in northwestern Spain. *Clin Endocrinol* (2001) 55:735–40. doi: 10.1046/j.1365-2265.2001.01406.x

2. Crespo I, Santos A, Valassi E, Pires P, Webb SM, Resmini E. Impaired decision making and delayed memory are related with anxiety and depressive symptoms in acromegaly. *Endocrine* (2015) 50:756–63. doi: 10.1007/s12020-015-0634-6

3. Cangiano B, Swee DS, Quinton R, Bonomi M. Genetics of congenital hypogonadotropic hypogonadism: Peculiarities and phenotype of an oligogenic disease. *Hum Genet* (2021) 140:77–111. doi: 10.1007/s00439-020-02147-1

4. Persani L, Brabant G, Dattani M, Bonomi M, Feldt-Rasmussen U, Fliers E, et al. European Thyroid association (ETA) guidelines on the diagnosis and management of central hypothyroidism. *Eur Thyroid J* (2018) 7:225–37. doi: 10.1159/000491388

5. Dekkers OM, Hammer S, deKeizer RJW, Roelfsema F, Schutte PJ, Smit JWA, et al. The natural course of non-functioning pituitary macroadenomas. *Eur J Endocrinol* (2007) 156:217–24. doi: 10.1530/eje.1.02334

6. Darzy KH, Shalet SM. Pathophysiology of radiation-induced growth hormone deficiency: Efficacy and safety of GH replacement. *Growth Horm IGF Res* (2006) 16:30–40. doi: 10.1016/j.ghir.2006.03.002

7. Rutter MM, Rose SR. Long-term endocrine sequelae of childhood cancer. *Curr Opin Pediatr* (2007) 19:480–7. doi: 10.1097/MOP.0b013e3282058b56

8. Hochberg Z, Kuten A, Hertz P, Tatcher M, Kedar A, Benderly A. The effect of single-dose radiation on cell survival and growth hormone secretion by rat anterior pituitary cells. *Radiat Res* (1983) 94:508–12. doi: 10.2307/3575908

9. Cordeiro D, Xu Z, Li CE, Iorio-Morin C, Mathieu D, Sisterson ND, et al. Gamma knife radiosurgery for the treatment of nelson's syndrome: a multicenter, international study. *J Neurosurg* (2019) 133:336–41. doi: 10.3171/2019.4.JNS19273

10. Knappe UJ, Petroff D, Quinkler M, Schmid SM, Schöfl C, Schopohl J, et al. Fractionated radiotherapy and radiosurgery in acromegaly: analysis of 352 patients from the German acromegaly registry. *Eur J Endocrinol* (2020) 182:275–84. doi: 10.1530/EJE-19-0784

11. Cohen-Inbar O, Ramesh A, Xu Z, Vance ML, Schlesinger D, Sheehan JP. Gamma knife radiosurgery in patients with persistent acromegaly or cushing's disease: long-term risk of hypopituitarism. *Clin Endocrinol* (2016) 84:524–31. doi: 10.1111/cen.12938

12. Caputo M, Prencipe N, Bisceglia A, Bona C, Maccario M, Aimaretti G, et al. Primary pituitary lymphoma as rare cause of a pituitary mass and hypopituitarism in adulthood. *Endocr Pract* (2020) 26:1337–50. doi: 10.4158/EP-2020-0286

13. Pekic S, Milicevic S, Colovic N, Colovic M, Popovic V. Intravascular large b-cell lymphoma as a cause of hypopituitarism: gradual and late reversal of hypopituitarism after long-term remission of lymphoma with immunochemotherapy. *Endocr* (2008) 34:11–6. doi: 10.1007/s12020-008-9109-3

14. Seejore K, Kyriakakis N, Murray RD. Is chemotherapy implicated in the development of hypopituitarism in childhood cancer survivors? *J Clin Endocrinol Metab* (2020) 105:e1897–900. doi: 10.1210/clinem/dgz132

15. Schneider HJ, Rovere S, Corneli G, Croce CG, Gasco V, Rudà R, et al. Endocrine dysfunction in patients operated on for non-pituitary intracranial tumors. *Eur J Endocrinol* (2006) 155:559–66. doi: 10.1530/eje.1.02272

16. Carpinteri R, Patelli I, Casanueva FF, Giustina A. Inflammatory and granulomatous expansive lesions of the pituitary. *Best Pract Res Clin Endocrinol Metab* (2009) 23:639–50. doi: 10.1016/j.beem.2009.05.009

17. Chiloiro S, Capoluongo ED, Tartaglione T, Giampietro A, Bianchi A, Giustina A, et al. The changing clinical spectrum of hypophysitis. *Trends Endocrinol Metab* (2019) 30:590–602. doi: 10.1016/j.tem.2019.06.004

18. Joshi MN, Whitelaw BC, Carroll PV. MECHANISMS IN ENDOCRINOLOGY: Hypophysitis: diagnosis and treatment. *Eur J Endocrinol* (2018) 179:R151–63. doi: 10.1530/EJE-17-0009

19. Takahashi Y. MECHANISMS IN ENDOCRINOLOGY: Autoimmune hypopituitarism: novel mechanistic insights. *Eur J Endocrinol* (2020) 182:R59–66. doi: 10.1530/EJE-19-1051

20. Bando H, Iguchi G, Fukuoka H, Taniguchi M, Yamamoto M, Matsumoto R, et al. The prevalence of IgG4-related hypophysitis in 170 consecutive patients with hypopituitarism and/or central diabetes insipidus and review of the literature. *Eur J Endocrinol* (2014) 170:161–72. doi: 10.1530/EJE-13-0642

21. Torino F, Barnabei A, Paragliola RM, Marchetti P, Salvatori R, Corsello SM. Endocrine side-effects of anti-cancer drugs: mAbs and pituitary dysfunction: clinical evidence and pathogenic hypotheses. *Eur J Endocrinol* (2013) 169:R153–164. doi: 10.1530/EJE-13-0434

22. Aimaretti G, Ambrosio MR, Di Somma C, Fusco A, Cannavò S, Gasperi M, et al. Traumatic brain injury and subarachnoid haemorrhage are conditions at high risk for hypopituitarism: screening study at 3 months after the brain injury. *Clin Endocrinol* (2004) 61:320–6. doi: 10.1111/j.1365-2265.2004.02094.x

23. Lieberman SA, Oberoi AL, Gilkison CR, Masel BE, Urban RJ. Prevalence of neuroendocrine dysfunction in patients recovering from traumatic brain injury. *J Clin Endocrinol Metabol* (2001) 86:5. doi: 10.1210/jcem.86.6.7592

24. Kelly DF, Gaw Gonzalo IT, Cohan P, Berman N, Swerdloff R, Wang C. Hypopituitarism following traumatic brain injury and aneurysmal subarachnoid hemorrhage: a preliminary report. *J Neurosurg* (2000) 93:743–52. doi: 10.3171/jns.2000.93.5.0743

25. Pekic S, Popovic V. DIAGNOSIS OF ENDOCRINE DISEASE: Expanding the cause of hypopituitarism. *Eur J Endocrinol* (2017) 176:R269–82. doi: 10.1530/EJE-16-1065

26. Golay V, Roychowdhary A, Dasgupta S, Pandey R. Hypopituitarism in patients with vasculotoxic snake bite envenomation related acute kidney injury: a prospective study on the prevalence and outcomes of this complication. *Pituitary* (2014) 17:125–31. doi: 10.1007/s11102-013-0477-1

27. Nawar RN, AbdelMannan D, Selman WR, Arafah BM. Analytic review: Pituitary tumor apoplexy: A review. *J Intensive Care Med* (2008) 23:75–90. doi: 10.1177/0885066607312992

28. Briet C, Salenave S, Bonneville J-F, Laws ER, Chanson P. Pituitary apoplexy. *Endocr Rev* (2015) 36:622–45. doi: 10.1210/er.2015-1042

29. Tanriverdi F, Dokmetas HS, Kebapcı N, Kilicli F, Atmaca H, Yarman S, et al. Etiology of hypopituitarism in tertiary care institutions in Turkish population: analysis of 773 patients from pituitary study group database. *Endocrine* (2014) 47:198–205. doi: 10.1007/s12020-013-0127-4

30. Diri H, Tanriverdi F, Karaca Z, Senol S, Unluhizarci K, Durak AC, et al. Extensive investigation of 114 patients with sheehan's syndrome: a continuing disorder. *Eur J Endocrinol* (2014) 171:311–8. doi: 10.1530/EJE-14-0244

31. Kucharska A, Łaguna P, Adamowicz-Salach A, Witkowska-Sędek E, Klukowska A. Growth hormone deficiency as a complication of haemophilia - a case report and

literature data. *Pediatr Endocrinol Diabetes Metab* (2020) 26:150–4. doi: 10.5114/pedm.2020.95619

32. Setian N, Tanaka CM, Damiani D, Dichtchekenian V, Carneiro JDA, D'Amico. Hypopituitarism EA. Deficiency of factors V and VIII and von willebrand factor: An uncommon association. *J Pediatr Endocrinol Metab* (2002) 15:331–4. doi: 10.1515/JPEM.2002.15.3.331

33. Klinge J, Auberger K, Auerswald G, Brackmann HH, Mauz-Körholz CH, Kreuz W, et al. Prevalence and outcome of intracranial haemorrhage in haemophiliacs – a survey of the paediatric group of the German society of thrombosis and haemostasis (GTH). *Eur J Pediatr* (1999) 158:S162–5. doi: 10.1007/PL00014346

34. Higham CE, Johannsson G, Shalet SM. Hypopituitarism. *Lancet* (2016) 388:2403–15. doi: 10.1016/S0140-6736(16)30053-8

35. Alatzoglou KS, Dattani MT. Genetic forms of hypopituitarism and their manifestation in the neonatal period. *Early Hum Dev* (2009) 85:705–12. doi: 10.1016/j.earlhumdev.2009.08.057

36. Steinberg A, Shechter FR, Segal HI. True pituitary addison's disease–a pituitary unitropic deficiency (fifteen-year follow-up)*. *J Clin Endocrinol Metab* (1954) 14:1519–29. doi: 10.1210/jcem-14-12-1519

37. Erichsen MM, Løvås K, Fougner KJ, Svartberg J, Hauge ER, Bollerslev J, et al. Normal overall mortality rate in addison's disease, but young patients are at risk of premature death. *Eur J Endocrinol* (2009) 160:233–7. doi: 10.1530/EJE-08-0550

38. Broersen LHA, van Haalen FM, Kienitz T, Dekkers OM, Strasburger CJ, Pereira AM, et al. The incidence of adrenal crisis in the postoperative period of HPA axis insufficiency after surgical treatment for cushing's syndrome. *Eur J Endocrinol* (2019) 181:201–10. doi: 10.1530/EJE-19-0202

39. Wright JJ, Powers AC, Johnson DB. Endocrine toxicities of immune checkpoint inhibitors. *Nat Rev Endocrinol* (2021) 17:389–99. doi: 10.1038/s41574-021-00484-3

40. Barroso-Sousa R, Barry WT, Garrido-Castro AC, Hodi FS, Min L, Krop IE, et al. Incidence of endocrine dysfunction following the use of different immune checkpoint inhibitor regimens: A systematic review and meta-analysis. *JAMA Oncol* (2018) 4:173–82. doi: 10.1001/jamaoncol.2017.3064

41. Vallotton MB. Endocrine emergencies. disorders of the adrenal cortex. *Baillieres Clin Endocrinol Metab* (1992) 6:41–56. doi: 10.1016/s0950-351x(05)80330-1

42. Ferrante E, Ferraroni M, Castrignanò T, Menicatti L, Anagni M, Reimondo G, et al. Non-functioning pituitary adenoma database: a useful resource to improve the clinical management of pituitary tumors. *Eur J Endocrinol* (2006) 155:823–9. doi: 10.1530/eje.1.02298

43. Téblick A, Gunst J, Van den Berghe G. Critical illness–induced corticosteroid insufficiency: What it is not and what it could be. *J Clin Endocrinol Metab* (2022) 107:2057–64. doi: 10.1210/clinem/dgac201

44. Odagaki T, Noguchi Y, Fukui T. Flexion contractures of the legs as the initial manifestation of adrenocortical insufficiency. *Intern Med* (2003) 42:710–3. doi: 10.2169/internalmedicine.42.710

45. Tamaya S, Ihara C, Tsuji K, Nanno M, Maekawa N, Matsumoto S, et al. [Isolated ACTH deficiency with severe muscle atrophy]. *Nihon Naika Gakkai Zasshi* (2000) 89:983–5. doi: 10.2169/naika.89.983

46. Komatsu T, Ohara N, Hirota N, Yoneoka Y, Tani T, Terajima K, et al. Isolated adrenocorticotropic hormone deficiency presenting with severe hyponatremia and rhabdomyolysis: A case report and literature review. *Am J Case Rep* (2019) 20:1857–63. doi: 10.12659/AJCR.918427

47. Pecori Giraldi F, Fatti LM, Cavagnini F. Isolated corticotrophin deficiency presenting with pericardial effusion. *J Endocrinol Invest* (2005) 28:831–3. doi: 10.1007/BF03347576

48. Mayinger B, Harsch IA, Axelos D, Hahn EG. [Isolated ACTH deficiency as a rare cause of recurrent syncope and hypoglycemia]. *Med Klin (Munich)* (2000) 95:701–5. doi: 10.1007/pl00002089

49. Otsuka F, Yamamoto K, Shimada N, Kageyama J, Ogura T, Makino H. Cholestatic jaundice: An unusual symptom of isolated adrenocorticotropin deficiency in adults. *J Endocrinol Invest* (2004) 27:404–5. doi: 10.1007/BF03351070

50. Taguchi T, Yoshida M, Terada Y. Petrified ear auricles with isolated adrenocorticotropic hormone deficiency. *Intern Med* (2017) 56:3263–4. doi: 10.2169/internalmedicine.9108-17

51. Atkin SL, Masson EA, White MC. Isolated adrenocorticotropin deficiency presenting as primary infertility. *J Endocrinol Invest* (1995) 18:456–9. doi: 10.1007/BF03349745

52. Kalambokis G, Vassiliou V, Vergos T, Christou L, Tsatsoulis A, Tsianos EV. Isolated ACTH deficiency associated with crohn's disease. *J Endocrinol Invest* (2004) 27:961–4. doi: 10.1007/BF03347541

53. Corcuff J-B, Lafranque P, Henry P, Roger P. Isolated corticotroph insufficiency associated to myasthenia gravis. *J Endocrinol Invest* (1997) 20:669–71. doi: 10.1007/BF03348029

54. Yonemura K, Yasuda H, Fujigaki Y, Oki Y, Hishida A. Adrenal insufficiency due to isolated adrenocorticotropin deficiency complicated by autosomal recessive polycystic kidney disease. *Renal Failure* (2003) 25:485–92. doi: 10.1081/JDI-120021162

55. Bando H, Iguchi G, Kanie K, Nishizawa H, Matsumoto R, Fujita Y, et al. Isolated adrenocorticotropic hormone deficiency as a form of paraneoplastic syndrome. *Pituitary* (2018) 21:480–9. doi: 10.1007/s11102-018-0901-7

56. Aanderud S, Jorde R. ACTH deficiency, hyperprolactinemia and benign intracranial hypertension. a case report. *Acta Endocrinol (Copenh)* (1988) 118:346–50. doi: 10.1530/acta.0.1180346

57. Oueslati I, Ben Jemaa M, Yazidi M, Chaker F, Chihaoui M. Late-onset isolated corticotrope deficiency in a woman with down syndrome. *Case Rep Endocrinol* (2021) 2021:5562831. doi: 10.1155/2021/5562831

58. Matsuo K, Koga M, Oishi M, Kawai M, Kanda T. Cognitive impairment caused by isolated adrenocorticotropic hormone deficiency without other hypo-adrenalism signs - autoimmune encephalopathy mimics. *Intern Med* (2020) 59:119–20. doi: 10.2169/internalmedicine.3234-19

59. Ishimura H. [A case of secondary adrenocortical insufficiency due to isolated ACTH deficiency that developed following a mental health disorder]. *Sangyo Eiseigaku Zasshi* (2019) 61:133–7. doi: 10.1539/sangyoeisei.2019-001-D

60. Raj R, Jacob A, Elshimy G, Smith J. Isolated adrenocorticotropic hormone deficiency secondary to chronic opiate use. *Cureus* (2020) 12:e9270. doi: 10.7759/cureus.9270

61. Ohara N, Kobayashi M, Tuchida M, Koda R, Yoneoka Y, Iino N. Isolated adrenocorticotropic hormone deficiency and primary hypothyroidism in a patient undergoing long-term hemodialysis: A case report and literature review. *Am J Case Rep* (2020) 21:e922376. doi: 10.12659/AJCR.922376

62. Kearney T, Robinson S, Johnston DG. Isolated corticotropin deficiency in chronic alcoholism. *J R Soc Med* (2000) 93:15–7. doi: 10.1177/014107680009300105

63. Miller MJ, Horst TV. Isolated ACTH deficiency and primary hypothyroidism. *Acta Endocrinol (Copenh)* (1982) 99:573–6. doi: 10.1530/acta.0.0990573

64. Martin-Du Pan RC, Rouiller D, Goumaz M. [Isolated ACTH deficiency and primary thyroid insufficiency in an atopic patient: hypophysitis?]. *Schweiz Med Wochenschr* (1994) 124:806–9.

65. Miyauchi S, Yamashita Y, Matsuura B, Onji M. Isolated ACTH deficiency with graves' disease: a case report. *Endocr J* (2004) 51:115–9. doi: 10.1507/endocrj.51.115

66. Giustina A, Candrina R, Cimino A, Romanelli G. Development of isolated ACTH deficiency in a man with type I diabetes mellitus. *J Endocrinol Invest* (1988) 11:375–7. doi: 10.1007/BF03349058

67. Kojima I, Nejima I, Ogata E. Isolated adrenocorticotropin deficiency associated with polyglandular failure. *J Clin Endocrinol Metab* (1982) 54:182–6. doi: 10.1210/jcem-54-1-182

68. Morita S, Tsuji T, Kishimoto S, Uraki S, Takeshima K, Iwakura H, et al. Isolated ACTH deficiency following immunization with the BNT162b2 SARS-CoV-2 vaccine: a case report. *BMC Endocr Disord* (2022) 22:185. doi: 10.1186/s12902-022-01095-3

69. Fleseriu M, Hashim IA, Karavitaki N, Melmed S, Murad MH, Salvatori R, et al. Hormonal replacement in hypopituitarism in adults: An endocrine society clinical practice guideline. *J Clin Endocrinol Metab* (2016) 101:3888–921. doi: 10.1210/jc.2016-2118

70. Kosak M, Duskova M, Starka L, Jandikova H, Pospisilova H, Sramkova M, et al. Can the gold standard be beaten? how reliable are various modifications of the synacthen test compared to the insulin tolerance test. *Physiol Res* (2017) 66:S387–95. doi: 10.33549/physiolres.933729

71. Daidoh H, Morita H, Mune T, Murayama M, Hanafusa J, Ni H, et al. Responses of plasma adrenocortical steroids to low dose ACTH in normal subjects. *Clin Endocrinol (Oxf)* (1995) 43:311–5. doi: 10.1111/j.1365-2265.1995.tb02037.x

72. Streeten DH, Anderson GHJr, Bonaventura MM. The potential for serious consequences from misinterpreting normal responses to the rapid adrenocorticotropin test. *J Clin Endocrinol Metab* (1996) 81:285–90. doi: 10.1210/jcem.81.1.8550765

73. Karaca Z, Grossman A, Kelestimur F. Investigation of the hypothalamo-pituitary-adrenal (HPA) axis: a contemporary synthesis. *Rev Endocr Metab Disord* (2021) 22:179–204. doi: 10.1007/s11154-020-09611-3

74. Leong KS, Walker AB, Martin I, Wile D, Wilding J, MacFarlane IA. An audit of 500 subcutaneous glucagon stimulation tests to assess growth hormone and ACTH secretion in patients with hypothalamic–pituitary disease. *Clin Endocrinol* (2001) 54:463–8. doi: 10.1046/j.1365-2265.2001.01169.x

75. Schneider HJ, Aimaretti G, Kreitschmann-Andermahr I, Stalla G-K, Ghigo E. Hypopituitarism. *Lancet* (2007) 369:1461–70. doi: 10.1016/S0140-6736(07)60673-4

76. Gasco V, Bima C, Geranzani A, Giannelli J, Marinelli L, Bona C, et al. Morning serum cortisol level predicts central adrenal insufficiency diagnosed by insulin tolerance test. *NEN* (2021) 111:1238–48. doi: 10.1159/000514216

77. Bioletto F, Berton AM, Varaldo E, Cuboni D, Bona C, Parasiliti-Caprino M, et al. Development and internal validation of a predictive score for the diagnosis of central adrenal insufficiency when morning cortisol is in the grey zone. *J Endocrinol Invest* (2022) 46(3):535–43. doi: 10.1007/s40618-022-01926-z

78. Reznik Y, Barat P, Bertherat J, Bouvattier C, Castinetti F, Chabre O, et al. SFE/SFEDP adrenal insufficiency French consensus: Introduction and handbook. *Annales d'Endocrinol* (2018) 79:1–22. doi: 10.1016/j.ando.2017.12.001

79. Prencipe N, Parasiliti-Caprino M, Gatti F, Penner F, Berton AM, Bona C, et al. Second-day morning cortisol levels after transsphenoidal surgery are accurate predictors of secondary adrenal insufficiency with diagnostic cut-offs similar to those in non-stressed conditions. *NEN* (2021) 111:639–49. doi: 10.1159/000509092

80. Prete A, Bancos I. Glucocorticoid induced adrenal insufficiency. *BMJ* (2021), 374:n1380. doi: 10.1136/bmj.n1380

81. Rose SR, Horne VE, Howell J, Lawson SA, Rutter MM, Trotman GE, et al. Late endocrine effects of childhood cancer. *Nat Rev Endocrinol* (2016) 12:319–36. doi: 10.1038/nrendo.2016.45

82. Gasco V, Prodam F, Pagano L, Grottoli S, Belcastro S, Marzullo P, et al. Hypopituitarism following brain injury: when does it occur and how best to test? *Pituitary* (2012) 15:20–4. doi: 10.1007/s11102-010-0235-6

83. Stelmachowska-Banaś M, Czajka-Oraniec I. Management of endocrine immune-related adverse events of immune checkpoint inhibitors: an updated review. *Endocr Connect* (2020) 9:R207–28. doi: 10.1530/EC-20-0342

84. Younes AK, Younes NK. Recovery of steroid induced adrenal insufficiency. *Transl Pediatr* (2017) 6:269–73. doi: 10.21037/tp.2017.10.01

85. Beck-Peccoz P, Rodari G, Giavoli C, Lania A. Central hypothyroidism - a neglected thyroid disorder. *Nat Rev Endocrinol* (2017) 13:588–98. doi: 10.1038/nrendo.2017.47

86. Faglia G, Bitensky L, Pinchera A, Ferrari C, Paracchi A, Beck-Peccoz P, et al. Thyrotropin secretion in patients with central hypothyroidism: evidence for reduced biological activity of immunoreactive thyrotropin. *J Clin Endocrinol Metab* (1979) 48:989–98. doi: 10.1210/jcem-48-6-989

87. Persani L, Ferretti E, Borgato S, Faglia G, Beck-Peccoz P. Circulating thyrotropin bioactivity in sporadic central hypothyroidism. *J Clin Endocrinol Metab* (2000) 85:3631–5. doi: 10.1210/jcem.85.10.6895

88. Chaker L, Razvi S, Bensenor IM, Azizi F, Pearce EN, Peeters RP. Hypothyroidism. *Nat Rev Dis Primers* (2022) 8:1–17. doi: 10.1038/s41572-022-00357-7

89. Lauffer P, Zwaveling-Soonawala N, Naafs JC, Boelen A, van Trotsenburg ASP. Diagnosis and management of central congenital hypothyroidism. *Front Endocrinol (Lausanne)* (2021) 12:686317. doi: 10.3389/fendo.2021.686317

90. Alexopoulou O, Beguin C, De Nayer P, Maiter D. Clinical and hormonal characteristics of central hypothyroidism at diagnosis and during follow-up in adult patients. *Eur J Endocrinol* (2004) 150:1–8. doi: 10.1530/eje.0.1500001

91. Andersen S, Pedersen KM, Bruun NH, Laurberg P. Narrow individual variations in serum T(4) and T(3) in normal subjects: a clue to the understanding of subclinical thyroid disease. *J Clin Endocrinol Metab* (2002) 87:1068–72. doi: 10.1210/jcem.87.3.8165

92. Ormston BJ, Cryer RJ, Garry R, Besser GM, Hall R. Thyrotrophin-releasing hormone as a thyroid-function test. *Lancet* (1971) 2:10–4. doi: 10.1016/s0140-6736(71)90005-5

93. van Tijn DA, de Vijlder JJM, Vulsma T. Role of the thyrotropin-releasing hormone stimulation test in diagnosis of congenital central hypothyroidism in infants. *J Clin Endocrinol Metab* (2008) 93:410–9. doi: 10.1210/jc.2006-2656

94. Atmaca H, Tanriverdi F, Gokce C, Unluhizarci K, Kelestimur F. Do we still need the TRH stimulation test? *Thyroid* (2007) 17:529–33. doi: 10.1089/thy.2006.0311

95. Obregon M-J, Escobar del Rey F, Morreale de Escobar G. The effects of iodine deficiency on thyroid hormone deiodination. *Thyroid* (2005) 15:917–29. doi: 10.1089/thy.2005.15.917

96. Burch HB. Drug effects on the thyroid. *New Engl J Med* (2019) 381(20):1980–1. doi: 10.1056/NEJMra1901214

97. Sherman SI, Gopal J, Haugen BR, Chiu AC, Whaley K, Nowlakha P, et al. Central hypothyroidism associated with retinoid X receptor-selective ligands. *N Engl J Med* (1999) 340:1075–9. doi: 10.1056/NEJM199904083401404

98. Russo M, Scollo C, Pellegriti G, Cotta OR, Squatrito S, Frasca F, et al. Mitotane treatment in patients with adrenocortical cancer causes central hypothyroidism. *Clin Endocrinol (Oxf)* (2016) 84:614–9. doi: 10.1111/cen.12868

99. Chang L-S, Barroso-Sousa R, Tolaney SM, Hodi FS, Kaiser UB, Min L. Endocrine toxicity of cancer immunotherapy targeting immune checkpoints. *Endocr Rev* (2019) 40:17–65. doi: 10.1210/er.2018-00006

100. Lupoli R, Di Minno A, Tortora A, Ambrosino P, Lupoli GA, Di Minno MND. Effects of treatment with metformin on TSH levels: a meta-analysis of literature studies. *J Clin Endocrinol Metab* (2014) 99:E143–148. doi: 10.1210/jc.2013-2965

101. Keen F, Chalishazar A, Mitchem K, Dodd A, Kalhan A. Central hypothyroidism related to antipsychotic and antidepressant medications: an observational study and literature review. *Eur Thyroid J* (2022) 11:e210119. doi: 10.1530/ETJ-21-0119

102. McConnell RJ. Abnormal thyroid function test results in patients taking salsalate. *JAMA* (1992) 267:1242–3. doi: 10.1001/jama.1992.03480090090033

103. Surks MI, DeFesi CR. Normal serum free thyroid hormone concentrations in patients treated with phenytoin or carbamazepine. *A paradox resolved JAMA* (1996) 275:1495–8. doi: 10.1001/jama.1996.03530430039036

104. Warner MH, Beckett GJ. Mechanisms behind the non-thyroidal illness syndrome: an update. *J Endocrinol* (2010) 205:1–13. doi: 10.1677/JOE-09-0412

105. Fliers E, Boelen A. An update on non-thyroidal illness syndrome. *J Endocrinol Invest* (2021) 44:1597–607. doi: 10.1007/s40618-020-01482-4

106. Miyai K. Congenital thyrotropin deficiency–from discovery to molecular biology, postgenome and preventive medicine. *Endocr J* (2007) 54:191–203. doi: 10.1507/endocrj.kr-107

107. Bonomi M, Proverbio MC, Weber G, Chiumello G, Beck-Peccoz P, Persani L. Hyperplastic pituitary gland, high serum glycoprotein hormone alpha-subunit, and variable circulating thyrotropin (TSH) levels as hallmark of central hypothyroidism due to mutations of the TSH beta gene. *J Clin Endocrinol Metab* (2001) 86:1600–4. doi: 10.1210/jcem.86.4.7411

108. Partsch C-J, Riepe FG, Krone N, Sippell WG, Pohlenz J. Initially elevated TSH and congenital central hypothyroidism due to a homozygous mutation of the TSH beta subunit gene: case report and review of the literature. *Exp Clin Endocrinol Diabetes* (2006) 114:227–34. doi: 10.1055/s-2006-924232

109. Beck-Peccoz P. Treatment of central hypothyroidism. *Clin Endocrinol (Oxf)* (2011) 74:671–2. doi: 10.1111/j.1365-2265.2011.04037.x

110. Ferretti E, Persani L, Jaffrain-Rea ML, Giambona S, Tamburrano G, Beck-Peccoz P. Evaluation of the adequacy of levothyroxine replacement therapy in patients with central hypothyroidism. *J Clin Endocrinol Metab* (1999) 84:924–9. doi: 10.1210/jcem.84.3.5553

111. Arafah BM. Increased need for thyroxine in women with hypothyroidism during estrogen therapy. *N Engl J Med* (2001) 344:1743–9. doi: 10.1056/NEJM200106073442302

112. Ross A, Bhasin S. Hypogonadism: Its prevalence and diagnosis. *Urol Clinics North America* (2016) 43:163–76. doi: 10.1016/j.ucl.2016.01.002

113. Young J, Xu C, Papadakis GE, Acierno JS, Maione L, Hietamäki J, et al. Clinical management of congenital hypogonadotropic hypogonadism. *Endocr Rev* (2019) 40:669–710. doi: 10.1210/er.2018-00116

114. Lima Amato LG, Latronico AC, Gontijo Silveira LF. Molecular and genetic aspects of congenital isolated hypogonadotropic hypogonadism. *Endocrinol Metab Clinics North America* (2017) 46:283–303. doi: 10.1016/j.ecl.2017.01.010

115. Casoni F, Malone SA, Belle M, Luzzati F, Collier F, Allet C, et al. Development of the neurons controlling fertility in humans: new insights from 3D imaging and transparent fetal brains. *Development* (2016) 143:3969–81. doi: 10.1242/dev.139444

116. Boehm U, Bouloux P-M, Dattani MT, de Roux N, Dodé C, Dunkel L, et al. Expert consensus document: European consensus statement on congenital hypogonadotropic hypogonadism–pathogenesis, diagnosis and treatment. *Nat Rev Endocrinol* (2015) 11:547–64. doi: 10.1038/nrendo.2015.112

117. Dwyer AA, Sykiotis GP, Hayes FJ, Boepple PA, Lee H, Loughlin KR, et al. Trial of recombinant follicle-stimulating hormone pretreatment for GnRH-induced fertility in patients with congenital hypogonadotropic hypogonadism. *J Clin Endocrinol Metab* (2013) 98:E1790–5. doi: 10.1210/jc.2013-2518

118. Laitinen E-M, Vaaralahti K, Tommiska J, Eklund E, Tervaniemi M, Valanne L, et al. Incidence, phenotypic features and molecular genetics of kallmann syndrome in Finland. *Orphanet J Rare Dis* (2011) 6:41. doi: 10.1186/1750-1172-6-41

119. Hanchate NK, Giacobini P, Lhuillier P, Parkash J, Espy C, Fouveaut C, et al. SEMA3A, a gene involved in axonal pathfinding, is mutated in patients with kallmann syndrome. *PloS Genet* (2012) 8:e1002896. doi: 10.1371/journal.pgen.1002896

120. Basaran Y, Bolu E, Unal HU, Sagkan RI, Taslipinar A, Ozgurtas T, et al. Multiplex ligation dependent probe amplification analysis of KAL1, GNRH1, GNRHR, PROK2 and PROKR2 in male patients with idiopathic hypogonadotropic hypogonadism. *Endokrynol Polska* (2013) 64:285–92. doi: 10.5603/EP.2013.0007

121. Stamou MI, Varnavas P, Plummer L, Koika V, Georgopoulos NA. Next-generation sequencing refines the genetic architecture of Greek GnRH-deficient patients. *Endocr Connect* (2019) 8:468–80. doi: 10.1530/EC-19-0010

122. Tommiska J, Känsäkoski J, Christiansen P, Jørgensen N, Lawaetz JG, Juul A, et al. Genetics of congenital hypogonadotropic hypogonadism in Denmark. *Eur J Med Genet* (2014) 57:345–8. doi: 10.1016/j.ejmg.2014.04.002

123. Kim S-H, Hu Y, Cadman S, Bouloux P. Diversity in fibroblast growth factor receptor 1 regulation: learning from the investigation of kallmann syndrome. *J Neuroendocrinol* (2008) 20:141–63. doi: 10.1111/j.1365-2826.2007.01627.x

124. Xu N, Qin Y, Reindollar RH, Tho SPT, McDonough PG, Layman LC. A mutation in the fibroblast growth factor receptor 1 gene causes fully penetrant normosmic isolated hypogonadotropic hypogonadism. *J Clin Endocrinol Metab* (2007) 92:1155–8. doi: 10.1210/jc.2006-1183

125. Tusset C, Trarbach EB, Silveira LFG, Beneduzzi D, Montenegro L, Latronico AC. Clinical and molecular aspects of congenital isolated hypogonadotropic hypogonadism. *Arquivos Brasileiros Endocrinol e Metab* (2011) 55:501–11. doi: 10.1590/s0004-27302011000800002

126. Pitteloud N, Boepple PA, Decruz S, Valkenburgh SB, Crowley Jr. WF, Hayes FJ. The fertile eunuch variant of idiopathic hypogonadotropic hypogonadism: Spontaneous reversal associated with a homozygous mutation in the gonadotropin-releasing hormone receptor. *J Clin Endocrinol Metab* (2001) 86:2470–5. doi: 10.1210/jc.86.6.2470

127. Seminara SB, Oliveira LMB, Beranova M, Hayes FJ, Crowley WF. Genetics of hypogonadotropic hypogonadism. *J Endocrinol Invest* (2000) 23:560–5. doi: 10.1007/BF03343776

128. Beneduzzi D, Trarbach EB, Min L, Jorge AAL, Garmes HM, Renk AC, et al. Role of gonadotropin-releasing hormone receptor mutations in patients with a wide spectrum of pubertal delay. *Fertil Steril* (2014) 102:838–846.e2. doi: 10.1016/j.fertnstert.2014.05.044

129. Corona G, Goulis DG, Huhtaniemi I, Zitzmann M, Toppari J, Forti G, et al. European Academy of andrology (EAA) guidelines on investigation, treatment and

monitoring of functional hypogonadism in males: Endorsing organization: European society of endocrinology. *Andrology* (2020) 8:970–87. doi: 10.1111/andr.12770

130. Gianetti E, Tusset C, Noel SD, Au MG, Dwyer AA, Hughes VA, et al. TAC3/TACR3 mutations reveal preferential activation of gonadotropin-releasing hormone release by neurokinin b in neonatal life followed by reversal in adulthood. *J Clin Endocrinol Metab* (2010) 95:2857–67. doi: 10.1210/jc.2009-2320

131. Zhu J, Choa RE-Y, Guo MH, Plummer L, Buck C, Palmert MR, et al. A shared genetic basis for self-limited delayed puberty and idiopathic hypogonadotropic hypogonadism. *J Clin Endocrinol Metab* (2015) 100:E646–54. doi: 10.1210/jc.2015-1080

132. Bonomi M, Vezzoli V, Krausz C, Guizzardi F, Vezzani S, Simoni M, et al. Characteristics of a nationwide cohort of patients presenting with isolated hypogonadotropic hypogonadism (IHH). *Eur J Endocrinol* (2018) 178:23–32. doi: 10.1530/EJE-17-0065

133. Quinton R, Duke VM, Robertson A, Kirk JMW, Matfin G, De Zoysa PA, et al. Idiopathic gonadotrophin deficiency: genetic questions addressed through phenotypic characterization*. *Clin Endocrinol* (2001) 55:163–74. doi: 10.1046/j.1365-2265.2001.01277.x

134. Bonomi M, Quinton R. Congenital GnRH deficiency: a complex and genetically heterogeneous disease affecting human fertility and sexual development. *Minerva Endocrinol* (2016) 41:183–7.

135. Gordon CM, Ackerman KE, Berga SL, Kaplan JR, Mastorakos G, Misra M, et al. Functional hypothalamic amenorrhea: An endocrine society clinical practice guideline. *J Clin Endocrinol Metab* (2017) 102:1413–39. doi: 10.1210/jc.2017-00131

136. Egalini F, Marinelli L, Rossi M, Motta G, Prencipe N, Rossetto Giaccherino R, et al. Endocrine disrupting chemicals: effects on pituitary, thyroid and adrenal glands. *Endocrine* (2022) 78:395–405. doi: 10.1007/s12020-022-03076-x

137. Gaudino R, De Filippo G, Bozzola E, Gasparri M, Bozzola M, Villani A, et al. Current clinical management of constitutional delay of growth and puberty. *Ital J Pediatr* (2022) 48:45. doi: 10.1186/s13052-022-01242-5

138. Bollino A, Cangiano B, Goggi G, Federici S, Duminuco P, Giovanelli L, et al. Pubertal delay: the challenge of a timely differential diagnosis between congenital hypogonadotropic hypogonadism and constitutional delay of growth and puberty. *Minerva Pediatr* (2020) 72:278–87. doi: 10.23736/S0026-4946.20.05860-0

139. Chaudhary S, Walia R, Bhansali A, Dayal D, Sachdeva N, Singh T, et al. FSH-stimulated inhibin b (FSH-iB): A novel marker for the accurate prediction of pubertal outcome in delayed puberty. *J Clin Endocrinol Metab* (2021) 106:e3495–505. doi: 10.1210/clinem/dgab357

140. Grinspon RP, Rey RA. New perspectives in the diagnosis of pediatric male hypogonadism: the importance of AMH as a sertoli cell marker. *Arq Bras Endocrinol Metabol* (2011) 55:512–9. doi: 10.1590/s0004-27302011000800003

141. Lewkowitz-Shpuntoff HM, Hughes VA, Plummer L, Au MG, Doty RL, Seminara SB, et al. Olfactory phenotypic spectrum in idiopathic hypogonadotropic hypogonadism: Pathophysiological and genetic implications. *J Clin Endocrinol Metab* (2012) 97:E136–44. doi: 10.1210/jc.2011-2041

142. De Souza MJ, Koltun KJ, Williams NI. The role of energy availability in reproductive function in the female athlete triad and extension of its effects to men: An initial working model of a similar syndrome in Male athletes. *Sports Med* (2019) 49:125–37. doi: 10.1007/s40279-019-01217-3

143. Nieschlag E, Vorona E. MECHANISMS IN ENDOCRINOLOGY: Medical consequences of doping with anabolic androgenic steroids: effects on reproductive functions. *Eur J Endocrinol* (2015) 173:R47–58. doi: 10.1530/EJE-15-0080

144. Tan RS, Scally MC. Anabolic steroid-induced hypogonadism – towards a unified hypothesis of anabolic steroid action. *Med Hypotheses* (2009) 72:723–8. doi: 10.1016/j.mehy.2008.12.042

145. Martin KA, Anderson RR, Chang RJ, Ehrmann DA, Lobo RA, Murad MH, et al. Evaluation and treatment of hirsutism in premenopausal women: An endocrine society* clinical practice guideline. *J Clin Endocrinol Metab* (2018) 103:1233–57. doi: 10.1210/jc.2018-00241

146. Cedars MI. Evaluation of female fertility-AMH and ovarian reserve testing. *J Clin Endocrinol Metab* (2022) 107:1510–9. doi: 10.1210/clinem/dgac039

147. Maione L, Dwyer AA, Francou B, Guiochon-Mantel A, Binart N, Bouligand J, et al. GENETICS IN ENDOCRINOLOGY: Genetic counseling for congenital hypogonadotropic hypogonadism and kallmann syndrome: new challenges in the era of oligogenism and next-generation sequencing. *Eur J Endocrinol* (2018) 178:R55–80. doi: 10.1530/EJE-17-0749

148. Nordenström A, Ahmed SF, van den Akker E, Blair J, Bonomi M, Brachet C, et al. Pubertal induction and transition to adult sex hormone replacement in patients with congenital pituitary or gonadal reproductive hormone deficiency: an endo-ERN clinical practice guideline. *Eur J Endocrinol* (2022) 186:G9–G49. doi: 10.1530/EJE-22-0073

149. Raivio T, Wikström AM, Dunkel L. Treatment of gonadotropin-deficient boys with recombinant human FSH: long-term observation and outcome. *Eur J Endocrinol* (2007) 156:105–11. doi: 10.1530/eje.1.02315

150. Kohva E, Huopio H, Hero M, Miettinen PJ, Vaaralahti K, Sidoroff V, et al. Recombinant human FSH treatment outcomes in five boys with severe congenital hypogonadotropic hypogonadism. *J Endocr Soc* (2018) 2:1345–56. doi: 10.1210/js.2018-00225

151. Raivio T, Toppari J, Perheentupa A, McNeilly AS, Dunkel L. Treatment of prepubertal gonadotrophin-deficient boys with recombinant human follicle-stimulating hormone. *Lancet* (1997) 350:263–4. doi: 10.1016/S0140-6736(05)62227-1

152. Naeraa RW, Nielsen J, Kastrup KW. Growth hormone and 17β-oestradiol treatment of turner girls — 2-year results. *Eur J Pediatr* (1994) 153:72–7. doi: 10.1007/BF01959210

153. Shah S, Forghani N, Durham E, Neely EK. A randomized trial of transdermal and oral estrogen therapy in adolescent girls with hypogonadism. *Int J Pediatr Endocrinol* (2014) 2014:12. doi: 10.1186/1687-9856-2014-12

154. Dumont A, Dewailly D, Plouvier P, Catteau-Jonard S, Robin G. Comparison between pulsatile GnRH therapy and gonadotropins for ovulation induction in women with both functional hypothalamic amenorrhea and polycystic ovarian morphology. *Gynecol Endocrinol* (2016) 32:999–1004. doi: 10.1080/09513590.2016.1191462

155. Quinton R, Cheow HK, Tymms DJ, Bouloux PM, Wu FC, Jacobs HS. Kallmann's syndrome: is it always for life? *Clin Endocrinol* (1999) 50:481–5. doi: 10.1046/j.1365-2265.1999.00708.x

156. Mao J-F, Xu H-L, Duan J, Chen R-R, Li L, Li B, et al. Reversal of idiopathic hypogonadotropic hypogonadism: a cohort study in Chinese patients. *Asian J Androl* (2015) 17:497–502. doi: 10.4103/1008-682X.145072

157. Sidhoum VF, Chan Y-M, Lippincott MF, Balasubramanian R, Quinton R, Plummer L, et al. Reversal and relapse of hypogonadotropic hypogonadism: Resilience and fragility of the reproductive neuroendocrine system. *J Clin Endocrinol Metab* (2014) 99:861–70. doi: 10.1210/jc.2013-2809

158. Sun T, Xu W, Chen Y, Niu Y, Wang T, Wang S, et al. Reversal of idiopathic hypogonadotropic hypogonadism in a Chinese male cohort. *Andrologia* (2022) 54(11): e14583. doi: 10.1111/and.14583

159. Yuen KCJ, Biller BMK, Radovick S, Carmichael JD, Jasim S, Pantalone KM, et al. American association of clinical endocrinologists and american college of endocrinology guidelines for management of growth hormone deficiency in adults and patients transitioning from pediaratic to adult care. *Endocr Pract* (2019) 25:1191–232. doi: 10.4158/GL-2019-0405

160. Sassolas G, Chazot FB, Jaquet P, Bachelot I, Chanson P, Rudelli CC, et al. GH deficiency in adults: an epidemiological approach. *Eur J Endocrinol* (1999) 141:595–600. doi: 10.1530/eje.0.1410595

161. Stochholm K, Gravholt CH, Laursen T, Jørgensen JO, Laurberg P, Andersen M, et al. Incidence of GH deficiency - a nationwide study. *Eur J Endocrinol* (2006) 155:61–71. doi: 10.1530/eje.1.02191

162. Allen DB, Backeljauw P, Bidlingmaier M, Biller BMK, Boguszewski M, Burman P, et al. GH safety workshop position paper: a critical appraisal of recombinant human GH therapy in children and adults. *Eur J Endocrinol* (2016) 174:P1–9. doi: 10.1530/EJE-15-0873

163. Nicolson A, Toogood AA, Rahim A, Shalet SM. The prevalence of severe growth hormone deficiency in adults who received growth hormone replacement in childhood [see comment]. *Clin Endocrinol (Oxf)* (1996) 44:311–6. doi: 10.1046/j.1365-2265.1996.671492.x

164. Mullis P E. Genetics of isolated growth hormone deficiency. *J Clin Res Pediatr Endocrinol* (2010) 2:52–62. doi: 10.4274/jcrpe.v2i2.52

165. Molitch ME. Nonfunctioning pituitary tumors and pituitary incidentalomas. *Endocrinol Metab Clin North Am* (2008) 37:151–71. doi: 10.1016/j.ecl.2007.10.011

166. Abs R, Mattsson AF, Bengtsson B-Å, Feldt-Rasmussen U, Góth MI, Koltowska-Häggström M, et al. Isolated growth hormone (GH) deficiency in adult patients: Baseline clinical characteristics and responses to GH replacement in comparison with hypopituitary patients. a sub-analysis of the KIMS database. *Growth Horm IGF Res* (2005) 15:349–59. doi: 10.1016/j.ghir.2005.06.018

167. Hernández LM, Lee PDK, Camacho-Hübner C. Isolated growth hormone deficiency. *Pituitary* (2007) 10:351–7. doi: 10.1007/s11102-007-0073-3

168. Bonfig W, Bechtold S, Bachmann S, Putzker S, Fuchs O, Pagel P, et al. Reassessment of the optimal growth hormone cut-off level in insulin tolerance testing for growth hormone secretion in patients with childhood-onset growth hormone deficiency during transition to adulthood. *J Pediatr Endocrinol Metab* (2008) 21:1049–56. doi: 10.1515/JPEM.2008.21.11.1049

169. Longobardi S, Merola B, Pivonello R, Di Rella F, Di Somma C, Colao A, et al. Reevaluation of growth hormone (GH) secretion in 69 adults diagnosed as GH-deficient patients during childhood. *J Clin Endocrinol Metab* (1996) 81:1244–7. doi: 10.1210/jcem.81.3.8772606

170. Melmed S. Idiopathic adult growth hormone deficiency. *J Clin Endocrinol Metab* (2013) 98:2187–97. doi: 10.1210/jc.2012-4012

171. Shalet SM, Toogood A, Rahim A, Brennan BM. The diagnosis of growth hormone deficiency in children and adults. *Endocr Rev* (1998) 19:203–23. doi: 10.1210/edrv.19.2.0329

172. Ezzat S, Asa SL, Couldwell WT, Barr CE, Dodge WE, Vance ML, et al. The prevalence of pituitary adenomas: a systematic review. *Cancer* (2004) 101:613–9. doi: 10.1002/cncr.20412

173. Arafah BM. Reversible hypopituitarism in patients with large nonfunctioning pituitary adenomas. *J Clin Endocrinol Metab* (1986) 62:1173–9. doi: 10.1210/jcem-62-6-1173

174. Roth C, Lakomek M, Schmidberger H, Jarry H. [Cranial irradiation induces premature activation of the gonadotropin-releasing-hormone]. *Klin Padiatr* (2001) 213:239–43. doi: 10.1055/s-2001-16854

175. Madaschi S, Sara M, Fiorino C, Claudio F, Losa M, Marco L, et al. Time course of hypothalamic-pituitary deficiency in adults receiving cranial radiotherapy for primary extrasellar brain tumors. *Radiother Oncol* (2011) 99:23–8. doi: 10.1016/j.radonc.2011.02.015

176. Lam KS, Tse VK, Wang C, Yeung RT, Ho JH. Effects of cranial irradiation on hypothalamic-pituitary function–a 5-year longitudinal study in patients with nasopharyngeal carcinoma. *Q J Med* (1991) 78:165–76. doi: 10.1016/j.radonc.2011.02.015

177. Littley MD, Shalet SM, Beardwell CG, Ahmed SR, Applegate G, Sutton ML. Hypopituitarism following external radiotherapy for pituitary tumours in adults. *Q J Med* (1989) 70:145–60.

178. Sathyapalan T, Dixit S. Radiotherapy-induced hypopituitarism: a review. *Expert Rev Anticancer Ther* (2012) 12:669–83. doi: 10.1586/era.12.27

179. Tölli A, Borg J, Bellander B-M, Johansson F, Höybye C. Pituitary function within the first year after traumatic brain injury or subarachnoid haemorrhage. *J Endocrinol Invest* (2017) 40:193–205. doi: 10.1007/s40618-016-0546-1

180. Tanriverdi F, Schneider HJ, Aimaretti G, Masel BE, Casanueva FF, Kelestimur F. Pituitary dysfunction after traumatic brain injury: A clinical and pathophysiological approach. *Endocr Rev* (2015) 36:305–42. doi: 10.1210/er.2014-1065

181. Gasco V, Cambria V, Bioletto F, Ghigo E, Grottoli S. Traumatic brain injury as frequent cause of hypopituitarism and growth hormone deficiency: Epidemiology, diagnosis, and treatment. *Front Endocrinol* (2021) 12:634415. doi: 10.3389/fendo.2021.634415

182. Kelestimur F, Tanriverdi F, Atmaca H, Unluhizarci K, Selcuklu A, Casanueva FF. Boxing as a sport activity associated with isolated GH deficiency. *J Endocrinol Invest* (2004) 27:RC28–32. doi: 10.1007/BF03345299

183. Tanriverdi F, Unluhizarci K, Coksevim B, Selcuklu A, Casanueva FF, Kelestimur F. Kickboxing sport as a new cause of traumatic brain injury-mediated hypopituitarism. *Clin Endocrinol* (2007) 66:360–6. doi: 10.1111/j.1365-2265.2006.02737.x

184. Schaefer S, Boegershausen N, Meyer S, Ivan D, Schepelmann K, Kann PH. Hypothalamic-pituitary insufficiency following infectious diseases of the central nervous system. *Eur J Endocrinol* (2008) 158:3–9. doi: 10.1530/EJE-07-0484

185. Tsiakalos A, Xynos ID, Sipsas NV, Kaltsas G. Pituitary insufficiency after infectious meningitis: a prospective study. *J Clin Endocrinol Metab* (2010) 95:3277–81. doi: 10.1210/jc.2010-0144

186. Booij HA, Gaykema WDC, Kuijpers K a. J, Pouwels MJM, den Hertog HM. Pituitary dysfunction and association with fatigue in stroke and other acute brain injury. *Endocr Connect* (2018) 7:R223–37. doi: 10.1530/EC-18-0147

187. Karamouzis I, Pagano L, Prodam F, Mele C, Zavattaro M, Busti A, et al. Clinical and diagnostic approach to patients with hypopituitarism due to traumatic brain injury (TBI), subarachnoid hemorrhage (SAH), and ischemic stroke (IS). *Endocrine* (2016) 52:441–50. doi: 10.1007/s12020-015-0796-2

188. Lillicrap T, Garcia-Esperon C, Walker FR, Ong LK, Nilsson M, Spratt N, et al. Growth hormone deficiency is frequent after recent stroke. *Front Neurol* (2018) 9:713. doi: 10.3389/fneur.2018.00713

189. Tritos NA, Biller BMK. Current concepts of the diagnosis of adult growth hormone deficiency. *Rev Endocr Metab Disord* (2021) 22:109–16. doi: 10.1007/s11154-020-09594-1

190. Boguszewski MCS, Cardoso-Demartini AA, Boguszewski CL, Chemaitilly W, Higham CE, Johannsson G, et al. Safety of growth hormone (GH) treatment in GH deficient children and adults treated for cancer and non-malignant intracranial tumors-a review of research and clinical practice. *Pituitary* (2021) 24:810–27. doi: 10.1007/s11102-021-01173-0

191. Gasco V, Caputo M, Cambria V, Beccuti G, Caprino MP, Ghigo E, et al. Progression of pituitary tumours: impact of GH secretory status and long-term GH replacement therapy. *Endocrine* (2019) 63:341–7. doi: 10.1007/s12020-018-1787-x

192. Buchfelder M, Kann PH, Wüster C, Tuschy U, Saller B, Brabant G, et al. Influence of GH substitution therapy in deficient adults on the recurrence rate of hormonally inactive pituitary adenomas: a case–control study. *Eur J Endocrinol* (2007) 157:149–56. doi: 10.1530/EJE-07-0164

193. Chung TT, Drake WM, Evanson J, Walker D, Plowman PN, Chew SL, et al. Tumour surveillance imaging in patients with extrapituitary tumours receiving growth hormone replacement. *Clin Endocrinol* (2005) 63:274–9. doi: 10.1111/j.1365-2265.2005.02338.x

194. Frajese G, Drake WM, Loureiro RA, Evanson J, Coyte D, Wood DF, et al. Hypothalamo-pituitary surveillance imaging in hypopituitary patients receiving long-term GH replacement therapy. *J Clin Endocrinol Metab* (2001) 86:5172–5. doi: 10.1210/jcem.86.11.8018

195. Hatrick AG, Boghalo P, Bingham JB, Ayres AB, Sonksen PH, Russell-Jones DL. Does GH replacement therapy in adult GH-deficient patients result in recurrence or increase in size of pituitary tumours? *Eur J Endocrinol* (2002) 146:807–11. doi: 10.1530/eje.0.1460807

196. Karavitaki N, Warner JT, Marland A, Shine B, Ryan F, Arnold J, et al. GH replacement does not increase the risk of recurrence in patients with craniopharyngioma. *Clin Endocrinol* (2006) 64:556–60. doi: 10.1111/j.1365-2265.2006.02508.x

197. Olsson DS, Buchfelder M, Schlaffer S, Bengtsson B-Å, Jakobsson K-E, Johannsson G, et al. Comparing progression of non-functioning pituitary adenomas in hypopituitarism patients with and without long-term GH replacement therapy. *Eur J Endocrinol* (2009) 161:663–9. doi: 10.1530/EJE-09-0572

198. de Boer H, Blok GJ, Voerman B, Derriks P, van der Veen E. Changes in subcutaneous and visceral fat mass during growth hormone replacement therapy in adult men. *Int J Obes Relat Metab Disord* (1996) 20:580–7.

199. Abs R, Bengtsson BA, Hernberg-Ståhl E, Monson JP, Tauber JP, Wilton P, et al. GH replacement in 1034 growth hormone deficient hypopituitary adults: demographic and clinical characteristics, dosing and safety. *Clin Endocrinol (Oxf)* (1999) 50:703–13. doi: 10.1046/j.1365-2265.1999.00695.x

200. Lissett CA, Thompson EG, Rahim A, Brennan BM, Shalet SM. How many tests are required to diagnose growth hormone (GH) deficiency in adults? *Clin Endocrinol (Oxf)* (1999) 51:551–7. doi: 10.1046/j.1365-2265.1999.00836.x

201. Corneli G, Di Somma C, Baldelli R, Rovere S, Gasco V, Croce CG, et al. The cut-off limits of the GH response to GH-releasing hormone-arginine test related to body mass index. *Eur J Endocrinol* (2005) 153:257–64. doi: 10.1530/eje.1.01967

202. Gasco V, Ferrero A, Bisceglia A, Prencipe N, Cambria V, Bioletto F, et al. The cut-off limits of growth hormone response to the insulin tolerance test related to body mass index for the diagnosis of adult growth hormone deficiency. *Neuroendocrinology* (2021) 111:442–50. doi: 10.1159/000508103

203. Kgosidialwa O, Hakami O, Muhammad Zia-Ul-Hussnain H, Agha A. Growth hormone deficiency following traumatic brain injury. *Int J Mol Sci* (2019) 20:3323. doi: 10.3390/ijms20133323

204. Gilis-Januszewska A, Kluczyński Ł, Hubalewska-Dydejczyk A. Traumatic brain injuries induced pituitary dysfunction: a call for algorithms. *Endocr Connections* (2020) 9:R112–23. doi: 10.1530/EC-20-0117

205. McKenna SP, Doward LC, Alonso J, Kohlmann T, Niero M, Prieto L, et al. The QoL-AGHDA: an instrument for the assessment of quality of life in adults with growth hormone deficiency. *Qual Life Res* (1999) 8:373–83. doi: 10.1023/a:1008987922774

206. Cerbone M, Dattani MT. Progression from isolated growth hormone deficiency to combined pituitary hormone deficiency. *Growth Horm IGF Res* (2017) 37:19–25. doi: 10.1016/j.ghir.2017.10.005

207. Toledano Y, Lubetsky A, Shimon I. Acquired prolactin deficiency in patients with disorders of the hypothalamic-pituitary axis. *J Endocrinol Invest* (2007) 30:268–73. doi: 10.1007/BF03346292

208. Kauppila A, Chatelain P, Kirkinen P, Kivinen S, Ruokonen A. Isolated prolactin deficiency in a woman with puerperal alactogenesis*. *J Clin Endocrinol Metab* (1987) 64:309–12. doi: 10.1210/jcem-64-2-309

209. Falk RJ. Isolated prolactin deficiency: a case report. *Fertil Steril* (1992) 58:1060–2. doi: 10.1016/s0015-0282(16)55460-0

210. Zargar AH, Masoodi SR, Laway BA, Shah NA, Salahudin M. Familial puerperal alactogenesis: possibility of a genetically transmitted isolated prolactin deficiency. *Br J Obstet Gynaecol* (1997) 104:629–31. doi: 10.1111/j.1471-0528.1997.tb11548.x

211. Douchi T, Nakae M, Yamamoto S, Iwamoto I, Oki T, Nagata Y. A woman with isolated prolactin deficiency. *Acta Obstet Gynecol Scandinavica* (2001) 80:368–70. doi: 10.1034/j.1600-0412.2001.080004368.x

212. Iwama S, Welt CK, Romero CJ, Radovick S, Caturegli P. Isolated prolactin deficiency associated with serum autoantibodies against prolactin-secreting cells. *J Clin Endocrinol Metab* (2013) 98:3920–5. doi: 10.1210/jc.2013-2411

213. Callejas L, Berens P, Nader S. Breastfeeding failure secondary to idiopathic isolated prolactin deficiency: report of two cases. *Breastfeed Med* (2015) 10:183. doi: 10.1089/bfm.2015.0003

214. Tolino A, Tedeschi A, Montemagno U. Influence of bromocriptine on plasma prolactin, human placental lactogen, beta-HCG and steroid hormones in early human pregnancy. *Biol Res Pregnancy Perinatol* (1985) 6:70–2.

215. Colao A, Di Sarno A, Guerra E, Pivonello R, Cappabianca P, Caranci F, et al. Predictors of remission of hyperprolactinaemia after long-term withdrawal of cabergoline therapy. *Clin Endocrinol (Oxf)* (2007) 67:426–33. doi: 10.1111/j.1365-2265.2007.02905.x

216. Lozano R, Marin R, Santacruz M-J. Prolactin deficiency by aripiprazole. *J Clin Psychopharmacol* (2014) 34:539–40. doi: 10.1097/JCP.0000000000000151

217. Decreased prolactin reserve in hemochromatosis* (Accessed November 13, 2022).

218. Isaac R, Merceron RE, Caillens G, Raymond JP, Ardaillou R. Effect of parathyroid hormone on plasma prolactin in man. *J Clin Endocrinol Metab* (1978) 47:18–23. doi: 10.1210/jcem-47-1-18

219. Krysiak R, Kowalcze K, Okopień B. Cabergoline-induced hypoprolactinemia may attenuate cardiometabolic effects of atorvastatin: A pilot study. *CRD* (2022), 147(5-6)::497–506. doi: 10.1159/000527333

220. Turkington RW. Phenothiazine stimulation test for prolactin reserve: the syndrome of isolated prolactin deficiency. *J Clin Endocrinol Metab* (1972) 34:246–9.

221. Powe CE, Allen M, Puopolo KM, Merewood A, Worden S, Johnson LC, et al. Recombinant human prolactin for the treatment of lactation insufficiency. *Clin Endocrinol (Oxf)* (2010) 73:645–53. doi: 10.1111/j.1365-2265.2010.03850.x

222. Academy Of Breastfeeding Medicine Protocol Committee. ABM clinical protocol #9: Use of galactogogues in initiating or augmenting the rate of maternal milk secretion (First revision January 2011). *Breastfeed Med* (2011) 6:41–9. doi: 10.1089/bfm.2011.9998

frontiers | Frontiers in Neuroscience

TYPE Original Research
PUBLISHED 20 March 2023
DOI 10.3389/fnins.2023.1098404

OPEN ACCESS

EDITED BY
Alexandre Benani,
Centre National de la Recherche Scientifique (CNRS), France

REVIEWED BY
Emanuele Ferrante,
IRCCS Ca' Granda Foundation Maggiore Policlinico Hospital, Italy
Aart J. Van Der Lely,
Erasmus University Rotterdam, Netherlands

*CORRESPONDENCE
Alessandro Maria Berton
✉ alessandro.m.berton@gmail.com
Mirko Parasiliti-Caprino
✉ mirko.parasiliticaprino@gmail.com

†These authors have contributed equally to this work and share first authorship

SPECIALTY SECTION
This article was submitted to Neuroendocrine Science, a section of the journal Frontiers in Neuroscience

RECEIVED 14 November 2022
ACCEPTED 03 March 2023
PUBLISHED 20 March 2023

CITATION
Berton AM, Parasiliti-Caprino M, Prencipe N, Bioletto F, Lopez C, Bona C, Caputo M, Rumbolo F, Ponzetto F, Settanni F, Gasco V, Mengozzi G, Ghigo E, Grottoli S, Maccario M and Benso AS (2023) Copeptin adaptive response to SGLT2 inhibitors in patients with type 2 diabetes mellitus: The GliRACo study. *Front. Neurosci.* 17:1098404. doi: 10.3389/fnins.2023.1098404

Copeptin adaptive response to SGLT2 inhibitors in patients with type 2 diabetes mellitus: The GliRACo study

Alessandro Maria Berton [1*†], Mirko Parasiliti-Caprino [1*†], Nunzia Prencipe[1], Fabio Bioletto[1], Chiara Lopez[1], Chiara Bona[1], Marina Caputo[2], Francesca Rumbolo[3], Federico Ponzetto[3], Fabio Settanni[3], Valentina Gasco[1], Giulio Mengozzi[3], Ezio Ghigo[1], Silvia Grottoli[1], Mauro Maccario[1] and Andrea Silvio Benso[1]

[1]Division of Endocrinology, Diabetes and Metabolism, Department of Medical Sciences, University of Turin, Turin, Italy, [2]Department of Health Sciences, University of Eastern Piedmont, Novara, Italy, [3]Clinical Biochemistry Laboratory, Department of Laboratory Medicine, AOU Città della Salute e della Scienza di Torino, University Hospital, Turin, Italy

Introduction: In type 2 diabetes mellitus (T2DM), the antidiuretic system participates in the adaptation to osmotic diuresis further increasing urinary osmolality by reducing the electrolyte-free water clearance. Sodium glucose co-transporter type 2 inhibitors (SGLT2i) emphasize this mechanism, promoting persistent glycosuria and natriuresis, but also induce a greater reduction of interstitial fluids than traditional diuretics. The preservation of osmotic homeostasis is the main task of the antidiuretic system and, in turn, intracellular dehydration the main drive to vasopressin (AVP) secretion. Copeptin is a stable fragment of the AVP precursor co-secreted with AVP in an equimolar amount.

Aim: To investigate the copeptin adaptive response to SGLT2i, as well as the induced changes in body fluid distribution in T2DM patients.

Methods: The GliRACo study was a prospective, multicenter, observational research. Twenty-six consecutive adult patients with T2DM were recruited and randomly assigned to empagliflozin or dapagliflozin treatment. Copeptin, plasma renin activity, aldosterone and natriuretic peptides were evaluated at baseline (T0) and then 30 (T30) and 90 days (T90) after SGLT2i starting. Bioelectrical impedance vector analysis (BIVA) and ambulatory blood pressure monitoring were performed at T0 and T90.

Results: Among endocrine biomarkers, only copeptin increased at T30, showing subsequent stability (7.5 pmol/L at T0, 9.8 pmol/L at T30, 9.5 pmol/L at T90; $p = 0.001$). BIVA recorded an overall tendency to dehydration at T90 with a stable proportion between extra- and intracellular fluid volumes. Twelve patients (46.1%) had a BIVA overhydration pattern at baseline and 7 of them (58.3%) resolved this condition at T90. Total body water content, extra and intracellular fluid changes were significantly affected by the underlying overhydration condition ($p < 0.001$), while copeptin did not.

Conclusion: In patients with T2DM, SGLT2i promote the release of AVP, thus compensating for persistent osmotic diuresis. This mainly occurs because of a proportional dehydration process between intra and extracellular fluid (i.e., intracellular dehydration rather than extracellular dehydration). The extent of fluid reduction, but not the copeptin response, is affected by the patient's baseline volume conditions.

Clinical trial registration: Clinicaltrials.gov, identifier NCT03917758.

KEYWORDS

arginine-vasopressin, sodium glucose co-transporter type 2 inhibitors, osmotic homeostasis, extracellular fluid, bioelectrical impedance vector analysis, renin-angiotensin-aldosterone system

Introduction

Copeptin, the C-terminal fragment of pre-provasopressin (CT-proAVP), represents a reliable biomarker of the activity of the antidiuretic system, being secreted by magnocellular hypothalamic neurons in equimolar amount with arginine-vasopressin (AVP) in response to osmotic, hemodynamic and stressful stimuli (Christ-Crain, 2019). The main task of AVP is to maintain osmotic homeostasis, promoting the passive reabsorption of water in the renal collecting ducts by activating the V2 receptors (V2R) located on the basal membrane of the principal cells.

It was shown that even in type 2 diabetes mellitus (T2DM) the antidiuretic system participates in the adaptation to osmotic diuresis, further increasing urinary osmolality by reducing the electrolyte-free water (EFW) clearance (Marton et al., 2021); in this context, sodium glucose co-transporter type 2 inhibitors (SGLT2i) appear to emphasize this mechanism, promoting persistent glycosuria and natriuresis.

In recent years, both empagliflozin (EMPA) and dapagliflozin (DAPA) have gained indication in the treatment not only of T2DM, but also of chronic heart failure (HF) with reduced ejection fraction and chronic kidney disease (CKD), thanks to their ability to reduce disease progression and exacerbations, together with overall cardiovascular mortality (Zinman et al., 2015; Wanner et al., 2016; McMurray et al., 2019; Wiviott et al., 2019).

The pathophysiological basis of these favorable effects is not yet fully understood, but one of the hypotheses is that SGLT2i could induce a greater reduction of interstitial fluids (ISF) than traditional diuretics, thus avoiding hypovolemia and acute kidney injury due to intravascular volume depletion (Lambers Heerspink et al., 2013; Hallow et al., 2018).

Indeed, significant losses of isotonic fluid able to reduce the effective circulating volume (ECV) cannot be immediately replaced by the water present in the interstitial space, since these two compartments share the same osmotic pressure. This process, called extracellular dehydration, leads to extensive neurohormonal activation, in turn associated with known harmful effects on the cardiovascular system when persisting for a long time (Cheuvront and Kenefick, 2014).

Conversely, hypotonic or electrolyte-free water losses are responsible for a mainly intracellular dehydration process, associated with a lower activation of the renin-angiotensin-aldosterone system (RAAS) and the sympathetic nervous system, in favor of an isolated osmotic response of the antidiuretic system (Cheuvront and Kenefick, 2014).

The aim of this proof-of-concept study was to investigate the copeptin adaptive response to persistent osmotic diuresis due to SGLT2i administration, as well as the induced changes in body fluid distribution, in T2DM.

Materials and methods

Design, population, observation times, and study setting

The GliRACo study was a prospective, multicenter research involving the Division of Endocrinology, Diabetes and Metabolism of the University Hospital "Città della Salute e della Scienza di Torino" in Turin, and the Division of Endocrinology of the University Hospital "Maggiore della Carità" in Novara. Both Local Ethics Committees of the two University Hospitals approved the study protocol (Turin: protocol n. D026280; Novara: protocol n. CE76/19) and the clinical research was conducted in accordance with the principles of Declaration of Helsinki.

Sixty-eight consecutive patients with T2DM (**Figure 1**) were evaluated at the Diabetic Outpatient Clinic of each Center for the following inclusion criteria: (1) age ≥18 years; (2) clinical indication for starting SGLT2i treatment, (3) written informed consent. Exclusion criteria were as follow: (1) past medical history positive for any disease able to alter RAAS or the antidiuretic system (i.e., primary aldosteronism, HF, CKD, liver cirrhosis, diabetes insipidus, syndrome of inappropriate antidiuresis–SIAD, adrenal insufficiency, Cushing syndrome); (2) impossibility to suspend any ongoing treatment known to alter copeptin levels or to interfere with the RAAS activity; (3) body mass index (BMI) ≥ 40 Kg/m^2; (4) HbA1c ≥ 86 mmol/mol or clinical signs suspected of poor glycaemic control (polyuria, weight loss, visual alteration); (5) any other ongoing antihyperglycemic treatment except for metformin.

Since recruitment, any antihypertensive treatment potentially interfering with RAAS or antidiuretic system was discontinued (i.e., angiotensin converting enzyme inhibitors–ACEi, angiotensin

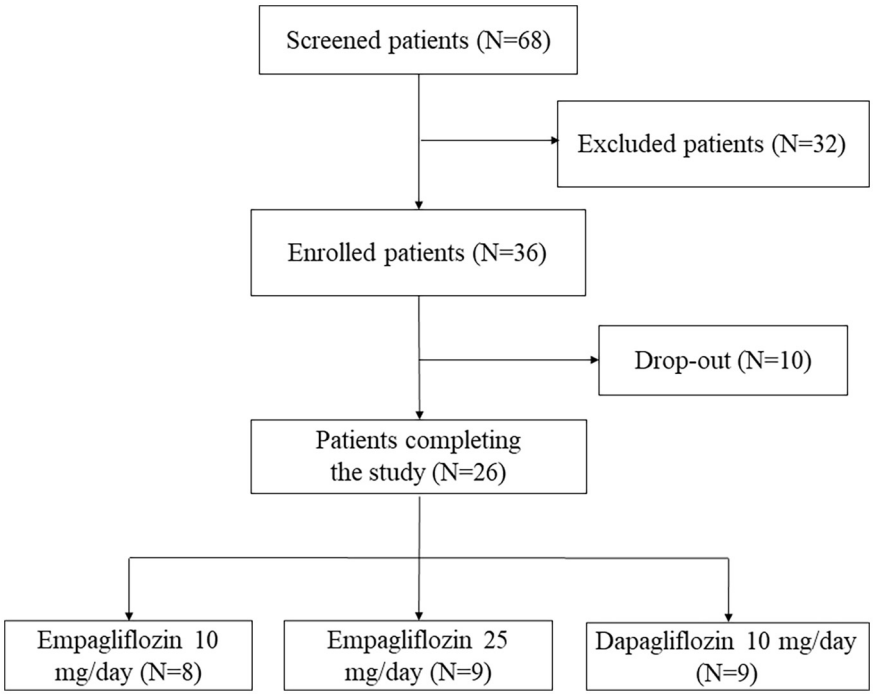

FIGURE 1
Recruitment process flow-chart.

receptor blockers - ARB, beta-blockers, diuretics) and substituted with alfa-blockers and/or calcium channel blockers. At the same time, all patients were instructed to follow controlled diet with 3–5 g of salt and up to 2 L of water per day.

Twenty days later, patients were randomly assigned to EMPA (10 or 25 mg/die, based on diabetic disease control) or DAPA (10 mg/die) alone or in addition to an ongoing metformin treatment. The day before SGLT2i starting (T0) and then at 30 (T30) and 90 days (T90) of treatment, a comprehensive fasting physical and biochemical evaluation (i.e., copeptin, plasma renin activity–PRA, aldosterone, NT-proBNP and MR-proANP) was performed; moreover, patients were instructed to avoid caffeine or nicotine on the day of study visit. In addition, at T0 and T90, all patients underwent to bioelectrical impedance vector analysis (BIVA) and 24-h ambulatory blood-pressure monitoring (ABPM).

Analytical methods

All the biochemical analysis were performed with automated assays in the same laboratory (Clinical Biochemistry Laboratory, "Città della Salute e della Scienza" University Hospital, Turin, Italy).

As previously reported (Pasero et al., 2020), copeptin and MR-proANP concentrations (pmol/L) were determined by the B.R.A.H.A.M.S. KRYPTOR compact PLUS (Thermo Fisher Scientific, Hennigsdorf, Germany) automated method using the TRACE (Time-Resolved Amplified Cryptate Emission) technique. The detection limit of the assay was 0.9 pmol/L for copeptin and 0.05 pmol/L for MR-proANP; intra and interassay coefficients of variation were, respectively, <7 and <12% for copeptin, <4 and <11% for MR-proANP.

Plasma samples for NT-proBNP determination were processed on Cobas e602 automated platform (Roche Diagnostics) by sandwich immunoassay with two monoclonal antibodies directed against N-terminal portion (1–76) of proBNP molecule (Elecsys proBNP II), using electrochemiluminescence analysis. The limit of detection was 5 pg/mL (0.6 pmol/L), with a 5–35,000 pg/ml (0.6–4,130 pmol/L) dynamic range, as well as intra and interassay coefficients of variation < 5% at three different concentrations (46, 125 and 14, 150 pg/ml).

Serum aldosterone levels were measured by liquid chromatography coupled to mass spectrometry (LC-MS) assays. LC-MS analyses were conducted employing the MassChrom Steroids in serum/plasma kit (Chromsystems Instruments and Chemicals GmbH, Gräfelfing, Germany) on a Nexera X2 LC system (Shimadzu, Tokyo, Japan) coupled to a Triple Quad 4500MD MS (AB Sciex, Toronto, Canada). The lower limit of quantification of the method was 14 pg/ml; the intra and interassay coefficient of variation ranges from 0.9 to 1.9% and from 3.9 to 5.9%, respectively. As previously described (Parasiliti-Caprino et al., 2020), PRA (ng/ml/h) was assessed by RIA RENCTK kit (DiaSorin, Saluggia, Italy). The sensitivity of the assay was 0.20 ng/ml; the intra and interassay coefficient of variation ranges from 5.4 to 9.9% and from 7.7 to 11.5%, respectively. We decided to adopt LC-MS method for aldosterone measurement and RIA for PRA determination, because these methods have been considered the most accurate for the expected hormone range values.

Sodium fractional excretion (FENa), solute-free water (SFW) and EFW clearance have been calculated according to the following formulas: FENa = s-creatinine × u-Na/s-Na × u-creatinine × 100; SFW clearance = 24 h urine volume × [1–(u-Osm/p-Osm)]; EFW clearance = 24 h urine volume × [1–(u-Na + u-K/s-Na)].

BIVA

Body fluid composition was evaluated by an impedance vector analyzer with measurement frequency of 50 kHz ± 1% (BIA101BIVA®, Akern, Loc. Montacchiello, Pisa, Italy). Both bioimpedance parameters (resistance–Rz, and reactance–Xc) were normalized according to the patients' height (H) and plotted on a Rz/H and Xc/H graph (Biavector, Bodygram Plus® version 1.31). This technique allows a reliable and reproducible assessment of the distribution of body fluids in several clinical settings (Lukaski et al., 2019), Rz reflecting conductivity through ionic solutions, Xc the impedance due to the membrane capacitance of metabolically active cells and, finally, phase angle (PhA) representing a derived parameter, which expresses the ratio between intracellular fluid (ICF) and extracellular fluid (ECF) volumes. Moreover, Biavector allows to compare the variations between repeated measurements on the same subject with the normal sex-specific ellipses of the general healthy population (Piccoli et al., 1995). Reliable thresholds for both overhydration and dehydration conditions have been previously identified at the lower and upper poles of the 75th sex-specific tolerance ellipse, respectively, (Piccoli et al., 1995).

ABPM

Ambulatory blood-pressure monitoring were performed using an automated, non-invasive oscillometric device (TM-2430; Intermed s.r.l., Milan, Italy). Recordings were made every 15′ for the daytime and every 20′ for the night-time. Valid 24-h ABPM had to have recorded >80% of successful measurements. Controlled ambulatory BP was defined according to current guidelines (Williams et al., 2018). Heart rate (HR) variability (HRV) was determined as the standard deviation (SD) of daytime, night-time and 24-h HR. For the assessment of the nocturnal BP profile, we considered reverse dipping when night-time BP was higher than daytime, reduced dipping a night reduction of 0–10%, normal dipping a night reduction of 10–20% and extreme dipping a night reduction >20%.

Statistical methods

Continuous variables were expressed as mean and SD or median and interquartile range (IQR) depending on their distribution; categorical variables were expressed as number and percentage. Normality was assessed using the Shapiro–Wilk test. Between-group comparisons for continuous variables were performed with the Student *t*-test or the Mann–Whitney *U*-test; repeated measures ANOVA or the Friedman test were used to identify longitudinal differences over time. Correlation between categorical variables were identified by the Chi-square test or Fisher's exact test, as appropriate. Multivariable linear regression models with stepwise backward variable selection were adopted to assess the relationship between continuous variables during treatment with SGLT2i. With respect to BIVA, mean vectors from independent groups were compared with the two-sample Hotelling's T2 test, while mean Biavectors' displacement between T0 and T90 was evaluated with the paired one-sample Hotelling's T2 test (Piccoli and Pastori, 2002).

The calculation of the sample size was based on the results reported in a recent study by Lytvyn et al. (2020), conducted in a population of 40 young type 1 diabetic subjects treated with EMPA 25 mg/die for 8 weeks, in which the authors observed a mean increase in copeptin levels equal to 1 pmol/L in normoglycemic state (i.e., 72–108 mg/dL) and 2.3 pmol/L in hyperglycemic condition (i.e., 172–198 mg/dl). Based on these data, in our analysis conducted in a real-life outpatient setting, an expected mean copeptin increase of 1.5 pmol/L in response to SGLT2i treatment was hypothesized. The expected SD was estimated to be equal to 2.2 pmol/L based on the results of the reference study (Lytvyn et al., 2020). A sample size of at least 25 patients was thus needed to obtain a statistical power of 90% (beta error 0.1) with an alpha error of 0.05.

Statistical analysis was performed using MedCalc® version 20 (MedCalc Software Ltd, Ostend, Belgium).

Results

Study population

Among the 68 patients with T2DM evaluated to enter the study, 32 did not meet the inclusion criteria, while 36 were finally enrolled (**Figure 1**) and randomized to EMPA (10 mg/day in 12 patients and 25 mg/day in other 12) or DAPA (10 mg/day, 12 patients). A complete urinalysis was performed at each scheduled visit to confirm SGLT2i intake based on the presence of marked glucosuria without significant hyperglycemia. Four patients prematurely discontinued SGLT2i treatment due to symptomatic urinary infections, and six additional patients were lost at follow-up because they missed some scheduled visits; the remaining 26 patients (16 males and 10 females; age, mean ± SD, 60.9 ± 11.1 years) completed the study protocol (eight EMPA 10 mg/day, nine EMPA 25 mg/day and nine DAPA 10 mg/day).

Considering only patients who completed the study protocol, 20 were already assuming metformin [median duration of disease 6.5 (IQR 1.7–11) years]; at T0, HbA1c was ≥75 mmol/mol in three patients and fasting glucose levels were >180 mg/dl in five. Fourteen patients were already on antihypertensive treatment (mean duration of disease 9.0 ± 4.5 years), while in seven others a first diagnosis of arterial hypertension was made at T0. Among hypertensive patients, all drugs potentially interfering with the RAAS or the antidiuretic system were stopped at least 20 days before T0 (eight patients stopped ACEi or ARB, three beta-blockers and six thiazides) and an acceptable control of blood pressure levels was achieved using alpha-blockers and/or calcium channel blockers (**Table 1**).

Anthropometric and metabolic variables

An early reduction in body weight was observed at T30 (82.3 Kg at T0 vs. 81.5 Kg at T0; $p = 0.004$) with subsequent stability. Fasting glucose, but not HbA1c, resulted significantly lower at

TABLE 1 Ambulatory blood pressure monitoring (ABPM) data at baseline and at the end of the study.

ABPM variables	Baseline	90 days	*P*-value
24 h results			
SBP (mmHg)	134.7 ± 11.9	133.8 ± 13.4	0.577
DBP (mmHg)	78.3 ± 6.6	78.0 ± 8.7	0.684
MAP (mmHg)	96.8 ± 7.8	96.3 ± 9.6	0.625
HR (bpm)	77.7 ± 10.4	78.3 ± 8.2	0.639
HRV (bpm)	10.9 (9.1–12.3)	12.2[(10.5–13.1)	**0.011**
PP (mmHg)	56.4 ± 8.2	55.8 ± 8.8	0.566
Day-time results			
SBP (mmHg)	139.6 ± 13.0	136.8 ± 12.7	0.245
DBP (mmHg)	82.1 ± 7.1	80.6 ± 8.2	0.320
MAP (mmHg)	100.9 ± 8.5	99.0 ± 9.1	0.261
HR (bpm)	81.8 ± 7.7	81.5 ± 8.4	0.980
HRV (bpm)	10.3 (8.7–12.5)	11.8 (10.6–13.1)	**0.006**
PP (mmHg)	57.6 ± 9.0	56.2 ± 8.6	0.299
Nigh-time results			
SBP (mmHg)	124.7 ± 15.0	126.0 ± 17.0	0.901
DBP (mmHg)	70.2 ± 8.1	70.9 ± 10.7	0.974
MAP (mmHg)	88.1 ± 9.8	88.9 ± 12.1	0.948
HR (bpm)	71.9 ± 9.9	69.2 ± 9.5	**0.023**
HRV (bpm)	5 (3.7–6.9)	5 (4.3–6.2)	0.395
PP (mmHg)	54.5 ± 10.1	55.1 ± 10.6	0.919
Nocturnal BP profile			
Reverse dipping	4.5%	0%	0.635
Reduced dipping	54.6%	47.8%	
Normal dipping	40.9%	47.8%	
Extreme dipping	0%	4.4%	
AASI	0.5 ± 0.1	0.5 ± 0.16	0.572

Paired samples *t*-test and Wilcoxon test significant results ($p < 0.05$) reported in bold. AASI, ambulatory arterial stiffness index; BP, blood pressure; bpm, beats per minute; DBP, diastolic blood pressure; HR, heart rate; HRV, heart rate variability; MAP, mean arterial pressure; PP, pulse pressure; SBS, systolic blood pressure.

T90 (122 mg/dl at T0 vs. 115.5 mg/dl at T90; $p = 0.041$). Both absolute urinary albumin (14.9 mg/die at T0 vs. 26.7 mg/die at T90; $p = 0.032$) and urine albumin to creatinine ratio (ACR) on spot urine collection (10.5 μg/mg at T0 vs. 23.6 μg/mg at T90; $p = 0.046$) increased at T90 (Table 2).

Hydro-electrolyte balance

As expected, during SGLT2i treatment u-Osm showed an early growth (522 mOsm/Kg at T0 vs. 734 mOsm/Kg at T30; $p = 0.001$), while SFW clearance further decreased (−1.8 L/die at T0 vs. −3.3 L/die at T30; $p = 0.0002$), with subsequent stability of both. Just transient increases in daily diuresis (2.0 L/die at T0 vs. 2.5 L/die at T30; $p = 0.001$) as well as in FENa were observed at T30 (0.76% at T0 vs. 0.84% at T30; $p = 0.015$), not associated to significant modification in absolute u-Na values. EFW clearance showed a slight upward trend at T30 (0.1 L/die at T0 vs. 0.38 L/die at T30; $p = 0.044$) and serum electrolytes remained stable. Of note, a significant increase in hematocrit (HCT) was recorded at T90 (42.5% at T0 vs. 46.3% at T90; $p < 0.0001$), without any significant change in p-Osm (Table 2).

Endocrine systems

Copeptin levels increased at T30, showing subsequent stability (7.5 pmol/L at T0, 9.8 pmol/L at T30 and 9.5 pmol/L at T90; $p = 0.001$). At all observation times p-Osm resulted a significant predictor of copeptin values (coefficient 0.06, standard error (SE) 0.03; $p = 0.022$), particularly at T30 (coefficient 0.08, SE 0.02; $p = 0.0002$) (Figure 2). Finally, at T90, copeptin was confirmed a significant predictor of log-normalized albuminuria, even if corrected for creatinine clearance or the presence of leukocyturia (coefficient 0.06, SE 0.02; $p = 0.009$). All other endocrine biomarkers remained essentially stable, in the absence of relevant clinical or biochemical signs of hypovolemia (Table 2).

ABPM

At T90, ABPM revealed an increase in daytime HRV (10.3 bpm at T0 vs. 11.8 bpm at T90; $p = 0.006$) together with a slight decrease in mean night HR (71.9 bpm at T0 vs. 69.2 bpm at T90; $p = 0.023$). Conversely, BP did not change significantly, as reported in Table 1.

BIVA

Bioelectrical impedance vector analysis recorded a tendency to dehydration at T90, estimating a prevailing reduction of the ECF (22.2 L at T0 vs. 21.2 L at T90; $p = 0.018$), although in the presence of normal and stable PhA (Table 3). Twelve patients (46.1%) had a BIVA overhydration pattern ($p < 0.0001$, Figure 3) at T0 and 7 of them (58.3%) resolved this condition at T90. At the same time, in overhydrated patients both Xc and Rz increased significantly ($p < 0.02$), while ECF and total body water (TBW) decreased ($p < 0.02$). Conversely, in normohydrated diabetic patients, none of these variables changed remarkably. Finally, a significant displacement of the Biavector was confirmed at T90 only in subjects overhydrated at T0 ($p < 0.001$) (Figure 4). Repeated measures ANOVA confirmed that all volume changes (ECF, TBW, and ICF) were significantly affected by the underlying overhydration condition ($p < 0.001$), while copeptin levels and daytime HRV did not.

Drugs

As attended, no significant differences in endocrine and hydro-electrolyte balance variables were detected between the three different arms of treatment. No treatment was significantly associated to over-hydration resolution at T90.

TABLE 2 Changes in anthropometric, metabolic, hydro-electrolyte, and hormonal variables during the study protocol.

Variables	Baseline	30 days	90 days	*P*-value
Anthropometric				
Weight (Kg)	82.3 ± 21.4	81.5 ± 21.4	80.5 ± 21.1	**0.01***†
BMI (Kg/m^2)	29.1 ± 6.0	28.8 ± 6.0	28.4 ± 5.7	**0.008***†
Waist circumference (cm)	101.5 ± 12.1	100.6 ± 11.6	100.2 ± 11.3	0.151
Metabolic				
HbA1c (mmol/mol)	54 (49–67)	53 (50.5–59.9)	53 (46–57)	*0.144*
P-glucose (mg/dl)	122 (113–153)	114.5 (102–144)	115.5 (104–142)	**0.038**†
S-creatinine (mg/dl)	0.83 (0.73–0.91)	0.83 (0.74–0.95)	0.83 (0.71–0.91)	*0.216*
Creatinine clearance (ml/min)	110 (86–127)	105.6 (76–132)	109.5 (71–146)	*0.359*
Urinary albumin (mg/die)	14.9 (11.6–31.7)	23.2 (16.5–36.2)	26.7 (19.5–43.4)	**0.016**†
ACR (μg/mg)	10.5 (7.8–25.4)	19.5 (14.1–34.2)	23.6 (14.4–33.1)	**0.027**†
Hydro-electrolyte balance				
S-Na (mmol/L)	141 (140–142)	141 (140–142)	141 (138–142)	0.743
S-K (mmol/L)	4.5 (4.2–4.8)	4.4 (4.1–4.7)	4.5 (4.3–4.9)	0.528
P-Osm (mOsm/Kg)	291.1 ± 4.5	291.7 ± 5.4	292.1 ± 4.1	0.274
HCT (%)	42.5 (40.4–45.5)	43.2 (41.2–45.3)	46.3 (42.2–48.1)	<**0.0001**†‡
Daily diuresis (L/die)	2.0 (1.5–2.5)	2.5 (2.0–2.8)	2.1 (1.7–2.6)	***0.0006****
U-Osm (mOsm/Kg)	552 (510–728)	734 (637–807)	772 (697–826)	<***0.001****†
U-Na (mmol/L)	99.6 ± 38.9	88.1 ± 23.3	89.5 ± 28.1	0.193
FENa (%)	0.76 (0.57–0.71)	0.84 (0.71–1.4)	0.89 (0.57–1.18)	***0.024****
EFW clearance (L/die)	0.1 ± 0.72	0.38 ± 0.45	0.28 ± 0.52	**0.042**
SFW clearance (L/die)	−1.8 (−2.7–1.5)	−3.3 (−4.5–2.5)	−3.6 (−4.5–2.6)	<**0.0001***†
Endocrine systems				
Copeptin (pmol/L)	7.5 (4.7–11.9)	9.8 (7.4–16.2)	9.5 (7.4–12.5)	***0.001****†
PRA (ng/ml/h)	0.4 (0.18–0.98)	0.66 (0.41–1.18)	0.51 (0.35–1.10)	*0.164*
Aldosterone (pg/ml)	50 (30–88)	89 (30–110)	45 (38–100)	*0.19*
ARR	112 (64.9–222.2)	69 (44.8–201.7)	94.1 (37–180)	*0.405*
NT-proBNP (pg/ml)	46 (23–77)	34 [15–67]	46.8 (16–73)	*0.33*
MR-proANP (pmol/L)	42 (36.7–79.1)	47.2 (28.5–81.5)	44.7 (30.7–72.6)	*0.16*

Repeated measures ANOVA and Friedman test significant results ($p < 0.05$) reported in bold; significant results of repeated measures ANOVA on log-normalized variables shown in italics.
*Significant difference between baseline and 30 days.
†Significant difference between baseline and 90 days.
‡Significant difference between 30 and 90 days after starting SGLT2i.
ACR, urine albumin-to-creatinine ratio; ARR, aldosterone-to-renin ratio; BMI, body mass index; bpm, beats per minute; DBP, diastolic blood pressure; EFW, electrolyte-free water; FENa, sodium fractional excretion; HbA1c, glycated hemoglobin; HCT, hematocrit; HR, heart rate; MR-proANP, mid-regional pro atrial natriuretic peptide; NT-proBNP, N-terminal prohormone of brain natriuretic peptide; p-glucose, plasma glucose; p-Osm, plasma osmolality; PRA, plasma renin activity; SBS, systolic blood pressure; s-creatinine, serum creatinine; SFW, solute-free water; s-Na, serum sodium; u-Na, urine sodium; u-Osm, urine osmolality.

Discussion

Our results confirm an isolated response of the antidiuretic system to the administration of SGLT2i in patients with T2DM. In particular, the increase in copeptin levels seems attributable to a prevalent intracellular dehydration phenomenon, in the absence of evident signs of hypovolemia or a wide neurohormonal activation. Moreover, the dehydration process due to SGLT2i treatment led to remarkable changes in body fluid distribution only in basally overhydrated patients.

SGLT2i represent new euglycemic drugs able to induce sustained glycosuria by the inhibition of glucose reabsorption in the renal proximal tubule. SGLT2i proved to be effective in reducing cardiovascular risk in patients with T2DM beyond glycemic control, even preventing HF exacerbation and CKD progression (Zinman et al., 2015; Wanner et al., 2016; Neal et al., 2017; Wiviott et al., 2019). Moreover, regardless of T2DM, SGLT2i treatment seems able to improve all hydro-retention states such as HF, liver cirrhosis, CKD and even the syndrome of inappropriate antidiuresis (Saffo and Taddei, 2018; McMurray et al., 2019; Refardt et al., 2020; Bioletto et al., 2023). So far, several hypotheses have been formulated to explain at least some of the unexpected pleiotropic effects associated with the administration of SGLT2i, some authors arguing that these drugs can allow effective drainage

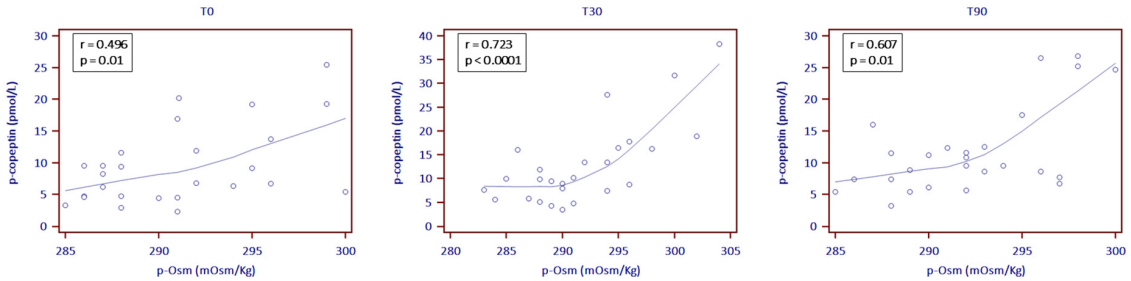

FIGURE 2
Correlation between plasma copeptin (p-copeptin) and plasma osmolality levels (p-Osm) the day before the start of SGLT2i (T0) and then at 30 (T30) and 90 (T90) treatment days (locally weighted scattered-pot smoother (LOESS) with a span of 80%).

TABLE 3 Measured bioimpedance parameters and estimated body fluid composition at both baseline and end of study in all patients and, particularly, in those who achieved significant resolution of overhydration condition on Biavector.

Number of patients	Variables	Baseline	90 days	*P*-value
All patients (26, 100%)	Rz (Ohm)	388 (317–477.8)	415 (345–467)	0.354
	Xc (Ohm)	39 (33–52)	45.12 (39–54)	**0.029**
	PhA (°)	5.9 (5.5–6.4)	5.8 (5.7–6.5)	0.447
	TBW (L)	48.9 ± 11.3	47.5 ± 10.3	0.183
	ECF (L)	22.2 ± 5.2	21.2 ± 4.6	**0.018**
	ICF (L)	26.7 ± 6.7	26.3 ± 6.4	0.574
Patients with overhydration resolution (7, 27%)	Rz (Ohm)	356 (303.5–366)	410 (359.7–443.2)	**0.031**
	Xc (Ohm)	34 (33–37)	39 (37.5–43.2)	**0.016**
	PhA (°)	5.9 (5.4–6.2)	5.7 (5.3–6.4)	0.469
	TBW (L)	52.6 ± 6	47.3 ± 4.7	**0.007**
	ECF (L)	24.2 ± 2.5	22 ± 2.4	**0.002**
	ICF (L)	28.4 ± 4.1	25.2 ± 3	**0.021**

Paired samples *t*-test and Wilcoxon test significant results ($p < 0.05$) reported in bold. ECF, extracellular fluid; ICF, intracellular fluid; PhA, phase angle; Rz, resistance; Xc, reactance; TBW total body water.

of interstitial fluid (ISF), thus avoiding hypovolemia and acute kidney injury (Lambers Heerspink et al., 2013; Hallow et al., 2018).

Indeed, consistent losses of body water and electrolytes, as observed during secretory diarrhea or loop diuretics administration, may be responsible for large ECF volume contraction, primarily involving the intravascular volume. In similar conditions of marked extracellular dehydration, the activation of baroreceptors determines a reduction in the tonic inhibition exerted on the release of AVP (Cheuvront and Kenefick, 2014). Furthermore, the baroreceptor reflex itself, together with the strong stimulation of AVP 1a receptors (V1aR) by the hypothalamic nonapeptide, induces the activation of the sympathetic nervous system and the RAAS, aiming to restore the ECV both through arterial vasoconstriction and through the reabsorption of sodium (Na^+) and water from the kidney. Unfortunately, a similar persistent neurohormonal activation also leads to harmful cardiovascular effects and cardiac remodeling, at least in part attributable to chronic water retention and the combined profibrotic action exerted by AVP, angiotensin II and aldosterone (Szczepanska-Sadowska et al., 2018).

Conversely, intracellular dehydration occurs during prevailing losses of electrolyte-free water. This condition produces a consequent flow of water from the ICF to the ECF and is detected by both the central and peripheral osmoreceptors, in turn responsible for an isolated stimulus to the release of AVP from the hypothalamus (Cheuvront and Kenefick, 2014).

Copeptin is co-secreted by the neurohypophysis in an equimolar proportion with AVP and in response to the same stimuli, being mainly osmoregulated. Due to low pre-analytical variability and reliable automated testing, copeptin levels are strongly correlated with p-Osm in healthy subjects, even better than AVP itself (Balanescu et al., 2011).

Copeptin levels were found slightly higher in patients with both type 1 and T2DM than in healthy individuals (Roussel et al., 2017; Jensen et al., 2019) and, in this regard, an acceleration in the turnover of body fluids due to glycosuria, as well as a reset of the osmostat have been hypothesized (Marton et al., 2021). Nevertheless, a definitive justification for this endocrine adaptation has not yet been provided (Bankir et al., 2001).

Furthermore, a modest increase in copeptin was previously observed even after a few weeks of treatment with SGLT2i (Heerspink et al., 2019; Lytvyn et al., 2020); thus, further supporting the theory of a compensatory mechanism to limit volume depletion in response to osmotic diuresis, but also of a possible adaptive mechanism alteration of the AVP-renal axis.

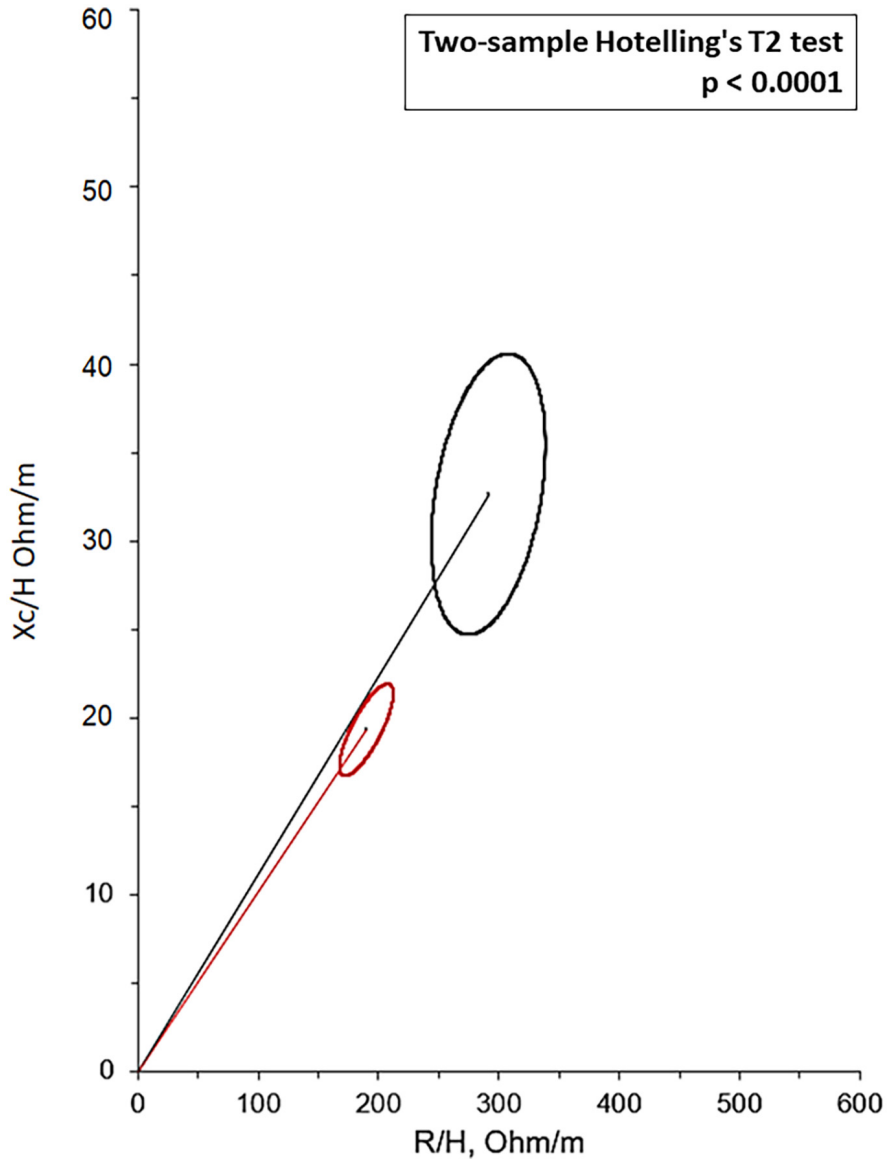

FIGURE 3
Mean Biavectors from overhydrated (red ellipse) and normohydrated patients (black ellipse), recorded the day before the start of SGLT2i (T0), compared with the two-sample Hotelling's T2 test ($p < 0.0001$).

In this context, our results show for the first time that copeptin adaptation to SGLT2i in diabetic patients persists for over 3 months and that its levels remain strongly associated with p-Osm even during long-term treatment. Most importantly, BIVA recorded a proportional dehydration process between ECF and ICF; this phenomenon was associated with a condition of basal hyperhydration, in the absence of significant RAAS activation.

These data support the hypothesis of a progressive and coupled reduction of both ECF and ICF, as observed in the process of intracellular dehydration, able to counteract ECF overload without inducing hypovolemia.

Indeed, our results confirm that treatment with SGLT2i in well-controlled diabetic subjects increases u-Osm inducing glycosuria, with only a transient increase in total daily diuresis and natriuresis.

A possible explanation for these findings is the unique mechanism of action of SGLT2i. As known, the natriuretic effect of SGLT2i is exerted by the selective inhibition of Na^+ reabsorption in the proximal tubule, with consequent increase of the luminal Na^+ content in the distal convoluted tubule and in the collecting duct. Increased luminal Na^+ and flow rate result in increased Na^+ reabsorption in the aldosterone-sensitive distal nephron *via* epithelial Na^+ channels (ENaC), thereby reducing effective Na^+ losses (Szczepanska-Sadowska et al., 2018). Finally, it should be considered that an increase in AVP release would further improve both ENaC and Na^+/K^+-ATPase activity in the kidney (Nicco et al., 2001; Mordasini et al., 2005).

On the other hand, in physiological conditions (i.e., euglycemic state), serum glucose substantially represents an ineffective osmole, due to its presence both in the extracellular and intracellular compartment (Verbalis, 2003); conversely, in severe hyperglycemic state, glucose significantly increases effective p-Osm by attracting water from the ICF.

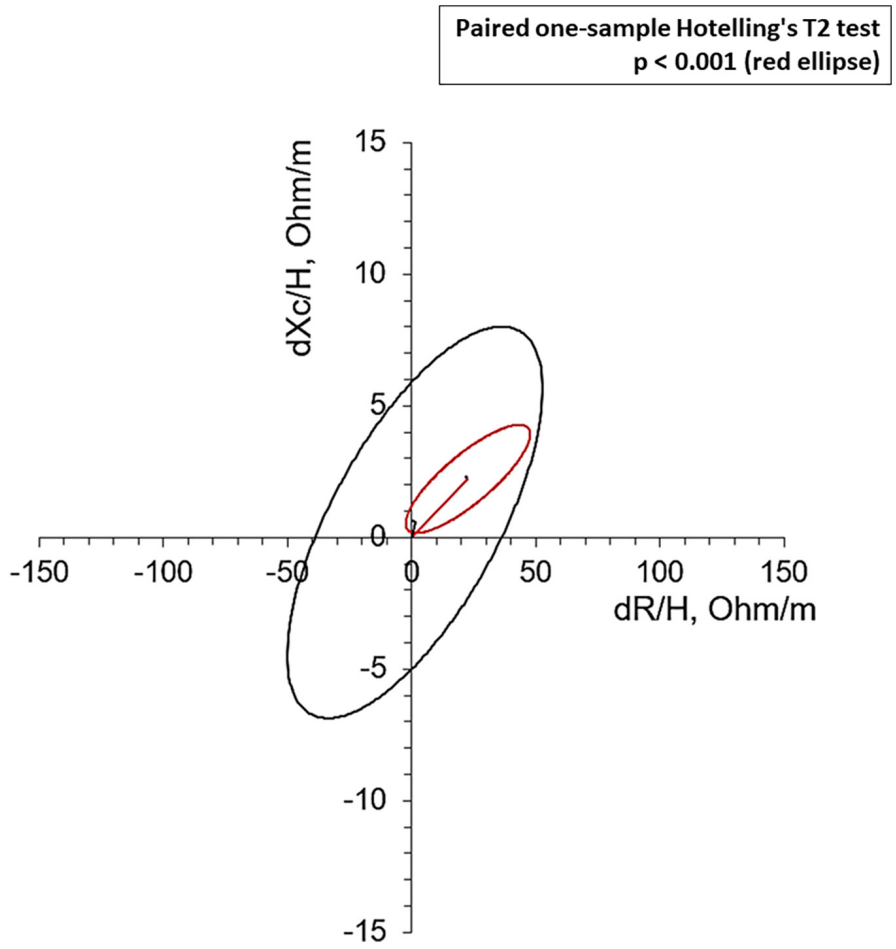

FIGURE 4
Mean Biavectors' displacement, between the day before the start of SGLT2i (T0) and 90 treatment days (T90), from overhydrated (red ellipse, $p < 0.001$) and normohydrated patients (black ellipse, not significant), compared with the paired one-sample Hotelling's T2 test.

The result of the sum of these combined effects is that, in a population of diabetic subjects not severely hyperglycemic, but affected by ECF overload, SGLT2i would favor a progressive loss of substantially hypotonic fluids compared to plasma; thus, determining a prevalent phenomenon of intracellular dehydration (**Figure 5**).

Noteworthy, our results also confirm an evident increase in HCT a few months after treatment with SGLT2i. Although HTC levels are reliable indicators of a prevalent extracellular dehydration phenomenon, several evidence gathered in recent years supports the hypothesis that this new class of drugs directly and indirectly improves erythropoietin production (Marathias et al., 2020; Kanbay et al., 2022).

We also found a significant increase in HRV in our population, accompanied by a reduction in mean nocturnal HR (**Table 2**), apparently not associated with resolution of fluid overload, as well as copeptin response.

Consistently, a recent Japanese study identified during SGLT2i administration a significant reduction in HR at rest, another well-known indicator of the autonomic nervous system activity (Sano, 2018). Taken together, these observations could suggest a beneficial reduction in sympathetic tone and an improvement in the function of the autonomic nervous system, notoriously impaired in diabetic subjects; although this constitutes a research area yet to be explored (Spallone et al., 2011). Conversely, ABPM did not show significant blood pressure variation during SGLT2i treatment, except for small reduction in diurnal values, of the order of 2–3 mmHg, in agreement with the results of other groups (Baker et al., 2017).

Finally, recent evidence, collected from large observational studies conducted on diabetic patients, has shown a clear association between the values of copeptin and albuminuria (Velho et al., 2013; Roussel et al., 2017). In our population, administration of SGLT2i led to a subclinical increase in both albuminuria and ACR, regardless of any sign of lower urinary tract infection (**Table 1**). Although there is evidence of a possible adverse effect of elevated circulating AVP levels on the degree of albuminuria, possibly mediated by V2R activation, a clear pathophysiological explanation for this phenomenon has not yet been provided (Bankir et al., 2001; Roussel et al., 2017). Most of all our patients were no longer receiving RAAS inhibitors at least 3 weeks prior to the initiation of SGLT2i and this could represent an explanation for a partially increased glomerular filtration pressure.

No variables among copeptin, HVR, TBW, ECF, and ICF were significantly associated with the arms of treatment in our

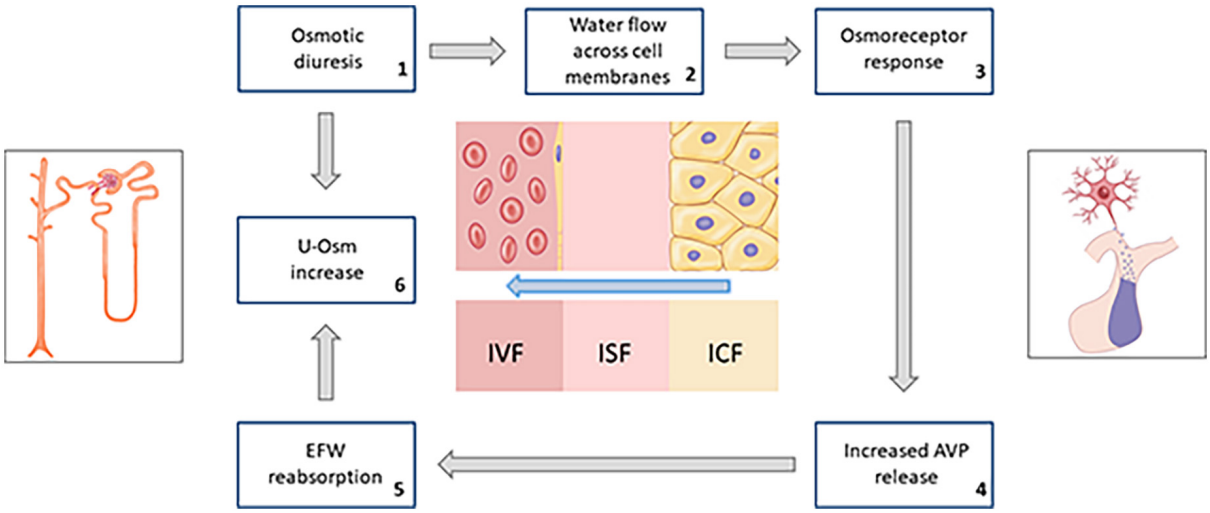

FIGURE 5
Schematic summary of the hypothesized response of osmoreceptors to water flow across cell membranes due to persistent osmotic diuresis during treatment with SGLT2i (AVP, arginine-vasopressin; EFW, electrolyte-free water; u-Osm, urine osmolality).

population. Although the number of subjects required for our study was calculated to find a significant difference in copeptin levels before and after SGLT2i treatment, these data support the hypothesis of a class effect; furthermore, a low dose of EMPA may be sufficient to achieve the same beneficial draining effect of ECF, as hypothesized based on other previous studies (Zinman et al., 2015).

The main strengths of our study are the prospective design, the outpatient population enrolled in real life and the extensive analysis conducted on the endocrine regulation of water and electrolyte balance. On the other hand, the absence of a control group and the small sample size certainly represent the main limitations of this research. Furthermore, there is a complex relationship between AVP and glucose metabolism, as V1aR activation induces both glycogenolysis and gluconeogenesis in the liver (Whitton et al., 1978; Keppens and de Wulf, 1979) and diabetic patients also exhibit an apparent enhanced AVP response to various stimuli (Bankir et al., 2001). In addition, previous studies have shown that AVP increases the release of insulin and glucagon by acting directly on pancreatic beta and alpha cells, in a glucose-dependent manner (Abu-Basha et al., 2002); whereas insulin may be able to reduce urinary Na^+ excretion, due to its ability to promote the adenylate cyclase system in the thick ascending limb of the nephron (Mandon et al., 1993).

Also for this reason we enrolled patients in good glycemic control to evaluate the copeptin response to SGLT2i; on the other hand this implies that our results are not applicable to a poorly controlled diabetic patient population.

Conclusion

In patients with T2DM, SGLT2i induces the release of AVP, thus compensating for persistent osmotic diuresis. This mainly occurs because of a proportional dehydration process between ECF and ICF (i.e., intracellular dehydration rather than extracellular dehydration). The extent of fluid reduction, but not the copeptin response, is affected by the patient's baseline volume conditions. In view of the known association between T2DM, essential arterial hypertension and volume overload, even in the absence of HF, our results offer some new insight into the pleiotropic benefits derived from SGLT2i treatment in patients with T2DM.

Data availability statement

The original contributions presented in this study are included in the article/supplementary material, further inquiries can be directed to the corresponding authors.

Ethics statement

The studies involving human participants were reviewed and approved by the Local Ethics Committees of the Turin and Novara University Hospitals (Turin: protocol *n*. D026280; Novara: protocol *n*. CE76/19). The patients/participants provided their written informed consent to participate in this study.

Author contributions

AMB and MP-C conceived and designed the study. FR, FP, and FS performed the biochemical analysis and collected the results. CL and CB performed the instrumental evaluation and edit the cases report form. AMB, MP-C, NP, MC, and FB performed the data analysis, the figures designing, and the manuscript writing. VG, GM were in charge for overall direction and planning. SG, MM, and ASB gave the needed encouragement and support to investigate and supervised the findings of this work. All authors revised

the manuscript for important intellectual content and approved the definitive version.

Funding

This research project was funded in 2020 by the University of Turin (ex 60%).

Acknowledgments

We thank Benedetta Romano and Federica Rosmini for collecting patients' data; Chiara Prencipe for her truly kind contribution in the design and graphic realization of the images of the manuscript. We wish to acknowledge the European Reference Network for rare endocrine conditions (Endo-ERN), of which several authors of this publication are members (Project ID No. 739543).

Conflict of interest

AMB received fees from Thermo Fisher Diagnostics for previous editorial collaborations and oral presentations.

The remaining authors declare that the research was conducted in the absence of any commercial or financial relationships that could be construed as a potential conflict of interest.

Publisher's note

References

Abu-Basha, E., Yibchok-Anun, S., and Hsu, W. (2002). Glucose dependency of arginine vasopressin-induced insulin and glucagon release from the perfused rat pancreas. *Metabolism* 51, 1184–1190. doi: 10.1053/meta.2002.34052

Baker, W., Buckley, L., Kelly, M., Bucheit, J., Parod, E. D., Brown, R., et al. (2017). Effects of sodium-glucose cotransporter 2 inhibitors on 24-hour ambulatory blood pressure: A systematic review and meta-analysis. *J. Am. Heart Assoc.* 6:e005686. doi: 10.1161/JAHA.117.005686

Balanescu, S., Kopp, P., Gaskill, M., Morgenthaler, N., Schindler, C., and Rutishauser, J. (2011). Correlation of plasma copeptin and vasopressin concentrations in hypo-, iso-, and hyperosmolar States. *J. Clin. Endocrinol. Metab.* 96, 1046–1052. doi: 10.1210/jc.2010-2499

Bankir, L., Bardoux, P., and Ahloulay, M. (2001). Vasopressin and diabetes mellitus. *Nephron* 87, 8–18. doi: 10.1159/000045879

Bioletto, F., Varaldo, E., Prencipe, N., Benso, A., and Berton, A. (2023). Long-term efficacy of empagliflozin as an add-on treatment for chronic SIAD: A case report and literature review. *Hormones (Athens)* doi: 10.1007/s42000-023-00430-0

Cheuvront, S., and Kenefick, R. (2014). Dehydration: Physiology, assessment, and performance effects. *Compr. Physiol.* 4, 257–285.

Christ-Crain, M. (2019). Vasopressin and copeptin in health and disease. *Rev. Endocr. Metab. Disord.* 20, 283–294. doi: 10.1007/s11154-019-09509-9

Hallow, K., Helmlinger, G., Greasley, P., McMurray, J., and Boulton, D. (2018). Why do SGLT2 inhibitors reduce heart failure hospitalization? A differential volume regulation hypothesis. *Diabetes Obes. Metab.* 20, 479–487. doi: 10.1111/dom.13126

Heerspink, H., Eickhoff, M., Dekkers, C., Kramers, B., Laverman, G., Frimodt-Møller, M., et al. (2019). Effects of dapagliflozin on volume status when added to renin-angiotensin system inhibitors. *J. Clin. Med.* 8:779. doi: 10.3390/jcm8060779

Jensen, T., Bjornstad, P., Johnson, R., Sippl, R., Rewers, M., and Snell-Bergeon, J. (2019). Copeptin and estimated insulin sensitivity in adults with and without type 1 diabetes: The CACTI study. *Can. J. Diabetes* 43, 34–39. doi: 10.1016/j.jcjd.2018.03.006

Kanbay, M., Tapoi, L., Ureche, C., Tanriover, C., Cevik, E., Demiray, A., et al. (2022). Effect of sodium-glucose cotransporter 2 inhibitors on hemoglobin and hematocrit levels in type 2 diabetes: A systematic review and meta-analysis. *Int. Urol. Nephrol.* 54, 827–841. doi: 10.1007/s11255-021-02943-2

Keppens, S., and de Wulf, H. (1979). The nature of the hepatic receptors involved in vasopressin-induced glycogenolysis. *Biochim. Biophys. Acta.* 588, 63–69. doi: 10.1016/0304-4165(79)90371-4

Lambers Heerspink, H., de Zeeuw, D., Wie, L., Leslie, B., and List, J. (2013). Dapagliflozin a glucose-regulating drug with diuretic properties in subjects with type 2 diabetes. *Diabetes Obes. Metab.* 15, 853–862. doi: 10.1111/dom.12127

Lukaski, H., Vega Diaz, N., Talluri, A., and Nescolarde, L. (2019). Classification of hydration in clinical conditions: Indirect and direct approaches using bioimpedance. *Nutrients* 11:809. doi: 10.3390/nu11040809

Lytvyn, Y., Bjornstad, P., Katz, A., Singh, S., Godoy, L., Chung, L., et al. (2020). SGLT2 inhibition increases serum copeptin in young adults with type 1 diabetes. *Diabetes Metab.* 46, 203–209. doi: 10.1016/j.diabet.2019.11.006

Mandon, B., Siga, E., Chabardes, D., Firsov, D., Roinel, N., and de Rouffignac, C. (1993). Insulin stimulates Na+, Cl-, Ca2+, and Mg2+ transports in TAL of mouse nephron: cross-potentiation with AVP. *Am. J. Physiol.* 265(3 Pt 2), F361–F369. doi: 10.1152/ajprenal.1993.265.3.F361

Marathias, K., Lambadiari, V., Markakis, K., Vlahakos, V., Bacharaki, D., Raptis, A., et al. (2020). Competing effects of renin angiotensin system blockade and sodium-glucose cotransporter-2 inhibitors on erythropoietin secretion in diabetes. *Am. J. Nephrol.* 51, 349–356. doi: 10.1159/000507272

Marton, A., Kaneko, T., Kovalik, J., Yasui, A., Nishiyama, A., Kitada, K., et al. (2021). Organ protection by SGLT2 inhibitors: Role of metabolic energy and water conservation. *Nat. Rev. Nephrol.* 17, 65–77. doi: 10.1038/s41581-020-00350-x

McMurray, J., DeMets, D., Inzucchi, S., Køber, L., Kosiborod, M., Langkilde, A., et al. (2019). A trial to evaluate the effect of the sodium–glucose co-transporter 2 inhibitor dapagliflozin on morbidity and mortality in patients with heart failure and reduced left ventricular ejection fraction (DAPA-HF). *Eur. J. Heart Fail.* 21, 665–675. doi: 10.1002/ejhf.1432

Mordasini, D., Bustamante, M., Rousselot, M., Martin, P., Hasler, U., and Féraille, E. (2005). Stimulation of Na+ transport by AVP is independent of PKA phosphorylation of the Na-K-ATPase in collecting duct principal cells. *Am. J. Physiol. Renal Physiol.* 289, F1031–F1039. doi: 10.1152/ajprenal.00128.2005

Neal, B., Perkovic, V., Mahaffey, K., de Zeeuw, D., Fulcher, G., Erondu, N., et al. (2017). Canagliflozin and cardiovascular and renal events in type 2 diabetes. *N. Engl. J. Med.* 377, 644–657. doi: 10.1056/NEJMoa1611925

Nicco, C., Wittner, M., DiStefano, A., Jounier, S., Bankir, L., and Bouby, N. (2001). Chronic exposure to vasopressin upregulates ENaC and sodium transport in the rat renal collecting duct and lung. *Hypertension* 38, 1143–1149. doi: 10.1161/hy1001.092641

Parasiliti-Caprino, M., Lopez, C., Prencipe, N., Lucatello, B., Settanni, F., Giraudo, G., et al. (2020). Prevalence of primary aldosteronism and association with cardiovascular complications in patients with resistant and refractory hypertension. *J. Hypertens.* 38, 1841–1848. doi: 10.1097/HJH.0000000000002441

Pasero, D., Berton, A., Motta, G., Raffaldi, R., Fornaro, G., Costamagna, A., et al. (2020). Neuroendocrine predictors of vasoplegia after cardiopulmonary bypass. *J. Endocrinol. Invest.* 44, 1533–1541. doi: 10.1007/s40618-020-01465-5

Piccoli, A., and Pastori, G. (2002). *BIVA software [Internet]*. Padova: University of Padova.

Piccoli, A., Nigrelli, S., Caberlotto, A., Bottazzo, S., Rossi, B., Pillon, L., et al. (1995). Bivariate normal values of the bioelectrical impedance vector in adult and elderly populations. *Am. J. Clin. Nutr.* 61, 269–270. doi: 10.1093/ajcn/61.2.269

Refardt, J., Imber, C., Sailer, C., Jeanloz, N., Potasso, L., Kutz, A., et al. (2020). A randomized trial of empagliflozin to increase plasma sodium levels in patients

with the syndrome of inappropriate antidiuresis. *J. Am. Soc. Nephrol.* 31, 615–624. doi: 10.1681/ASN.2019090944

Roussel, R., Velho, G., and Bankir, L. (2017). Vasopressin and diabetic nephropathy. *Curr. Opin. Nephrol. Hypertens.* 26, 311–318. doi: 10.1097/MNH.0000000000000335

Saffo, S., and Taddei, T. (2018). SGLT2 inhibitors and cirrhosis: A unique perspective on the comanagement of diabetes mellitus and ascites. *Clin. Liver Dis.* 11, 141–144. doi: 10.1002/cld.714

Sano, M. (2018). A new class of drugs for heart failure: SGLT2 inhibitors reduce sympathetic overactivity. *J. Cardiol. Jpn. Coll. Cardiol. (Nippon Sinzobyo Gakkai)* 71, 471–476. doi: 10.1016/j.jjcc.2017.12.004

Spallone, V., Ziegler, D., Freeman, R., Bernardi, L., Frontoni, S., Pop-Busui, R., et al. (2011). Cardiovascular autonomic neuropathy in diabetes: Clinical impact, assessment, diagnosis, and management. *Diabetes Metab. Res. Rev.* 27, 639–653.

Szczepanska-Sadowska, E., Czarzasta, K., and Cudnoch-Jedrzejewska, A. (2018). Dysregulation of the renin-angiotensin system and the vasopressinergic system interactions in cardiovascular disorders. *Curr. Hypertens. Rep.* 20:19. doi: 10.1007/s11906-018-0823-9

Velho, G., Bouby, N., Hadjadj, S., Matallah, N., Mohammedi, K., Fumeron, F., et al. (2013). Plasma copeptin and renal outcomes in patients with type 2 diabetes and albuminuria. *Diabetes Care* 36, 3639–3645. doi: 10.2337/dc13-0683

Verbalis, J. (2003). Disorders of body water homeostasis. *Best Pract. Res. Clin. Endocrinol. Metab.* 17, 471–503. doi: 10.1016/S1521-690X(03)00049-6

Wanner, C., Inzucchi, S., Lachin, J., Fitchett, D., von Eynatten, M., Mattheus, M., et al. (2016). Empagliflozin and progression of kidney disease in type 2 diabetes. *N. Engl. J. Med.* 375, 323–334. doi: 10.1056/NEJMoa1515920

Whitton, P., Rodrigues, L., and Hems, D. (1978). Stimulation by vasopressin, angiotensin and oxytocin of gluconeogenesis in hepatocyte suspensions. *Biochem. J.* 176, 893–898. doi: 10.1042/bj1760893

Williams, B., Mancia, G., Spiering, W., Rosei, E., Azizi, M., Burnier, M., et al. (2018). 2018 practice guidelines for the management of arterial hypertension of the European society of cardiology and the European society of hypertension ESC/ESH task force for the management of arterial hypertension. *J. Hypertens.* 36, 2284–2309. doi: 10.1097/HJH.0000000000001961

Wiviott, S., Raz, I., Bonaca, M., Mosenzon, O., Kato, E., Cahn, A., et al. (2019). Dapagliflozin and cardiovascular outcomes in type 2 diabetes. *N. Engl. J. Med.* 380, 347–357. doi: 10.1056/NEJMoa1812389

Zinman, B., Wanner, C., Lachin, J., Fitchett, D., Bluhmki, E., Hantel, S., et al. (2015). Empagliflozin, cardiovascular outcomes, and mortality in type 2 diabetes. *N. Engl. J. Med.* 373, 2117–2128. doi: 10.1056/NEJMoa1504720

frontiers | Frontiers in Endocrinology

TYPE Original Research
PUBLISHED 03 April 2023
DOI 10.3389/fendo.2023.1140886

OPEN ACCESS

EDITED BY
Alexandre Benani,
Centre National de la Recherche Scientifique (CNRS), France

REVIEWED BY
Chen-Che Jeff Huang,
Auburn University, United States
Wilson CJ Chung,
Kent State University, United States

*CORRESPONDENCE
Delphine Franssen
dfranssen@uliege.be

SPECIALTY SECTION
This article was submitted to Neuroendocrine Science, a section of the journal Frontiers in Endocrinology

RECEIVED 09 January 2023
ACCEPTED 03 March 2023
PUBLISHED 03 April 2023

CITATION
Franssen D, Johansson HKL, Lopez-Rodriguez D, Lavergne A, Terwagne Q, Boberg J, Christiansen S, Svingen T and Parent A-S (2023) Perinatal exposure to the fungicide ketoconazole alters hypothalamic control of puberty in female rats.
Front. Endocrinol. 14:1140886.
doi: 10.3389/fendo.2023.1140886

Perinatal exposure to the fungicide ketoconazole alters hypothalamic control of puberty in female rats

Delphine Franssen[1]*, Hanna K. L. Johansson[2], David Lopez-Rodriguez[1], Arnaud Lavergne[3], Quentin Terwagne[1], Julie Boberg[2], Sofie Christiansen[2], Terje Svingen[2] and Anne-Simone Parent[1,4]

[1]Neuroendocrinology Unit, GIGA Neurosciences, University of Liège, Liège, Belgium, [2]National Food Institute, Technical University of Denmark, Kgs. Lyngby, Denmark, [3]GIGA-Bioinformatics, GIGA Institute, Université de Liège, Liège, Belgium, [4]Department of Pediatrics, University Hospital Liege, Liege, Belgium

Introduction: Estrogenic endocrine disrupting chemicals (EDCs) such as diethylstilbestrol (DES) are known to alter the timing of puberty onset and reproductive function in females. Accumulating evidence suggests that steroid synthesis inhibitors such as ketoconazole (KTZ) or phthalates may also affect female reproductive health, however their mode of action is poorly understood. Because hypothalamic activity is very sensitive to sex steroids, we aimed at determining whether and how EDCs with different mode of action can alter the hypothalamic transcriptome and GnRH release in female rats.

Design: Female rats were exposed to KTZ or DES during perinatal (DES 3-6-12µg/kg.d; KTZ 3-6-12mg/kg.d), pubertal or adult periods (DES 3-12-48µg/kg.d; KTZ 3-12-48mg/kg.d).

Results: Ex vivo study of GnRH pulsatility revealed that perinatal exposure to the highest doses of KTZ and DES delayed maturation of GnRH secretion before puberty, whereas pubertal or adult exposure had no effect on GnRH pulsatility. Hypothalamic transcriptome, studied by RNAsequencing in the preoptic area and in the mediobasal hypothalamus, was found to be very sensitive to perinatal exposure to all doses of KTZ before puberty with effects persisting until adulthood. Bioinformatic analysis with Ingenuity Pathway Analysis predicted "Creb signaling in Neurons" and "IGF-1 signaling" among the most downregulated pathways by all doses of KTZ and DES before puberty, and "PPARg" as a common upstream regulator driving gene expression changes. Deeper screening ofRNAseq datasets indicated that a high number of genes regulating the activity of the extrinsic GnRH pulse generator were consistently affected by all the doses of DES and KTZ before puberty. Several, including MKRN3, DNMT3 or Cbx7, showed similar alterations in expression at adulthood.

Conclusion: nRH secretion and the hypothalamic transcriptome are highly sensitive to perinatal exposure to both DES and KTZ. The identified pathways should be exploredfurther to identify biomarkers for future testing strategies for EDC identification and when enhancing the current standard information requirements in regulation.

KEYWORDS

endocrine disrupting chemicals (EDCs), hypothalamus, puberty, transcriptome, reproduction

1 Introduction

Age distribution of pubertal signs in humans has been changing over the last decades. It is characterized by an extended distribution towards earliness for initial pubertal stages and towards lateness for final pubertal stages (1). This phenomenon is concomitant with an increased incidence rate in reproductive disorders (1, 2). Such rapid trends suggest that environmental factors play a causal role. Indeed, the programming of pubertal maturation and fertility is finely tuned by sex steroids and highly sensitive to environmental factors (3, 4). A growing body of evidence points towards an association between exposure to endocrine disrupting chemicals (EDCs) and recent changes in pubertal timing or reproductive health (5). While initial studies reported an impact of such environmental factors on male fertility (6), epidemiological data, together with animal models, now indicate that female reproductive health is also sensitive to environmental chemicals (7–10). Epidemiological studies reported associations between prenatal or childhood exposure to estrogenic EDCs such as dichlorodiphenyltrichloroethane (DDT) or bisphenol A with early or late puberty in girls (11–13). Impaired fecundity or premature menopause have also been reported after exposure to diethylstilbestrol (DES) (14, 15), PCOS after exposure to bisphenol A (16), and premature ovarian failure after exposure to perfluoroalkyl chemicals (17). Following such observations, initial animal studies focused on modeling effects of developmental and adult exposure to estrogenic EDCs on pubertal development, ovulation, and fertility. Estrogenic EDCs such as DES, bisphenol A and dichlorodiphenyltrichloroethane have been shown to alter the timing of vaginal opening or first estrus (18–22); reviewed in (1) and disrupt the preovulatory luteinizing hormone (LH) surge, ovarian follicle maturation and fertility in rodents (23–25). In addition, steroid synthesis inhibitors such as phthalates and the fungicide ketoconazole (KTZ) which are known to alter male reproductive function (26–28), have been recently described to impair female reproductive health (29, 30).

We recently showed that perinatal exposure to KTZ and DES delays vaginal opening in female rats without affecting bodyweight (21). This opened up the question of possible effects on central regulation of puberty onset. In the present study, we investigate the brain from the same animal litters to explore hypothalamic mechanisms potentially involved in the disruption of puberty. The reproductive organs have long been considered the major target of EDCs, but brain structures such as the hypothalamus, also appear to be highly sensitive to EDCs (31). GnRH neurons regulate all aspects of reproduction through their pattern of release. The secretory activity of GnRH neurons depends on trans-synaptic and glial inputs mediated by neurotransmitters and cell-cell signaling molecules produced in the preoptic area (POA) and the mediobasal hypothalamus (MBH) (32). New methods have provided more information regarding the transcriptional regulation of the hypothalamic network coordinating reproduction (33–35). This tightly organized network controlling GnRH secretion throughout development appears to be exquisitely sensitive to EDCs (10, 36).

KTZ is a first-generation antifungal imidazole known to disrupt steroid hormone synthesis by inhibiting various cytochrome P450 (CYP) enzymes (37–39). Recent data showed that KTZ, at low concentration (0.041-1.2 µM) induced an inhibition of CYP17A1 as it led to an accumulation of progestagens and corticosteroids and a decrease in androgens and estrogens. At higher concentrations, KTZ suppressed all steroids synthesis (40). DES is a synthetic estrogen (41–43). Its effects appear to be mediated by ERα as mice deficient in ERα (ERαKO) do not develop genital anomalies observed in wild-type mice after DES exposure (44–47). DES activate MAP kinase and PI3K pathways and induce ERK phosphorylation (48, 49).

Although deleterious effects of EDCs on reproductive function are now well recognized, current regulations are still insufficient for identifying windows of sensitivity and effects on female reproductive health (50). Better test methods to identify EDCs are necessary and require a better understanding of modes of action as well as the identification of biomarkers. To address this issue, this study aimed to determine the influence of two EDCs with different modes of action on the hypothalamic transcriptome governing GnRH release.

2 Methods

2.1 Chemicals

Ketoconazole (KTZ - CAS no. 65,277-42-1, purity 98%) was purchased from BOC Sciences Inc. (USA), and diethylstilbestrol (DES- CAS no. 56-53-1, purity ≥ 99%) from Sigma/Aldrich (cat.no. D4628). To use as control and vehicle, corn oil was purchased from Sigma/Aldrich (cat.no. C8267).

2.2 Animals and experimental design

Housing and exposure of the rats were performed in the National Food Institute facilities, Technical University of Denmark (Lyngby, Denmark). Ethical approval was obtained from the Danish Animal Experiments Inspectorate under the authorization number 2015-15-0201-00553. The National Food Institutes In-house Animal Welfare Committee for animal care and use oversaw the experiments. The animals were housed in High Temperature Polysulfone (PSU) cages with Tapvei wooden shelters. The cages were placed in ScanTainers (Ventilated Cabinets from Scanbur) with controlled environmental conditions: 12 h light (21.00 - 9.00 h): 12 h dark (9.00–21.00 h) cycle, humidity 55% ± 5, temperature 22°C ± 1°C and ventilation changing air 50–60 times per hour. Animals were fed Altromin 1314 (soy and alfalfa free) and tap water (BPA free bottles 84- ACBT0702SU; Polysulfone 700 mL w/ring square) ad libitum. As illustrated in Figure 1, three different exposure scenarios were used: *perinatal*, *pubertal*, and *adult*. For perinatal exposure (21), time-mated nulliparous Sprague-Dawley rats (CD IGS Rat, Crl : CD(SD), Charles River Laboratories,

10.3389/fendo.2023.1140886

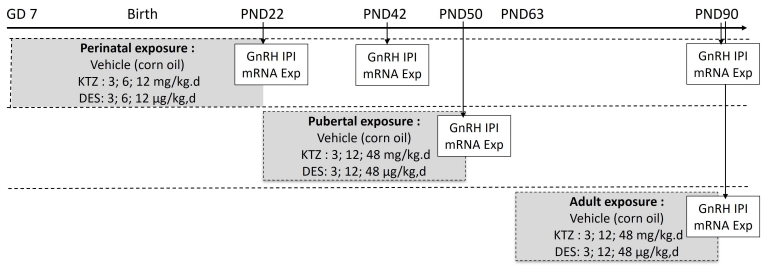

FIGURE 1
Exposure protocol. Rats were exposed to vehicle or diethylstilbestrol (DES) or ketoconazole (KTZ) during the perinatal period (gestation day (GD) 7 to postnatal day (PD) 22), pubertal period (PD22 to PD50) or adulthood (PD63 to PD90). Arrows indicate the age at which GnRH secretion and hypothalamic mRNA studies were conducted. GnRH IPI, GnRH interpulse interval; mRNA Exp, mRNA expression.

Sandhofer Weg 7, Sulzfeld, Germany) were supplied on gestation day (GD) 3. The day when a vaginal plug was detected was designated GD 1. On GD 4, animals were pseudo-randomly distributed into seven groups with similar body weight distributions. Dams were exposed by oral gavage with either chemical or vehicle once daily from GD 7 until birth and from the day after birth until postnatal (PND) 22. Doses for DES were 0; 3; 6; 12 µg/kg bw/day and doses for KTZ were 0; 3; 6; 12 mg/kg bw/day. For pubertal and adult exposure, females were exposed by oral gavage with either chemical or vehicle once daily from PND 23 to 49-52 or from PND 63 to 91-94, respectively. The exact day of study termination differed in a four-day interval to enable dissection in the di-estrous stage. The doses for DES were 0; 3; 12; 48 µg/kg bw/day and the doses for KTZ were 0; 3; 12; 48 mg/kg bw/day.

2.3 Hypothalamic explant incubation and GnRH assay

In order to assess the effect of DES or KTZ exposure on GnRH frequency, GnRH interpulse interval was measured using a hypothalamic explant incubation system followed by a GnRH radioimmunoassay, as described previously (51, 52). For the perinatally exposed animals, hypothalamic explant incubation was conducted for low and high dose groups of both DES and KTZ on PND 22, 42 and 90. For animals exposed during pubertal and adult periods all doses of DES and KTZ were included and hypothalamic explant incubation conducted on PND 50 and 90 respectively. Briefly, after decapitation, brains were collected to dissect the hypothalamus. Hypothalamic explants were transferred into an individual chamber, in a static incubator, submerged in MEM. The *ex vivo* explants incubation chamber contained a water-saturated atmosphere of O_2 at 37.5°C. Incubation medium was then collected and renewed every 7.5 min for a period of 4 hours. The GnRH released into the incubation medium was measured in duplicate using a radioimmunoassay method as described previously (53). In short, samples were preincubated with CR11-B81 (AB_2687904) rabbit anti-GnRH antiserum (initial dilution 1:20,000) (provided by Dr.V.D.Ramirez, Urbana, Illinois) during 24h at 4°C. GnRH labeled with ^{125}I (30,000 CPM) and rabbit serum (dilution 1:100) were added for 24h at 4°C. Finally, precipitation was induced by a solution of sheep anti-rabbit antiserum (dilution 1:200; CER Groupe), polyethylene glycol (60g=L), tween, and cellulose. Radioactivity was counted on a gamma-counter (Wallac CliniGamma). The intra-assay and inter-assay coefficients of variation were 7% and 10% and the limit of detection was 5pg/100 µl.

2.4 Hypothalamic mRNA extraction

Expression of hypothalamic genes in females was analyzed by RNA-seq after perinatal exposure (at PND22, PND42 and PND90) and by real-time RT-PCR after pubertal and adult exposures. After decapitation, the pre-optic area (POA) and the mediobasal hypothalamus (MBH) were rapidly dissected and frozen. The brain was placed ventral side up. The dissection began by two sagittal incisions along the lateral hypothalamic sulci. Two transversal incisions were made 2 mm ahead from the anterior boundaries of the optic chiasm and along the caudal margin of the mammillary bodies. Finally, a frontal incision was made under the ventral surface of the hypothalamus. Total RNA was extracted from the MBH and POA using Universal RNA mini kit (Qiagen,Venlo, Netherlands) following the manufacturer's instructions.

2.5 RNA sequencing

RNA-seq analysis was carried out on total RNA extracted from MBH and POA of female rats at PND22, PND42 and PND90 after perinatal exposure to vehicle, DES (3; 6; 12 µg/kg bw/day) or KTZ (3; 6; 12 mg/kg bw/day) (n = 5/each group; 210 samples in total). Library preparation and sequencing were performed at the GIGA Genomics facility (University of Liège, Belgium). RNA integrity was verified on the Agilent Bioanalyser with RNA 6000 Nano chips, RIN scores were > 7.5 for all samples. Illumina Truseq stranded mRNA Sample Preparation kit was used to prepare libraries from 1

microgram of total RNA. Libraries were quantified by qPCR with the KAPA Library Quantification Kits for Illumina® platforms. Sequencing was performed on Illumina® NovaSeq™6000 Sequencing System. The average read-depth of the data is ~25-30M reads. The data were processed through the nf-core "rnaseq" pipeline version 1.4.2 (https://nf-co.re/rnaseq/1.4.2). The quality control of the samples was assessed with FastQC software v0.11.8 (https://www.bioinformatics.babraham.ac.uk/projects/fastqc/). Reads were aligned on the Rattus Norvegicus genome, using Rnor_6.0 genome build and annotations from the Ensembl release v102 (ensembl.org) using STAR software v2.6.1d (https://github.com/alexdobin/STAR). Gene expression was determined using featureCounts v1.6.4. QCs of mapping and quantification were assessed with ~80-85% of mapping rate and ~65-70% of assignation rate. Raw data were deposited on the GEO repository under accession number GSE225359.

2.6 RNA-seq data analysis

The count matrix was imported in R environment and analyzed using the *DESeq2* package (54). Differentially Gene Expression Analyses were performed by pairwise comparisons using classical *DESeq2* methods, and differentially expressed genes were selected using an adjusted p-value (FDR) lower than 0.05 and no threshold on the log2 Fold Change (Log2FC). Samples were clustered using Principal Component Analysis while we used Venn Diagram (using ggVennDiagram) to cross results from the different groups.

2.7 Ingenuity pathway analysis

Datasets generated by the RNA-seq analysis, including log2-fold change and adjusted p-value, were imported into the Ingenuity Pathway Analysis Tool (v01-20-04 version). In IPA, differentially expressed genes (DEG) are mapped to genetic networks available in the Ingenuity database and then ranked by score. The score is generated based on hypergeometric distribution, where the negative logarithm of the significance level is obtained by Fisher's exact test at the right tail (55, 56). The Z-score >2 was defined as the threshold of significant activation, whilst Z-score <–2 was defined as the threshold of significant inhibition. The Comparison Analysis tool of IPA was used to study canonical pathways and upstream regulators among the different doses of KTZ and DES. The threshold for significance for the heat map of canonical pathways was a Z-score >2. The heatmap were then filtered for "*Neurotransmitters & other nervous system signaling*", "*Hormone biosynthesis*", "*Nuclear receptor signaling*" and "*Growth factor signaling*" representing around 100 canonical pathways.

2.8 RT-qPCR

Reverse transcription of 500 nanograms of RNA for each sample (n= 6/group) was performed using the Transcriptor first strand cDNA synthesis kit (Roche, Germany). For real-time semi quantitative RT.PCR reactions (RT-qPCR), FastStart Universal SYBR Green Master (Rox) (Roche, Germany) and a LightCycler 480 system (Roche, Germany) were used. Four microliters of cDNA (previously 10-fold diluted) were added to a mix of 5 µl of SYBR green, 0.3 µl of both forward and reverse primers and 0.4 µl of nuclease-free water. Cycle threshold (Ct) values were obtained from each individual amplification curve and the average Ct was calculated for each target gene in each sample. Quantification of relative gene expression was performed according to the 2–ΔΔCt method, which takes into account reaction efficiency depending on primers (57). All assays had amplification efficiencies between 1.9 and 2.1. β-actin was used as normalizing gene. The primer sequences and information are provided in Supplemental Table 1.

2.9 Statistics

For the analyses of GnRH interval interpulse and the RT-qPCR, numerical values were expressed as mean ± SEM. As the data followed a normal distribution, a one-way ANOVA followed by a Newman-Keuls multiple test were performed. For the analysis of the RNAsequencing analysis, the DEGs were identified by adjusted p-value >0.05.

3 Results

3.1 Perinatal exposure to KTZ or DES slows down maturation of GnRH pulsatile secretion

We previously showed that perinatal exposure to DES or KTZ delays vaginal opening in female rats without affecting bodyweight (21). Because puberty results from the activation of GnRH secretion, this opened up the question of a potential delayed activation of GnRH secretion caused by exposure to DES and KTZ. Pulsatile GnRH secretion from individually incubated hypothalamic explants displays a developmental acceleration between day 5 and day 25, before the onset of puberty (58). Consistently, exposures to EDCs that advance or delay pubertal onset are associated with an acceleration or retardation of GnRH release, respectively (9, 19, 20), indicating the sensitivity of such an assay. We aimed to study the effect of perinatal exposure to KTZ or DES on GnRH secretion on PND22. GnRH interpulse interval (GnRH IPI) was significantly increased by exposure to EDCs ($F_{4,18}$ = 4.727; p=0.0088). *Post hoc* analyses indicated that the exposures to 12 µg/kg/d of DES and 12 mg/kg/d of KTZ significantly increased GnRH interpulse interval at 22 days of age compared to the Control group (p = 0.02 and p = 0.02 respectively; Figure 2A), indicating a delay of the maturation of GnRH secretion. This was consistent with the significant delay in vaginal opening reported in the same animals for all doses of DES or KTZ at 6 mg/kg/d (21).

To determine whether the effects of DES and KTZ persisted later in life, we studied GnRH pulsatile release after puberty: at PND42 and during adulthood (diestrus stage) at PND90. ANOVA analysis of GnRH interpulse interval at PND 42 showed a significant effect of

10.3389/fendo.2023.1140886

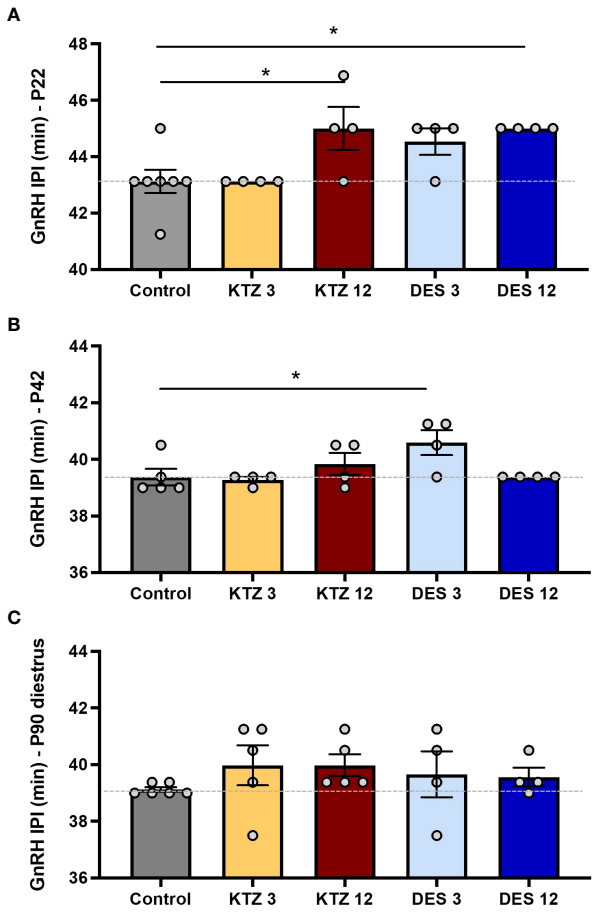

FIGURE 2
Effects of perinatal exposure to KTZ and DES on pulsatile GnRH secretion from hypothalamic explants *in vitro*. **(A)** GnRH interpulse interval *ex vivo* using hypothalamic explants obtained on PND 22 from female rats perinataly exposed to vehicle (control), DES (3 or 12 µg/kg bw/day) or ketoconazole (3 or 12 mg/kg bw/day). **(B)** and **(C)** GnRH interpulse interval *ex vivo* using hypothalamic explants after perinatal exposure to vehicle, DES or KTZ and obtained on PND 42 and PND 90 respectively. Data are mean (n=4-6) +/- SEM; *p < 0.05 versus control at the same age. The dotted line indicates the mean interpulse interval for the control group.

exposure ($F_{4,16}$ = 3.312; p=0.0371). *Post hoc* analyses revealed that only the lowest dose of DES (3 µg/kg/d) significantly increased GnRH interpulse interval on PND 42 (p = 0.0301; Figure 2B). Alterations of GnRH release caused by exposure to DES or KTZ before puberty did not persist on PND90 (Figure 2B, C).

3.2 Pubertal or adult exposure to KTZ or DES did not affect GnRH pulsatile secretion

We also aimed at determining whether there was a sensitive exposure window for DES and KTZ effects on GnRH secretion. GnRH pulsatile release was studied immediately after pubertal or adult (diestrus stage) exposure to DES and KTZ. The ANOVA tests did not indicate any significant disruption of GnRH pulsatility after pubertal ($F_{6,27}$ = 0.347; p=0.905) or adult exposure ($F_{6,28}$ = 1.109; p=0.382) (Supplemental Figure 1).

3.3 Perinatal exposure to KTZ or DES disrupts the hypothalamic transcriptome

Because gestational and lactational exposure to DES and KTZ delayed vaginal opening and maturation of GnRH secretion, we hypothesized that the transcriptional activity of the glial and neuronal network governing GnRH secretion, in the mediobasal hypothalamus (MBH) and in preoptic area (POA), would be sensitive to perinatal exposure to KTZ or DES. To explore this hypothesis, RNA-seq was performed on MBH or POA total RNA obtained from females at different developmental time points (PND 22, 42 and 90) after perinatal exposure to the three doses of KTZ or DES (5 biological replicates per group).

In the MBH, the principal component analysis (PCA plot, Figure 3) indicated that the transcriptional profiles of control and EDC exposed samples were readily distinguishable at specific ages. At PND22, the three doses of KTZ or DES were clearly separated from the control group. The first two components explained 68% of total point variance for KTZ (Figure 3A) and 58% of total variability for DES (Figure 3C). At PND42, there were no clear clustering between EDC samples and control. At PND90, the three groups exposed to KTZ, or the highest dose of DES were clearly separated from the controls (Figure 3A, C).

We conducted differential expression analysis with an adjusted p-value threshold of 0.05 on each set of raw expression measures. The MBH appeared to be very sensitive to perinatal exposure to DES or KTZ before puberty as the mRNA expression of 1896 hypothalamic genes was significantly affected by all three doses of KTZ (Figure 3B); and 1084 genes by all three doses of DES (Figure 3D) on PND22. On PND 42, 48 genes were affected by all 3 doses of KTZ and 100 genes by the 3 doses of DES. On PND90, 2433 genes are affected by the three doses of KTZ while only the highest dose of DES altered a high number of genes (2496). The list of DEG was deposited on the Figshare repository under accession link: https://figshare.com/s/778fbb8f785c97d5d9ee.

RNA-seq of the preoptic area (POA) indicated a milder effect of perinatal exposure to KTZ or DES on the transcriptome compared to MBH. The principal component analysis (PCA plot, Figure 4C) revealed no distinction between the control and the DES clusters leading to an absence of genes affected by all three doses of DES. After KTZ exposure, 593 genes were commonly affected by the three doses at PN22 but only 18 at PND42 (Figure 4B). At PND 90, 13 genes were affected by all 3 doses of KTZ but the intermediate and the high doses shared 3284 affected genes (Figure 4B).

3.4 Perinatal exposure to KTZ or DES affects common hypothalamic pathways in the MBH before puberty

To investigate possible biological interactions of differentially regulated genes in the MBH at PN22, RNA-seq datasets were imported into the Ingenuity Pathway Analysis Tool. Ingenuity Pathway Analysis (IPA) was used to predict enriched canonical pathways and their activation or inhibition. Heatmaps comparing the most enriched canonical pathways for the 3 doses of KTZ or

10.3389/fendo.2023.1140886

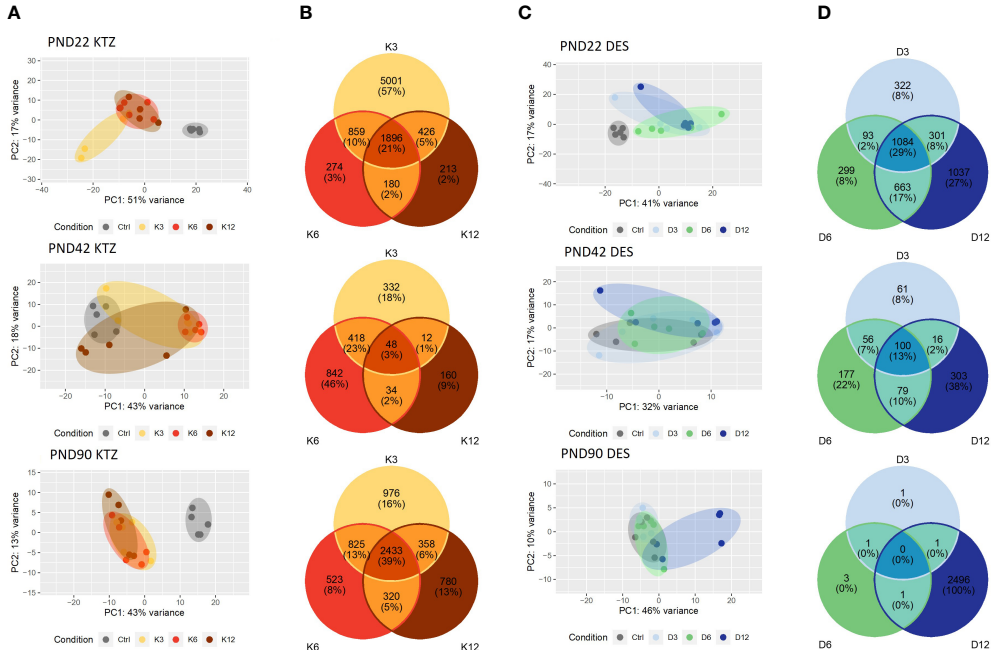

FIGURE 3
Effects of perinatal exposure to KTZ or DES on the mediobasal hypothalamus transcriptome. **(A, C)** Principal activity component (PCA) plot showing the dispersion of the transcriptome of MBH samples on PND 22, 42 or 90 after perinatal exposure to vehicle (control) or DES (D3: 3; D6: 6; or D12: 12 µg/kg bw/day) or KTZ (K3: 3; K6: 6; or K12: 12 mg/kg bw/day). Panels **(B, D)**: Venn diagrams representing the number of differentially expressed transcripts based on an adjusted p-value of 0.05 for all 3 doses of KTZ **(B)** or DES **(D)** compared to controls. N=5 samples/group.

DES were generated by ranking pathways according to the Z-score and by applying thresholds and filters as described in the material and methods. A Z-score >2 was defined as the threshold for significant activation, whilst Z-score <−2 was defined as the threshold for significant inhibition (55, 56). The heatmaps comparing the 20 most enriched canonical pathways for the 3 doses of KTZ and the three doses of DES are shown in Figure 5. Several important canonical pathways were shared among the three doses of each EDC. *"Estrogen biosynthesis", "Creb signaling in Neurons", "IGF-1 signaling"* and *"Oxytocin in brain signaling"* are critical pathways for reproductive function. The prediction of their activation or inhibition were also similar between the doses of each EDC and between both EDCs. As illustrated by the heatmaps (Figure 5B) representing the Log2-fold change of the 10 most up- or downregulated genes for these 4 selected pathways, it appears that the consequences of KTZ and DES exposure led to similar transcriptional effects. For instance, the oxytocin transcript (*Oxt*) was upregulated by the 3 doses of KTZ but also by the three doses of DES. The subcellular representations of these 4 pathways are provided in Supplemental Figures 2–5.

The heatmaps comparing the 20 most enriched canonical pathways after exposure to the 3 doses of KTZ in the POA at PND22 (Supplemental Figure 6), also revealed critical pathways for reproductive function such as "*Creb signaling pathway*" and "*oxytocin in brain signaling*" that are predicted to be downregulated. The two pathways that are predicted to be activated in the POA involve PPAR signaling. Notably, the Log2FC of the differentially expressed genes (DEG) in the POA are smaller than DEG changes observed in the MBH.

3.5 PPAR, a common upstream target of KTZ and DES

Using IPA upstream regulator analysis to identify potential upstream signals that may be driving changes in gene expression in the MBH, "PPARγ" was identified for all doses of KTZ and DES when compared with controls, with a z-score > 2.

Figure 6 provides a heatmap identifying the top 15 up- and downregulated genes regulated by PPARγ in the MBH after exposure to the 3 doses of KTZ or DES. The comprehensive gene list is provided in Supplementary Table 2. As an illustration, the subcellular localization of the DEG products after KTZ 3mg/kg.d exposure in the MBH at PND22 is shown in Figure 6B. This figure represents the direct interactions between the upstream regulator (PPARγ) and the downstream top upregulated (labelled in red) or downregulated (labelled in green) genes. The upregulation of 10 and the downregulation of 5 of those genes are consistent with PPARγ activation (orange and blue arrows respectively). Two upregulated genes and 5 downregulated genes are inconsistent with PPARγ activation.

The IPA tool, Tox Lists, helps to link experimental data to toxicological responses by providing sets of molecules that are known to be involved in a particular type of toxicity. In the Ingenuity Tox lists, "*PPARα/RXRα activation*" is systematically found among the most significant pathways for each EDC dose compared to control (KTZ 3_p-value =2.29x107; KTZ 6_p-value =5.88x103, KTZ 12_p-value =2.43x102; DES 3_p-value =4.89 x102; DES 6_p-value =2.45 x102; DES 12_p-value =5.88 x103) with an overlap of 15 to 48% between the genes of this pathway and the DEG

10.3389/fendo.2023.1140886

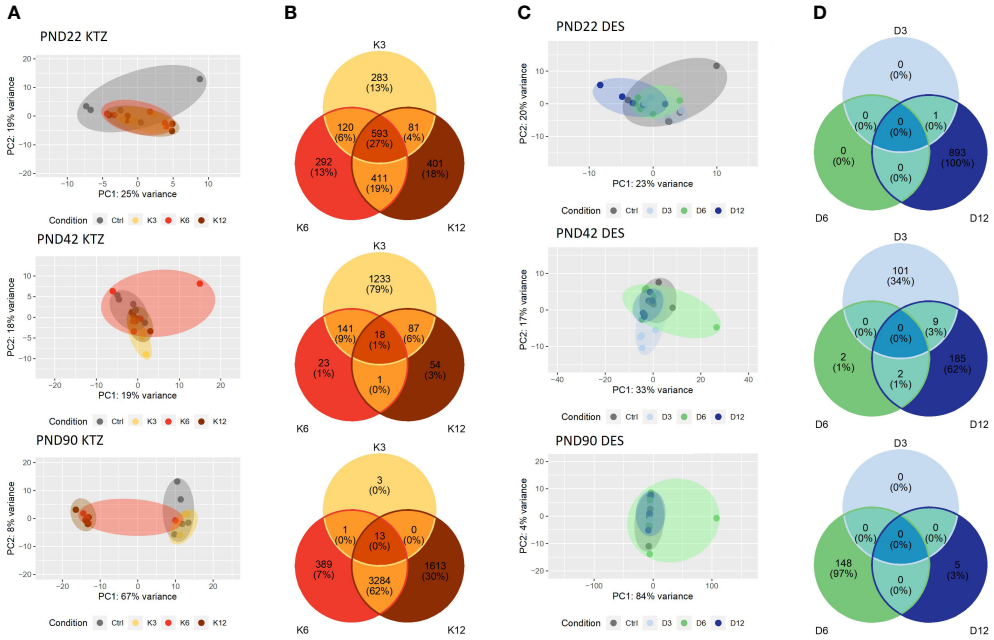

FIGURE 4
Effects of perinatal exposure to KTZ or DES on the Preoptic area (POA) transcriptome. **(A, C)** Principal activity component (PCA) plot showing the dispersion of the transcriptome of POA samples on PND 22, 42 or 90 after perinatal exposure to vehicle (control) or DES (D3: 3; D6: 6; or D12: 12 µg/kg bw/day) or KTZ (K3: 3; K6: 6; or K12: 12 mg/kg bw/day). Panels **(B, D)**: Venn diagrams representing the number of differentially expressed transcripts based on an adjusted p-value of 0.05 for all 3 doses of KTZ **(B)** or DES **(D)** compared to controls. N=5 samples/group.

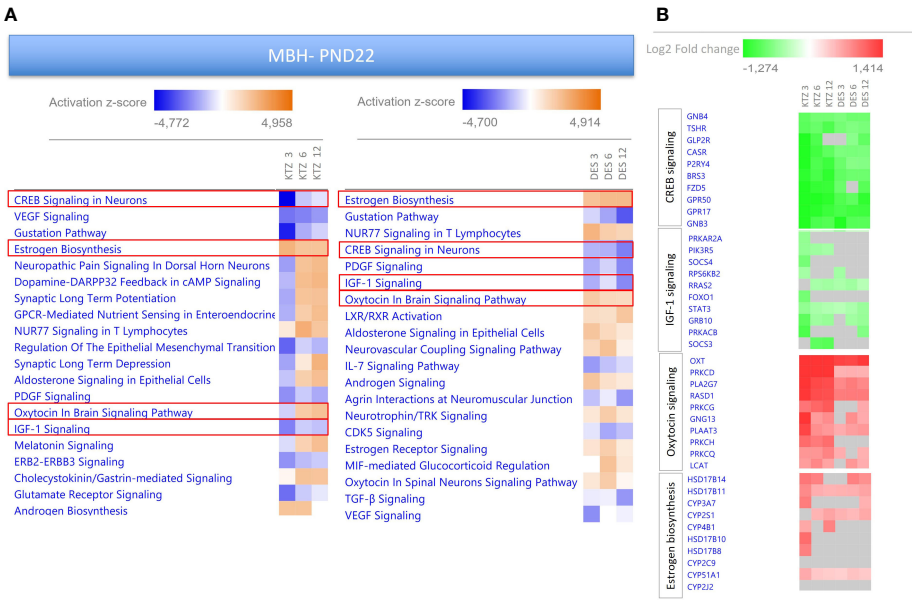

FIGURE 5
Enriched pathways differentially expressed in the MBH of PND22 females after perinatal exposure to KTZ or DES compared to controls. **(A)** Heatmaps comparing the most enriched canonical pathways for the 3 doses of KTZ or DES were generated by ranking pathways according to the Z-score and applying threshold and filters as described in the material and methods section. The z-score predicts whether a canonical pathway or diseases and biological functions are increased (positive z-score, orange) or decreased (negative z-score, blue) in accordance with the experimental dataset. Darker colors indicate higher absolute z-scores. **(B)** Heatmaps representing the Log2FC of the 10 most affected up- or downregulated genes for 4 selected pathways. Red or green colors indicate a significant change in expression (adjusted p-value < 0.05). Grey indicates non-significant changes.

10.3389/fendo.2023.1140886

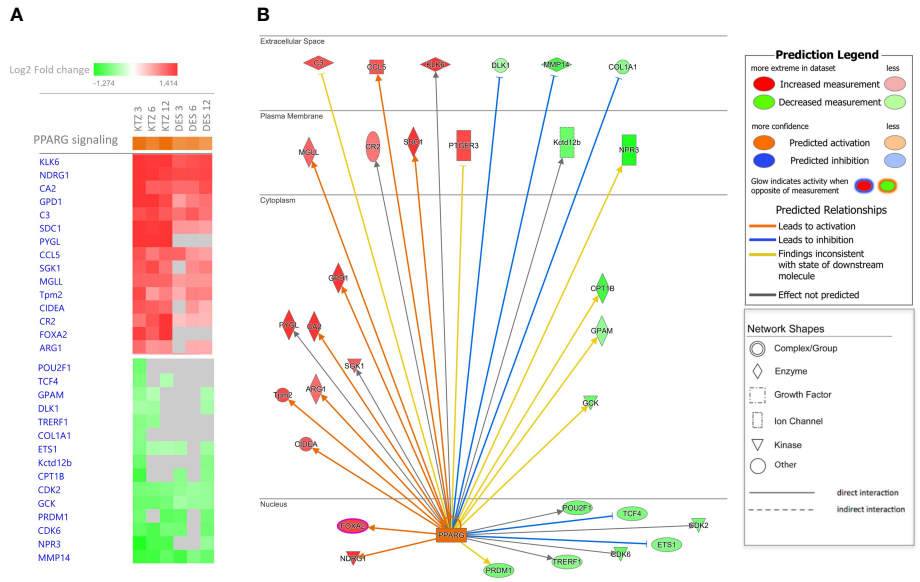

FIGURE 6
Ingenuity Pathway Analysis (IPA) identified PPARγ as upstream regulators. **(A)** The heatmap provides the top 15 up- and downregulated genes regulated by PPARγ in the MBH after exposure to the 3 doses of KTZ or DES. **(B)** The subcellular localization of the DEG products after KTZ 3 mg/kg bw/day exposure in the MBH at PND22, represents the direct interactions between the upstream regulator (PPARγ) and the downstream upregulated (labelled in red) or downregulated (labelled in green) genes. The upregulation of 10 and the downregulation of 5 of those genes are consistent with PPARγ activation (orange and blue arrows respectively). Two upregulated genes and 5 downregulated genes are inconsistent with PPARγ activation.

of each EDC dose. This toxicological activation is systematically found in the 4 canonical pathways, affected in the same direction by three doses of each EDC in the MBH on PD22 (*"Estrogen biosynthesis", "Creb signaling in Neurons", "IGF-1 signaling"* and *"Oxytocin in brain signaling"*) (Supplemental Figures 2 to 5).

3.6 Perinatal exposure to KTZ or DES affects mRNA expression of genes critical for puberty onset

As we previously shown, perinatal exposure to the three doses of DES and the intermediate dose of KTZ led to a significant delay in vaginal opening without affecting bodyweight (21). This observation is consistent with the delayed maturation of GnRH secretion induced by exposure to the two highest doses of KTZ and DES (Figure 2). We screened the PND 22 MBH RNA-seq data set for all genes known to be associated with hypogonadotropic hypogonadism or familial self-limited delayed puberty (59, 60) in order to identify potential target genes involved in delayed puberty caused by KTZ or DES. Table 1 indicates the level of expression of genes known to be mutated in pathological conditions leading to a delay of puberty and significantly affected by at least 2 doses of KTZ on PND22 in the MBH. The comprehensive gene list is provided in Supplemental Table 3. Among them, *Igsf10*, for which loss-of-function mutations lead to delayed puberty, is downregulated by all doses of DES and KTZ at PND22 (61).

In addition, we screened the RNA-seq data set for genes known to regulate GnRH neuron activity directly or indirectly and compared their level of expression after perinatal exposure to the three doses of KTZ and DES in the MBH at PND22 (Table 2). The data indicates that a high number of genes involved in the

TABLE 1 Genes known to be mutated in pathological conditions leading to a delay of puberty and significantly affected by at least 2 doses of KTZ at PND22 in the MBH.

	KTZ 3		KTZ 6		KTZ 12		DES 3		DES 6		DES 12	
	Log2FC	Padj	Log2FC	Padj	Log2FC	Padj	Log2FC	Padj	Log2FC	Padj	Log2FC	Padj
Sema7a	1,09	3,57E-07	1,13	2,83E-07	1,25	1,00E-08	0,73	8,37E-03	0,75	5,41E-03	0,77	3,10E-03
Nsmf	1,59	4,16E-09	1,17	3,79E-05	1,15	6,26E-05	0,65	2,34E-02	0,79	3,84E-03	0,77	4,32E-03
Fezf1	-0,82	1,06E-03	-0,60	3,73E-02	-0,70	1,47E-02	-0,56	7,21E-02	-0,36	2,58E-01	-0,57	4,63E-02
Igsf10	-1,10	1,35E-06	-0,83	7,86E-04	-0,93	1,40E-04	-0,62	1,39E-02	-0,83	3,55E-04	-0,83	2,49E-04
Sema3a	-1,12	2,97E-05	-0,62	5,10E-02	-1,00	6,17E-04	-0,83	1,45E-03	-0,54	5,32E-02	-0,80	1,84E-03
Pnpla6	-0,45	2,54E-04	-0,31	2,66E-02	-0,13	4,53E-01	-0,10	5,44E-01	-0,21	1,26E-01	-0,24	6,67E-02

TABLE 2 Genes known to regulate GnRH activity and their level of expression (Log2FC) after perinatal exposure to the three doses of KTZ and DES in the MBH at PND22 and PND90.

		KTZ						DES					
		P22			P90			P22			P90		
Pathway	Gene	K3	K6	K12	K3	K6	K12	D3	D6	D12	D3	D6	D12
Transcriptional and epigenetic control of puberty and reproduction	*Cbx7*	0.493***	0.614***	0.630***	0.704***	0.754***	0.695***	0.578***	0.529***	0.540***			0.400**
	Dnmt3a	-1.263***	-0.804**	-0.694*	-0.975***	-0.928***	-0.892***	-0.651*	-0.595*	-0.824**			-0.417**
	Dnmt3b	-1.030***	-0.959**	-0.556			-0.478*	-0.794**	-0.604*	-0.924***			
	Ezh1	0.335*	0.481**	0.569***	0.451***	0.519***	0.620***	0.500***	0.424***	0.421***			0.357***
	Ezh2	-0.429*	-0.560**	-0.544**	-0.788***	-0.843***	-0.896***	-0.685***	-0.361*	-0.591***			-0.418*
	Mkrn3	-0.686**	-0.918***	-0.778***	-0.922***	-0.926***	-1.043***	-0.808***	-0.777***	-0.709**			
	Gata3	0.871**	0.814*	1.270***									
	Sema7a	1.092***	1.130***	1.246***			0.502**	0.725**	0.748**	0.775**			
	Prc1				-0.479**	-0.612***	-0.528**						
	Sirt2		-0.354*	-0.393*	-1.031***	-1.114***	-1.136***	-0.415**	-0.328*				-0.427*
	Per3	-0.932***	-0.598**	-0.421*	-0.287*	-0.342*	-0.401**	-0.528*	-0.433*	-0.657**			-0.394***
Gabaergic signaling	*Gabbr1*	0.154*	0.191*	0.213**	0.135*			0.235*					
	Gabbr2	0.476*	0.629**	0.750***			0.324*	0.520*					
	Gabra4	1.234***	1.372***	1.336***					0.555*				
	Gabra5	-0.462***	-0.352***	-0.515***				-0.424***	-0.467***	-0.425***			
	Gabrd	2.143***	2.011***	2.138***			0.307*	0.372***	0.445***	0.353***			
	Gabre	-1.711***	-1.509***	-1.555***	-0.782***	-0.786***	-0.856***	-0.897**	-1.102***	-1.022***			-0.421*
	Gabrq	-1.287***	-0.739*	-0.833*						-0.863**			
	Slc32a1												
	Abat				0.393***	0.439***	0.287**						0.256**
	Gnai2				0.322***	0.279***	0.210**						
	Trak2	0.955***	0.715***	0.607**	0.414*	0.421*		0.489**	0.524**	0.758***			0.391**
Calcium signaling	*Cacna1i*	-0.716***			-0.310**	-0.236*	-0.311**						-0.344**
	Cacna1h	-0.781***	-0.778***	-0.524*	-0.401**	-0.336*	-0.356*		-0.501*	-0.504*			-0.481***
	Cacna2d3	0.370*	0.493*	0.515*									

(Continued)

10.3389/fendo.2023.1140886

TABLE 2 Continued

		KTZ						DES					
		P22			P90			P22			P90		
Pathway	Gene	K3	K6	K12	K3	K6	K12	D3	D6	D12	D3	D6	D12
	Cacna2d4	0.944**	0.785*							0.618*			
	Cacnb1	-0.550***	-0.556***	-0.434**	-0.372***	-0.402***	-0.320**	-0.325*	-0.311*	-0.353*			-0.286***
	Cacng3	0.239*	0.319*	0.285*			0.331*		0.334*				
	Cacng4				-0.220***	-0.296***	-0.217***						-0.152*
Glutamatergic signaling	*Grid2ip*	1.938***	2.068***	2.232***				0.652***	0.753***	0.725***			
	Grik2	-0.579***	-0.334*	-0.405*	-0.338**				-0.391*	-0.420*			
	Grm3	1.168***	1.365***	1.308***	0.658***	0.606***	0.802***	1.210***	1.198***	1.219***			0.474**
	Grm4	0.755**	0.693**	0.993***		-0.434*							
	Neto1	-1.163***	-0.526*	-0.703**	-0.539***		-0.389*	-0.543*		-0.692**			
	Slc17a7	1.832***	1.744***	1.877***				0.388***	0.544***	0.511***			
	Adcy6	-0.745***	-0.527***	-0.420**	-0.479***	-0.448***	-0.414***	-0.449**	-0.499**	-0.469**			-0.369***
	Itpr1		0.631**	0.587**	0.414**	0.503**	0.612***						0.409***
	Slc38a3		-0.248**		-0.252**	-0.349***	-0.427***			-0.264**			
Neuropeptides and receptors controlling reproductive function	*Crhr2*	-1.019***	-0.962***	-1.043***				-0.588*	-0.735**				-0.360*
	Esr1	-1.130***	-0.571*	-0.860***									
	Esrra	0.854***	0.516*	0.580**					0.591*	0.519*			
	Ghr	-0.846***	-0.561**	-0.701***			-0.346*	-0.533*	-0.541**	-0.666***			
	Gpr37	0.345*	0.452**	0.625***	0.266*		0.447***	0.585***	0.491***	0.521***			
	Rxra	-0.539***	-0.397**	-0.325*						-0.369*			
	Rxrg	-0.509***	-0.570***	-0.585***					-0.414*				
	Tshr	-0.935***	-0.851***	-1.008***				-0.794**	-0.720**	-0.765**			
	Oxt	2.509***	2.014***	1.651***	0.427*			1.300***	1.271***	1.369***			
	Pdyn	-0.624***	-0.708***	-0.775***					-0.498*	-0.697**			
	Pgf	0.900***	0.507*	0.477*	0.607***	0.459**	0.384*	0.509*	0.607**	0.572**			

(Continued)

10.3389/fendo.2023.1140886

TABLE 2 Continued

		KTZ						DES					
		P22			P90			P22			P90		
Pathway	Gene	K3	K6	K12	K3	K6	K12	D3	D6	D12	D3	D6	D12
Control of metabolism	*Adora1*	0.777***	0.710***	0.672***				0.473*	0.482*	0.503*			0.306*
	Agrp	-0.620*	-1.027***	-1.032***			-0.584**						
	Arg1	1.023***	0.725***	0.769***					0.568*	0.563*			
	Avp	1.994***	1.337***	1.129***	0.869***		0.779***	0.847***	0.789***	0.895***			
	Car2	1.520***	1.103***	1.132***	0.783***	0.655***	0.805***	1.024***	1.030***	1.211***			0.476**
	Cck	1.897***	1.486***	1.529***				0.363*	0.603**	0.435*			
	Gpr12	0.464*	0.547*	0.549*					0.529*	0.547*			
	Gpr17	-1.488***	-1.207***	-1.109***	-2.211***	-2.306***	-2.182***	-1.035***	-1.096***	-1.101***			-0.380*
	Igfbp5	0.579***	0.715***	0.697***	0.701***	0.587***	0.718***	0.837***	0.750***	0.572***			0.472**
	Insig1	0.628***	0.527***	0.575***			0.344*	0.501**	0.444**	0.467**			
	Mc3r	-0.529*	-0.666**	-0.606**					-0.502*	-0.621**			
	Npw	-3.104***	-3.317***	-3.315***	-1.996***	-1.898***	-2.049***	-2.525***	-2.524***	-2.524***			-0.426**
	Npy2r	-1.257***	-0.684*	-0.806**						-0.679*			
	Nr5a1	-1.278***	-1.333***	-0.969***	-0.465*			-0.761*		-0.809**			-0.413*
	Stat3	-0.619***	-0.491**	-0.440*				-0.405*	-0.470**	-0.571***			

Upregulated (font color po ay red) or Downregulated (font color po ay green) genes /*p<0,05 ; **p<0,01 ; ***p<0,001.

10.3389/fendo.2023.1140886

10.3389/fendo.2023.1140886

transcriptional and epigenetic control of GnRH secretion are very consistently affected by the 3 doses of DES and KTZ at PN22. Notably, *Mkrn3*, known to act as a brake on GnRH secretion and puberty onset (62), was downregulated by all doses of DES and KTZ. Glutamatergic and GABAergic pathways appeared also very sensitive to KTZ and DES. The glutamatergic receptor, *Grm3*, was upregulated by all the doses of KTZ and DES while seven subunits of GABA receptor were significantly affected by the 3 doses of KTZ and by some doses of DES. In addition, the mRNA expression of other receptors able to modulate reproductive function, such as *Ghr, Gpr37, Esrra* or *Tshr*, were also altered in the same direction by all the doses of KTZ and nearly all doses of DES. The two neuropeptides, arginine vasopressin (*Avp*) and oxytocin (*Oxt*) synthesized in magnocellular neurons located mainly in the supraoptic (SON) and paraventricular (PVN) nuclei of the hypothalamus, appear to be upregulated by all the doses of KTZ and DES. The expression of *Npw*, neuropeptide identified to play a role in regulating energy homeostasis during postnatal development (63), was also strongly downregulated by all doses of KTZ and DES.

3.7 Consequences of exposure to KTZ or DES on adult transcriptome

As depicted in Figures 3, 4, perinatal exposure to KTZ but not DES appeared to significantly affect hypothalamic (MBH and POA) transcriptional activity in adulthood. The heatmaps presented in Figure 7 compares the 20 most enriched canonical pathways in the MBH or POA after perinatal exposure to the 3 doses of KTZ. IPA mainly predicted a strong inhibition of the most affected pathways in the MBH and a moderate activation of a limited number of pathways in the POA. Several enriched pathways appeared conserved between PND 22 and PND 90 in the MBH. "*Creb signaling in Neurons*", "*IGF-1 signaling*" and "*Glutamate receptor signaling*" were still predicted to be downregulated. The comparison also revealed "*GnRH signaling pathways*" among the top downregulated pathways.

Several DEGs at PND22 in the MBH showed similar alterations at PND90 after KTZ exposure. Three PolyComb genes important for the epigenetic regulation of reproductive genes (64), *Cbx7, Ezh1* and *Ezh2*, were all affected by the three doses of KTZ at both ages. The glutamatergic receptor, *Grm3*, and the ϵ subunit of GABAergic receptor were still upregulated and downregulated, respectively, at PND90. The expression of the neuropeptide, *Npw* was also strongly downregulated by all doses of KTZ at PND90.

Finally, we assessed by RT-qPCR the mRNA expression of six genes after pubertal and adult exposures to KTZ and DES. These six genes were chosen because they were differentially affected by the perinatal exposure to most of the doses of KTZ and DES at PND22 and PND90. Only *Dnmt3* mRNA expression was affected by pubertal or adult exposure to one dose of KTZ (Supplemental Figure 7).

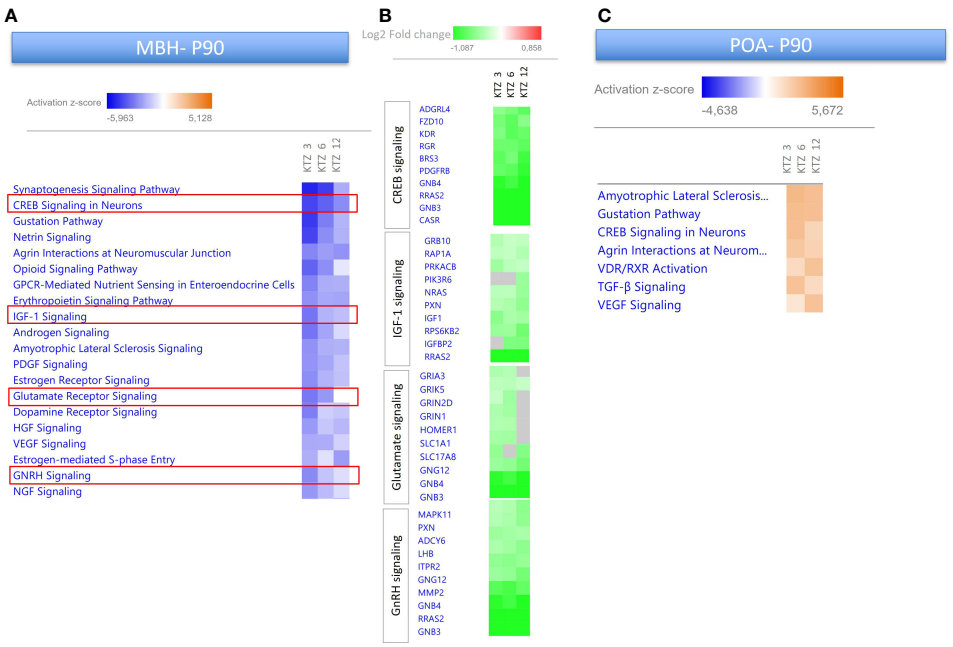

FIGURE 7
Enriched pathways differentially expressed in the MBH and POA of PND90 females after perinatal exposure to KTZ compared to controls. **(A)** Heatmaps comparing the most enriched canonical pathways for the 3 doses of KTZ were generated by ranking pathways according to the Z-score and applying threshold and filters as described in the material and methods section. The z-score predicts whether a canonical pathway or diseases and biological functions are increased (positive z-score, orange) or decreased (negative z-score, blue) in accordance with the experimental dataset. Darker colors indicate higher absolute z-scores. **(B)** Heatmaps representing the Log2FC of the 10 most downregulated genes for 4 selected pathways. Green color indicates a significant change in expression (adjusted p-value < 0.05). Grey indicates non-significant changes. **(C)** Heatmaps comparing the most enriched canonical pathways in the POA for the 3 doses of KTZ were generated by ranking pathways according to the Z-score.

4 Discussion

This study assessed the consequences of exposure to two EDCs with different mode of action, ketoconazole (steroidogenesis inhibitor) and diethylstilbestrol (strong estrogen), on the hypothalamic transcriptome governing GnRH release in female rats. To consolidate the study, multiple doses and different windows of exposure were tested. We found that perinatal exposure to KTZ and DES delayed the maturation of GnRH secretion in female rats which is consistent with the delay in vaginal opening we previously reported for the same animals (21). Our results underline the exquisite sensitivity of the mediobasal hypothalamus to developmental exposure to EDCs. In particular, the transcription of crucial actors of the GnRH network was affected by the developmental exposure to both estrogenic and anti-androgenic compounds.

4.1 GnRH release is sensitive to EDC exposure

We have previously shown that developmental exposure to estrogenic EDCs can disrupt the hypothalamic control of puberty (19, 20, 65). Our hypothalamic incubation model retains the pulsatile characteristics of GnRH secretion which are defined by a physiological acceleration before the onset of puberty (51). This model is thus well suited to detect the central effects of EDCs on GnRH secretion *ex vivo*. We previously documented that delayed vaginal opening caused by developmental exposure to EDCs can be explained by a slowdown of GnRH pulsatile release before puberty. Exposure to DES at 1 µg/kg.day during the first 5 postnatal days led to a slower release of GnRH at PND 25 and to delayed vaginal opening (19). The same observation was made after exposure to 25 ng/kg.day of BPA during the first 5 or 15 postnatal days while a higher dose of 5 mg/kg.day accelerated maturation of GnRH secretion and advanced puberty (20). In this study, we observed that perinatal exposure to 12 µg/kg.day DES and 12 mg/kg.day KTZ slowed down GnRH secretion consistent with the reported delayed vaginal opening (21). The prepubertal period was the most sensitive in detecting the impact of EDCs on GnRH release as the impact of DES and KTZ on GnRH secretion was less pronounced at later ages (PND 42 and 90). This indicates that the mechanisms that trigger the activation of the GnRH pulse generator at puberty onset may be more sensitive to KTZ or DES than the mechanisms maintaining GnRH secretion later in life (66, 67). The activation of GnRH release around puberty results from a loss in trans-synaptic inhibition together with a rise in excitatory input (34). This is explained by a shift in expression of puberty activating and inhibitory genes. Our results suggest that early exposure to KTZ or DES disrupt the shift in expression of key inhibitory or excitatory factors which are responsible for GnRH secretion acceleration at puberty. In addition, our data identified the perinatal period as a critical window of sensitivity, as exposure to DES or KTZ during that period led to an alteration of GnRH pulsatility while pubertal or adult exposures had no impact on GnRH pulse frequency in our model. However, we cannot exclude that such later exposure could affect other parameters such as the amplitude of GnRH pulses *ex vivo* which is physiologically increased during the afternoon of the proestrus (68).

4.2 EDC exposure disrupts extrinsic GnRH pulse generator

We show here that a very high number of hypothalamic genes is affected by perinatal exposure to KTZ and DES when studied during the prepubertal period (PND 22). This illustrates the high sensitivity of the hypothalamic transcriptional regulation to EDC exposure. The cell bodies of GnRH neurons are located in the POA. Their projections cross the MBH to end in the median eminence where GnRH is released in a pulsatile manner. Compelling data indicate that the pulse generator is not intrinsic to GnRH neurons, but rather is extrinsic and located within the arcuate nucleus and MBH (32, 67, 69). In our study, the MBH transcriptome appeared more sensitive to KTZ and DES exposure than the POA, as shown by the higher number of DEGs and the broad amplitude of expression changes. KNDy (expressing Kisspeptin, Neurokinin B and Dynorphin) and GABAergic neurons appear to be major actors of the GnRH pulse generator (32, 67, 69). Recent work by Herbison demonstrated that the inhibitory GABAergic signalization on GnRH dendrons requires $GABA_B$ receptor and voltage-gated calcium channels (VGCC)(70). In our study, the expression of two subunits of $GABA_B$ receptor and two subunits of VGCC, *Cacna2d3* and *Cacng3*, are upregulated by all doses of KTZ in the MBH at PND22, which is consistent with a delay in the activation of the extrinsic GnRH pulse generator and slowdown of GnRH pulsatile secretion. The opposite observation is made for the P22 downregulation of *Mkrn3*, that has been recently demonstrated to prevent puberty initiation, at least in part, by repressing the transcription of the genes coding for Kisspeptin and Neurokinin B (62). Finally, we cannot exclude that the delay in GnRH secretion maturation is due to the disruption of embryonic migration or development of GnRH neurons by DES or KTZ. *Igsf10* mutations are associated with abnormal GnRH neuronal migration resulting in delayed puberty (61). Notably, in our study, *Igsf10* is downregulated by all doses of KTZ and DES at PND22. Additionally, epigenetic factors driving fgf8-dependent GnRH neuron development such as *Dnmt* and *Ezh2* (71), were downregulated by the developmental exposure to KTZ.

4.3 Biomarkers of KTZ and DES exposure

To identify potential biomarkers of exposure, we focused on DEGs and pathways that were affected by all 3 doses of KTZ and DES. *Ingenuity pathway analysis®(IPA)* is a powerful analysis and interpretation tool built on the comprehensive and manually selected content of the QIAGEN Knowledge Base. Using IPA, we identified pathways predicted to be up or down regulated by perinatal exposure to KTZ and DES. At PND 22, the top pathway predicted to be activated by DES and KTZ was "*estrogen biosynthesis*". The role of neuroestrogens in the regulation of

GnRH and puberty is still incompletely understood. Terasawa et al. showed that neuroestradiol, locally synthesized in the hypothalamus, could be a component of the central inhibition of GnRH release before puberty in monkeys (72). Estradiol (E_2) levels in the median eminence are higher before than during puberty onset when GnRH release begins to increase (73). Because neuroestrogens appear to halt puberty, the activation of this pathway seems consistent with the delay of maturation of GnRH release observed in our model of exposure.

The "*Creb signaling pathway*" was systematically identified as downregulated by the three doses of KTZ in the MBH at PND22 and PND90 and in the POA at PND22. DES exposure similarly led to a downregulation of this pathway in the MBH at PND22. cAMP response element-binding protein (Creb) is a transcription factor which binds to cAMP response element (CRE) of the promoter of its target genes. As illustrated in Supplemental Figure 2, Creb can act as a second messenger upon activation of glutamate receptors, growth factor receptors or an intracellular Ca2+ influx (74, 75). GnRH neurons express Creb which acts as a mediator of E2 negative feedback (76). Creb has already been reported to be a target of anti-androgenic EDC in the hippocampus (77–79) and the testes (80).

The "*Igf-1 (insulin--like growth factor 1) signaling pathway*" was another pathway constantly affected by perinatal exposure to KTZ and DES. Igf1 is a metabolic signal activating and enhancing GnRH secretion at the time of puberty 81). IGF1 effect on GnRH neurons is mediated by glial production of PGE2 (81) and by neurokinin B release by KNDys neurons (82). Its expression is sensitive to EDCs, as it is upregulated in the arcuate nucleus after perinatal exposure to BPA or DES (83). Recent data indicates that precocious puberty in female rats following peripubertal exposure to 5 mg/kg/day of DEHP was associated with an upregulation of the hypothalamic Igf-1/Pi3k/Akt/mTor pathway. Inhibition of Igf-1R and mTor prevented the action of DEHP by decreasing Kiss-1, Gpr54, and GnRH expression (84). These reports support Igf1 as an interesting biomarker of EDC impact on the hypothalamic network.

We identified *Oxt* and *Avp* as potential biomarkers, as they were among the genes most affected by perinatal exposure to KTZ and DES at PND 22 and PND 90. The pathway "*Oxytocin in brain signaling*" was also identified by IPA analyses. Oxytocin appears to play a key role in pubertal onset and ovulation in several species. In rats, oxytocin facilitates female pubertal development through a mechanism involving Pge2 release by glial cell and increases the expression of several actors of the GnRH network including kisspeptin (85–87). In fish, studies suggest a modulation of the hypothalamo-pituitary-gonadal axis by oxytocin (88). In women, oxytocin is involved in the physiological regulation of LH through the ovulatory cycle (89). Hypothalamic oxytocin appears to be sensitive to EDC exposure. In our previous study, a perinatal exposure to a mixture of estrogenic and anti-androgenic EDCs led to a transgenerational downregulation of *Oxt* mRNA expression in the hypothalamus of prepubertal female rats (65). In the present study, we observed an opposite effect. *Oxt* was upregulated after both KTZ and DES perinatal exposure. These changes appear to contradict the delayed maturation of GnRH secretion and puberty. but could be seen as reactive rather than causal as previously seen for BPA effects on hypothalamic expression of enzymes involved in GABA synthesis (20). Thus, *Oxt* appears as a sensitive target, and a potential biomarker, of developmental exposure to EDCs.

Our results indicate that PPARγ could be one of the upstream regulators driving the changes in gene expression caused by KTZ and DES in the MBH. PPARγ is a nuclear receptor and a transcription factor. It regulates the expression of genes responsible for adipocyte differentiation, placental differentiation, lipid and glucose homeostasis, control of inflammatory responses and steroidogenesis (90). PPARγ is also expressed by hypothalamic AgRP and NPY neurons which are involved in the control of energy balance in mice and rats (91, 92). Those neurons send projections to GnRH neurons and regulate their activity (reviewed in (93)). One could hypothesize that PPARγ expressed by AgRP/NPY neurons could mediate EDC effects on GnRH secretion. However, the role of PPARγ as a metabolic sensor regulating GnRH activity remains to be determined. Several studies indicate that PPARγ expression and activity are sensitive to EDCs. It has been identified as a major mediator of the obesogenic effects of phthalates or bisphenol A, in adipocytes (94, 95). PPARγ is also expressed in the ovary where its activity is induced by mono-(2-ethylhexyl) phthalate (MEHP)(96) or Perfluoroalkyl and polyfluoroalkyl substances (PFAS) (97). All together, these data suggest that PPARγ could also be a potent effector and biomarker of EDC effects on female reproduction and lend further support to a previously developed putative AOP that proposes a PPARγ-mediated reduction in aromatase to explain irregular ovarian cycling and impaired fertility in adult females (*AOP-Wiki*).

It should be considered that our transcriptome data were obtained from whole MBH or POA, both of which are made up of various cell populations. Thus, it can be difficult to separate changes to general cellularity (a shift in cell populations) from bona fide changes in gene transcription. This is a prevailing challenge for RNA-seq analysis of heterogenous tissues. Future studies including single-cell RNA-seq could be used to identify specific cell populations sensitive to EDC exposure by deconvolution approaches. Nevertheless, our data suggests that a large proportion of DEGs represent changes in transcription, as we did not observe any obvious trend of all (or most) genes specific to certain cell types were moving in one direction; either up- or down-regulated.

4.4 Mode of action of ketoconazole

KTZ is mostly known to inhibit various P450 cytochrome enzymes involved in steroidogenesis and thereby interfering with both androgen and estrogen synthesis (39, 40). However, the role and expression of aromatase in the brain during puberty onset has been poorly studied. Aromatase (*Cyp19a1*) mRNA expression in the hypothalamus is very low during the infantile period (98, 99) and almost undetectable in the POA at P21 (100). Recent studies using

modified mice where EGFP transcription is coupled to the physiological activation of Cyp19A1, show that aromatase is well expressed in the medial preoptic area of the hypothalamus during embryonic life (101) and during adulthood (102). However, infantile, and pubertal periods have not been studied with this technology. This suggests that KTZ exposure during gestation and lactation could impact aromatase transcription or activity during the embryonic period. During this period, aromatase plays a crucial role in sexual differentiation of the brain. The classical view of brain sexual differentiation in mammals holds that sex differences mostly depend on the production of testosterone by the testes (103). Depending on the species, some of the effects of testosterone result from the action of estradiol derived from aromatization of testosterone locally in the male brain. For this reason, any compound which interferes with estrogen-dependent processes, as estrogenic or anti-androgenic compounds, in the developing brain can disrupt the sexual differentiation and consequently also the programming of puberty and reproductive function. Thus, we cannot exclude that the hypothalamic disruption is indirect and due to an altered release of peripheral steroids as KTZ can inhibit steroidogenic P450 enzymes in the adrenal cortex (104, 105) and gonads (105, 106). A recent review also reported that azole fungicides may affect all levels of the hypothalamo-pituitary-adrenal & gonadal axes in fish (107).

5 Conclusions

GnRH secretion and the hypothalamic transcriptome of female rats are sensitive to perinatal exposure to both DES and KTZ. Our results point toward similar transcriptional consequences after exposure to a steroidogenesis inhibitor (KTZ) or an estrogenic compound (DES). In particular, perinatal exposure to KTZ strongly impacted hypothalamic gene expression before puberty with consequences persisting until adulthood. Several enriched pathways as well as differentially expressed genes that were affected at PND 22 were still altered at PND 90. These pathways should be explored further to identify biomarkers for future EDC testing strategies and be part of future standard information requirement in risk assessment of chemicals.

Data availability statement

The original contributions presented in the study are publicly available. This data can be found here: 10.6084/m9.figshare.21842124.

Ethics statement

The animal study was reviewed and approved by Danish Animal Experiments Inspectorate; authorization number 2015-15-0201-00553.

Author contributions

DF: Conceptualization, Formal analysis, Data interpretations, Writing – Original draft, Writing – review & editing. HJ: Conceptualization, Data interpretations, Writing – review & editing. DL-R: Formal analysis, Data interpretations, Writing – review & editing. AL: Data interpretations, Formal analysis, Writing – review & editing. QT: Technical support, Formal analysis. JB: Conceptualization, Writing – review & editing, Funding acquisition. SC: Conceptualization, Writing – review & editing. TS: Conceptualization, Writing – review & editing, Funding acquisition. A-SP: Conceptualization, Data interpretations, Writing – Original draft, Writing – review & editing, Funding acquisition. All authors contributed to the article and approved the submitted version.

Funding

This work was funded by the EU Horizon 2020 project FREIA [grant number 825100] van Duursen et al. (50).

Acknowledgments

We would like to thank laboratory technicians Dorte Lykkegaard Korsbech, Lillian Sztuk, Heidi Broksø Letting, Mette Voigt Jessen, as well as the personnel in the Bio Facility at the National Food Institute for their excellent work during the animal studies.

Conflict of interest

The authors declare that the research was conducted in the absence of any commercial or financial relationships that could be construed as a potential conflict of interest.

Publisher's note

Supplementary material

The Supplementary Material for this article can be found online at: https://www.frontiersin.org/articles/10.3389/fendo.2023.1140886/full#supplementary-material

References

1. Parent A-S, Franssen D, Fudvoye J, Gérard A, Bourguignon J-P. Developmental variations in environmental influences including endocrine disruptors on pubertal timing and neuroendocrine control: Revision of human observations and mechanistic insight from rodents. *Front Neuroendocrinol* (2015) 38:12–36. doi: 10.1016/j.yfrne.2014.12.004

2. Skakkebæk NE, Lindahl-Jacobsen R, Levine H, Andersson AM, Jørgensen N, Main KM, et al. Environmental factors in declining human fertility. *Nat Rev Endocrinol* (2022) 18:139–57. doi: 10.1038/s41574-021-00598-8

3. Goy RW, Bercovitch FB, McBrair MC. Behavioral masculinization is independent of genital masculinization in prenatally androgenized female rhesus macaques. *Hormones Behav* (1988) 22(4):552–71. doi: 10.1016/0018-506X(88)90058-X

4. Herbosa-Encarnación C, Kosut SS, Foster DL, Wood RI. Prenatal androgens time neuroendocrine puberty in the sheep: Effect of testosterone dose*. *Endocrinology* (1997) 138(3):1072–7. doi: 10.1210/endo.138.3.4993

5. Gore AC, Chappell VA, Fenton SE, Flaws JA, Nadal A, Prins GS, et al. EDC-2: The endocrine society's second scientific statement on endocrine-disrupting chemicals. *Endocrine Rev* (2015) 36(6):E1–E150. doi: 10.1210/er.2015-1010

6. Skakkebaek NE. Sperm counts, testicular cancers, and the environment. *BMJ* (2017) 359. doi: 10.1136/bmj.j4517

7. Johansson HKL, Svingen T, Fowler PA, Vinggaard AM, Boberg J. Environmental influences on ovarian dysgenesis-developmental windows sensitive to chemical exposures. *Nat Rev Endocrinol* (2017) 13:400–14. doi: 10.1038/nrendo.2017.36

8. Johansson HKL, Damdimopoulou P, van Duursen MBM, Boberg J, Franssen D, de Cock M, et al. Putative adverse outcome pathways for female reproductive disorders to improve testing and regulation of chemicals. *Arch Toxicol* (2020) 400–14. doi: 10.1007/s00204-020-02834-y

9. Lopez-Rodriguez D, Franssen D, Heger S, Parent AS. Endocrine-disrupting chemicals and their effects on puberty. *Best Pract Res: Clin Endocrinol Metab* (2021) 35. doi: 10.1016/j.beem.2021.101579

10. Franssen D, Svingen T, Lopez Rodriguez D, Van Duursen M, Boberg J, Parent AS. A putative adverse outcome pathway network for disrupted female pubertal onset to improve testing and regulation of endocrine disrupting chemicals. *Neuroendocrinology* (2022) 112(2):101–14. doi: 10.1159/000515478

11. Krstevska-Konstantinova M, Charlier C, Craen M, Du Caju M, Heinrichs C, De Beaufort C, et al. Sexual precocity after immigration from developing countries to Belgium: Evidence of previous exposure to organochlorine pesticides. *Hum Reprod* (2001) 16(5):1020–6. doi: 10.1093/humrep/16.5.1020

12. Ouyang F, Perry MJ, Venners SA, Chen C, Wang B, Yang F, et al. Serum DDT, age at menarche, and abnormal menstrual cycle length. *Occup Environ Med* (2005) 62 (12):878–84. doi: 10.1136/oem.2005.020248

13. Den Hond E, Dhooge W, Bruckers L, Schoeters G, Nelen V, van de Mieroop E, et al. Internal exposure to pollutants and sexual maturation in Flemish adolescents. *J exposure Sci Environ Epidemiol* (2011) 21(3):224–33. doi: 10.1038/jes.2010.2

14. Hatch EE, Troisi R, Wise LA, Hyer M, Palmer JR, Titus-Ernstoff L, et al. Age at natural menopause in women exposed to diethylstilbestrol *in utero*. *Am J Epidemiol* (2006) 164(7):682–8. doi: 10.1093/aje/kwj257

15. Palmer JR, Wise LA, Hatch EE, Troisi R, Titus-Ernstoff L, Strohsnitter W, et al. Prenatal diethylstilbestrol exposure and risk of breast cancer. *Cancer Epidemiol Biomarkers Prev* (2006) 15(8):1509–14. doi: 10.1158/1055-9965.EPI-06-0109

16. Palioura E, Diamanti-Kandarakis E. Polycystic ovary syndrome (PCOS) and endocrine disrupting chemicals (EDCs). *Rev Endocrine Metab Disord* (2015) 16:365–71. doi: 10.1007/s11154-016-9326-7

17. Zhang S, Tan R, Pan R, Xiong J, Tian Y, Wu J, et al. Association of perfluoroalkyl and polyfluoroalkyl substances with premature ovarian insufficiency in Chinese women. *J Clin Endocrinol Metab* (2018) 103(7):2543–51. doi: 10.1210/jc.2017-02783

18. Rasier G, Parent A-S, Gérard A, Lebrethon M-C, Bourguignon J-P. Early maturation of gonadotropin-releasing hormone secretion and sexual precocity after exposure of infant female rats to estradiol or dichlorodiphenyltrichloroethane. *Biol Reprod* (2007) 77(4):734–42. doi: 10.1095/biolreprod.106.059303

19. Franssen D, Ioannou YS, Alvarez-real A, Gérard A, Mueller JK, Heger S, et al. Pubertal timing after neonatal diethylstilbestrol exposure in female rats: Neuroendocrine vs peripheral effects and additive role of prenatal food restriction. *Reprod Toxicol* (2014) 44(0):63–72. doi: 10.1016/j.reprotox.2013.10.006

20. Franssen D, Gérard A, Hennuy B, Donneau AF, Bourguignon JP, Parent AS. Delayed neuroendocrine sexual maturation in female rats after a very low dose of bisphenol a through altered gabaergic neurotransmission and opposing effects of a high dose. *Endocrinology* (2016) 157(5):1740–50. doi: 10.1210/en.2015-1937

21. Johansson HKL, Christiansen S, Draskau MK, Svingen T, Boberg J. Classical toxicity endpoints in female rats are insensitive to the human endocrine disruptors diethylstilbestrol and ketoconazole. *Reprod Toxicol* (2021) 101:9–17. doi: 10.1016/j.reprotox.2021.01.003

22. Castillo LY, Ríos-Carrillo J, González-Orozco JC, Camacho-Arroyo I, Morin JP, Zepeda RC, et al. Juvenile exposure to BPA alters the estrous cycle and differentially increases anxiety-like behavior and brain gene expression in adult Male and female rats. *Toxics* (2022) 10(9):513. doi: 10.3390/toxics10090513

23. Newbold RR. Lessons learned from perinatal exposure to diethylstilbestrol. *Toxicol Appl Pharmacol* (2004) 199(2):142–50. doi: 10.1016/j.taap.2003.11.033

24. Karavan JR, Pepling ME. Effects of estrogenic compounds on neonatal oocyte development. *Reprod Toxicol* (2012) 34(1):51–6. doi: 10.1016/j.reprotox.2012.02.005

25. Lopez-Rodriguez D, Franssen D, Sevrin E, Gerard A, Balsat C, Blacher S, et al. Persistent vs transient alteration of folliculogenesis and estrous cycle after neonatal vs adult exposure to bisphenol a. *Endocrinology* (2019) 160(11):2558–72. doi: 10.1210/en.2019-00505

26. Heckman WR, Kane BR, Pakyz RE, Cosentino MJ. The effect of ketoconazole on endocrine and reproductive parameters in Male mice and rats. *J Androl* (1992) 13 (3):191–8. doi: 10.1002/j.1939-4640.1992.tb00298.x

27. Skakkebaek NE, Rajpert-De Meyts E, Buck Louis GM, Toppari J, Andersson AM, Eisenberg ML, et al. Male Reproductive disorders and fertility trends: Influences of environment and genetic susceptibility. *Physiol Rev* (2015) 96(1):55–97. doi: 10.1152/physrev.00017.2015

28. Jorgensen A, Svingen T, Miles H, Chetty T, Stukenborg JB, Mitchell RT. Environmental impacts on Male reproductive development: Lessons from experimental models. *Hormone Res Paediatrics* (2021), 303–19. doi: 10.1159/000519964

29. Mesquita I, Lorigo M, Cairrao E. Update about the disrupting-effects of phthalates on the human reproductive system. *Mol Reprod Dev* (2021) 88(10):650–72. doi: 10.1002/mrd.23541

30. Basso CG, de Araújo-Ramos AT, Martino-Andrade AJ. Exposure to phthalates and female reproductive health: A literature review. *Reprod Toxicol* (2022) 109:61–79. doi: 10.1016/j.reprotox.2022.02.006

31. Pinson A, Franssen D, Gérard A, Parent A-S, Bourguignon J-P. Neuroendocrine disruption without direct endocrine mode of action: Polychloro-biphenyls (PCBs) and bisphenol a (BPA) as case studies. *Comptes rendus biologies* (2017) 340(9–10):432–8. doi: 10.1016/j.crvi.2017.07.006

32. Herbison AE. The gonadotropin-releasing hormone pulse generator. *Endocrinology* (2018) 159(11):3723–36. doi: 10.1210/en.2018-00653

33. Heger S, Mastronardi C, Dissen GA, Lomniczi A, Cabrera R, Roth CL, et al. Enhanced at puberty 1 (EAP1) is a new transcriptional regulator of the female neuroendocrine reproductive axis. *J Clin Invest* (2007) 117(8):2145–54. doi: 10.1172/JCI31752

34. Lomniczi A, Wright H, Ojeda SR. Epigenetic regulation of female puberty. *Front Neuroendocrinol* (2015) 36:90–107. doi: 10.1016/j.yfrne.2014.08.003

35. Aylwin CF, Vigh-Conrad K, Lomniczi A. The emerging role of chromatin remodeling factors in female pubertal development. *Neuroendocrinology* (2019) 109 (3):208–17. doi: 10.1159/000497745

36. Lopez-Rodriguez D, Franssen D, Bakker J, Lomniczi A, Parent AS. Cellular and molecular features of EDC exposure: consequences for the GnRH network. *Nat Rev Endocrinol* (2021) 17(2):83–96. doi: 10.1038/s41574-020-00436-3

37. Mason JI, Carr BR, Murry BA. Imidazole antimycotics: selective inhibitors of steroid aromatization and progesterone hydroxylation. *Steroids* (1987) 50(1–3):179–89. doi: 10.1016/0039-128X(83)90070-3

38. Oates JA, Wood AJJ, Sonino N. The use of ketoconazole as an inhibitor of steroid production. *New Engl J Med* (1987) 317(13):812–8. doi: 10.1056/NEJM198709243171307

39. Kjærstad MB, Taxvig C, Nellemann C, Vinggaard AM, Andersen HR. Endocrine disrupting effects *in vitro* of conazole antifungals used as pesticides and pharmaceuticals. *Reprod Toxicol* (2010) 30(4):573–82. doi: 10.1016/j.reprotox.2010.07.009

40. Munkboel CH, Rasmussen TB, Elgaard C, Olesen MLK, Kretschmann AC, Styrishave B. The classic azole antifungal drugs are highly potent endocrine disruptors *in vitro* inhibiting steroidogenic CYP enzymes at concentrations lower than therapeutic cmax. *Toxicology* (2019) 425:152247. doi: 10.1016/j.tox.2019.152247

41. Folmar LC, Hemmer MJ, Denslow ND, Kroll K, Chen J, Cheek A, et al. A comparison of the estrogenic potencies of estradiol, ethynylestradiol, diethylstilbestrol, nonylphenol and methoxychlor *in vivo* and *in vitro*. *Aquat Toxicol* (2002) 60(1–2):101–10. doi: 10.1016/S0166-445X(01)00276-4

42. Han DH, Denison MS, Tachibana H, Yamada K. Relationship between estrogen receptor-binding and estrogenic activities of environmental estrogens and suppression by flavonoids. *Biosci biotechnol Biochem* (2002) 66(7):1479–87. doi: 10.1271/BBB.66.1479

43. Brion F, Le Page Y, Piccini B, Cardoso O, Tong SK, Chung BC, et al. Screening estrogenic activities of chemicals or mixtures *in vivo* using transgenic (cyp19a1b-GFP) zebrafish embryos. *PloS One* (2012) 7(5):e36069. doi: 10.1371/JOURNAL.PONE.0036069

44. Korach KS, McLachlan JA. The role of the estrogen receptor in diethylstilbestrol toxicity. *Arch Toxicol Supplement* (1985) 8:33–42. doi: 10.1007/978-3-642-69928-3_4

45. Kuiper GG, Lemmen JG, Carlsson B, Corton JC, Safe SH, van der Saag PT, et al. Interaction of estrogenic chemicals and phytoestrogens with estrogen receptor beta. *Endocrinology* (1998) 139(10):4252–63. doi: 10.1210/endo.139.10.6216

46. Blair RM, Fang H, Branham WS, Hass BS, Dial SL, Moland CL, et al. The estrogen receptor relative binding affinities of 188 natural and xenochemicals: structural diversity of ligands. *Toxicological Sci* (2000) 54(1):138–53. doi: 10.1093/TOXSCI/54.1.138

47. Couse JF, Dixon D, Yates M, Moore AB, Ma L, Maas R, et al. Estrogen receptor-alpha knockout mice exhibit resistance to the developmental effects of neonatal diethylstilbestrol exposure on the female reproductive tract. *Dev Biol* (2001) 238 (2):224–38. doi: 10.1006/DBIO.2001.0413

48. Bulayeva NN, Watson CS. Xenoestrogen-induced ERK-1 and ERK-2 activation *via* multiple membrane-initiated signaling pathways. *Environ Health perspectives* (2004) 112(15):1481–7. doi: 10.1289/ehp.7175

49. Li X, Zhang S, Safe S. Activation of kinase pathways in MCF-7 cells by 17beta-estradiol and structurally diverse estrogenic compounds. *J Steroid Biochem Mol Biol* (2006) 98(2–3):122–32. doi: 10.1016/J.JSBMB.2005.08.018

50. van Duursen MBM, Boberg J, Christiansen S, Connolly L, Damdimopoulou P, Filis P, et al. Safeguarding female reproductive health against endocrine disrupting chemicals–the FREIA project. *Int J Mol Sci* (2020) 21(9):3215. doi: 10.3390/ijms21093215

51. Bourguignon JP, Franchimont P. Puberty-related increase in LHRH release from rat hypothalamus *in vitro*. *Endocrinology* (1984) 114(5):1941–3. doi: 10.1210/endo-114-5-1941

52. Matagne V, Rasier G, Lebrethon M-CC, Gérard A, Bourguignon J-PP. Estradiol stimulation of pulsatile gonadotropin-releasing hormone secretion *in vitro*: correlation with perinatal exposure to sex steroids and induction of sexual precocity *in vivo*. *Endocrinology* (2004) 145(6):2775–83. doi: 10.1210/en.2003-1259

53. Bourguignon JP, Gérard A, Franchimont P. Direct activation of gonadotropin-releasing hormone secretion through different receptors to neuroexcitatory amino acids. *Neuroendocrinology* (1989) 49(4):402–8. doi: 10.1159/000125145

54. Love MI, Huber W, Anders S. Moderated estimation of fold change and dispersion for RNA-seq data with DESeq2. *Genome Biol* (2014) 15(12):550. doi: 10.1186/s13059-014-0550-8

55. Thomas S, Bonchev D. A survey of current software for network analysis in molecular biology. *Hum Genomics* (2010) 4(5):353–60. doi: 10.1186/1479-7364-4-5-353

56. Krämer A, Green J, Pollard J, Tugendreich S. Causal analysis approaches in ingenuity pathway analysis. *Bioinformatics* (2014) 30(4):523–30. doi: 10.1093/bioinformatics/btt703

57. Pfaffl MW. A new mathematical model for relative quantification in real-time RT-PCR. *Nucleic Acids Res* (2001) 29(9):45. doi: 10.1093/nar/29.9.e45

58. Bourguignon J-PP, Gerard A, Alvarez Gonzalez ML, Franchimont P, Gonzalez MA, Franchimont P. Neuroendocrine mechanism of onset of puberty. sequential reduction in activity of inhibitory and facilitatory n-methyl-p-aspartate receptors. *J Clin Invest* (1992) 90(5):1736–44. doi: 10.1172/JCI116047

59. Howard SR. The genetic basis of delayed puberty. *Front Endocrinol* (2019) 40 (2):669–710. doi: 10.3389/fendo.2019.00423

60. Young J, Xu C, Papadakis GE, Acierno JS, Maione L, Hietamäki J, et al. Clinical management of congenital hypogonadotropic hypogonadism. *Endocrine Rev* (2019), 669–710. doi: 10.1210/er.2018-00116

61. Howard SR, Guasti L, Ruiz-Babot G, Mancini A, David A, Storr HL, et al. IGSF10 mutations dysregulate gonadotropin-releasing hormone neuronal migration resulting in delayed puberty. *EMBO Mol Med* (2016) 8(6):626–42. doi: 10.15252/EMMM.201606250

62. Abreu AP, Toro CA, Song YB, Navarro VM, Bosch MA, Eren A, et al. MKRN3 inhibits the reproductive axis through actions in kisspeptin-expressing neurons. *J Clin Invest* (2020) 140(8):4486–500. doi: 10.1172/JCI136564

63. Motoike T, Skach AG, Godwin JK, Sinton CM, Yamazaki M, Abe M, et al. Transient expression of neuropeptide W in postnatal mouse hypothalamus - a putative regulator of energy homeostasis. *Neuroscience* (2015) 301:323–37. doi: 10.1016/j.neuroscience.2015.06.014

64. Toro CA, Aylwin CF, Lomniczi A. Hypothalamic epigenetics driving female puberty. *J Neuroendocrinol* (2018) 30(7):e12589. doi: 10.1111/jne.12589

65. López-Rodríguez D, Aylwin CF, Delli V, Sevrin E, Campanile M, Martin M, et al. Multi- and transgenerational outcomes of an exposure to a mixture of endocrine-disrupting chemicals (EDCs) on puberty and maternal behavior in the female rat. *Environ Health Perspect* (2021) 129(8):87003. doi: 10.1289/EHP8795

66. Herbison AE. Control of puberty onset and fertility by gonadotropin-releasing hormone neurons. *Nat Rev Endocrinol* (2016) 12(8):452–66. doi: 10.1038/nrendo.2016.70

67. Goodman RL, Herbison AE, Lehman MN, Navarro VM. Neuroendocrine control of gonadotropin-releasing hormone: Pulsatile and surge modes of secretion. *J Neuroendocrinol* (2022) 34(5):e13094. doi: 10.1111/jne.13094

68. Parent AS, Lebrethon MC, Gerard A, Vandersmissen E, Bourguignon J-P. Leptin effects on pulsatile gonadotropin releasing hormone secretion from the adult rat hypothalamus and interaction with cocaine and amphetamine regulated transcript peptide and neuropeptide y. *Regul Peptides* (2000) 92:17–24. doi: 10.1016/S0167-0115(00)00144-0

69. Terasawa E. Mechanism of pulsatile GnRH release in primates: Unresolved questions. *Mol Cell Endocrinol* (2019) 498:110578. doi: 10.1016/j.mce.2019.110578

70. Liu X, Porteous R, Herbison AE. Robust GABAergic regulation of the GnRH neuron distal dendron. *Endocrinology* (2022) 164(1):bqac194. doi: 10.1210/endocr/bqac194

71. Linscott ML, Chung WCJ. Epigenomic control of gonadotrophin-releasing hormone neurone development and hypogonadotrophic hypogonadism. *J Neuroendocrinol* (2020) 32(6):e12860. doi: 10.1111/JNE.12860

72. Terasawa E. The mechanism underlying the pubertal increase in pulsatile GnRH release in primates. *J Neuroendocrinol* (2022) 34(5):e13119. doi: 10.1111/jne.13119

73. Kenealy BP, Keen KL, Kapoor A, Terasawa E. Neuroestradiol in the stalk median eminence of female rhesus macaques decreases in association with puberty onset. *Endocrinology* (2016) 157(1):70–6. doi: 10.1210/en.2015-1770

74. Ghosh A, Ginty DD, Bading H, Greenberg ME. Calcium regulation of gene expression in neuronal cells. *J Neurobiol* (1994) 25(3):294–303. doi: 10.1002/neu.480250309

75. Altarejos JY, Montminy M. CREB and the CRTC co-activators: Sensors for hormonal and metabolic signals. *Nat Rev Mol Cell Biol* (2011) 12:141–51. doi: 10.1038/nrm3072

76. Kwakowsky A, Herbison AE, Ábrahám IM. The role of cAMP response element-binding protein in estrogen negative feedback control of gonadotropin-releasing hormone neurons. *J Neurosci* (2012) 32(33):11309–17. doi: 10.1523/JNEUROSCI.1333-12.2012

77. Li X, Jiang L, Cheng L, Chen H. Dibutyl phthalate-induced neurotoxicity in the brain of immature and mature rat offspring. *Brain Dev* (2014) 36(8):653–60. doi: 10.1016/j.braindev.2013.09.002

78. Min A, Liu F, Yang X, Chen M. Benzyl butyl phthalate exposure impairs learning and memory and attenuates neurotransmission and CREB phosphorylation in mice. *Food Chem Toxicol* (2014) 71:81–9. doi: 10.1016/j.fct.2014.05.021

79. Qiu F, Zhou Y, Deng Y, Yi J, Gong M, Liu N, et al. Knockdown of TNFAIP1 prevents di-(2-ethylhexyl) phthalate-induced neurotoxicity by activating CREB pathway. *Chemosphere* (2020) 241:125114. doi: 10.1016/j.chemosphere.2019.125114

80. Plummer SM, Dan D, Quinney J, Hallmark N, Phillips RD, Millar M, et al. Identification of transcription factors and coactivators affected by dibutylphthalate interactions in fetal rat testes. *Toxicological Sci* (2013) 132(2):443–57. doi: 10.1093/toxsci/kft016

81. Dees WL, Hiney JK, Srivastava VK. IGF-1 influences gonadotropin-releasing hormone regulation of puberty. *Neuroendocrinology* (2021) 111(12):1151–63. doi: 10.1159/000514217

82. Dees WL, Hiney JK, Srivastava VK. Regulation of prepubertal dynorphin secretion in the medial basal hypothalamus of the female rat. *J Neuroendocrinol* (2019) 31(12):e12810. doi: 10.1111/jne.12810

83. Roepke TA, Yang JA, Yasrebi A, Mamounis KJ, Oruc E, Zama AM, et al. Regulation of arcuate genes by developmental exposures to endocrine-disrupting compounds in female rats. *Reprod Toxicol (Elmsford N.Y.)* (2016) 62:18–26. doi: 10.1016/j.reprotox.2016.04.014

84. Shao P, Wang Y, Zhang M, Wen X, Zhang J, Xu Z, et al. The interference of DEHP in precocious puberty of females mediated by the hypothalamic IGF-1/PI3K/Akt/mTOR signaling pathway. *Ecotoxicol Environ Saf* (2019) 181:362–9. doi: 10.1016/j.ecoenv.2019.06.017

85. Parent A-S, Lebrethon M-C, Gérard A, Bourguignon J-P. Factors accounting for perinatal occurrence of pulsatile gonadotropin-releasing hormone secretion *in vitro* in rats. *Biol Reprod* (2005) 72(1):143–9. doi: 10.1095/biolreprod.104.033167

86. Parent AS, Rasier G, Matagne V, Lomniczi A, Lebrethon MC, Gérard A. Oxytocin facilitates female sexual maturation through a glia to neuron signaling pathway. *Endocrinology* (2008) 149(3):1358–65. doi: 10.1210/en.2007

87. Salehi MS, Khazali H, Mahmoudi F, Janahmadi M. Oxytocin intranasal administration affects neural networks upstream of GNRH neurons. *J Mol Neurosci* (2017) 62(3–4):356–62. doi: 10.1007/s12031-017-0943-8

88. Mennigen JA, Ramachandran D, Shaw K, Chaube R, Joy KP, Trudeau VL. Reproductive roles of the vasopressin/oxytocin neuropeptide family in teleost fishes. *Front Endocrinol* (2022) 13:1005863. doi: 10.3389/fendo.2022.1005863

89. Evans JJ, Reid RA, Wakeman SA, Croft LB, Benny PS. Evidence that oxytocin is a physiological component of LH regulation in non-pregnant women. *Hum Reprod* (2003) 18(7):1428–31. doi: 10.1093/humrep/deg291

90. Escher P, Wahli W. Peroxisome proliferator-activated receptors: Insight into multiple cellular functions. *Mutat Res - Fundam Mol Mech Mutagenesis* (2000) 448 (2):121–38. doi: 10.1016/S0027-5107(99)00231-6

91. Mouihate A, Boissé L, Pittman QJ. A novel antipyretic action of 15-Deoxy-Δ 12,14-prostaglandin J2 in the rat brain. *J Neurosci* (2004) 24(6):1312–8. doi: 10.1523/JNEUROSCI.3145-03.2004

92. Sarruf DA, Yu F, Nguyen HT, Williams DL, Printz RL, Niswender KD, et al. Expression of peroxisome proliferator-activated receptor-γ in key neuronal subsets regulating glucose metabolism and energy homeostasis. *Endocrinology* (2009) 150 (2):707–12. doi: 10.1210/en.2008-0899

93. Manfredi-Lozano M, Roa J, Tena-Sempere M. Connecting metabolism and gonadal function: Novel central neuropeptide pathways involved in the metabolic control of puberty and fertility. *Front Neuroendocrinol* (2018) 48:37–49. doi: 10.1016/j.yfrne.2017.07.008

94. Desvergne B, Feige JN, Casals-Casas C. PPAR-mediated activity of phthalates: A link to the obesity epidemic? *Mol Cell Endocrinol Mol Cell Endocrinol* (2009) 304(1-2):43–8. doi: 10.1016/j.mce.2009.02.017

95. Nappi F, Barrea L, Di Somma C, Savanelli MC, Muscogiuri G, Orio F, et al. Endocrine aspects of environmental "obesogen" pollutants. *Int J Environ Res Public Health* (2016) 13(8):765. doi: 10.3390/ijerph13080765

96. Lovekamp-Swan T, Jetten AM, Davis BJ. Dual activation of PPARα and PPARγ by mono-(2-ethylhexyl) phthalate in rat ovarian granulosa cells. *Mol Cell Endocrinol* (2003) 201(1–2):133–41. doi: 10.1016/S0303-7207(02)00423-9

97. Ding N, Harlow SD, Randolph JF, Loch-Caruso R, Park SK. Perfluoroalkyl and polyfluoroalkyl substances (PFAS) and their effects on the ovary. *Hum Reprod Update* (2020) 26(5):724–52. doi: 10.1093/humupd/dmaa018

98. Colciago A, Casati L, Mornati O, Vergoni A V, Santagostino A, Celotti F, et al. Chronic treatment with polychlorinated biphenyls (PCB) during pregnancy and lactation in the rat part 2: Effects on reproductive parameters, on sex behavior, on memory retention and on hypothalamic expression of aromatase and 5alpha-reductases in the offs. *Toxicol Appl Pharmacol* (2009) 239(1):46–54. doi: 10.1016/j.taap.2009.04.023

99. Kanaya M, Tsuda MC, Sagoshi S, Nagata K, Morimoto C, Thu CKT, et al. Regional difference in sex steroid action on formation of morphological sex differences in the anteroventral periventricular nucleus and principal nucleus of the bed nucleus of the stria terminalis. *PloS One* (2014) 9(11):e112616. doi: 10.1371/journal.pone.0112616

100. Kanaya M, Morishita M, Tsukahara S. Temporal expression patterns of genes related to sex steroid action in sexually dimorphic nuclei during puberty. *Front Endocrinol* (2018) 9:213. doi: 10.3389/fendo.2018.00213

101. Wartenberg P, et al. Sexually dimorphic neurosteroid synthesis regulates neuronal activity in the murine brain. *J Neurosci* (2021) 41(44):9177–91. doi: 10.1523/JNEUROSCI.0885-21.2021

102. Stanić D, Dubois S, Chua HK, Tonge B, Rinehart N, Horne MK, et al. Characterization of aromatase expression in the adult Male and female mouse brain. i. coexistence with oestrogen receptors α and β, and androgen receptors. *PloS One* (2014) 9(3):e90451. doi: 10.1371/journal.pone.0090451

103. McCarthy MM, Arnold AP, Ball GF, Blaustein JD, de Vries GJ. Sex differences in the brain: The not so inconvenient truth. *J Neurosci* (2012) 32(7):2241–7. doi: 10.1523/JNEUROSCI.5372-11.2012

104. Loose DS, Kan PB, Hirst MA, Marcus RA, Feldman D. Ketoconazole blocks adrenal steroidogenesis by inhibiting cytochrome P450-dependent enzymes. *J Clin Invest* (1983) 71(5):1495–9. doi: 10.1172/JCI110903

105. Medda F, et al. Short term treatment with ketoconazole: effects on gonadal and adrenal steroidogenesis in women(1987) (Accessed 14 February 2023).

106. Kugathas I, Johansson HKL, Chan Sock Peng E, Toupin M, Evrard B, Darde TA, et al. Transcriptional profiling of the developing rat ovary following intrauterine exposure to the endocrine disruptors diethylstilbestrol and ketoconazole. *Arch Toxicol* (2023) 97(3):849–63. doi: 10.1007/S00204-023-03442-2

107. Huang T, Zhao Y, He J, Cheng H, Martyniuk CJ. Endocrine disruption by azole fungicides in fish: A review of the evidence. *Sci total Environ* (2022) 822:153412. doi: 10.1016/J.SCITOTENV.2022.153412

frontiers | Frontiers in Endocrinology

TYPE Review
PUBLISHED 27 June 2023
DOI 10.3389/fendo.2023.1202089

OPEN ACCESS

EDITED BY
Alexandre Benani,
Centre National de la Recherche Scientifique (CNRS), France

REVIEWED BY
Kazuki Harada,
University of Tokyo, Japan
Yousuke Tsuneoka,
Toho University, Japan

*CORRESPONDENCE
Natalie Jane Michael
natalie.michael@pha.ulaval.ca

†These authors contributed equally to this work and share first authorship

RECEIVED 07 April 2023
ACCEPTED 06 June 2023
PUBLISHED 27 June 2023

CITATION
Khouma A, Moeini MM, Plamondon J, Richard D, Caron A and Michael NJ (2023) Histaminergic regulation of food intake. *Front. Endocrinol.* 14:1202089. doi: 10.3389/fendo.2023.1202089

Histaminergic regulation of food intake

Axelle Khouma[1,2†], Moein Minbashi Moeini[1,2†], Julie Plamondon[1], Denis Richard[1,3], Alexandre Caron[1,2,4] and Natalie Jane Michael[1,2*]

[1]Institut Universitaire de Cardiologie et de Pneumologie de Québec, Quebec, QC, Canada, [2]Faculté de Pharmacie, Université Laval, Québec, QC, Canada, [3]Faculté de Medicine, Université Laval, Québec, QC, Canada, [4]Montreal Diabetes Research Center, Montreal, QC, Canada

Histamine is a biogenic amine that acts as a neuromodulator within the brain. In the hypothalamus, histaminergic signaling contributes to the regulation of numerous physiological and homeostatic processes, including the regulation of energy balance. Histaminergic neurons project extensively throughout the hypothalamus and two histamine receptors (H1R, H3R) are strongly expressed in key hypothalamic nuclei known to regulate energy homeostasis, including the paraventricular (PVH), ventromedial (VMH), dorsomedial (DMH), and arcuate (ARC) nuclei. The activation of different histamine receptors is associated with differential effects on neuronal activity, mediated by their different G protein-coupling. Consequently, activation of H1R has opposing effects on food intake to that of H3R: H1R activation suppresses food intake, while H3R activation mediates an orexigenic response. The central histaminergic system has been implicated in atypical antipsychotic-induced weight gain and has been proposed as a potential therapeutic target for the treatment of obesity. It has also been demonstrated to interact with other major regulators of energy homeostasis, including the central melanocortin system and the adipose-derived hormone leptin. However, the exact mechanisms by which the histaminergic system contributes to the modification of these satiety signals remain underexplored. The present review focuses on recent advances in our understanding of the central histaminergic system's role in regulating feeding and highlights unanswered questions remaining in our knowledge of the functionality of this system.

KEYWORDS

histamine, food intake, hypothalamus, neurometabolism, melanocortin, leptin, histamine receptors, GPCR

Introduction

Histamine is a small biological molecule (biogenic amine) that is widely distributed throughout the body. Although probably best recognized for its importance in arousal regulation and allergic inflammatory reactions, histamine plays a role in a diverse range of biological functions. This includes the regulation of energy balance, sleep and wakefulness,

10.3389/fendo.2023.1202089

thermoregulation, gastrointestinal function, immune responses, and learning and memory (1–3). Within the central nervous system (CNS), a population of neurons located in the posterior hypothalamus provide the sole source of neuronal histamine to the brain (4–6) and can be identified based on the expression of histidine decarboxylase (HDC), the enzyme required for histamine synthesis (7, 8). These histaminergic neurons project extensively throughout the CNS, and strongly innervate multiple hypothalamic nuclei known to influence energy homeostasis and feeding behaviors (9–11). While histamine is known to impact food intake via its actions in the hypothalamus (12, 13), the precise mechanisms by which it does so are still being uncovered. The present review focuses on recent advances in understanding of the central histaminergic system's role in regulating food intake, including potential interactions with satiety signals and neuropeptide/neurotransmitter systems implicated in energy balance regulation.

Histaminergic neurons

Histaminergic neuron somas are confined to the tuberomammillary nucleus (TMN) in the posterior hypothalamus (Figure 1) but have widespread projections that extensively innervate the CNS. This includes major brain regions including the cortex, brainstem, hippocampus, striatum, nucleus accumbens, amygdala, and substantia nigra, as well as multiple intrahypothalamic projections (9–11, 14). The diffuse projection patterns correlate with the multiple functions associated with histaminergic neurons, which have been comprehensively

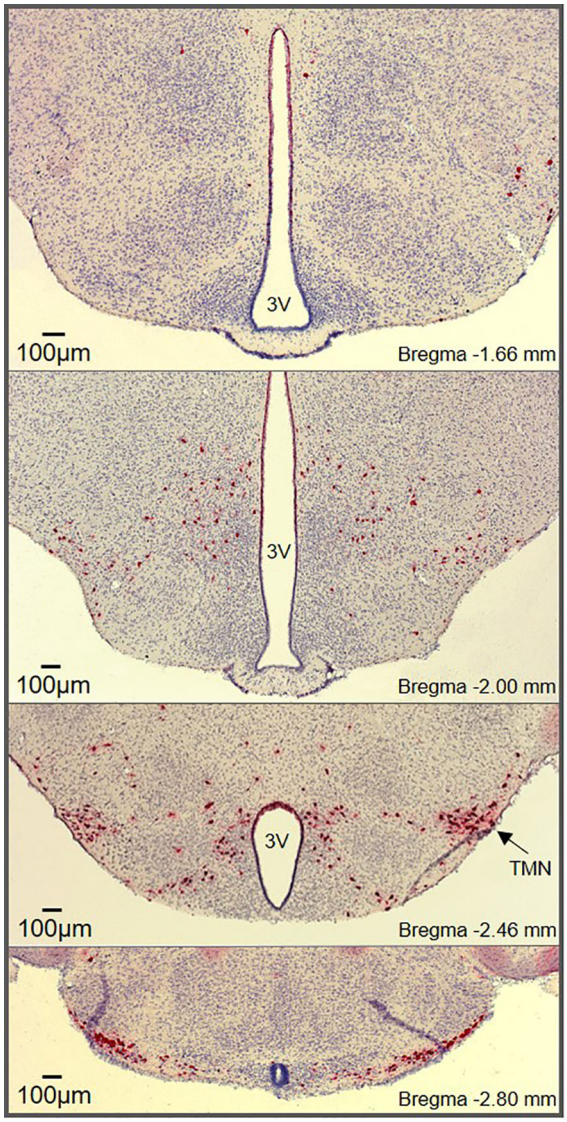

FIGURE 1
Histaminergic neuron distribution throughout the hypothalamus. RNAscope® *in situ* hybridization (ISH) targeting *Hdc* shows histaminergic neurons (red) densely packed in the core region of the tuberomammillary nucleus (marked TMN) along with diffusely scattered histaminergic neurons throughout the hypothalamus. The RNAscope® ISH was performed on hypothalamic brain slices (25µm) from male mice according to the manufacturer's instructions (Advanced Cell Diagnostics, Inc., USA).

reviewed elsewhere (1, 3, 15). In contrast to the diffuse and well characterized projections of histaminergic neurons, difficulties occurred with initial attempts to identify afferent inputs to the histaminergic neurons, likely due to the inherent limitations of retrograde tracing studies, including potential spread to surrounding tissue and labeling of fibers of passage (16, 17). However, significant afferent input to the histaminergic neurons has since been identified, with inputs originating from the ventrolateral preoptic area (VLPO) (17–19) and the lateral hypothalamus (20–23). Importantly, the TMN can be subdivided into 3-5 different subregions depending on the classification method used (9, 24, 25). While histaminergic neurons are usually acknowledged to reside in the 'TMN core', their distribution within the hypothalamus (including the dorsal and bridge regions of the TMN) is much more widespread than typically appreciated (Figure 1), with some degree of variability observed between species (26, 27). However, the anatomical location of the histaminergic neurons and distribution of fibers throughout the brain appears comparable in humans to that described in rodents (28).

The location of the histaminergic neurons within the hypothalamus raises the potential for their involvement in the regulation of feeding. Many of the histaminergic neurons lay in close proximity to the third ventricle or are located on the ventral surface of the brain, suggesting, like other hypothalamic neurons, a potential for the detection of circulating hormones and neuropeptides (29). Moreover, histaminergic neuron fibers densely innervate the hypothalamus, including key hypothalamic nuclei known to regulate energy balance. While early studies required colchicine treatment to visualize histamine containing neurons (4), targeting of HDC (the enzyme required for histamine synthesis) allowed for the identification of dense fiber networks throughout the hypothalamus (6). Studies examining HDC immunoreactivity alone or in combination with paired retrograde tracer studies reveal high to very high density of histaminergic fibers in hypothalamic regions that regulate energy homeostasis. This includes the paraventricular nucleus of the hypothalamus (PVH), ventromedial hypothalamus (VMH), lateral hypothalamus (LH), dorsomedial hypothalamus (DMH) and the arcuate nucleus (ARC) (6, 9, 10). Use of newer immunohistochemical methods, with increased sensitivity for the visualization of histamine immunoreactive fibers and terminals, provided additional support for a moderate density of histaminergic fibers in the PVH, VMH, DMH, LH, and ARC (11). While identification of fiber tracts does not necessarily indicate functional connections, the presence of histamine receptors in these regions supports the role of histamine in regulating the activity of key metabolic neurons located in these areas of the hypothalamus.

Histamine receptor signaling

Histamine exerts its pleiotropic effects by binding to four subtypes of histamine receptors (HR), three of which are located within the brain (H1R, H2R, and H3R) (30–33). HRs belong to the family of G protein–coupled receptors (GPCRs), which interact with G proteins located in the plasma membrane. When a ligand binds to a GPCR, it causes a conformational change that triggers the interaction between the GPCR and nearby heterotrimeric G proteins. This promotes the exchange of a GDP for a GTP on the Gα subunit, resulting in its dissociation from Gβγ (34). There are four main families of Gα subunits: Gαi, Gαq, Gαs, and Gα12 (35). Gα subunits and Gβγ can activate different signaling pathways.

Identified in 1966, the H1R subclass of histamine receptors (gene symbol: HRH1) primarily couples to Gαq, resulting in the activation of the phospholipase C (PLC) signaling pathway (36–40) (Figure 2). This leads to the subsequent cleavage of phosphatidylinositol 4,5-bisphosphate (PIP2) into diacyl glycerol (DAG) and inositol 1,4,5-trisphosphate (IP3). These second messengers respectively activate protein kinase C (PKC) and promote the mobilization of Ca^{2+} (41). Accumulation of IP3, DAG and Ca^{2+} following histamine was shown to be prevented with the H1R inverse antagonist pyrilamine (42–45), while the H1R inverse agonist chlorpheniramine was reported to block the stimulatory effect of histamine on PLC and Ca^{2+} (46), confirming the involvement of H1R in the Gαq-dependent actions of histamine. One report also suggests that activation of H1R by histamine increases cAMP levels through Gβγ, an effect that is prevented by the H1R inverse agonist pyrilamine (47). As such, H1R activation and stimulation of it signaling cascade has excitatory effects and is associated with membrane depolarization in neurons (48–52).

The H2R subclass of histamine receptors (gene symbol: HRH2), often referred to as the histamine gastric receptor, couples to both Gαq and Gαs proteins (39, 53). As a consequence, histamine binding to H2R stimulates both PLC and adenylate cyclase (AC) through Gαq and Gαs proteins respectively (53) (Figure 2). Activation of Gαs proteins in turn increases cAMP, an effect that is prevented by the HRH2 antagonist lafutidine (54). Increased cytosolic cAMP then leads to the activation of protein kinase A (PKA), which has been shown to stimulate neurons (55). Therefore, histamine binding to H2Rs also has excitatory actions within the brain, and results in depolarization of neurons through increased Ca^{2+}, cAMP and PKA (56, 57).

The H3R subclass of histamine receptors (gene symbol: HRH3, previously known as GPCR97) primarily couples to Gαi proteins (39, 58) and functions as an inhibitory auto- or hetero-receptor in the brain (59–62). Activation of H3R results in AC inhibition and a subsequent reduction of cAMP levels (63, 64) (Figure 2). In contrast to the excitatory effects of H1R and H2R, binding of the H3R by histamine results in a suppression of neuronal activity and inhibition of neurotransmitter release (15, 60, 65, 66). Several mechanisms can contribute to the inhibitory effects of H3R. First, the Gβγ subunit of Gαi-coupled receptors has been shown to activate G protein-gated inwardly rectifying potassium (GIRK) channels (66, 67). Second, H3R activation can reduce neurotransmitter release by inhibiting N- and P/Q-type voltage-gated calcium channels again through the Gβγ subunit (68, 69). Third, H3R activation has been shown to reduce the activity of the

10.3389/fendo.2023.1202089

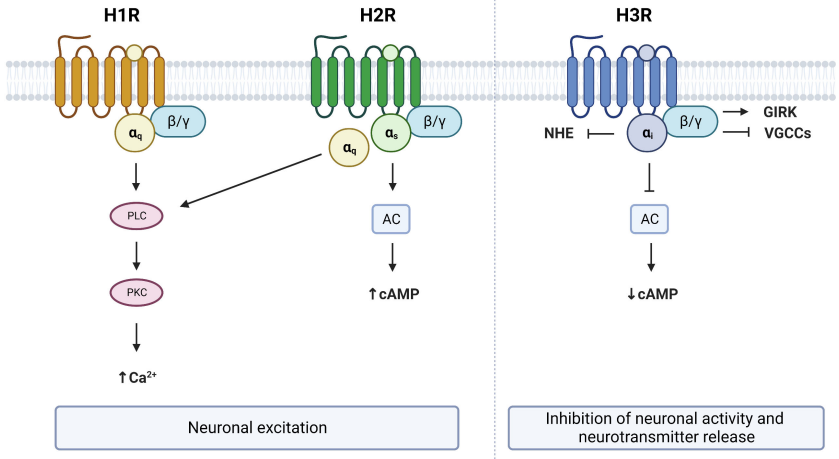

FIGURE 2
G protein–coupled receptor (GPCR) signaling from brain expressed histamine receptors. Histamine activation of H1R and H2R lead to neuronal excitation via Gαq and/or Gαs dependent mechanisms respectively. Activation of H3R leads to neuronal inhibition and suppression of neurotransmitter release. PLC, phospholipase C; PKC, protein kinase C; AC, adenylate cyclase; NHE, sodium–proton exchanger; GIRK, G protein-gated inwardly rectifying potassium channels; VGCCs, voltage-gated calcium channels; cAMP, cyclic adenosine monophosphate. Figure created with BioRender.com.

sodium–proton exchanger (NHE), which is under the control of Gαi (70, 71). Therefore, activation of H3R has opposite effects on neuronal activity to that of H1R or H2R activation.

Central histaminergic system and the regulation of feeding

Histamine synthesis

The central histaminergic system has been implicated in the regulation of food intake through multiple different strategies used to manipulate the system. This includes altering the body's ability to produce histamine. Genetic knock-out of histidine decarboxylase (HDC-KO) has been used to prevent the synthesis of histamine, resulting in histamine deficient mice. Studies using these mice suggest that HDC-KO animals are more susceptible to develop obesity as they age, or after consumption of a high fat diet (72–74). Detailed analyses of food intake in these mice are lacking, however, one study suggests that HDC-KO mice are not hyperphagic, but have an increased feed efficiency (72). However, the increased body weight in HDC-KO mice could be confounded by the decreased locomotor activity observed in these animals (75–77). An alternate method to deplete histamine is the use of α-Fluromethyl-[S]-histidine (α-FMH) which is a suicide inhibitor of histamine synthesis. Chemical inhibition of histamine synthesis with α-FMH has consistently been associated with an increase in food intake (78–82), suggesting that overall, histamine may be anorexigenic. However, such genetic or chemical methods preventing histamine synthesis provide limited and unspecific information regarding histamine's ability to influence feeding, due to a loss of histaminergic tone at all histamine receptors simultaneously.

H1R activation suppresses food intake

The H1R is generally accepted to mediate the suppression of food intake induced by histamine (Figure 3). Early studies demonstrated that intracerebroventricular (ICV) injection of H1R antagonists stimulated feeding (12, 83). Moreover, the effects of pharmacological strategies increasing brain histamine levels, which are associated with a suppression of food intake, are attenuated, or abolished in the presence of H1R antagonists (78, 84). These actions are consistent with the increased food intake and weight gain seen with first-generation antihistamines used to treat allergies (85–87) which are all inverse agonists of the H1R (88).

More recently, global H1R knockout (H1R-KO) mice have been developed (89) and food intake and body weight studies in these mice overwhelmingly backed up that obtained with pharmacological ligands targeting the H1R. The ability of α-FMH to stimulate food intake is lost in H1R-KO mice (79) and histamine's ability to suppress food intake and body weight is reduced in H1R-KO mice compared to control mice (90). Moreover, the ability of betahistine, which enhances histamine levels and acts as an agonist of H1R, to reduce food intake and body weight is absent in H1R-KO mice (91). Together, these data strongly support the idea that histamine's actions at the H1R are anorexigenic. Interestingly, H1R-KO mice do not show any changes in food intake or body weight when fed a standard chow diet (90, 92). However, with age or high fat diet feeding, H1R-KO mice

10.3389/fendo.2023.1202089

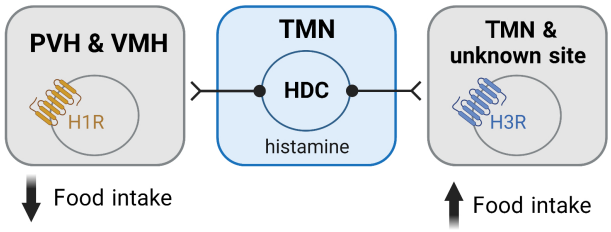

FIGURE 3
Histamine mediates its effects on feeding via activation of histamine receptors within the hypothalamus. Activation of the H1R is associated with an anorexigenic effect and is believed to be mediated via H1Rs expressed in the PVH and VMH. In contrast, activation of the H3R is orexigenic and occurs via autoinhibition of the histaminergic neurons. H3Rs in unidentified sites may also contribute to the orexigenic effects of H3R activation. Figure created with BioRender.com.

accumulate fat mass and develop obesity (90, 92, 93), which is consistent with what was seen in mice completely deficient of histamine (HDC-KO) as discussed above. Additionally, H1R-KO mice display a decreased anorexigenic response to thyrotropin releasing hormone (TRH), neurotensin, nesfatin-1, and estradiol (94–97), suggesting that the H1R may contribute to the suppression of feeding normally induced by these anorexigenic peptides.

While the ability of histamine to suppress feeding is well demonstrated to occur via H1R, the exact neuronal populations and mechanisms responsible for these effects are not well understood. Studies where H1R antagonists were directly infused into different hypothalamic nuclei have demonstrated that blockade of H1R only in the paraventricular (PVH) and ventromedial (VMH) hypothalamus stimulate feeding (12, 13) (Figure 3). Similarly, micro infusion of α-FMH to decrease local histamine concentrations, only has effects on food intake when infused in the PVH and VMH (78, 82, 98). While H1R agonists have been shown to induce markers of cell activity (c-Fos) only in the PVH (91), extracellular recording techniques demonstrate that the H1R antagonist chlorpheniramine inhibits neurons in the VMH (83). Despite these studies suggesting that the PVH and VMH are the sites where H1R activation has its anorexigenic effects, future studies are required to further elucidate the mechanisms involved, including the chemical phenotype of the cells in these nuclei mediating the anorexigenic effects of H1R activation.

H2R activation does not influence food intake

When it comes to central H2Rs, there is limited evidence indicating that they have any role in regulating feeding. Importantly, H2R antagonists administered ICV or directly to hypothalamic regions have no effect on food intake (12, 83, 99, 100). Furthermore, the H2R antagonist ranitidine has been shown to have no effect on histamine-induced suppression of food intake, whereas both H1R and H3R antagonists influenced this effect (84). It should be noted that while H2R antagonists can influence feeding when taken orally or infused directly into the gut, peripheral mechanisms including H2R effects on gastric acid secretion and gut hormones likely contribute to these effects (101–103). Furthermore, it is unsurprising that centrally expressed H2Rs do not influence food intake given that these receptors are most strongly expressed in extrahypothalamic regions such as the cortex, hippocampus, striatum, basal ganglia, and amygdala (30, 33, 104). Together, these data strongly suggest that central H2Rs do not contribute to the homeostatic regulation of food intake.

H3R activation stimulates food intake

Pharmacological studies indicate that activation of the H3R is orexigenic, with H3R agonist delivery directly to the brain stimulating food intake (105–107) (Figure 3). In line with these observations, blockade or inverse agonism of the H3R suppresses food intake (78, 82, 84, 100, 107, 108). The capacity of H3R inverse agonists/antagonists to reduce food intake has also been shown to minimize weight gain occurring in models of diet-induced obesity and to reduce body weight in obese rodents (108–112). Moreover, H3R inverse agonists/antagonists suppress food intake in conditions associated with an increased orexigenic drive, i.e., in the fasted state or following neuropeptide Y (NPY) administration (105, 113). In one study, food intake in rats that received a single dose of thioperamide, a H3R antagonist, was significantly less for two days compared to controls (82). The suppression of food intake induced by H3R antagonists has also been demonstrated to occur in non-rodent species including pigs and non-human primates (114). Together, these studies demonstrate that histamine's actions at the H3R stimulate feeding, and blockade of this receptor is associated with anorexigenic effects.

The ability of H3R inverse agonists/antagonists to suppress food intake is largely assumed to occur by removing the normal auto-inhibition of histaminergic neurons (Figure 3), thereby increasing histamine levels and enhancing action at the anorexigenic H1R (78, 105, 115). However, the H3R also functions as a heteroreceptor and has been shown to be expressed in several brain regions other than the TMN (32, 58, 60, 116). Importantly, the H3R can suppress the release of multiple neurotransmitters including serotonin (117,

118), dopamine (119, 120), noradrenaline (118, 121), acetylcholine (122, 123) and GABA (124–126), neurotransmitters that are implicated in the regulation of feeding. This raises the potential for H3R inverse agonism/antagonism to influence food intake via transmitters other than histamine (Figure 3). However, such a possibility has not been comprehensively assessed.

In comparison with pharmacological studies targeting the H3R, experiments using global H3R-KO mice have generated diverging and less consistent findings. H3R-KO mice were shown to consume more food and have an increase in body weight from approximately 10 weeks of age (127). Such findings seem counterintuitive considering that the KO of H3Rs should remove the auto-inhibition of the histaminergic neurons and enhance anorexigenic actions at the H1R. However, it has been demonstrated that H3R-KO mice actually have decreased histamine levels in the hypothalamus and cortex (127, 128) potentially contributing to this effect. In contrast to the food intake effects reported by Takahashi et al. (127), others have suggested that a decrease in food intake occurs in H3R-KO mice, however, food intake was normalized to body weight, making any absolute changes difficult to assess (129). While genetic mouse models can reveal important insights into the mechanistic underpinnings of physiology and behavior, developmental and compensatory actions can occur, especially in relation to fundamental processes such as eating. Moreover, the function of the H3R as a heteroreceptor adds another level of complexity, whereby knockout of H3R could simultaneously influence multiple neurotransmitter systems. Despite some conflicting results obtained in knockout animals, it is clear that the H3R plays an important role in regulating food intake, and its activation is generally orexigenic.

Histaminergic system and interaction with key metabolic signals

Leptin

In addition to histamine's ability to influence feeding, the central histaminergic system has been suggested to interact with other signals reflective of the metabolic state. This includes leptin, a hormone produced by adipose tissue that acts in the CNS to regulate energy metabolism (130). Circulating leptin levels occur in proportion to fat mass and decrease with periods of fasting (131, 132), therefore, acting as a signal of energy reserves to the brain. Exogenous leptin administration is associated with a suppression of food intake, a reduction in body weight, and an upregulation of uncoupling protein 1 (UCP1) expression in adipose tissue depots, all of which have been suggested to require a fully functioning histaminergic system (79, 80, 92, 133). Studies in which histamine synthesis was chemically inactivated failed to observe the normal leptin-induced suppression of food intake and decrease in body weight (79, 80, 133). These effects have been linked to the H1R, as studies performed in mice globally lacking H1R show similar effects. In H1R-KO mice, leptin's effect on food intake and body weight is suppressed or absent compared to that seen in control animals (79, 92). Additionally, leptin's ability to decrease body fat percentage and upregulate UCP1 in brown adipose tissue was suppressed in H1R-KO mice (92). Moreover, genetic disruption of histamine synthesis (HDC-KO mice) leads to impairments in leptin sensing and regulation (72, 74, 134). While these studies suggest that the histaminergic system may mediate some of the anorexigenic effects of leptin, the mechanisms by which the histaminergic system regulates the actions of leptin in the CNS remains to be determined. Interestingly, the core region of the TMN, where the histaminergic neurons reside, does not express the long form of the leptin receptor (LepR) (135), which likely precludes direct effects of leptin on the histaminergic neurons themselves. In contrast, LepR is expressed in sub-populations of neurons located in the lateral hypothalamus (136–138) a region known to directly and indirectly influence the histaminergic neurons (139, 140). However, the potential for leptin to influence the activity of histaminergic neurons via presynaptic inputs has not previously been investigated. Future studies are required to determine the sites and mechanisms by which histamine and leptin signaling may converge within the brain.

Melanocortin system

The central melanocortin system is one of the best-characterized brain circuits regulating food intake and energy expenditure (141–144). Melanocortin peptides, derived from the proopiomelanocortin (POMC) pre-prohormone, form a crucial component of this system and act at cognate melanocortin receptors to influence energy balance (145, 146). Importantly, recent work has identified that histaminergic neurons are sensitive to activation of the melanocortin 4 receptor (MC4R) (147). Using single neuron *ex vivo* electrophysiological recordings from genetically identified histaminergic (HDC) neurons, we demonstrated that approximately 40% of histaminergic neurons are excited by the non-selective MC3R/MC4R agonist melanotan II (MTII) or a selective MC4R agonist (THIQ) (147). These MC4R-mediated effects were shown to modify glutamatergic tone to the histaminergic neurons (147). Moreover, the interaction between the melanocortin and histaminergic systems was shown to be important for feeding regulation. Chemogenetic inhibition of the histaminergic neurons using an inhibitory Designer Receptor Exclusively Activated by Designer Drugs (DREADD) approach (148–150), enhanced the anorexigenic response to central infusion of MTII (147). This study found that melanocortin system activation results in unabated anorexia once the histaminergic neurons are silenced and suggests that, under normal conditions, the melanocortin-dependent activation of histaminergic neurons acts naturally as a negative feedback loop of the anorexigenic effects of the melanocortin system (147). Despite this important observation demonstrating histaminergic neurons are sensitive to key metabolic signals conveyed by the melanocortin system, the downstream mechanisms by which histaminergic neurons restrain the anorexigenic effects of melanocortin system activation remain to be identified.

Other appetite-related hormones

The ability of other appetite-related hormones to influence the activity and function of the histaminergic neurons has not been intensively investigated. One previous study suggested that ghrelin may activate the histaminergic neurons, as increased c-Fos expression, an indirect marker of cellular activity, was observed in the TMN following central administration of ghrelin (151). However, the receptor for ghrelin, the growth hormone secretagogue receptor (GHSR), is not expressed in the TMN (152) and *Ghsr* mRNA is not detected in transcriptomic profiling of histaminergic neurons (153). This likely prevents any direct post-synaptic modulation of histaminergic neurons by ghrelin. Similarly, *in vivo* work has suggested that the histaminergic system is influenced by glucagon-like peptide-1 (GLP-1), as central GLP-1 infusion has been shown to increase histamine and histamine metabolite levels in the hypothalamus (154). The same study also indicated that the histaminergic system was required for the full anorexigenic effect of GLP-1, as inhibition of histamine synthesis (with α-FMH) attenuated the GLP-1 induced suppression of food intake (154). While there are descriptions of GLP-1 receptor (GLP-1R) expression in the TMN (155) and tuberal region (156), and GLP-1R agonists have been reported to activate (c-Fos) in the ventral region of the TMN (157) and the tuberal region (158), single cell sequencing fails to detect *Glp1r* mRNA in histaminergic neurons (153). Interestingly, the LH, a region strongly innervating the TMN, has been shown to express *Glp1r* mRNA (155, 156) and is involved in mediating some of the anorexigenic effects of GLP-1 (159). Thus, any influence of GLP-1 on the histaminergic neurons may be indirect via neurons of the LH.

The pancreatic hormone insulin may also have a role in regulating histaminergic neuron function. One study demonstrated that a very small percentage of histaminergic neurons displayed c-Fos expression following insulin-induced hypoglycemia (160). Further work would be required to delineate whether histaminergic neuron activation in these conditions was mediated by the hypoglycemia or insulin itself. However, histaminergic neurons have been shown to express the insulin receptor (153). Another metabolically relevant neuropeptide known to target the histaminergic neurons is orexin (also known as hypocretin). Orexin is a potent stimulator of feeding and the neurons synthesizing this orexigenic neuropeptide are located in the LH (161, 162). Importantly, histaminergic neurons express the orexin receptor type 2 (OxR2/Hcrt2) (153, 163) and are excited by orexin-A (164, 165). Orexin actions on histaminergic neurons have largely been demonstrated to influence arousal control (165, 166). However, it is important to note that the orexin neurons also co-express glutamate and can signal to the downstream histaminergic neurons via glutamatergic currents (22, 167). Moreover, the glutamatergic tone at histaminergic neurons, arising from the LH, has been linked to the modulation of food intake (147). While it is interesting to speculate about the different functional consequences of orexin neuronal transmission to histaminergic neurons, delineating such multifunctionality remains understudied. Overall, it appears that the ability of histaminergic neurons to detect, and interact with, metabolic signals occur via indirect (presynaptic) mechanisms, or via actions downstream of the histaminergic neurons themselves, i.e. on neurons expressing the histamine receptors.

Medications regulating body weight via the histaminergic system

Psychiatric medications for the treatment of schizophrenia

Supporting the importance of histamine receptors in the regulation of energy balance, antipsychotic medications that interact with the histaminergic system are associated with clinically significant weight gain (168, 169). Notably, the atypical antipsychotics with the largest weight gain profiles, olanzapine and clozapine, also display high affinities for the H1R (170–173). Atypical antipsychotics act to antagonize histamine's endogenous actions at the H1R, which may partially explain the increased food intake seen with these medications (174–177). While the exact mechanisms underlying atypical antipsychotic-induced weight gain remain somewhat elusive, these medications have been shown to downregulate hypothalamic expression of the H1R (178). In addition, atypical antipsychotics have been shown to increase orexigenic neuropeptide Y (NPY) expression and activate the cellular energy sensor AMP-activated protein kinase (AMPK) in the hypothalamus, effects that are dependent on functional H1Rs (171, 179). Moreover, combination therapies including betahistine, a H1R agonist/H3R antagonist, have been shown to reduce weight gain in people treated with olanzapine (180). Although the histaminergic system is not the only transmitter system implicated in atypical antipsychotic-induced weight gain, strong evidence suggests its ability to influence food intake, and sensitivity to these medications, plays a contributing role.

Therapeutic potential for the treatment of obesity

Following the cloning of the H3R in 1999 (58), numerous ligands were developed to manipulate the function of the receptor, and the H3R was subsequently proposed as a potential therapeutic target for the treatment of obesity (81, 116, 181, 182). In addition to food intake effects of H3R antagonists/inverse agonists, as discussed in this review, pre-clinical work demonstrated that these compounds also improve metabolic health and are associated with decreased body weight and fat mass, improved glucose homeostasis, and increased insulin sensitivity (108–111). These properties saw multiple pharmaceutical companies including Novo Nordisk, Abbott Laboratories, and Gliatech pursue H3R ligands for the treatment of obesity (183). While there was a brief surge in interest in these compounds for their metabolic effects, few ligands transitioned from the pre-clinical stage. Abbott laboratories H3R antagonist (A-331440) was found to have the potential for

genotoxic effects which prohibited its further development as an anti-obesity therapeutic (184). Contradictory results were obtained between ligands with some studies failing to demonstrate consistent effects on food intake and anti-obesity properties (81, 185). Additionally, human trials with betahistine, a H1R agonist/H3R antagonist, failed to identify any striking weight loss effects in obese women (186), or on food intake when presented a buffet meal following a single day of betahistine treatment (187). Differences in ligand affinity for the H3R found between species may also contribute to some discrepancies observed among rodent and human studies (63, 188). Even though the pharmaceutical industry appears to have largely withdrawn its interest in pursuing the H3R as an anti-obesity target (189), work endures to optimize H3R ligands and explore their potential to influence food intake and body weight, and H3R antagonists/inverse agonists continue to be proposed for the treatment of obesity (190, 191).

Considerations and future directions

The central histaminergic system has received considerable interest for its ability to regulate energy balance, however, many unanswered questions remain. Generally, histamine is considered an anorexigenic substance, as activation of H1Rs decrease food intake, effects that are believed to be mediated through actions in the PVH and VMH (12, 13). However, these hypothalamic nuclei consist of multiple cell types, and the chemical phenotype or identity of the cells mediating H1R agonism-induced suppression of food intake remain unidentified. Moreover, the view of histamine as an anorexigenic compound seems somewhat contradictory given that feeding occurs during waking hours when histaminergic neurons are active and histamine levels are highest (192–196). It appears that the picture is more complex and likely involves numerous interactions, some of which have yet to be uncovered.

Pharmacological and genetic knockout studies have provided important insights into the functioning of the histaminergic system, but the expression of histamine receptors in both the brain and periphery, and effects of the H3R on multiple neurotransmitter systems, likely complicate the interpretation of some of these findings. The field now requires the ability to manipulate individual histamine receptors in a cell-type specific way (e.g., histamine receptor floxed mice) to further delineate the precise actions of histamine in different nuclei and different cell types, and to overcome some of the inherent limitations of global knockout models.

Evidence also continues to emerge that the histaminergic neurons are heterogeneous. Differences have been demonstrated in their basal electrophysiological properties, transcriptional makeup, and their response to various pharmacological agents (163, 197–199). Such heterogeneity combined with multiple histamine receptors, differentially expressed within the hypothalamus and in multiple cell types, contributes to the complexity of the histaminergic system and highlights multiple ways histamine may serve to influence neuronal activity and food intake. Additionally, histamine itself has been proposed to function more like a neuromodulator or neuropeptide than a classical "neurotransmitter" (1, 200). Histaminergic neurons rarely form close synaptic contacts (201, 202), preventing their potential for traditional fast synaptic signaling to clearly defined post-synaptic targets. Rather, histaminergic neurons are believed to communicate via volume transmission, with histamine being released non-synaptically, allowing it to have longer lasting actions, and modulate neurotransmission at extra synaptic sites similar to other monoamines (203). The ability of histamine to signal in this fashion raises the potential for histaminergic neurons to "prime" other neurons' responsiveness to additional incoming (metabolic) stimuli during waking hours when histaminergic tone is highest. However, future studies will be required to address such a possibility.

Conclusion

In summary, histamine functions as a neuromodulator in the brain and contributes to the central regulation of energy homeostasis. Its effects on food intake largely depend on the histamine receptor subtype activated, with agonism of H1Rs being anorexigenic and agonism of H3Rs causing an orexigenic response. These important metabolic effects of HR activation contribute towards the weight gain side effects of some common medications and have seen HR ligands proposed as anti-obesity therapeutics. The histaminergic system has also been demonstrated to interact with key metabolic signals in the brain. It is clear that the histaminergic system has a powerful ability to influence food intake. Now we must turn our attention to elucidating the exact mechanisms by which it does so and the circumstances in which histaminergic signaling may contribute to an altered homeostatic drive to eat.

Author contributions

All authors contributed to the article and approved the submitted version.

Funding

This research was supported by the Sentinel North Initiative funded by the Canada First Research Excellence Fund (Partnered Research Chair in Sleep Pharmacometabolism to NJM), the Fonds de recherche du Québec - Santé (FRQS) (J1 Research Scholar award to NJM), the Natural Sciences and Engineering Research Council of Canada (NSERC) (to NJM), the Fondation de l'Insitut Universitaire de Cardiologie et de Pneumologie de Québec (FIUCPQ) (to NJM and MMM), and the Canada Research Chairs Program (to AC).

Conflict of interest

The authors declare that the research was conducted in the absence of any commercial or financial relationships that could be construed as a potential conflict of interest.

Publisher's note

References

1. Schwartz JC, Arrang JM, Garbarg M, Pollard H, Ruat M. Histaminergic transmission in the mammalian brain. *Physiol Rev* (1991) 71(1):1–51. doi: 10.1152/physrev.1991.71.1.1

2. Schneider E, Rolli-Derkinderen M, Arock M, Dy M. Trends in histamine research: new functions during immune responses and hematopoiesis. *Trends Immunol* (2002) 23(5):255–63. doi: 10.1016/s1471-4906(02)02215-9

3. Haas HL, Sergeeva OA, Selbach O. Histamine in the nervous system. *Physiol Rev* (2008) 88(3):1183–241. doi: 10.1152/physrev.00043.2007

4. Panula P, Yang HY, Costa E. Histamine-containing neurons in the rat hypothalamus. *Proc Natl Acad Sci USA* (1984) 81(8):2572–6. doi: 10.1073/pnas.81.8.2572

5. Takeda N, Inagaki S, Shiosaka S, Taguchi Y, Oertel WH, Tohyama M, et al. Immunohistochemical evidence for the coexistence of histidine decarboxylase-like and glutamate decarboxylase-like immunoreactivities in nerve cells of the magnocellular nucleus of the posterior hypothalamus of rats. *Proc Natl Acad Sci USA* (1984) 81 (23):7647–50. doi: 10.1073/pnas.81.23.7647

6. Watanabe T, Taguchi Y, Shiosaka S, Tanaka J, Kubota H, Terano Y, et al. Distribution of the histaminergic neuron system in the central nervous system of rats; a fluorescent immunohistochemical analysis with histidine decarboxylase as a marker. *Brain Res* (1984) 295(1):13–25. doi: 10.1016/0006-8993(84)90811-4

7. Taylor KM, Snyder SH. Isotopic microassay of histamine, histidine, histidine decarboxylase and histamine methyltransferase in brain tissue. *J Neurochem* (1972) 19 (5):1343–58. doi: 10.1111/j.1471-4159.1972.tb01459.x

8. Green JP, Prell GD, Khandelwal JK, Blandina P. Aspects of histamine metabolism. *Agents Actions* (1987) 22(1-2):1–15. doi: 10.1007/bf01968810

9. Ericson H, Watanabe T, Kohler C. Morphological analysis of the tuberomammillary nucleus in the rat brain: delineation of subgroups with antibody against l-histidine decarboxylase as a marker. *J Comp Neurol* (1987) 263(1):1–24. doi: 10.1002/cne.902630102

10. Inagaki N, Yamatodani A, Ando-Yamamoto M, Tohyama M, Watanabe T, Wada H. Organization of histaminergic fibers in the rat brain. *J Comp Neurol* (1988) 273(3):283–300. doi: 10.1002/cne.902730302

11. Panula P, Pirvola U, Auvinen S, Airaksinen MS. Histamine-immunoreactive nerve fibers in the rat brain. *Neuroscience* (1989) 28(3):585–610. doi: 10.1016/0306-4522(89)90007-9

12. Sakata T, Ookuma K, Fukagawa K, Fujimoto K, Yoshimatsu H, Shiraishi T, et al. Blockade of the histamine H1-receptor in the rat ventromedial hypothalamus and feeding elicitation. *Brain Res* (1988) 441(1-2):403–7. doi: 10.1016/0006-8993(88)91423-0

13. Ookuma K, Yoshimatsu H, Sakata T, Fujimoto K, Fukagawa F. Hypothalamic sites of neuronal histamine action on food intake by rats. *Brain Res* (1989) 490(2):268–75. doi: 10.1016/0006-8993(89)90244-8

14. Lin W, Xu L, Zheng Y, An S, Zhao M, Hu W, et al. Whole-brain mapping of histaminergic projections in mouse brain. *Proc Natl Acad Sci USA* (2023) 120(14): e2216231120. doi: 10.1073/pnas.2216231120

15. Haas H, Panula P. The role of histamine and the tuberomamillary nucleus in the nervous system. *Nat Rev Neurosci* (2003) 4(2):121–30. doi: 10.1038/nrn1034

16. Saper CB, Stornetta RL. Central autonomic system. In: Paxinos G, editor. *The rat nervous system, 4th Edition*. Amsterdam: Academic Press (2015). p. 629–73.

17. Sherin JE, Elmquist JK, Torrealba F, Saper CB. Innervation of histaminergic tuberomammillary neurons by GABAergic and galaninergic neurons in the ventrolateral preoptic nucleus of the rat. *J Neurosci Off J Soc Neurosci* (1998) 18 (12):4705–21. doi: 10.1523/JNEUROSCI.18-12-04705.1998

18. Sherin JE, Shiromani PJ, McCarley RW, Saper CB. Activation of ventrolateral preoptic neurons during sleep. *Science* (1996) 271(5246):216–9. doi: 10.1126/science.271.5246.216

19. Chung S, Weber F, Zhong P, Tan CL, Nguyen TN, Beier KT, et al. Identification of preoptic sleep neurons using retrograde labelling and gene profiling. *Nature* (2017) 545(7655):477–81. doi: 10.1038/nature22350

20. Peyron C, Tighe DK, van den Pol AN, de Lecea L, Heller HC, Sutcliffe JG, et al. Neurons containing hypocretin (orexin) project to multiple neuronal systems. *J Neurosci Off J Soc Neurosci* (1998) 18(23):9996–10015. doi: 10.1523/JNEUROSCI.18-23-09996.1998

21. Chemelli RM, Willie JT, Sinton CM, Elmquist JK, Scammell T, Lee C, et al. Narcolepsy in orexin knockout mice: molecular genetics of sleep regulation. *Cell* (1999) 98(4):437–51. doi: 10.1016/s0092-8674(00)81973-x

22. Schone C, Cao ZF, Apergis-Schoute J, Adamantidis A, Sakurai T, Burdakov D. Optogenetic probing of fast glutamatergic transmission from hypocretin/orexin to histamine neurons in situ. *J Neurosci Off J Soc Neurosci* (2012) 32(36):12437–43. doi: 10.1523/JNEUROSCI.0706-12.2012

23. Jego S, Glasgow SD, Herrera CG, Ekstrand M, Reed SJ, Boyce R, et al. Optogenetic identification of a rapid eye movement sleep modulatory circuit in the hypothalamus. *Nat Neurosci* (2013) 16(11):1637–43. doi: 10.1038/nn.3522

24. Kohler C, Swanson LW, Haglund L, Wu JY. The cytoarchitecture, histochemistry and projections of the tuberomammillary nucleus in the rat. *Neuroscience* (1985) 16(1):85–110. doi: 10.1016/0306-4522(85)90049-1

25. Inagaki N, Toda K, Taniuchi I, Panula P, Yamatodani A, Tohyama M, et al. An analysis of histaminergic efferents of the tuberomammillary nucleus to the medial preoptic area and inferior colliculus of the rat. *Exp Brain Res* (1990) 80(2):374–80. doi: 10.1007/bf00228164

26. Karlstedt K, Nissinen M, Michelsen KA, Panula P. Multiple sites of l-histidine decarboxylase expression in mouse suggest novel developmental functions for histamine. *Dev Dyn* (2001) 221(1):81–91. doi: 10.1002/dvdy.1127

27. Airaksinen MS, Panula P. The histaminergic system in the guinea pig central nervous system: an immunocytochemical mapping study using an antiserum against histamine. *J Comp Neurol* (1988) 273(2):163–86. doi: 10.1002/cne.902730204

28. Panula P, Airaksinen MS, Pirvola U, Kotilainen E. A histamine-containing neuronal system in human brain. *Neuroscience* (1990) 34(1):127–32. doi: 10.1016/0306-4522(90)90307-p

29. Reiner PB, Semba K, Watanabe T, Wada H. En bloc immunohistochemistry reveals extensive distribution of histidine decarboxylase-immunoreactive neurons on the ventral surface of the rat hypothalamus. *Neurosci Lett* (1987) 77(2):137–42. doi: 10.1016/0304-3940(87)90575-1

30. Martinez-Mir MI, Pollard H, Moreau J, Arrang JM, Ruat M, Traiffort E, et al. Three histamine receptors (H1, H2 and H3) visualized in the brain of human and non-human primates. *Brain Res* (1990) 526(2):322–7. doi: 10.1016/0006-8993(90)91240-h

31. Bouthenet ML, Ruat M, Sales N, Garbarg M, Schwartz JC. A detailed mapping of histamine H1-receptors in guinea-pig central nervous system established by autoradiography with [125I]iodobolpyramine. *Neuroscience* (1988) 26(2):553–600. doi: 10.1016/0306-4522(88)90167-4

32. Pollard H, Moreau J, Arrang JM, Schwartz JC. A detailed autoradiographic mapping of histamine H3 receptors in rat brain areas. *Neuroscience* (1993) 52(1):169–89. doi: 10.1016/0306-4522(93)90191-h

33. Vizuete ML, Traiffort E, Bouthenet ML, Ruat M, Souil E, Tardivel-Lacombe J, et al. Detailed mapping of the histamine H2 receptor and its gene transcripts in guinea-pig brain. *Neuroscience* (1997) 80(2):321–43. doi: 10.1016/s0306-4522(97)00010-9

34. Weis WI, Kobilka BK. The molecular basis of G protein-coupled receptor activation. *Annu Rev Biochem* (2018) 87:897–919. doi: 10.1146/annurev-biochem-060614-033910

35. Pfleger J, Gresham K, Koch WJ. G Protein-coupled receptor kinases as therapeutic targets in the heart. *Nat Rev Cardiol* (2019) 16(10):612–22. doi: 10.1038/s41569-019-0220-3

36. Ash AS, Schild HO. Receptors mediating some actions of histamine. *Br J Pharmacol Chemother* (1966) 27(2):427–39. doi: 10.1111/j.1476-5381.1966.tb01674.x

37. Gutowski S, Smrcka A, Nowak L, Wu DG, Simon M, Sternweis PC. Antibodies to the alpha q subfamily of guanine nucleotide-binding regulatory protein alpha subunits attenuate activation of phosphatidylinositol 4,5-bisphosphate hydrolysis by hormones. *J Biol Chem* (1991) 266(30):20519–24. doi: 10.1016/S0021-9258(18)54955-3

38. Leopoldt D, Harteneck C, Nurnberg B. G Proteins endogenously expressed in sf 9 cells: interactions with mammalian histamine receptors. *Naunyn-Schmiedeberg's Arch Pharmacol* (1997) 356(2):216–24. doi: 10.1007/pl00005044

39. Harding SD, Armstrong JF, Faccenda E, Southan C, Alexander SPH, Davenport AP, et al. The IUPHAR/BPS guide to PHARMACOLOGY in 2022: curating pharmacology for COVID-19, malaria and antibacterials. *Nucleic Acids Res* (2022) 50(D1):D1282–D94. doi: 10.1093/nar/gkab1010

40. Leurs R, Traiffort E, Arrang JM, Tardivel-Lacombe J, Ruat M, Schwartz JC. Guinea Pig histamine H1 receptor. II. stable expression in Chinese hamster ovary cells reveals the interaction with three major signal transduction pathways. *J Neurochem* (1994) 62(2):519–27. doi: 10.1046/j.1471-4159.1994.62020519.x

41. Harding SD, Sharman JL, Faccenda E, Southan C, Pawson AJ, Ireland S, et al. The IUPHAR/BPS guide to PHARMACOLOGY in 2018: updates and expansion to

encompass the new guide to IMMUNOPHARMACOLOGY. *Nucleic Acids Res* (2018) 46(D1):D1091–D106. doi: 10.1093/nar/gkx1121

42. Lo WW, Fan TP. Histamine stimulates inositol phosphate accumulation via the H1-receptor in cultured human endothelial cells. *Biochem Biophys Res Commun* (1987) 148(1):47–53. doi: 10.1016/0006-291x(87)91074-6

43. Li H, Choe NH, Wright DT, Adler KB. Histamine provokes turnover of inositol phospholipids in guinea pig and human airway epithelial cells via an H1-receptor/G protein-dependent mechanism. *Am J Respir Cell Mol Biol* (1995) 12(4):416–24. doi: 10.1165/ajrcmb.12.4.7695921

44. De Backer MD, Gommeren W, Moereels H, Nobels G, Van Gompel P, Leysen JE, et al. Genomic cloning, heterologous expression and pharmacological characterization of a human histamine H1 receptor. *Biochem Biophys Res Commun* (1993) 197(3):1601–8. doi: 10.1006/bbrc.1993.2662

45. Tilly BC, Tertoolen LG, Lambrechts AC, Remorie R, de Laat SW, Moolenaar WH. Histamine-H1-receptor-mediated phosphoinositide hydrolysis, Ca2+ signalling and membrane-potential oscillations in human HeLa carcinoma cells. *Biochem J* (1990) 266(1):235–43. doi: 10.1042/bj2660235

46. Markwardt KL, Magnino PE, Pang IH. Effect of histamine on phosphoinositide turnover and intracellular calcium in human ciliary muscle cells. *Exp Eye Res* (1996) 62 (5):511–20. doi: 10.1006/exer.1996.0062

47. Maruko T, Nakahara T, Sakamoto K, Saito M, Sugimoto N, Takuwa Y, et al. Involvement of the betagamma subunits of G proteins in the cAMP response induced by stimulation of the histamine H1 receptor. *Naunyn-Schmiedeberg's Arch Pharmacol* (2005) 372(2):153–9. doi: 10.1007/s00210-005-0001-x

48. Segal M. Histamine modulates reactivity of hippocampal CA3 neurons to afferent stimulation in vitro. *Brain Res* (1981) 213(2):443–8. doi: 10.1016/0006-8993(81)90251-1

49. McCormick DA, Williamson A. Modulation of neuronal firing mode in cat and guinea pig LGNd by histamine: possible cellular mechanisms of histaminergic control of arousal. *J Neurosci Off J Soc Neurosci* (1991) 11(10):3188–99. doi: 10.1523/JNEUROSCI.11-10-03188.1991

50. Smith BN, Armstrong WE. The ionic dependence of the histamine-induced depolarization of vasopressin neurones in the rat supraoptic nucleus. *J Physiol* (1996) 495(Pt 2):465–78. doi: 10.1113/jphysiol.1996.sp021607

51. Reiner PB, Kamondi A. Mechanisms of antihistamine-induced sedation in the human brain: H1 receptor activation reduces a background leakage potassium current. *Neuroscience* (1994) 59(3):579–88. doi: 10.1016/0306-4522(94)90178-3

52. Billups D, Billups B, Challiss RA, Nahorski SR. Modulation of gq-protein-coupled inositol trisphosphate and Ca2+ signaling by the membrane potential. *J Neurosci Off J Soc Neurosci* (2006) 26(39):9983–95. doi: 10.1523/JNEUROSCI.2773-06.2006

53. Kuhn B, Schmid A, Harteneck C, Gudermann T, Schultz G. G Proteins of the gq family couple the H2 histamine receptor to phospholipase c. *Mol Endocrinol* (1996) 10 (12):1697–707. doi: 10.1210/mend.10.12.8961278

54. Fukushima Y, Otsuka H, Ishikawa M, Asano T, Anai M, Katsube T, et al. Potent and long-lasting action of lafutidine on the human histamine H(2) receptor. *Digestion* (2001) 64(3):155–60. doi: 10.1159/000048856

55. Pedarzani P, Storm JF. PKA mediates the effects of monoamine transmitters on the k+ current underlying the slow spike frequency adaptation in hippocampal neurons. *Neuron* (1993) 11(6):1023–35. doi: 10.1016/0896-6273(93)90216-e

56. Yanovsky Y, Haas HL. Histamine increases the bursting activity of pyramidal cells in the CA3 region of mouse hippocampus. *Neurosci Lett* (1998) 240(2):110–2. doi: 10.1016/s0304-3940(97)00925-7

57. Selbach O, Brown RE, Haas HL. Long-term increase of hippocampal excitability by histamine and cyclic AMP. *Neuropharmacology* (1997) 36(11-12):1539–48. doi: 10.1016/s0028-3908(97)00144-5

58. Lovenberg TW, Roland BL, Wilson SJ, Jiang X, Pyati J, Huvar A, et al. Cloning and functional expression of the human histamine H3 receptor. *Mol Pharmacol* (1999) 55(6):1101–7. doi: 10.1124/mol.55.6.1101

59. Schlicker E, Malinowska B, Kathmann M, Gothert M. Modulation of neurotransmitter release via histamine H3 heteroreceptors. *Fundam Clin Pharmacol* (1994) 8(2):128–37. doi: 10.1111/j.1472-8206.1994.tb00789.x

60. Nieto-Alamilla G, Marquez-Gomez R, Garcia-Galvez AM, Morales-Figueroa GE, Arias-Montano JA. The histamine H3 receptor: structure, pharmacology, and function. *Mol Pharmacol* (2016) 90(5):649–73. doi: 10.1124/mol.116.104752

61. Arrang JM, Garbarg M, Schwartz JC. Auto-inhibition of brain histamine release mediated by a novel class (H3) of histamine receptor. *Nature* (1983) 302(5911):832–7. doi: 10.1038/302832a0

62. Arrang JM, Garbarg M, Schwartz JC. Autoregulation of histamine release in brain by presynaptic H3-receptors. *Neuroscience* (1985) 15(2):553–62. doi: 10.1016/0306-4522(85)90233-7

63. Lovenberg TW, Pyati J, Chang H, Wilson SJ, Erlander MG. Cloning of rat histamine H(3) receptor reveals distinct species pharmacological profiles. *J Pharmacol Exp Ther* (2000) 293(3):771–8.

64. Wieland K, Bongers G, Yamamoto Y, Hashimoto T, Yamatodani A, Menge WM, et al. Constitutive activity of histamine h(3) receptors stably expressed in SK-N-MC cells: display of agonism and inverse agonism by H(3) antagonists. *J Pharmacol Exp Ther* (2001) 299(3):908–14.

65. Arrang JM, Garbarg M, Lancelot JC, Lecomte JM, Pollard H, Robba M, et al. Highly potent and selective ligands for histamine H3-receptors. *Nature* (1987) 327 (6118):117–23. doi: 10.1038/327117a0

66. Parks GS, Olivas ND, Ikrar T, Sanathara NM, Wang L, Wang Z, et al. Histamine inhibits the melanin-concentrating hormone system: implications for sleep and arousal. *J Physiol* (2014) 592(10):2183–96. doi: 10.1113/jphysiol.2013.268771

67. Kano H, Toyama Y, Imai S, Iwahashi Y, Mase Y, Yokogawa M, et al. Structural mechanism underlying G protein family-specific regulation of G protein-gated inwardly rectifying potassium channel. *Nat Commun* (2019) 10(1):2008. doi: 10.1038/s41467-019-10038-x

68. Zamponi GW, Currie KP. Regulation of Ca(V)2 calcium channels by G protein coupled receptors. *Biochim Biophys Acta* (2013) 1828(7):1629–43. doi: 10.1016/j.bbamem.2012.10.004

69. Takeshita Y, Watanabe T, Sakata T, Munakata M, Ishibashi H, Akaike N. Histamine modulates high-voltage-activated calcium channels in neurons dissociated from the rat tuberomammillary nucleus. *Neuroscience* (1998) 87(4):797–805. doi: 10.1016/s0306-4522(98)00152-3

70. Silver RB, Mackins CJ, Smith NC, Koritchneva IL, Lefkowitz K, Lovenberg TW, et al. Coupling of histamine H3 receptors to neuronal Na+/H+ exchange: a novel protective mechanism in myocardial ischemia. *Proc Natl Acad Sci USA* (2001) 98 (5):2855–9. doi: 10.1073/pnas.051599198

71. van Willigen G, Nieuwland R, Nurnberg B, Gorter G, Akkerman JW. Negative regulation of the platelet Na+/H+ exchanger by trimeric G-proteins. *Eur J Biochem* (2000) 267(24):7102–8. doi: 10.1046/j.1432-1327.2000.01813.x

72. Fulop AK, Foldes A, Buzas E, Hegyi K, Miklos IH, Romics L, et al. Hyperleptinemia, visceral adiposity, and decreased glucose tolerance in mice with a targeted disruption of the histidine decarboxylase gene. *Endocrinology* (2003) 144 (10):4306–14. doi: 10.1210/en.2003-0222

73. Jorgensen EA, Vogelsang TW, Knigge U, Watanabe T, Warberg J, Kjaer A. Increased susceptibility to diet-induced obesity in histamine-deficient mice. *Neuroendocrinology* (2006) 83(5-6):289–94. doi: 10.1159/000095339

74. Kennedy L, Hargrove L, Demieville J, Bailey JM, Dar W, Polireddy K, et al. Knockout of l-histidine decarboxylase prevents cholangiocyte damage and hepatic fibrosis in mice subjected to high-fat diet feeding via disrupted Histamine/Leptin signaling. *Am J Pathol* (2018) 188(3):600–15. doi: 10.1016/j.ajpath.2017.11.016

75. Dere E, De Souza-Silva MA, Spieler RE, Lin JS, Ohtsu H, Haas HL, et al. Changes in motoric, exploratory and emotional behaviours and neuronal acetylcholine content and 5-HT turnover in histidine decarboxylase-KO mice. *Eur J Neurosci* (2004) 20 (4):1051–8. doi: 10.1111/j.1460-9568.2004.03546.x

76. Kubota Y, Ito C, Sakurai E, Sakurai E, Watanabe T, Ohtsu H. Increased methamphetamine-induced locomotor activity and behavioral sensitization in histamine-deficient mice. *J Neurochem* (2002) 83(4):837–45. doi: 10.1046/j.1471-4159.2002.01189.x

77. Acevedo SF, Ohtsu H, Benice TS, Rizk-Jackson A, Raber J. Age-dependent measures of anxiety and cognition in male histidine decarboxylase knockout (Hdc-/-) mice. *Brain Res* (2006) 1071(1):113–23. doi: 10.1016/j.brainres.2005.11.067

78. Ookuma K, Sakata T, Fukagawa K, Yoshimatsu H, Kurokawa M, Machidori H, et al. Neuronal histamine in the hypothalamus suppresses food intake in rats. *Brain Res* (1993) 628(1-2):235–42. doi: 10.1016/0006-8993(93)90960-u

79. Morimoto T, Yamamoto Y, Mobarakeh JI, Yanai K, Watanabe T, Watanabe T, et al. Involvement of the histaminergic system in leptin-induced suppression of food intake. *Physiol Behav* (1999) 67(5):679–83. doi: 10.1016/s0031-9384(99)00123-7

80. Toftegaard CL, Knigge U, Kjaer A, Warberg J. The role of hypothalamic histamine in leptin-induced suppression of short-term food intake in fasted rats. *Regul Peptides* (2003) 111(1-3):83–90. doi: 10.1016/s0167-0115(02)00260-4

81. Yoshimoto R, Miyamoto Y, Shimamura K, Ishihara A, Takahashi K, Kotani H, et al. Therapeutic potential of histamine H3 receptor agonist for the treatment of obesity and diabetes mellitus. *Proc Natl Acad Sci USA* (2006) 103(37):13866–71. doi: 10.1073/pnas.0506104103

82. Sakata T, Fukagawa K, Ookuma K, Fujimoto K, Yoshimatsu H, Yamatodani A, et al. Hypothalamic neuronal histamine modulates ad libitum feeding by rats. *Brain Res* (1990) 537(1-2):303–6. doi: 10.1016/0006-8993(90)90373-j

83. Fukagawa K, Sakata T, Shiraishi T, Yoshimatsu H, Fujimoto K, Ookuma K, et al. Neuronal histamine modulates feeding behavior through H1-receptor in rat hypothalamus. *Am J Physiol* (1989) 256(3 Pt 2):R605–11. doi: 10.1152/ajpregu.1989.256.3.R605

84. Lecklin A, Tuomisto L. The blockade of H1 receptors attenuates the suppression of feeding and diuresis induced by inhibition of histamine catabolism. *Pharmacol Biochem Behav* (1998) 59(3):753–8. doi: 10.1016/s0091-3057(97)00465-6

85. Orthen-Gambill N. Antihistaminic drugs increase feeding, while histidine suppresses feeding in rats. *Pharmacol Biochem Behav* (1988) 31(1):81–6. doi: 10.1016/0091-3057(88)90315-2

86. Comer SD, Haney M, Fischman MW, Foltin RW. Cyproheptadine produced modest increases in total caloric intake by humans. *Physiol Behav* (1997) 62(4):831–9. doi: 10.1016/s0031-9384(97)00246-1

87. Greaves MW. Antihistamines. *Dermatol Clin* (2001) 19(1):53–62. doi: 10.1016/S0733-8635(05)70229-1

88. Leurs R, Church MK, Taglialatela M. H1-antihistamines: inverse agonism, anti-inflammatory actions and cardiac effects. *Clin Exp Allergy* (2002) 32(4):489–98. doi: 10.1046/j.0954-7894.2002.01314.x

89. Inoue I, Yanai K, Kitamura D, Taniuchi I, Kobayashi T, Niimura K, et al. Impaired locomotor activity and exploratory behavior in mice lacking histamine H1 receptors. *Proc Natl Acad Sci USA* (1996) 93(23):13316–20. doi: 10.1073/pnas.93.23.13316

90. Masaki T, Yoshimatsu H, Chiba S, Watanabe T, Sakata T. Central infusion of histamine reduces fat accumulation and upregulates UCP family in leptin-resistant obese mice. *Diabetes* (2001) 50(2):376–84. doi: 10.2337/diabetes.50.2.376

91. Masaki T, Chiba S, Yasuda T, Noguchi H, Kakuma T, Watanabe T, et al. Involvement of hypothalamic histamine H1 receptor in the regulation of feeding rhythm and obesity. *Diabetes* (2004) 53(9):2250–60. doi: 10.2337/diabetes.53.9.2250

92. Masaki T, Yoshimatsu H, Chiba S, Watanabe T, Sakata T. Targeted disruption of histamine H1-receptor attenuates regulatory effects of leptin on feeding, adiposity, and UCP family in mice. *Diabetes* (2001) 50(2):385–91. doi: 10.2337/diabetes.50.2.385

93. Wang KY, Tanimoto A, Yamada S, Guo X, Ding Y, Watanabe T, et al. Histamine regulation in glucose and lipid metabolism via histamine receptors: model for nonalcoholic steatohepatitis in mice. *Am J Pathol* (2010) 177(2):713–23. doi: 10.2353/ajpath.2010.091198

94. Gotoh K, Masaki T, Chiba S, Higuchi K, Kakuma T, Shimizu H, et al. Hypothalamic neuronal histamine signaling in the estrogen deficiency-induced obesity. *J Neurochem* (2009) 110(6):1796–805. doi: 10.1111/j.1471-4159.2009.06272.x

95. Gotoh K, Fukagawa K, Fukagawa T, Noguchi H, Kakuma T, Sakata T, et al. Hypothalamic neuronal histamine mediates the thyrotropin-releasing hormone-induced suppression of food intake. *J Neurochem* (2007) 103(3):1102–10. doi: 10.1111/j.1471-4159.2007.04802.x

96. Gotoh K, Masaki T, Chiba S, Ando H, Shimasaki T, Mitsutomi K, et al. Nesfatin-1, corticotropin-releasing hormone, thyrotropin-releasing hormone, and neuronal histamine interact in the hypothalamus to regulate feeding behavior. *J Neurochem* (2013) 124(1):90–9. doi: 10.1111/jnc.12066

97. Ohinata K, Shimano T, Yamauchi R, Sakurada S, Yanai K, Yoshikawa M. The anorectic effect of neurotensin is mediated via a histamine H1 receptor in mice. *Peptides* (2004) 25(12):2135–8. doi: 10.1016/j.peptides.2004.07.009

98. Sakata T, Ookuma K, Fujimoto K, Fukagawa K, Yoshimatsu H. Histaminergic control of energy balance in rats. *Brain Res Bull* (1991) 27(3-4):371–5. doi: 10.1016/0361-9230(91)90127-6

99. Itowi N, Nagai K, Nakagawa H, Watanabe T, Wada H. Changes in the feeding behavior of rats elicited by histamine infusion. *Physiol Behav* (1988) 44(2):221–6. doi: 10.1016/0031-9384(88)90142-4

100. Doi T, Sakata T, Yoshimatsu H, Machidori H, Kurokawa M, Jayasekara LA, et al. Hypothalamic neuronal histamine regulates feeding circadian rhythm in rats. *Brain Res* (1994) 641(2):311–8. doi: 10.1016/0006-8993(94)90160-0

101. Stoa-Birketvedt G, Waldum HL, Vonen B, Florholmen J. Effect of cimetidine on basal and postprandial plasma concentrations of cholecystokinin and gastrin in humans. *Acta Physiol Scand* (1997) 159(4):321–5. doi: 10.1046/j.1365-201X.1997.00122.x

102. Stoa-Birketvedt G, Lovhaug N, Vonen B, Florholmen J. H2-receptor antagonist reduces food intake and weight gain in rats by non-gastric acid secretory mechanisms. *Acta Physiol Scand* (1997) 161(4):489–94. doi: 10.1046/j.1365-201X.1997.00249.x

103. Stoa-Birketvedt G. Effect of cimetidine suspension on appetite and weight in overweight subjects. *BMJ* (1993) 306(6885):1091–3. doi: 10.1136/bmj.306.6885.1091

104. Ruat M, Traiffort E, Bouthenet ML, Schwartz JC, Hirschfeld J, Buschauer A, et al. Reversible and irreversible labeling and autoradiographic localization of the cerebral histamine H2 receptor using [125I]iodinated probes. *Proc Natl Acad Sci USA* (1990) 87(5):1658–62. doi: 10.1073/pnas.87.5.1658

105. Clapp RH, Luckman SM. Proxyfan acts as a neutral antagonist of histamine H3 receptors in the feeding-related hypothalamic ventromedial nucleus. *Br J Pharmacol* (2012) 167(5):1099–110. doi: 10.1111/j.1476-5381.2012.02056.x

106. Chiba S, Itateyama E, Sakata T, Yoshimatsu H. Acute central administration of immepip, a histamine H3 receptor agonist, suppresses hypothalamic histamine release and elicits feeding behavior in rats. *Brain Res Bull* (2009) 79(1):37–40. doi: 10.1016/j.brainresbull.2008.12.012

107. Jethwa PH, Barrett P, Turnbull Y, Enright RA, Warner A, Murphy M, et al. The role of histamine 3 receptors in the control of food intake in a seasonal model of obesity: the Siberian hamster. *Behav Pharmacol* (2009) 20(2):155–65. doi: 10.1097/FBP.0b013e32832a8099

108. Malmlof K, Zaragoza F, Golozoubova V, Refsgaard HH, Cremers T, Raun K, et al. Influence of a selective histamine H3 receptor antagonist on hypothalamic neural activity, food intake and body weight. *Int J Obes (Lond)* (2005) 29(12):1402–12. doi: 10.1038/sj.ijo.0803036

109. Kotanska M, Mika K, Regula K, Szczepanska K, Szafarz M, Bednarski M, et al. KSK19 - novel histamine H3 receptor ligand reduces body weight in diet induced obese mice. *Biochem Pharmacol* (2019) 168:193–203. doi: 10.1016/j.bcp.2019.07.006

110. Kotanska M, Kuder KJ, Szczepanska K, Sapa J, Kiec-Kononowicz K. The histamine H3 receptor inverse agonist pitolisant reduces body weight in obese mice. *Naunyn-Schmiedeberg's Arch Pharmacol* (2018) 391(8):875–81. doi: 10.1007/s00210-018-1516-2

111. Hancock AA, Bennani YL, Bush EN, Esbenshade TA, Faghih R, Fox GB, et al. Antiobesity effects of a-331440, a novel non-imidazole histamine H3 receptor antagonist. *Eur J Pharmacol* (2004) 487(1-3):183–97. doi: 10.1016/j.ejphar.2004.01.015

112. Hancock AA, Diehl MS, Fey TA, Bush EN, Faghih R, Miller TR, et al. Antiobesity evaluation of histamine H3 receptor (H3R) antagonist analogs of a-331440 with improved safety and efficacy. *Inflamm Res* (2005) 54 (Suppl 1):S27–9. doi: 10.1007/s00011-004-0412-z

113. Itoh E, Fujimiya M, Inui A. Thioperamide, a histamine H3 receptor antagonist, suppresses NPY-but not dynorphin a-induced feeding in rats. *Regul Peptides* (1998) 75-76:373–6. doi: 10.1016/s0167-0115(98)00090-1

114. Malmlof K, Hastrup S, Wulff BS, Hansen BC, Peschke B, Jeppesen CB, et al. Antagonistic targeting of the histamine H3 receptor decreases caloric intake in higher mammalian species. *Biochem Pharmacol* (2007) 73(8):1237–42. doi: 10.1016/j.bcp.2007.01.034

115. Schneider EH, Neumann D, Seifert R. Modulation of behavior by the histaminergic system: lessons from HDC-, H3R- and H4R-deficient mice. *Neurosci Biobehav Rev* (2014) 47:101–21. doi: 10.1016/j.neubiorev.2014.07.020

116. Leurs R, Bakker RA, Timmerman H, de Esch IJ. The histamine H3 receptor: from gene cloning to H3 receptor drugs. *Nat Rev Drug Discovery* (2005) 4(2):107–20. doi: 10.1038/nrd1631

117. Schlicker E, Betz R, Gothert M. Histamine H3 receptor-mediated inhibition of serotonin release in the rat brain cortex. *Naunyn-Schmiedeberg's Arch Pharmacol* (1988) 337(5):588–90. doi: 10.1007/BF00182737

118. Smits RP, Mulder AH. Inhibitory effects of histamine on the release of serotonin and noradrenaline from rat brain slices. *Neurochem Int* (1991) 18(2):215–20. doi: 10.1016/0197-0186(91)90188-j

119. Schlicker E, Fink K, Detzner M, Gothert M. Histamine inhibits dopamine release in the mouse striatum via presynaptic H3 receptors. *J Neural Transm Gen Sect* (1993) 93(1):1–10. doi: 10.1007/BF01244933

120. Medhurst AD, Atkins AR, Beresford IJ, Brackenborough K, Briggs MA, Calver AR, et al. GSK189254, a novel H3 receptor antagonist that binds to histamine H3 receptors in alzheimer's disease brain and improves cognitive performance in preclinical models. *J Pharmacol Exp Ther* (2007) 321(3):1032–45. doi: 10.1124/jpet.107.120311

121. Schlicker E, Fink K, Hinterthaner M, Gothert M. Inhibition of noradrenaline release in the rat brain cortex via presynaptic H3 receptors. *Naunyn-Schmiedeberg's Arch Pharmacol* (1989) 340(6):633–8. doi: 10.1007/BF00717738

122. Ichinose M, Barnes PJ. Inhibitory histamine H3-receptors on cholinergic nerves in human airways. *Eur J Pharmacol* (1989) 163(2-3):383–6. doi: 10.1016/0014-2999(89)90212-4

123. Arrang JM, Drutel G, Schwartz JC. Characterization of histamine H3 receptors regulating acetylcholine release in rat entorhinal cortex. *Br J Pharmacol* (1995) 114(7):1518–22. doi: 10.1111/j.1476-5381.1995.tb13379.x

124. Garcia M, Floran B, Arias-Montano JA, Young JM, Aceves J. Histamine H3 receptor activation selectively inhibits dopamine D1 receptor-dependent [3H]GABA release from depolarization-stimulated slices of rat substantia nigra pars reticulata. *Neuroscience* (1997) 80(1):241–9. doi: 10.1016/s0306-4522(97)00100-0

125. Jang IS, Rhee JS, Watanabe T, Akaike N, Akaike N. Histaminergic modulation of GABAergic transmission in rat ventromedial hypothalamic neurones. *J Physiol* (2001) 534(Pt 3):791–803. doi: 10.1111/j.1469-7793.2001.00791.x

126. Barrett P, van den Top M, Wilson D, Mercer JG, Song CK, Bartness TJ, et al. Short photoperiod-induced decrease of histamine H3 receptors facilitates activation of hypothalamic neurons in the Siberian hamster. *Endocrinology* (2009) 150(8):3655–63. doi: 10.1210/en.2008-1620

127. Takahashi K, Suwa H, Ishikawa T, Kotani H. Targeted disruption of H3 receptors results in changes in brain histamine tone leading to an obese phenotype. *J Clin Invest* (2002) 110(12):1791–9. doi: 10.1172/JCI15784

128. Toyota H, Dugovic C, Koehl M, Laposky AD, Weber C, Ngo K, et al. Behavioral characterization of mice lacking histamine H(3) receptors. *Mol Pharmacol* (2002) 62(2):389–97. doi: 10.1124/mol.62.2.389

129. Nuutinen S, Lintunen M, Vanhanen J, Ojala T, Rozov S, Panula P. Evidence for the role of histamine H3 receptor in alcohol consumption and alcohol reward in mice. *Neuropsychopharmacol Off Publ Am Coll Neuropsychopharmacol* (2011) 36(10):2030–40. doi: 10.1038/npp.2011.90

130. Campfield LA, Smith FJ, Guisez Y, Devos R, Burn P. Recombinant mouse OB protein: evidence for a peripheral signal linking adiposity and central neural networks. *Science* (1995) 269(5223):546–9. doi: 10.1126/science.7624778

131. Frederich RC, Hamann A, Anderson S, Lollmann B, Lowell BB, Flier JS. Leptin levels reflect body lipid content in mice: evidence for diet-induced resistance to leptin action. *Nat Med* (1995) 1(12):1311–4. doi: 10.1038/nm1295-1311

132. Ahima RS, Prabakaran D, Mantzoros C, Qu D, Lowell B, Maratos-Flier E, et al. Role of leptin in the neuroendocrine response to fasting. *Nature* (1996) 382(6588):250–2. doi: 10.1038/382250a0

133. Yoshimatsu H, Itateyama E, Kondou S, Tajima D, Himeno K, Hidaka S, et al. Hypothalamic neuronal histamine as a target of leptin in feeding behavior. *Diabetes* (1999) 48(12):2286–91. doi: 10.2337/diabetes.48.12.2286

134. Hegyi K, Fulop KA, Kovacs KJ, Falus A, Toth S. High leptin level is accompanied with decreased long leptin receptor transcript in histamine deficient transgenic mice. *Immunol Lett* (2004) 92(1-2):193–7. doi: 10.1016/j.imlet.2003.11.029

135. Elmquist JK, Bjorbaek C, Ahima RS, Flier JS, Saper CB. Distributions of leptin receptor mRNA isoforms in the rat brain. *J Comp Neurol* (1998) 395(4):535–47. doi: 10.1002/(SICI)1096-9861(19980615)395:4<535::AID-CNE9>3.0.CO;2-2

136. Cui H, Sohn JW, Gautron L, Funahashi H, Williams KW, Elmquist JK, et al. Neuroanatomy of melanocortin-4 receptor pathway in the lateral hypothalamic area. *J Comp Neurol* (2012) 520(18):4168–83. doi: 10.1002/cne.23145

137. Mickelsen LE, Kolling FW, Chimileski BR, Fujita A, Norris C, Chen K, et al. Neurochemical heterogeneity among lateral hypothalamic Hypocretin/Orexin and melanin-concentrating hormone neurons identified through single-cell gene expression analysis. *eNeuro* (2017) 4(5):1–24. doi: 10.1523/ENEURO.0013-17.2017

138. Leinninger GM, Jo YH, Leshan RL, Louis GW, Yang H, Barrera JG, et al. Leptin acts via leptin receptor-expressing lateral hypothalamic neurons to modulate the mesolimbic dopamine system and suppress feeding. *Cell Metab* (2009) 10(2):89–98. doi: 10.1016/j.cmet.2009.06.011

139. Venner A, De Luca R, Sohn LT, Bandaru SS, Verstegen AMJ, Arrigoni E, et al. An inhibitory lateral hypothalamic-preoptic circuit mediates rapid arousals from sleep. *Curr Biol CB* (2019) 29(24):4155–68 e5. doi: 10.1016/j.cub.2019.10.026

140. Bonnavion P, Mickelsen LE, Fujita A, de Lecea L, Jackson AC. Hubs and spokes of the lateral hypothalamus: cell types, circuits and behaviour. *J Physiol* (2016) 594 (22):6443–62. doi: 10.1113/JP271946

141. Cone RD. Anatomy and regulation of the central melanocortin system. *Nat Neurosci* (2005) 8(5):571–8. doi: 10.1038/nn1455

142. Schwartz MW, Woods SC, Porte D, Seeley RJ, Baskin DG. Central nervous system control of food intake. *Nature* (2000) 404(6778):661–71. doi: 10.1038/35007534

143. Millington GW. The role of proopiomelanocortin (POMC) neurones in feeding behaviour. *Nutr Metab* (2007) 4:18. doi: 10.1186/1743-7075-4-18

144. Belgardt BF, Okamura T, Bruning JC. Hormone and glucose signalling in POMC and AgRP neurons. *J Physiol* (2009) 587(Pt 22):5305–14. doi: 10.1113/jphysiol.2009.179192

145. Ellacott KL, Cone RD. The role of the central melanocortin system in the regulation of food intake and energy homeostasis: lessons from mouse models. *Philos Trans R Soc Lond B Biol Sci* (2006) 361(1471):1265–74. doi: 10.1098/rstb.2006.1861

146. Mountjoy KG. Pro-opiomelanocortin (POMC) neurones, POMC-derived peptides, melanocortin receptors and obesity: how understanding of this system has changed over the last decade. *J Neuroendocrinol* (2015) 27(6):406–18. doi: 10.1111/jne.12285

147. Michael NJ, Caron A, Castorena CM, Lee CE, Lee S, Zigman JM, et al. Melanocortin regulation of histaminergic neurons via perifornical lateral hypothalamic melanocortin 4 receptors. *Mol Metab* (2020) 35:100956. doi: 10.1016/j.molmet.2020.01.020

148. Zhu H, Aryal DK, Olsen RH, Urban DJ, Swearingen A, Forbes S, et al. Cre-dependent DREADD (Designer receptors exclusively activated by designer drugs) mice. *Genesis* (2016) 54(8):439–46. doi: 10.1002/dvg.22949

149. Roth BL. DREADDs for neuroscientists. *Neuron* (2016) 89(4):683–94. doi: 10.1016/j.neuron.2016.01.040

150. Armbruster BN, Li X, Pausch MH, Herlitze S, Roth BL. Evolving the lock to fit the key to create a family of G protein-coupled receptors potently activated by an inert ligand. *Proc Natl Acad Sci United States America* (2007) 104(12):5163–8. doi: 10.1073/pnas.0700293104

151. Nakazato M, Murakami N, Date Y, Kojima M, Matsuo H, Kangawa K, et al. A role for ghrelin in the central regulation of feeding. *Nature* (2001) 409(6817):194–8. doi: 10.1038/35051587

152. Zigman JM, Jones JE, Lee CE, Saper CB, Elmquist JK. Expression of ghrelin receptor mRNA in the rat and the mouse brain. *J Comp Neurol* (2006) 494(3):528–48. doi: 10.1002/cne.20823

153. Campbell JN, Macosko EZ, Fenselau H, Pers TH, Lyubetskaya A, Tenen D, et al. A molecular census of arcuate hypothalamus and median eminence cell types. *Nat Neurosci* (2017) 20(3):484–96. doi: 10.1038/nn.4495

154. Gotoh K, Fukagawa K, Fukagawa T, Noguchi H, Kakuma T, Sakata T, et al. Glucagon-like peptide-1, corticotropin-releasing hormone, and hypothalamic neuronal histamine interact in the leptin-signaling pathway to regulate feeding behavior. *FASEB J Off Publ Fed Am Societies Exp Biol* (2005) 19(9):1131–3. doi: 10.1096/fj.04-2384fje

155. Ten Kulve JS, van Bloemendaal L, Balesar R, RG IJ, Swaab DF, Diamant M, et al. Decreased hypothalamic glucagon-like peptide-1 receptor expression in type 2 diabetes patients. *J Clin Endocrinol Metab* (2016) 101(5):2122–9. doi: 10.1210/jc.2015-3291

156. Jensen CB, Pyke C, Rasch MG, Dahl AB, Knudsen LB, Secher A. Characterization of the glucagonlike peptide-1 receptor in Male mouse brain using a novel antibody and *In situ* hybridization. *Endocrinology* (2018) 159(2):665–75. doi: 10.1210/en.2017-00812

157. Gu G, Roland B, Tomaselli K, Dolman CS, Lowe C, Heilig JS. Glucagon-like peptide-1 in the rat brain: distribution of expression and functional implication. *J Comp Neurol* (2013) 521(10):2235–61. doi: 10.1002/cne.23282

158. Salinas CBG, Lu TT, Gabery S, Marstal K, Alanentalo T, Mercer AJ, et al. Integrated brain atlas for unbiased mapping of nervous system effects following liraglutide treatment. *Sci Rep* (2018) 8(1):10310. doi: 10.1038/s41598-018-28496-6

159. Lopez-Ferreras L, Richard JE, Noble EE, Eerola K, Anderberg RH, Olandersson K, et al. Lateral hypothalamic GLP-1 receptors are critical for the control of food reinforcement, ingestive behavior and body weight. *Mol Psychiatry* (2018) 23(5):1157–68. doi: 10.1038/mp.2017.187

160. Miklos IH, Kovacs KJ. Functional heterogeneity of the responses of histaminergic neuron subpopulations to various stress challenges. *Eur J Neurosci* (2003) 18(11):3069–79. doi: 10.1111/j.1460-9568.2003.03033.x

161. Sakurai T, Amemiya A, Ishii M, Matsuzaki I, Chemelli RM, Tanaka H, et al. Orexins and orexin receptors: a family of hypothalamic neuropeptides and G protein-coupled receptors that regulate feeding behavior. *Cell* (1998) 92(4):573–85. doi: 10.1016/s0092-8674(00)80949-6

162. de Lecea L, Kilduff TS, Peyron C, Gao X, Foye PE, Danielson PE, et al. The hypocretins: hypothalamus-specific peptides with neuroexcitatory activity. *PNAS* (1998) 95(1):322–7. doi: 10.1073/pnas.95.1.322

163. Mickelsen LE, Flynn WF, Springer K, Wilson L, Beltrami EJ, Bolisetty M, et al. Cellular taxonomy and spatial organization of the murine ventral posterior hypothalamus. *eLife* (2020) 9:e58901. doi: 10.7554/eLife.58901

164. Eriksson KS, Sergeeva O, Brown RE, Haas HL. Orexin/hypocretin excites the histaminergic neurons of the tuberomammillary nucleus. *J Neurosci Off J Soc Neurosci* (2001) 21(23):9273–9. doi: 10.1523/JNEUROSCI.21-23-09273.2001

165. Mochizuki T, Arrigoni E, Marcus JN, Clark EL, Yamamoto M, Honer M, et al. Orexin receptor 2 expression in the posterior hypothalamus rescues sleepiness in narcoleptic mice. *Proc Natl Acad Sci USA* (2000) 108(11):4471–6. doi: 10.1073/pnas.1012456108

166. Huang ZL, Qu WM, Li WD, Mochizuki T, Eguchi N, Watanabe T, et al. Arousal effect of orexin a depends on activation of the histaminergic system. *Proc Natl Acad Sci United States America* (2001) 98(17):9965–70. doi: 10.1073/pnas.181330998

167. Schone C, Apergis-Schoute J, Sakurai T, Adamantidis A, Burdakov D. Coreleased orexin and glutamate evoke nonredundant spike outputs and computations in histamine neurons. *Cell Rep* (2014) 7(3):697–704. doi: 10.1016/j.celrep.2014.03.055

168. Wetterling T. Bodyweight gain with atypical antipsychotics. a comparative review. *Drug Saf* (2001) 24(1):59–73. doi: 10.2165/00002018-200124010-00005

169. Reynolds GP, Kirk SL. Metabolic side effects of antipsychotic drug treatment–pharmacological mechanisms. *Pharmacol Ther* (2010) 125(1):169–79. doi: 10.1016/j.pharmthera.2009.10.010

170. Kroeze WK, Hufeisen SJ, Popadak BA, Renock SM, Steinberg S, Ernsberger P, et al. H1-histamine receptor affinity predicts short-term weight gain for typical and atypical antipsychotic drugs. *Neuropsychopharmacol Off Publ Am Coll Neuropsychopharmacol* (2003) 28(3):519–26. doi: 10.1038/sj.npp.1300027

171. Kim SF, Huang AS, Snowman AM, Teuscher C, Snyder SH. Antipsychotic drug-induced weight gain mediated by histamine H1 receptor-linked activation of hypothalamic AMP-kinase. *Proc Natl Acad Sci United States America* (2007) 104 (9):3456–9. doi: 10.1073/pnas.0611417104

172. Wirshing DA, Wirshing WC, Kysar L, Berisford MA, Goldstein D, Pashdag J, et al. Novel antipsychotics: comparison of weight gain liabilities. *J Clin Psychiatry* (1999) 60(6):358–63. doi: 10.4088/JCP.v60n0602

173. Humbert-Claude M, Davenas E, Gbahou F, Vincent L, Arrang JM. Involvement of histamine receptors in the atypical antipsychotic profile of clozapine: a reassessment *in vitro* and in vivo. *Psychopharmacology* (2012) 220(1):225–41. doi: 10.1007/s00213-011-2471-5

174. Gothelf D, Falk B, Singer P, Kairi M, Phillip M, Zigel L, et al. Weight gain associated with increased food intake and low habitual activity levels in male adolescent schizophrenic inpatients treated with olanzapine. *Am J Psychiatry* (2002) 159(6):1055–7. doi: 10.1176/appi.ajp.159.6.1055

175. Fountaine RJ, Taylor AE, Mancuso JP, Greenway FL, Byerley LO, Smith SR, et al. Increased food intake and energy expenditure following administration of olanzapine to healthy men. *Obes (Silver Spring)* (2010) 18(8):1646–51. doi: 10.1038/oby.2010.6

176. Davoodi N, Kalinichev M, Korneev SA, Clifton PG. Hyperphagia and increased meal size are responsible for weight gain in rats treated sub-chronically with olanzapine. *Psychopharmacol (Berl)* (2009) 203(4):693–702. doi: 10.1007/s00213-008-1415-1

177. Coccurello R, Caprioli A, Ghirardi O, Conti R, Ciani B, Daniele S, et al. Chronic administration of olanzapine induces metabolic and food intake alterations: a mouse model of the atypical antipsychotic-associated adverse effects. *Psychopharmacol (Berl)* (2006) 186(4):561–71. doi: 10.1007/s00213-006-0368-5

178. Han M, Deng C, Burne TH, Newell KA, Huang XF. Short- and long-term effects of antipsychotic drug treatment on weight gain and H1 receptor expression. *Psychoneuroendocrinology* (2008) 33(5):569–80. doi: 10.1016/j.psyneuen.2008.01.018

179. Chen X, Yu Y, Zheng P, Jin T, He M, Zheng M, et al. Olanzapine increases AMPK-NPY orexigenic signaling by disrupting H1R-GHSR1a interaction in the hypothalamic neurons of mice. *Psychoneuroendocrinology* (2020) 114:104594. doi: 10.1016/j.psyneuen.2020.104594

180. Poyurovsky M, Fuchs C, Pashinian A, Levi A, Weizman R, Weizman A. Reducing antipsychotic-induced weight gain in schizophrenia: a double-blind placebo-controlled study of reboxetine-betahistine combination. *Psychopharmacol (Berl)* (2013) 226(3):615–22. doi: 10.1007/s00213-012-2935-2

181. Esbenshade TA, Fox GB, Cowart MD. Histamine H3 receptor antagonists: preclinical promise for treating obesity and cognitive disorders. *Mol Interv* (2006) 6 (2):77–88, 59. doi: 10.1124/mi.6.2.5

182. Hancock AA, Brune ME. Assessment of pharmacology and potential anti-obesity properties of H3 receptor antagonists/inverse agonists. *Expert Opin Investig Drugs* (2005) 14(3):223–41. doi: 10.1517/13543784.14.3.223

183. Celanire S, Wijtmans M, Talaga P, Leurs R, de Esch IJ. Keynote review: histamine H3 receptor antagonists reach out for the clinic. *Drug Discov Today* (2005) 10(23-24):1613–27. doi: 10.1016/S1359-6446(05)03625-1

184. Hancock AA, Diehl MS, Faghih R, Bush EN, Krueger KM, Krishna G, et al. *In vitro* optimization of structure activity relationships of analogues of a-331440 combining radioligand receptor binding assays and micronucleus assays of potential antiobesity histamine H3 receptor antagonists. *Basic Clin Pharmacol Toxicol* (2004) 95 (3):144–52. doi: 10.1111/j.1742-7843.2004.950307.x

185. Barbier AJ, Berridge C, Dugovic C, Laposky AD, Wilson SJ, Boggs J, et al. Acute wake-promoting actions of JNJ-5207852, a novel, diamine-based H3 antagonist. *Br J Pharmacol* (2004) 143(5):649–61. doi: 10.1038/sj.bjp.0705964

186. Barak N, Greenway FL, Fujioka K, Aronne LJ, Kushner RF. Effect of histaminergic manipulation on weight in obese adults: a randomized placebo controlled trial. *Int J Obes (Lond)* (2008) 32(10):1559–65. doi: 10.1038/ijo.2008.135

187. Ali AH, Yanoff LB, Stern EA, Akomeah A, Courville A, Kozlosky M, et al. Acute effects of betahistine hydrochloride on food intake and appetite in obese women: a randomized, placebo-controlled trial. *Am J Clin Nutr* (2010) 92(6):1290–7. doi: 10.3945/ajcn.110.001586

188. Ligneau X, Morisset S, Tardivel-Lacombe J, Gbahou F, Ganellin CR, Stark H, et al. Distinct pharmacology of rat and human histamine H(3) receptors: role of two amino acids in the third transmembrane domain. *Br J Pharmacol* (2000) 131(7):1247–50. doi: 10.1038/sj.bjp.0703712

189. Provensi G, Blandina P, Passani MB. The histaminergic system as a target for the prevention of obesity and metabolic syndrome. *Neuropharmacology* (2016) 106:3–12. doi: 10.1016/j.neuropharm.2015.07.002

190. Szczepanska K, Pockes S, Podlewska S, Horing C, Mika K, Latacz G, et al. Structural modifications in the distal, regulatory region of histamine H(3) receptor antagonists leading to the identification of a potent anti-obesity agent. *Eur J Med Chem* (2021) 213:113041. doi: 10.1016/j.ejmech.2020.113041

191. Kumar A, Pasam VR, Thakur RK, Singh M, Singh K, Shukla M, et al. Novel tetrahydroquinazolinamines as selective histamine 3 receptor antagonists for the treatment of obesity. *J Med Chem* (2019) 62(9):4638–55. doi: 10.1021/acs.jmedchem.9b00241

192. Vanni-Mercier G, Sakai K, Jouvet M. Neurons specifiques de l'eveil dans l'hypothalamus posterieur du chat. *C R Acad Sci III* (1984) 298(7):195–200.

193. Mochizuki T, Yamatodani A, Okakura K, Horii A, Inagaki N, Wada H. Circadian rhythm of histamine release from the hypothalamus of freely moving rats. *Physiol Behav* (1992) 51(2):391–4. doi: 10.1016/0031-9384(92)90157-w

194. Tuomisto L, Tuomisto J. Diurnal variations in brain and pituitary histamine and histamine-n-methyltransferase in the rat and guinea pig. *Med Biol* (1982) 60(4):204–9.

195. Strecker RE, Nalwalk J, Dauphin LJ, Thakkar MM, Chen Y, Ramesh V, et al. Extracellular histamine levels in the feline preoptic/anterior hypothalamic area during natural sleep-wakefulness and prolonged wakefulness: an *in vivo* microdialysis study. *Neuroscience* (2002) 113(3):663–70. doi: 10.1016/s0306-4522(02)00158-6

196. Dong H, Li M, Yan Y, Qian T, Lin Y, Ma X, et al. Genetically encoded sensors for measuring histamine release both in vitro and *in vivo*. *Neuron* (2023) 11(10):1564–76.e6. doi: 10.1016/j.neuron.2023.02.024

197. Michael NJ, Zigman JM, Williams KW, Elmquist JK. Electrophysiological properties of genetically identified histaminergic neurons. *Neuroscience* (2020) 444:183–95. doi: 10.1016/j.neuroscience.2020.06.031

198. Sergeeva OA, Eriksson KS, Sharonova IN, Vorobjev VS, Haas HL. GABA(A) receptor heterogeneity in histaminergic neurons. *Eur J Neurosci* (2002) 16(8):1472–82. doi: 10.1046/j.1460-9568.2002.02221.x

199. Giannoni P, Passani MB, Nosi D, Chazot PL, Shenton FC, Medhurst AD, et al. Heterogeneity of histaminergic neurons in the tuberomammillary nucleus of the rat. *Eur J Neurosci* (2009) 29(12):2363–74. doi: 10.1111/j.1460-9568.2009.06765.x

200. Prell GD, Green JP. Histamine as a neuroregulator. *Annu Rev Neurosci* (1986) 9:209–54. doi: 10.1146/annurev.ne.09.030186.001233

201. Takagi H, Morishima Y, Matsuyama T, Hayashi H, Watanabe T, Wada H. Histaminergic axons in the neostriatum and cerebral cortex of the rat: a correlated light and electron microscopic immunocytochemical study using histidine decarboxylase as a marker. *Brain Res* (1986) 364(1):114–23. doi: 10.1016/0006-8993(86)90992-3

202. Tohyama M, Tamiya R, Inagaki N, Tagaki H. Morphology of histaminergic neurons with histidine decarboxy-lase as a marker. In: Watanabe T, Wada H, editors. *Histaminergic neurons: morphology and function*. Boca Raton, FL: CRC Press (1991). p. 107–26.

203. Wada H, Inagaki N, Yamatodani A, Watanabe T. Is the histaminergic neuron system a regulatory center for whole-brain activity? *Trends Neurosci* (1991) 14(9):415–8. doi: 10.1016/0166-2236(91)90034-r

frontiers | Frontiers in Endocrinology

TYPE Original Research
PUBLISHED 13 July 2023
DOI 10.3389/fendo.2023.1131995

OPEN ACCESS

EDITED BY
Alexandre Benani,
Centre National de la Recherche Scientifique (CNRS), France

REVIEWED BY
Elizabeth Hampson,
Western University, Canada
Katherine Bottenhorn,
Florida International University, United States
Anira Escrichs,
Pompeu Fabra University, Spain

*CORRESPONDENCE
Esmeralda Hidalgo-Lopez
esmehl@umich.edu
Belinda Pletzer
belinda.pletzer@plus.ac.at

RECEIVED 26 December 2022
ACCEPTED 09 June 2023
PUBLISHED 13 July 2023

CITATION
Hidalgo-Lopez E, Noachtar I and Pletzer B (2023) Hormonal contraceptive exposure relates to changes in resting state functional connectivity of anterior cingulate cortex and amygdala. *Front. Endocrinol.* 14:1131995. doi: 10.3389/fendo.2023.1131995

Hormonal contraceptive exposure relates to changes in resting state functional connectivity of anterior cingulate cortex and amygdala

Esmeralda Hidalgo-Lopez[1,2]*, Isabel Noachtar[1,2] and Belinda Pletzer[1,2]*

[1]Centre for Cognitive Neuroscience, University of Salzburg, Salzburg, Austria, [2]Department of Psychology, University of Salzburg, Salzburg, Austria

Introduction: Hormonal contraceptives (HCs), nowadays one of the most used contraceptive methods, downregulate endogenous ovarian hormones, which have multiple plastic effects in the adult brain. HCs usually contain a synthetic estrogen, ethinyl-estradiol, and a synthetic progestin, which can be classified as androgenic or anti-androgenic, depending on their interaction with androgen receptors. Both the anterior cingulate cortex (ACC) and the amygdala express steroid receptors and have shown differential functionality depending on the hormonal status of the participant and the use of HC. In this work, we investigated for the first time the relationship between ACC and amygdala resting state functional connectivity (rs-FC) and HC use duration, while controlling for progestin androgenicity.

Methods: A total of 231 healthy young women participated in five different magnetic resonance imaging studies and were included in the final analysis. The relation between HC use duration and (i) gray matter volume, (ii) fractional amplitude of low-frequency fluctuations, and (iii) seed-based connectivity during resting state in the amygdalae and ACC was investigated in this large sample of women.

Results: In general, rs-FC of the amygdalae with frontal areas, and between the ACC and temporoparietal areas, decreased the longer the HC exposure and independently of the progestin's androgenicity. The type of HC's progestin did show a differential effect in the gray matter volume of left ACC and the connectivity between bilateral ACC and the right inferior frontal gyrus.

KEYWORDS

resting state fMRI, brain connectivity, hormonal contraceptives, progestins, amygdala, anterior cingulate cortex

1 Introduction

Consistent evidence has demonstrated ongoing plastic changes in the adult brain, including those related to ovarian hormones (1, 2). From neurogenesis to remyelination, the neuroactive actions of ovarian hormones are vast and still not fully understood (1, 3). In humans, brain network dynamics are also affected by ovarian hormone fluctuations, and more importantly, these effects appear to be suppressed during the use of hormonal contraceptives (HCs) (4). While women experienced physiological fluctuations of ovarian hormones throughout their adulthood, HCs, nowadays one of the most used contraceptive methods (5), abolish this cycle. In general, HCs downregulate the hypothalamic–pituitary–gonadal axis, decreasing the endogenous ovarian hormones' production and maintaining their levels low, comparable to the levels observed in naturally cycling women during menses (6). In general, the synthetic hormones' bioavailability remains stable during the active HC use and prevents follicle growth and ovulation (7, 8). HCs usually contain a synthetic estrogen, ethinyl-estradiol, but on the side of synthetic progestins, the range of compounds is wider. The latter can be classified into androgenic or anti-androgenic, depending on their interaction with androgen receptors (9, 10). On the one hand, those progestins derived from 19-nortestosterone (i.e., norethindrone, desogestrel, gestodene, and norgestimate) can be classified as androgenic due to their rapid metabolism to levonorgestrel, which demonstrates agonistic binding to the androgen receptor (11). On the other hand, those progestins derived from spironolactone (i.e., drospirenone), or from 17-hydroxyprogesterone (i.e., chlormadinone acetate or cyproterone acetate), can be classified as anti-androgenic due to their antagonistic actions at the androgen receptor (12). Additionally, dienogest, although derived from 19-nortestosterone, also exhibits anti-androgenic activities (13).

Despite the sparsity of literature regarding HC effects on the female brain, animal research and a few human studies hint at structural (14, 15) and functional changes (see reviews by 16, 17) related to HC use. Among the most consistently reported brain areas in ovarian hormones research are those belonging to the salience network. This network, crucial for emotion processing, is of special interest given that adverse mood effects are the major reason to discontinue HC use (18, 19). Both the anterior cingulate cortex (ACC) and the amygdala, at the core of this network, express steroid receptors (1, 3), and have shown differential functionality depending on the hormonal status of the participant (20–22). ACC not only shows differences in activation across the menstrual cycle, but also has been reported to be thinner (23) and to increase its activation to emotional stimuli (24) in HC users compared to naturally cycling women. Likewise, amygdala structure (25) and response to emotional stimuli differs between naturally cycling women and HC users (26), and across the menstrual cycle (27, 28).

Resting state functional connectivity (rs-FC), assessed as the correlated activity of different brain areas in the absence of an explicit task, offers a valuable measure to understand the brain's intrinsic network organization (29, 30). Nowadays, we can investigate changes in rs-FC to disentangle the dynamics of the healthy brain functioning. Within this framework, neuroimaging studies have shown differences in the intrinsic connectivity of the salience network across menstrual cycle phase, and between naturally cycling women and HC users (for a review, see 16). Across the natural menstrual cycle, rs-FC between the ACC with the middle frontal, superior temporal, transverse temporal, and postcentral gyri (31) increased during the luteal phase when progesterone levels are high (31). In a recent study, we also described increased effective connectivity from the middle frontal gyrus to the ACC, but decreased effective connectivity from the medial prefrontal cortex to the ACC during the luteal phase (22). However, decreased rs-FC between ACC, middle frontal gyrus, and cuneus has also been described for luteal woman (32). Also, during this phase, the amygdala rs-FC with the right middle frontal gyrus, superior frontal gyrus, and paracentral lobule has been reported to increase (31). During the late luteal phase, though, rs-FC between the left amygdala and left angular gyrus and posterior cingulate cortex was decreased compared to the mid-follicular phase (33).

Regarding the HC effects on rs-FC, Engman et al. (31) investigated changes in the ACC and amygdala connectivity in response to a levonorgestrel containing HC in a randomized, placebo-controlled trial. They observed an increased rs-FC of the right ACC with the precuneus and left superior frontal gyrus and a decreased rs-FC between the right amygdala and the left postcentral gyrus, during HC intake (31). Additionally, between-group comparisons revealed increased rs-FC between the left ACC and precuneus, and left amygdala and left postcentral gyrus and precuneus for the naturally cycling luteal women compared to the HC users (31). Active HC users have also shown an increased rs-FC of the ACC within the salience network compared to naturally cycling women (34), but decreased rs-FC between the salience network and the left middle frontal gyrus, compared to both HC inactive phase and naturally cycling women (32). Lisofsky et al. (25) followed women before and after the start of HC use and reported decreased rs-FC between the left amygdala and the right IFG. However, these latter studies did not control for the androgenicity of the HC used, and it remains unclear whether androgenic and anti-androgenic HCs differentially modulate rs-FC of the salience network. Given that exogenous testosterone in women decreases connectivity between ACC and the inferior frontal gyrus (35), and between amygdala and the orbitofrontal cortex (36), it seems relevant to account for the type of progestin that the HCs contain. In this work, we investigated for the first time the relationship between ACC/amygdala rs-FC and HC use, while controlling for the progestin's androgenicity.

Furthermore, while Engman et al. (31) investigated the effects of short-term HC-use (one intake cycle) on rs-FC of the salience network nodes, Petersen et al. (32) included long-term HC users. Given that results differ between the two studies, it is an interesting question whether changes in rs-FC of the salience network accumulate over time. Previous animal research has shown cumulative effects of sex steroids on the brain substrate, ranging from molecular to cellular levels (see reviews: 3, 37–40). In rodents, DNA de-methylation through the estrogen receptor is time-dependent (38), while continuous vs. sequential administration of progesterone elicits a differential gene expression profile in the hippocampus (40). After neural damage,

progesterone-dependent recovery is affected by treatment duration, alongside differential effects on the cytoarchitectural structure (39). Relatedly, time-dependent effects on synaptic transmission are mediated by changes in shape and density of dendrites (39) and neurotransmitter's receptors (41). Other steroids' cumulative effects found in rodents include changes in the glial cells and consequent myelination, with an important role in neuroprotection (37, 42). Finally, and given that the reversibility of HC effects on the brain is still in question, we further explored if the effects found in HC users were replicated in previous HC users. Accordingly, we here opted for studying in a large sample of women those time-dependent associations that may accumulate over HC use duration, differentiating between androgenic and anti-androgenic progestins. In addition to addressing the temporal dynamics of HC effect or rs-FC of the salience network, the pattern of associations might shed some light into the endocrinological mechanisms underlying these effects. At the moment, it remains unclear whether changes in rs-FC during HC use are related to the progestagenic or androgenic/anti-androgenic actions of the progestin component, estrogenic actions of ethinyl-estradiol, or a by-product of HC effects on endogenous neurosteroids.

Given that the contraceptive effects of HC depend largely on the progestin component, the focus with regard to neuroplastic changes in response to HC is usually on the activation of progesterone receptors. Synthetic progestins possess a higher binding affinity for intracellular progesterone receptors than the endogenous hormone (43). If cumulative effects of HC on the salience network depend on progestagenic actions, we can expect effects as observed in the luteal phase (e.g., increased connectivity of the ACC and amygdalae to the middle frontal gyrus; 22, 31) to increase with increasing use duration, irrespective of the androgenicity of the progestin. Furthermore, one important consideration is that most of the effects of endogenous progesterone are exerted through its metabolite allopregnanolone. Synthetic progestins, however, are not metabolized to allopregnanolone, which is a potent modulator of one of the receptors for inhibitory neurotransmitter γ-aminobutyric acid (GABA) (for review, see 40). Although women under HC have increased synthetic progestin levels with high affinity for progesterone receptors, their circulating allopregnanolone levels seem to be decreased (androgenic HC: 44; anti-androgenic HC: 45). Accordingly, if previously reported effects along the natural menstrual cycle were related to endogenous allopregnanolone rather than actions on the progesterone receptor, we expect longer HC duration, related to decreased ACC connectivity with the temporal lobe, middle frontal and postcentral gyri connectivity (22, 31) while increased ACC connectivity with the medial prefrontal cortex (22). Likewise, for the amygdala, decreased connectivity with the middle, superior frontal gyrus and paracentral lobule (31) would be expected. These hypotheses are in line with results obtained from long-term HC users in previous studies (32). On the other hand, animal research hints a more complex scenario, in which allopregnanolone levels depend on the type of progestin (see systematic review, 46). In general, while androgenic progestins decrease allopregnanolone levels in the brain; anti-androgenic progestins increase them. If this is also the case in humans, further differential effects are expected for androgenic vs. anti-androgenic HCs related to levels of allopregnanolone.

More importantly, related to the differential modulation of androgen receptors by different progestins, opposite associations to the duration of androgenic vs. anti-androgenic progestin use can be expected. Although we would expect androgenic HC to have similar effects as testosterone (e.g., decreased ACC–inferior frontal gyrus and amygdala–orbitofrontal cortex connectivity; 35, 36), it is noteworthy that endogenous testosterone is metabolized to estradiol, acting also on estrogen receptors (47). Regarding estrogenic effects on the salience network, higher rs-FC between the amygdala and prefrontal and temporal areas has been reported after an estradiol challenge in postmenopausal women (48). Within naturally cycling women, increased connectivity between the amygdala and cuneus, inferior frontal fyrus, precentral gyrus, supramarginal gyrus, and temporal lobe has been described in the presence of high estradiol levels, while increased connectivity between amygdalae and the ACC has been described for low estradiol levels (49). Accordingly, if cumulative HC effects on the salience network are derived from the estrogenic actions of ethinyl-estradiol, we expect connectivity between the amygdalae and fronto-temporal areas to increase with use duration irrespective of the androgenicity of the progestin.

In general, a decreased rs-FC of the ROIs with frontal areas like middle frontal gyrus and inferior frontal gyrus is expected, related to longer HC exposure (25, 32). We also expect an increased rs-FC of the ACC with the precuneus and left superior frontal gyrus and a decreased rs-FC between the amygdalae and the left postcentral gyrus and precuneus, especially for HC with androgenic progestins (31). Further differential effects of androgenic vs. anti-androgenic HC will be explored.

2 Methods

2.1 Participants and procedure

A total of 231 healthy young women (105 current HC users and 126 past HC users and currently naturally cycling) were included in the final analysis, from five different MRI studies (50–52). Participants were recruited via flyers at the University of Salzburg and via online advertisements. Most of the participants were university students and all of them were right-handed. Main exclusionary criteria for women were neurological, psychiatric, or endocrine disorders, any medication intake, or any brain abnormalities displayed on structural MRI. Note that differential brain organization may underlie women's susceptibility to HC adverse mood side effects, which is the major reason for HC discontinuation (19, 53).

In all studies, scanning sessions were scheduled in the active phase of HC use for current HC users (second or third week of the intake cycle), or locked to their menstrual cycle for naturally cycling women (past users). For the latter, the majority of sessions were scheduled during the early follicular phase (cycle days 1–8), except for six participants that were in their mid-luteal phase (3–10 days

before onset of next menses). Participants had to confirm the onset of next menses in retrospect.

As part of our standard screening questionnaire, information on previous contraceptive use was collected. The participants were subdivided into HC users with current androgenic HC use (A-HC; n = 62) and current anti-androgenic HC use (AA-HC; n = 43), and naturally cycling women with previous androgenic HC use (A-NC; n = 45), previous anti-androgenic HC use (AA-NC; n = 52), and unknown androgenicity of the HC (n = 29). Further details regarding the categorization of progestins into androgenic or anti-androgenic and the subsample size of each specific progestogenic component can be found in the Supplementary Material.

Only women currently or previously using HCs with only one and the same type of progestin (either A or AA) were included. Specifically for naturally cycling women, only participants who had not been using any HCs or IUDs for the past 6 months and had a regular menstrual cycle, defined as between 21 and 35 days, and less than 7 days of cycle length variability (54), were included. All participants gave their signed written consent to participate in each study. Every study was approved by the University of Salzburg's ethics committee and conforms to the Code of Ethics of the World Medical Association (Declaration of Helsinki).

The androgenicity of HC was coded as a categorical variable with the following levels: level "A": androgenic, level "AA": anti-androgenic, and level "unknown". Further details are described in the following paragraphs. In order to compare age and HC use duration between androgenic and anti-androgenic users, independent-samples t-test was performed. For women currently using HC, there was a significant difference in age between A-HC (M = 21.31, SD = 2.55) and AA-HC (M = 22.58, SD = 3.57); $t_{(103)} = -2.13$, $p = 0.04$. Anti-androgenic users were, on average, approximately 1 year older than androgenic users. Likewise, use duration was significantly different between A-HC (M = 4.00, SD = 2.47) and AA-HC (M = 5.12, SD = 2.92); $t(103) = -2.12$, $p = 0.04$. The HC use duration for anti-androgenic users was, on average, approximately 1 year longer than the androgenic duration. For the naturally cycling women, age and HC use duration were not significantly different between women who had previously taken androgenic or anti-androgenic HC ($t > |2.5|$, $p > 0.05$) (Table 1). HC use duration was not related to ethinyl-estradiol levels ($r < 0.01$, $p = 0.23$), and the distribution of HC use duration by each different type of progestin followed similar distributions.

In order to control for possible moderation effects of ethinyl-estradiol levels and given previously reported dose-dependent cognitive effects (55), the following analyses were further performed controlling for the levels present in the HC. No interactive effect of pill duration by ethinyl-estradiol levels was observed, and therefore, the rest of the analyses and results will focus on the main effect of HC use duration and interaction with HC androgenicity.

2.2 fMRI data acquisition

For each study, a resting state scan of approximately 9 min duration was performed at the beginning of the scanning session. Participants were instructed to close their eyes, relax, and let their mind wander. One of the studies, however, instructed the participants to leave their eyes open (HC = 20, 19% of the final sample; NC = 28, 22% of the final sample). When the sample from this study was excluded, partial correlations between HC use duration and brain connectivity effects remained significant ($pr_{\text{age, type of scanner}} > |0.35|$, $p < 0.05$). Therefore, participants from all five studies were included in the following analyses. Two types of scanners were used: a Siemens Magnetom TIM Trio 3 Tesla and a Siemens Magnetom Prisma Fit 3 Tesla, both of them with a 64ch head coil (see Table 1 for demographics). Although we add a regressor for potential confounding effects of the type of scanner in all of the analyses, the combination of these datasets still poses a conceptual limitation. The impact of Siemens Tim Trio to Prisma upgrade has been assessed in different quantitative MRI measures (56) and proton magnetic resonance spectroscopy (57). Higher reliability was identified in most of the MRI outputs that were investigated across the Prisma upgrade (56) and inter-scanner variation had average values of approximately 2.2%–3.8% (56). Although there is also a fair level of intra-vendor consistency in individual scans (58), the present datasets also differed in their respective sequences' TR. Therefore, we explored additional interactions of the type of scanner with the HC used duration effects herein presented. No significant interactive effects were found.

For the first four studies, functional and high-resolution structural images were acquired on the TIM Trio scanner following a field map acquisition. Functional images consisted of

TABLE 1 Participants' demographics.

	Current HC users				Past HC users				
Type of scanner	TRIO		PRISMA		TRIO			PRISMA	
Type of progestin	A	AA	A	AA	A	AA	Unknown	A	AA
Sample size (n)	32	20	30	23	24	32	29	21	20
HC use duration in years M (SD)	4.71 (2.80)	4.89 (2.34)	3.25 (1.82)	5.32 (3.39)	4.24 (3.00)	4.65 (4.33)	2.09 (2.00)	3.97 (3.01)	3.80 (3.50)
Age M (SD)	22.53 (2.77)	21.80 (2.84)	20.00 (1.44)	23.26 (4.05)	25.96 (4.62)	24.47 (3.72)	25.45 (5.51)	24.24 (3.32)	25.00 (4.00)

HC, hormonal contraceptive; A, androgenic; AA, anti-androgenic; M, mean; SD, standard deviation.

a T2-weighted gradient echo planar sequence with 36 transversal slices oriented parallel to the AC-PC line (whole-brain coverage, TE = 30 ms, TR = 2,250 ms, flip angle 70°, slice thickness 3.0 mm, matrix 192 × 192, FOV 192 mm). For structural images, we acquired a T1-weigthed 3D MPRAGE sequence (160 sagittal slices, slice thickness = 1 mm, TE = 2.91 ms, TR = 2,300 ms, TI delay 900 ms, flip angle 9°, FOV 256 × 256 mm). For the most recent study, functional and high-resolution structural images were acquired on the same MRI device, upgraded to the Prisma Fit system. Functional images consisted of a T2-weighted gradient echo planar sequence with 64 transversal slices oriented parallel to the AC-PC line (whole-brain coverage, multi-slice interleaved, TE = 30 ms, TR = 1,400 ms, flip angle 69°, slice thickness 2.3 mm, matrix 202 × 202, FOV 202 mm). For structural images, we acquired a T1-weigthed 3D MPRAGE sequence (176 sagittal slices, slice thickness = 1 mm, TE = 2.91 ms, TR = 2,300 ms, TI delay 900 ms, flip angle 9°, FOV 256 × 256 mm). In the Prisma scanner study, in order to create unwrapped field maps that can be used to do B0 inhomogeneity distortion correction of the functional scans, two echo planar images (EPI) with opposite phase encode directions were acquired right before the resting state.

2.3 fMRI data analyses

For functional images, the first six images of each session were discarded. The remaining scans were despiked using 3d-despiking as implemented in AFNI (afni.nimh.nih.gov). The resulting images were pre-processed using SPM12 standard procedures and templates including (i) realignment and unwarping of the functional images using the field map, (ii) segmentation of the structural images using CAT12, (iii) co-registration of the functional images to the structural images, (iv) normalization of functional images using the normalization parameters as estimated by CAT12, and (v) spatial smoothing using a 6-mm kernel. Additionally, for the Prisma scanner, the field map was calculated from the two EPI images with opposite phase encoding using the FSL "topup" tool (http://fsl.fmrib.ox.ac.uk/fsl/fslwiki/TOPUP; 59), and the Field Map Toolbox from SPM12 was used to calculate a voxel displacement map to correct the BOLD EPI images (https://lcni.uoregon.edu/kb-articles/kb-0003; 60). Pre-processing quality control procedures included the automatic exclusion of participants with excessive movement (>3 mm translation, >2° rotation), visual inspection of structural and functional scans ensuring adequate coregistration, and visually checking the normalization to a standard T1 and an EPI MNI template. Finally, we perform ICA-AROMA non-aggressive removal of artifactual components on the resulting images. ICA-AROMA has been shown to reduce motion-induced variation in fMRI signal, while preserving the signal of interest (61).

2.3.1 Gray matter volume and fractional amplitude of low-frequency fluctuations

Gray matter volumes from bilateral ACC and amygdala were extracted using the get_totals script by G. Ridgeway (http://www0.cs.ucl.ac.uk/staff/gridgway/vbm/get_totals.m), each region of interest (ROI) defined with the AAL atlas (62).

The fractional amplitude of low-frequency fluctuation (fALFF) maps were calculated from pre-processed resting state images using the DPABI toolbox (63). The fALFF is a measure of oscillatory activity at the resting state, relative to the whole frequency range (64). It is defined as the ratio of the power spectrum of low frequency (0.01–0.08 Hz) to the average square root of each frequencies power within this range (64, 65).

In order to assess the duration of the HC use*androgenicity interactive effect on (i) gray matter volume and (ii) fALFF, they were introduced as dependent variables in linear models in R Version 1.4.1717, using the lm function from the stats package (66). For all models, HC use duration, androgenicity, and their interaction were included as fixed effects. In case no significant interaction between androgenicity and HC use duration was observed, the interaction was removed from the model and the main effect of HC use duration was calculated across both groups. For every model, age and type of scanner were added as nuisance regressors (e.g., fALFF ~ duration of HC use*androgenicity + age + type of scanner). For the models including gray matter volume, we used the total intracranial volume (TIV) as an additional covariate (e.g., GM IFG ~ duration of HC use*androgenicity +TIV + age + type of scanner). All continuous variables were scaled prior to analyses to allow for interpretation of effect sizes based on standard deviations.

2.3.2 Seed-to-voxel connectivity analysis

We investigated bilateral ACC and amygdala functional connectivity with AAL atlas-defined region of interest (ROI) (62). Seed-to-voxel connectivity maps from these ROIs were estimated for each subject using the CONN-toolbox standard procedures and templates (67). The six movement parameters as well as five white matter and cerebrospinal fluid components were used as regressors during the denoising step. A band-pass filter of 0.008–0.09 Hz was applied. For the group-level analysis, full factorial models were used to evaluate the overall connectivity relation to HC use duration. For each of the ROIs, the first-level contrast images were introduced into a full factorial design in order to investigate the interactive effect of duration of HC use and HC group (androgenic vs. anti-androgenic). In case no significant interaction between androgenicity and HC duration was observed, the main effect of HC use duration was calculated across both groups. In order to control for age and scanning upgrade, their interaction with the HC group was additionally modeled as nuisance regressors. For this second level, results were masked with an SPM gray matter template, and we used an extent threshold of $k = 20$ voxels, an uncorrected primary threshold of $p < 0.001$, and a secondary cluster-level FWE-corrected threshold of $p < 0.05$ (indicated as pFWE). In case a cluster of significant interaction between androgenicity and HC use duration emerged, eigenvalues were extracted from this cluster and partial correlations controlling for age and type of scanner were performed separately for androgenic and anti-androgenic HC users. In a follow-up analysis, we checked if the effects in HC users were replicated in naturally cycling

previous HC users. The first eigenvector of the time series across voxels was extracted from the significant FWE-corrected clusters found in HC current users, and partial correlations for naturally cycling previous HC users were performed controlling for both age and type of scanner. In case of no significant interaction between androgenicity and HC use duration, the level "unknown" from HC androgenicity variable was included in the partial correlation. Otherwise, only known "A" and "AA" previous HC users were included and partial correlations were explored separately.

3 Results

3.1 Gray matter volume and fractional amplitude of low-frequency fluctuations

For the gray matter volume of the ROIs, there was an interactive effect of HC use duration and androgenicity in the left ACC [$b = -0.31$, $SE_b = 0.15$, $t_{(98)} = -1.99$, $p = 0.049$]. Current androgenic users showed a smaller GM volume of the left ACC the longer the duration of HC use (Figure S1). However, partial correlations were separated by androgenicity, and controlling for age, TIV and scanner type did not survive the significance threshold [$pr_{age,\ type\ of\ scanner,\ TIV} = -0.05$, $p_{(57)} = 0.73$ for A-HC, and $pr_{age,\ type\ of\ scanner,\ TIV} = -0.23$, $p_{(38)} = 0.15$ for AA-HC].

No further significant relations were found for right ACC or bilateral amygdala gray matter volume. Neither ACC nor amygdala showed any previous HC use duration effect [all $pr_{age,\ type\ of\ scanner} < |0.015|$, $p_{(122)} > 0.05$].

No significant relations were found for bilateral ACC or amygdala between fALFF and duration of HC use.

3.2 Seed-to-voxel connectivity analysis

Whole brain connectivity maps of bilateral ACC and amygdalae are displayed in the Supplementary Material (S2–S5). For the ACC, positive connectivity maps included insular and medio-temporal areas, while negative connectivity maps included superior parietal lobes and inferior frontal gyri. Positive connectivity maps for the amygdalae included insular, middle cingulate, and ventromedial prefrontal cortices, among other medio-temporal areas, putamen, and thalamus. Negative connectivity maps for the amygdalae included superior, middle frontal, and angular gyri, among others.

3.2.1 Main effect of HC use duration

For the ACC connectivity, we observed an inversed main effect of current HC use duration and connectivity between the right ACC and left post-central gyrus ([-54, -22, 49], 79 voxels, $T = 4.63$, $p_{FWE} = 0.001$), right posterior insula ([36, -16, 10], 67 voxels, $T = 4.58$, $p_{FWE} = 0.003$), and right pre/post-central gyrus ([39, -16, 61], 121 voxels, $T = 4.54$, $p_{FWE} < 0.001$). Functional connectivity between the right ACC and these three clusters was lower the longer the use of HC in current users, irrespective of the androgenicity (Figure 1A). Connectivity between the right ACC and these three clusters of interest did not show any previous HC use duration effect [all $pr_{age,\ type\ of\ scanner"} < |0.015|$, $p_{(122)} > 0.05$].

We also observed an inversed main effect of HC use duration on connectivity between bilateral amygdalae and prefrontal cortex. Connectivity between bilateral amygdalae and the left middle frontal gyrus ([-30, 35, 40], 37 voxels, $T = 3.79$, $p_{FWE} = 0.042$, for the left amygdala; [-30, 26, 46], 62 voxels, $T = 4.42$, $p_{FWE} = 0.004$, for the right amygdala) and between the right amygdala and the ventral part of the superior frontal gyrus ([-21, 56, -5], 37 voxels, $T = 4.47$, $p_{FWE} = 0.042$) was lower the longer the duration of HC, irrespective of the androgenicity (Figure 1B). Only for the connectivity between the right amygdala and the left superior frontal gyrus did we observe a similar effect of previous HC use duration in naturally cycling participants [$pr_{age,\ type\ of\ scanner} = -0.19$, $p_{(122)} = 0.035$]. Independently of the androgenicity type, the connectivity between the right amygdala and the ventral part of the superior frontal gyrus ([-21, 56, -5], 37 voxels) was lower the longer the use of HC in previous users (Figure S6).

3.2.2 Interactive effect of HC use duration and HC androgenicity

We further observed an interactive effect of HC use duration and androgenicity in the connectivity between left and right ACC with the triangular part of the right inferior frontal gyrus ([45, 47, -2], 50 voxels, $T = 4.18$, $p_{FWE} = 0.012$, for the left ACC; [39, 47, -5], 39 voxels, $T = 4.35$, $p_{FWE} = 0.038$, for the right ACC). For current users of an androgenic HC, the connectivity between bilateral ACC and the right inferior frontal gyrus was lower the longer the HC use [$pr_{age,\ type\ of\ scanner} = -0.46$, $p_{(58)} < 0.001$ for the left ACC; $pr_{age,\ type\ of\ scanner} = -0.44$, $p_{(58)} < 0.001$ for the right ACC]; for anti-androgenic HC users, connectivity strength was higher the longer the HC use [$pr_{age,\ type\ of\ scanner} = 0.34$, $p_{(39)} = 0.03$ for the left ACC; $pr_{age,\ type\ of\ scanner} = 0.31$, $p_{(39)} = 0.04$ for the right ACC; Figure 2]. Connectivity between the ACC and inferior frontal gyrus did not show any previous HC use duration effect in naturally cycling participants [all $pr_{age,\ type\ of\ scanner} < |0.015|$, $p_{(122)} > 0.05$]. No interactive effect of androgenicity and HC use duration was observed for the rs-FC of the amygdalae.

In summary, for the current HC users, the connectivity between the right ACC and right insula/bilateral post-central gyrus, and between bilateral amygdalae and left prefrontal cortex, was lower the longer the use of HC, irrespective of the androgenicity. For androgenic HC users, the connectivity between bilateral ACC and the right IFG was lower the longer the HC use; for anti-androgenic HC users, connectivity strength was higher the longer the HC use.

4 Discussion

In this study, we investigated for the first time the differences in the resting state functional connectivity (rs-FC) network of the anterior cingulate cortices (ACC) and the amygdalae related to the duration of androgenic (A) or anti-androgenic (AA) HC use. In general, rs-FC of the ACC and temporoparietal areas, and between the amygdalae with frontal areas, decreased the longer the HC

10.3389/fendo.2023.1131995

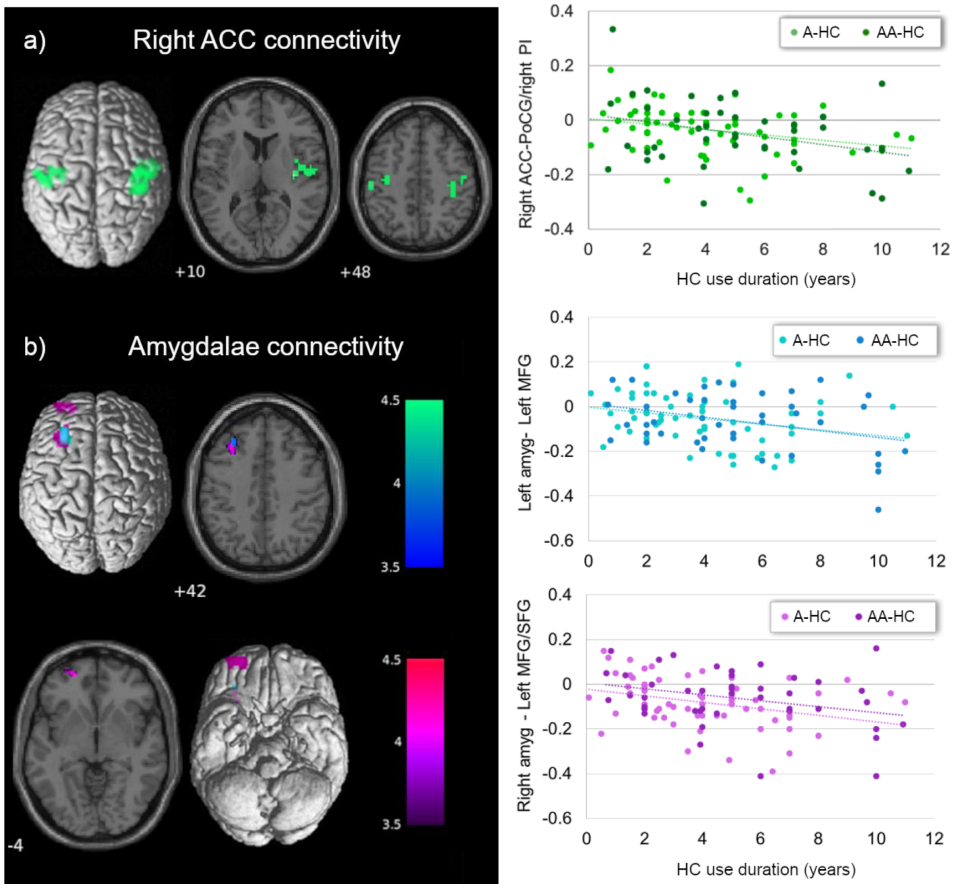

FIGURE 1
Main effect of current HC use duration on ACC and amygdala connectivity. **(A)** Current HC users showed lower connectivity between the right ACC and right insula/bilateral post-central gyrus, the longer the use of HC, irrespective of the androgenicity (in green). **(B)** Independently of the androgenicity of the HC, current users showed lower connectivity between left (in blue) and right (in purple) amygdala with left prefrontal cortex the longer the use of the HC. ACC, anterior cingulate cortex; PoCG, post-central gyrus; PI, posterior insula; amyg, amygdala; MFG, middle frontal gyrus; SFG, superior frontal gyrus; HC, hormonal contraceptive; A, androgenic; AA, anti-androgenic.

exposure and independently of the progestin androgenicity. Androgenicity did show a differential effect in the connectivity between bilateral ACC and the right inferior frontal gyrus (IFG).

Longer HC use duration, irrespective of the androgenicity, was related to decreased connectivity between the ACC and the insular cortex, both involved in the salience network. Although naturally cycling women show within salience network connectivity increased related to enhanced endogenous progesterone (22, 53), this effect was absent in women during HC use (53). The impact of HC on salience-dependent processes such as motivation and reward-oriented behavior has been related to a decrease of the insula activation, for example, to sexual cues (68). In animal models, this sexual behavior has been shown to be impaired by exogenous hormonal treatment, changes suggested to be mediated by the blunted levels of allopregnanolone (69). Conversely, Sharma et al. (34) reported an increased salience within-network connectivity with the medial superior frontal gyrus for the HC users compared to the naturally cycling women (34). It needs to be noted, though, that pubertal-onset HC users were included in this comparison and given that this sub-group was reported to show significantly general increased connectivity compared to the adult-onset sub-group, it is unclear to which extent they drove the direction of the results.

Contrary to our expectations, we did not find a decreased connectivity between the amygdala and the postcentral gyrus and precuneus (31). Instead, it was the ACC that showed decreased connectivity to the bilateral pre/postcentral gyri the longer the HC use. In a recent study analyzing effective connectivity in a placebo-controlled trial, connections between the dorsal ACC and parietal areas decreased during androgenic HC treatment (53). In naturally cycling women, connectivity between the ACC and postcentral gyrus increased during the luteal phase (31), and the connectivity of the somatosensorial cortices was also positively related to progesterone levels (70). Connectivity between amygdalae with superior and middle frontal gyrus was also found decreased the longer the HC use in the present sample, in line with Petersen et al. (32). Moreover, although it did not survive the FWE correction in the whole-brain analysis, the right amygdala also showed reduced connectivity with the ipsilateral middle frontal gyrus, the longer the HC use duration (see Supplementary Material, Figure S7). Conversely, increased connectivity between these areas has been

10.3389/fendo.2023.1131995

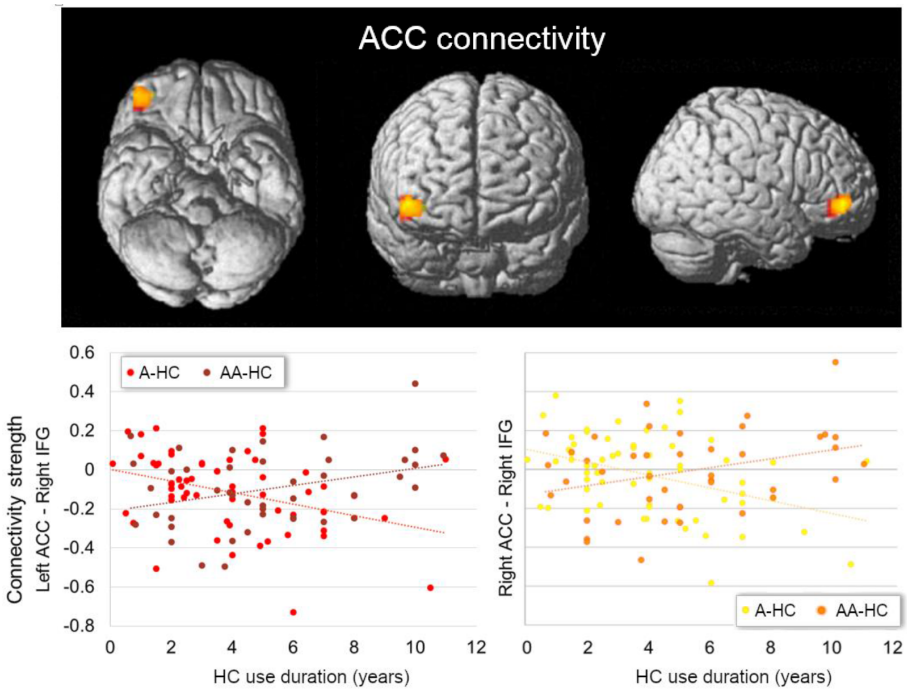

FIGURE 2
Interactive effect of current HC use duration and androgenicity on the connectivity between left (in red) and right ACC (in orange) with right inferior frontal gyrus (IFG). Current users of an androgenic HC (A-HC) showed lower connectivity between bilateral ACC and the right IFG the longer the HC use. In contrast, current users of an anti-androgenic HC (AA-HC) showed stronger connectivity between bilateral ACC and the right IFG the longer the HC use. ACC, anterior cingulate cortex; IFG, inferior frontal gyrus HC, hormonal contraceptive; A, androgenic; AA, anti-androgenic.

reported before during the progesterone-dominated luteal phase in naturally cycling women (31).

Following the argument that while HC women have increased synthetic progestin levels, their allopregnanolone levels remain decreased (44, 45), and that some effects of endogenous progesterone are exerted through this metabolite, these changes in opposite directions may suggest that the ACC-insular/somatosensorial and prefrontal–amygdalar connectivity positively relates to allopregnanolone levels, which, in turn, remains decreased during HC use. Relatedly, exogenous administration of progesterone, which significantly increased allopregnanolone levels, selectively increased amygdala reactivity (71). However, although animal research corroborates these effects for androgenic progestins, except for drospirenone (72), anti-androgenic progestins appear to increase allopregnanolone levels in the rodent brain (73, 74). On the other hand, although ethinyl-estradiol has a greater affinity for estrogen receptors than endogenous estradiol (75), it is administered in a much lower dose and also shows a differential selectivity for the alpha receptor type over the beta receptor type (76). The present findings could be a consequence of the cumulative effect of synthetic hormones, the abolishment of cyclic endogenous hormonal fluctuations, or the combination of both.

Contrary to our hypotheses, we only found an interactive effect of androgenicity and use duration for bilateral ACC. The connectivity of these areas with the right inferior frontal gyrus was lower the longer the androgenic HC use, while it was stronger the longer the anti-androgenic HC use. In post-menopausal women, connectivity between these areas during memory tasks is positively related to estradiol levels (77). Conversely, in pre-menopausal women using HC, bilateral ACC–inferior frontal gyrus connectivity has been reported to decrease after testosterone administration, during an empathy-related task (35). In male patients, anabolic androgen users showed decreased dorsal attention network connectivity with superior and inferior frontal gyri (SFG/IFG) and the ACC, related to use duration (78). Opposed effects of HC depending on the androgenicity of their progestin have also been extended to the behavioral level by some studies (see review, 79). Although these findings indicate opposite cumulative effects of androgenic vs. estrogenic modulation, both androgenic and anti-androgenic progestins reduce overall testosterone bioavailability (80, 81). Therefore, HC's androgenicity impact needs to be further elucidated, preferably in longitudinal placebo-controlled trials.

Most of the effects observed in current HC users did not replicate for previous HC users, which could be interpreted as reversibility for such effects. Only the connectivity between the right amygdala and the ventral area of the left superior frontal gyrus still showed a decrease the longer the duration of previous HC use. We have previously described an effect of HC exposure on gray matter volume of subcortical structures, some of which also appear to remain after discontinuation (82). Although some studies hint at a chronic decrease in endogenous hormone levels many years after cessation of HC use (83), and long-term effects in task performance (84), the extent to which fronto-amygdalar connectivity is directly influenced by a prolonged HC use is still undetermined. Further

longitudinal randomized placebo-controlled studies need to be carried out in order to fully disentangle the causal effect of HC and its reversibility after discontinuation.

Some remarks and limitations need to be noted. First, and important for the interpretations of these results, is that while a cross-sectional group comparison could identify those effects that emerge after the first months of use, but do not accumulate over time, here we investigated time-dependent associations. Therefore, for those results conflicting with previous literature, an alternative explanation is that following this early impact (that would explain the group differences), the changes adapt/regress over time. Further inconsistencies could also be partly attributable to the small sample and effect sizes of past studies. Second, although the categorization of progestins used here corresponds to their androgenic vs. anti-androgenic effects, this does not always reflect the corresponding androgenicity of the HCs. Progestins with a stronger androgenic effect may be found in lower doses in the HC and therefore have lower androgenic effects in the body once dosage is taken into account (85).Third, HC-related differences could be modulated by a continued suppression of the endogenous hormones, by the exposure to synthetic hormones, and/or by the interaction of both effects. As previously described, endogenous estradiol has a lower affinity for estrogen receptors than ethinyl-estradiol, and endogenous progesterone also differs to the different types of synthetic progestins in their extra-progestogenic effects. For example, they present a different affinity and agonist or antagonist modulation of gluco- and mineralocorticoid receptors (86). Furthermore, the involvement of these receptors in the regulation of the stress response is of special importance when considering potential long-term effects of HC on the brain. Last, but not least, we selected the present ROIs based on previous literature and delimited by the AAL atlas (62) for replication purposes (31). However, there are conceptual and practical challenges when selecting a specific parcellation, including the lack of precision in terms of inter-individual homologous correspondence in brain cortex (87, 88). Additional bias towards smaller sub-networks instead of larger brain systems has also been suggested for seed-based analyses (89).

Overall, these results in a large sample of women suggest cumulative changes in functional connectivity patterns at rest related to the extent of exposure to HC and the abolishment of the endogenous fluctuation of ovarian hormones. Differential effects of the type of progestin arose for some of these functional changes. Given the widespread use of HC among women, and the early onset of HC use, usually starting during adolescence, elucidating the synthetic progestins effects and the functional implications of these findings is of the utmost importance.

Data availability statement

Data and scripts are openly available at https://osf.io/5ezw9/. MR images are available upon request from the corresponding author.

Ethics statement

Every study was approved by the University of Salzburg's ethics committee and conforms to the Code of Ethics of the World Medical Association (Declaration of Helsinki). The patients/participants provided their written informed consent to participate in this study.

Author contributions

BP designed and made the concept of the study. BP, EH-L, and IN were responsible for acquiring the data. EH-L was responsible for data curation and analysis, interpreting the results, and drafting and revising the manuscript. BP supervised the analysis, contributed in the results' interpretation, and revised the manuscript. All authors contributed to the article and approved the submitted version.

Funding

This research was funded by the Austrian Science Fund (FWF) Project P32276 supporting BP; the PhD Programme "Imaging the Mind: Connectivity and Higher Cognitive Function" [W 1233-G17] supporting EH-L and IN; and the European Research Council (ERC) Starting Grant 850953 supporting BP and EH-L.

Conflict of interest

The authors declare that the research was conducted in the absence of any commercial or financial relationships that could be construed as a potential conflict of interest.

Publisher's note

Supplementary material

The Supplementary Material for this article can be found online at: https://www.frontiersin.org/articles/10.3389/fendo.2023.1131995/full#supplementary-material

References

1. McEwen B. Estrogen actions throughout the brain. *Recent Prog Hormone Res* (2002) 57(FEBRUARY 2002):357–84. doi: 10.1210/rp.57.1.357

2. Wendler A, Albrecht C, Wehling M. Nongenomic actions of aldosterone and progesterone revisited. *Steroids* (2012) 77(10):1002–6. doi: 10.1016/j.steroids.2011.12.023

3. Brinton RD, Thompson RF, Foy MR, Baudry M, Wang JM, Finch CE, et al. Progesterone receptors: form and function in brain. *Front Neuroendocrinol* (2008) 29 (2):313–39. doi: 10.1016/j.yfrne.2008.02.001

4. Pritschet L, Santander T, Taylor CM, Layher E, Yu S, Miller MB, et al. Functional reorganization of brain networks across the human menstrual cycle. *NeuroImage* (2020) 220:117091. doi: 10.1016/j.neuroimage.2020.117091

5. United Nations. (2022). United Nations, Department of Economic and Social Affairs, Population Division. Available at: https://www.un.org/development/desa/pd/sites/www.un.org.development.desa.pd/files/undesa_pd_2022_wcu_fp-indicators_documentation.pdf.

6. Fleischman DS, Navarrete CD, Fessler DMT. Oral contraceptives suppress ovarian hormone production. *psychol Sci* (2010) 21(5):750–2. doi: 10.1177/0956797610368062/ASSET/0956797610368062.FP.PNG_V03

7. Turgeon JL, Carr MC, Maki PM, Mendelsohn ME, Wise PM. Complex actions of sex steroids in adipose tissue, the cardiovascular system, and brain: insights from basic science and clinical studies. *Endocr Rev* (2006) 27(6):575–605. doi: 10.1210/er.2005-0020

8. Jensen JT. Evaluation of a new estradiol oral contraceptive: estradiol valerate and dienogest. *Expert Opin Pharmacother* (2010) 11(7):1147–57. doi: 10.1517/14656561003724713

9. Kuhl H. Pharmacology of estrogens and progestogens: influence of different routes of administration. *Climacteric* (2005) 8(SUPPL. 1):3–63. doi: 10.1080/13697130500148875

10. Pletzer BA, Kerschbaum HH. 50 years of hormonal contraception - time to find out, what it does to our brain. *Front Neurosci* (2014) 8 JUL:256. doi: 10.3389/fnins.2014.00256

11. Knopp RH, Broyles FE, Cheung M, Moore K, Marcovina S, Chandler WL. Comparison of the lipoprotein, carbohydrate, and hemostatic effects of phasic oral contraceptives containing desogestrel or levonorgestrel. *Contraception* (2001) 63(1):1–11. doi: 10.1016/s0010-7824(00)00196-7

12. Sech LA, Mishell DR. Oral steroid contraception. *Women's Health* (2015) 11 (6):743–8. doi: 10.2217/WHE.15.82

13. Foster RH, Wilde MI. Dienogest. *Drugs* (1998) 56(5):825–33. doi: 10.2165/00003495-199856050-00007

14. Pletzer B, Kronbichler M, Aichhorn M, Bergmann J, Ladurner G, Kerschbaum HH. Menstrual cycle and hormonal contraceptive use modulate human brain structure. *Brain Res* (2010) 1348:55–62. doi: 10.1016/j.brainres.2010.06.019

15. De Bondt T, Van Hecke W, Veraart J, Leemans A, Sijbers J, Sunaert S, et al. Does the use of hormonal contraceptives cause microstructural changes in cerebral white matter? preliminary results of a DTI and tractography study. *Eur Radiol* (2013) 23 (1):57–64. doi: 10.1007/s00330-012-2572-5

16. Brønnick MK, Økland I, Graugaard C, Brønnick KK. The effects of hormonal contraceptives on the brain: a systematic review of neuroimaging studies. *Front Psychol* (2020) 11:556577. doi: 10.3389/fpsyg.2020.556577

17. Casto KV, Jordan T, Petersen N. Hormone-based models for comparing menstrual cycle and hormonal contraceptive effects on human resting-state functional connectivity. *Front Neuroendocrinol* (2022) 67:101036. doi: 10.1016/J.YFRNE.2022.101036

18. Lindh I, Blohm F, Andersson-Ellström A, Milsom I. Contraceptive use and pregnancy outcome in three generations of Swedish female teenagers from the same urban population. *Contraception* (2009) 80(2):163–9. doi: 10.1016/j.contraception.2009.01.019

19. Poromaa IS, Segebladh B. Adverse mood symptoms with oral contraceptives. *Acta Obstet Gynecol Scand* (2012) 91(4):420–7. doi: 10.1111/j.1600-0412.2011.01333.x

20. Toffoletto S, Lanzenberger R, Gingnell M, Sundström-Poromaa I, Comasco E. Emotional and cognitive functional imaging of estrogen and progesterone effects in the female human brain: a systematic review. *Psychoneuroendocrinology* (2014) 50:28–52. doi: 10.1016/j.psyneuen.2014.07.025

21. Dubol M, Epperson CN, Sacher J, Pletzer B, Derntl B, Lanzenberger R, et al. Neuroimaging the menstrual cycle: a multimodal systematic review. *Front Neuroendocrinol* (2021) 60. doi: 10.1016/J.YFRNE.2020.100878

22. Hidalgo-Lopez E, Zeidman P, Harris TA, Razi A, Pletzer B. Spectral dynamic causal modelling in healthy women reveals brain connectivity changes along the menstrual cycle. *Commun Biol* (2021) 4:954. doi: 10.1038/s42003-021-02447-w

23. Petersen N, Touroutoglou A, Andreano JM, Cahill L. Oral contraceptive pill use is associated with localized decreases in cortical thickness. *Hum Brain Mapp* (2015) 36 (7):2417–851. doi: 10.1002/hbm.22797

24. Miedl SF, Wegerer M, Kerschbaum H, Blechert J, Wilhelm FH. Neural activity during traumatic film viewing is linked to endogenous estradiol and hormonal contraception. *Psychoneuroendocrinology* (2018) 87:20–6. doi: 10.1016/j.psyneuen.2017.10.006

25. Lisofsky N, Riediger M, Gallinat J, Lindenberger U, Kühn S. Hormonal contraceptive use is associated with neural and affective changes in healthy young women. *NeuroImage* (2016) 134:597–606. doi: 10.1016/j.neuroimage.2016.04.042

26. Petersen N, Cahill L. Amygdala reactivity to negative stimuli is influenced by oral contraceptive use. *Soc Cogn Affect Neurosci* (2014) 10(9):1266–72. doi: 10.1093/scan/nsv010

27. Amin Z, Epperson CN, Constable RT, Canli T. Effects of estrogen variation on neural correlates of emotional response inhibition. *NeuroImage* (2006) 32(1):457–64. doi: 10.1016/j.neuroimage.2006.03.013

28. Andreano JM, Cahill L. Menstrual cycle modulation of medial temporal activity evoked by negative emotion. *NeuroImage* (2010) 53(4):1286–93. doi: 10.1016/j.neuroimage.2010.07.011

29. Greicius MD, Krasnow B, Reiss AL, Menon V. Functional connectivity in the resting brain: a network analysis of the default mode hypothesis. *Proc Natl Acad Sci U States America* (2003) 100(1):253–8. doi: 10.1073/pnas.0135058100

30. Deco G, Ponce-Alvarez A, Mantini D, Romani GL, Hagmann P, Corbetta M. Resting-state functional connectivity emerges from structurally and dynamically shaped slow linear fluctuations. *J Neurosci* (2013) 33(27):11239–52. doi: 10.1523/JNEUROSCI.1091-13.2013

31. Engman J, Sundström Poromaa I, Moby L, Wikström J, Fredrikson M, Gingnell M. Hormonal cycle and contraceptive effects on amygdala and salience resting-state networks in women with previous affective side effects on the pill. *Neuropsychopharmacology* (2018) 43(3):555–63. doi: 10.1038/npp.2017.157

32. Petersen N, Kilpatrick LA, Goharzad A, Cahill L. Oral contraceptive pill use and menstrual cycle phase are associated with altered resting state functional connectivity. *NeuroImage* (2014) 90:24–32. doi: 10.1016/j.neuroimage.2013.12.016

33. Petersen N, Ghahremani DG, Rapkin AJ, Berman SM, Wijker N, Liang L, et al. Resting-state functional connectivity in women with PMDD. *Trans Psychiatry* (2019) 9:339. doi: 10.1038/s41398-019-0670-8

34. Sharma R, Fang Z, Smith A, Ismail N. Oral contraceptive use, especially during puberty, alters resting state functional connectivity. *Hormones Behav* (2020) 126 (February):104849. doi: 10.1016/j.yhbeh.2020.104849

35. Bos PA, Hofman D, Hermans EJ, Montoya ER, Baron-Cohen S, van Honk J. Testosterone reduces functional connectivity during the "Reading the mind in the eyes" test. *Psychoneuroendocrinology* (2016) 68:194–201. doi: 10.1016/j.psyneuen.2016.03.006

36. van Wingen G, Mattern C, Verkes RJ, Buitelaar J, Fernández G. Testosterone reduces amygdala-orbitofrontal cortex coupling. *Psychoneuroendocrinology* (2010) 35 (1):105–13. doi: 10.1016/j.psyneuen.2009.09.007

37. Chowen JA, Azcoitia I, Cardona-Gomez GP, Garcia-Segura LM. Sex steroids and the brain: lessons from animal studies. *J Pediatr Endocrinol Metab* (2000) 13 (8):1045–66. doi: 10.1515/JPEM.2000.13.8.1045

38. Finch CE, Felicio LS, Mobbs CV, Nelson JF. Ovarian and steroidal influences on neuroendocrine aging processes in female rodents. *Sci Aging Knowledge Environ* (2002) 2002(37):cp19–9. doi: 10.1126/sageke.2002.37.cp19

39. Deutsch ER, Espinoza TR, Atif F, Woodall E, Kaylor J, Wright DW. Progesterone's role in neuroprotection, a review of the evidence. *Brain Res* (2013) 1530:82–105. doi: 10.1016/j.brainres.2013.07.014

40. Schumacher M, Mattern C, Ghoumari A, Oudinet JPP, Liere P, Labombarda F, et al. Revisiting the roles of progesterone and allopregnanolone in the nervous system: resurgence of the progesterone receptors. *Prog Neurobiol* (2014) 113:6–39. doi: 10.1016/j.pneurobio.2013.09.004

41. Follesa P, Concas A, Porcu P, Sanna E, Serra M, Mostallino MC, et al. Role of allopregnanolone in regulation of GABAA receptor plasticity during long-term exposure to and withdrawal from progesterone. *Brain Res Rev* (2001) 37(1–3):81–90. doi: 10.1016/S0165-0173(01)00125-4

42. Garcia-Segura LM, Melcangi RC. Steroids and glial cell function. In: *GLIA*, vol. 54. John Wiley & Sons, Ltd (2006). p. 485–98. doi: 10.1002/glia.20404

43. Kuhl H. Pharmacology of progestogens. *J Reproduktionsmed Endokrinol* (2011) 8:157–77.

44. Rapkin AJ, Morgan M, Sogliano C, Biggio G, Concas A. Decreased neuroactive steroids induced by combined oral contraceptive pills are not associated with mood changes. *Fertil Steril* (2006) 85(5):1371–8. doi: 10.1016/j.fertnstert.2005.10.031

45. Paoletti AM, Lello S, Fratta S, Orrù M, Ranuzzi F, Sogliano C, et al. Psychological effect of the oral contraceptive formulation containing 3 mg of drospirenone plus 30 µg of ethinyl estradiol. *Fertil Steril* (2004) 81(3):645–51. doi: 10.1016/j.fertnstert.2003.08.030

46. Pletzer B, Winkler-Crepaz K, Hillerer K. Progesterone and contraceptive progestin actions on the brain: a systematic review of animal studies and comparison to human neuroimaging studies. *Front Neuroendocrinol* (2023) 101060. doi: 10.1016/J.YFRNE.2023.101060

47. Shay DA, Vieira-Potter VJ, Rosenfeld CS. Sexually dimorphic effects of aromatase on neurobehavioral responses. *Front Mol Neurosci* (2018) 11:374/BIBTEX. doi: 10.3389/FNMOL.2018.00374/BIBTEX

48. Ottowitz WE, Derro D, Dougherty DD, Lindquist MA, Fischman AJ, Hall JE. Analysis of amygdalar-cortical network covariance during pre- versus post-menopausal estrogen levels: potential relevance to resting state networks, mood, and cognition. *Neuro Endocrinol Lett* (2008) 29(4):467.

49. Engman J, Linnman C, Van Dijk KRA, Milad MR. Amygdala subnuclei resting-state functional connectivity sex and estrogen differences. *Psychoneuroendocrinology* (2016) 63:34–42. doi: 10.1016/J.PSYNEUEN.2015.09.012

50. Pletzer B, Harris TA, Scheuringer A, Hidalgo-Lopez E. The cycling brain: menstrual cycle related fluctuations in hippocampal and fronto-striatal activation and connectivity during cognitive tasks. *Neuropsychopharmacology* (2019) 44 (11):1867–75. doi: 10.1038/s41386-019-0435-3

51. Menting-Henry S, Hidalgo-Lopez E, Aichhorn M, Kronbichler M, Kerschbaum H, Pletzer B. Oral contraceptives modulate the relationship between resting brain activity, amygdala connectivity and emotion recognition – a resting state fMRI study. *Front Behav Neurosci* (2022) 16:775796. doi: 10.3389/fnbeh.2022.775796

52. Noachtar I, Harris T-A, Hidalgo-Lopez E, Pletzer B. Sex and strategy effects on brain activation during a 3D-navigation task. *Commun Biol* (2022) 5(1):1–14. doi: 10.1038/s42003-022-03147-9

53. Hidalgo-Lopez E, Engman J, Poromaa IS, Gingnell M, Pletzer B. Triple network model of brain connectivity changes related to adverse mood effects in an oral contraceptive placebo-controlled trial. *Transl Psychiatry* (2023) 13:209. doi: 10.1038/s41398-023-02470-x

54. Fehring RJ, Schneider M, Raviele K. Variability in the phases of the menstrual cycle. *JOGNN - J Obstet Gynecol Neonatal Nurs* (2006) 35:376–84.

55. Beltz AM, Hampson E, Berenbaum SA. Oral contraceptives and cognition: a role for ethinyl estradiol. *Hormones Behav* (2015) 74:209–17. doi: 10.1016/j.yhbeh.2015.06.012

56. Gracien RM, Maiworm M, Brüche N, Shrestha M, Nöth U, Hattingen E, et al. How stable is quantitative MRI? – assessment of intra- and inter-scanner-model reproducibility using identical acquisition sequences and data analysis programs. *NeuroImage* (2020) 207:116364. doi: 10.1016/j.neuroimage.2019.116364

57. Plitman E, Bussy A, Valiquette V, Salaciak A, Patel R, Cupo L, et al. The impact of the Siemens Tim trio to prisma upgrade and the addition of volumetric navigators on cortical thickness, structure volume, and 1H-MRS indices: an MRI reliability study with implications for longitudinal study designs. *NeuroImage* (2021) 238:118172. doi: 10.1016/j.neuroimage.2021.118172

58. Badhwar AP, Collin-Verreault Y, Orban P, Urchs S, Chouinard I, Vogel J, et al. Multivariate consistency of resting-state fMRI connectivity maps acquired on a single individual over 2.5 years, 13 sites and 3 vendors. *NeuroImage* (2020) 205:116210. doi: 10.1016/j.neuroimage.2019.116210

59. Andersson JLR, Skare S, Ashburner J. How to correct susceptibility distortions in spin-echo echo-planar images: application to diffusion tensor imaging. *NeuroImage* (2003) 20(2):870–88. doi: 10.1016/S1053-8119(03)00336-7

60. Chang H, Fitzpatrick JM. A technique for accurate magnetic resonance imaging in the presence of field inhomogeneities. *IEEE Trans Med Imaging* (1992) 11(3):319–29. doi: 10.1109/42.158935

61. Pruim RHR, Mennes M, van Rooij D, Llera A, Buitelaar JK, Beckmann CF. ICA-AROMA: A robust ICA-based strategy for removing motion artifacts from fMRI data. *Neuroimage* (2015) 112:267–77.

62. Tzourio-Mazoyer N, Landeau B, Papathanassiou D, Crivello F, Etard O, Delcroix N, et al. Automated anatomical labeling of activations in SPM using a macroscopic anatomical parcellation of the MNI MRI single-subject brain. *Neuroimage* (2002) 15:273–89.

63. Yan C-GG, Wang X-D, Di Zuo X-NN, Zang Y-FF. DPABI: Data processing & analysis for (Resting-State) brain imaging. *Neuroinformatics* (2016) 14:339–51.

64. Zou QH, Zhu CZ, Yang Y, Zuo XN, Long XY, Cao QJ, et al. An improved approach to detection of amplitude of low-frequency fluctuation (ALFF) for resting-state fMRI: fractional ALFF. *J. Neurosci. Methods* (2008) 172:137–41.

65. Zang YF, Yong H, Chao-Zhe Z, Qing-Jiu C, Man-Qiu S, Meng L, et al. ltered baseline brain activity in children with ADHD revealed by resting-state functional MRI. *Brain Dev* (2007) 29:83–91.

66. R Core Team. A language and environment for statistical computing. In: *R foundation for statistical computing* (2018).

67. Whitfield-Gabrieli S, Nieto-Castanon A. *Conn*: a functional connectivity toolbox for correlated and anticorrelated brain networks. *Brain Connectivity* (2012) 2(3):125–41. doi: 10.1089/brain.2012.0073

68. Abler B, Kumpfmüller D, Grön G, Walter M, Stingl J, Seeringer A. Neural correlates of erotic stimulation under different levels of female sexual hormones. *PloS One* (2013) 8(2):e54447. doi: 10.1371/journal.pone.0054447

69. Santoru F, Berretti R, Locci A, Porcu P, Concas A. Decreased allopregnanolone induced by hormonal contraceptives is associated with a reduction in social behavior and sexual motivation in female rats. *Psychopharmacology* (2014) 231(17):3351–64. doi: 10.1007/s00213-014-3539-9

70. Arélin K, Mueller K, Barth C, Rekkas PV, Kratzsch JJ, Burmann I, et al. Progesterone mediates brain functional connectivity changes during the menstrual cycle-a pilot resting state MRI study. *Front Neurosci* (2015) 9:44(FEB). doi: 10.3389/fnins.2015.00044

71. Van Wingen GA, Van Broekhoven F, Verkes RJ, Petersson KM, Bäckström T, Buitelaar JK, et al. Progesterone selectively increases amygdala reactivity in women. *Mol Psychiatry* (2008) 13(3):325–33. doi: 10.1038/sj.mp.4002030

72. Genazzani AR, Pluchino N, Begliuomini S, Pieri M, Centofanti M, Freschi L, et al. Drospirenone increases central and peripheral β-endorphin in ovariectomized female rats. *Menopause* (2007) 14(1):63–73. doi: 10.1097/01.gme.0000230348.05745.7d

73. Lenzi E, Pluchino N, Begliuomini S, Ninni F, Freschi L, Centofanti M, et al. Effects of nomegestrol acetate administration on central and peripheral beta-endorphin and allopregnanolone in ovx rats. *J Steroid Biochem Mol Biol* (2008) 110(1–2):67–75. doi: 10.1016/j.jsbmb.2008.02.002

74. Pluchino N, Lenzi E, Casarosa E, Cela V, Begliuomini S, Ninni F, et al. Dydrogesterone increases allopregnanolone in selected brain areas and in serum of female rats. *Fertil Steril* (2008) 89(5 Suppl):1384–9. doi: 10.1016/J.FERTNSTERT.2007.03.077

75. Blair RM, Fang H, Branham WS, Hass BS, Dial SL, Moland CL, et al. The estrogen receptor relative binding affinities of 188 natural and xenochemicals: structural diversity of ligands. *Toxicol Sci* (2000) 54(1):138–53. doi: 10.1093/toxsci/54.1.138

76. Harris HA, Bapat AR, Gonder DS, Frail DE. The ligand binding profiles of estrogen receptors α and β are species dependent. *Steroids* (2002) 67(5):379–84. doi: 10.1016/S0039-128X(01)00194-5

77. Schroeder RA, Thurston RC, Wu M, Aizenstein HJ, Derby CA, Maki PM. Distinctive roles of estrone and estradiol in shaping verbal memory circuitry in postmenopausal women. *Alzheimer's Dementia* (2020) 16(S4):e043110. doi: 10.1002/alz.043110

78. Westlye LT, Kaufmann T, Alnæs D, Hullstein IR, Bjørnebekk A. Brain connectivity aberrations in anabolic-androgenic steroid users. *NeuroImage: Clin* (2017) 13:62–9. doi: 10.1016/j.nicl.2016.11.014

79. Tronson NC, Schuh KM. Hormonal contraceptives, stress, and the brain: the critical need for animal models. *Front Neuroendocrinol* (2022) 67:101035. doi: 10.1016/j.yfrne.2022.101035

80. Zimmerman Y, Eijkemans MJC, Coelingh Bennink HJT, Blankenstein MA, Fauser BCJM. The effect of combined oral contraception on testosterone levels in healthy women: a systematic review and meta-analysis. *Hum Reprod Update* (2014) 20 (1):76–105. doi: 10.1093/humupd/dmt038

81. Hilz EN. Methods and considerations for the use of hormonal contraceptives in rat models of neurobehavior. *Front Neuroendocrinol* (2022) 66. doi: 10.1016/j.yfrne.2022.101011

82. Pletzer B, Harris TA, Hidalgo-Lopez E. Previous contraceptive treatment relates to grey matter volumes in the hippocampus and basal ganglia. *Sci Rep* (2019) 9(1):2417-851. doi: 10.1038/s41598-019-47446-4

83. Chan MF, Dowsett M, Folkerd E, Wareham N, Luben R, Welch A, et al. Past oral contraceptive and hormone therapy use and endogenous hormone concentrations in postmenopausal women. *Menopause* (2008) 15(2):332–9. doi: 10.1097/gme.0b013e31806458d9

84. Egan KR, Gleason CE. Longer duration of hormonal contraceptive use predicts better cognitive outcomes later in life. *J Women's Health* (2012) 21(12):1259–66. doi: 10.1089/jwh.2012.3522

85. Hampson E. Oral contraceptives in the central nervous system: basic pharmacology, methodological considerations, and current state of the field. *Front Neuroendocrinol* (2023) 68. doi: 10.1016/j.yfrne.2022.101040

86. Regidor PA. The clinical relevance of progestogens in hormonal contraception: present status and future developments. *Oncotarget* (2018) 9(77):34628–38. doi: 10.18632/oncotarget.26015

87. Poldrack RA. Region of interest analysis for fMRI. *Soc Cogn Affect Neurosci* (2007) 2(1):67–70. doi: 10.1093/scan/nsm006

88. Evans AC, Janke AL, Collins DL, Baillet S. Brain templates and atlases. *NeuroImage* (2012) 62(2):911–22. doi: 10.1016/J.NEUROIMAGE.2012.01.024

89. Cole DM, Smith SM, Beckmann CF. Advances and pitfalls in the analysis and interpretation of resting-state FMRI data. *Front Syst Neurosci* (2010) 8. doi: 10.3389/fnsys.2010.00008

frontiers | Frontiers in Endocrinology

TYPE Case Report
PUBLISHED 12 September 2023
DOI 10.3389/fendo.2023.1224381

OPEN ACCESS

EDITED BY
Alexandre Benani,
Centre National de la Recherche Scientifique (CNRS), France

REVIEWED BY
Romesh Khardori,
Eastern Virginia Medical School, United States
Natale Calomino,
Surgery and Neuroscience, University of Siena, Italy
Hiraku Kameda,
Cedars Sinai Medical Center, United States

*CORRESPONDENCE
Qiaoying You
youqiaoy@aliyun.com

RECEIVED 17 May 2023
ACCEPTED 25 August 2023
PUBLISHED 12 September 2023

CITATION
Zhang X, Huang D, Pan X, Si Q and You Q (2023) ACTH-producing small cell neuroendocrine carcinoma from the gallbladder: a case report and literature review.
Front. Endocrinol. 14:1224381.
doi: 10.3389/fendo.2023.1224381

ACTH-producing small cell neuroendocrine carcinoma from the gallbladder: a case report and literature review

Xiaofang Zhang, Dihua Huang, Xiaojie Pan, Qiya Si and Qiaoying You*

Department of Endocrinology, Shaoxing People's Hospital, Shaoxing, Zhejiang, China

Ectopic adrenocorticotropic hormone syndrome (EAS) is a condition of hypercortisolism caused by non-pituitary tumors that secrete adrenocorticotropic hormone (ACTH). A rare occurrence of this syndrome is due to an ACTH-producing neuroendocrine tumor that originates from the gallbladder. One patient with severe hypokalemia and alkalosis was admitted to our hospital. Clinical presentations and radiographic findings confirmed the diagnosis of an aggressive ACTH-producing gallbladder malignancy with multiple liver metastases. The diagnosis was verified by pathological and immunohistochemical measurements from a biopsy of the hepatic metastasis. A literature review identified only four similar cases had been reported. Despite being rare and having a poor prognosis, hormone-producing neuroendocrine tumors that derive from the gallbladder should be considered in the differential diagnosis of ectopic ACTH syndrome.

KEYWORDS

Cushing syndrome, ectopic adrenocorticotropic hormone syndrome, neuroendocrine tumor, gallbladder, case report

Introduction

Neuroendocrine neoplasms (NENs) are a heterogeneous group of tumors originating from neuroendocrine cells and are able to secrete amines or peptides as their neurotransmitters, such as 5-hydroxytryptamine, vasoactive polypeptide, insulin, growth hormone, adrenocorticotropic hormone, gastrin, somatostatin pancreatic polypeptide, and calcitonin. Ectopic adrenocorticotropic hormone syndrome (EAS) develops as a result of neuroendocrine tumors outside of the pituitary gland, which secrete either adrenocorticotropic hormone (ACTH) and/or corticotropin-releasing hormone, leading to a clinical presentation that resembles Cushing disease, characterized by hirsutism, muscular wasting, truncal-central obesity, hypertension, diabetes mellitus, and

osteoporosis (1). The most common cause of ectopic ACTH is neuroendocrine tumors derived from the lung and anterior mediastinum. According to the largest published series (involving 383 EAS patients), lung NETs are the most common neoplasm (25%), followed by small-cell lung cancer (SCLC) (20%). Other common tumors are thymic (11%) and pancreatic NETs (8%), medullary thyroid carcinoma (6%), and pheochromocytoma (5%) (2). Tumors originating from the gallbladder and biliary duct were rarely reported.

We reported a case of severe hypokalemia and alkalosis caused by an aggressive ACTH-secreting gallbladder malignancy with numerous liver metastases. Only four comparable cases have been reported (3–6), according to a comprehensive literature review.

Case report

A 65-year-old man was admitted to our hospital with complaints of progressive weakness and anorexia that had persisted for ten days. Prior to this, the patient had been in a normal state. His condition began to deteriorate rapidly, as he claimed to have experienced accelerated fatigue, decreased appetite, and a weight loss of 1 kg. The patient denied experiencing any abdominal pain or diarrhea. His previous medical history included hypertension for the past 8 years and type 2 diabetes mellitus for the past 5 years. Glycemia was well controlled with insulin Aspart30 during the past two years, but it has deteriorated in the last month. Additionally, he underwent a bladder mass resection surgery in 2015, but the pathology of the mass could not be traced. He had a history of smoking for over 20 years and alcohol consumption for 30 years (100 ml per day). There was also a positive family history of hypertension and diabetes mellitus. Physical examination indicated that the patient had facial blushing, central obesity with thin extremities, and proximal muscle wasting. Pitting edema was also observed in both lower limbs. Skin hyperpigmentation was not obvious. His height measured at 159 cm, weight at 64 kg, and his blood pressure at 162/102 mmHg.

Laboratory tests showed that the hematocrit and leukocyte count were normal, the platelet count decreased to 62 $\times 10^9$/L. Liver function manifested slightly elevated GGT (81.2 U/L) and total bilirubin (31.3 μmol/L). Hypoproteinemia was observed (serum albumin: 31.7 g/L). HbA1c was 7.5%, indicating that blood glucose levels had not been well controlled for the past 3 months. Notable analysis revealed a hypokalemia of 1.98 mmol/L and metabolic alkalosis. Urinary potassium excretion (138.53 mmol/24 h) markedly increased. Additional tests revealed that the patient had disrupted circadian biorhythms of plasma ACTH and cortisol (as shown in Table 1). The plasma ACTH level at 8 a.m. was highly elevated at 820 pg/mL (N 7-46 pg/mL). Both serum and 24-hour urine cortisol levels were remarkably beyond the upper limit of detection, and could not be suppressed by high-dose dexamethasone (administered orally, 2 mg every 6 hours for 2 days). Tumor markers, especially CEA, CA199, and AFP, were elevated. All these data raised suspicion of ACTH-dependent Cushing syndrome, and further imaging examinations were conducted in an attempt to locate the tumors. Enhanced CT (Figure 1A) and MRI (Figure 1B) scans consistently detected a mass in the gallbladder invading the liver. Multiple metastases were discovered in the liver. The pituitary gland appeared normal except for a Rathke cyst (Figure 1C). Bilateral adrenal hyperplasia, possibly caused by elevated ACTH, was also noted (Figure 1D). A CT-guided transdermal biopsy of liver metastasis was successfully performed. Immunohistochemical analysis revealed a small cell neuroendocrine tumor with positive staining of chromogranin A, synaptophysin, and ACTH (Figure 2) (7). Based on the evidence, a diagnosis of an ectopic ACTH-production tumor with hepatic metastases derived from the gallbladder was made.

As for the treatment, the patient received a daily dosage of 180 mg spironolactone (divided into three times) and 134 mmol of potassium. This eventually helped to maintain the serum potassium level at 3.7 mmol/L. Radical resection of gallbladder malignancy and hepatic metastases was unattainable on account of the patient's delicate condition. Chemotherapy, molecular targeted therapy, somatostatin analogues, and peptide receptor radionuclide therapy were openly discussed with the patient and his family members. The patient initially declined these therapeutic measures. He died of advanced gallbladder malignancy, liver function failure, malnutrition, and chronic gastrointestinal bleeding, hypoxemia after one month.

TABLE 1 The main laboratory results in the patient with gallbladder EAS.

Items	Result	Normal range
Serum cortisol (nmol/L, 8 a.m.)	>1380	138-690
Serum cortisol (nmol/L, 0 a.m.)	>1380	138-690
ACTH (pg/ml, 8 a.m.)	820	0-46
24h-UFC (nmol)	>5114	157-645
Serum cortisol after large dose dexamethasone test (nmol/L, 8 a.m.)	>1380	≤138
CEA (ng/ml)	22.9	0-5
APF (ng/ml)	52.73	0-13.4
CA199 (U/ml)	844.19	0-37

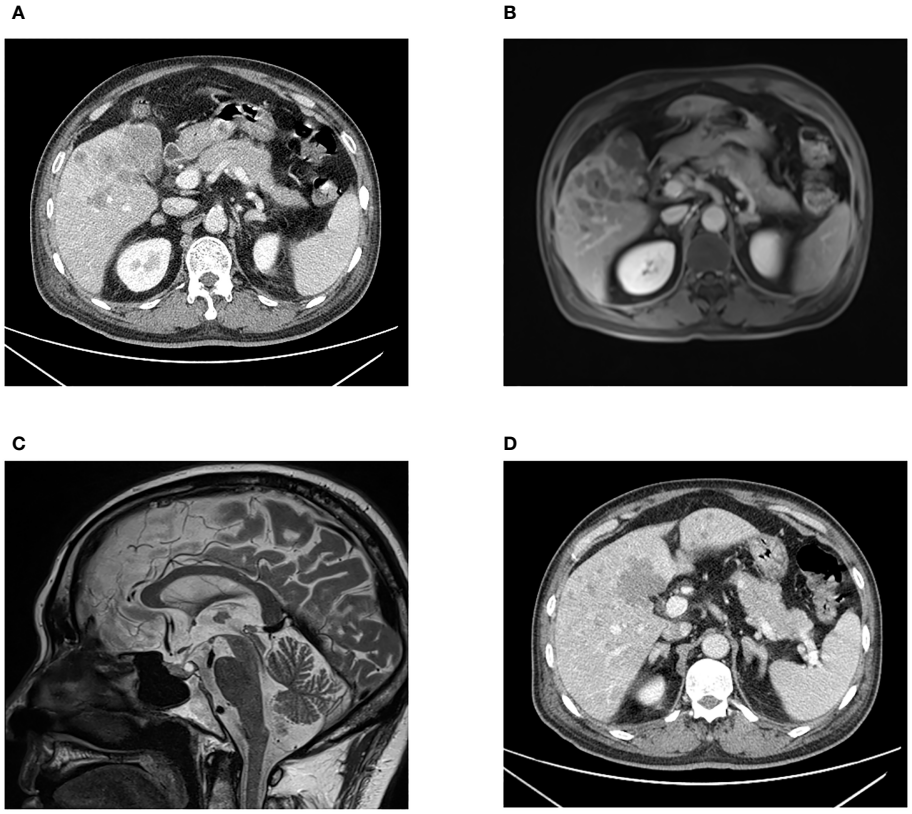

FIGURE 1
CT scan **(A)** and MRI scan **(B)** images presenting an irregular shaped mass in the gallbladder fossa, and multiple intrahepatic nodular lesions. Pituitary MRI **(C)** showing a Rathke cyst in the posterior pituitary gland with high signal intensity on T2WI. Bilaterally enlarged adrenal glands are displayed **(D)**.

Literature review found that 4 cases of gallbladder EAS were reported. Three patients had gallbladder malignancy, and one patient had cholangiocarcinoma. The main clinical characteristics are listed in Table 2.

Discussion

In this patient, elevated ACTH and serum cortisol levels supported the diagnosis of ACTH-dependent Cushing syndrome. The next challenge is to identify the tumor responsible for producing ACTH. High doses of dexamethasone may partially or completely suppress ACTH secretion for most pituitary corticotrophin tumors but not for most ectopic ACTH-secreting tumors (8). However, the high-dose dexamethasone suppression test (HDDST) is considered to have relatively low diagnostic accuracy (9). In some well-differentiated neuroendocrine tumor cases (in particular bronchial, thymic, and pancreatic carcinoids), ACTH secretion can be suppressed by high doses of dexamethasone (10). IPSS (inferior petrosal sinus sampling) is the gold standard to reliably differentiate ectopic ACTH syndrome from pituitary ACTH adenoma. For some EAS patients with indolent tumors, 68Ga-DOTATATE can be used as a tracer in PET imaging to detect criminal tumors (11). For our patients, the diagnosis of ectopic ACTH syndrome caused by a gallbladder mass could be established based on the following evidence: Firstly, high-dose dexamethasone could not suppress serum and urine cortisol levels, indicating the presence of ectopic ACTH-producing tumors. Secondly, a normal pituitary MR image ruled out the existence of an ACTH macroadenoma. Thirdly, biopsy of the hepatic metastasis revealed positive ACTH staining.

According to the new WHO classification, neuroendocrine carcinomas (NECs) are defined as >10 mitoses per 2 mm^2 and Ki-67 >20% (often associated with a Ki-67 >55%). The carcinomas are further subtyped as small cell and large cell neuroendocrine carcinomas based on cytomorphological characteristics (12). In this patient's case, a diagnosis of EAS led to the identification of an ACTH-producing neuroendocrine tumor derived from the gallbladder with multiple intra-hepatic metastases. Pathological and immunohistochemical examination showed positive ACTH in liver metastases with a Ki-67 of 67%, confirming the diagnosis of small cell neuroendocrine carcinoma. His general condition deteriorated rapidly and he had a poor outcome, which is consistent with the typical presentation of carcinoma.

Medical management of EAS is a complex matter. The aim is to reduce excessive cortisol levels and eliminate neuroendocrine tumors. The optimal treatment strategy is complete surgical

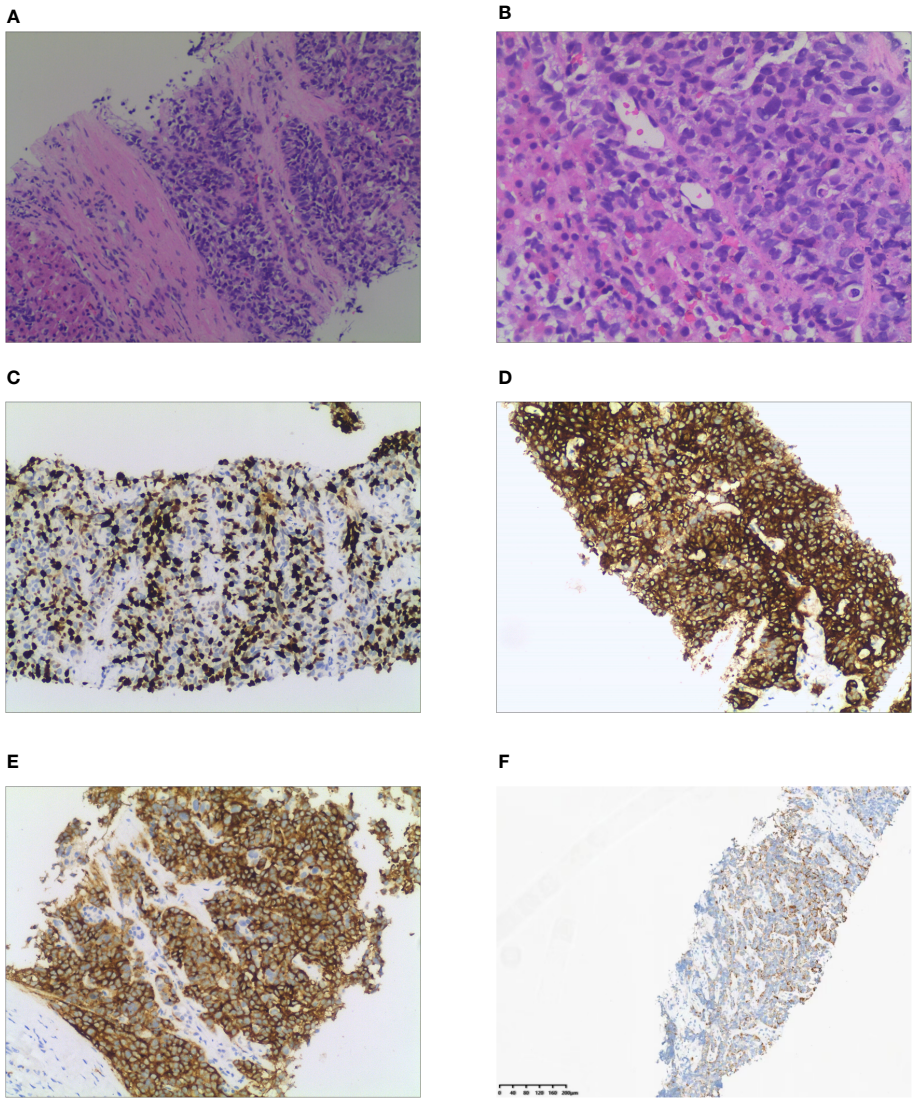

FIGURE 2
Histological and immunohistochemical examination of liver metastasis. **(A)** Tumor cells gather into nests or sheets and infiltrate the fibrous stroma (H&E stain, x100). **(B)** Cellularity is very high with hyperchromatic nuclei and no discernible nucleoli is observed (x200). **(C)** Immunohistochemical staining of Ki 67. Tumor cells demonstrate a Ki 67 index of 67%. **(D)** Tumor cells demonstrate positive expression of chromogranin A. **(E)** Positive expression of synaptophysin is observed in tumor cells. **(F)** ACTH is diffusively expressed in the cytoplasm of tumor cells.

resection of the tumor. However, most patients are at a late stage of disease when they get a final diagnosis, and only 10–30% of them have a chance for curative resection of the tumors. A combination of active chemotherapy, radiotherapy, targeted therapy, somatostatin analogues, and other multimodal treatments should be considered to minimize tumor size and prolong survival time (13). When the tumor is unresectable, management to reduce hypercortisolism should be conducted, including pharmacological agents to suppression of cortisone production or bilateral adrenalectomy. In this case, a multidisciplinary team was organized to deliberate on treatment strategies. Surgical removal of the gallbladder mass and hepatic metastases seemed impossible. Unfortunately, the patient died one month later without attempting any other therapeutic choices due to the rapid progression and deterioration of the disease.

We systematically reviewed the previous reports on ACTH-secreting gallbladder endocrine tumors. Four cases had been reported at present (3–6). All were female patients with severe hypokalemia. The neoplasms presented with highly aggressive atypical carcinoids and produced remarkably high level of ACTH and cortisol. One located in the bile duct, and the other three located in the gallbladder. Three cases had liver metastasis. All patients had rapid progression and a dismal prognosis. In our case, ACTH-producing gallbladder neuroendocrine carcinoma was confirmed by a positive ACTH immunocytochemical stain in biopsy from hepatic metastasis, which provides a novel and simple way to diagnosis.

In conclusion, ACTH-producing neuroendocrine carcinomas located in the gallbladder are rare. We present a case of a male patient with a gallbladder NEC that secretes

TABLE 2 Ectopic ACTH syndrome caused by malignancy from the gallbladder and biliary: patient details, pathology, and tumor location.

Case Number	Sex/ Age (year)	Symptom and sign	K+ (mmol/ l)	ACTH (8 a.m.) (pg/ml)	Cortisol (8 a.m.) (nmol/ L)	24h-UFC (nmol)	Pathology	Management and follow up	Tumor location	Reference
P1	F/44	depression hysteria, weight gain, weakness, oedema, facial plethora, hirsutism, striae and bruise, quadriceps wasting	2.5	161 (N 10-46)	137.48 (N 270-540)	ND.	poorly differentiated anaplastic adenocarcinoma	bilateral adrenalectomy; died in three months;	in the gallbladder, with a secondary tumor in the liver	(3)
P2	F/68	Not given	2.1	1459	2500	ND.	atypical carcinoid	metyrapone; died;	in the gallbladder with liver metastasis	(4)
P3	F/61	edema of the lower extremities, weight gain, moon face, truncal fat deposition, hirsutism, skin hyperpigmentation	2.1	1340	>1380	> 900	liver adenocarcinoma of bile duct origin	cholecystostomy; died one month after surgery	in the bile duct with metastatic deposit in liver	(5)
P4	F/65	weakness, anorexia, proximal muscle weakness hirsutism, moon face, buffalo hump	1.8	224	Not given	Not given	ACTH-producing large cell neuroendocrine carcinoma	cholecystectomy and wedge-shaped liver resection, followed by arterial embolization; died;	in the gallbladder	(6)

Conversion for plasma cortisol: 1 μg/dl = 27.64 nmol/l; ND, not done.

ACTH. The disease advanced rapidly and had a poor prognosis. Recognition of its clinical condition by laboratory measurements, radiological and immunohistochemical examinations may benefit in an earlier diagnosis and a better chance of life-saving management.

Data availability statement

The original contributions presented in the study are included in the article/supplementary material. Further inquiries can be directed to the corresponding author.

Ethics statement

The studies involving humans were approved by the ethics committee of Shaoxing People's Hospital. The studies were conducted in accordance with the local legislation and institutional requirements. The participants provided their written informed consent to participate in this study. Written informed consent was obtained from the individual(s) for the publication of any potentially identifiable images or data included in this article.

Author contributions

XZ and DH are co-first authors of this case report. XZ conducted the writing and literature search. DH performed the acquisition, analysis and interpretation. XP and QS carried out the medical practice. QY is the corresponding author supervising this work. All authors contributed to the article and have approved the submitted version.

Funding

This work was supported by Zhejiang Medical and Health Science and Technology Program (2023KY365)

Conflict of interest

The authors declare that the research was conducted in the absence of any commercial or financial relationships that could be construed as a potential conflict of interest.

Publisher's note

References

1. Isidori AM, Kaltsas GA, Pozza C, Frajese V, Newell-Price J, Reznek RH, et al. The ectopic adrenocorticotropin syndrome: clinical features, diagnosis, management, and longterm follow-up. *J Clin Endocrinol Metab* (2006) 91(2):371–7. doi: 10.1210/jc.2005-1542

2. Isidori AM, Lenzi A. Ectopic ACTH syndrome. *Arq Bras Endocrinol Metabol* (2007) 51(8):1217–25. doi: 10.1590/s0004-27302007000800007

3. Spence RW, Burns-Cox CJ. ACTH-secreting 'apudoma' of gallbladder. *Gut* (1975) 16(6):473–6. doi: 10.1136/gut.16.6.473

4. Howlett TA, Drury PL, Perry L, Doniach I, Rees LH, Besser GM. Diagnosis and management of ACTH-dependent Cushing's syndrome: comparison of the features in ectopic and pituitary ACTH production. *Clin Endocrinol (Oxf)* (1986) 24(6):699–713. doi: 10.1111/j.1365-2265.1986.tb01667.x

5. Papastratis G, Zografos GN, Pappis HC, Kontogeorgos G, Anagnostopoulos G, Kounadi T, et al. ACTH-producing cholangiocarcinoma associated with Cushing's Syndrome. *Endocr Pathol* (1999) 10(3):259–63. doi: 10.1007/BF02738888

6. Lin D, Suwantarat N, Kwee S, Miyashiro M. Cushing's syndrome caused by an ACTH-producing large cell neuroendocrine carcinoma of the gallbladder. *World J Gastrointest Oncol* (2010) 2(1):56–8. doi: 10.4251/wjgo.v2.i1.56

7. Lamberts SW, Hofland LJ, Nobels FR. Neuroendocrine tumor markers. *Front Neuroendocrinol* (2001) 22(4):309–39. doi: 10.1006/frne.2001.0218

8. Liddle GW. Tests of pituitary-adrenal suppressibility in the diagnosis of Cushing's syndrome. *J Clin Endocrinol Metab* (1960) 20(12):1539–60. doi: 10.1210/jcem-20-12-1539

9. Fleseriu M, Auchus R, Bancos I, Ben-Shlomo A, Bertherat J, Biermasz NR, et al. Consensus on diagnosis and management of Cushing's disease: a guideline update. *Lancet Diabetes Endocrinol* (2021) 9(12):847–75. doi: 10.1016/S2213-8587(21)00235-7

10. Raff H, Carrol T. Cushing's syndrome: from physiological principles to diagnosis and clinical care. *J Physiol* (2015) 593(3):493–506. doi: 10.1113/jphysiol.2014.282871

11. Wannachalee T, Turcu AF, Bancos I, Amir Habra M, Avram AM, Chuang HH, et al. The clinical impact of [^{68} Ga]-DOTATATE PET/CT for the diagnosis and management of ectopic adrenocorticotropic hormone - secreting tumors. *Clin Endocrinol (Oxf)* (2019) 91(2):288–94. doi: 10.1111/cen.14008

12. Mete O, Wenig BM. Update from the 5th edition of the World Health Organization classification of head and neck tumors: overview of the 2022 WHO classifcation of head and neck neuroendocrine neoplasms. *Head Neck Pathol* (2022) 16 (1):123–42. doi: 10.1007/s12105-022-01435-8

13. Kaltsas GA, Besser GM, Grossman AB. The diagnosis and medical management of advanced neuroendocrine tumors. *Endocr Rev* (2004) 25(3):458–511. doi: 10.1210/er.2003-0014

frontiers | Frontiers in Endocrinology

TYPE Original Research
PUBLISHED 29 November 2023
DOI 10.3389/fendo.2023.1290176

OPEN ACCESS

EDITED BY
Alexandre Benani,
Centre National de la Recherche Scientifique (CNRS), France

REVIEWED BY
Charlotte Steenblock,
Technical University Dresden, Germany
Brandon Peter Lucke-Wold,
University of Florida, United States
Hipólito Nzwalo,
University of Algarve, Portugal

*CORRESPONDENCE
Anqiang Yang
717289270@qq.com
Xuhui Hui
huixuhui0806@126.com

RECEIVED 07 September 2023
ACCEPTED 01 November 2023
PUBLISHED 29 November 2023

CITATION
Yang S, Liu Y, Wang S, Cai Z, Yang A and Hui X (2023) Association between high serum blood glucose lymphocyte ratio and all-cause mortality in non-traumatic cerebral hemorrhage: a retrospective analysis of the MIMIC-IV database. *Front. Endocrinol.* 14:1290176. doi: 10.3389/fendo.2023.1290176

Association between high serum blood glucose lymphocyte ratio and all-cause mortality in non-traumatic cerebral hemorrhage: a retrospective analysis of the MIMIC-IV database

Shiqiang Yang [1,2], Yanwei Liu [3], Shiqiang Wang [4], Zhonghai Cai [1], Anqiang Yang [1]* and Xuhui Hui [2]*

[1]Department of Neurosurgery, First People's Hospital of Yibin, Yibin, Sichuan, China, [2]Department of Neurosurgery, West China Hospital, Sichuan University, Chengdu, Sichuan, China, [3]Department of Neurology, First People's Hospital of Yibin, Yibin, Sichuan, China, [4]Department of Neuro-Oncology, Cancer Hospital, Chongqing University, Chongqing, China

Background: This study aimed to evaluate the association between the glucose-to-lymphocyte ratio (GLR) and all-cause mortality in intensive care unit (ICU) patients with Non-traumatic cerebral hemorrhage.

Methods: This is a retrospective cohort study. Baseline data and in-hospital prognosis from patients with non-traumatic cerebral hemorrhage admitted to the intensive care unit. Multivariate COX regression analysis was applied and adjusted hazard ratios (HR) and 95% predictive values with confidence intervals (CI) were calculated. Survival curves for the two groups of cases were plotted using K-M curves, and subgroup analyses were performed in one step. Using restricted cubic spline curves, we analyzed the potential linear relationship between GLR and outcome indicators.

Results: In the Medical Information Mart for Intensive Care IV (MIMIC-IV database), we extracted 3,783 patients with nontraumatic intracerebral hemorrhage, and 1,806 patients were finally enrolled in the study after exclusion of missing values and patients with a short hospital stay. The overall ICU mortality rate was 8.2% (148/1806) and the in-hospital mortality rate was 12.5% (225/1806). The use of curve fitting yielded a significant linear relationship between GLR and both ICU mortality and in-hospital mortality. It also suggested a reference point at GLR=3.9. These patients were categorized into high and low subgroups based on the median value of their GLR (GLR = 3.9). Model comparisons based on multivariate COX regression analysis showed that in-hospital mortality was higher in the high GLR group after adjusting for all confounders (HR = 1.31, 95% CI: 1.04-1.47), while the ICU mortality in the high GLR group was (HR = 1.73, 95% CI: 1.18-2.52). Stratified analyses based on age, gender, race, GCS, BMI, and disease type showed stable correlations between the high GLR group and in-hospital and ICU mortality.

10.3389/fendo.2023.1290176

Conclusion: Based on our retrospective analysis, it is known that as the GLR increased, the in-hospital mortality rate and ICU mortality rate of patients with nontraumatic cerebral hemorrhage also increased progressively in the United States in a clear linear relationship. However, further studies are needed to confirm these findings.

KEYWORDS

glucose-to-lymphocyte ratio, nontraumatic cerebral hemorrhage, medical information mart for intensive care IV, mortality, linear relationship, intensive care unit

Introduction

Acute non-traumatic cerebral hemorrhage, including diseases such as hypertensive cerebral hemorrhage, spontaneous subarachnoid hemorrhage, and hemorrhage of auto-vascular causes, is a group of diseases that seriously endanger the lives of patients. It ranks as the second most prevalent type of stroke, severity, swift advancement, elevated rates of mortality and disability, thereby constituting a significant peril to the global population (1, 2). Despite the implementation of optimal care within the intensive care unit and during hospitalization, patients afflicted with nontraumatic intracerebral hemorrhage continue to exhibit a considerable in-hospital mortality rate (3).Epidemiological surveys have shown that the in-hospital mortality rate for non-traumatic intracerebral hemorrhage is as high as 20%, and even higher in developing countries (3, 4). Considering the serious life-threatening nature of this group of patients, there is an urgent need for non-invasive and inexpensive tests to identify those at greater risk of death and to prevent death (5).

Numerous clinical studies have determined that patients who experience intracerebral hemorrhage exhibit a concurrent systemic inflammatory response. Furthermore, patients with severe cerebral hemorrhage have demonstrated signs of immune cell activation and abnormal host reactions (6, 7). Moreover, various systemic inflammatory biomarkers, such as the neutrophil-lymphocyte ratio (NLR) (8), platelet-lymphocyte ratio (PLR) (9), and lymphocyte-monocyte ratio (LMR) (10), have been linked to critical cerebrovascular disease and unfavorable prognosis in patients. The presence of immune cell deficiency and dysfunction is widely recognized as significant contributors to secondary infections and unfavorable prognosis in critically ill patients. Consequently, variations in the quantity and functionality of immune cells may be linked to mortality rates in this patient population. Among the key effector cells implicated in the systemic inflammatory response of critically ill patients, lymphocytes play a prominent role (11). Consequently, lymphocyte counts, serving as indicators of immune system status, appear to hold predictive value for the prognosis of critically ill patients suffering from intracerebral hemorrhage (12).

Furthermore, Patients with acute cerebral hemorrhage are at increased risk of stress hyperglycemia of varying intensity, and glycemic management may be challenging. A maladaptive mechanism caused by acute stress and inflammatory states antagonizes insulin-mediated glucose uptake through excess cortisol. In addition to hormonal changes, studies have found that cytokines such as TNF-alpha and interleukin-1 are involved in the dysregulation of insulin signaling. Patients progressively develop a hyperglycemic state after the onset of the disease. In addition, it has been shown that there is a correlation between hyperglycemia and poor prognosis in intensive care unit patients, including increased mortality, hospital-acquired infections, wound complications, prolonged intensive care unit stays, and an increased incidence of intensive care neuropathy (11, 13).Acute hyperglycemia, in particular, emerges as an autonomous risk factor for mortality in critically ill individuals (14). Differences between the two indicators, blood glucose and absolute blood lymphocyte values, become apparent through changes in the GLR, an increase in the GLR implying an imbalance in glucose regulation and immune response. This disparity results in the occurrence of organ failure, metabolic disturbances, compromised immune function, and an imbalance between oxygen availability and demand, ultimately culminating in mortality. Increasing evidence suggests a significant correlation between heightened blood glucose levels and diminished lymphocyte counts, indicating the severity of critical cerebral hemorrhage in patients (15). The elevated GLR may serve as an indicator of the combined impact of hyperglycemia and immune dysfunction in critically ill individuals. Current clinical studies suggest that elevated GLR is an important predictor of acute mortality and prognosis in patients with gastric cancer (16), hepatocellular carcinoma (17), breast cancer, thyroid cancer, rectal cancer (18), acute respiratory distress syndrome and acute exacerbation of chronic obstructive pulmonary disease (11).Therefore, it has important clinical significance in terms of malignant tumor disease burden and respiratory disease burden. The aim of this study was to evaluate the correlation between GLR at admission and prognosis of hospitalization in patients with non-traumatic cerebral hemorrhage. GLR, a composite measure encompassing both glucose levels and systemic inflammation, may offer a novel basis and benchmark for the clinical treatment of individuals with severe cerebral hemorrhage. This will contribute to the early identification of critically ill patients in the clinic by these easily available biomarkers and individualized targeted therapy to save patients' lives to a greater extent.

Materials

Study population

This retrospective cohort study adhered to the Guidelines for Enhancing the Reporting of Observational Studies in Epidemiology. The researchers accessed health-related data from the MIMIC-IV (version 2.2) database, a comprehensive and well-maintained general-purpose database created by the MIT Computational Physiology Laboratory. This database contains comprehensive and reliable medical records of patients admitted to the Intensive Care Unit at Beth Israel Deaconess Medical Center. One author (Shiqiang Yang) complied with requirements for access to the database and was responsible for the data extraction(certification number 52945707). Patients diagnosed with non-traumatic cerebral hemorrhage according to the International Classification of Diseases, 9th and 10th editions, were included in this study. Between 2008 and 2019, over 50,000 adult patients were admitted to the ICU at Beth Israel Deaconess Medical Center, Boston. Of these, a total of 3783 patients with non-traumatic cerebral hemorrhage were selected based on records from ICD-9 codes 430 and 431, and I60, I601 ~ I609 and I610 ~ I619 in ICD10 codes. Exclusion criteria were as follows: First, we excluded 679 patients who were not admitted to the ICU for the first time from all 3783 data. Second, 356 patients who were admitted to the ICU for less than 24 hours were excluded from the remaining data. Finally, 742 patients without clear blood glucose and blood lymphocyte counts were excluded. We provided adequate explanations for the exclusion of patients. Finally, a total of 1,806 patients were included in this study (Figure 1).

Data collection

The data for this study was collected by executing Structured Query Language (SQL) using PostgresSQL (version 13.9.9) and Navicate Premium (version 16.1.7) software. The variables selected for analysis can be classified into five main categories: (1) demographic characteristics such as age, gender, weight, height, and BMI; (2) vital signs encompassing systolic blood pressure, diastolic blood pressure, respiration rate, heart rate, temperature, oxygen saturation, length of stay in the intensive care unit (ICU) and hospital, and ICU and hospital mortality.(3) Various scoring systems such as the Glasgow Score (GCS), Sequential Organ Failure Score (SOFA), and Logistic Organ Dysfunction System (LODS) are utilized. (4) Comorbidities encompass pulmonary disease, coagulation abnormalities, heart failure, renal disease, and liver disease. (5) Laboratory indicators encompass blood glucose, white blood cells (WBC), hemoglobin, platelets, serum sodium, serum creatinine, PTT, anion gap, bicarbonate, chloride, and other relevant factors.

The follow-up period began upon admission and ended upon death for deceased patients or discharge for surviving patients. The GLR index was calculated by dividing the fasting blood glucose (mmol/L) by the serum lymphocyte (10^9 cells/L) on the first day of admission. All laboratory variables and disease severity scores were obtained from data recorded for the first instance after the patient's admission to the intensive care unit. To minimize potential bias, when missing values were found for the glucose, serum lymphocyte, and death outcome variables during cleaning of the raw data, we deleted this one case. Covariates with missing values exceeding 10% were excluded. Covariates with less than 10% missing data were processed by the multiple interpolation scheme of the Free Statistics software version 1.7 (Beijing, China) and the statistical software packages R 3.3.2. (Table 1).

Clinical outcomes

The primary endpoint of this study was all-cause mortality in the ICU, and the second endpoint was all-cause mortality in hospital.

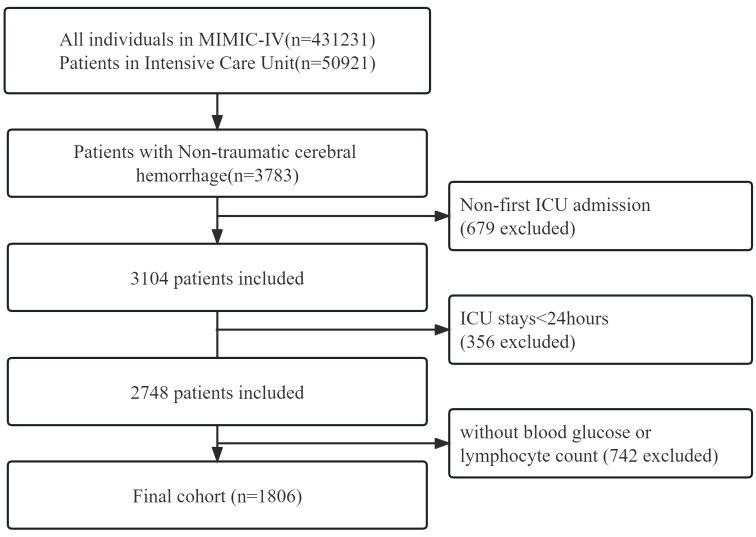

FIGURE 1
A flowchart of study patients.

10.3389/fendo.2023.1290176

TABLE 1 Details of missing values.

Variables	The number of missing values	The percent of missing values(%)
Hemoglobin	17	0.94%
Platelets	21	1.16%
Sodium	25	1.38%
Potassium	26	1.43%
Bicarbonate	27	1.49%
Aniongap	34	1.88%
Chloride	35	1.94%
Calcium	41	2.21%
partial thromboplastin time	64	3.54%
Blood glucose	92	5.09%
Blood lymphocyte	650	35.99%

Statistical analysis

Continuous variables were reported as mean ± standard deviation (SD) or median interquartile range (IQR), while categorical variables were expressed as percentages. The patients were divided into two groups based on the GLR index using the upper quartile. The Q1 group included patients with a low index (GLR<3.9, n=843), while the Q2 group consisted of patients with a high index (BAR≥3.9, n=963). Fisher's exact test, chi-square test, or Kruskal-Wallis test were used to assess the statistical differences between the two groups for each variable. The study employed the restricted cubic splines regression analysis to elucidate the linear correlation between the GLR index and both ICU and hospital all-cause mortality in individuals suffering from acute nontraumatic cerebral hemorrhage.

Additionally, a multivariate Cox proportional hazards model was utilized to evaluate the relationship between the GLR index and both ICU mortality and in-Hospital mortality. Confounding variables were chosen through a combination of clinical expertise, previous research, and effect values surpassing 10% for baseline variables. In the crude Model, the covariates were left unadjusted. In Model I, the covariates were adjusted for age, sex, race, and BMI. In Model II, the covariates were adjusted for the covariates in Model I, along with Glasgow Coma Scale score, Sequential Organ Failure Assessment score, and Logistic Organ Dysfunction System score. In Model III, the covariates from Model II were adjusted for, along with additional variables including WBC, aniongap, bicarbonate, BUN, chloride, creatinine, sodium, PTT, hemoglobin, and platelets. A sensitivity analysis was conducted to assess the reliability of the data analysis.

Kaplan-Meier (K-M) survival curves were utilized to visually depict the relationship between two GLR groups and the occurrence of ICU mortality and in-hospital mortality. Moreover, the study conducted interaction and stratification analyses, considering variables such as age, sex, race, BMI, GCS, and type of disease. The results were presented as hazard ratios (HR) accompanied by a 95% confidence interval (CI), and statistical significance was determined by p values less than 0.05. The statistical software packages R 3.3.2 and Free Statistics software version 1.7.1 (Beijing, China) were employed for all statistical analyses.

Results

Population

In total, 3783 patients were identified according to the non-traumatic cerebral hemorrhage criterion. Of these, 1977 patients without GLR values and other specific conditions were excluded, and 1806 with non-traumatic cerebral hemorrhage criterion were included in the final cohort (Figure 1 shows a flow chart).Out of 1806 patients, 148 patients died in the ICU with a rate of 8.2. In total, 225 patients had a fatal outcome during hospitalization with an incidence rate of 12.5%.

Baseline characteristics

This study included a cohort of 1806 patients out of the total 3783 individuals diagnosed with non-traumatic cerebral hemorrhage and undergoing treatment in the intensive care unit (ICU), as depicted in Figure 1. Among these patients, 1043 were males, with an average age of 64.7 ± 16.9 years. The patients were divided into two groups based on their GLR index, and the distribution of baseline population characteristics for all patients and subgroups can be found in Table 1. Patients in the high GLR index group (≥3.9) exhibited significantly higher scores in SOFA and LODS, as well as higher rates of ICU and in-hospital mortality compared to the low GLR index group. The detailed Baseline characteristics of this study is detailed in Table 2.

Curve fitting analysis

Restricted cubic spline models were utilized to construct smooth curves representing the mortality risk indexed by GLR for both ICU all-cause mortality and hospital all-cause mortality. The solid black line depicts the smooth curve fit between the variables, while the gray bands indicate the 95% confidence intervals. Following the adjustment for covariates, a statistically significant association was observed between GLR levels and all-cause mortality in both the ICU and hospital settings. Specifically, the all-cause mortality in patients with nontraumatic cerebral hemorrhage exhibited a linear increase with higher GLR levels, as depicted in Figure 2. The two curves were separately analyzed to identify inflection points.

Kaplan–Meier curves

In addition, KM survival curves showed that patients in the high GLR score group (GLR≥3.9) at admission had lower ICU survival and in-Hospital survival (both $p < 0.05$), as shown in Figure 3.

10.3389/fendo.2023.1290176

TABLE 2 The clinical characteristics of patients with non-traumatic intracranial hemorrhage.

Characteristics	GLR: blood glucose-to-lymphocyte ratio			*p*-value
	Total (n = 1806)	Tertile1 (<3.9) (n = 843)	Tertile2 ((≥3.9) (n = 963)	
Age, years	64.7 ± 16.9	63.8 ± 17.5	65.5 ± 16.5	0.038
Gender, Male (%)	1043 (57.8)	497 (59)	546 (56.7)	0.332
Race, White (%)	1200 (66.4)	588 (69.8)	612 (63.6)	0.005
BMI,Kg/m^2	27.5 ± 5.4	27.2 ± 4.8	27.8 ± 5.9	0.025
SOAI, hours	4.7 (3.0, 6.0)	4.8 (2.0, 4.0)	4.4 (2.0, 5.5)	0.151
Vital signs				
SBP,mmHg	118.4 ± 17.2	117.9 ± 16.7	118.9 ± 17.7	0.234
DBP,mmHg	64.0 ± 11.6	63.6 ± 11.5	64.3 ± 11.7	0.239
MBP,mmHg	78.6 ± 11.6	78.1 ± 11.4	79.0 ± 11.8	0.131
RR,beats/min	19.5 ± 3.9	19.1 ± 3.6	19.8 ± 4.1	< 0.001
HR,beats/min	85.6 ± 15.6	84.1 ± 15.0	86.9 ± 15.9	< 0.001
Temperature,°C	37.1 ± 0.7	37.0 ± 0.7	37.1 ± 0.8	0.008
SpO2, (%)	96.8 ± 2.4	97.0 ± 2.2	96.7 ± 2.5	0.028
Hospitalization status				
ICU length of stay, days	2.0 (1.1, 4.0)	2.0 (1.1, 3.8)	2.1 (1.1, 4.1)	0.127
ICU mortality, n (%)	148 (8.2)	40 (4.7)	108 (11.2)	< 0.001
Hospital length of stay, days	7.1 (4.0, 12.1)	7.0 (4.1, 12.1)	7.4 (4.0, 12.2)	0.609
Hospital mortality, n (%)	225 (12.5)	84 (10)	141 (14.6)	0.003
Scoring systems				
GCS	12.7 ± 3.4	12.8 ± 3.3	12.7 ± 3.4	0.539
SOFA	5.3 ± 3.8	5.0 ± 3.6	5.6 ± 3.9	< 0.001
LODS	4.8 ± 3.3	4.4 ± 3.1	5.1 ± 3.4	< 0.001
Comorbidities, n (%)				
Chronic pulmonary disease, n (%)	319(17.7)	132(15.7)	187(19.4)	0.031
Coagulation abnormality, n (%)	301(16.7)	133(15.8)	168(17.4)	0.52
Liver diseases, n (%)	185(10.2)	80(9.5)	105(10.9)	0.141
Cardiovascular diseases, n (%)	398(22.0)	170(20.2)	228(23.7)	0.006
Malignancy, n (%)	124 (6.9)	47 (5.6)	77 (8)	0.304
Renal diseases, n (%)	317(17.6)	136(16.1)	181(18.8)	0.008
Laboratory tests				
Hemoglobin, (g/dL)	11.4 ± 2.2	11.4 ± 2.2	11.5 ± 2.2	0.624
Platelets, (10^9/L)	235.1 ± 68.1	234.8 ± 60.5	235.3 ± 64.5	0.936
WBC, (10^9/L)	14.1 ± 10.0	14.4 ± 11.4	13.8 ± 8.5	0.252
Anion gap	17.0 ± 5.2	16.0 ± 4.4	17.8 ± 5.6	< 0.001
Bicarbonate, (mmol/L)	24.6 ± 4.6	24.7 ± 4.5	24.4 ± 4.7	0.216
Creatinine, (mmol/L)	1.7 ± 2.0	1.6 ± 2.0	1.7 ± 1.9	0.297
Sodium, (mmol/L)	139.8 ± 5.1	139.5 ± 4.7	140.1 ± 5.4	0.02

(Continued)

TABLE 2 Continued

Characteristics	GLR: blood glucose-to-lymphocyte ratio			*p*-value
	Total (n = 1806)	Tertile1 (<3.9) (n = 843)	Tertile2 ((≥3.9) (n = 963)	
PTT, seconds	44.0 ± 31.4	42.4 ± 29.1	45.4 ± 33.2	0.042
Glucose,(mmol/L)	7.9 (6.4, 10.6)	6.8 (5.8, 8.2)	9.4 (7.2, 13.2)	< 0.001
Lymphocytes,(10^9/L)	2.1 (1.4, 3.0)	2.9 (2.3, 3.5)	1.4 (1.1, 2.0)	< 0.001

GLR:serum blood glucose/lymphocyte count; BMI,Body mass index; SOAI, stroke onset to the admission to ICU; SBP, systolic blood pressure; DBP, diastolic blood pressure; MBP, mean blood pressure; RR, respiratory rate; HR, heart rate; SpO2, percutaneous oxygen saturation; GCS, Glasgow Coma Score; SOFA, Sequential organ function score; LODS, The Logistic organ dysfunction system; WBC, white blood cell; PTT, Partial thromboplastin time.

Univariate Cox regression analysis

In this study, a univariate Cox regression analysis was conducted to examine the independent effects of various variables on ICU mortality and in-hospital mortality. The findings indicated statistically significant effects of age, GCS, LODS, SOFA, blood glucose, SBP, DBP, MBP, Temperature, respiratory rate, heart rate, SpO2, WBC, Anion gap, Bicarbonate, and BUN, along with GLR (all p<0.05, Table Supplementary 1).

Multi-variable Cox regression analysis

In this study, three multivariate Cox regression models were constructed to examine the independent impact of GLR on in-ICU and Hospital mortality. The resulting effect sizes (HRs) and their corresponding 95% confidence intervals are presented in Table 3. It was observed that the unadjusted model HRs remained statistically significant ($p < 0.05$) across all three models. Specifically, in the unadjusted model, a one-unit increase in GLR was found to be associated with a 5% increase in the difference in ICU mortality (HR = 1.05, 95% CI: 1.02-1.08).In the minimally adjusted model (model I), an increase of one unit in GLR was found to be associated with a 5% increase in the difference in ICU mortality (HR = 1.05, 95% CI: 1.02-1.08). In Model II, which was further adjusted for Model I + GCS + SOFA + LODS, the difference in ICU mortality increased by 3% for each unit increase in GLR (HR = 1.03, 95% CI: 1-1.06).However, in the fully adjusted model (Model III), which accounted for various covariates such as age, gender, race, GCS, SOFA, LODS, pneumonia, stroke onset to the admission to ICU, hemoglobin, platelets, WBC, anion gap, bicarbonate, BUN, chloride, creatinine, sodium, and PTT, the difference in in-ICU mortality increased by 2% for each unit increase in GLR (HR = 1.02 CI: 0.97 to 1.04).In the unadjusted model, the effect value of GLR on hospitalization mortality was (HR = 1.02, 95% CI: 1.01-1.05). In the minimally adjusted model (Model I), the effect value was (HR = 1.02, 95% CI: 1-1.05). In model II,the effect value was (HR = 1.01, 95% CI: 0.98-1.04).In the fully adjusted model (Model III), the effect size was (HR =0.99, 95% CI: 0.96-1.02).

To conduct further sensitivity analyses, we transformed the continuous variable GLR into a categorical variable (median GLR), with the low GLR group (Q1) serving as the baseline reference. The

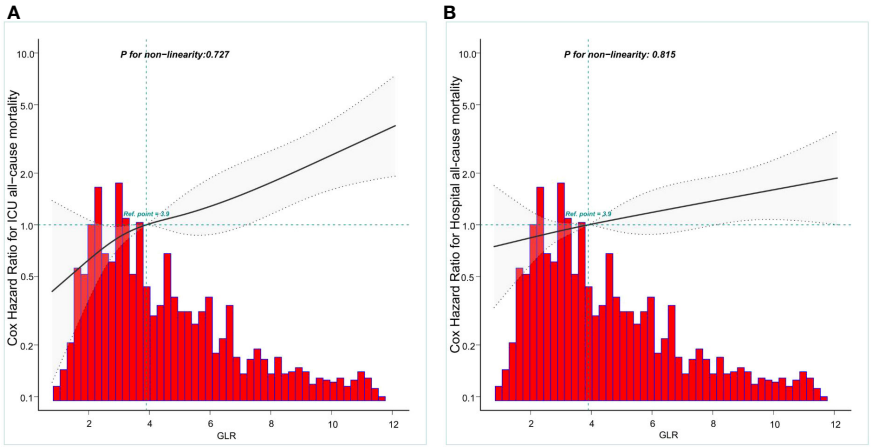

FIGURE 2
Construction of smooth curve describing the risk of mortality against GLR using a restricted cubic spline model. **(A)** ICU all-cause mortality; **(B)** Hospital all-cause mortality. The solid black line represents the smooth curve fit between variables. Grey bands present the 95% confidence interval. Data were adjusted for age, gender, race, BMI,GCS, SOFA,LODS,hemoglobin, Platelets, WBC,anion gap,bicarbonate,BUN, chloride, creatinine sodium and partial thromboplastin time.

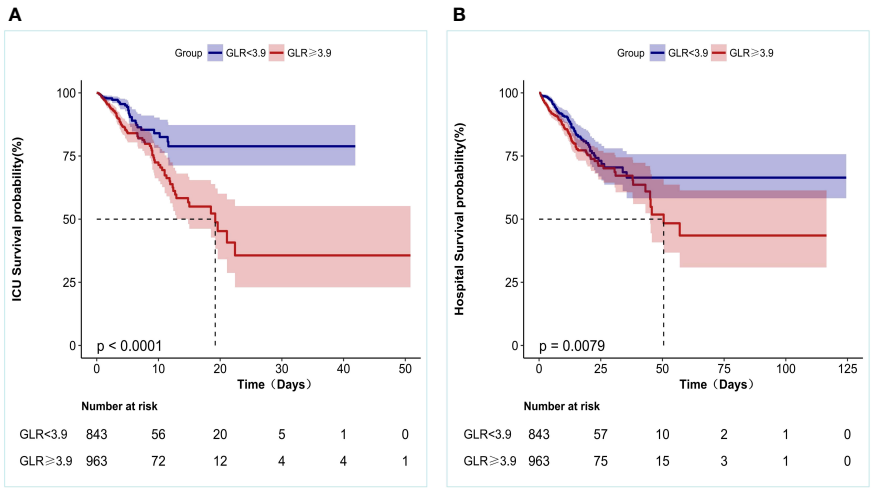

FIGURE 3
Kaplan-Meier survival curves for patients with Non-traumatic intracranial hemorrhage based on GLR group. **(A)** ICU all-cause mortality; **(B)** Hospital all-cause mortality. x-Axis: survival time (days). y-Axis: survival probability.

association between the categorical variable GLR and intensive care unit and hospitalized all-cause mortality was evaluated using the low subgroup (GLR <3.9) as the reference group. In the initial analysis, the high subgroup (GLR ≥3.9) exhibited a significantly elevated risk of intensive care unit (HR: 2.25, 95% CI: 1.56 to 3.23) and in-hospital all-cause mortality (HR: 1.44, 95% CI: 1.19 to 1.89).In the minimally adjusted model I, the heightened risk of ICU mortality (HR: 2.19, 95% CI: 1.52 to 3.15) and in-hospital all-cause mortality (HR: 1.4, 95% CI: 1.17 to 1.83) remained statistically significant even after controlling for age, sex, race, and body mass index. In Model II, which was further adjusted for Model I + GCS + SOFA + LODS, the hazard ratios for ICU mortality (HR: 1.85, 95% CI: 1.28 to 2.67) and hospitalized all-cause mortality (HR: 1.42, 95% CI: 1.13 to 1.61) continued to demonstrate significance. Similarly, in the fully adjusted Model III, the hazard ratios for ICU mortality (HR: 1.71, 95% CI: 1.16 to 2.54) and hospitalized all-cause mortality (HR: 1.33, 95% CI: 1.04 to 1.49) continued to demonstrate significance. Thus, the heightened risk of mortality in patients belonging to the high GLR group remained statistically significant.

Subgroup analysis

Subgroup analyses were conducted to examine the association between the GLR index and all-cause mortality in both ICUs and hospitals. The findings revealed a statistically significant correlation between elevated GLR index values and increased all-cause mortality rates across various subgroups within ICUs and hospitals, encompassing factors such as age, gender, race, body mass index, Glasgow Coma Scale (GCS) score, and disease type. Specifically, patients classified in the high BAR index group exhibited a significantly heightened risk of all-cause mortality in both ICUs and hospitals when compared to those in the low BAR group, thereby aligning with the overall study outcomes (Table Supplementary 2, 3) (Figures 4, 5).

Discussion

This study aimed to evaluate the association between ICU mortality and in-hospital mortality among patients with nontraumatic cerebral hemorrhage who were admitted to the intensive care unit, taking into account the GLR and adjusting for variables related to population-based analysis. Our findings showed a significant linear increasing relationship between GLR when used as a continuous variable and ICU mortality and in-hospital mortality among patients with nontraumatic cerebral hemorrhage of all races in the United States. Furthermore, by employing curve fitting techniques, it was determined that the reference point for GLR was 3.9, and the HR trend exhibited consistency on either side of this reference point. When we applied the median to divide them into high and low subgroups and then analyzed them, we found that patients in the high subgroups had higher ICU mortality and in-hospital mortality than those in the low subgroups. And the statistical difference was significant.

Nontraumatic cerebral hemorrhage is distinguished by non-specific metabolic changes in various organs of the central nervous system and the entire body. Prior research has demonstrated that both inflammatory reactions and hyperglycemia play a role in comparable pathophysiological mechanisms subsequent to an incident of cerebral hemorrhage (ICH) (6, 19). Disrupted oxygen consumption, heightened levels of circulating substrates, impaired glucose and lipid oxidation, and malfunctioning mitochondria are linked to multiorgan dysfunction and unfavorable outcomes in animal models and patients. Acute stress can be triggered following a spontaneous cerebral hemorrhage, which disrupts glucose homeostasis and subsequently leads to hyperglycemia (20). This hyperglycemia has detrimental effects on immune function and metabolism, ultimately resulting in adverse outcomes. The mechanisms underlying glucose dysregulation in this context are multifaceted. Furthermore, neuroendocrine stress can lead to hypersecretion of adrenocorticotropic hormone, which affects hyperglycogenism, glucose metabolism, and insulin resistance

TABLE 3 Multivariable cox regression models evaluating the association between GLR and ICU and Hospital all-cause mortality.

Variable	Crude		Model I		Model II		Model III	
	HR (95%CI)	*P*-value	HR (95%CI)	*P*-value	HR (95%CI)	*P*-value	HR (95%CI)	*P*-value
ICU all-cause mortality								
GLR	1.05 (1.02~1.08)	0.001	1.05 (1.02~1.08)	0.001	1.03 (1~1.06)	0.063	1.02 (0.97-1.04)	0.673
GLR<3.9	1 (Ref)		1 (Ref)		1 (Ref)		1 (Ref)	
GLR≥3.9	2.25 (1.56~3.23)	<0.001	2.19 (1.52~3.15)	<0.001	1.85 (1.28~2.67)	0.001	1.71 (1.16~2.54)	0.005
Hospital all-cause mortality								
GLR	1.02 (1.01~1.05)	0.002	1.02 (1~1.05)	0.099	1.01 (0.98~1.04)	0.56	0.99 (0.97~1.03)	0.531
GLR<3.9	1 (Ref)		1 (Ref)		1 (Ref)		1 (Ref)	
GLR≥3.9	1.44 (1.19~1.89)	0.008	1.4 (1.17~1.83)	0.015	1.42 (1.13~1.61)	0.018	1.33 (1.04~1.49)	0.032

>Crude model: adjusted for none; Model I: adjusted for age, gender, race and BMI; Model II:adjusted for Model I +GCS+SOFA+LODS;
Model III: adjusted for Model II +SOAI+hemoglobin+Platelets+WBC+anion gap+bicarbonate+BUN+chloride+creatinine+sodium+PTT.

(21). Additionally, low lymphocyte counts may be correlated with reduced survival time in individuals with nontraumatic cerebral hemorrhage (7).Previously available clinical studies have demonstrated that in individuals with cerebral hemorrhage, the post-onset stimulus is predominantly inflammatory, accompanied by the release of diverse anti-inflammatory cytokines into the bloodstream. This concomitant release of anti-inflammatory cytokines can trigger immunosuppression, resulting in the apoptosis of a substantial number of lymphocytes. Lymphopenia, a prevalent characteristic of immunosuppression following an all-inflammatory response, hinders the clearance of microbes and consequently gives rise to secondary, more severe infections. These infections are the primary cause of mortality among patients with cerebral hemorrhage (6, 12, 22).

The precise mechanism underlying the correlation between increased GLR levels and unfavorable prognosis in individuals with nontraumatic cerebral hemorrhage remains unclear. In recent times, there has been a growing interest among various researchers in integrating blood glucose levels and inflammation-associated lymphocytes to forecast prognostic biomarkers in specific medical conditions (10, 12, 14, 23). Yılmaz A and colleagues (17) have discovered that GLR prior to sorafenib therapy serves as a novel prognostic biomarker, accurately predicting survival rates in patients diagnosed with advanced hepatocellular carcinoma. The prognostic significance of the GLR has been demonstrated in studies involving metastatic gastric cancer (mGC) and metastatic breast cancer (MBC) patients receiving Cdk 4/6 inhibitors (16). Additionally, in patients with type 2 diabetes and MBC, the preoperative hyperglycemia to lymphocyte ratio was found to be an independent predictor of preoperative central lymph node metastasis (18). Constructing a column-line graph could enhance the predictive accuracy of preoperative central lymph node metastasis in these patients. In the realm of research pertaining to cerebral hemorrhage, prior researchers have established a correlation between the neutrophil-to-lymphocyte ratio (NLR) and blood glucose level (BGL), indicating an independent association between the two variables (8, 9). Consequently, it can be inferred that the intricate interplay of various pathological mechanisms potentially influences the progression of inflammatory response and hyperglycemia, thereby exacerbating secondary brain damage. Although the detrimental impact of acute stress and inflammatory response on the outcome of cerebral hemorrhage (ICH) has been acknowledged, the underlying mechanisms remain unidentified (24). The research conducted by Sérgio Fonseca et al. aimed to assess the impact of neutrophil-to-lymphocyte ratio (NLR) on the outcome of intracerebral hemorrhage (ICH), specifically focusing on hematoma expansion and early brain edema (25). Fei Wang et al. analyzed the relationship between neutrophil and lymphocyte ratios and 30-day mortality in patients with acute cerebral hemorrhage, further exploring the role of inflammatory response in disease progression in patients with cerebral hemorrhage (26). While Shaafi S et al. studied the correlation between erythrocyte distribution width, neutrophil-to-lymphocyte ratio, and neutrophil-to-platelet ratio with 3-month prognosis in patients with cerebral hemorrhage, respectively (27, 28). In contrast, our study directly examined the association between the GLR upon admission and mortality rates during hospitalization and in the ICU among nontraumatic cerebral hemorrhage patients admitted to the ICU. We assessed the inflammatory response and glycemic combo of these patients on admission and then conducted a comprehensive analysis of the impact of the main findings.

The potential synergistic effect of septic immune impairment and hyperglycemia should be taken into account when considering the significance of GLR (29, 30). This study presents novel findings on the association between GLR, a readily accessible biomarker, and the mortality rates in ICU and in-hospital settings among patients with nontraumatic cerebral hemorrhage. To the best of our knowledge, this is the first report to establish a distinct correlation between GLR and the mortality rates in both ICU and in-hospital settings among ICU patients with non-traumatic cerebral hemorrhage. This study has the potential to contribute to the development of a diagnostic or predictive model for in-hospital mortality in future research by incorporating the Generalized Linear Regression technique along with other clinical features of spontaneous cerebral hemorrhage. In summary, our study possesses

10.3389/fendo.2023.1290176

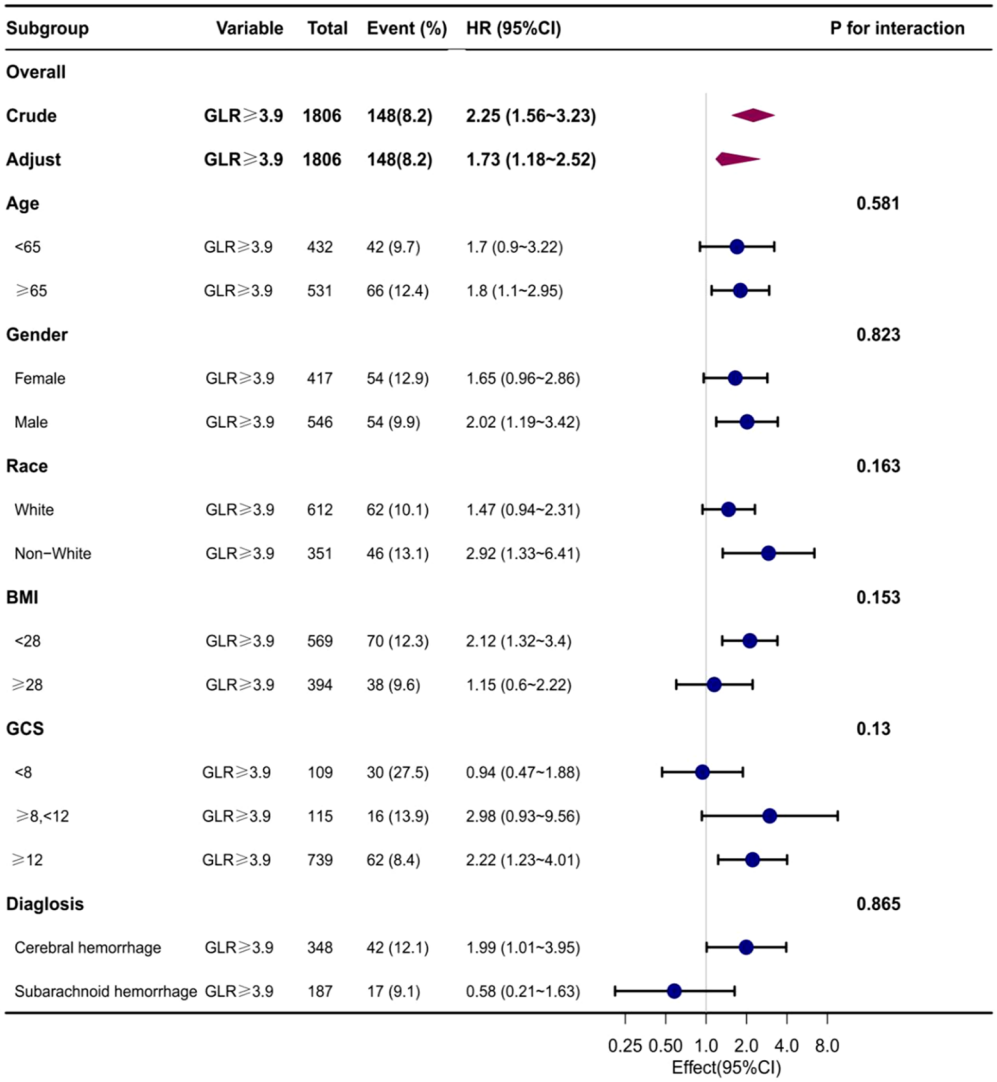

FIGURE 4
Subgroup analyses of the effect of on ICUall-cause mortality. Data were adjusted for age, gender, race, BMI, GCS, SOFA, LODS, hemoglobin, Platelets, WBC, anion gap, sodium bicarbonate, BUN, chloride, creatinine, and partial thromboplastin time.

several notable strengths. Firstly, it utilized a large and diverse population to ensure the validity and generalizability of the findings. Second, rigorous statistical adjustments were used in this retrospective observational study to mitigate the effects of potential residual confounding variables. In addition, the implementation of effect-corrected factor analysis improved data utilization and produced more resilient results across subgroups.

There are some noteworthy limitations to this study. Initially, within the MIMIC-IV database, we encountered limitations in acquiring comprehensive data pertaining to calcitoninogen levels, organ function, and the administration of antithrombotic medications among all patients. Consequently, our ability to accurately distinguish between distinct subtypes of cerebral hemorrhage, determine the extent of hemorrhage volumes, and ascertain the usage of antithrombotic medications in the study cohort was compromised. Furthermore, we encountered challenges in obtaining precise information regarding the treatment protocols employed for the enrolled patients, including the administration of ventilation. Additionally, there may exist residual confounding factors that were not accounted for in our analysis. In addition, some patients with nontraumatic cerebral hemorrhage were excluded from our study due to the lack of necessary data, which may have led to biased findings. Secondly, our researchers do not have access to precise treatment protocols and antibiotic use. We contend that this subject holds significant importance and shall serve as the focal point of our forthcoming research endeavors. Thirdly, our study encompassed a population afflicted with severe non-traumatic cerebral hemorrhage, originating solely from a solitary medical facility. Furthermore, it is worth noting that GLR values undergo dynamic fluctuations throughout the course of hospitalization. However, the GLR values utilized in this study were derived from static measurements taken on the initial day of admission to the intensive care unit (ICU) or hospital, rather than from continuously evolving measurements throughout the course of the disease. Consequently, these values solely reflect the

10.3389/fendo.2023.1290176

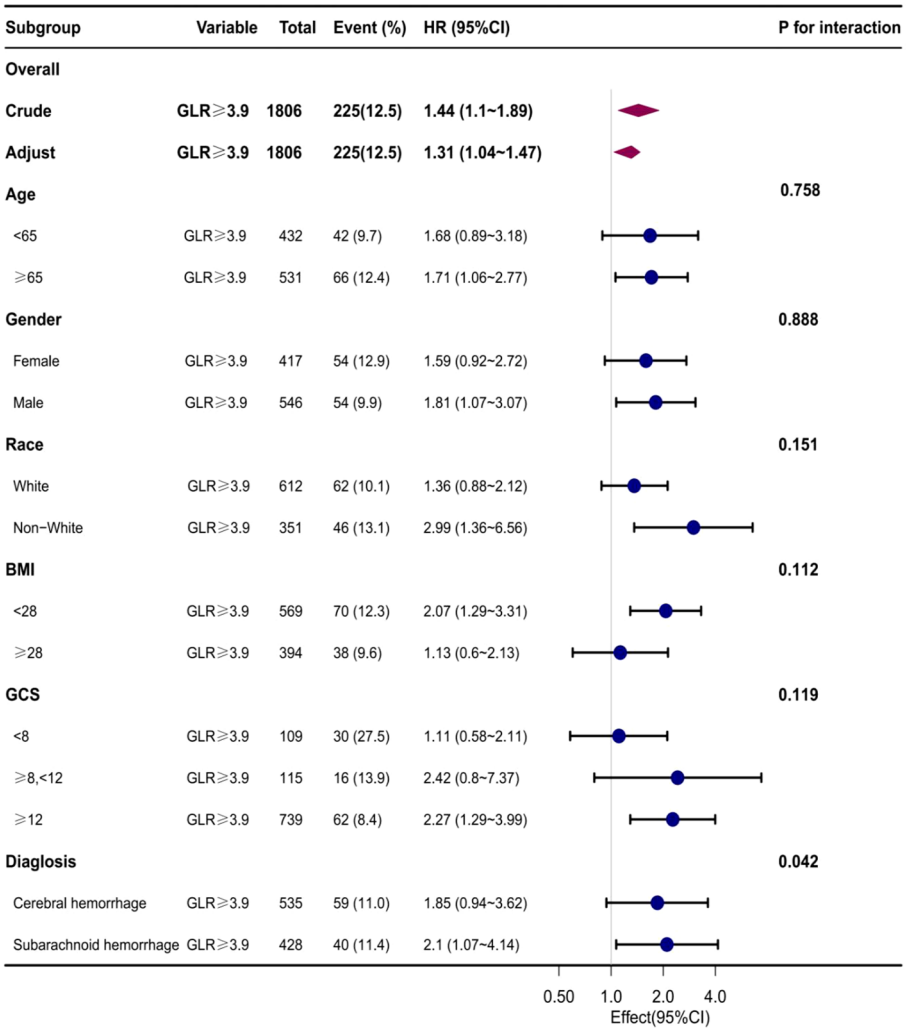

FIGURE 5
Subgroup analyses of the effect of on Hospital all-cause mortality. Data were adjusted for age, gender, race, BMI, GCS, SOFA, LODS, hemoglobin, Platelets, WBC, anion gap, sodium bicarbonate, BUN, chloride, creatinine, and partial thromboplastin time.

impact of the patient's physical condition at the time of hospital admission on the study outcomes. In light of the retrospective nature of our investigation, which relied on data from the MIMIC-IV database. Therefore, it is imperative to conduct further prospective studies of high quality in order to validate the association between GLR and prognosis. A comprehensive examination of the correlation between prognosis in individuals with nontraumatic cerebral hemorrhage could be undertaken by utilizing sequential BAR measurements as an indicator, when circumstances allow. This endeavor would enhance the prompt detection of severely ill patients within the clinical setting through the utilization of readily accessible biomarkers, thereby facilitating tailored therapeutic interventions aimed at significantly improving patient survival rates.

Conclusion

In patients with nontraumatic cerebral hemorrhage, GLR were significantly and linearly associated with both ICU mortality and hospital mortality. When GLR was used as a reference point at 3.9, patients in the higher GLR group had significantly higher ICU mortality and hospitalization mortality than those in the lower group.

Data availability statement

Publicly available datasets were analyzed in this study. This data can be found here: https://mimic.mit.edu/.

Ethics statement

The studies involving humans were approved by Ethics Committee of Yibin First People's Hospital, Yibin First People's Hospital. The studies were conducted in accordance with the local legislation and institutional requirements. The ethics committee/institutional review board waived the requirement of written informed consent for

participation from the participants or the participants' legal guardians/next of kin because This was a retrospective study in a public database, so informed consent was not required.

Author contributions

SY: Writing – original draft. YL: Data curation, Investigation, Writing – original draft. SW: Data curation, Software, Writing – original draft. ZC: Data curation, Investigation, Writing – original draft. AY: Funding acquisition, Supervision, Writing – review & editing. XH: Supervision, Validation, Visualization, Writing – review & editing.

Funding

The author(s) declare financial support was received for the research, authorship, and/or publication of this article. This study was supported by the Sichuan Medical Association's Special Research on Hypertensive Diseases (2019TG27).

Acknowledgments

We would like to thank the Massachusetts Institute of Technology and the Beth Israel Deaconess Medical Center for the MIMIC-IV database. We thank the Sichuan Provincial Medical Association for supporting this study. We thank Prof. Jie Liu (General Hospital of the People's Liberation Army, Beijing, China) and the team of clinician-scientists for their help and support.

Conflict of interest

The authors declare that the research was conducted in the absence of any commercial or financial relationships that could be construed as a potential conflict of interest.

Publisher's note

Supplementary material

The Supplementary Material for this article can be found online at: https://www.frontiersin.org/articles/10.3389/fendo.2023.1290176/full#supplementary-material

References

1. GBD 2019 Diseases and Injuries Collaborators. Global burden of 369 diseases and injuries in 204 countries and territories, 1990-2019: a systematic analysis for the Global Burden of Disease Study 2019. *Lancet* (2020) 396(10258):1204–22. doi: 10.1016/S0140-6736(20)30925-9

2. GBD 2016 Lifetime Risk of Stroke Collaborators, Feigin VL, Nguyen G, Cercy K, Johnson CO, Alam T, et al. Global, regional, and country-specific lifetime risks of stroke, 1990 and 2016. *N Engl J Med* (2018) 379(25):2429–37. doi: 10.1056/NEJMoa1804492

3. Wu S, Wu B, Liu M, Chen Z, Wang W, Anderson CS, et al. Stroke in China: advances and challenges in epidemiology, prevention, and management. *Lancet Neurol* (2019) 18(4):394–405. doi: 10.1016/S1474-4422(18)30500-3

4. Wang W, Jiang B, Sun H, Ru X, Sun D, Wang L, et al. Prevalence, incidence, and mortality of stroke in China: results from a nationwide population-based survey of 480687 adults. *Circulation* (2017) 135(8):759–71. doi: 10.1161/CIRCULATIONAHA.116.025250

5. Wafa HA, Wolfe CDA, Emmett E, Roth GA, Johnson CO, Wang Y. Burden of stroke in Europe: thirty-year projections of incidence, prevalence, deaths, and disability-adjusted life years. *Stroke* (2020) 51(8):2418–27. doi: 10.1161/STROKEAHA.120.029606

6. Keep RF, Hua Y, Xi G. Intracerebral haemorrhage: mechanisms of injury and therapeutic targets. *Lancet Neurol* (2012) 11(8):720–31. doi: 10.1016/S1474-4422(12)70104-7

7. Claude Hemphill J 3rd, Lam A. Emergency neurological life support: intracerebral hemorrhage. *Neurocrit Care* (2017) 27(Suppl 1):89–101. doi: 10.1007/s12028-017-0453-0

8. Khanzadeh S, Lucke-Wold B, Eshghyar F, Rezaei K, Clark A. The neutrophil to lymphocyte ratio in poststroke infection: A systematic review and meta-analysis. *Dis Markers* (2022) 2022:1983455. doi: 10.1155/2022/1983455

9. Muresan EM, Golea A, Vesa SC, Givan I, Perju-Dumbrava L. Admission emergency department point-of-care biomarkers for prediction of early mortality in spontaneous intracerebral hemorrhage. *In Vivo* (2022) 36(3):1534–43. doi: 10.21873/invivo.12864

10. Reznik ME, Kalagara R, Moody S, Drake J, Margolis SA, Cizginer S, et al. Common biomarkers of physiologic stress and associations with delirium in patients with intracerebral hemorrhage. *J Crit Care* (2021) 64:62–7. doi: 10.1016/j.jcrc.2021.03.009

11. Cai S, Wang Q, Ma C, Chen J, Wei Y, Zhang L, et al. Association between glucose-to-lymphocyte ratio and in-hospital mortality in intensive care patients with sepsis: A retrospective observational study based on Medical Information Mart for Intensive Care IV. *Front Med (Lausanne)* (2022) 9:922280. doi: 10.3389/fmed.2022.922280

12. Luo S, Yang WS, Shen YQ, Chen P, Zhang SQ, Jia Z, et al. The clinical value of neutrophil-to-lymphocyte ratio, platelet-to-lymphocyte ratio, and D-dimer-to-fibrinogen ratio for predicting pneumonia and poor outcomes in patients with acute intracerebral hemorrhage. *Front Immunol* (2022) 13:1037255. doi: 10.3389/fimmu.2022.1037255

13. Michel M, Lucke-Wold B. Diabetes management in spinal surgery. *J Clin Images Med Case Rep* (2022) 3(6):1906.

14. Kawata K, Liu CY, Merkel SF, Ramirez SH, Tierney RT, Langford D. Blood biomarkers for brain injury: What are we measuring? *Neurosci Biobehav Rev* (2016) 68:460–73. doi: 10.1016/j.neubiorev.2016.05.009

15. Cao C, Yu M, Chai Y. Pathological alteration and therapeutic implications of sepsis-induced immune cell apoptosis. *Cell Death Dis* (2019) 10:782. doi: 10.1038/s41419-019-2015-1

16. Hannarici Z, Yılmaz A, Buyukbayram ME, Turhan A, Çağlar AA, Biliciet M, et al. The value of pretreatment glucose-to-lymphocyte ratio for predicting survival of metastatic gastric cancer. *Future Oncol* (2023) 19(4):315–25. doi: 10.2217/fon-2022-0579

17. Yılmaz A, Şimşek M, Hannarici Z, Büyükbayram ME, Bilici M, Tekin SB. The importance of the glucose-to-lymphocyte ratio in patients with hepatocellular carcinoma treated with sorafenib. *Future Oncol* (2021) 17(33):4545–59. doi: 10.2217/fon-2021-0457

18. Jin L, Zheng D, Mo D, Guan Y, Wen J, Zhang X, et al. Glucose-to-lymphocyte ratio (GLR) as a predictor of preoperative central lymph node metastasis in papillary

thyroid cancer patients with type 2 diabetes mellitus and construction of the nomogram. *Front Endocrinol (Lausanne)* (2022) 13:829009. doi: 10.3389/fendo.2022.829009

19. Zhang Z, Zhang Z, Lu H, Yang Q, Wu H, Wang J. Microglial polarization and inflammatory mediators after intracerebral hemorrhage. *Mol Neurobiol* (2017) 54 (3):1874–86. doi: 10.1007/s12035-016-9785-6

20. Preau S, Vodovar D, Jung B, Lancel S, Zafrani L, Flatres A, et al. Energetic dysfunction in sepsis: a narrative review. *Ann Intensive Care* (2021) 11:104. doi: 10.1186/s13613-021-00893-7

21. Navas-Marrugo SZ, Alvis-Miranda HR, Moscote-Salazar LR. Manejo neurocrítico de la glicemia en la hemorragia intracerebral espontánea: revisión de la literatura [Neuro-critical management of glycemia in spontaneous intracerebral hemorrhage: review of the literature]. *Bol Asoc Med P R* (2014) 106(1):60–8.

22. Morotti A, Marini S, Jessel MJ, Schwab K, Kourkoulis C, Ayres A, et al. Lymphopenia, infectious complications, and outcome in spontaneous intracerebral hemorrhage. *Neurocrit Care* (2017) 26(2):160–6. doi: 10.1007/s12028-016-0367-2

23. Geraghty JR, Lung TJ, Hirsch Y, Katz EA, Cheng T, Saini NS, et al. Systemic immune-inflammation index predicts delayed cerebral vasospasm after aneurysmal subarachnoid hemorrhage. *Neurosurgery* (2021) 89(6):1071–9. doi: 10.1093/neuros/nyab354

24. Chen S, Li L, Peng C, Bian CJ, Ocak PE, Zhang JH, et al. Targeting oxidative stress and inflammatory response for blood-brain barrier protection in intracerebral hemorrhage. *Antioxid Redox Signal* (2022) 37(1-3):115–34. doi: 10.1089/ars.2021.0072

25. Fonseca S, Costa F, Seabra M, Dias R, Soares A, Dias C, et al. Systemic inflammation status at admission affects the outcome of intracerebral hemorrhage by increasing perihematomal edema but not the hematoma growth. *Acta Neurol Belg* (2021) 121(3):649–59. doi: 10.1007/s13760-019-01269-2

26. Wang F, Hu S, Ding Y, Ju X, Wang L, Lu Q, et al. Neutrophil-to-lymphocyte ratio and 30-day mortality in patients with acute intracerebral hemorrhage. *J Stroke Cerebrovasc Dis* (2016) 25(1):182–7. doi: 10.1016/j.jstrokecerebrovasdis.2015.09.013

27. Shaafi S, Bonakdari E, Sadeghpour Y, Nejadghaderi SA. Correlation between red blood cell distribution width, neutrophil to lymphocyte ratio, and neutrophil to platelet ratio with 3-month prognosis of patients with intracerebral hemorrhage: a retrospective study. *BMC Neurol* (2022) 22(1):191. doi: 10.1186/s12883-022-02721-2

28. Pereira M, Batista R, Marreiros A, Nzwalo H. Neutrophil-to-leukocyte ratio and admission glycemia as predictors of short-term death in very old elderlies with lobar intracerebral hemorrhage. *Brain Circ* (2023) 9(2):94–8. doi: 10.4103/bc.bc_5_23

29. Bahadar GA, Shah ZA. Intracerebral hemorrhage and diabetes mellitus: blood-brain barrier disruption, pathophysiology and cognitive impairments. *CNS Neurol Disord Drug Targets* (2021) 20(4):312–26. doi: 10.2174/1871527320666210223145112

30. Li Z, Li M, Shi SX, Yao N, Cheng X, Guo A, et al. Brain transforms natural killer cells that exacerbate brain edema after intracerebral hemorrhage. *J Exp Med* (2020) 217 (12):e20200213. doi: 10.1084/jem.20200213

frontiers | Frontiers in Endocrinology

TYPE Original Research
PUBLISHED 30 November 2023
DOI 10.3389/fendo.2023.1289558

OPEN ACCESS

EDITED BY
Alexandre Benani,
Centre National de la Recherche Scientifique (CNRS), France

REVIEWED BY
Raoni C. Dos-Santos,
Tulane University, United States
Ifechukwude J. Biose,
Louisiana State University, United States

*CORRESPONDENCE
Mingmei Zhou
zhoumm368@163.com
Xiaojun Gou
gouxiaojun1975@163.com
Ying Huang
huangying0518@126.com

†These authors have contributed equally to this work

‡These authors have contributed equally to this work and share first authorship

RECEIVED 06 September 2023
ACCEPTED 13 November 2023
PUBLISHED 30 November 2023

CITATION
Liu R, Cao S, Cai Y, Zhou M, Gou X and Huang Y (2023) Brain and serum metabolomic studies reveal therapeutic effects of san hua decoction in rats with ischemic stroke.
Front. Endocrinol. 14:1289558.
doi: 10.3389/fendo.2023.1289558

Brain and serum metabolomic studies reveal therapeutic effects of san hua decoction in rats with ischemic stroke

Ruisi Liu[1‡], Shengxuan Cao[2‡], Yufeng Cai[2], Mingmei Zhou[1,3*†], Xiaojun Gou[4*†] and Ying Huang[2*†]

[1]Institute of Interdisciplinary Integrative Medicine Research, Shanghai University of Traditional Chinese Medicine, Shanghai, China, [2]Experimental Research Center, China Academy of Chinese Medical Sciences, Beijing Key Laboratory of Research of Chinese Medicine on Prevention and Treatment for Major Diseases, Beijing, China, [3]Shanghai Frontiers Science Center of TCM Chemical Biology, Shanghai University of Traditional Chinese Medicine, Shanghai, China, [4]Central Laboratory, Baoshan District Hospital of Integrated Traditional Chinese and Western Medicine of Shanghai, Shanghai University of Traditional Chinese Medicine, Shanghai, China

San Hua Decoction (SHD) is a traditional four-herbal formula that has long been used to treat stroke. Our study used a traditional pharmacodynamic approach combined with systematic and untargeted metabolomics analyses to further investigate the therapeutic effects and potential mechanisms of SHD on ischemic stroke (IS). Male Sprague-Dawley rats were randomly divided into control, sham-operated, middle cerebral artery occlusion reperfusion (MCAO/R) model and SHD groups. The SHD group was provided with SHD (7.2 g/kg, i.g.) and the other three groups were provided with equal amounts of purified water once a day in the morning for 10 consecutive days. Our results showed that cerebral infarct volumes were reduced in the SHD group compared with the model group. Besides, SHD enhanced the activity of SOD and decreased MDA level in MCAO/R rats. Meanwhile, SHD could ameliorate pathological abnormalities by reducing neuronal damage, improving the structure of damaged neurons and reducing inflammatory cell infiltration. Metabolomic analysis of brain and serum samples with GC-MS techniques revealed 55 differential metabolites between the sham and model groups. Among them, the levels of 12 metabolites were restored after treatment with SHD. Metabolic pathway analysis showed that SHD improved the levels of 12 metabolites related to amino acid metabolism and carbohydrate metabolism, 9 of which were significantly associated with disease. SHD attenuated brain inflammation after ischemia-reperfusion. The mechanisms underlying the therapeutic effects of SHD in MCAO/R rats are related to amino acid and carbohydrate metabolism.

KEYWORDS

Chinese medicine formula, ischemic stroke, inflammation, metabolomics, GC-MS

1 Introduction

Stroke is recognized as one of the most serious health and life-threatening diseases. Although the incidence of stroke has stabilized and mortality has decreased in recent years, the global burden of stroke continues to grow (1). Strokes are generally classified as hemorrhagic or ischemic stroke (IS), with the latter accounting for approximately 85% of all stroke types (2). IS is severe brain tissue necrosis due to stenosis or obstruction of the arteries supplying blood to the brain (carotid and vertebral arteries), as well as inadequate blood supply to the brain. Its disability rate and mortality rate are also much higher than other types (3).

The clinical treatment options for stroke are very limited and the time window for treatment is also quite narrow. Many contraindications place limitations on the treatment of stroke (4). Tissue-type plasminogen activator (tPA) is currently the only thrombolytic agent approved by the U.S. Food and Drug Administration (FDA) for the treatment of IS (5). However, delayed thrombolytic therapy with tPA has great potential to increase this aspect of hemorrhagic transformation. Thus, there is a pressing need to find better treatment options to overcome the limitations and adverse effects of clinical treatment.

Traditional Chinese medicine (TCM) has been widely used in the treatment of stroke due to its rich application experience and unique theoretical system (6, 7). TCM and has significant advantages in terms of safety, efficacy and multi-target profiling in the treatment of IS (8). According to the development level of IS, different herbal formulas can be selected for treatment (9). It has been shown that some bioactive components in Chinese herbs promote endogenous neurogenesis by affecting the proliferation, migration and differentiation of neural stem cells after reperfusion, which has great therapeutic effects in improving neurological function and cerebral infarct area (6). Salvianolic acid A administration significantly reduced infarct volume and vascular embolization in MCAO/R rats, ameliorated pathological damage in the hippocampus and striatum as well as neurological deficits (10). Ginseng Shouwu extract improved learning and memory abilities in vascular dementia rats. It also promoted the increase in the number of newborn neurons and brain microvessel density by inhibiting the TLR4/NF-κB/NLRP3 inflammatory signaling pathway after IS in rats (11). Baimi Decoction improved neuronal function and neurogenesis by decreasing neuronal loss, vacuolization, neuronal atrophy and neuronal structural disruption, and modulation of the expression of vascular endothelial growth factor, caspase-3 and NF-κB to alleviate pathological abnormalities in MCAO/R rats (12). In addition, Chinese herbal medicine has been shown to reduce the side effects of tPA thrombolysis for acute IS as an adjunctive therapy (13).

San Hua Decoction (SHD) is a symbolic traditional Chinese herbal fomula for IS, first included in "Suwen Bingji Qiyi Baomingji" (a traditional Chinese medicine classic of 1188 A.D. in Jin Dynasty). Clinically, SHD ameliorates hemiplegia due to stroke and stroke sequelae. It has been shown that SHD can effectively improve the prognosis and blood rheology of patients with acute stroke by regulating phosphorylated tau levels, promoting endogenous neurogenesis and reducing cerebral infarction after ischemia-reperfusion injury, and facilitating patient recovery (14). In addition, SHD also has a preventive effect on IS and can be used to improve cerebral embolism and hypertensive crisis (15). SHD contains four herbs, Rhei Radix et Rhizoma (*Rheum palmatum* L. [Polygonaceae], Dahuang) (RR), Notopterygii Rhizoma et Radix (*Notopterygium incisum* Ting ex H. T. [Apiaceae], ChangQianghuo) (NR), Magnoliae Officinalis Cortex (*Magnolia officinalis* Rehd.et Wils. [Magnoliaceae], Houpu) (MO), and Aurantii Fructus Immaturus (*Citrus aurantium* L. [Rutaceae], Zhishi) (AF). Modern pharmacological studies have found that all four herbs have effects related to IS therapy. RR inhibits platelet aggregation and protects neurons damaged from hypoxic-ischemic brain injury (16). The anthraquinone constituent of RR has a protective effect against IS (17). NR can increase cerebral blood flow and improve cerebral blood circulation to reduce neuropathic pain (18). MO can protect nerves from ischemic and reperfusion injury through suppression of encephalitis and improvement of BBB dysfunction. It has preventive and therapeutic effects on neurological and psychiatric diseases (19, 20). The peel extract of AF has been shown to have anti-inflammatory, antioxidant and anti-apoptotic effects through AMPK and NRF2-related signaling, alleviating liver damage in mice (21). The potential therapeutic mechanisms of SHD for IS remain unclear, but we hypothesize that SHD can influence disease progression by improving metabolism.

In this research, we evaluated the therapeutic effects of SHD in a rat model of middle cerebral artery occlusion reperfusion (MCAO/R) with conventional pharmacodynamic indicators, combining a metabolomics approach to identify differential metabolites in brain and serum to elucidate the potential mechanisms of SHD on IS.

Abbreviations: AF, Aurantii Fructus Immaturus; CCA, common carotid artery; ECA, external carotid artery; GC-MS, gas chromatography–mass spectrometry; H&E, hematoxylin and eosin; IS, ischemic stroke; IR, ischemia-reperfusion; ICA, internal carotid artery; MCAO/R, middle cerebral artery occlusion reperfusion; MDA, malondialdehyde; MO, Magnoliae Officinalis Cortex; MCA, middle cerebral artery; NR, Notopterygium Rhizoma Et Radix; NMDAR, N-methyl-D-aspartate receptors; OPLS-DA, orthogonal partial least squares-discriminant analysis; RR, Radix et Rhizoma Rhei; SHD, San Hua Decoction; SOD, superoxide dismutase; TTC, 2,3,5-triphenyl tetrazolium chloride; TCM, traditional Chinese medicine; tPA, tissue-type plasminogen activator; VIP, variable importance in the projection.

2 Materials and methods

2.1 Materials and reagents

Methanol, methoxamine and N, O-Bis (trimethylsilyl) trifluoroacetamide (BSTFA with 1% TMCS) were provided by Sigma-Aldrich Co., Ltd. (Germany); chloroform and pyridine were obtained from Sinopharm Chemical Reagent Co., Ltd (Shanghai, China); heptadecanoic acid was purchased from Aladdin Reagent Co., Ltd. (Shanghai, China). All reagents are analytical grade.

2.2 Preparation of san hua decoction

SHD consists of 4 traditional Chinese herbs, namely Rhei Radix et Rhizoma (RR), Notopterygii Rhizoma et Radix (NR), Magnoliae

Officinalis Cortex (MO) and Aurantii Fructus Immaturus (AF). The medicinal parts of RR, NR, MO and AF were the dried roots, dried barks (including root and branch barks), and dried fruits of the original herbs, respectively. All Chinese medicine decoction slices were purchased from Beijing Tongrentang Co., Ltd. (Beijing, China) and authenticated by Dr. Xirong He (China Academy of Chinese Medical Sciences). The herbs used in SHD were tested for the detection of microorganisms, heavy metals and pesticide residues before they were sold. All test results are in accordance with Chinese safety standards. The quality identification standards of the herbs used were in compliance with the 2020 edition Chinese Pharmacopoeia.

In preparation of SHD, the crude herbs (RR, NR, MO and AF) were mixed in a ratio of 1:1:1:1. The 4 herbs were ground into powder and mixed well to obtain 80 g of raw herb powder, then boiled in 10 times volume of sterile water for 30 minutes. The herbs were then decocted for 2 h, filtered and concentrated to obtain water-based decoctions containing 1 g/mL of the raw herbs. In our previous study, we used an HPLC method to analyze the main components of SHD. SHD mainly contains six active ingredients for the treatment of ischemic stroke, namely Rhein, Emodin, Chrysophanol, Neohesperidin, Magnolol and Notopterol (22).

2.3 Experimental animals

Male Sprague-Dawley rats (SD rats, 8 weeks, body weight 230-250 g) were obtained from Beijing Huafukang Biotechnology Co., Ltd (Beijing, China, SCXK (JING) 2019-0008). All animal experiments complied with the standards of the Principles for Laboratory Animals and were conducted under the guidance of the Bioethics Committee of Experimental Research center of China Academy of Chinese Medical Sciences (license number: ERCCACMS21-2307-03). The rats were housed in an environment with the temperature of 23–25°C and the humidity of 50% with 12 h day and night cycle. The rats were kept for 3 days before performing experiments. Normal rodent chow and water are available to all rats without restriction.

2.4 Grouping and drug administration

The 32 rats were grouped at random into control (Con), sham-operated (Sham), MCAO/R model (Model), and SHD groups, with 8 rats in each group by using the randomized numerical table method. The Con group received no treatment. Sham group received sham operation, Model group and SHD group received MCAO/R treatment. According to the weight of rats, the SHD group was treated with SHD by intragastric administration. The dose administered to rats in the SHD group was converted from the patient's daily clinical dose, which was 7.2 g/kg administered at 10 a.m. daily. The Con, Sham and Model groups were given equal volumes of purified water in same manner, once a day for 10 days. The administration in all groups was uniformly done at the end of modeling and was a therapeutic intervention.

2.5 MCAO/R model establishment

The MCAO rat model was set up by the suture-occluded method according to our previous methods (23). Rats were anesthetized with 1% pentobarbital (40 mg/kg BW, i.p.). The right common carotid artery (CCA), internal carotid artery (ICA) and external carotid artery (ECA) of rats were exposed and carefully isolated without stimulating the vagus nerve. After ligating the CCA and ECA with a thin wire 5 mm from the bifurcation of the ECA and ICA and at the end of the CCA, respectively, the ICA blood flow is blocked by pulling the preloaded wire. A small incision was made at the bifurcation of ICA and CCA, and the monofilament was inserted. Loosened the thread and slowly advanced approximately 18–20 mm until resistance occurred. The ICA is then ligated, leaving the thread in place to prevent the monofilament from falling out. After 90 minutes of cerebral ischemia, the monofilament was gently removed from the ICA to perform reperfusion. Different from the Model group, the monofilament in the Sham group was only inserted 10 mm in the ICA, not the MCA. The wound was disinfected with iodine and sutured.

2.6 Cerebral infarct area measurement and histopathological examination

Rats were anaesthetized with 1% pentobarbital (40 mg/kg, *i.p.*) by intraperitoneal injection, 24 hours after the last administration of the drug. The brain was isolated after craniotomy. MCAO/R-induced cerebral infarct areas were confirmed by 2,3,5-triphenyltetrazolium chloride (TTC) staining. The brain tissue was cut into six posterior coronal slices before incubation with 2% TTC. The cerebral infarct area percentage was calculated by using the Image J 1.41 software (24). For histopathological examination, brain tissues from the ischemic area were fixed in 4% paraformaldehyde for 12 hours. The brain tissues was then subjected to gradient dehydration and transparency with xylene for 1 hour. Finally, the brain tissues were embedded in paraffin, sectioned and stained with hematoxylin and eosin (H&E).

2.7 Serum biochemical examination

The levels of superoxide dismutase (SOD) and malondialdehyde (MDA), two oxidative stress-related indicators, were measured using the appropriate assy kits.

2.8 Metabolomic studies

2.8.1 Sample collection and procession

Metabolite profiles were analyzed using gas chromatography-mass spectrometry (GC-MS). 24 hours after the last dose, 1% pentobarbital (40 mg/kg *i.p.*) was used to anesthetize rats and blood was obtained from the abdominal aorta. Serum samples

were obtained by centrifugation at 4°C, 3500 rpm for 15 minutes, and the supernatant was gathered. Brain tissue was put into normal saline (NS) to remove blood. The collected serum and brain samples were then frozen at -80°C. Subsequent analyses were performed by GC-MS within 48 hours.

2.8.2 Sample preparation for GC-MS

Samples were thawed at room temperature before processing. The 50 mg of brain tissue was taken and 500 µl of methanol-water-chloroform (5:2:2, v/v/v) mixture was added. The mixture was vortexed for 1 minute and then sonicated for 5 min. The 50 µL of serum was placed in a 1.5 mL centrifuge tube. Centrifuge tubes were placed at -20°C and incubated for 20 minutes. After being centrifuged at 13,000 rpm for 10 min at 4°C, the supernatant was removed. The 10uL of heptadecanoic acid-methanol solution (1.0 mg/mL) was added into 200 µL of supernatant as internal standard. After being blow-dried, 50 µL of methoxyamine-pyridine hydrochloride solution (15 mg/mL) was added to the residue and shaken at 30°C for 90 min. After adding 50 µL of methoxylamine-pyridine hydrochloride solution (15 mg/mL) to the residue, it was shaken at 30°C for 90 min. The mixture was then methylsilylated at 70°C for 1 h after adding 50 µL of BSTFA with 1% TMCS to the mixture. The samples were left at room temperature for 1h and waited for analysis.

2.8.3 GC-MS conditions

The Agilent 6890N gas chromatograph with the Agilent 5975B mass selective detector and an inert electron impact ionization (EI) source comprise the GC-MS analysis system. The column was an Agilent J&W DB-5ms Ultra Inert chromatography column (30m x 0.25mm, 0.25µm). The carrier gas consisting of high purity helium (99.9996%) was delivered at a constant flow rate of 1.0 mL/min. Split injection was performed with the split ratio of 2:1 and injection volume of 1.0mL. The temperature of both the mass spectrometry interface and the injection port is 260°C. The temperatures of the ion source and the quadrupole were 230°C and 150°C, respectively. The ionization voltage is 70 eV. The data was acquired in full scan mode with a scanning range of 50-500 m/z. A randomized cross-feeding order was used for all samples.

The brain is analyzed under the following conditions: an starting temperature of the GC was set at 90°C for 1 minute. The temperature is increased to 180°C at a rate of 10°C/min, then to 240°C at a rate of 5°C/min. The final temperature is raised to 290°C at 25°C/min for 11 minutes. The solvent delay time was 5 minutes.

The serum is analyzed under the following conditions: an starting temperature of the GC was set at 80°C for 2 minute. The temperature is increased to 240°C at a rate of 5°C/min, then to 290°C at a rate of 25°C/min for 10 minutes. The solvent delay time was 7 minutes.

2.8.4 Data processing and pattern recognition analysis

The pre-processing of raw data was performed using R software. The data were further analyzed using SIMCA software, including orthogonal partial least squares discriminant analysis (OPLS-DA), S-plot and permutation validation. Metabolite changes between the two groups were analyzed using OPLS-DA. Permutation validation was performed prior to the OPLS-DA analysis. The parameters R2 and Q2 were used to assess whether the model was valid, so as to avoid the risk of overfitting. S-plots were obtained on the basis of variable importance in projection (VIP) values calculated by OPLS-DA with VIP values > 1.0.

2.9 Statistical analysis

All of the experimental measurements were presented as mean ± SD. Differential metabolite finding was analyzed by SPSS software for independent samples t-test. Determination of differential metabolites depended on VIP values > 1.0 and p-values < 0.05 from Student's t-tests. GraphPad Prism software was used to analyze oxidative stress levels and differential metabolite levels. Shapiro–Wilk normality test to verify normality. One-way ANOVA was used for analyzing the statistics of four groups. The *post hoc* test used was the Dunnett-t test. Correlations between different metabolite levels and disease were determined by Spearman's correlation analysis. The significant differences were indicated by: * $p < 0.05$, ** $p < 0.01$, *** $p < 0.001$.

2.10 Pathway analysis of metabolites

The different patterns of specific metabolites obtained by screening were analyzed using MetaboAnalyst 5.0 to identify their metabolic pathways. In this study, pathways with pathway impact >0.10 were categorized as potential metabolic pathways. All metabolic pathways were linked through the Kyoto Encyclopedia of Genes and Genomes (KEGG, http://www.genome.jp/kegg/).

3 Results

3.1 The influence of SHD on cerebral infarct area in rats with cerebral ischemia-reperfusion

The cerebral infarct area is an important indicator of brain damage. Compared with the Sham group, the cerebral infarct area of brain tissue in rats in the Model group was drastically higher, with statistical differences ($p < 0.01$). Compared with the Model group, the cerebral infarct area in the SHD group was significantly lower, with statistical differences ($p < 0.01$). Detailed data can be found in Supplementary Figure 1, Supplementary Table 1.

3.2 The influence of SHD on oxidative stress levels

The results of SOD and MDA measurements showed a beneficial role of SHD in regulating oxidative stress markers. Compared with the Sham group, MDA levels were significantly higher ($p < 0.01$) and SOD levels were not significantly changed in the Model group, while SOD was significantly higher in the SHD group ($p < 0.01$). Compared with the Model group, the SHD group showed an increase in SOD levels ($p < 0.05$) and a significant decrease in MDA levels ($p < 0.01$). (Figure 1, Supplementary Table 2).

3.3 The influence of SHD on the histopathological abnormality of brain

After H&E staining, the morphological characteristics of neurons were evaluated. Brain tissue morphology in the Con and Sham groups was essentially normal, with intact cytoarchitecture and neatly arranged cells, and no pathological abnormalities were observed (Figures 2A, B). In the Model group, the brain tissue in the ischemic area was extensively necrotic, with some cortical areas showing a highly sparse sieve reticular structure, unclear cell structure, significantly reduced number of brain tissue cells, and degeneration and necrosis of neurons (Figure 2C). The SHD group showed less cell necrosis and lesions, neater cell alignment, and less inflammatory cell infiltration compared to the Model group. (Figure 2D).

3.4 The influence of SHD on differential metabolites

3.4.1 Multivariate data analysis for brain and serum samples

We used OPLS-DA, S-plot scores and permutation validation in supervised mode to analyze data from Sham, Model and SHD groups (Figures 3, 4) to investigate the effect of SHD on the metabolic pattern of MCAO/R rats. A clear separation was observed between the Sham and Model groups (Figure 3A), indicating that the composition of brain tissue metabolites was significantly influenced by the MCAO/R procedure. The samples in the SHD group were significantly separated from the Model group (Figure 3B). The separation between the two groups indicates that the metabolites in the two groups are significantly different. This result confirms the effect of SHD treatment in ameliorating brain injury by modulating certain metabolic pathways.

3.4.2 Identification of potential endogenous metabolites

Screening for differential metabolites between the two groups associated with IS was performed by the OPLS-DA model. Significance levels were set at $p < 0.05$ and VIP > 1. We identified differential metabolites in the model and Sham groups. There were 28 different endogenous metabolites identified in the brain samples (Table 1). There were 34 different endogenous metabolites identified in the serum samples (Table 2). The overlap of

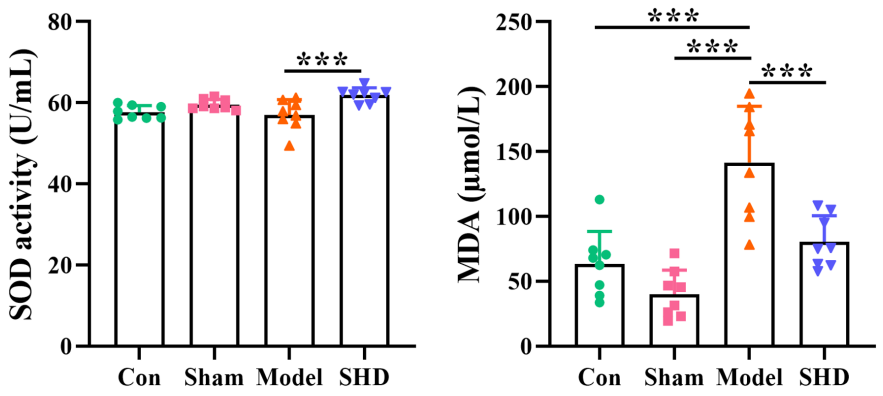

FIGURE 1
Effect of SHD on SOD and MDA in serum of rats with cerebral ischemia-reperfusion. ***$p < 0.001$ relative to the Model group.

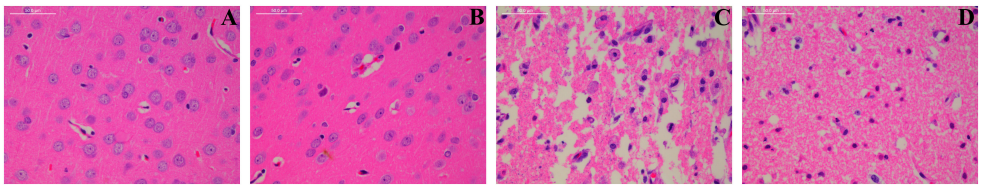

FIGURE 2
Effect of BMD on histopathological abnormality of brain tissue. Original magnification: ×4 and ×10. **(A)** Con group; **(B)** Sham group; **(C)** Model group; and **(D)** SHD group.

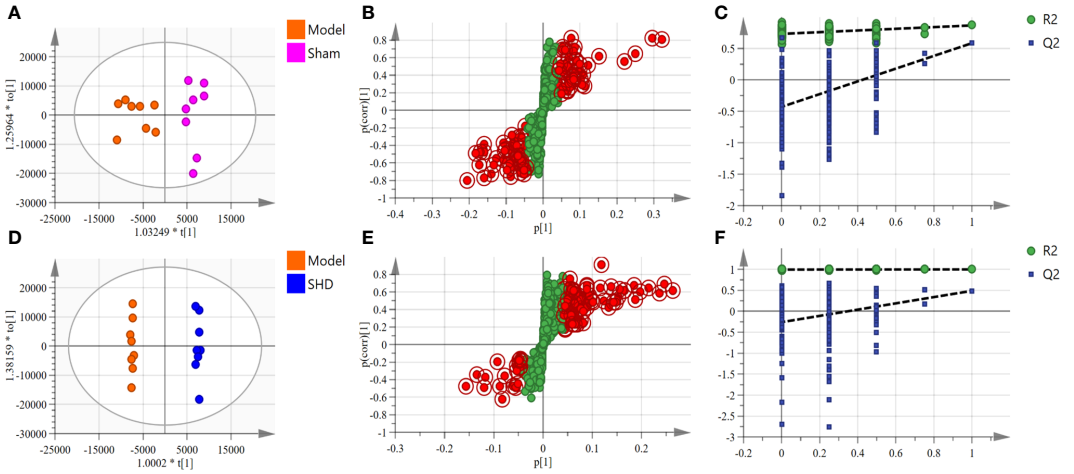

FIGURE 3
OPLS-DA scores, S-plot and permutation validation of the brain samples. **(A–C)** Sham group vs. Model group; **(D–F)** Model group vs. SHD group. (n = 8).

endogenous metabolites in brain and serum samples was analyzed using Venn diagrams (Figure 5). The results showed that the following metabolites were present in serum and brain samples, phosphoric acid, L-isoleucine, 2-butenedioic acid, propanoic acid, butanoic acid, L- (−)-sorbose, D-allose,D-Glucose and myo-inositol. After SHD treatment, levels of a total of 12 of these 55 different endogenous metabolites were restored in MCAO/R rats. Of these 12 metabolites, 7 were in the brain and 5 in the serum. The 7 metabolites in the brain are 2-piperidinecarboxylic acid, urea, glycine, L-proline, gluconic acid, butyric acid and phosphoric acid (Figure 6). The five metabolites in the serum were acetic acid, DL-ornithine, L-ornithine, D-allose and myo-inositol (Figure 7).

3.4.3 Verification of metabolic pathway analysis and relevant targets

The cluster analysis of metabolites in the brain and serum is shown as a heat map in Figure 8A. Metabolic pathway analysis was conducted on four groups of differential metabolites, to explore correlations between metabolites and major metabolic pathways, with the MetaboAnalyst 5.0 online database. Based on statistical analysis, metabolic pathways with $p < 0.05$ and impact > 0.10 were the major metabolic pathways. The results of metabolic pathway analysis revealed common pathways between the Model and SHD groups, suggesting that SHD acts primarily by affecting these 4 metabolic pathways in MCAO/R rats: glyoxylate and dicarboxylate metabolism, arginine and proline metabolism, inositol phosphate metabolism, and glycine, serine and threonine metabolism (Figure 8B). In the KEGG database, 4 major metabolic pathways were linked into a complete metabolic network, elucidating the key metabolic pathways through which SHDs exert their therapeutic effects. (Figure 9).

3.4.4 SHD improves disease-related metabolites levels

To elucidate the relationship between alterations in these 12 associated metabolites and IS, we performed Spearman

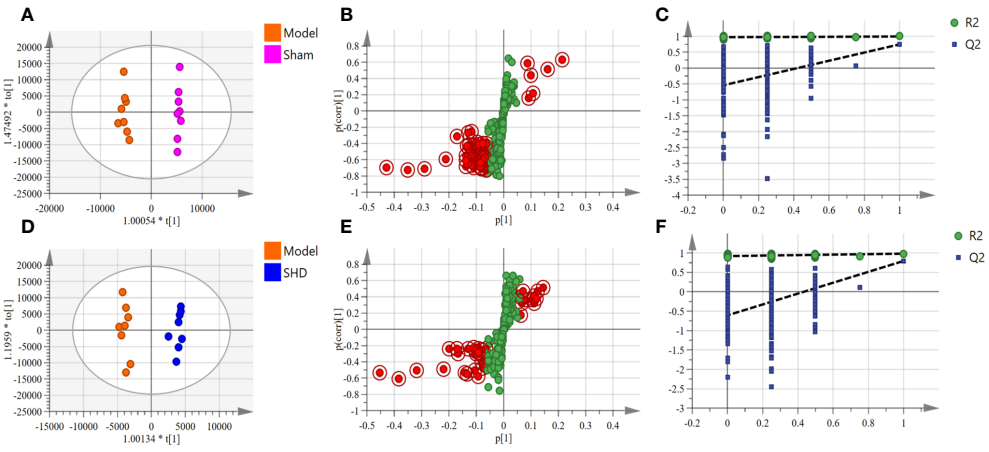

FIGURE 4
OPLS-DA scores, S-plot and permutation validation of the serum samples. **(A–C)** Sham group vs. Model group; **(D–F)** Model group vs. SHD group. (n = 8).

10.3389/fendo.2023.1289558

TABLE 1 Statistical analysis results of identified metabolite changes in the brain.

NO.	Name	Molecular Formula	P value	VIP	M/Z	RT	Fold Change	HMDB
1	Acetic acid	C8H20O3Si2	0.044	1.407	146.9	5.161	0.80	HMDB0000042
2	l-Alanine	C9H23NO2Si2	0.045	1.444	243.9	5.377	0.81	HMDB0000161
3	Propanedioic acid	C9H20O4Si2	0.019	1.604	151.9	6.036	0.69	HMDB0000691
4	Phosphoric acid	C7H21O4PSi2	0.017	1.885	261	6.469	0.32	HMDB0002142
5	L-Valine	C11H27NO2Si2	0.033	1.625	144	6.936	1.39	HMDB0000883
6	Urea	C7H20N2OSi2	0.024	1.674	189	7.475	0.55	HMDB0000294
7	L-Isoleucine	C12H29NO2Si2	0.034	1.628	158	7.955	1.38	HMDB0000172
8	2-Butenedioic acid	C10H20O4Si2	0.001	2.362	43.1	8.669	1.72	HMDB0000176
9	Gluconic acid	C16H35NO6Si3	0.002	2.178	155.9	10.635	0.50	HMDB0000625
10	Propanoic acid	C13H33NO2Si3	0.026	1.468	146.95	10.990	0.76	HMDB0000237
11	Butanoic acid	C13H33NO2Si3	0.015	1.922	174.1	11.021	0.76	HMDB0000039
12	3-Iodo-L-tyrosine	C18H34INO3Si3	0.018	1.691	176.9	12.315	1.41	HMDB0000021
13	L-Asparagine	C13H32N2O3Si3	0.032	1.649	257.9	12.841	0.71	HMDB0000168
14	N-Acetyl-D-glucosamine	C21H50N2O6Si4	0.007	1.946	97	13.463	0.82	HMDB0000215
15	2-Propanone	C15H40NO6PSi4	0.019	1.762	114	14.532	0.67	HMDB0001659
16	L-(-)-Sorbose	C22H55NO6Si5	0.044	1.401	73	15.872	1.28	HMDB0001266
17	D-(-)-Fructose	C22H55NO6Si5	0.026	1.777	308	15.952	1.40	HMDB0000660
18	D-Allose	C22H55NO6Si5	0.022	1.880	146.9	16.105	1.86	HMDB0001151
19	D-Galactose	C22H55NO6Si5	0.003	2.107	73	16.290	1.54	HMDB0000143
20	D-Glucose	C22H55NO6Si5	0.038	1.707	103	16.295	3.33	HMDB0000122
21	Inositol	C24H60O6Si6	0.022	1.678	190.9	19.469	1.31	HMDB0000211
22	Myo-inositol	C24H60O6Si6	0.001	2.060	73	19.481	0.85	HMDB0000211
23	D-(+)-Galactose	C24H61NO6Si6	0.043	1.813	146.9	20.252	1.69	HMDB0000143
24	Heptadecanoic acid	C20H42O2Si	0.029	1.708	73	20.491	0.91	HMDB0002259
25	Octadecanoic acid	C21H44O2Si	0.005	1.834	127.9	22.050	0.67	HMDB0000827
26	11-Eicosenoic acid	C23H46O2Si	0.014	1.619	83	23.876	0.74	HMDB0034296
27	3-Indoleacrylic acid	C23H37NO2Si2	0.050	1.565	173.9	24.224	0.70	HMDB0000734
28	D-Altro-2-Heptulose	C29H74NO10PSi7	0.002	2.147	285.9	24.827	1.57	HMDB0003219

correlation analyses, plotted correlation heat maps (Figure 10A), and screened 10 metabolites that were significantly associated with cerebral infarct area, MDA, and SOD. The correlations for the other 2 metabolites (Figures 10I, K) were not significant. The results showed that brain 2-piperidinecarboxylic acid (Figure 10B), brain phosphoric acid (Figure 10C), and brain glycine (Figure 10F) were negatively correlated with cerebral infarct area, and serum uridine (Figure 10D) and serum L-fucose (Figure 10E) were positively correlated with cerebral infarct area. Serum uridine (Figure 10G) and serum L-fucose (Figure 10H) were negatively correlated with MDA levels. Serum mannopyranose (Figure 10J) was negatively correlated with SOD, and brain butanedioic acid (Figure 10L) and brain urea (Figure 10M) were positively correlated with SOD. This suggests that SHD may ameliorate ischemic necrosis of brain tissue in tMCAO rats by affecting the levels of disease-related metabolites.

4 Discussion

Stroke is the second leading cause of death worldwide. In stroke, the blood supply to certain areas of the brain is interrupted or blocked, preventing the delivery of adequate nutrients and oxygen to brain tissue and ultimately leading to neuronal damage. IS due to embolism is often associated with atrial fibrillation and severe neurological syndromes (25). The incidence of IS is increasing, with high mortality and disability rates. Improving early diagnosis

10.3389/fendo.2023.1289558

TABLE 2 Statistical analysis results of identified metabolite changes in the serum.

NO.	Name	Molecular Formula	P value	VIP	M/Z	RT	Fold Change	HMDB
1	Glycine	C9H23NO2Si2	0.028	1.59968	173.9	7.414	1.27	HMDB0000123
2	D-(-)-Lactic acid	C9H22O3Si2	0.013	1.67382	73	7.642	0.90	HMDB0001311
3	Propanoic acid	C9H22O3Si2	0.015	1.6416	74.1	7.667	1.19	HMDB0000237
4	L-(+)-Lactic acid	C9H22O3Si2	0.013	1.64365	147	7.675	1.16	HMDB0000190
5	Butanoic acid	C10H24O3Si2	0.010	1.70604	131	9.261	1.78	HMDB0000039
6	1H-Indole-3-ethanamine	C16H28N2Si2	0.001	1.89296	175	12.895	1.87	HMDB0000303
7	Benzaldehyde	C8H7FO3	0.014	1.46248	169.9	13.148	1.30	HMDB0006115
8	L-Isoleucine	C12H29NO2Si2	0.002	1.85282	159	13.585	1.56	HMDB0000172
9	L-Norleucine	C12H29NO2Si2	0.003	1.82305	158	13.587	1.53	HMDB0001645
10	L-Proline	C11H25NO2Si2	0.030	1.30067	142	13.702	1.46	HMDB0000162
11	L-Homoserine	C13H33NO3Si3	0.040	1.41885	73	15.945	1.28	HMDB0000719
12	(R*,S*)-2,3-Dihydroxybutanoic acid	C13H32O4Si3	0.034	1.41502	291	15.948	1.40	HMDB0000498
13	Butanedioic acid	C13H30O5Si3	0.000	2.01385	147.9	18.494	1.88	HMDB0000254
14	2-Butenedioic acid	C10H20O4Si2	0.017	1.49511	73	18.500	1.44	HMDB0000176
15	2-Piperidinecarboxylic acid	C12H27NO2Si2	0.026	1.45946	219	19.226	1.54	HMDB0000070
16	2-Pentanone	C8H18OSi	0.016	1.53469	146.9	20.022	1.61	HMDB0034235
17	Phosphoric acid	C9H22NO4PSSi2	0.007	1.62415	188	21.077	2.35	HMDB0002142
18	Glutamic acid	C14H33NO4Si3	0.014	1.56212	246	21.595	1.61	HMDB0000148
19	1H-Indole-2,3-dione	C17H25NO2Si	0.009	1.63988	73	21.598	1.57	HMDB0061933
20	Pentadecane	C21H44	0.031	1.22446	174	24.455	1.87	HMDB0059886
21	DL-Ornithine	C17H44N2O2Si4	0.046	1.09941	73	25.832	1.51	HMDB32455
22	L-Ornithine	C17H44N2O2Si4	0.012	1.40929	146.9	25.846	1.59	HMDB0000214
23	1,5-Anhydro-D-sorbitol	C18H44O5Si4	0.005	1.72214	75	26.527	1.63	HMDB0002712
24	D-Fructose	C22H55NO6Si5	0.013	1.71509	73	26.913	1.51	HMDB0000660
25	L-(-)-Sorbose	C22H55NO6Si5	0.016	1.709	335.1	26.915	1.70	HMDB0001266
26	D-Allose	C24H61NO6Si6	0.005	1.56378	205	27.434	0.84	HMDB0001151
27	D-Mannose	C24H61NO6Si6	0.034	1.27105	319.1	27.463	0.92	HMDB0000169
28	D-Glucose	C24H61NO6Si6	0.027	1.4162	208	27.467	1.15	HMDB0000122
29	L-Tyrosine	C18H35NO3Si3	0.003	1.63524	218	28.271	1.85	HMDB0000158
30	Myo-Inositol	C24H60O6Si6	0.009	1.36863	305	28.539	2.45	HMDB0000211
31	L-Tryptophan	C20H36N2O2Si3	0.021	1.44616	45.1	33.277	1.60	HMDB0000929
32	D-Glucuronic acid	C21H50O7Si5	0.013	1.46307	217	34.439	2.44	HMDB0000127
33	D-Ribose	C17H42O5Si4	0.050	1.37958	331.15	34.465	2.43	HMDB0000283
34	Probucol	C31H48O2S2	0.015	1.66934	279	44.309	0.19	HMDB0015537

and intervention in IS and developing new therapeutic strategies is now a top priority (26). Vascular interventions and thrombolytic therapy remain the most desirable options for the treatment of IS, but only in certain stroke patients and with very low cure rates and associated with severe adverse effects (27). In almost all patients with IS, secondary ischemia-reperfusion (IR) injury after revascularization is an inevitable consequence (28, 29). IR is the most important cause of cellular necrosis in infarcted lesions, which is further exacerbated by vascular injury or even vascular occlusion (30).

SHD is a well-known classic traditional Chinese medicine prescription for IS. SHD is still used consistently and extensively

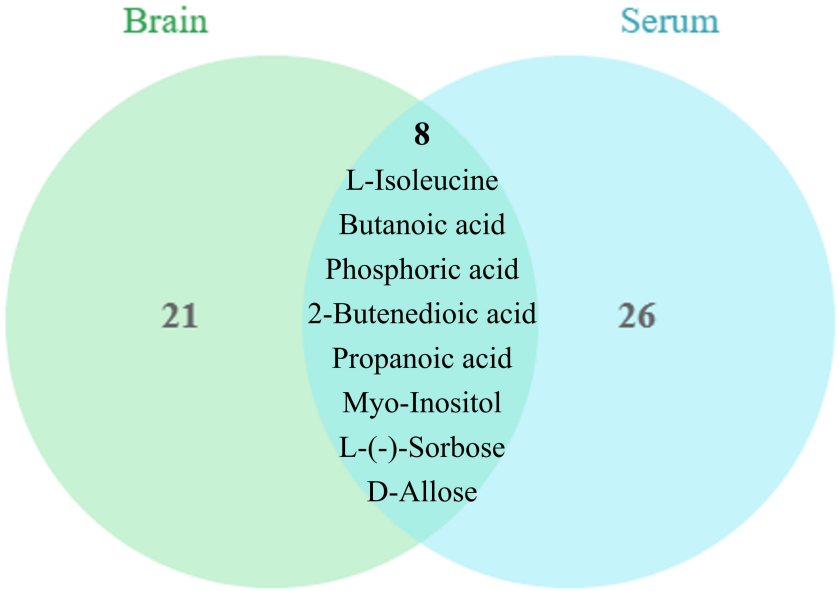

FIGURE 5
Metabolite differences between brain and serum samples. The brain and serum have 9 common differential metabolites, phosphoric acid, L-isoleucine, 2-butenedioic acid, propanoic acid, butanoic acid, L-(-)-sorbose, D-allose, D-Glucose and myo-inositol.

in modern society for stroke treatment. However, the mechanism of treatment of acute IS by SHD remains uncertain. To confirm the protective effect of SHD, we analyzed cerebral infarct areas in MCAO/R rats. All results indicated that SHD improved the neurological damage and cerebral infarct area in rats. Examination of biochemical indicators showed a significant increase in MDA after MCAO/R operation and in the period of ischemia. It indicated that free radicals and reactive oxygen species cause severe oxidative damage. Meanwhile, SOD may be affected by the ischemia-reperfusion state of the brain due to the imbalance of the antioxidant system. After SHD treatment, the levels of SOD and MDA were restored to alleviate the oxidative stress damage. Stress caused by redox imbalance is an influential factor in ischemia-reperfusion injury and is the initial marker of brain damage. In IR-induced long-term injury, neuroinflammation causes systemic inflammation, which further

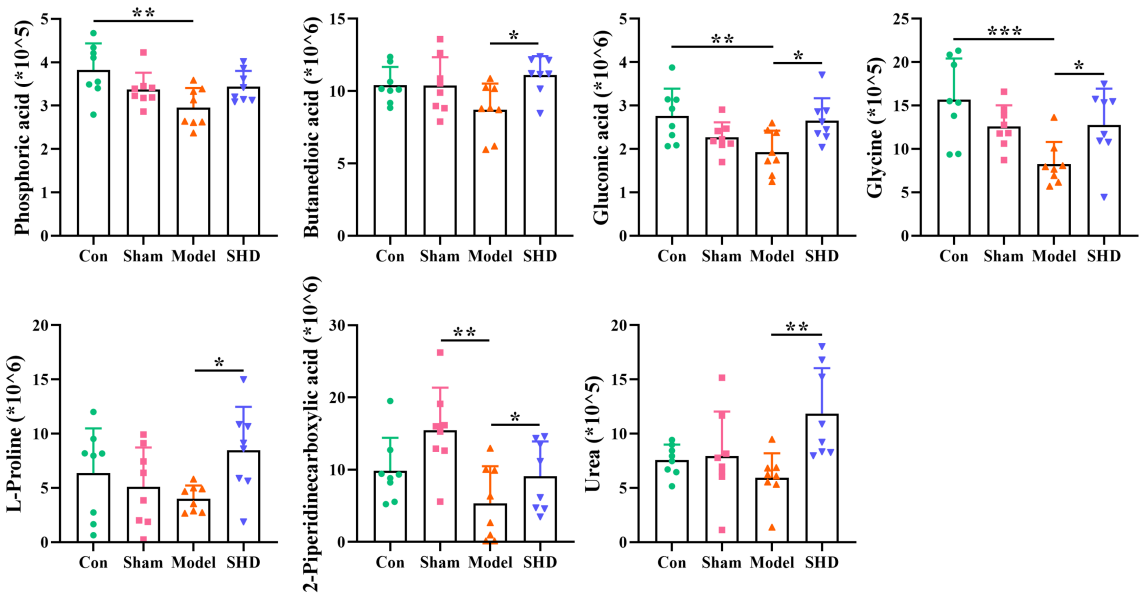

FIGURE 6
Differential metabolite changes in Model with SHD intervention in the brain. All values were presented as the mean ± SD. *$p < 0.05$, **$p < 0.01$, ***$p < 0.001$ relative to the Model group.

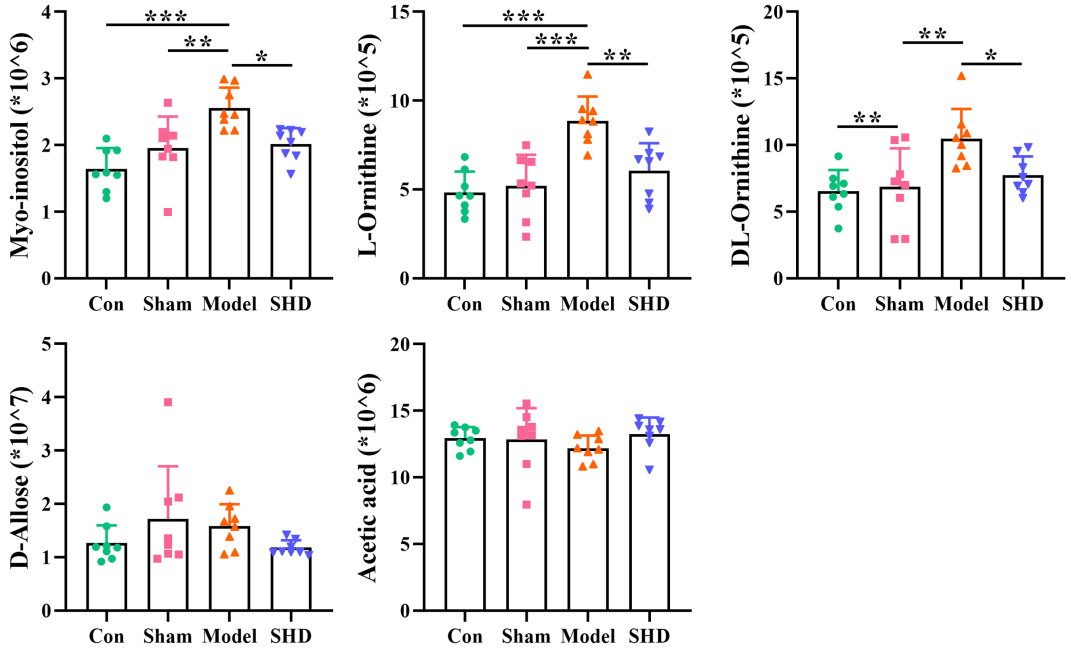

FIGURE 7
Differential metabolite changes in Model with SHD intervention in the serum. All values were presented as the mean ± SD. *$p < 0.05$, **$p < 0.01$, ***$p < 0.001$ relative to the Model group.

leads to progressive dysfunction of peripheral organs (31). The results of brain pathology sections indicated that SHD had a ameliorative effect on brain damage after IR by decreasing neuronal necrosis and improving neuronal cell structure and inflammatory cell infiltration. At the same time, no significant side effects of SHD on other organs were observed, suggesting that SHD is safe at the doses at which it exerts its therapeutic effects.

In recent years, a growing number of studies have identified the same signature metabolites from patients with cerebral ischemia and animal models that improve the diagnosis and predict the outcome of IS (32). Gender is an important variable in the prevalence of stroke. There are 55,000 more women than men who suffer a stroke each year. Women bear a greater risk of disease than men (33). The aim of this study was to determine the therapeutic effect of SHD on ischemic stroke. To exclude female-unique factors such as sex hormones, exogenous estrogens, and pregnancy, we performed a GC-MS based metabolomics study using male rats. Brain and serum metabolite analyses were utilized to assess the therapeutic effects and potential mechanisms of SHD in MCAO/R rats.

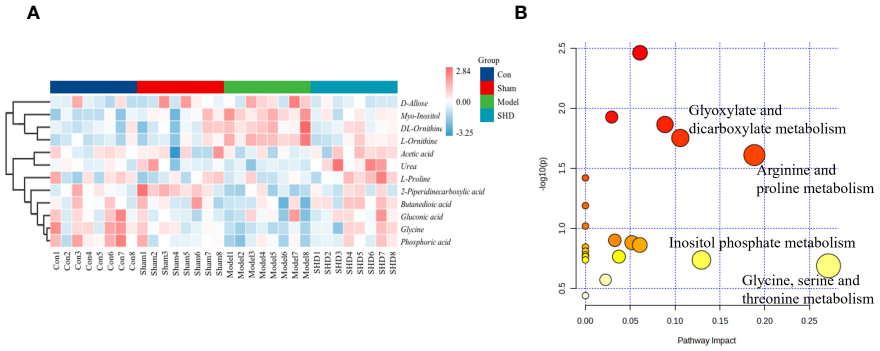

FIGURE 8
Analysis of differential metabolites in brain and serum in MCAO/R rats after SHD intervention. **(A)** Heat map of metabolite content in serum and brain samples of four groups. **(B)** Pathway analysis of SHD intervention. The metabolic pathways involved in the protection effects of SHD on MCAO/R rats.

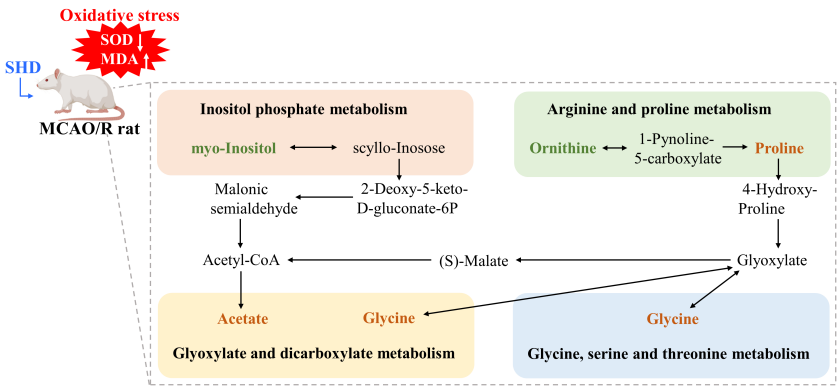

FIGURE 9
Schematic diagram of the metabolic pathways. Orange and green represent the increase and decrease of d metabolite levels after SHD intervention, respectively.

We identified 55 differential metabolites between the Sham and Model groups. These 55 altered metabolites are potential biomarkers of IS, which will facilitate later monitoring of disease progression in the clinic. After SHD intervention, the levels of 7 and 5 differential metabolites were restored in brain and serum, respectively. Of these 12 differential metabolites that were restored, changes in 8 were significantly different. The Model group had decreased levels of urea, glycine, L-proline, gluconic acid and butanedioic acid, and increased levels of myo-inositol, L-ornithine, and DL-ornithine compared with the Sham group. After treatment with SHD, the levels of the above metabolites were restored. These 12 metabolites were mainly related to 4 metabolic pathways, including glyoxylate and dicarboxylate metabolism, arginine and proline metabolism, inositol phosphate metabolism, and glycine, serine and threonine metabolism. Many metabolic problems have been shown to lead to stroke or stroke-like episodes (34).

Glyoxalate and dicarboxylic acid metabolism is closely correlated with the TCA cycle. The chain cycle of oxidative decarboxylation of glyoxylate serves as a native metabolic cycle analog of the TCA cycle. In the TCA cycle, glyoxylate can be converted to carbon dioxide and produce aspartate (35). Gluconic acid is associated with oxidative stress and is a predictor of hyperglycemia and cytotoxic brain injury after stroke (36). Arginine and proline metabolism have been shown to be associated with axon regeneration, and arginine is a necessary raw material for axon regeneration (37). L-ornithine produced during its metabolism has recently been shown to be one of the biomarkers used for early detection of stroke (38). L-ornithine transcarbamylase deficiency leads to elevated ornithine levels, which in turn cause impaired urea cycling that can lead to stroke-like episodes (39), impaired mitochondrial function and reduced antioxidant capacity (40). After IS, plasma L-proline levels are reduced (41). Excitotoxicity mediated by N-methyl-D-aspartate receptors (NMDARs) regulated by L-proline, and is one of the main reasons of neuronal death after stroke (42, 43). It has been shown that neuroprotection and neurorepair can be promoted in acute ischemic stroke models by inhibiting L-proline uptake in the brain (43). Glycine can regulate microglial polarization after IS and indirectly inhibit ischemia-induced neuronal death and functional recovery (44). Through the miR-19a-3p/AMPK/GSK-3β/HO-1 pathway, glycine ameliorates apoptosis, inflammatory response and dysregulated glucose metabolism in IS (45). In addition, *in vitro* experiments showed that low doses of glycine improved NMDAR function, but high doses of glycine induced NMDAR internalization and thus neuroprotective effects in IS (46). Inositol phosphate metabolism has been shown to be abnormal in a rat stroke model (47). Inositol and phosphatidylinositol reduce insulin resistance, improve insulin sensitivity, and have unique roles in energy metabolism and metabolic disorders (48). Phosphatidylinositol 3-kinase is a phosphorylation product of inositol phospholipids and is involved in the immune response. Electrical stimulation of the cerebral cortex exerts anti-apoptotic, angiogenic and anti-inflammatory effects via the phosphatidylinositol 3-kinase/Akt pathway in rats with IS (49). Taken together, amino acid metabolism and carbohydrate metabolism are closely related to IS. The present study showed that the differences of metabolite between the Model group and the Sham group had improved to some extent after SHD intervention, and some metabolite levels were restored. This suggested that therapeutic effect of SHD on IR-induced metabolic disorders.

5 Conclusion

In this research, we integrated pharmacodynamic and metabolomic approaches to investigate firstly the therapeutic effects of SHD on the MCAO/R rat model and its underlying mechanisms. Our findings indicated that SHD treatment ameliorated MCAO/R-induced IS symptoms, ameliorated oxidative stress, attenuated brain damage and had a protective

10.3389/fendo.2023.1289558

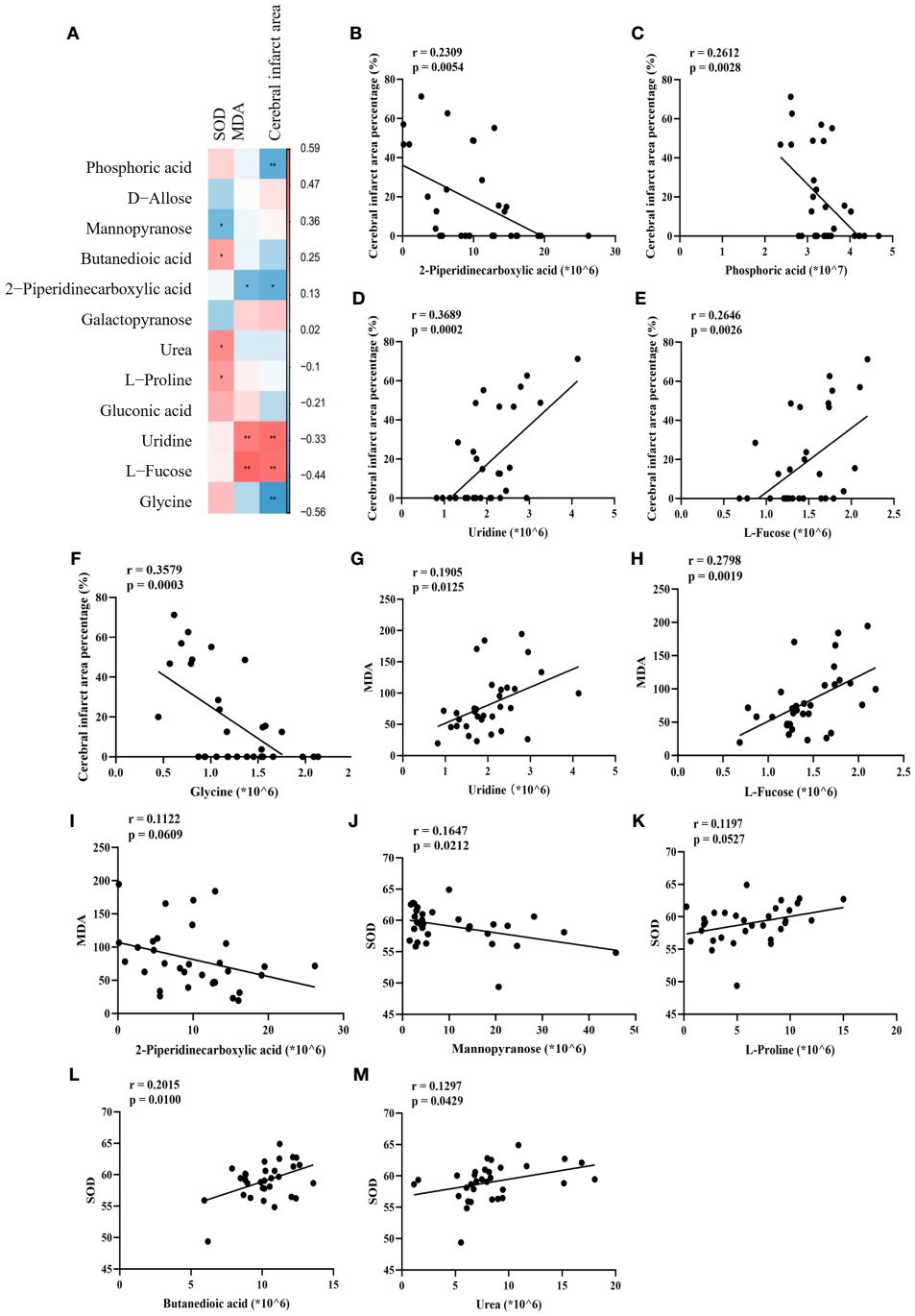

FIGURE 10
Correlation of disease-related metabolites with disease markers. **(A)** Heat map of Spearman correlation between cerebral infarct area, SOD, MDA and metabolites. **(B–M)** Spearman correlation analysis between percentage of cerebral infarcted area, MDA and SOD with phosphoric acid, mannopyranose, butanedioic acid, 2-piperidinecarboxylic acid, urea, L-proline, uridine, L(-)-fucose and glycine.

effect on damaged nerves. Brain and serum metabolomic analyses suggested that SHD treatment could significantly affect 4 metabolic pathways. The neuroprotective effects of SHD were primarily mediated through modulation of amino acid metabolism and carbohydrate metabolism, and nine metabolites that were altered after SHD treatment were significantly associated with disease. In conclusion, these findings deepen the understanding of the mechanisms by which SHD treats IS and suggests that SHD is promising drug candidate for intervening in the developmental process of IS.

Data availability statement

The original contributions presented in the study are included in the article/Supplementary Material. Further inquiries can be directed to the corresponding authors.

Ethics statement

The animal study was approved by China Academy of Chinese Medical Sciences. The study was conducted in accordance with the local legislation and institutional requirements.

Author contributions

RL: Writing – original draft. SC: Writing – original draft. YC: Writing – review & editing. MZ: Conceptualization, Writing – review & editing. XG: Data curation, Writing – review & editing. YH: Writing – review & editing.

Funding

The author(s) declare financial support was received for the research, authorship, and/or publication of this article. This study was financially supported by the Fundamental Research Funds for the Central Public Welfare Research Institutes (JJPY2022024).

Conflict of interest

The authors declare that the research was conducted in the absence of any commercial or financial relationships that could be construed as a potential conflict of interest.

Publisher's note

All claims expressed in this article are solely those of the authors and do not necessarily represent those of their affiliated organizations, or those of the publisher, the editors and the reviewers. Any product that may be evaluated in this article, or claim that may be made by its manufacturer, is not guaranteed or endorsed by the publisher.

Supplementary material

The Supplementary Material for this article can be found online at: https://www.frontiersin.org/articles/10.3389/fendo.2023.1289558/full#supplementary-material

References

1. Hankey GJ. Stroke. *Lancet* (2017) 389:641–54. doi: 10.1016/S0140-6736(16)30962-X

2. Wang X-G, Zhu D-D, Li N, Huang Y-L, Wang Y-Z, Zhang T, et al. Scorpion venom heat-resistant peptide is neuroprotective against cerebral ischemia-reperfusion injury in association with the NMDA-MAPK pathway. *Neurosci Bull* (2020) 36:243–53. doi: 10.1007/s12264-019-00425-1

3. Pénzes M, Túrós D, Máthé D, Szigeti K, Hegedűs N, Rauscher AÁ, et al. Direct myosin-2 inhibition enhances cerebral perfusion resulting in functional improvement after ischemic stroke. *Theranostics* (2020) 10:5341–56. doi: 10.7150/thno.42077

4. Catanese L, Tarsia J, Fisher M. Acute ischemic stroke therapy overview. *Circ Res* (2017) 120:541–58. doi: 10.1161/CIRCRESAHA.116.309278

5. IST-3 collaborative group, Sandercock P, Wardlaw JM, Lindley R, Dennis M, Cohen G, et al. The benefits and harms of intravenous thrombolysis with recombinant tissue plasminogen activator within 6 h of acute ischaemic stroke (the third international stroke trial [IST-3]): a randomised controlled trial. *Lancet* (2012) 379:2352–63. doi: 10.1016/S0140-6736(12)60768-5

6. Seto S-W, Chang D, Jenkins A, Bensoussan A, Kiat H. Angiogenesis in ischemic stroke and angiogenic effects of Chinese herbal medicine. *J Clin Med* (2016) 5:56. doi: 10.3390/jcm5060056

7. Wang M, Yao M, Liu J, Takagi N, Yang B, Zhang M, et al. Ligusticum chuanxiong exerts neuroprotection by promoting adult neurogenesis and inhibiting inflammation in the hippocampus of ME cerebral ischemia rats. *J Ethnopharmacology* (2020) 249:112385. doi: 10.1016/j.jep.2019.112385

8. Zhou X, Seto SW, Chang D, Kiat H, Razmovski-Naumovski V, Chan K, et al. Synergistic effects of chinese herbal medicine: A comprehensive review of methodology and current research. *Front Pharmacol* (2016) 7:201. doi: 10.3389/fphar.2016.00201

9. Liu N, Liu C, Yang Y, Ma G, Wei G, Liu S, et al. Xiao-Xu-Ming decoction prevented hemorrhagic transformation induced by acute hyperglycemia through inhibiting AGE-RAGE-mediated neuroinflammation. *Pharmacol Res* (2021) 169:105650. doi: 10.1016/j.phrs.2021.105650

10. Zhang S, Kong D, Ma G, Liu C, Yang Y, Liu S, et al. Long-term administration of salvianolic acid A promotes endogenous neurogenesis in ischemic stroke rats through activating Wnt3a/GSK3β/β-catenin signaling pathway. *Acta Pharmacol Sin* (2022) 43:2212–25. doi: 10.1038/s41401-021-00844-9

11. Li Y, Liang W, Guo C, Chen X, Huang Y, Wang H, et al. Renshen Shouwu extract enhances neurogenesis and angiogenesis via inhibition of TLR4/NF-κB/NLRP3 signaling pathway following ischemic stroke in rats. *J Ethnopharmacology* (2020) 253:112616. doi: 10.1016/j.jep.2020.112616

12. Yang L, Su X, Lu F, Zong R, Ding S, Liu J, et al. Serum and brain metabolomic study reveals the protective effects of Bai-Mi-Decoction on rats with ischemic stroke. *Front Pharmacol* (2022) 13:1005301. doi: 10.3389/fphar.2022.1005301

13. Ye Y, Zhu Y, Xin X, Zhang J, Zhang H, Li D. Efficacy of Chinese herbal medicine for tPA thrombolysis in experimental stroke: A systematic review and meta-analysis. *Phytomedicine* (2022) 100:154072. doi: 10.1016/j.phymed.2022.154072

14. Fu D-L, Li J-H, Shi Y-H, Zhang X-L, Lin Y, Zheng G-Q. Sanhua decoction, a classic herbal prescription, exerts neuroprotection through regulating phosphorylated tau level and promoting adult endogenous neurogenesis after cerebral ischemia/reperfusion injury. *Front Physiol* (2020) 11:57. doi: 10.3389/fphys.2020.00057

15. Zheng L, Meng L, Liang H, Yang J. Sanhua decoction: Current understanding of a traditional herbal recipe for stroke. *Front Neurosci* (2023) 17:1149833. doi: 10.3389/fnins.2023.1149833

16. Liu T, Zhou J, Cui H, Li P, Luo J, Li T, et al. iTRAQ-based quantitative proteomics reveals the neuroprotection of rhubarb in experimental intracerebral hemorrhage. *J Ethnopharmacology* (2019) 232:244–54. doi: 10.1016/j.jep.2018.11.032

17. Li X, Chu S, Liu Y, Chen N. Neuroprotective effects of anthraquinones from rhubarb in central nervous system diseases. *Evidence-Based Complementary Altern Med* (2019) 2019:e3790728. doi: 10.1155/2019/3790728

18. Ruan Y, Jin X, Ji H, Zhu C, Yang Y, Zhou Y, et al. Water extract of Notopterygium incisum alleviates cold allodynia in neuropathic pain by regulation of TRPA1. *J Ethnopharmacology* (2023) 305:116065. doi: 10.1016/j.jep.2022.116065

19. Zhu S, Liu F, Zhang R, Xiong Z, Zhang Q, Hao L, et al. Neuroprotective potency of neolignans in magnolia officinalis cortex against brain disorders. *Front Pharmacol* (2022) 13:857449. doi: 10.3389/fphar.2022.857449

20. Liu X, Chen X, Zhu Y, Wang K, Wang Y. Effect of magnolol on cerebral injury and blood brain barrier dysfunction induced by ischemia-reperfusion in *vivo* and in *vitro*. *Metab Brain Dis* (2017) 32:1109–18. doi: 10.1007/s11011-017-0004-6

21. Choi B-K, Kim T-W, Lee D-R, Jung W-H, Lim J-H, Jung J-Y, et al. A polymethoxy flavonoids-rich Citrus aurantium extract ameliorates ethanol-induced

liver injury through modulation of AMPK and Nrf2-related signals in a binge drinking mouse model. *Phytotherapy Res* (2015) 29:1577–84. doi: 10.1002/ptr.5415

22. Lu Y, Huang Y, Sun M, Li W. Determination of active ingredients and prediction of targetin Sanhua Decoction for cerebral ischemia based on HPLC and network pharmacology methods. *Int J Traditional Chin Med* (2021) 43:1109–15. doi: 10.3760/cma.j.cn115398-20210413-00140

23. YingHuang U, Gao S, Gong Z, Li W, Xiao-junGou U, Sun J, et al. Mechanism of sanhua decoction in the treatment of ischemic stroke based on network pharmacology methods and experimental verification. *BioMed Res Int* (2022) 2022:e7759402. doi: 10.1155/2022/7759402

24. Benedek A, Móricz K, Jurányi Z, Gigler G, Lévay G, Hársing LG, et al. Use of TTC staining for the evaluation of tissue injury in the early phases of reperfusion after focal cerebral ischemia in rats. *Brain Res* (2006) 1116:159–65. doi: 10.1016/j.brainres.2006.07.123

25. Hart RG. Atrial fibrillation and prevention of embolic stroke. *Stroke* (2021) 52: e55–7. doi: 10.1161/STROKEAHA.120.030420

26. Mao R, Zong N, Hu Y, Chen Y, Xu Y. Neuronal death mechanisms and therapeutic strategy in ischemic stroke. *Neurosci Bull* (2022) 38:1229–47. doi: 10.1007/s12264-022-00859-0

27. Pirson FAV, Boodt N, Brouwer J, Bruggeman AAE, den Hartog SJ, Goldhoorn R-JB, et al. Endovascular treatment for posterior circulation stroke in routine clinical practice: results of the multicenter randomized clinical trial of endovascular treatment for acute ischemic stroke in the Netherlands registry. *Stroke* (2022) 53:758–68. doi: 10.1161/STROKEAHA.121.034786

28. Villringer K, Cuesta BES, Ostwaldt A-C, Grittner U, Brunecker P, Khalil AA, et al. DCE-MRI blood–brain barrier assessment in acute ischemic stroke. *Neurology* (2017) 88:433–40. doi: 10.1212/WNL.0000000000003566

29. Arba F, Piccardi B, Palumbo V, Biagini S, Galmozzi F, Iovene V, et al. Blood–brain barrier leakage and hemorrhagic transformation: The Reperfusion Injury in Ischemic StroKe (RISK) study. *Eur J Neurol* (2021) 28:3147–54. doi: 10.1111/ene.14985

30. Jayaraj RL, Azimullah S, Beiram R, Jalal FY, Rosenberg GA. Neuroinflammation: friend and foe for ischemic stroke. *J Neuroinflamm* (2019) 16:142. doi: 10.1186/s12974-019-1516-2

31. DeLong JH, Ohashi SN, O'Connor KC, Sansing LH. Inflammatory responses after ischemic stroke. *Semin Immunopathol* (2022) 44:625–48. doi: 10.1007/s00281-022-00943-7

32. Zhang R, Meng J, Wang X, Pu L, Zhao T, Huang Y, et al. Metabolomics of ischemic stroke: insights into risk prediction and mechanisms. *Metab Brain Dis* (2022) 37:2163–80. doi: 10.1007/s11011-022-01011-7

33. Demel SL, Kittner S, Ley SH, McDermott M, Rexrode KM. Stroke risk factors unique to women. *Stroke* (2018) 49:518–23. doi: 10.1161/STROKEAHA.117.018415

34. Mastrangelo M, Ricciardi G, Giordo L, Michele MD, Toni D, Leuzzi V. Stroke and stroke-like episodes in inborn errors of metabolism: Pathophysiological and clinical implications. *Mol Genet Metab* (2022) 135:3–14. doi: 10.1016/j.ymgme.2021.12.014

35. Springsteen G, Yerabolu JR, Nelson J, Rhea CJ, Krishnamurthy R. Linked cycles of oxidative decarboxylation of glyoxylate as protometabolic analogs of the citric acid cycle. *Nat Commun* (2018) 9:91. doi: 10.1038/s41467-017-02591-0

36. Ament Z, Bevers MB, Wolcott Z, Kimberly WT, Acharjee A. Uric acid and gluconic acid as predictors of hyperglycemia and cytotoxic injury after stroke. *Transl Stroke Res* (2021) 12:293–302. doi: 10.1007/s12975-020-00862-5

37. Zhang J, Jiang C, Liu X, Jiang C, Cao Q, Yu B, et al. The metabolomic profiling identifies N, N-dimethylglycine as a facilitator of dorsal root ganglia neuron axon regeneration after injury. doi: 10.1096/fj.202101698R

38. Tao S, Xiao X, Li X, Na F, Na G, Wang S, et al. Targeted metabolomics reveals serum changes of amino acids in mild to moderate ischemic stroke and stroke mimics. *Front Neurol* (2023) 14:1153193. doi: 10.3389/fneur.2023.1153193

39. Gowda VK, Gupta P, Shivappa SK, Benakappa N. Recurrent stroke like episodes secondary to ornithine transcarbamylase deficiency. *Indian J Pediatr* (2020) 87:852–3. doi: 10.1007/s12098-020-03193-3

40. Zanatta Â, Rodrigues MDN, Amaral AU, Souza DG, Quincozes-Santos A, Wajner M. Ornithine and homocitrulline impair mitochondrial function, decrease antioxidant defenses and induce cell death in menadione-stressed rat cortical astrocytes: potential mechanisms of neurological dysfunction in HHH syndrome. *Neurochem Res* (2016) 41:2190–8. doi: 10.1007/s11064-016-1933-x

41. Fan D, Krishnamurthi R, Harris P, Barber PA, Guan J. Plasma cyclic glycine proline/IGF-1 ratio predicts clinical outcome and recovery in stroke patients. *Ann Clin Trans Neurol* (2019) 6:669–77. doi: 10.1002/acn3.743

42. Goulart VAM, Sena MM, Mendes TO, Menezes HC, Cardeal ZL, Paiva MJN, et al. Amino acid biosignature in plasma among ischemic stroke subtypes. *BioMed Res Int* (2019) 2019:e8480468. doi: 10.1155/2019/8480468

43. Carvalho GA, Chiareli RA, Marques BL, Parreira RC, de Souza Gil E, de Carvalho FS, et al. L-proline transporter inhibitor (LQFM215) promotes neuroprotection in ischemic stroke. *Pharmacol Rep* (2023) 75:276–92. doi: 10.1007/s43440-023-00451-x

44. Liu R, Liao X-Y, Pan M-X, Tang J-C, Chen S-F, Zhang Y, et al. Glycine Exhibits Neuroprotective Effects in Ischemic Stroke in Rats through the Inhibition of M1 Microglial Polarization via the NF-κB p65/Hif-1α Signaling Pathway. *J Immunol* (2019) 202:1704–14. doi: 10.4049/jimmunol.1801166

45. Chen Z-J, Zhao X-S, Fan T-P, Qi H-X, Li D. Glycine improves ischemic stroke through miR-19a-3p/AMPK/GSK-3β/HO-1 pathway. *DDDT* (2020) 14:2021–31. doi: 10.2147/DDDT.S248104

46. Cappelli J, Khacho P, Wang B, Sokolovski A, Bakkar W, Raymond S, et al. Glycine-induced NMDA receptor internalization provides neuroprotection and preserves vasculature following ischemic stroke. *iScience* (2022) 25:103539. doi: 10.1016/j.isci.2021.103539

47. Lin TN, Liu TH, Xu J, Hsu CY, Sun GY. Brain polyphosphoinositide metabolism during focal ischemia in rat cortex. *Stroke* (1991) 22:495–8. doi: 10.1161/01.STR.22.4.495

48. Chatree S, Thongmaen N, Tantivejkul K, Sitticharoon C, Vucenik I. Role of inositols and inositol phosphates in energy metabolism. *Molecules* (2020) 25:5079. doi: 10.3390/molecules25215079

49. Baba T, Kameda M, Yasuhara T, Morimoto T, Kondo A, Shingo T, et al. Electrical stimulation of the cerebral cortex exerts antiapoptotic, angiogenic, and anti-inflammatory effects in ischemic stroke rats through phosphoinositide 3-kinase/akt signaling pathway. *Stroke* (2009) 40:e598–605. doi: 10.1161/STROKEAHA.109.563627

frontiers | Frontiers in Endocrinology

TYPE Original Research
PUBLISHED 11 June 2024
DOI 10.3389/fendo.2024.1388871

OPEN ACCESS

EDITED BY
Alexandre Benani,
Centre National de la Recherche Scientifique (CNRS), France

REVIEWED BY
Omer Iqbal,
Loyola University Chicago, United States
Vladimir Tesar,
Charles University, Czechia

*CORRESPONDENCE
Aimin Li
liaimin_6529@126.com
Yong Sun
sunyong@njmu.edu.cn

†These authors have contributed equally to this work and share first authorship

RECEIVED 20 February 2024
ACCEPTED 29 May 2024
PUBLISHED 11 June 2024

CITATION
Yang S, Li K, Huang Z, Xu Y, Liang J, Sun Y and Li A (2024) Risk factors of acute ischemic stroke and the role of angiotensin I in predicting prognosis of patients undergoing endovascular thrombectomy.
Front. Endocrinol. 15:1388871.
doi: 10.3389/fendo.2024.1388871

Risk factors of acute ischemic stroke and the role of angiotensin I in predicting prognosis of patients undergoing endovascular thrombectomy

Shengkai Yang[1,2†], Kemian Li[1,2†], Zhengqian Huang[1], Yingda Xu[1], Jingshan Liang[1], Yong Sun[1*] and Aimin Li[1*]

[1]Department of Neurosurgery, The Affiliated Lianyungang Hospital of Xuzhou Medical University, Lianyungang, Jiangsu, China, [2]Department of Neurosurgery, Binhai County People's Hospital Affiliated to Kangda College of Nanjing Medical University, Yancheng, Jiangsu, China

Purpose: The interaction between the renin-angiotensin system (RAS) and the acute ischemic stroke (AIS) is definite but not fully understood. This study aimed to analyze the risk factors of AIS and explore the role of serum indicators such as angiotensin I (Ang I) in the prognosis of patients undergoing endovascular thrombectomy (EVT).

Patients and methods: Patients with AIS who underwent EVT and healthy controls were retrospectively enrolled in this study, and the patients were divided into a good or a poor prognosis group. We compared Ang I, blood routine indexes, biochemical indexes, electrolyte indexes, and coagulation indexes between patients and controls. We used univariate and multivariate logistic regression analyses to evaluate possible risk factors for AIS and the prognosis of patients undergoing EVT. Independent risk factors for the prognosis of patients undergoing EVT were identified through multifactorial logistic regression analyses to construct diagnostic nomograms, further assessed by receiver operating characteristic curves (ROC).

Results: Consistent with previous studies, advanced age, high blood glucose, high D-dimer, and high prothrombin activity are risk factors for AIS. In addition, Ang I levels are lower in AIS compared to the controls. The level of Ang I was higher in the good prognosis group. Furthermore, we developed a nomogram to evaluate its ability to predict the prognosis of AIS after EVT. The AUC value of the combined ROC model (Ang I and albumin-globulin ratio (AGR)) was 0.859.

Conclusions: In conclusion, advanced age, high blood glucose, high D-dimer, and high prothrombin activity are risk factors for AIS. The combined Ang I and AGR model has a good predictive ability for the prognosis of AIS patients undergoing arterial thrombectomy.

KEYWORDS

acute ischemic stroke, risk factors, endovascular thrombectomy, angiotensin I, nomograms

Introduction

Acute ischemic stroke (AIS) is a disorder of blood flow supply to brain tissue caused by various reasons, which is characterized by high morbidity, disability, and mortality (1). According to statistics, the number of deaths due to ischemic stroke (IS) in the world ranks first in the number of deaths from cardiovascular and cerebrovascular diseases. It is one of the third leading causes of death in the world. China is a country with a high incidence of stroke. The incidence of stroke was 170/100,000 and 620/100,000 in males and females, respectively, and the prevalence rate was 620/100,000.

There are many pathogenic factors and complex pathological mechanisms of AIS. At present, it is generally believed that the occurrence of AIS is caused by atherosclerosis. Oxidative stress and vascular endothelial dysfunction are the primary pathogenesis of atherosclerosis. In recent years, with the deepening of research, people have found that the renin-angiotensin system (RAS) activation is closely related to AIS, which can directly or indirectly induce the occurrence and influence the development of AIS.

RAS is an endocrine regulatory system composed of peptide hormones and corresponding enzymes as the main components. It comprises six parts: renin, angiotensinogen, angiotensin, angiotensin-converting enzyme, angiotensin receptor, and aldosterone. Renin is an acid-hydrolytic protease produced by the juxtaglomerular cells of the kidney. Sodium depletion, sympathetic excitation, and decreased renal blood flow stimulate the release of renin, which acts on the hepatic production of angiotensinogen to convert it to angiotensin I (Ang I). Ang I has no biological activity and is further hydrolyzed to angiotensin II (Ang II) by the action of angiotensin-converting enzyme I. Ang II can be further decomposed into angiotensin (1–7) and angiotensin III and angiotensin IV by the step of angiotensin-converting enzyme II and aminopeptidase A, respectively (2).

Over-activation of RAS can produce a series of pathophysiological effects. At present, it is believed that circulating RAS mainly acts through the following two axes: (1) angiotensin-converting enzyme 1-Ang II-AT1R axis: the binding of Ang I-IV to AT1R leads to vasoconstriction, tissue cell fibrosis, and oxidative stress; (2) Angiotensin-converting enzyme 2-Ang (1–7)-Mas receptor axis: The binding of angiotensin domain with AT2R and Ang (1–7) with Mas receptor can resist the pathological effects of AT1R, dilate blood vessels, anti-inflammation, anti-tissue cell fibrosis, reduce cell apoptosis, and have protective effects on heart, brain, kidney, blood vessels and other organs (2). Studies on the pathological mechanism of RAS causing AIS mainly focus on Ang II, and the relationship between other components of RAS and AIS is relatively few.

The preferred treatment for AIS is intravenous thrombolysis within the time window. Still, due to the strict time window, the proportion of patients who can benefit from it is relatively low, and the treatment effect is poor (3). In recent years, with the continuous development of various endovascular therapy (EVT) devices and techniques, EVT has shown a good application prospect in treating AIS. Some domestic and foreign AIS treatment guidelines (4) recommend EVT as the first choice of treatment when intravenous thrombolysis is contraindicated or ineffective. Studies have shown that the overexpression of inflammatory factors and abnormal secretion of neurohormones in the pathogenesis of AIS aggravates the degree of neurological impairment and affects the prognosis of patients (5).

At present, the content of clinical evaluation of the development and prognosis of AIS mainly includes serological indicators and imaging examinations, among which serological indicators have the advantages of being simple, fast, and highly accurate and have become an essential means to guide clinical diagnosis and treatment. The primary objective of this study is to analyze the risk factors related to the occurrence of AIS, and the secondary aim is to explore the role of serum indicators such as neurohormones, blood routine, liver and kidney function, electrolytes, and coagulation function in the prognosis of patients undergoing endovascular thrombectomy (EVT).

Abbreviations: RAS, renin-angiotensin system; AIS, acute ischemic stroke; Ang I, angiotensin I; EVT, endovascular thrombectomy; ROC, receiver operating characteristic curves; AGR, albumin-globulin ratio; IS, ischemic stroke; Ang I, angiotensin I; DSA, digital subtraction angiography; AUC, area under the curve; RAAS, renin-angiotensin-aldosterone system.

Materials and methods

Patients

In this study, the alpha value was 0.05, the beta value was 0.2, and the test power was 0.8. The difference of Ang I between the patients and the controls was expected to be about 1–3 ng/ml. According to the 1:1 ratio between the case group and the control group, about 33 patients should be enrolled. Ultimately, seventy-two patients with AIS who underwent EVT at the Neurosurgery department of the First People's Hospital of Lianyungang from December 2022 to October 2023 were retrospectively enrolled in this study. At the same time, 60 subjects who underwent regular physical examinations during the same period were included, and a total of 132 cases were included. This study met the criteria outlined in the Declaration of Helsinki. The ethics committee approved it, and the institutional review board of the First People's Hospital of Lianyungang (ethics numbers: SHSY-IECKY-4.0/18–68/01 and ZDKYSB077). Written informed consent was obtained from this study's patients and their relatives.

Inclusion and exclusion criteria

Inclusion criteria: (1). Age over 18 years old; (2). AIS diagnosed by imaging (CT and MRI); (3). Undergo EVT.

Exclusion criteria: (1). Cerebral hemorrhage was confirmed by imaging examination; (2). Patients who have received thrombolytic therapy; (3). Concurrent diagnosis of other malignant tumors that may seriously affect survival; (4). Accompanied with severe infectious diseases or liver and kidney dysfunction; (5). Severe bleeding tendency; (6). Patients with previous IS and severe motor dysfunction.

Based on the above criteria, 7 patients accept thrombolytic therapy, 2 patients had severe liver and kidney dysfunction, and 3 patients had IS previously and severe motor dysfunction. We excluded 12 patients, and 60 patients were finally included in this study. According to the above criteria, we divided the 120 subjects into two groups: normal group and disease group. To further analyze the effect of different

variables on the prognosis of patients with AIS who underwent EVT, 60 patients in the disease group were divided into good prognosis group (0–2 scores) and poor prognosis group (3–5 scores) according to the modified Rankin scale score at discharge.

Study variables

The clinical data of inpatients in the Department of Neurosurgery of the First People's Hospital of Lianyungang were collected retrospectively, including age, sex, blood routine indexes, biochemical indexes, electrolyte indexes, and coagulation indexes. Blood samples were collected within 72 hours after surgery for further analysis. All blood samples were obtained from either the left or right femoral vein. Rapidlab 1200 series equipment (Laboratory equipment of the First People's Hospital of Lianyungang City) was used to analyze blood samples. Ang I ELISA assay: To measure the concentration of Ang I, quantitative factor high-sensitivity ELISA [R&D; Human angiotensin: BY-EH111540 (sensitivity 0.1 ng/mL)] was used to detect the concentration of Ang I in serum. Patients who underwent EVT were followed up by outpatient examination or telephone.

Surgical methods of endovascular thrombectomy

The patient was conventionally given local anesthesia, and if the patient has agitation, general anesthesia or intravenous combined anesthesia will be selected. The patient was asked to take the supine position, the femoral artery puncture was performed, and the 8F artery

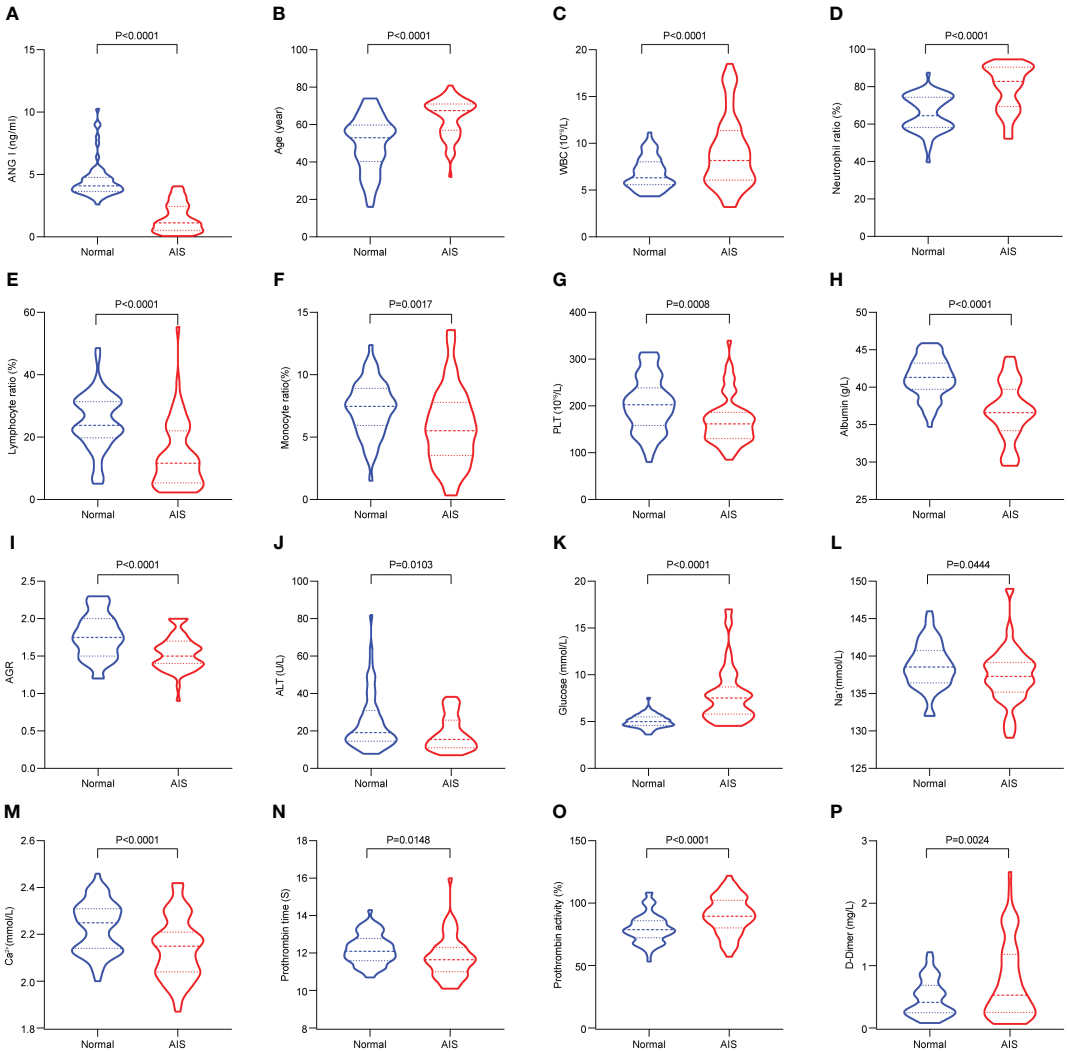

FIGURE 1
The significant differences in demographic data and clinical information between the controls and AIS patients. **(A)** Comparison of Ang I. **(B)** Comparison of age. **(C)** Comparison of WBC. **(D)** Comparison of neutrophil ratio. **(E)** Comparison of lymphocyte ratio. **(F)** Comparison of monocyte ratio. **(G)** Comparison of PLT. **(H)** Comparison of albumin. **(I)** Comparison of AGR. **(J)** Comparison of ALT. **(K)** Comparison of globulin. **(L)** Comparison of Na+. **(M)** Comparison of Ca2+. **(N)** Comparison of prothrombin time. **(O)** Comparison of prothrombin activity. **(P)** Comparison of D-Dimer. AIS, acute ischemic stroke; Ang I, angiotensin I; WBC, white blood cell; PLT, platelets; AGR, albumin-globulin ratio; ALT, alanine aminotransferase.

10.3389/fendo.2024.1388871

TABLE 1 Baseline demographic and clinical characteristics of AIS patients and controls.

Characteristic	Total (n=120)	Controls (n=60)	AIS patients (n=60)	*P value*
Age	56.925±14.282	49.883±14.418	63.967±10.133	< 0.001
Sex				0.099
Female	55 (45.833)	32 (53.333)	23 (38.333)	
Male	65 (54.167)	28 (46.667)	37 (61.667)	
Ang I (ng/ml)	3.026±2.007	4.531±1.487	1.52±1.141	< 0.001
Anticoagulation				0.347
No	109 (90.833)	56 (93.333)	53 (88.333)	
Yes	11 (9.167)	4 (6.667)	7 (11.667)	
Atrial fibrillation				0.127
No	100 (83.333)	54 (90)	48 (80)	
Yes	20 (16.667)	6 (10)	12 (20)	
RAS receptor blocker therapy				0.228
No	86 (71.667)	46 (76.667)	40 (66.667)	
Yes	34 (28.333)	14 (23.333)	20 (33.333)	
Blood routine indexes				
WBC (10^9/L)	7.882±3.123	6.796±1.687	8.968±3.798	< 0.001
RBC (10^12/L)	4.244±0.596	4.267±0.684	4.222±0.497	0.68
Hb (g/L)	127.092±15.068	125.6±15.192	128.583±14.922	0.28
HCT (%)	38.453±4.435	37.922±4.302	38.985±4.537	0.19
Neutrophil ratio (%)	72.61±12.922	65.657±9.612	79.563±12.086	< 0.001
Lymphocyte ratio (%)	19.473±11.161	24.987±8.919	13.96±10.482	< 0.001
Monocyte ratio (%)	6.514±2.719	7.283±2.144	5.745±3.019	0.002
PLT (10^9/L)	185.525±56.71	202.617±57.649	168.433±50.686	< 0.001
Biochemical indexes				
Albumin (g/L)	38.977±3.972	41.233±2.621	36.72±3.819	< 0.001
Globulin (g/L)	24.212±4.436	24.095±4.686	24.33±4.207	0.773
AGR (%)	1.653±0.284	1.763±0.291	1.542±0.231	< 0.001
ALT (U/L)	21.609±12.614	24.542±14.871	18.677±9.071	0.011
AST (U/L)	24.677±8.581	25.303±9.469	24.05±7.619	0.426
BUN (mmol/L)	5.139±1.767	5.15±1.357	5.129±2.111	0.947
Cr (umol/L)	68.265±19.563	65.483±15.683	71.047±22.588	0.12
Uric acid (umol/L)	292.733±81.525	293.817±73.876	291.65±89.136	0.885
Glucose (mmol/L)	6.452±2.564	5.056±0.691	7.848±2.97	< 0.001
Electrolyte indexes				
K+ (mmol/L)	3.802±0.361	3.802±0.284	3.803±0.428	0.982
Na+ (mmol/L)	138.031±3.481	138.668±3.044	137.393±3.787	0.044
Cl- (mmol/L)	104.177±3.22	104.315±3.07	104.04±3.384	0.642
Ca2+ (mmol/L)	2.185±0.127	2.23±0.108	2.14±0.13	< 0.001

(Continued)

TABLE 1 Continued

Characteristic	Total (n=120)	Controls (n=60)	AIS patients (n=60)	*P value*
Coagulation indexes				
Prothrombin time (s)	11.995±0.98	12.212±0.789	11.778±1.103	0.015
Prothrombin activity (%)	85.014±14.312	79.538±11.556	90.49±14.785	< 0.001
INR	1.048±0.095	1.061±0.096	1.036±0.094	0.147
Partial thromboplastin time (s)	27.007±4.896	26.257±3.091	27.757±6.136	0.094
Thrombin time (s)	17.652±4.736	17.795±1.442	17.508±6.567	0.742
Fibrinogen (g/L)	2.849±0.746	2.847±0.525	2.852±0.919	0.971
D-Dimer (mg/L)	0.615±0.497	0.479±0.293	0.751±0.612	0.003

AIS, acute ischemic stroke; Ang I, angiotensin I; WBC, white blood cell; RBC, red blood cell; HCT, hematocrit; PLT, platelets; AGR, albumin-globulin ratio; ALT, alanine aminotransferase; AST, aspartate transaminase; BUN, blood urea nitrogen; INR, international normalized ratio.

TABLE 2 Univariate and multivariate analysis of AIS patients and controls.

Characteristic	Univariate analysis		Multivariate analysis	
	Odds Ratio (95% CI)	*P value*	Odds Ratio (95% CI)	*P value*
Age	1.098(1.057-1.141)	<0.001	1.137(0.99-1.306)	0.07
Ang I (ng/ml)	0.048(0.013-0.184)	<0.001	0.019(0.001-0.266)	0.003
Blood routine indexes				
WBC (10^9/L)	1.327(1.131-1.557)	<0.001	–	0.764
RBC (10^12/L)	0.879(0.480-1.612)	0.677		
Hb (g/L)	1.013(0.989-1.038)	0.278		
HCT (%)	1.057(0.973-1.148)	0.190		
Neutrophil ratio (%)	1.114(1.070-1.160)	<0.001	–	0.764
Lymphocyte ratio (%)	0.892(0.852-0.934)	<0.001	–	0.484
Monocyte ratio (%)	0.797(0.687-0.925)	0.003	–	0.514
PLT (10^9/L)	0.988(0.981-0.996)	0.002	–	0.406
Biochemical indexes				
Albumin (g/L)	0.652(0.556-0.764)	<0.001	0.614(0.391-0.964)	0.034
Globulin (g/L)	1.012(0.933-1.098)	0.771		
AGR (%)	0.039(0.008-0.193)	<0.001	–	0.384
ALT (U/L)	0.959(0.927-0.992)	0.015	–	0.881
AST (U/L)	0.983(0.942-1.025)	0.423		
BUN (mmol/L)	0.993(0.810-1.217)	0.947		
Cr (umol/L)	1.015(0.996-1.036)	0.125		
Uric acid (umol/L)	1.000(0.995-1.004)	0.884		
Glucose (mmol/L)	4.512(2.454-8.295)	<0.001	4.731(0.712-31.448)	0.108
Electrolyte indexes				
K+ (mmol/L)	1.012(0.374-2.734)	0.982		
Na+ (mmol/L)	0.895(0.801-0.999)	0.049	–	0.606

(Continued)

TABLE 2 Continued

Characteristic	Univariate analysis	Multivariate analysis		
	Odds Ratio (95% CI)	*P value*	Odds Ratio (95% CI)	*P value*
Electrolyte indexes				
Cl- (mmol/L)	0.974(0.871-1.089)	0.639		
Ca2+ (mmol/L)	0.002(0.000-0.054)	<0.001	–	0.729
Coagulation indexes				
Prothrombin time (s)	0.614(0.410-0.920)	0.018	–	0.304
Prothrombin activity (%)	1.064(1.032-1.097)	<0.001	–	0.103
INR	0.055(0.001-2.890)	0.151		
Partial thromboplastin time (s)	1.082(0.981-1.193)	0.113		
Thrombin time (s)	0.987(0.914-1.066)	0.740		
Fibrinogen (g/L)	1.009(0.623-1.634)	0.970		
D-Dimer (mg/L)	3.515(1.480-8.351)	0.004	–	0.246

AIS, acute ischemic stroke; Ang I, angiotensin I; WBC, white blood cell; RBC, red blood cell; HCT, hematocrit; PLT, platelets; AGR, albumin-globulin ratio; ALT, alanine aminotransferase; AST, aspartate transaminase; BUN, blood urea nitrogen; INR, international normalized ratio.

TABLE 3 Comparison of good prognosis and poor prognosis in AIS patients.

Characteristic	Total (n=60)	Good prognosis (n=25)	Poor prognosis (n=35)	P value
Age	63.967±10.133	58.24±10.887	68.057±7.292	< 0.001
Sex				0.164
Female	23 (38.333)	7 (28)	16 (45.714)	
Male	37 (61.667)	18 (72)	19 (54.286)	
Ang I (ng/ml)	1.52±1.141	2.205±1.256	1.031±0.745	< 0.001
Blood routine indexes				
WBC (10^9/L)	8.968±3.798	8.612±2.343	9.222±4.583	0.504
RBC (10^12/L)	4.222±0.497	4.239±0.402	4.21±0.56	0.816
Hb (g/L)	128.583±14.922	130.96±16.349	126.886±13.805	0.316
HCT (%)	38.985±4.537	39.72±4.57	38.46±4.506	0.295
Neutrophil ratio (%)	79.563±12.086	78.512±11.196	80.314±12.791	0.565
Lymphocyte ratio (%)	13.96±10.482	15.868±11.538	12.597±9.598	0.252
Monocyte ratio (%)	5.745±3.019	5.385±2.896	6.003±3.12	0.434
PLT (10^9/L)	168.433±50.686	172.8±48.267	165.314±52.816	0.571
Biochemical indexes				
Albumin (g/L)	36.72±3.819	36.748±3.481	36.7±4.094	0.961
Globulin (g/L)	24.33±4.207	23±2.992	25.28±4.708	0.026
AGR (%)	1.54±0.23	1.62±0.23	1.48±0.21	0.018
ALT (U/L)	18.677±9.071	18.608±9.039	18.726±9.226	0.961
AST (U/L)	24.05±7.619	21.04±6.248	26.2±7.858	0.006
BUN (mmol/L)	5.129±2.111	4.858±2.242	5.322±2.023	0.415

(Continued)

TABLE 3 Continued

Characteristic	Total (n=60)	Good prognosis (n=25)	Poor prognosis (n=35)	P value
Biochemical indexes				
Cr (umol/L)	71.047±22.588	69.84±24.781	71.909±21.214	0.737
Uric acid (umol/L)	291.65±89.136	302.176±73.593	284.131±99.119	0.422
Glucose (mmol/L)	7.848±2.97	7.521±2.891	8.081±3.045	0.472
Electrolyte indexes				
K+ (mmol/L)	3.803±0.428	3.992±0.337	3.668±0.438	0.002
Na+ (mmol/L)	137.393±3.787	137.632±2.255	137.223±4.608	0.651
Cl- (mmol/L)	104.04±3.384	104.148±3.603	103.963±3.27	0.839
Ca2+ (mmol/L)	2.14±0.13	2.143±0.133	2.139±0.13	0.909
Coagulation indexes				
Prothrombin time (s)	11.778±1.103	11.496±1.241	11.98±0.962	0.11
Prothrombin activity (%)	90.49±14.785	96.064±14.444	86.509±13.888	0.013
INR	1.036±0.094	1.025±0.109	1.043±0.083	0.484
Partial thromboplastin time (s)	27.757±6.136	29.352±8.704	26.617±2.941	0.142
Thrombin time (s)	17.508±6.567	19.056±9.626	16.403±2.533	0.19
Fibrinogen (g/L)	2.852±0.919	2.654±0.683	2.993±1.043	0.134
D-Dimer (mg/L)	0.751±0.612	0.717±0.67	0.776±0.576	0.726

AIS, acute ischemic stroke; Ang I, angiotensin I; WBC, white blood cell; RBC, red blood cell; HCT, hematocrit; PLT, platelets; AGR, albumin-globulin ratio; ALT, alanine aminotransferase; AST, aspartate transaminase; BUN, blood urea nitrogen; INR, international normalized ratio.

sheath was inserted. The whole brain digital subtraction angiography (DSA) was performed to determine the infarction site. For patients without large artery occlusion, 100,000 U urokinase was injected into the artery on the opposite side of the lesion or the poor development side. Then 20, 000 U/min urokinase was maintained according to the patient's condition. The vital signs of the patients were closely monitored. For patients with large artery occlusion, an 8F MPA1 guide catheter was placed at the distal end of the common carotid artery, and a 5F-125 Naven intermediate catheter was placed at the distal end of the internal carotid artery along the guide catheter. Under the guidance of a 0.014 microguide wire, a Rebar-18 microcatheter was used to pass through the occlusion vessel to the distal end of the thrombus. Microcatheter angiography was performed to confirm the patency of the thrombus site and the distal end of the occluded vessel. The Solitaire AB stent was placed through the microcatheter. After 5 minutes, to ensure the full release of the stent, the stent was withdrawn with the microcatheter, and the blood was quickly aspirated with a 50 mL syringe. DSA examination was performed again after thrombectomy to confirm vascular recanalization.

Statistical analysis

Customarily distributed values were calculated as parametric tests and mean ± standard deviation, while non-normally distributed values were calculated as median. Categorical variables were analyzed by chi-square or Fisher's exact test, and continuous variables were analyzed by unpaired t-test. The chi-square or Kruskal-Wallis test was used to evaluate the correlation between Ang I, blood routine indexes, biochemical indexes, electrolyte indexes, coagulation indexes, and clinicopathological features. The ROC curve and the area under the curve (AUC) were used to compare the ability of the models to predict AIS and outcome status. Univariate and multivariate logistic regression analyses were used to analyze the risk factors of AIS. Multivariate logistic regression was used to analyze the independent risk factors for the prognosis of AIS, and a diagnostic nomogram was constructed. All data were analyzed by SPSS software (version 27.0), GraphPad Prism software (version 8.3.1), and RStudio software (4.3.0). A value of 0.05 was considered statistically significant.

Results

Demographic and clinical characteristics

Figure 1; Table 1 show the demographic data and various clinical information data between the controls and disease groups included in the study and the levels of significance of differences between groups. The median age of 120 patients was 56.925 ± 14.282 years old. The median age of 60 controls was 49.883 ± 14.418 years old, and the median age of 60 patients was 63.967 ± 10.133 years old (p<0.001). The level of Ang I in the disease group (1.52 ± 1.141) was significantly lower

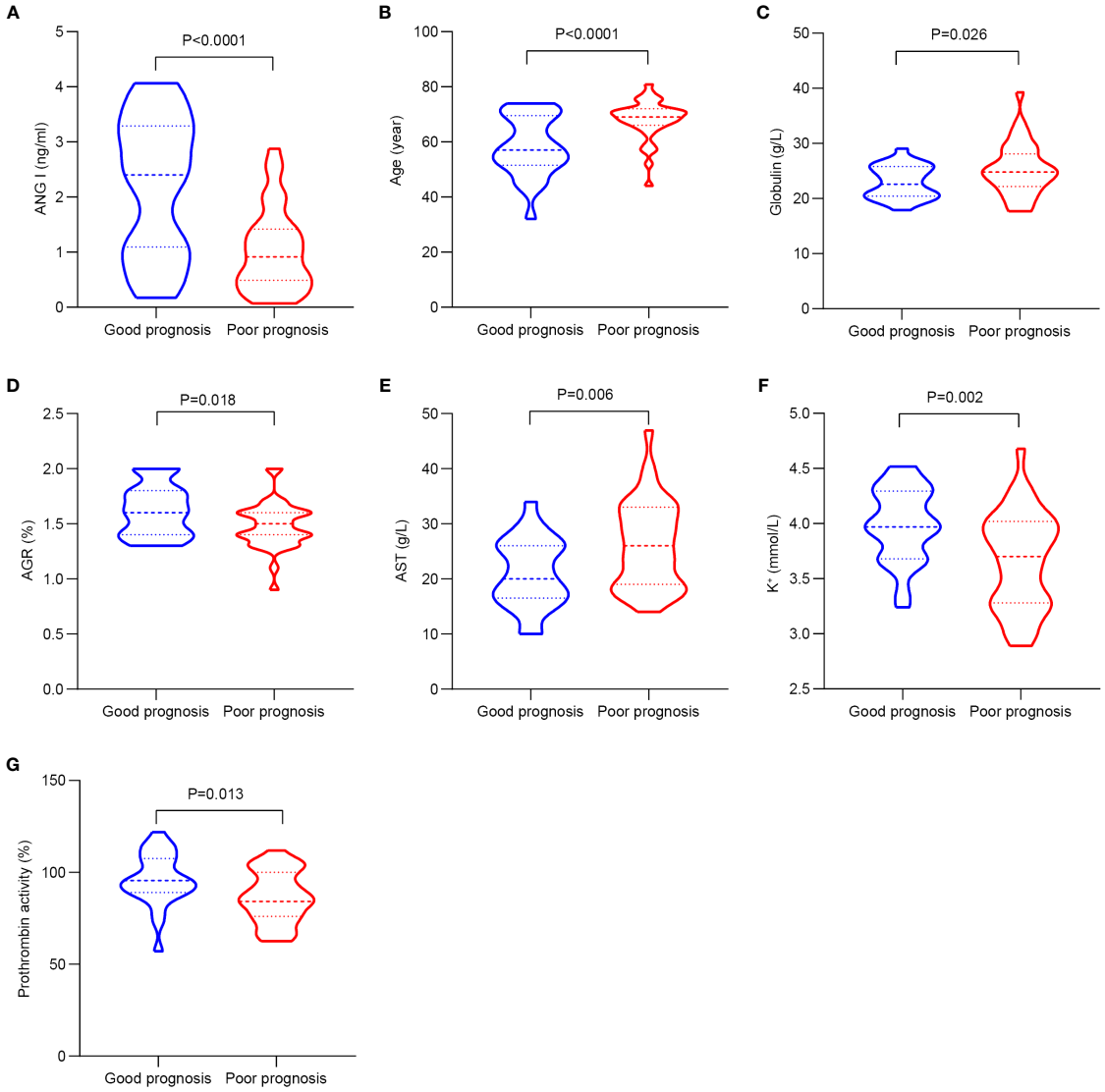

FIGURE 2
The significant differences in demographic data and clinical information between the good and poor prognosis groups of AIS patients. **(A)** Comparison of Ang I. **(B)** Comparison of age. **(C)** Comparison of globulin. **(D)** Comparison of AGR. **(E)** Comparison of AST. **(F)** Comparison of K+. **(G)** Comparison of prothrombin activity. AIS, acute ischemic stroke; Ang I, angiotensin I; AGR, albumin-globulin ratio; AST, aspartate transaminase.

than that in the control group (4.531 ± 1.487) (p<0.001). WBC, neutrophil ratio, lymphocyte ratio, monocyte ratio, PLT in blood routine indexes; albumin, albumin-globulin ratio (AGR), ALT, glucose in biochemical indexes; K+, Ca2+ in electrolyte; prothrombin time, prothrombin activity and D-dimer all had significant differences between the normal group and the disease group (p<0.05).

Risk factors for AIS

We explored the influencing factors of AIS occurrence by univariate and multivariate Logistic regression analyses (Table 2). Multivariate Logistic regression analysis showed that older age (OR: 1.098, 95%CI: 1.057–1.141, p<0.001), high leukocyte expression (OR: 1.327, 95%CI: 1.131–1.557, p<0.001), high neutrophil ratio (OR: 1.114, 95%CI: 1.070–1.160, p<0.001), hyperglycemia (OR: 4.512, 95%CI: 2.454–8.295, p<0.001), high prothrombin activity (OR: 1.064, 95%CI: 1.032–1.097, p<0.001), high D-dimer (OR: 3.515, 95%CI: 1.480–8.351, p=0.004) might be more likely to have AIS.

The higher Ang I (OR: 0.048, 95%CI: 0.013–0.184, p<0.001), the higher lymphocyte ratio (OR: 0.892, 95%CI: 0.852–0.934, p<0.001), higher monocyte ratio (OR: 0.797, 95%CI: 0.687–0.925, p=0.003), higher PLT (OR: 0.988, 95%CI: 0.981–0.996, p=0.002), and higher albumin (OR: 0.797, 95%CI: 0.687–0.925, p=0.002). 0.652, 95% CI 0.556–0.764, p<0.001), AGR (OR: 0.039, 95%CI: 0.008–0.193, p=0.049), ALT (OR: 0.959, 95%CI: 0.927–0.992, p=0.015), and Na+ (OR: 0.959, 95%CI: 0.927–0.992, p=0.015). 0.895, 95%CI = 0.801–0.999, p=0.049), and the higher Ca2+ (OR: 0.002, 95%CI = 0.000–0.054, p<0.001) and longer prothrombin time (OR<: 0.614, 95%CI: 0.410–0.920, p=0.018) might reduce the risk of AIS.

10.3389/fendo.2024.1388871

Demographic and clinical characteristics of patients with different prognosis

Table 3; Figure 2 show the demographic data and various clinical information data between the good and poor prognosis groups of AIS patients and the levels of significance of differences between groups. The median age of 60 patients was 63.967 ± 10.133 years old. The median age of 25 patients in the good prognosis group was 58.24 ± 10.887 years old, and the median age of 35 patients in the poor prognosis group was 68.057 ± 7.292 years old (p<0.001). The level of Ang I was significantly different between the good prognosis group (2.205 ± 1.256) and the poor prognosis group (1.031 ± 0.745) (p<0.001). Significant differences existed in the expression of globulin, AGR, ALT, K+, and prothrombin activity between the good and poor prognoses groups (p<0.05).

Identification of prognostic factors for AIS

To further explore the clinical diagnostic predictive value of serum Ang I, blood routine indexes, biochemical indexes, electrolyte indexes, and coagulation indexes for the prognosis of AIS, the good prognosis group was used as negative samples, and the poor prognosis group was used as positive samples. The ROC curve diagnostic analysis model was established. Ang I, K+, and prothrombin activity all had high diagnostic and predictive value. The AUC of Ang I was 0.763, 95% CI was 0.633–0.894, p<0.001; The AUC of K+ in electrolyte was 0.715, 95%CI was 0.585–0.846, p=0.005; The AUC of prothrombin activity in coagulation function was 0.705, 95%CI was 0.568–0.841, p=0.007 (Table 4; Figure 3).

Factors associated with the prognosis of AIS

We explored the influencing factors of AIS outcome by univariate and multivariate logistic regression (Table 5). The results showed that the higher Ang I (OR: 0.336, 95%CI: 0.184–0.616, p<0.001), the higher lymphocyte ratio (OR: 0.892, 95%CI: 0.852–0.934, p<0.001), higher AGR (OR = 0.053, 95%CI: 0.004–0.687, p=0.025), higher K+ (OR = 0.124, 95%CI: 0.028–0.555, p=0.006), and higher prothrombin activity (OR = 0.124, 95%CI: 0.028–0.555, p=0.006). 0.952, 95%CI: 0.914–0.991, p=0.017) might have a better prognosis.

High expression of globulin (OR: 1.164, 95%CI: 1.004–1.349, p=0.045), increased expression of ALT (OR: 1.111, 95%CI: 1.022–1.207, p=0.013), and high admission NIHSS score (OR: 1.203, 95%CI: 1.046–1.384, p=0.010) might have a poor prognosis of AIS. Multivariate Logistic regression analysis of variables with significant differences in univariate logistic regression showed that Ang I (OR: 0.260, 95%CI: 0.124–0.547, p<0.001) and high AGR (OR: 0.011, 95%CI: 0.000–0.306, p=0.008) were still statistically significant.

TABLE 4 AUC of different factors for AIS.

Characteristic	AUC	Odds Ratio (95% CI)	P value
Ang I (ng/ml)	0.763	0.633-0.894	0.001
Blood routine indexes			
WBC (10^9/L)	0.520	0.372-0.668	0.793
RBC (10^12/L)	0.523	0.373-0.673	0.759
Hb (g/L)	0.573	0.421-0.725	0.341
HCT (%)	0.577	0.426-0.728	0.311
Neutrophil ratio (%)	0.575	0.426-0.723	0.326
Lymphocyte ratio (%)	0.597	0.449-0.744	0.205
Monocyte ratio (%)	0.468	0.314-0.622	0.675
PLT (10^9/L)	0.569	0.419-0.719	0.364
Biochemical indexes			
Albumin (g/L)	0.504	0.354-0.654	0.958
Globulin (g/L)	0.639	0.498-0.781	0.067
AGR (%)	0.663	0.521-0.805	0.033
ALT (U/L)	0.498	0.344-0.652	0.982
AST (U/L)	0.687	0.553-0.822	0.014
BUN (mmol/L)	0.591	0.443-0.739	0.233
Cr (umol/L)	0.530	0.380-0.680	0.691
Uric acid (umol/L)	0.609	0.460-0.758	0.152
Glucose (mmol/L)	0.557	0.402-0.712	0.458
Electrolyte indexes			
K+ (mmol/L)	0.715	0.585-0.846	0.005
Na+ (mmol/L)	0.569	0.422-0.715	0.368
Cl- (mmol/L)	0.539	0.388-0.690	0.61
Ca2+ (mmol/L)	0.501	0.350-0.652	0.994
Coagulation indexes			
Prothrombin time (s)	0.673	0.532-0.813	0.024
Prothrombin activity (%)	0.705	0.568-0.841	0.007
INR	0.606	0.458-0.753	0.165
Partial thromboplastin time (s)	0.574	0.421-0.726	0.333
Thrombin time (s)	0.526	0.373-0.526	0.73
Fibrinogen (g/L)	0.583	0.437-0.729	0.277
D-Dimer (mg/L)	0.573	0.414-0.732	0.337

AIS, acute ischemic stroke; Ang I, angiotensin I; WBC, white blood cell; RBC, red blood cell; HCT, hematocrit; PLT, platelets; AGR, albumin-globulin ratio; ALT, alanine aminotransferase; AST, aspartate transaminase; BUN, blood urea nitrogen; INR, international normalized ratio.

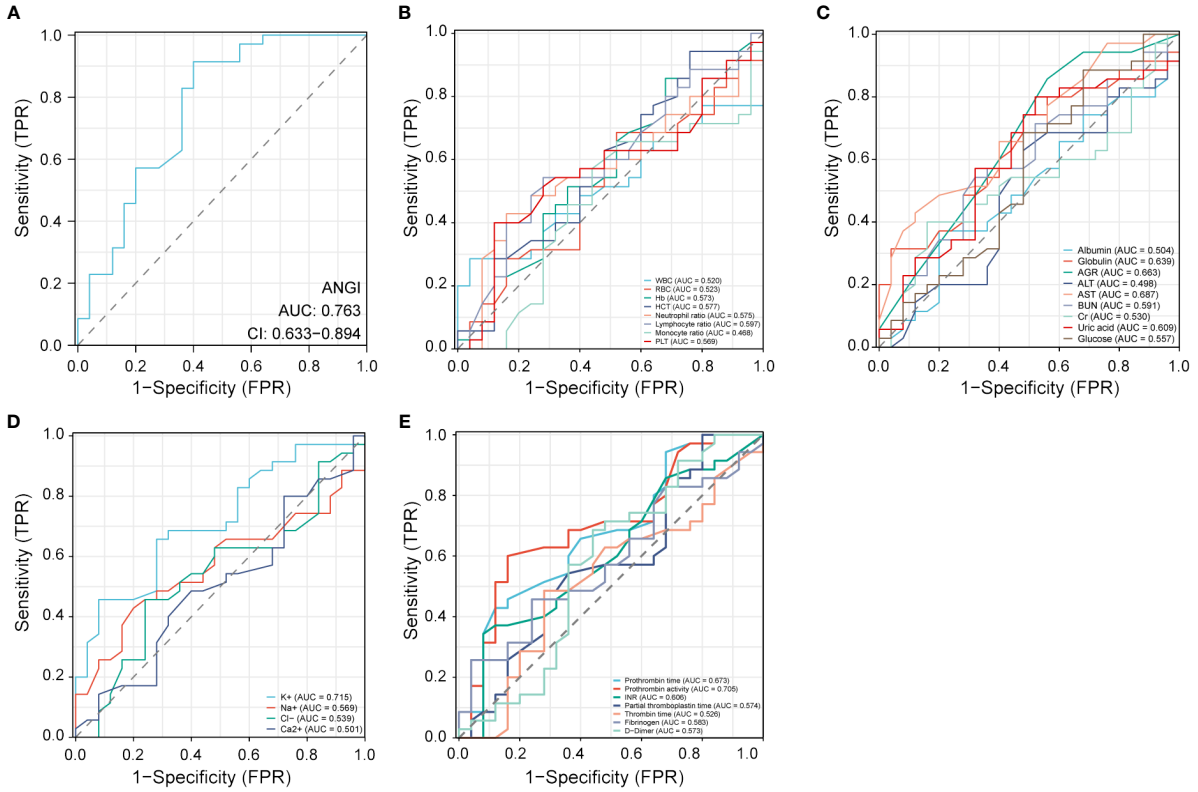

FIGURE 3
Receiver operating characteristic (ROC) curve analysis of different factors for the prognosis of AIS. **(A)** Ang I. **(B)** Blood routine indexes. **(C)** Biochemical indexes. **(D)** Electrolyte indexes. **(E)** Coagulation indexes. AIS, acute ischemic stroke; Ang I, angiotensin I; WBC, white blood cell; RBC, red blood cell; HCT, hematocrit; PLT, platelets; AGR, albumin-globulin ratio; ALT, alanine aminotransferase; AST, aspartate transaminase; BUN, blood urea nitrogen; INR, international normalized ratio.

TABLE 5 Univariate and multivariate analysis of good and poor prognosis AIS.

Characteristic	Univariate analysis		Multivariate analysis	
	Odds Ratio (95% CI)	*P value*	Odds Ratio (95% CI)	*P value*
Ang I (ng/ml)	0.336(0.184-0.616)	<0.001	0.26(0.124-0.547)	<0.001
Blood routine indexes				
WBC (10^9/L)	1.045(0.909-1.201)	0.538		
RBC (10^12/L)	0.887(0.312-2.520)	0.822		
Hb (g/L)	0.981(0.947-1.017)	0.297		
HCT (%)	0.939(0.836-1.055)	0.289		
Neutrophil ratio (%)	1.013(0.970-1.057)	0.567		
Lymphocyte ratio (%)	0.970(0.922-1.021)	0.240		
Monocyte ratio (%)	1.073(0.900-1.279)	0.433		
PLT (10^9/L)	0.997(0.987-1.007)	0.571		
Biochemical indexes				
Albumin (g/L)	0.997(0.870-1.141)	0.961		
Globulin (g/L)	1.164(1.004-1.349)	0.045	–	0.997
AGR (%)	0.053(0.004-0.687)	0.025	0.011(0.000-0.306)	0.008

(Continued)

TABLE 5 Continued

Characteristic	Univariate analysis		Multivariate analysis	
	Odds Ratio (95% CI)	*P value*	Odds Ratio (95% CI)	*P value*
Biochemical indexes				
ALT (U/L)	1.001(0.946-1.060)	0.960		
AST (U/L)	1.111(1.022-1.207)	0.013	–	0.081
BUN (mmol/L)	1.118(0.861-1.451)	0.403		
Cr (umol/L)	1.004(0.981-1.028)	0.725		
Uric acid (umol/L)	0.998(0.992-1.004)	0.439		
Glucose (mmol/L)	1.070(0.891-1.284)	0.471		
Electrolyte indexes				
K+ (mmol/L)	0.124(0.028-0.555)	0.006	–	0.263
Na+ (mmol/L)	0.971(0.847-1.114)	0.678		
Cl- (mmol/L)	0.984(0.844-1.147)	0.833		
Ca2+ (mmol/L)	0.789(0.015-42.147)	0.907		
Coagulation indexes				
Prothrombin time (s)	1.577(0.915-2.716)	0.101		
Prothrombin activity (%)	0.952(0.914-0.991)	0.017	–	0.106
INR	8.858(0.028-2822.600)	0.458		
Partial thromboplastin time (s)	0.910(0.805-1.029)	0.134		
Thrombin time (s)	0.933(0.846-1.029)	0.165		
Fibrinogen (g/L)	1.559(0.834-2.915)	0.164		
D-Dimer (mg/L)	1.174(0.499-2.759)	0.713		
Prothrombin time (s)	1.203(1.046-1.384)	0.010	–	0.194

AIS, acute ischemic stroke; Ang I, angiotensin I; WBC, white blood cell; RBC, red blood cell; HCT, hematocrit; PLT, platelets; AGR, albumin-globulin ratio; ALT, alanine aminotransferase; AST, aspartate transaminase; BUN, blood urea nitrogen; INR, international normalized ratio.

Nomogram construction and validation

According to the results of multivariate logistic regression, Ang I and AGR were selected to construct a diagnostic nomogram for the prognosis of AIS, and the ROC curve was used to verify the diagnostic nomogram to test its predictive efficacy for the prognosis of patients. The AUC value of the combined model was 0.859 (95% CI: 0.765–0.954). According to the above results, it was suggested that the model had a solid predictive ability, as shown in Figure 4.

Discussion

In this retrospective study, univariate and multivariate logistic regression were used to analyze the risk factors for AIS. Consistent with previous studies, advanced age, high blood glucose, high D-dimer, and high prothrombin activity are risk factors for acute ischemic AIS. We also found that the increase of white blood cells and the increase of neutrophil ratio in blood routine examination also have specific suggestive significance. In addition, we found that the higher Ang I was, the lower the risk of AIS was. The level of Ang I was higher in the good prognosis group. Significant differences existed in the expression of globulin, AGR, ALT, K+, and prothrombin activity between the good and the poor prognosis group. As previously mentioned, our study found that Ang I and AGR had a non-negligible impact on the prognosis of patients with AIS, so we developed a nomogram to evaluate its ability to predict the prognosis of AIS.

Risk factors for AIS include age, smoking, obesity, atrial fibrillation, hypertension, diabetes, etc. (6), of which hypertension is the most critical risk factor. Excluding other risk factors for AIS, a 10mmHg increase in systolic blood pressure was associated with a 49% increased risk of AIS, and a 5mmHg rise in diastolic blood pressure was associated with a 46% increased risk of AIS (7). Experimental results showed that the vascular shear stress was increased in hypertensive patients compared with normal people, which caused vascular endothelial damage (8). At the same time, endothelial injury also affects NO activity and increases the synthesis and release of endothelin and Ang II, resulting in vasomotor dysfunction (8). Wallace et al. found that after endothelial injury, endothelial cells will release a large number of

10.3389/fendo.2024.1388871

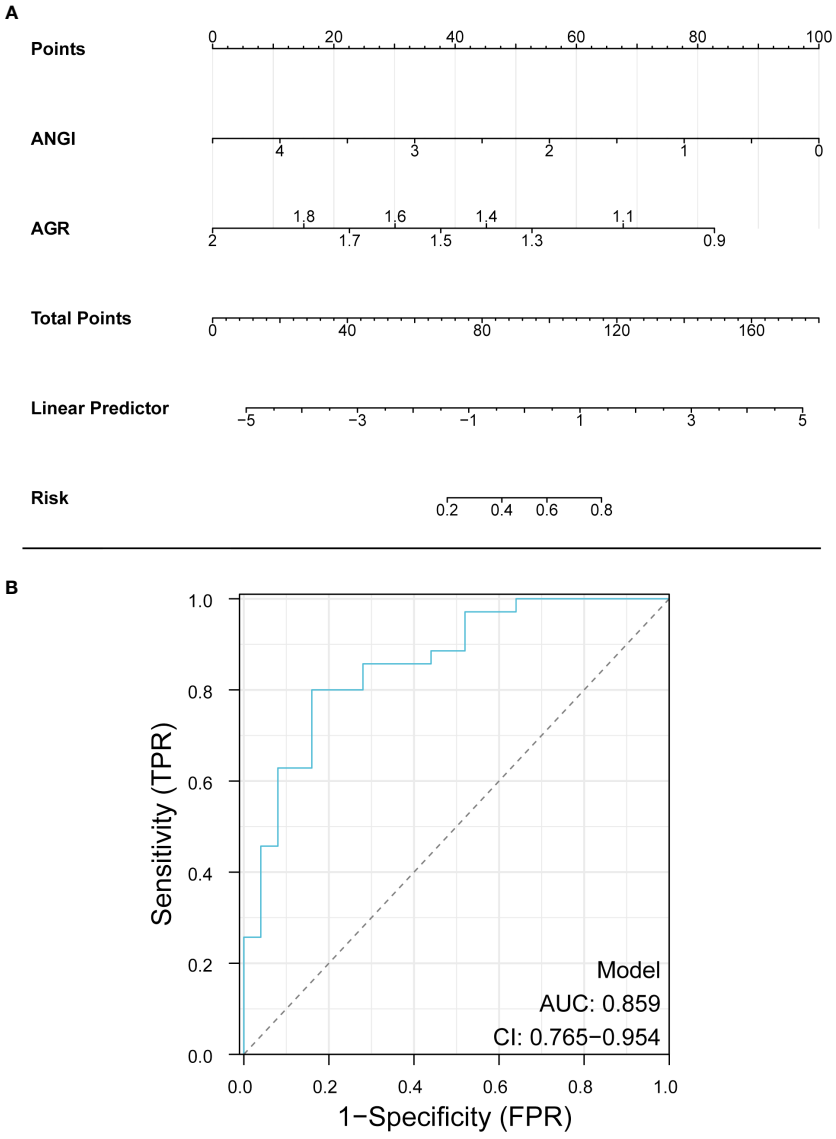

FIGURE 4
Nomogram for predicting the prognosis of AIS. Ang I, angiotensin I; AGR, albumin-globulin ratio.

active substances, including adenosine triphosphate, 5-hydroxytryptamine, etc., which can promote the synthesis and release of endothelin, increasing blood pressure, and then damage endothelial cells again, forming a vicious circle (9). The primary pathogenesis of AIS is as follows: The damage of vascular endothelial cells leads to atherosclerosis, which leads to occlusion of cerebral arteries and cerebral ischemia. Neurons in the ischemic center release the injury-related molecular pattern to activate the immune response (10–12).

Hyperactivation of the local renin-angiotensin-aldosterone system (RAAS) in hypertensive patients is also an important reason for vascular endothelial injury (13). RAAS is an essential regulatory system to maintain the body's balance of water and electrolyte. Its dysfunction will lead to vasoconstriction and aggravate the degree of ischemic injury in cerebrovascular diseases. And affect the rate of vascular recanalization after treatment (14, 15). The mechanism of RAAS activation is as follows: firstly, angiotensinogen is converted into Ang I under the stimulation of renin, and then Ang I is converted into Ang II by ACE. Ang II increases aldosterone secretion through the sympathetic nervous system, resulting in water and sodium retention and increasing blood pressure (16).

Some studies have shown that the serum Ang II level of patients after intravenous thrombolysis or EVT treatment is significantly lower than that before treatment, and the serum Ang II level of patients in the EVT group is lower than that in intravenous thrombolysis group, suggesting that EVT can significantly reduce the neurohormone level of AIS patients (17–22). How does the level of Ang I change? Our study focused on the changes of Ang I.

Our study found that Ang I levels were lower in AIS patients than in controls and higher in the group with a good prognosis. One study had similar results to ours. The level of Ang I decreased while

the level of Ang II remained unchanged, accompanied by an increase in ACE activity. This phenomenon can be explained by the decrease in renin caused by the negative feedback after the rise in blood pressure. Increased ACE activity can convert all available Ang I to Ang II (16). Another reason for maintaining a steady Ang II concentration may be the up-regulation of local AT1 and AT2 receptors in and around the infarct area. Animal experiments have also confirmed that RAAS promotes brain oxidative stress response, further promoting RAAS and sympathetic nervous system activation to mobilize peripheral organ responses (23).

Nomograms are highly effective in areas such as diagnosis and prediction. Compared with traditional scoring systems for IS (24, 25), the nomogram model can estimate the probability of adverse outcomes after EVT, which often provides a better-personalized assessment to help management decisions. In addition, the graph has higher accuracy and better-discriminating ability and is more convenient to use. Several studies have predicted poor outcomes in patients with IS. Zhang et al. established a nomogram model to predict the 3-month risk of death in IS patients with anterior circulation arterial occlusion who successfully received endovascular thrombolysis, composed of age, pretreatment collateral status, baseline blood glucose level, symptomatic intracranial hemorrhage, and baseline National Institutes of Health Stroke Scale score (26). Du et al. determined that age, baseline National Institutes of Health Stroke Scale score, collateral circulation, rapid blood glucose levels, and recirculation were independent predictors of malignant cerebral edema after EVT (27). A study from Japan also focused on whether imaging technology, low relative diffusion-weighted imaging (DWI) signal intensity, can predict good clinical outcomes after EVT in patients with acute IS. Forty-nine patients were included in the analysis, and the results showed that the relative DWI signal intensity of the group with a good prognosis was significantly lower than that of the group with a poor prognosis. Low relative DWI signal intensity was associated with a good prognosis after EVT (28). In this study, Ang I and AGR, two readily available variables, have good discriminative ability, and the AUC value of the combined ROC model is 0.859. Therefore, the combined Ang I and AGR model can predict the prognosis of AIS patients, thus achieving a more accurate therapeutic effect and better serving the patient population.

The small sample size limits our study, and the sample size will be expanded. This is a retrospective single-center study, and the results must be further prospectively verified in multiple centers. Our study has established the role of Ang I in the prognosis of patients undergoing EVT. Still, there was no study of the other components, including angiotensinogen and Ang II, so further studies are needed to explore the mechanisms and other parts of the RAAS system.

Conclusion

The study's findings suggested advanced age, high blood glucose, high D-dimer, and high prothrombin activity are risk factors in patients with AIS. The higher the ANG I and AGR, the better the prognosis of AIS surgery. Furthermore, the combined ANG I and AGR model has a good predictive ability for the prognosis of patients undergoing arterial thrombectomy.

Data availability statement

The original contributions presented in the study are included in the article/supplementary material. Further inquiries can be directed to the corresponding authors.

Ethics statement

The studies involving humans were approved by The institutional review board of the First People's Hospital of Lianyungang. The studies were conducted in accordance with the local legislation and institutional requirements. The participants provided their written informed consent to participate in this study.

Author contributions

SY: Conceptualization, Data curation, Formal Analysis, Writing – original draft. KL: Methodology, Software, Visualization, Writing – review & editing. ZH: Validation, Writing – review & editing. YX: Validation, Writing – review & editing. JL: Validation, Writing – review & editing. YS: Funding acquisition, Investigation, Resources, Supervision, Writing – review & editing. AL: Conceptualization, Project administration, Supervision, Writing – review & editing.

Funding

The author(s) declare financial support was received for the research, authorship, and/or publication of this article. This research was funded by [Multi-factor analysis of cognitive dysfunction in elderly patients with ischemic stroke after thrombectomy] grant number [L202301].

Acknowledgments

The authors thank the participants in the study.

Conflict of interest

The authors declare that the research was conducted in the absence of any commercial or financial relationships that could be construed as a potential conflict of interest.

Publisher's note

References

1. Gravbrot N, McDougall R, Aguilar-Salinas P, Avila MJ, Burket AR, Dumont TM. National trends in endovascular thrombectomy and decompressive craniectomy for acute ischemic stroke: A study using national inpatient sample data from 2006 to 2016. *J Clin Neurosci*. (2022) 101:234–8. doi: 10.1016/j.jocn.2022.04.027

2. Holappa M, Vapaatalo H, Vaajanen A. Many faces of renin-angiotensin system - focus on eye. *Open Ophthalmol J*. (2017) 11:122–42. doi: 10.2174/1874364101711010122

3. Marko M, Posekany A, Szabo S, Scharer S, Kiechl S, Knoflach M, et al. Trends of R-tpa (Recombinant tissue-type plasminogen activator) treatment and treatment-influencing factors in acute ischemic stroke. *Stroke*. (2020) 51:1240–7. doi: 10.1161/strokeaha.119.027921

4. Powers WJ, Rabinstein AA, Ackerson T, Adeoye OM, Bambakidis NC, Becker K, et al. Guidelines for the early management of patients with acute ischemic stroke: A guideline for healthcare professionals from the American heart association/American stroke association. *Stroke*. (2018) 49:e46–e110. doi: 10.1161/str.0000000000000158

5. Jafari M, Katlowitz K, de la Garza C, Sellers A, Moore S, Hall H, et al. Impact of systemic inflammatory response syndrome on acute ischemic stroke patients treated with mechanical thrombectomy. *J Neurol Sci*. (2021) 430:119988. doi: 10.1016/j.jns.2021.119988

6. Alloubani A, Saleh A, Abdelhafiz I. Hypertension and diabetes mellitus as a predictive risk factors for stroke. *Diabetes Metab Syndr*. (2018) 12:577–84. doi: 10.1016/j.dsx.2018.03.009

7. Kannel WB, Wolf PA, Verter J, McNamara PM. Epidemiologic assessment of the role of blood pressure in stroke: the framingham study. *JAMA*. (1996) 276:1269–78.

8. Li WJ, Liu Y, Wang JJ, Zhang YL, Lai S, Xia YL, et al. "Angiotensin ii memory" Contributes to the development of hypertension and vascular injury via activation of nadph oxidase. *Life Sci*. (2016) 149:18–24. doi: 10.1016/j.lfs.2016.02.037

9. Wallace SM, Yasmin, McEniery CM, Mäki-Petäjä KM, Booth AD, Cockcroft JR, et al. Isolated systolic hypertension is characterized by increased aortic stiffness and endothelial dysfunction. *Hypertension*. (2007) 50:228–33. doi: 10.1161/hypertensionaha.107.089391

10. Hurford R, Sekhar A, Hughes TAT, Muir KW. Diagnosis and management of acute ischaemic stroke. *Pract Neurol*. (2020) 20:304–16. doi: 10.1136/practneurol-2020–002557

11. Zhao Y, Zhang X, Chen X, Wei Y. Neuronal injuries in cerebral infarction and ischemic stroke: from mechanisms to treatment (Review). *Int J Mol Med*. (2022) 49. doi: 10.3892/ijmm.2021.5070

12. Maida CD, Norrito RL, Daidone M, Tuttolomondo A, Pinto A. Neuroinflammatory mechanisms in ischemic stroke: focus on cardioembolic stroke, background, and therapeutic approaches. *Int J Mol Sci*. (2020) 21(18):6454. doi: 10.3390/ijms21186454

13. Montezano AC, Nguyen Dinh Cat A, Rios FJ, Touyz RM. Angiotensin ii and vascular injury. *Curr Hypertens Rep*. (2014) 16:431. doi: 10.1007/s11906–014-0431–2

14. Ames MK, Atkins CE, Pitt B. The renin-angiotensin-aldosterone system and its suppression. *J Vet Intern Med*. (2019) 33:363–82. doi: 10.1111/jvim.15454

15. McFall A, Nicklin SA, Work LM. The counter regulatory axis of the renin angiotensin system in the brain and ischaemic stroke: insight from preclinical stroke studies and therapeutic potential. *Cell Signal*. (2020) 76:109809. doi: 10.1016/j.cellsig.2020.109809

16. Back C, Thiesen KL, Skovgaard K, Edvinsson L, Jensen LT, Larsen VA, et al. Raas and stress markers in acute ischemic stroke: preliminary findings. *Acta Neurol Scand*. (2015) 131:132–9. doi: 10.1111/ane.12298

17. Ahmetović H, Jerković A, Vidaković MR, Košta V. The comparison of mechanical thrombectomy and symptomatic therapy on early outcome of acute ischemic stroke in patients older than 80 years: A retrospective cohort study. *Clin Neurol Neurosurg*. (2022) 221:107378. doi: 10.1016/j.clineuro.2022.107378

18. Collette SL, Bokkers RPH, Mazuri A, Lycklama À Nijeholt GJ, van Oostenbrugge RJ, LeCouffe NE, et al. Intra-arterial thrombolytics during endovascular thrombectomy for acute ischaemic stroke in the mr clean registry. *Stroke Vasc Neurol*. (2023) 8:17–25. doi: 10.1136/svn-2022–001677

19. Pan J, Wu H, Wu T, Geng Y, Yuan R. Association between post-procedure cerebral blood flow velocity and severity of brain edema in acute ischemic stroke with early endovascular therapy. *Front Neurol*. (2022) 13:906377. doi: 10.3389/fneur.2022.906377

20. Weller JM, Dorn F, Meissner JN, Stösser S, Beckonert NM, Nordsiek J, et al. Endovascular thrombectomy in young patients with stroke. *Int J Stroke*. (2023) 18:453–61. doi: 10.1177/17474930221119602

21. Tokunaga K, Tokunaga S, Hara K, Yasaka M, Okada Y, Kitazono T, et al. Fluid-attenuated inversion recovery vascular hyperintensity-diffusion-weighted imaging mismatch and functional outcome after endovascular reperfusion therapy for acute ischemic stroke. *Interv Neuroradiol*. (2022) 30(2):189–94. doi: 10.1177/15910199221113900

22. Zhong W, Chen Z, Yan S, Zhou Y, Zhang R, Luo Z, et al. Multi-mode imaging scale for endovascular therapy in patients with acute ischemic stroke (Meta). *Brain Sci*. (2022) 12(7):821. doi: 10.3390/brainsci12070821

23. Takahashi H, Yoshika M, Komiyama Y, Nishimura M. The central mechanism underlying hypertension: A review of the roles of sodium ions, epithelial sodium channels, the renin-angiotensin-aldosterone system, oxidative stress and endogenous digitalis in the brain. *Hypertens Res*. (2011) 34:1147–60. doi: 10.1038/hr.2011.105

24. Ong CJ, Gluckstein J, Laurido-Soto O, Yan Y, Dhar R, Lee JM. Enhanced detection of edema in Malignant anterior circulation stroke (Edema) score: A risk prediction tool. *Stroke*. (2017) 48:1969–72. doi: 10.1161/strokeaha.117.016733

25. Battey TW, Karki M, Singhal AB, Wu O, Sadaghiani S, Campbell BC, et al. Brain edema predicts outcome after nonlacunar ischemic stroke. *Stroke*. (2014) 45:3643–8. doi: 10.1161/strokeaha.114.006884

26. Zhang X, Yuan K, Wang H, Gong P, Jiang T, Xie Y, et al. Nomogram to predict mortality of endovascular thrombectomy for ischemic stroke despite successful recanalization. *J Am Heart Assoc*. (2020) 9:e014899. doi: 10.1161/jaha.119.014899

27. Du M, Huang X, Li S, Xu L, Yan B, Zhang Y, et al. A nomogram model to predict Malignant cerebral edema in ischemic stroke patients treated with endovascular thrombectomy: an observational study. *Neuropsychiatr Dis Treat*. (2020) 16:2913–20. doi: 10.2147/ndt.S279303

28. Kishi F, Nakagawa I, Park H, Kotsugi M, Myouchin K, Motoyama Y, et al. Low relative diffusion weighted image signal intensity can predict good prognosis after endovascular thrombectomy in patients with acute ischemic stroke. *J neurointerv Surg*. (2022) 14:618–22. doi: 10.1136/neurintsurg-2021–017583

frontiers | Frontiers in Endocrinology

TYPE Review
PUBLISHED 24 June 2024
DOI 10.3389/fendo.2024.1408677

OPEN ACCESS

EDITED BY
Alexandre Benani,
UMR6265 Centre des Sciences du Goût et de l'Alimentation (CSGA) Dijon, France

REVIEWED BY
Carolina Dalmasso,
University of Kentucky, United States
Rosaria Meccariello,
University of Naples Parthenope, Italy
Ebtesam Abdullah Al-Suhaimi,
King Abdulaziz and His Companions Foundation for Giftedness and Creativity, Saudi Arabia

*CORRESPONDENCE
Lydie Naulé
lydie.naule@sorbonne-universite.fr

RECEIVED 28 March 2024
ACCEPTED 29 May 2024
PUBLISHED 24 June 2024

CITATION
Torres T, Adam N, Mhaouty-Kodja S and Naulé L (2024) Reproductive function and behaviors: an update on the role of neural estrogen receptors alpha and beta. *Front. Endocrinol.* 15:1408677. doi: 10.3389/fendo.2024.1408677

Reproductive function and behaviors: an update on the role of neural estrogen receptors alpha and beta

Thomas Torres, Nolwenn Adam, Sakina Mhaouty-Kodja and Lydie Naulé*

Sorbonne Université, CNRS UMR8246, INSERM U1130, Neuroscience Paris Seine – Institut de Biologie Paris Seine, Paris, France

Infertility is becoming a major public health problem, with increasing frequency due to medical, environmental and societal causes. The increasingly late age of childbearing, growing exposure to endocrine disruptors and other reprotoxic products, and increasing number of medical reproductive dysfunctions (endometriosis, polycystic ovary syndrome, etc.) are among the most common causes. Fertility relies on fine-tuned control of both neuroendocrine function and reproductive behaviors, those are critically regulated by sex steroid hormones. Testosterone and estradiol exert organizational and activational effects throughout life to establish and activate the neural circuits underlying reproductive function. This regulation is mediated through estrogen receptors (ERs) and androgen receptor (AR). Estradiol acts mainly via nuclear estrogen receptors ERα and ERβ. The aim of this review is to summarize the genetic studies that have been undertaken to comprehend the specific contribution of ERα and ERβ in the neural circuits underlying the regulation of the hypothalamic-pituitary-gonadal axis and the expression of reproductive behaviors, including sexual and parental behavior. Particular emphasis will be placed on the neural role of these receptors and the underlying sex differences.

KEYWORDS

estrogen receptors, hypothalamic-pituitary-gonadal axis, reproductive behaviors, sex steroids, neuroendocrinology

10.3389/fendo.2024.1408677

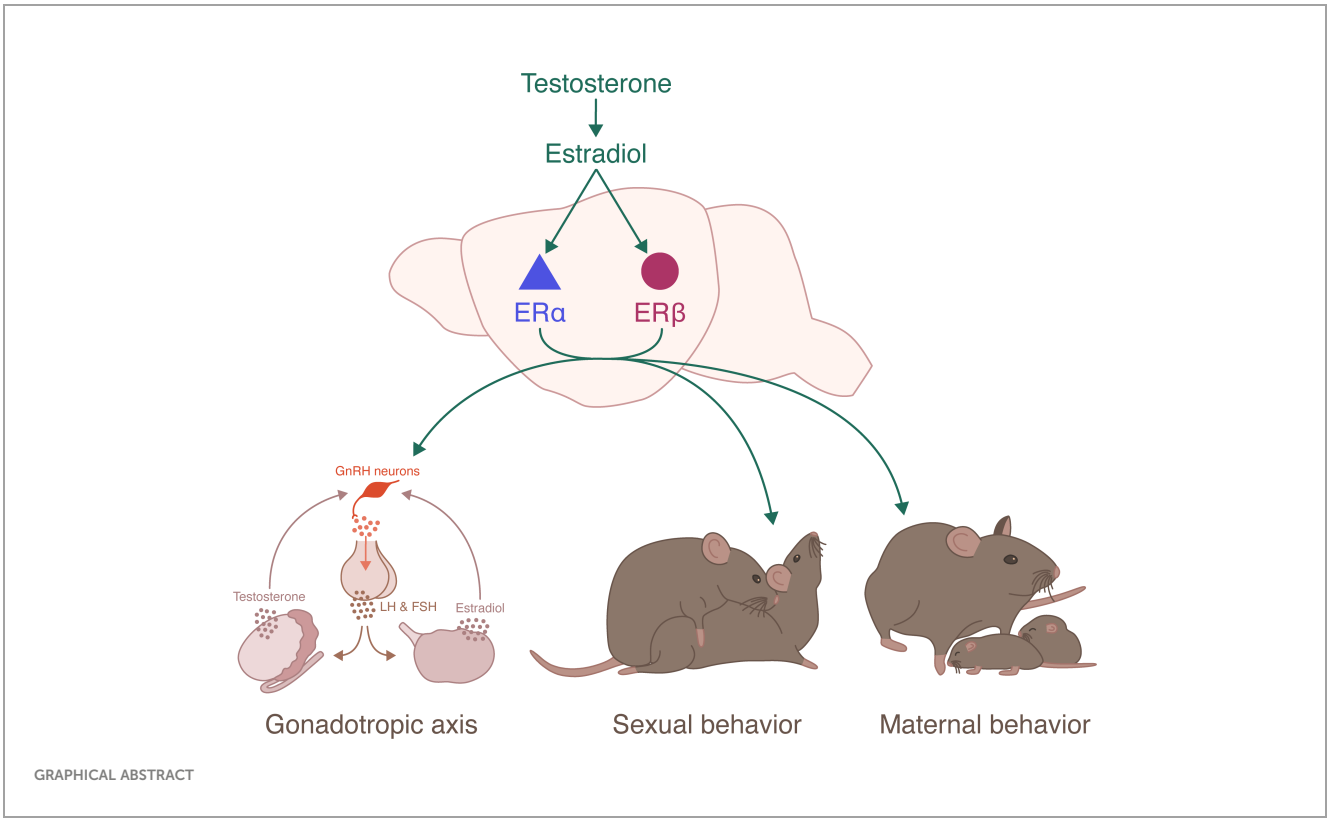

GRAPHICAL ABSTRACT

1 Introduction

In mammals, fertility allows the perpetuation of the species. Fertility relies on a fine regulation of reproductive function involving both adequate neuroendocrine regulation of the hypothalamic-pituitary-gonadal (HPG) axis, and synchronized expression of male and female sexually dimorphic reproductive behaviors.

Within the HPG axis, the pulsatile release of gonadotropin releasing hormone (GnRH) from hypothalamic GnRH neurons in the hypothalamic-pituitary portal system activates the neuroendocrine secretion of the gonadotropins luteinizing hormone (LH) and follicle-stimulating hormone (FSH) (Figure 1). LH and FSH stimulate the gonads and trigger gametogenesis and secretion of gonadal steroid hormones. Sex steroid hormones in turn exert a feedback control on the HPG axis (1). In males, testicular testosterone exerts a negative feedback control on hypothalamic GnRH and pituitary LH release (2). In females, estradiol negatively regulates hypothalamic GnRH secretion for most of the estrous cycle, except during the proestrus phase. During this phase, the growth of ovarian follicles is associated with a rise in circulating estradiol concentration that exerts hypothalamic and pituitary positive feedbacks, leading to the LH discharge necessary for ovulation and induction of female receptivity (3, 4). GnRH neurons activity is finely regulated by a complex neural network including kisspeptin-, neurokinin B-, glutamate- and GABA-expressing neurons. Glial cells, especially astrocytes and tanycytes, also participate in this regulation (5). Kisspeptin neurons are located in two distinct hypothalamic regions, the arcuate nucleus (ARC) and the rostral periventricular area of the third ventricle (RP3V). ARC kisspeptin neurons, referred to as KNDy neurons because of their coexpression of kisspeptin, neurokinin B and dynorphin, participate in estradiol negative feedback and coordination of GnRH pulses (6). RP3V kisspeptin neurons are essential to the regulation of estradiol

Abbreviations: AAV, Associated adenovirus; AOB, Accessory olfactory bulb; AR, Androgen receptor; ARC, Arcuate nucleus; AVPV, Anteroventral periventricular nucleus; BNST, Bed nucleus of the stria terminalis; BNSTpr, Principal subdivision of the BNST; DEG, Differentially expressed genes; EGFP, Enhanced green fluorescent protein; ER, Estrogen receptor; ERαΔ4, Estrogen receptor alpha delta 4; ER-X, Estrogen receptor X; FSH, Follicle-stimulating hormone; GnRH, Gonadotropin-releasing hormone; GPR30, G protein-coupled receptor 30; HPG, Hypothalamic-pituitary-gonadal; KNDy, Kisspeptin neurokininB dynorphin; LH, Luteinizing hormone; MAPK, Mitogen-activated-protein kinase; MeA, Medial amygdala; mER, Mebrane estrogen receptor; MERFISH, Multiplexed error-robust fluorescence *in situ* hybridization; mER-Gαq, Membrane estrogen receptor G alpha q; mGluR, Membrane metabotropic glutamate receptor; MOB, Main olfactory bulb; mPOA, Medial preoptic area; PAG, Periaqueductal gray matter; PI-3K, Phosphotidyl inositol 3 kinase; PKA, Protein kinase A; PKC, Protein kinase C; PND, Postnatal day; POA, Preoptic area; PVN, Paraventricular nucleus; RFP, Red fluorescent protein; RP3V, Rostral periventricular area of the third ventricle; scRNA-seq, Single-cell RNA-seq; shRNA, Small-hairpin RNA; STXBP, Saxitoxin binding protein; TRAPseq, Translating ribosome affinity purification and sequencing; T-types, Transcriptomic cell types; VMH, Ventromedial nucleus of the hypothalamus; VTA, Ventral tegmental area; ZFN, Zinc finger nuclease.

10.3389/fendo.2024.1408677

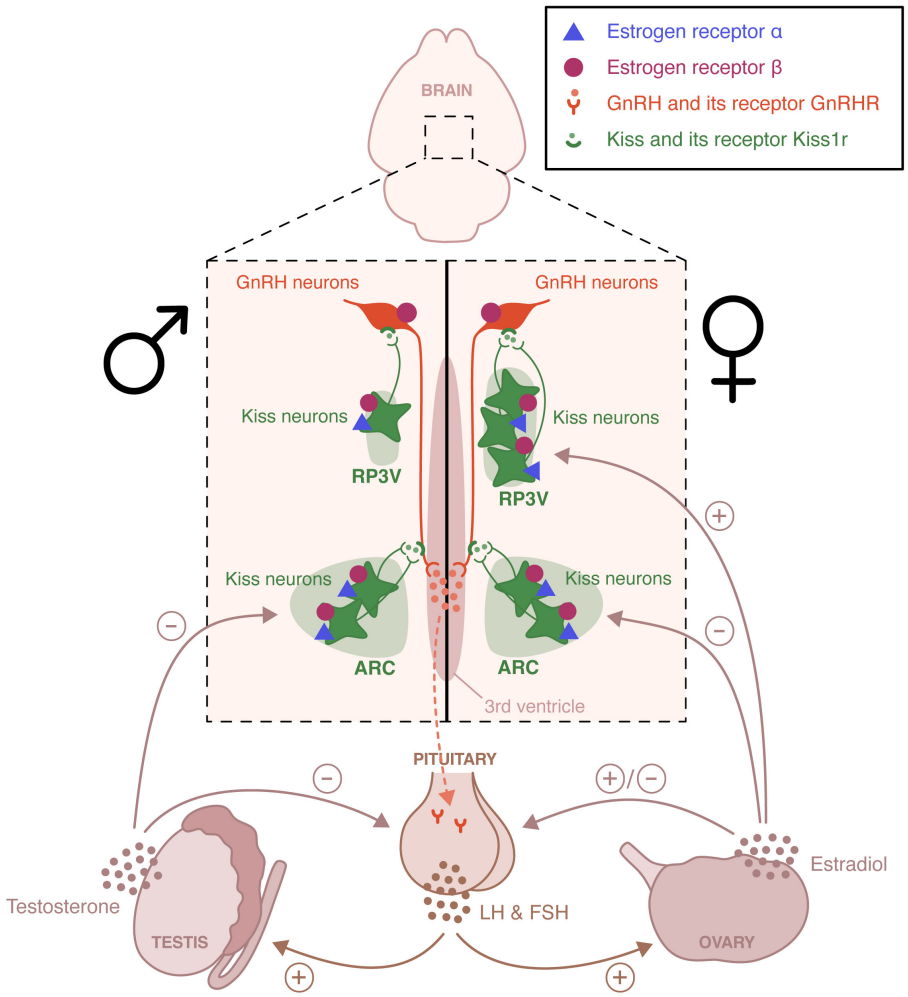

FIGURE 1
Schematic representation of the neural circuits involved in the estradiol regulation of the hypothalamic-pituitary-gonadal axis. Estrogen receptor (ER) α and ERβ are expressed in the rostral periventricular area of the third ventricle (RP3V) and the arcuate nucleus (ARC) of both males and females. These two hypothalamic nuclei are essential to the control of estradiol positive and negative feedback, respectively. The loss of the positive feedback in males is an example of sexual dimorphism. ERβ, unlike ERα is also expressed in gonadotropin-releasing hormone (GnRH) neurons and appears to participate to the pubertal activation of the hypothalamic-pituitary-axis. LH, Luteinizing hormone; FSH, follicle-stimulating hormone.

positive feedback driving the generation of the female LH surge (7). This positive feedback is lost in males. It is a primary example of sexual dimorphism.

In addition to a functional HPG axis, fertility requires appropriate and optimal display of reproductive behaviors, including sexual and parental behavior. Sexual behavior is sexually dimorphic. In rodents, it includes an appetitive phase, during which both sexes actively stimulate their partners by releasing pheromones and displaying appetitive behaviors. These behaviors include ano-genital investigations, series of approaches and solicitations, as well as male emission of ultrasonic vocalizations. These are followed by a consummatory phase, where male mounts are associated with female display of the lordosis posture, favoring intromission (8). Males express a continuous sexual activity, while females are only receptive during the proestrus phase of the estrous cycle, after the sequential rise in estrogen and progesterone (9). Sexual behavior relies on the activation of complex, sexually dimorphic neural circuits (10) (Figure 2). It is triggered by the detection of sensory stimuli, especially pheromones, that are detected by chemosensory neurons located in the vomeronasal organ and the main olfactory epithelium (11, 12). These neurons project to the main olfactory bulb (MOB) and the accessory olfactory bulb (AOB), which innervates among other structures, the medial amygdala (MeA) (13, 14). Neurons from the MeA then project to the bed nucleus of the stria terminalis (BNST), the medial preoptic area (mPOA), and the ventromedial nucleus of the hypothalamus (VMH). In males, the mPOA plays a critical role in the expression of sexual behavior. Projections from the hypothalamic paraventricular nucleus (PVN) are sent to the spinal centers that promote erection and ejaculation (15, 16). In females, the VMH is essential for the activation of sexual behavior. It sends projections to the periaqueductal gray matter (PAG) that project to the brainstem and spinal cord, which innervate the axial muscles involved in the lordosis posture (17). There is also an inhibitory circuit for lordosis behavior involving the ARC and the POA (18).

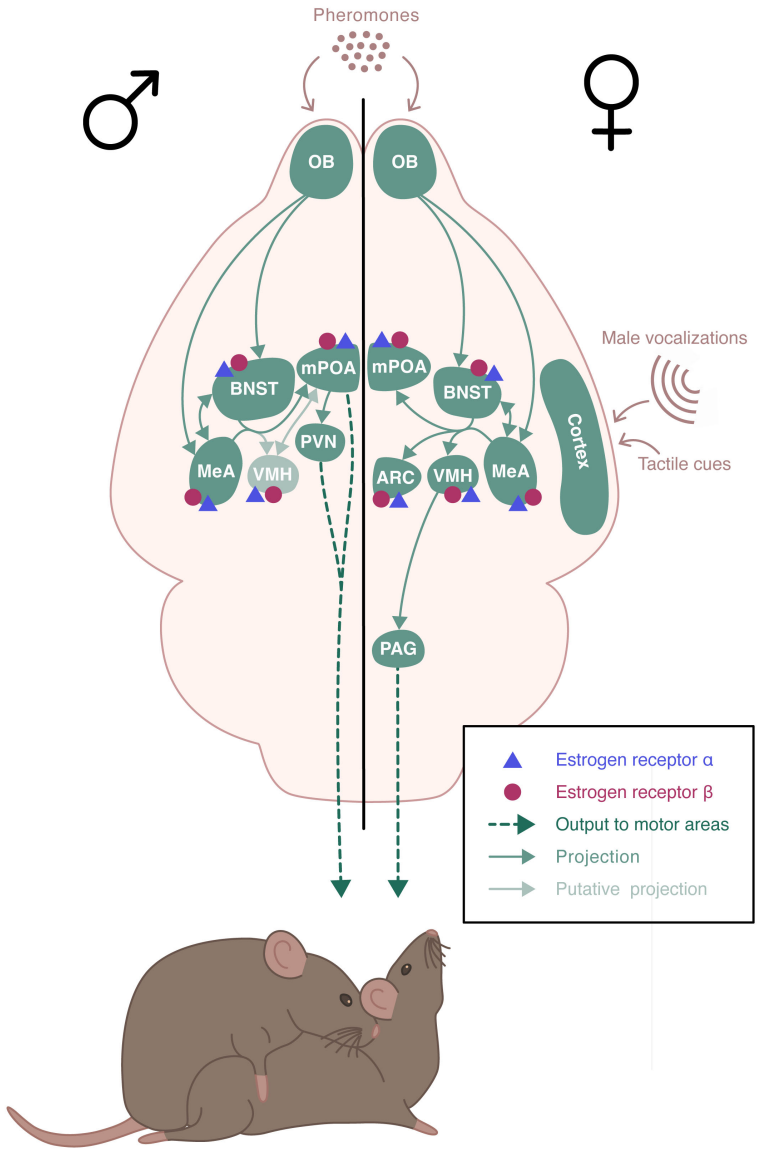

FIGURE 2
Schematic representation of the neural circuits involved in the estradiol regulation of sexual behaviors. Estrogen receptor (ER) α and ERβ receptors are expressed throughout the neural circuit involved in the expression of sexual behaviors in a sexually dimorphic manner. Sexual behavior is triggered by pheromones that are detected by chemosensory neurons. These neurons project to the olfactory bulb (OB) which innervates the medial amygdala (MeA) and the bed nucleus of the stria terminalis (BNST), which send projections to the medial preoptic area (mPOA) and the ventromedial nucleus of the hypothalamus (VMH). In males, mPOA plays a critical role in the expression of sexual behavior. Projections from the hypothalamic paraventricular nucleus (PVN) are sent to the spinal centers that promote erection and ejaculation. In females, VMH is essential for the activation of sexual behavior. It sends projections to the periaqueductal gray matter (PAG) that project to the brainstem and spinal cord, which innervate the axial muscles involved in the lordosis posture. There is also an inhibitory circuit for lordosis behavior involving the ARC and the POA.

Parental behavior occurs primarily in females and is minimal or absent in males of many mammalian species. In rodents, parental behavior is exhibited by the mother, with the exception of few species that display biparental care, such as the prairie vole or the California mouse (19). Parental behavior defines all behaviors exhibited to increase pups' chances of survival and development (20). Typically, rodents tend to avoid pups, or even exhibit aggressive behavior and infanticide towards them. A behavioral "switch" occurs in the early days of gestation, with females displaying an intensive nest building and increased aggressivity towards intruders. At birth, dams show a strong interest in newborns and become highly responsive to gustatory, olfactory, and tactile cues. Dams also rapidly respond to ultrasonic vocalizations emitted by pups, by retrieving them safely to the nest (21, 22). Pup's sensory information is integrated into a neural circuitry that includes the MeA and the BNST (Figure 3). These regions project to the mPOA that promotes pup attractivity. In turn, the mPOA projects to various downstream regions that facilitate the establishment and maintenance of maternal behavior, including the PVN rich in oxytocinergic neurons, and the ventral tegmental area (VTA) of the dopaminergic system (23). Males and virgin or non-lactating females of uniparental species can

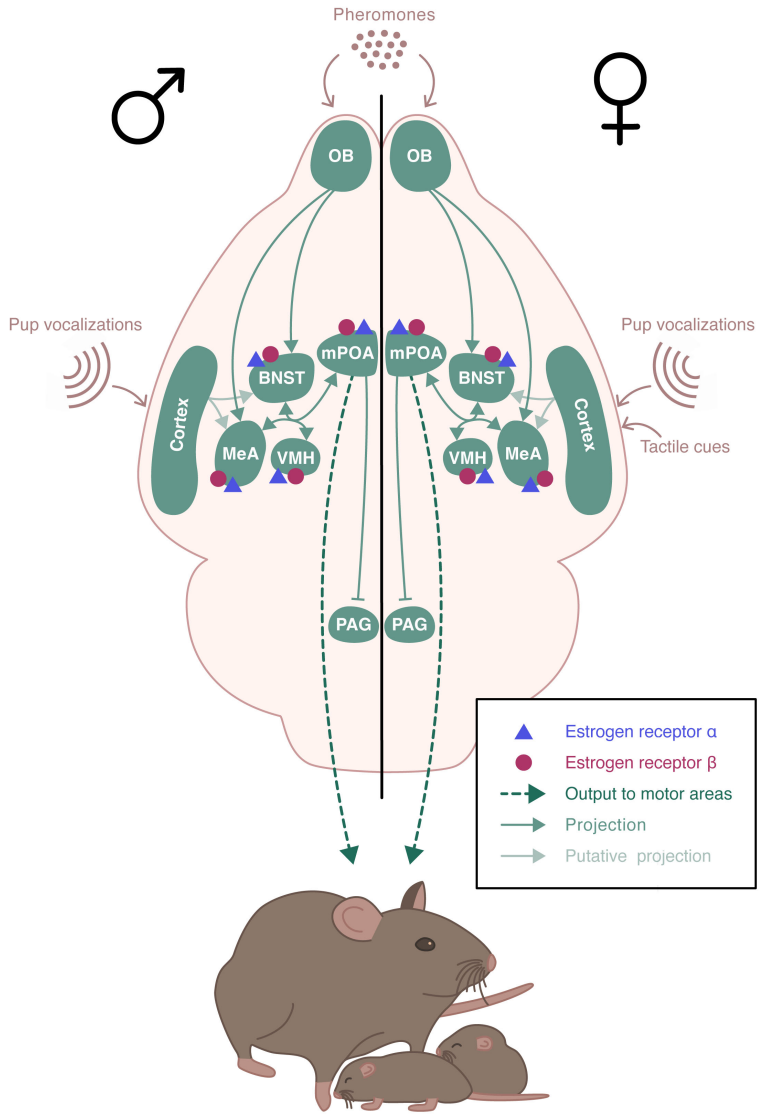

FIGURE 3
Schematic representation of the neural circuits involved in the estradiol regulation of parental behavior. ERα and ERβ receptors are expressed in the brain regions involved in the expression of parental behavior. Pup's sensory information is integrated into a neural circuitry that includes the medial amygdala (MeA) and the bed nucleus of the stria terminalis (BNST). These regions project to the medial preoptic area (mPOA) which send projections to various downstream regions including the hypothalamic paraventricular nucleus (PVN) and regions of the dopaminergic system. The neural pathway underlying paternal behavior remains unclear, but it seems to be similar to the one for maternal behavior, with mPOA as a key region.

also exhibit parental behavior. This occurs spontaneously in most strains of laboratory mice, although the level of pup care is much lower than that given by dams (24). The neural pathway underlying paternal behavior seems to be similar to the one for maternal behavior, with mPOA as a key region (19).

The reproductive function and behavior are tightly regulated by sex steroid hormones. The sexually dimorphic hormonal control of mating was first demonstrated by the pioneer work of Phoenix and collaborators in 1959 (25). This study, and those that followed, demonstrated the existence of both organizational and activational effects of sex steroids (26). Androgens and estrogens act at specific periods of development to organize, in a sex-dependent manner, the neural circuits controlling reproductive function and behavior, which are then activated by sex steroids in adulthood.

Organizational changes occur during sensitive periods of development. Although initially assumed to affect only males during perinatal life, increasing evidence supports that organization takes place in both sexes at multiple developmental windows, including the perinatal, postnatal, and pubertal periods. It is well known that perinatal masculinization of the male brain results from two testosterone bursts occurring before and after birth. In addition, brain feminization in females appears to occur later as circulating estradiol increases during postnatal and prepubertal development (27–31). These organizational and activational effects of testosterone and estradiol are mediated through their receptors: estrogen receptors (ERs) and androgen receptor (AR). In males, testosterone can also be aromatized due to neural expression of cytochrome p450 aromatase into neural 17β-estradiol, which then acts on ERs (32, 33).

The present review focuses on the neural role of the ERs in male and female reproduction (for a review of the role of AR in the central nervous system see (34)). In particular, we will review genetic evidence using transgenic mouse models and recent technological tools that have provided a better understanding of the role of ERs in estradiol-induced regulation of the HPG axis and reproductive behaviors.

2 Estrogen receptors: types and neural expression

In the mouse, ERα (66 kDa) and ERβ (54 kDa) are encoded by estrogen receptor 1 (*Esr1*) and estrogen receptor 2 (*Esr2*) genes located on chromosomes 10 and 12, respectively (35, 36). These receptors belong to the nuclear receptor superfamily and act as transcription factors. The primary regulation of gene expression involves direct binding of the receptor to EREs sequences as it is the case for example for progesterone receptor (*Pgr*) (37), Kiss-1 metastasis suppressor (*Kiss1*) (38), dynorphin (*Dyn*) (39) and brain derived neurotrophic factor (*Bdnf*) (40). In addition to its slow genomic action, rapid effects of estradiol have been observed. These nongenomic effects are generally initiated by the binding of estradiol to membrane receptors including the classical ERs and other receptors such as estrogen receptor alpha delta 4 (ERαΔ4), membrane estrogen receptor G alpha q (mER-Gαq), G protein-coupled receptor 30 (GPR30), estrogen receptor X (ER-X) and saxitoxin binding protein (STXBP) (41). Binding of estradiol to these receptors activates intracellular signaling pathways such as the mitogen-activated-protein kinase (MAPK), protein kinase C (PKC), protein kinase A (PKA), or phosphotidyl inositol 3 kinase (PI-3K) pathways (42). Mechanisms by which these membrane ERs (mERs) activate these pathways remain unclear. For example, in female rats, mER interaction with membrane metabotropic glutamate receptors (mGluR) was shown to participate in lordosis behavior, through μ-opioid receptor internalization and activation of the fast calcium response, and could also affect long term genetic expression via CREB phosphorylation (43–46). The present review focuses on nuclear ERα and ERβ given their critical and well-identified roles in male and female reproduction.

ERα and ERβ are expressed throughout the neural circuits that control reproductive function and behavior. In adult mice, *Esr1* mRNA and protein have been detected in the BNST, VMH, mPOA and ARC (47–49). *Esr2* mRNA is also present, less abundantly than *Esr1*, in the VMH, mPOA and ARC (50–52). Given the lack of selectivity of anti-ERβ antibodies (49, 53), several transgenic ERβ-enhanced green fluorescent protein (EGFP)/-red fluorescent protein (RFP) mouse lines were used and confirmed that the localization of the ERβ protein was similar to that of the transcript (48, 54, 55). During the development, ERα and ERβ are present in the mouse nervous system as early as embryonic day (E) 13 (56). ERα and ERβ mRNA and protein levels change considerably during development in a regional and sex-specific manner. For example, in the anteroventral periventricular nucleus (AVPV), the number of ERα-expressing cells decreases from postnatal day (PND) 0 to PND14 in females, then increases with age, in contrast to males, which show no significant variations over time. In this region, the number of ERβ-expressing cells is highest at PND0 in both sexes and decreases with age in males but not in females (54, 55). In the VMH, ERα-expressing cells are present in both sexes with maximal expression at PND0, followed by a reduction from PND0 to PND14. Then, females show an increase in expression at the end of the pubertal period (PND42-PND56). In males, ERα-expressing cells remain low, and are therefore lower than in females. The number of ERβ-expressing cells in the VMH is also highest at PND0 for both sexes, but more important in females than in males at PND0 and PND7. A sharp decrease is then observed in both sexes that abolishes sex differences after PND7 (54, 55). In the BNST, a greater number of ERα-expressing cells has been described in adult female compared to male mice (57). Indeed, ERα-expression increases in female during development, while remaining constant in males (except for a transient increase at PND28). ERβ-expressing cells remains constant in females, whereas it gradually increases in males to reach its highest level at PND42 and PND56 (55).

3 ERα versus ERβ in estradiol-induced regulation of the hypothalamic-pituitary-gonadal axis

Many studies have focused on the sites of action of estradiol in the regulation of the HPG axis. Does it act directly on GnRH-expressing neurons or indirectly via other cells within the GnRH network? This question was raised by data showing that GnRH neurons do not express *Esr1*. Of note, they also do not express *Ar*. Nevertheless, these neurons do express *Esr2* and present detectable levels of ERβ protein in mice, rats, and humans (58–62) (Figure 1).

3.1 Role of ERα in the regulation of the HPG axis

3.1.1 Models of ubiquitous *Esr1* deletion

Mouse models with ubiquitous deletion for *Esr1* (ERαKO) were obtained by homologous recombination targeting exon 2 (63) or exon 3 (64–69). ERαKO males showed a structurally normal urogenital tract, but with a strong decrease of testis weight and sperm count (63, 70). Females ERαKO uterus and vagina were hypoplastic with no cyclic morphological changes. They exhibited a polycystic ovary phenotype with an absence of corpora lutea, and anovulation (66). Both ERαKO males and females were infertile (63–66, 70). Circulating levels of testosterone were slightly increased in ERαKO males but circulating LH levels were unchanged showing no alteration of the negative feedback (70–72). In contrary, ERαKO females showed no negative or positive feedback of estradiol. Indeed, basal LH level was greatly increased in intact ERαKO female, and estradiol treatment in ovariectomized ERαKO females did not trigger the LH surge, unlike wildtypes (68, 69, 72–75).

The role of non-classical ERα signaling pathways was also investigated using a mouse model carrying a mutation in the ERα DNA recognition sequence that abolishes ERα signaling through

ERE binding mechanisms (ERα$^{+/AA}$ animals (76);). ERα$^{+/AA}$ males were fertile and showed normal testosterone levels suggesting that ERE-independent ERα signaling is sufficient for some male reproductive function (77). Mutant females, however, were sterile due to uterine defects and anovulation (76). A knocking mutant allele model that selectively restores ERE-independent signaling in ERαKO mice (ERα$^{-/AA}$ animals) revealed that these signaling were able to partially restore estrogen negative feedback on LH secretion, but were not sufficient to mediate estrogen positive feedback, increase GnRH neuron firing to generate the LH surge or mediate spontaneous ovulation (75, 78).

3.1.2 Models of brain specific *Esr1* deletion

ERα is thus essential for fertility in both sexes and required for both estradiol positive and negative feedback in females. Nevertheless, ERα is present in many peripheral tissues including male and female reproductive tracts, thus the effects described in ERαKO animals, especially the infertility, do not allow to distinguish between neural and peripheral effects. Studies using more restricted deletion models are reported below.

A mouse line selectively deleted for *Esr1* in forebrain neurons (including in the cortex, hippocampus, BNST, amygdala, olfactory bulb, striatum, thalamus and hypothalamus) and pituitary was generated by crossing mice carrying loxP sites on either side of exon 3 of *Esr1* with mice expressing Cre recombinase under the control of the calcium/calmodulin-dependent protein kinase IIα promoter (ERα$^{fl/fl}$; CamKIIα-Cre) (69). Both male and female mutants were infertile. ERα$^{fl/fl}$; CamKIIα-Cre females showed strong abnormalities of their reproductive organs, an absence of estrous cycle and defect in ovulation (69, 79). Similar to ubiquitous ERαKO mice, estradiol injection in mutant females did not trigger the LH surge (69). Basal LH level of ERα$^{fl/fl}$; CamKIIα-Cre female was no different from that of control females, but mutant mice did not show an increase in circulating LH levels after ovariectomy (79). The importance of ERα in adulthood in this negative feedback was revealed using an inducible tamoxifen-based Cre-LoxP model, which triggered more than 50% reduction in the number of ERα-expressing cells (79). This treatment resulted in lack of estrous cyclicity and disruption of negative feedback. Indeed, the increase in LH observed after ovariectomy was decreased in mutant mice, and estradiol treatment failed to restore baseline LH levels. These results revealed the importance of ERα in forebrain/pituitary in regulating both positive and acute negative feedback of estradiol.

Deletion of *Esr1* selectively in neural cells was generated by crossing ERα$^{fl/fl}$ females with males expressing the Cre recombinase under the control of the promoter and nervous system-specific enhancer of nestin (ERα^{Nescre} (80)). This model allowed the deletion of *Esr1* in both neuronal and glial cells but not in the pituitary. Females ERα^{Nescre} presented early puberty initiation with advanced vaginal opening and first estrus. In adulthood, mutant females showed a diminution in ovary weight with absence of corpora lutea and estrous cycle arrest. This was accompanied with a decrease in the number of kisspeptin cells in the RP3V in females. An increase in uterine weight was also reported, related to elevated levels of circulating estradiol in mutant females, similar to what has been observed in other ERαKO mouse model. In adult males, seminal vesicles weight and testosterone level were increased in mutant mice compared to controls, but no modification in testis weight was observed. In contrary to females, mutant males were fertile. Thus, while neural ERα is critical for normal cyclicity, fertility and regulation of both estradiol positive and negative feedback on LH secretion, sex differences are observed, with a more critical role in females than in males. Several studies, described below, aimed to decipher the specific cell population and neural circuits involved in ERα-mediated regulation of estradiol. Because ERα is not present in GnRH neurons, estradiol appears to act indirectly via afferent circuits.

Kisspeptin neurons have been widely studied for their potent activation of GnRH neurons and are known to be regulated by estradiol through ERα. ERα is expressed in around two-third of RP3V kisspeptin-expressing cells and nearly all ARC kisspeptin cells (81). Estradiol inhibits kisspeptin expression in the ARC while activating its expression in the RP3V (38, 82). This opposing regulation of estradiol on kisspeptin expression was abolished in ERαKO mice (38). To investigate further, a mouse model to delete *Esr1* specifically in kisspeptin expressing cells (KERKO) was generated by crossing mice floxed for exon 3 of *Esr1* with mice expressing Cre recombinase under the control of kisspeptin promoter (81, 83, 84). Mice carrying this mutation showed advanced vaginal opening, disruption of ovarian cyclicity, complete absence of corporal lutea leading to infertility. Adult females KERKO exhibited a reduced LH secretory response to ovariectomy compared to control suggesting an alteration of the estradiol negative feedback. Nevertheless, estradiol treatment following ovariectomy was still able to reduce LH levels (82). Estradiol injection failed to induce the LH surge in KERKO animals indicating a loss of estradiol positive feedback (82). In addition, KERKO mice lost the LH response to kisspeptin and showed a decreased LH response to GnRH injections (85). Along with these findings, electrophysiological studies demonstrated that RP3V kisspeptin cell activity was increased during estradiol positive feedback in control animals, but to a lesser extent in KERKO females (85). In contrast, ARC kisspeptin neurons activity was reduced during estradiol positive feedback in controls, but instead increased in KERKO females. These results were further confirmed using calcium imaging with protein-based indicators (GCaMP) fiber photometry approach, where KERKO mice showed an increased ARC *Kiss1*-expressing cell activity compared with intact controls, that was similar to ovariectomized controls (84). Thus, in females, ERα is required in kisspeptin neurons for complete maturation of the HPG axis and control of estradiol negative and positive feedback on GnRH/LH secretion. Although not studied in detail, the authors mentioned that KERKO males did not show modification in testicular weight or alterations in the LH response to castration (83), suggesting that ERα in kisspeptin neurons is not indispensable for estradiol regulation of male HPG axis.

KERKO animals have *Esr1* deleted in both RP3V and ARC kisspeptin neuronal populations. The role of ERα in KNDy neurons of the ARC was studied using a mouse model deleted for *Esr1* in *Tac2*-expressing cells, by crossing *Tac2*^{Cre} mice with *Esr1*^{flox} animals (ERα^{Tac2}KO (81)). Nearly all *Tac2*-expressing cells co-express ERα. ERα^{Tac2}KO females presented morphological

abnormalities in ovaries and uteri, precocious puberty and impaired cyclicity. Basal LH levels were elevated in mutant animals compared to control showing an impairment of estradiol negative feedback (81). The role of this cell population in the estradiol positive feedback needs to be further detailed. It is important to note that *Kiss1* has been detected in ovaries and *Tac3* in both pituitary and ovaries (86–88). Thus, it is likely that in these KERKO and ERα^{Tac2}KO models, *Esr1* was deleted in some cells outside the brain.

Esr1 is also expressed in GABAergic and glutamatergic neurons in key hypothalamic regions including the RP3V and the ARC. These neurons are known to project directly to GnRH neurons. In females, mouse models deleted for *Esr1* in GABAergic neurons (*Vgat*-ires-Cre;*Esr1*$^{lox/lox}$) showed no modification of the age of puberty onset or estradiol regulation of the negative feedback. Indeed, basal LH levels were unchanged and mutant mice responded similarly to control to ovariectomy and estradiol replacement. However, *Vgat*-ires-Cre; *Esr1*$^{lox/lox}$ females presented abnormal cyclicity, infertility and did not show the normal estradiol positive feedback rise in LH (89). In males, deletion of *Esr1* in GABAergic neurons did not modify testicular weight, serum testosterone levels or fertility compared to controls, suggesting that this population is not necessary for proper functioning of the male HPG axis (90).

In parallel, the deletion of *Esr1* in glutamatergic neurons in females (*Vglut2*-ires-Cre;*Esr1*$^{lox/lox}$) induced advanced puberty onset, disturbed cyclicity and infertility. Mutant females showed an impairment of estradiol negative feedback with elevated basal LH levels compared to control and abnormal response to ovariectomy and estradiol replacement. In addition, *Vglut2*-ires-Cre;*Esr1*$^{lox/lox}$ females were unable to present an LH surge from estradiol injection, illustrating a lack of estradiol positive feedback in these animals (89). Although studied with less detail, *Vglut2*-ires-Cre;*Esr1*$^{lox/lox}$ males were fertile, showed normal testicular weight but with a significant increase in serum testosterone levels compared with control animals, suggesting a role for this neuronal population in the control of negative feedback in males (90). These results highlight the existence of strong sex differences in the role of *Esr1* in GABAergic and glutamatergic neuron for the control of the HPG axis.

3.1.3 Models of region-specific and time-dependent *Esr1* deletion

The genetic models discussed above all have the caveat that ERα was deleted early during development, and thus did not allow for a distinction between developmental (organizational) and adult (activational) roles of this receptor. In addition, these models did not target a specific region, resulting in a lack of precision in understanding the neural network. Targeted viral vector injection in adulthood has permitted the reduction of *Esr1* expression in a hypothalamic nucleus-specific and time-dependent manner.

Ablation of *Esr1* specifically in the ARC has been achieved by stereotactic injection of an adeno-associated virus containing Cre recombinase (AAV-Cre) specifically into ERα$^{flox/flox}$ mice (91). The deletion of 60–90% of ERα-expressing cells in the ARC induced a disturbance in ovarian cyclicity. Basal LH level in mutant mice was similar to those in control females, but the increase in LH after ovariectomy was reduced, suggesting an activational role of ERα-expressing cells in the ARC for estradiol negative feedback (91).

More recently, the combination of CRISPR-Cas9 technique with targeted injection of viral vectors has enabled the deletion of *Esr1* in RP3V or ARC kisspeptin-expressing cells in adult females (AAV-*Esr1*) (84, 92). *Esr1* deletion in RP3V kisspeptin neurons in adulthood did not modify estrus cyclicity but blunted the estradiol-induced LH surge confirming the important role of this neural population in the control of estradiol positive feedback. This effect was linked to a decrease in electrophysiological excitability of RP3V kisspeptin neurons in RP3V-AAV-*Esr1* females compared to controls (92). Using the same technique, *Esr1* was deleted, in adulthood, in ARC kisspeptin neurons (ARC-AAV-*Esr1*). Depending on the study, these females showed either disrupted (92) or normal estrous cyclicity (84). A reduced LH response to kisspeptin or GnRH treatment compared to control was observed in Wang et al. (2019). Variability of effects was observed with regards to negative feedback regulation. No modification of LH pulse frequency or basal LH levels was observed between ARC-AAV-*Esr1* and control females (92). In this study, CRISPR-mediated *Esr1* knockdown was achieved in 60% of cell population. Mc Quillan et al. (2022) observed that the phenotype of the animals depended on the efficacy of the knockdown generated by CRISPR technology. Indeed, an *Esr1* knockdown greater than 70–80% in ARC kisspeptin neurons was necessary to generate an increased pattern of synchronization similar to that observed in control animals after ovariectomy (84). Thus, the high percentage of *Esr1* deletion required to alter LH secretion could explain the difference between the effects observed in these two studies. These results show that ERα in RP3V and ARC kisspeptin cells has activational roles in regulating estradiol positive and negative feedback, respectively.

3.2 Role of ERβ in the regulation of the HPG axis

ERβ, unlike ERα, is expressed in GnRH neurons. In addition to the indirect regulation of the HPG axis via ERα-expressing neurons, in particular kisspeptin neurons, estradiol could act directly on GnRH neurons via ERβ.

3.2.1 Models of ubiquitous *Esr2* deletion

The two first models of ubiquitous deletion of *Esr2* were obtained by homologous recombination by targeting exon 3 of *Esr2* (66, 93). ERβKO males had normal urogenital tract, testicular function and spermatogenesis and were fertile (66, 93). Nevertheless, castrated ERβKO males showed higher LH levels than wildtypes indicating a role for ERβ in estradiol negative feedback (94). In females, ERβKO induced variable reproductive phenotypes ranging from mild hypofertility to complete infertility (66, 93). Genital tracts of ERβKO females were similar to control animals (66). Adult ERβKO ovaries were macroscopically normal and had normal antral follicles, but with fewer corpora lutea than

controls, suggesting less efficient ovulation due to impaired ovarian function (66, 93). Ubiquitous deletion of *Esr2* had no major impact on female positive and negative feedbacks exerted by estradiol. Basal LH levels of ERβKO females were either normal (73) or slightly increased (74). Treatment of ovariectomized females with estradiol resulted in a similar induction of the LH surge in both control and mutant mice (69). Furthermore, the distribution and number of GnRH neurons were unchanged and the opposite estradiol regulation of kisspeptin expression in the RP3V and ARC was maintained in ERβKO mice (38, 69). ERβ appeared, however, to be involved in the rapid action of estradiol on GnRH neurons. Rapid modulation of the phosphorylation state of the cAMP response element-binding protein (CREB) in GnRH neurons was abolished in mutant females (95). Importantly, these models were later shown to still express transcripts from alternative splicing of *Esr2* (53), which could be the cause of these variable fertility phenotypes. Therefore, a line devoid of any *Esr2* transcripts was generated using the Cre/loxP technique (named $ERβ_{ST}^{L-/L-}$ (96)). Mutant males and females from this model showed complete infertility. In females, it was due to drastic impairment of cyclicity and ovarian function. In males, the reason was unclear, as testis and epididymis histology and apparent motility of spermatozoa appeared normal (96).

3.2.2 Models of brain specific *Esr2* deletion

ERβ is highly expressed in both female and male urogenital tracts, including the ovary, prostate and epididymis (97, 98). Thus, similarly to ERα, the infertility induced by the complete and ubiquitous deletion of *Esr2* did not allow the study of its neural effects. Although fewer in number than for ERα, more restrictive approaches have been used.

A mouse model selectively deleted for *Esr2* in the forebrain and pituitary has been generated by crossing $Esr2^{flox}$ mice (96) with CamKIIα-Cre mice (79). Mutant females showed normal cyclicity, basal LH levels and a normal increase in LH level after ovariectomy. However, their inability to reduce LH secretion after acute estradiol injection suggested a contribution of forebrain/pituitary ERβ in acute negative feedback of estradiol (79).

The role of neural ERβ was studied using an $ERβ^{NesCre}$ mouse line (99). Mutant $ERβ^{NesCre}$ females presented delayed puberty initiation with delayed vaginal opening and first estrus and delay of uterine growth (99). This pubertal delay was linked to a delay in postnatal expression of kisspeptin neurons in the RP3V. In adulthood, the number of GnRH neurons in the POA was unchanged, as was kisspeptin-immunoreactivity in the RP3V and ARC. Adult $ERβ^{NesCre}$ females showed no change in estradiol levels, nor in LH response to ovariectomy, and had regular estrous cyclicity and fertility (99). The initiation of male puberty has not yet been evaluated in this model. In adulthood, $ERβ^{NesCre}$ males were fertile, with seminal vesicles weights and testosterone levels unchanged from control littermates (100).

Selective *Esr2* deletion in GnRH neurons (GnRH-Cre;$ERβ^{loxP/loxP}$) did not disrupt cyclicity, basal LH level, or LH response to estradiol. However, there was a reduced increase in LH secretion after ovariectomy in mutant mice compared to controls, suggesting a minor role for ERβ-expressing GnRH neurons in controlling estradiol negative feedback (79). Another study using a different mouse model observed a more drastic phenotype in GnRH-ERβ-KO (GERβKO) females, which exhibited ovarian morphology abnormalities, delayed puberty initiation, impaired fertility and reduced basal and surge LH levels without altering estradiol-negative feedback (101). While studied in less details, GERβKO males showed normal basal LH levels and no change in the timing of preputial separation (101). Although not totally clear, the use of different genetic background strains and knockout approaches could explain some of these discrepancies. Lastly, another study demonstrated that the rapid action of estradiol to phosphorylate CREB in GnRH neurons involved ERβ expressed by GnRH neurons themselves (102).

Overall, these genetic studies showed that neural ERα is essential for fertility and both positive and negative feedback controls exerted by estradiol on the HPG axis in females. These studies also suggest that neural ERα participates in the prepubertal regulation of the female HPG axis, necessary for its activation at puberty. The lack of studies in males makes it difficult to draw definite conclusions, although neural ERα does not appear to be essential for maintaining fertility in males. Its role in estradiol negative feedback remains to be clarified. Regarding neural ERβ, further work will be needed to understand the discrepancies observed in the different mouse models generated. Nevertheless, neural ERβ appears to be less critical for fertility than ERα, since it seems to play a more subtle role in regulating estradiol positive and negative feedback through both classical and non-classical signaling pathways. Interestingly, ERβ appears to play an activating role in puberty initiation, and additional studies will be crucial to understanding the underlying mechanisms of action.

4 ERα versus ERβ in estradiol-induced regulation of sexual behavior

Alongside their role in regulating the HPG axis, ERα and ERβ receptors are present throughout the neural circuits involved in the expression of sexual behavior (Figure 2). The specific involvement of either receptor in the regulation of sexual behavior by estradiol has been addressed in genetic studies presented below.

4.1 Role of ERα in the regulation of sexual behavior

The predominant expression of ERα in brain regions involved in the expression of sexual behavior, including the MeA, BNST, VMH, MPOA and ARC, has made it the primary target of research on ERs.

4.1.1 Models of ubiquitous *Esr1* deletion

All studies carried out on ubiquitous ERαKO mouse lines showed a very strong disturbance of sexual behavior in both intact and hormonal-replaced males and females. ERαKO males

show altered sexual behavior manifested by a sharp decrease in frequency of intromissions and an increase in latencies (103–106). In addition, no (106, 107) or little ejaculation (70, 103) was observed in ERαKO males. Different results have been reported regarding the number and latency times of mounts, which were found to be equivalent (103) or reduced (106) compared to wildtype mice. Various observations were also made regarding the role of ERα in regulating olfactory preference in males. ERαKO male mice were first shown to have similar interest in the odors of receptive female mice as controls (108). Other studies have observed altered olfactory preference for receptive females in ERαKO males compared to controls (71, 109, 110).

In ERαKO females, lordosis behavior was severely impaired compared to wildtype mice (63, 111–114). This effect was linked to a marked reduction in induction of progesterone receptor (PR) expression by estradiol in the VMH of mutant females (113). In addition, ERαKO females exhibited a strong deficit in proceptive behavioral interactions. While the number of mount attempts by males was similar between mutant and wildtype females, ERαKO mice vigorously rejected mounts from males that were unable to intromit (112, 114). However, stud males were equally attracted to ERαKO as to wildtype females during preference tests, suggesting that ERα was not critical to female attractivity (114). It is important to note that ubiquitous *Esr1* deletion induced elevated levels of estrogen and testosterone in mutant animals compared to wildtypes, which may affected brain functions through developmental processes (70, 71, 115).

The role of ERα in ERE-independent mechanisms of estradiol was investigated using the ERα$^{-/AA}$ mice model. In this model, ERα signaling through ERE binding mechanisms was abolished (76, 77). ERα$^{-/AA}$ males showed a strong deficit in sexual behaviors suggesting that ERE-independent ERα signaling was not sufficient to maintain sexual behavior in males and that genomic action of estradiol is critical (77). Another model harboring a mutation of the ERα palmitoylation site, which prevents membrane ERα signaling, showed no change in female sexual behavior but a strong reduction in male sexual behavior, suggesting an involvement of ERα membrane-initiated estrogen signaling in the organization of male sexual behavior (116).

4.1.2 Models of brain specific *Esr1* deletion

To understand the specific role of neural ERα in the regulation of sexual behavior, several studies have used more restricted deletion models.

Sexual behavior was assessed in both ERα^{NesCre} males and females (80). Female sexual behavior, under normalized hormonal levels, was completely abolished with mutant females never exhibiting lordosis posture in response to male mounts. This impairment was linked with a drastic decrease in the number of progesterone receptor (PR)-expressing cells in the VMH of mutant animals compared to control littermates. In males, neural *Esr1* deletion induced a less severe behavioral phenotype (80). Mutant males were able to emit courtship vocalizations although with reduced number and duration of syllables. They also initiated mounts, intromissions and reached ejaculation, but with disturbance in the numbers and latencies of the events, provoking a less effective sexual behavior compared to control littermates and to mutants lacking both neural *Esr1* and *Ar* (80). Olfactory preference tests showed that both ERα^{NesCre} females and males presented similar preference toward males or receptive females as control littermates, suggesting an effect of *Esr1* deletion downstream the olfactory system (80). In particular, immunohistochemical analyses showed feminized calbindin and tyrosine hydroxylase neuronal populations of the mPOA, suggesting an implication of ERα in the perinatal organization of the neural circuitry underlying male sexual behavior (80).

To determine the role of ERα in either excitatory (glutamatergic) versus inhibitory (GABAergic) neurons, *Vglut2*-Cre;*Esr1*$^{lox/lox}$ and *Vgat*-Cre;*Esr1*$^{lox/lox}$ males were subjected to sexual behavior phenotyping (90). To date, female sexual behavior has not been tested in these models. In adult males, ERα-expressing neurons are mostly GABAergic in the mPOA, BNST and posterior dorsal MeA while they are predominantly glutamatergic in the VMHvl and posterior ventral MeA. Analysis demonstrated that the percentage of animals displaying mounting, intromission and ejaculation behaviors during the 30 min test was unchanged between *Vglut2*-Cre;*Esr1*$^{lox/lox}$ and wildtype males. In contrast, *Vgat*-Cre;*Esr1*$^{lox/lox}$ males showed similar mounting and intromission behaviors, but with a deficit in the ability to ejaculate, with only 25% of mutant males reaching it compared to controls, suggesting a role for GABAergic signaling in controlling male sexual behavior (90).

4.1.3 Models of region-specific and time dependent *Esr1* deletion

Further studies addressed the developmental versus activational roles of ERα and the hypothalamic nuclei involved.

In males, using viral mediated RNA interference technique, deletion of *Esr1* specifically in adulthood or during prepuberty, in the mPOA or VMH, altered components of male sexual behavior illustrated by a reduced number of mounts and intromissions during the 30-minute test (29, 117). In contrast, adult deletion in the MeA did not affect these behaviors, while prepubertal deletion resulted in a reduced number of mounts and intromissions in adulthood. Ejaculation was not analyzed in this paradigm (29, 117). These results suggested that ERα within the mPOA and VMH is essential for the activational role of estradiol on male sexual behavior, whereas ERα in the MeA may not be crucial in adulthood but is necessary for the organization of the neural circuits underlying sexual behavior during prepuberty. Going further, calcium recordings of *Esr1*+ neurons activity in the mPOA, using fiber photometry, confirmed that mPOA-*Esr1*+ neurons were activated during male mounts. Optogenetic stimulation of these neurons elicited mounting behavior, while the inhibition reduced it (118, 119). mPOA-*Esr1*+ neurons are mostly GABAergic (80%), and specific optogenetic activation of mPOA-*Esr1*+-*Vgat*+ neurons increased the mounting response compared to activation of all mPOA-*Esr1*+ neurons (119). Importantly, in both studies, activation of mPOA-*Esr1*+ or mPOA-*Esr1*+-*Vgat*+ neurons promoted male-typical mounting

behavior also in females suggesting that female adult mPOA maintains the functional neural circuits to execute this behavior (118, 119). Thus, it is suggested that sexually dimorphic activation of mPOA-*Esr1*+ cells would underlie sex differences in the expression of reproductive behaviors. Indeed, as detailed in section 5, the activation of mPOA-*Esr1*+ cells also regulate female-typical pup retrieval behavior.

Regarding the role of the VMH in regulating male sexual behavior, additional studies showed that unlike the mPOA, adult inhibition of the VMHvl or VMHvl-*Esr1*+ neurons did not disrupt mounting behavior (120). This suggests that while the mPOA is critical for the expression of male-typical mounting behavior, the VMH may contribute but is not necessary. Although defensive behaviors are not the focus of this review, in males the VMH and especially ERα expressing neurons in this region have been shown to control aggressive behavior (119–121).

Another region known to control sexual behavior is the BNST, a major upstream region of the mPOA and the VMH. *Esr1*+ neurons of the principal subdivision of the BNST (BNSTpr) were chemogenetically silenced during ongoing social behaviors. The results showed reduced male mounting behavior towards a female when silencing took place during the approach phase, but this reduction was not observed during female mounting (122). However, silencing during the attack interrupted this behavior. Going further with optogenetic silencing of BNST projections, the authors showed that the appetitive phase of male sexual behavior (sniffing to mount) depended primarily on the activity of BNSTpr-mPOA projections, while aggression was triggered by BNST-VMHvl projections. BNST is also a node for olfactory sex recognition, with optogenetic inhibition of BNST-*Esr1*+ neurons reducing olfactory preference for females over males (122, 123). Interestingly, single-cell calcium measurements showed that different BNST-*Esr1*+ cell populations responded to male versus female stimuli. The same was observed in the mPOA and VMH-*Esr1*+ populations. BNSTpr-*Esr1*+ neurons were therefore found involved in controlling the transition between the appetitive and consummatory phases of male sexual behavior (122).

In females, the ablation of *Esr1* specifically in the VMH, in adulthood, was performed by RNA interference, using AAV vectors encoding for small hairpin RNA (shRNA) targeting the *Esr1* gene. An 80% reduction in *Esr1* expression abolished proceptive as well as lordosis behaviors in female mice (124) and rats (125), in association with a reduced estradiol-induced PR expression in this region (124). In the VMH, the neurons expressing *Pgr* (coding for PR) co-express *Esr1*. This neuronal population has been shown to project to the RP3V, the POA and the PAG (126). Interestingly, projections to RP3V showed strong structural plasticity, with more projections in females in estrus stage than in diestrus, suggesting a role for this neuronal population in linking sexual behavior and ovulation. This hormone-driven change was not observed for projections to the POA or PAG. Going further, using electrophysiological and optogenetics studies, the authors showed that these VMH-RP3V projections were mostly glutamatergic, and that ovarian sex hormones enhanced these excitatory projections by increasing the number of glutamatergic synapses formed into RP3V neurons (126).

Regarding the role of MeA or POA in female sexual behavior, the suppression of ERα in the MeA of female rats did not show any effects (125), but the reduction of *Esr1* expression specifically in the mPOA increased lordosis behavior in mutant females compared to controls, without modification of proceptive behaviors (127). These results suggested that ERα is involved in the inhibitory action of the mPOA on lordosis behavior. Surprisingly, a study in female mice showed that reduction of *Esr1* expression in the mPOA induced a small decrease in receptive behaviors compared to control (128). However, these experiments were performed on gonadally intact female mice that expressed low levels of lordosis behaviors, making it difficult to compare the estradiol-induced effects between control and mutants.

4.2 Role of ERβ in the regulation of sexual behavior

Although ERβ is less expressed than ERα, it is found in most regions involved in the expression of sexual behavior. Fewer studies have investigated its function in the regulation of sexual behavior.

4.2.1 Models of ubiquitous *Esr2* deletion

Behavioral characterization of the first lines of ERβKO mice (93) showed no disturbance in any aspects of male (latency and number of mounts and intromissions) or female sexual behaviors (lordosis quotient) evaluated at adulthood (129, 130). Olfactory preference was also unaffected in ERβKO males (130). Nevertheless, a role for ERβ in the defeminization of the brain has been suggested by the increase in female-like lordosis behavior displayed by adult ERβKO males when primed with estradiol and progesterone (130). In addition, a delay in behavioral pubertal maturation was observed, with ERβKO males showing a delay in the age of first ejaculatory behavior (94). Interestingly, ERβKO displayed elevated testosterone levels in pubertal and young adults (5–12 weeks), not found in older mice, supporting a potential role for ERβ during pubertal development (131). It is important to note that in this ERβKO mouse line, some *Esr2* transcripts were still present. Different results were observed using the genetic model devoid of all *Esr2* transcripts ($ERβ_{ST}^{L-/L-}$ (96);). Indeed, in this model, mutant males exhibited mild alteration of sexual behavior, with an increase in the number of mounts and intromissions and in the latency to ejaculate compared to controls. Differences observed between controls and mutants declined with sexual experience (132). In females, $ERβ_{ST}^{L-/L-}$ mice showed reduced attractiveness and lordosis behavior (132).

4.2.2 Models of brain specific *Esr2* deletion

The first studies were carried out in female rats, in which adult intracerebroventricular administration of an *Esr2* antisense oligonucleotide showed no effect on lordosis behavior (133). Then, the role of neural ERβ in regulating sexual behavior was evaluated using $ERβ^{NesCre}$ males and females (99, 100). In males, neural *Esr2* deletion had no impact on the expression of sexual behavior, with mutant animals displaying the full range of sexual behaviors and achieving ejaculation similarly to wildtypes (100). No

change in olfactory preference was observed either. In contrast to what was observed in ubiquitous ERβKO males, the analysis of female-like lordosis behavior in castrated $ERβ^{NesCre}$ males primed with estradiol and progesterone did not reveal any significant change between mutants and controls (100). Regarding the females, $ERβ^{NesCre}$ animals displayed unchanged olfactory preference and lordosis behavior compared with controls (99). These results showed that neural ERβ is not necessary for the proper expression of male and female sexual behaviors at adulthood.

4.2.3 Model of region-specific and time dependent *Esr2* deletion

Few studies have gone further in discriminating between potential developmental versus activational roles of ERβ, and hypothalamic neural pathways involved.

In males, site-specific knockdown of ERβ in MeA and mPOA was obtained by injecting small-hairpin RNA (shRNA)-associated adenoviruses (AAV) into these regions during prepuberty (PND21) or at adulthood (134). Prepubertal or adult silencing of *Esr2* in mPOA or MeA did not alter the latencies and numbers of mounts and intromissions in adult males. An alteration in olfactory preference towards receptive versus non-receptive females was observed with adult *Esr2* silencing. No alteration was observed when tested for preference between a receptive female and a male (134). Going further, fiber photometry recording did show higher activity of MeA-ERβ+ cells when sniffing a receptive female than when sniffing a non-receptive one or a gonadally intact male. Interestingly, chemogenetic inhibition of these neurons abolished the preference for a receptive female over a non-receptive female, but did not change the preference for a receptive female over a male. The authors also identified that MeA-ERβ+ neuronal projections to the BNST participate in this olfactory preference based on female receptivity but not on sex (135). In the MeA, ERβ appeared to be involved in distinguishing receptive states of female mice.

Very few studies have been done in females. In rats, the silencing of ERβ by injection of an shRNA-associated AAV in the VMH, did not modify the lordosis response (136). In addition, in female mice, injection of shRNA-associated AAV into the dorsal raphe nucleus to specifically knockdown ERβ in adulthood, did not modify the lordosis response on the day of estrus, but led to a sustained lordosis response on the day following behavioral estrus (137). The same observations have been made previously in ubiquitous ERβKO females, suggesting a role for ERβ in the inhibitory regulation of female sexual behavior outside the estrus phase (129).

Collectively, these genetic studies have demonstrated the crucial role of neural ERα in regulating both male and female sexual behavior. Its roles and mechanisms of action are extremely complex and depend on sex, age and brain region. Recent elegant studies, using a combination of innovative techniques, have paved the way for establishing the precise neural pathways at play in the control of these behaviors. Fewer studies have focused on the role of ERβ, as the data indicate a less important role for this receptor in the control of sexual behavior. Indeed, ERβ appears to be more involved in the control of other social and mood related behaviors (99, 138). Nevertheless, studies suggest that ERβ participates in the pubertal organization of neural circuits involved in the control of sexual behavior, at least in males (94, 131). Further studies will be instrumental to go deeper into the mechanism of action and establish whether the same is true in females.

5 Estradiol regulation of parental behavior

In addition to their role in regulating sexual behaviors, several neural regions that express ERα and ERβ are also known to control parental behavior, especially the POA, VMH, BNST, and MeA. Parental behavior is crucial for species survival and offspring development (Figure 3). These brain regions exhibited an increase in *Fos* expression, a marker of neural activation, in response to the display of maternal behavior. Between 25% and 45% of these *Fos*+ immunoreactive cells co-expressed ERα, suggesting that maternal behavior possibly involved neural ERα activity (139). Furthermore, natural variations in the level of maternal care were associated with changes in *Esr1* expression, but not that of *Esr2* (140). This suggests a potential role of ERα in regulating maternal behavior, which was further investigated in the genetic studies described below. To date, no genetic studies have addressed the role of ERβ in the expression of parental behavior.

5.1 Role of ERα in the regulation of parental behavior

5.1.1 Models of ubiquitous *Esr1* deletion

Studies using ubiquitous ERαKO animals were performed in mice (104, 111, 112) and more recently in rats (141, 142). Due to the infertility of ERαKO animals, analysis of parental behavior was carried out in nulliparous animals following a pup sensitization process, which involves repeated exposure of the animals to pups produced by donor lactating mothers. Maternal behavior of ERαKO mice was strongly disturbed in both intact and gonadectomized females. Mutant females displayed impaired pup-retrieving behavior and a high level of infanticide (111, 112). In male mice, ubiquitous *Esr1* deletion had no effects on pup retrieval, but ERαKO males showed a high percentage of infanticide, that was abolished after gonadectomy (104). The authors suggested that the increase in testosterone levels observed in ERαKO males could be sufficient to promote infanticide, by acting on AR. Surprisingly, in rats, juvenile and adult ERαKO females showed no modification in maternal behavior. The latency score for retrieving and regrouping the pups and adopting a crouched position over them was identical in mutant and control animals (141, 142). Only a slight impairment was observed when the experimental tests were performed in a novel cage (142). The discrepancy with the data obtained in mice is not yet understood, but could result from different underlying mechanisms controlling maternal behavior in the two species. Moreover, deletion strategies diverged between the two ERαKO

animal lines, with homologous recombination targeting exon 2 in mice (63, 143), and zinc finger nucleases (ZFNs)-mediated genome editing targeting exon 3 in rats (144). In juvenile male rats, ubiquitous *Esr1* deletion did not alter the pup retrieval latency score compared with controls. The level of infanticide was not analyzed in these animals (141).

The discrepancies observed in these models underline the need to conduct genetic research under physiological conditions and to use more targeted approaches of *Esr1* deletion in the neural regions of interest. Maternal behavior was only studied in nulliparous females, which did not experience the hormonal changes that occur during gestation and parturition in preparation for behavioral processing. Moreover, males and females lacked stimulation of the ERα signaling pathway during embryonic, postnatal and pubertal development periods, which could interfere with the organization of the neural pathways underlying parental behavior.

5.1.2 Models of region-specific and time dependent *Esr1* deletion

Over the last decades, a growing number of studies have focused on region-specific deletions of *Esr1*, with particular emphasis on the mPOA, the main region controlling parental behavior.

In female mice, reduction of *Esr1* expression in the mPOA, via targeted viral-vector mediated siRNA silencing, significantly diminished pup retrieving behavior in sexually naive females (128). A similar behavioral impairment was observed when mPOA-*Esr1*+ cells were ablated (118) or chemogenetically inhibited (145) in naive and lactating females. In addition, experiments performed optogenetic inhibition of mPOA-*Esr1*+ neurons at specific time points in the behavioral sequence. This study demonstrated the critical role of these neurons in promoting pup contacts once females have initiated pup approach, and in facilitating the completion of pup retrieval once females have initiated this behavior (118). However, inhibition of these mPOA-*Esr1*+ neurons after the females had initiated crouching over the pups had no effect on this behavior. Conversely, optogenetic activation of mPOA-*Esr1*+ cells increased pup retrieval in both naive and lactating females (118, 145). With regards to the expression of other maternal behaviors, the reduction in *Esr1*+ expression in the mPOA decreased the time the female spent licking and nursing the pups without affecting maternal aggression (128). Fang et al., 2018 also reported that chemogenetic inhibition of mPOA-*Esr1*+ cells had no effect on sniffing, grooming, and crouching over the pups (145).

In the mPOA, galanin-expressing neurons (mPOA-*gal*) are crucial for the expression of parental behavior in mice (146, 147). They represent about 20% of mPOA neurons, and the majority of them express ERα. A recent study showed that AAV-mediated ablation of *Esr1* in mPOA-*gal* neurons drastically reduced the expression of pregnancy-induced maternal behaviors, including intensive nest building and pup retrieval behaviors, that occur from the first days of gestation. The parental behavior of these animals remained impaired after birth, indicating that these effects could not be compensated for by the effect of the hormonal milieu during parturition (148). Interestingly, the authors also demonstrated that estradiol play a role in the neural modeling of the mPOA-gal neurons during pregnancy, by transiently silencing mPOA-gal neurons and contradictively increasing their excitability. The deletion of *Esr1* in mPOA-*gal* neurons prevented this remodeling (148). These results indicated that within the mPOA, ERα signaling appears to facilitate pup care behaviors.

Other studies have focused on other parameters of parental behavior, such as increased interest in the pups leading to a reduction in infanticide, while there is an increased aggressivity towards intruders. In this context, Mei et al. (2023) uncovered a neural circuit between the BNSTp and the mPOA that modulates the display of female infanticide towards pups (149). Indeed, although the mechanism underlying this state-dependent switch remains unclear, sexually naive females often kill their pups, while lactating females show maternal care. Interestingly, chemogenetic inhibition of mPOA-*Esr1*+ cells projecting to the BNSTp increased pup attacks by females, while chemogenetic activation of these cells reduced infanticide. On the contrary, blocking the input from BNSTp-*Esr1*+ to the mPOA suppressed infanticide, while activating this projection suppressed maternal behavior. Furthermore, *in vitro* current-clamp recording showed that BNSTp-*Esr1*+ neuronal population switched from excitable in naive females to less excitable in lactating dams, in contrast to mPOA-*Esr1*+ cells which became more excitable in lactating dams than in naive females (149). These results support the existence of a neural circuitry remodeling between mPOA and BNSTp during motherhood that is dependent on estrogen signaling. In particular, there appears to be reciprocal inhibition between these two regions to control the levels of infanticide versus maternal behavior.

On the other hand, females typically display low levels of aggression, except during gestation and lactation, when dams show high levels of maternal aggression towards perceived threats to their offspring (150). This behavior is displayed from the first days of gestation, in response to the hormonal changes occurring with pregnancy. The ventrolateral part of the VMH (VMHvl) has been identified as a key hypothalamic region controlling maternal aggression in females. The same region has been extensively studied for its role in territorial aggression in males (151). Importantly, the role of VMHvl neural population in controlling female aggression is dependent on the genetic background and the reproductive state of the animals. Focusing on experiments using lactating females only, it has been showed that VMHvl-*Esr1*+ cells are critical for maternal aggression. Indeed, using the GCaMP fiber photometry approach, it was shown that VMHvl-*Esr1*+ cells were activated during attacks by a lactating female towards a juvenile or adult male intruder, but not when the lactating female was investigating or retrieving pups. Moreover, inhibition of VMHvl-*Esr1*+ cells in these mice drastically decreased aggression against intruders (152). Further studies, described below in 6., have used omics analyses to identify specific neural populations located in the POA and VMH which mediate maternal behaviors, and have differentiated them from cell clusters specifically activated during sexual behavior.

Collectively, these studies provide evidence that ERα regulates maternal behavior in mice. Within the mPOA, ERα appears to facilitate pup care behaviors, while it seems implicated in regulating infanticide in the BNSTp, and maternal aggression in the VMHvl.

Because mouse strains used in laboratory experiments are a monoparental species, the investigation of paternal behavior remains very limited. One study in male mice showed that ablation of mPOA-*Esr1*+ neurons had no effect on pup retrieval behavior, whereas optogenetic activation of these cells induced this behavior (118). These results suggested that unlike in females, mPOA-*Esr1*+ neurons may not be necessary for the display of pup retrieval in males. Nevertheless, additional studies are needed to establish the role of estradiol in the regulation of paternal behavior, especially using biparental species like prairie voles or Californian mice.

5.2 Lack of models of *Esr2* deletions

No genetic study has addressed the role of ERβ in the regulation of parental behavior. Yet this receptor appears to be tightly associated with oxytocin, a key hormone that facilitates maternal behavior. It has been shown that estrogen treatment increased oxytocin gene expression in the rat paraventricular nucleus (153). Oxytocin neurons in this region were found essential for the regulation of emotional and social behaviors, including parental care (for reviews: Acevedo-Rodriguez, Mani & Handa, (154); Neumann, (155)). In the paraventricular nucleus, approximately 84% of oxytocin neurons co-express ERβ, a colocalization not observed in other oxytocinergic regions such as the supraoptic nucleus (156). Estradiol treatment also increased oxytocin expression in the paraventricular nucleus of both male and female mice. This effect was not observed in ERβKO animals (157, 158). These data highlight the need for genetic studies to unravel the implication of ERβ in the regulation of parental behavior, notably in relation to oxytocin.

6 Molecular profiling of brain circuits controlling sex- and reproductive state- dependent reproductive behaviors

In recent years, several innovative techniques have allowed the identification of specific neural populations that control especially male versus female behaviors in the main regions controlling reproductive behaviors (POA, VMH, BNST and MeA).

Combination of single-cell RNA-seq (scRNA-seq) and multiplexed error-robust fluorescence *in situ* hybridization (MERFISH) analysis of the POA allowed the identification of 70 transcriptomic cell types (T-types), including T-types preferentially activated in females or males during specific social behaviors, particularly parenting, aggression, and mating (159). In this study, by including fos probes in MERFISH measurements, it was shown that cell clusters activated by parenting and mating (i.e. enriched in fos-positive cells) appeared to belong to two transcriptionally distinct cell populations localized into distinct preoptic nuclei (159). Interestingly, *Esr1* expression has been found in nearly all behaviorally activated clusters. With regard to mating, it was shown that some clusters enriched in fos-positive cells were activated in both sexes after mating, while a few clusters exhibited sexually dimorphic activation (159).

Several clusters expressing *Esr1* in the VMH have also been found to be enriched in a sexually dimorphic manner. For example, *Esr1*+ cells located in the VMHvl have been shown to co-express PR and control especially female sexual behavior and male aggression (120, 160–162). In males, calcium imaging analysis of VMHvl-*Esr1*+ neurons showed distinct cell populations activated by male versus female stimuli during resident-intruder assays. Intriguingly, these differences appeared with social and sexual experience, since in naive animals, male and female intruders activated overlapping neuronal populations (163). Going further into synaptic connectivity, viral-genetic tracing in *Esr1*-Cre male and female mice revealed that most inputs and outputs of VMHvl-*Esr1*+ neurons were located in the hypothalamus and extended amygdala with a high degree of bidirectional connectivity (164). scRNA-seq analysis identified 17 different sub-types of cells in the VMHvl, including seven *Esr1*+ T-types (162). Among them, the authors identified two anatomically distinct subsets of VMHvl-*Esr1*+ neurons, which preferably project to dPAG or mPOA, and would therefore play a role in the control of behavior, or provide feedback to hypothalamic and amygdala circuits, respectively (162, 164). A female-specific cluster has also been identified and subsequently confirmed to be specifically activated during mating (162, 165). Indeed, in females, a reproductive state-dependent switch in female behavior has been revealed, with molecularly distinct subpopulations of VMHvl-*Esr1*+ neurons excited during maternal aggression or sexual behavior (152, 165). The use of activity-dependent single-cell RNA sequencing allowed the identification of VMHvl T-types specifically activated in either lactating females exhibiting attack or virgins exhibiting lordosis (165). Among these clusters, using several optogenetic manipulations, the authors identified two transcriptomically distinct VMHvl-*Esr1*+ subtypes and were able to assign causal roles in mating versus aggression in virgins and lactating mothers, respectively. Interestingly, aggression-specific cells displayed changes in bulk-calcium activity depending on the reproductive status, showing an increase in response to social cues (male or female intruders) across the transition from virginity to lactation (165).

A broader approach used translating ribosome affinity purification and sequencing (TRAPseq), and scRNA-seq to identify differentially expressed genes (DEGs) between males and females (comprising females at two estrous stages, estrus and diestrus), specifically in *Esr1*+ neuronal population. These analyses were carried out in the BNSTpr, MeA, POA and VMHvl. The authors identified 1,415 DEGs between sexes and estrous stages, divided in 137 *Esr1*+ cell types (166). Almost all *Esr1*+ cell types co-expressed PR and AR, showing a strong hormonal influence on these populations. This study also confirmed that BNSTpr and POA are mostly GABAergic, the MeA composed of both excitatory and inhibitory neurons, whereas the VMHvl is largely glutamatergic. Nevertheless, a small population of *Esr1*+ inhibitory neurons was identified in the VMHvl (166). The authors focused on the behavioral role of two specific cell types.

First, BNSTpr-*Esr1*+-*Tac1*+ GABAergic neurons were found to be the most enriched in males compared with females,

independently of their estrous stage. Chemogenetic inhibition of this population in adult males reduced sex recognition, mounting and intromission during mating, but also attacks during aggression. Interestingly, these effects were not observed when inhibiting BNSTpr-*Esr1*+-*Tac1*- neurons, showing the specific involvement of cells expressing both *Esr1* and *Tac1* in BNSTpr for the regulation of male reproductive behaviors (166). Further studies showed that BNSTpr-*Esr1*+-*Tac1*+ neurons project in the POA to POA-*Tacr1*+ neurons (167) and that these projections regulated male mating but not aggression. POA-*Tacr1*+ neurons co-express *Esr1*, and fiber photometry imaging showed that these neurons were activated during mounting and intromission toward females, but not activated during male-male attacks. The neuropeptide substance P encoded by the tachykinin 1 gene (*Tac1*), is the ligand for the tachykinin receptor 1 (Tac1r). Its release by BNSTpr-*Tac1*+ cells was shown to potentiate the activation of POA-*Tacr1*+ neurons and initiate male mating. The authors also revealed that POA-*Tacr1*+ projections to VTA and PAG control male sexual behavior (167).

Secondly, in females, the authors identified the VMHvl-*Esr1*+-*Cckar*+ glutamatergic cell type enriched in females in estrus compared to diestrus. Chemogenetic inhibition of this population highly reduced lordosis behavior without altering maternal behaviors, including pup retrieval and maternal aggression. An additional viral strategy showed that these VMHvl-*Esr1*+-*Cckar*+ neurons project preferentially to the AVPV and that these projections peak at estrus. These effects were specific to *Esr1*+-*Cckar*+ cells and were not observed in VMHvl-*Esr1*+-*Cckar*- neurons. Interestingly, there was no change in the number of projections to the PAG or POA, indicating a specific projection pattern for this neuronal population. In addition, inhibiting VMHvl-*Esr1*+-*Cckar*- neurons did not affect lordosis behavior in female but inhibited male mounting behavior and abolished maternal aggression (166).

Altogether these innovative techniques open the way to deciphering the specific neural pathways that control sexually dimorphic reproductive behaviors. Indeed, discrete cell populations appear to be involved in the activation/repression of specific behaviors, according to sex and hormonal state.

7 Discussion and perspectives

Survival of the species relies on the proper regulation of the HPG axis and optimal expression of sexual and parental behavior. These reproductive function and behaviors are strongly influenced by hormonal regulation, especially by estradiol. Extensive research has been carried out since the 1950s, leading to a better comprehension of the specific role of ERα and ERβ and their underlying mechanisms of action. Importantly, all this research points to the existence of an extremely complex neural circuit, which is regulated in different ways according to sex, hormonal status, and age. Recent technological progress has rendered increasingly possible the differentiation of these different parameters in order to obtain a precise view of the neural populations and neural circuits involved in these neuroendocrine and behavioral functions.

The data presented here show that neural ERα is mandatory for the activation and functioning of the gonadotropic axis, expression of sexual and parental behavior in females. In males, it plays a critical role, but it is not indispensable. Indeed, testosterone and its neural metabolite estradiol act in a complementary manner via both AR and ERs in males, with a crucial role established for AR (34, 80). The role of neural ERβ is not entirely clear, but it appears that it is not required for fertility and instead plays a more subtle role in modulating the HPG axis in adults of both sexes. Nevertheless, it is important to bear in mind that the majority of studies analyzing the role of estradiol in regulating the HPG axis have been carried out in females, and that further studies in males are needed to achieve a more thorough understanding. Evidence reported so far has revealed the important role of ERα signaling in the control of maternal behaviors. Further studies, especially in males, will be instrumental in gaining a better understanding of the estradiol regulation of parental behavior.

The recent studies monitoring the activity of *Esr1*+ cell populations during very specific reproductive behaviors, in different brain regions, as a function of sex and/or hormonal state highlight the existence of a strong neuroplasticity of the brain circuits controlling distinct reproductive behaviors. Interestingly, within the same hypothalamic nucleus, sexually dimorphic activation of different cell clusters corresponds to sexually dimorphic expression of behaviors. Further studies are needed to understand the role of estradiol and other sex steroids in the organization of these neural circuits. Indeed, most of the region-specific deletions have been carried-out in adulthood, but as techniques improve, it is becoming possible to make these genetic modifications at younger ages. It would be particularly interesting with regard to ERβ, whose role in adulthood seems more subtle, but for which several indications point to an implication during pubertal development. It is important to note that, while outside the scope of this review, ERβ is known to play important roles in estradiol regulation of emotional state and social behaviors (99, 138).

Finally, a better understanding of ERs signaling pathways in the regulation of reproductive function and behaviors has an important translational perspective. Indeed, human fertility is under the control of estrogens and *ESR1* and/or *ESR2* gene mutations and polymorphisms have been associated with reproductive defects in both men and women, including abnormal timing of puberty and infertility (168–175). Loss-of-function mutations in *ESR1* induce estrogen resistance in both men and women. The first men case reported normal pubertal development with normal male genitalia and sperm density (168). In addition, the patient had tall stature and delayed skeletal maturation and osteoporosis, with at adulthood a bone age of 15 years old. Indeed, while not in the scope of this review, it is well known that estrogen plays critical role in bone development and mineralization during puberty in both sexes. Testosterone concentrations were normal while estrogen and FSH and LH serum levels were increased. He indicated having sexual interests and had normal functioning, including morning erections and nocturnal emissions. The treatment with estrogen had no detectable effect (168). A loss-of-function *ESR1* mutation was identified in a woman without breast development, primary

amenorrhea, a small uterus and multicystic ovaries (170). She also had elevated estrogen serum levels, mildly elevated gonadotropins and delayed bone age. Estrogen treatment did not change breast development but diminished ovarian and cyst size (170). Subsequently, few other *ESR1* mutations (2 females and 1 male) were identified describing similar clinical phenotypes (174). All suggested estrogen resistance syndrome and were in accordance with the reproductive phenotype of *Esr1* ubiquitous knockout mouse models described in section 4.1.1. *ESR2* mutations are even rarer. Monoallelic and biallelic *ESR2* variants have been identified in one syndromic and two nonsyndromic 46, XY patients with differences of sex development, presenting absent gonadal development or partial and complete gonadal dysgenesis. This suggested a role for ERβ in early gonadal development (175). In addition, a point mutation in *ESR2* was identified in a young woman with absent puberty without breast development, a small infantile uterus, no detectable ovaries and severe osteoporosis (173). In contrast to *ESR1*-deficient patients, estrogen levels were low. Estrogen and progestin replacement therapy enabled breast development, menarche and uterine maturation (173). These results suggest that *ESR2* is also necessary for human ovarian development and that *ESR1* is not sufficient to support ovarian function in human. *ESR1* and *ESR2* are expressed in human gonads, making it difficult to distinguish peripheral from central effects in these patients. Some studies have also associated *ESR1* and *ESR2* gene polymorphisms with infertility and assisted reproduction outcomes (171, 172). Further studies will be needed to understand the neural role of ERα and ERβ in regulating reproductive function in humans. The acquisition of greater knowledge could lead to the development of sex- and age-specific therapeutic strategies for fertility disorders, which represent a major public health issue as their frequency are increasing due to medical, environmental and societal causes.

Author contributions

TT: Writing – original draft, Writing – review & editing. NA: Writing – original draft, Writing – review & editing. SMK: Writing – review & editing. LN: Writing – original draft, Writing – review & editing.

Funding

The author(s) declare financial support was received for the research, authorship, and/or publication of this article. This work was supported by a French Society of Endocrinology Research award 2023 (to LN) and the Agence Nationale de la Recherche (Phtailure, 2018) in France (to SM-K).

Conflict of interest

The authors declare that the research was conducted in the absence of any commercial or financial relationships that could be construed as a potential conflict of interest.

Publisher's note

All claims expressed in this article are solely those of the authors and do not necessarily represent those of their affiliated organizations, or those of the publisher, the editors and the reviewers. Any product that may be evaluated in this article, or claim that may be made by its manufacturer, is not guaranteed or endorsed by the publisher.

References

1. Herbison AE. Chapter 11 - physiology of the adult gonadotropin-releasing hormone neuronal network. In: Plant TM, Zeleznik AJ, editors. *Knobil and Neill's Physiology of Reproduction, 4th ed.* Academic Press, San Diego (2015). p. 399–467. Available at: https://www.sciencedirect.com/science/article/pii/B9780123971753000119

2. Tilbrook AJ, Clarke IJ. Negative feedback regulation of the secretion and actions of gonadotropin-releasing hormone in males. *Biol Reprod*. (2001) 64:735–42. doi: 10.1095/biolreprod64.3.735

3. Herbison AE. Estrogen positive feedback to gonadotropin-releasing hormone (GnRH) neurons in the rodent: the case for the rostral periventricular area of the third ventricle (RP3V). *Brain Res Rev*. (2008) 57:277–87. doi: 10.1016/j.brainresrev.2007.05.006

4. Naftolin F, Garcia-Segura LM, Horvath TL, Zsarnovszky A, Demir N, Fadiel A, et al. Estrogen-induced hypothalamic synaptic plasticity and pituitary sensitization in the control of the estrogen-induced gonadotrophin surge. *Reprod Sci Thousand Oaks Calif*. (2007) 14:101–16. doi: 10.1177/1933719107301059

5. Naulé L, Maione L, Kaiser UB. Puberty, A sensitive window of hypothalamic development and plasticity. *Endocrinology*. (2021) 162:bqaa209. doi: 10.1210/endocr/bqaa209

6. Navarro VM, Gottsch ML, Chavkin C, Okamura H, Clifton DK, Steiner RA. Regulation of gonadotropin-releasing hormone secretion by kisspeptin/dynorphin/neurokinin B neurons in the arcuate nucleus of the mouse. *J Neurosci Off J Soc Neurosci*. (2009) 29:11859–66. doi: 10.1523/JNEUROSCI.1569-09.2009

7. Clarkson J, d'Anglemont de Tassigny X, Moreno AS, Colledge WH, Herbison AE. Kisspeptin-GPR54 signaling is essential for preovulatory gonadotropin-releasing hormone neuron activation and the luteinizing hormone surge. *J Neurosci Off J Soc Neurosci*. (2008) 28:8691–7. doi: 10.1523/JNEUROSCI.1775-08.2008

8. Beach FA. Sexual attractivity, proceptivity, and receptivity in female mammals. *Horm Behav*. (1976) 7:105–38. doi: 10.1016/0018-506X(76)90008-8

9. Powers JB. Hormonal control of sexual receptivity during the estrous cycle of the rat. *Physiol Behav*. (1970) 5:831–5. doi: 10.1016/0031-9384(70)90167-8

10. Mhaouty-Kodja S, Naulé L, Capela D. Sexual behavior: from hormonal regulation to endocrine disruption. *Neuroendocrinology*. (2018) 107:400–16. doi: 10.1159/000494558

11. Karlson P, Luscher M. Pheromones': a new term for a class of biologically active substances. *Nature*. (1959) 183:55–6. doi: 10.1038/183055a0

12. Brennan PA, Zufall F. Pheromonal communication in vertebrates. *Nature*. (2006) 444:308–15. doi: 10.1038/nature05404

13. Kevetter GA, Winans SS. Connections of the corticomedial amygdala in the golden hamster. I. Efferents of the "vomeronasal amygdala." *J Comp Neurol*. (1981) 197:81–98. doi: 10.1002/cne.901970107

14. Kang N, Baum MJ, Cherry JA. A direct main olfactory bulb projection to the 'vomeronasal' amygdala in female mice selectively responds to volatile pheromones from males. *Eur J Neurosci*. (2009) 29:624–34. doi: 10.1111/j.1460-9568.2009.06638.x

15. Hull EM, Dominguez JM. Sexual behavior in male rodents. *Horm Behav*. (2007) 52:45–55. doi: 10.1016/j.yhbeh.2007.03.030

16. Sakamoto H. Brain–spinal cord neural circuits controlling male sexual function and behavior. *Neurosci Res*. (2012) 72:103–16. doi: 10.1016/j.neures.2011.11.002

17. Kow LM, Pfaff DW. Physiology of somatosensory and estrogenic control over the lordosis reflex. *Exp Brain Res*. (1981) Suppl 3:262–73. doi: 10.1007/978-3-642-45525-4_21

18. Sinchak K, Micevych PE. Progesterone blockade of estrogen activation of mu-opioid receptors regulates reproductive behavior. *J Neurosci Off J Soc Neurosci*. (2001) 21:5723–9. doi: 10.1523/JNEUROSCI.21-15-05723.2001

19. Bales KL, Saltzman W. Fathering in rodents: Neurobiological substrates and consequences for offspring. *Horm Behav*. (2016) 77:249–59. doi: 10.1016/j.yhbeh.2015.05.021

20. Keller M, Vandenberg LN, Charlier TD. The parental brain and behavior: A target for endocrine disruption. *Front Neuroendocrinol*. (2019) 54:100765. doi: 10.1016/j.yfrne.2019.100765

21. Numan M, Insel TR. *The neurobiology of parental behavior [Internet]*. New York: Springer (2003). Available at: http://site.ebrary.com/id/10130203

22. McRae BR, Andreu V, Marlin BJ. Integration of olfactory and auditory cues eliciting parental behavior. *J Neuroendocrinol*. (2023) 35:e13307. doi: 10.1111/jne.13307

23. Adam N, Mhaouty-Kodja S. Behavioral effects of exposure to phthalates in female rodents: evidence for endocrine disruption? *Int J Mol Sci*. (2022) 23:2559. doi: 10.3390/ijms23052559

24. Rosenblatt JS. Nonhormonal basis of maternal behavior in the rat. *Science*. (1967) 156:1512–4. doi: 10.1126/science.156.3781.1512

25. Phoenix CH, Goy RW, Gerall AA, Young WC. Organizing action of prenatally administered testosterone propionate on the tissues mediating mating behavior in the female Guinea pig. *Endocrinology*. (1959) 65:369–82. doi: 10.1210/endo-65-3-369

26. Wallen K. The Organizational Hypothesis: Reflections on the 50th anniversary of the publication of Phoenix, Goy, Gerall, and Young (1959). *Horm Behav*. (2009) 55:561–5. doi: 10.1016/j.yhbeh.2009.03.009

27. Lenz KM, McCarthy MM. Organized for sex – steroid hormones and the developing hypothalamus. *Eur J Neurosci*. (2010) 32:2096–104. doi: 10.1111/j.1460-9568.2010.07511.x

28. Bakker J, Honda SI, Harada N, Balthazart J. The aromatase knock-out mouse provides new evidence that estradiol is required during development in the female for the expression of sociosexual behaviors in adulthood. *J Neurosci*. (2002) 22:9104–12. doi: 10.1523/JNEUROSCI.22-20-09104.2002

29. Sano K, Nakata M, Musatov S, Morishita M, Sakamoto T, Tsukahara S, et al. Pubertal activation of estrogen receptor α in the medial amygdala is essential for the full expression of male social behavior in mice. *Proc Natl Acad Sci USA*. (2016) 113:7632–7. doi: 10.1073/pnas.1524907113

30. Juraska JM, Sisk CL, DonCarlos LL. Sexual differentiation of the adolescent rodent brain: Hormonal influences and developmental mechanisms. *Horm Behav*. (2013) 64:203–10. doi: 10.1016/j.yhbeh.2013.05.010

31. Schulz KM, Zehr JL, Salas-Ramirez KY, Sisk CL. Testosterone Programs Adult Social Behavior before and during, But Not after, Adolescence. *Endocrinology*. (2009) 150:3690–8. doi: 10.1210/en.2008-1708

32. George FW, Ojeda SR. Changes in aromatase activity in the rat brain during embryonic, neonatal, and infantile development*. *Endocrinology*. (1982) 111:522–9. doi: 10.1210/endo-111-2-522

33. Roselli CE, Resko JA. Aromatase activity in the rat brain: Hormonal regulation and sex differences. *J Steroid Biochem Mol Biol*. (1993) 44:499–508. doi: 10.1016/0960-0760(93)90254-T

34. Mhaouty-Kodja S. Role of the androgen receptor in the central nervous system. *Mol Cell Endocrinol*. (2018) 465:103–12. doi: 10.1016/j.mce.2017.08.001

35. Sluyser M, Rijkers AWM, De Goeij CCJ, Parker M, Hilkens J. Assignment of estradiol receptor gene to mouse chromosome 10. *J Steroid Biochem*. (1988) 31:757–61. doi: 10.1016/0022-4731(88)90283-X

36. Tremblay GB, Tremblay A, Copeland NG, Gilbert DJ, Jenkins NA, Labrie F, et al. Cloning, chromosomal localization, and functional analysis of the murine estrogen receptor β. *Mol Endocrinol*. (1997) 11:353–65. doi: 10.1210/mend.11.3.9902

37. Alves SE, Mcewen BS, Hayashi S, Korach KS, Pfaff DW, Ogawa S. Estrogen-regulated progestin receptors are found in the midbrain raphe but not hippocampus of estrogen receptor alpha (ER)? gene-disrupted mice. *J Comp Neurol*. (2000) 427:185–95. doi: 10.1002/1096-9861(20001113)427:2<185::AID-CNE2>3.0.CO;2-G

38. Smith JT, Cunningham MJ, Rissman EF, Clifton DK, Steiner RA. Regulation of kiss1 gene expression in the brain of the female mouse. *Endocrinology*. (2005) 146:3686–92. doi: 10.1210/en.2005-0488

39. Gottsch ML, Navarro VM, Zhao Z, Glidewell-Kenney C, Weiss J, Jameson JL, et al. Regulation of *Kiss1* and *Dynorphin* gene expression in the murine brain by classical and nonclassical estrogen receptor pathways. *J Neurosci*. (2009) 29:9390–5. doi: 10.1523/JNEUROSCI.0763-09.2009

40. Deb P, Chini A, Guha P, Rishi A, Bhan A, Brady B, et al. Dynamic regulation of BDNF gene expression by estradiol and lncRNA HOTAIR. *Gene*. (2023) 897:148055. doi: 10.1016/j.gene.2023.148055

41. Sinchak K, Wagner EJ. Estradiol signaling in the regulation of reproduction and energy balance. *Front Neuroendocrinol*. (2012) 33:342–63. doi: 10.1016/j.yfrne.2012.08.004

42. Micevych P, Dominguez R. Membrane estradiol signaling in the brain. *Front Neuroendocrinol*. (2009) 30:315–27. doi: 10.1016/j.yfrne.2009.04.011

43. Dewing P, Boulware MI, Sinchak K, Christensen A, Mermelstein PG, Micevych P. Membrane estrogen receptor-α Interactions with metabotropic glutamate receptor 1a modulate female sexual receptivity in rats. *J Neurosci*. (2007) 27:9294–300. doi: 10.1523/JNEUROSCI.0592-07.2007

44. Dewing P, Christensen A, Bondar G, Micevych P. Protein kinase C signaling in the hypothalamic arcuate nucleus regulates sexual receptivity in female rats. *Endocrinology*. (2008) 149:5934–42. doi: 10.1210/en.2008-0847

45. Grove-Strawser D, Boulware MI, Mermelstein PG. Membrane estrogen receptors activate the metabotropic glutamate receptors mGluR5 and mGluR3 to bidirectionally regulate CREB phosphorylation in female rat striatal neurons. *Neuroscience*. (2010) 170:1045–55. doi: 10.1016/j.neuroscience.2010.08.012

46. Johnson CS, Mermelstein PG. The interaction of membrane estradiol receptors and metabotropic glutamate receptors in adaptive and maladaptive estradiol-mediated motivated behaviors in females. *Int Rev Neurobiol*. (2023) 168:33–91. doi: 10.1016/bs.irn.2022.11.001

47. Mozhui K, Lu L, Armstrong WE, Williams RW. Sex-specific modulation of gene expression networks in murine hypothalamus. *Front Neurosci*. (2012) 6:63/abstract. doi: 10.3389/fnins.2012.00063/abstract

48. Milner TA, Thompson LI, Wang G, Kievits JA, Martin E, Zhou P, et al. Distribution of estrogen receptor β containing cells in the brains of bacterial artificial chromosome transgenic mice. *Brain Res*. (2010) 1351:74–96. doi: 10.1016/j.brainres.2010.06.038

49. Mitra SW, Hoskin E, Yudkovitz J, Pear L, Wilkinson HA, Hayashi S, et al. Immunolocalization of estrogen receptor β in the mouse brain: comparison with estrogen receptor α. *Endocrinology*. (2003) 144:2055–67. doi: 10.1210/en.2002-221069

50. Osterlund M, Kuiper GG, Gustafsson JA, Hurd YL. Differential distribution and regulation of estrogen receptor-alpha and -beta mRNA within the female rat brain. *Brain Res Mol Brain Res*. (1998) 54:175–80. doi: 10.1016/S0169-328X(97)00351-3

51. Shughrue PJ, Lane MV, Merchenthaler I. Comparative distribution of estrogen receptor-alpha and -beta mRNA in the rat central nervous system. *J Comp Neurol*. (1997) 388:507–25. doi: 10.1002/(SICI)1096-9861(19971201)388:4<507::AID-CNE1>3.0.CO;2-6

52. Orikasa C, Kondo Y, Hayashi S, McEwen BS, Sakuma Y. Sexually dimorphic expression of estrogen receptor beta in the anteroventral periventricular nucleus of the rat preoptic area: implication in luteinizing hormone surge. *Proc Natl Acad Sci USA*. (2002) 99:3306–11. doi: 10.1073/pnas.052707299

53. Snyder MA, Smejkalova T, Forlano PM, Woolley CS. Multiple ERβ antisera label in ERβ knockout and null mouse tissues. *J Neurosci Methods*. (2010) 188:226–34. doi: 10.1016/j.jneumeth.2010.02.012

54. Zuloaga DG, Zuloaga KL, Hinds LR, Carbone DL, Handa RJ. Estrogen receptor β expression in the mouse forebrain: age and sex differences. *J Comp Neurol*. (2014) 522:358–71. doi: 10.1002/cne.23400

55. Lana LC, Hatsukano T, Sano K, Nakata M, Ogawa S. Sex and age differences in the distribution of estrogen receptors in mice. *Neurosci Lett*. (2023) 793:136973. doi: 10.1016/j.neulet.2022.136973

56. Gerlach JL, McEwen BS, Toran-Allerand CD, Friedman WJ. Perinatal development of estrogen receptors in mouse brain assessed by radioautography, nuclear isolation and receptor assay. *Dev Brain Res*. (1983) 11:7–18. doi: 10.1016/0165-3806(83)90197-9

57. Kelly DA, Varnum MM, Krentzel AA, Krug S, Forger NG. Differential control of sex differences in estrogen receptor α in the bed nucleus of the Stria terminalis and anteroventral periventricular nucleus. *Endocrinology*. (2013) 154:3836–46. doi: 10.1210/en.2013-1239

58. Herbison AE, Pape JR. New evidence for estrogen receptors in gonadotropin-releasing hormone neurons. *Front Neuroendocrinol*. (2001) 22:292–308. doi: 10.1006/frne.2001.0219

59. Hrabovszky E, Shughrue PJ, Merchenthaler I, Hajszán T, Carpenter CD, Liposits Z, et al. Detection of estrogen receptor-beta messenger ribonucleic acid and 125I-estrogen binding sites in luteinizing hormone-releasing hormone neurons of the rat brain. *Endocrinology*. (2000) 141:3506–9. doi: 10.1210/endo.141.9.7788

60. Hrabovszky E, Kalló I, Szlávik N, Keller E, Merchenthaler I, Liposits Z. Gonadotropin-releasing hormone neurons express estrogen receptor-beta. *J Clin Endocrinol Metab*. (2007) 92:2827–30. doi: 10.1210/jc.2006-2819

61. Legan SJ, Tsai HW. Oestrogen receptor-alpha and -beta immunoreactivity in gonadotropin-releasing hormone neurones after ovariectomy and chronic exposure to oestradiol. *J Neuroendocrinol*. (2003) 15:1164–70. doi: 10.1111/j.1365-2826.2003.01115.x

62. Skynner MJ, Sim JA, Herbison AE. Detection of estrogen receptor alpha and beta messenger ribonucleic acids in adult gonadotropin-releasing hormone neurons. *Endocrinology*. (1999) 140:5195–201. doi: 10.1210/endo.140.11.7146

63. Lubahn DB, Moyer JS, Golding TS, Couse JF, Korach KS, Smithies O. Alteration of reproductive function but not prenatal sexual development after insertional disruption of the mouse estrogen receptor gene. *Proc Natl Acad Sci USA*. (1993) 90:11162–6. doi: 10.1073/pnas.90.23.11162

64. Antonson P, Omoto Y, Humire P, Gustafsson JÅ. Generation of ERα-floxed and knockout mice using the Cre/LoxP system. *Biochem Biophys Res Commun*. (2012) 424:710–6. doi: 10.1016/j.bbrc.2012.07.016

65. Chen M, Wolfe A, Wang X, Chang C, Yeh S, Radovick S. Generation and characterization of a complete null estrogen receptor alpha mouse using Cre/LoxP technology. *Mol Cell Biochem*. (2009) 321:145–53. doi: 10.1007/s11010-008-9928-9

66. Dupont S, Krust A, Gansmuller A, Dierich A, Chambon P, Mark M. Effect of single and compound knockouts of estrogen receptors alpha (ERalpha) and beta

(ERbeta) on mouse reproductive phenotypes. *Dev Camb Engl.* (2000) 127:4277–91. doi: 10.1242/dev.127.19.4277

67. Feng Y, Manka D, Wagner KU, Khan SA. Estrogen receptor-alpha expression in the mammary epithelium is required for ductal and alveolar morphogenesis in mice. *Proc Natl Acad Sci USA*. (2007) 104:14718–23. doi: 10.1073/pnas.0706933104

68. Hewitt SC, Kissling GE, Fieselman KE, Jayes FL, Gerrish KE, Korach KS. Biological and biochemical consequences of global deletion of exon 3 from the ER alpha gene. *FASEB J Off Publ Fed Am Soc Exp Biol*. (2010) 24:4660–7. doi: 10.1096/fj.10-163428

69. Wintermantel TM, Campbell RE, Porteous R, Bock D, Gröne HJ, Todman MG, et al. Definition of estrogen receptor pathway critical for estrogen positive feedback to gonadotropin-releasing hormone neurons and fertility. *Neuron*. (2006) 52:271–80. doi: 10.1016/j.neuron.2006.07.023

70. Eddy EM, Washburn TF, Bunch DO, Goulding EH, Gladen BC, Lubahn DB, et al. Targeted disruption of the estrogen receptor gene in male mice causes alteration of spermatogenesis and infertility. *Endocrinology*. (1996) 137:4796–805. doi: 10.1210/endo.137.11.8895349

71. Rissman EF, Wersinger SR, Taylor JA, Lubahn DB. Estrogen receptor function as revealed by knockout studies: neuroendocrine and behavioral aspects. *Horm Behav*. (1997) 31:232–43. doi: 10.1006/hbeh.1997.1390

72. Wersinger SR, Haisenleder DJ, Lubahn DB, Rissman EF. Steroid feedback on gonadotropin release and pituitary gonadotropin subunit mRNA in mice lacking a functional estrogen receptor alpha. *Endocrine*. (1999) 11:137–43. doi: 10.1385/ENDO:11:2:137

73. Couse JF, Yates MM, Walker VR, Korach KS. Characterization of the hypothalamic-pituitary-gonadal axis in estrogen receptor (ER) Null mice reveals hypergonadism and endocrine sex reversal in females lacking ERalpha but not ERbeta. *Mol Endocrinol Baltim Md*. (2003) 17:1039–53. doi: 10.1210/me.2002-0398

74. Dorling AA, Todman MG, Korach KS, Herbison AE. Critical role for estrogen receptor alpha in negative feedback regulation of gonadotropin-releasing hormone mRNA expression in the female mouse. *Neuroendocrinology*. (2003) 78:204–9. doi: 10.1159/000073703

75. Glidewell-Kenney C, Hurley LA, Pfaff L, Weiss J, Levine JE, Jameson JL. Nonclassical estrogen receptor alpha signaling mediates negative feedback in the female mouse reproductive axis. *Proc Natl Acad Sci USA*. (2007) 104:8173–7. doi: 10.1073/pnas.0611514104

76. Jakacka M, Ito M, Martinson F, Ishikawa T, Lee EJ, Jameson JL. An estrogen receptor (ER)alpha deoxyribonucleic acid-binding domain knock-in mutation provides evidence for nonclassical ER pathway signaling *in vivo*. *Mol Endocrinol Baltim Md*. (2002) 16:2188–201. doi: 10.1210/me.2001-0174

77. McDevitt MA, Glidewell-Kenney C, Weiss J, Chambon P, Jameson JL, Levine JE. Estrogen response element-independent estrogen receptor (ER)-alpha signaling does not rescue sexual behavior but restores normal testosterone secretion in male ERalpha knockout mice. *Endocrinology*. (2007) 148:5288–94. doi: 10.1210/en.2007-0673

78. Christian CA, Glidewell-Kenney C, Jameson JL, Moenter SM. Classical estrogen receptor alpha signaling mediates negative and positive feedback on gonadotropin-releasing hormone neuron firing. *Endocrinology*. (2008) 149:5328–34. doi: 10.1210/en.2008-0520

79. Cheong RY, Porteous R, Chambon P, Abrahám I, Herbison AE. Effects of neuron-specific estrogen receptor (ER) α and ERβ deletion on the acute estrogen negative feedback mechanism in adult female mice. *Endocrinology*. (2014) 155:1418–27. doi: 10.1210/en.2013-1943

80. Trouillet AC, Ducroq S, Naulé L, Capela D, Parmentier C, Radovick S, et al. Deletion of neural estrogen receptor alpha induces sex differential effects on reproductive behavior in mice. *Commun Biol*. (2022) 5:383. doi: 10.1038/s42003-022-03324-w

81. Greenwald-Yarnell ML, Marsh C, Allison MB, Patterson CM, Kasper C, MacKenzie A, et al. ERα in Tac2 neurons regulates puberty onset in female mice. *Endocrinology*. (2016) 157:1555–65. doi: 10.1210/en.2015-1928

82. Dubois SL, Acosta-Martínez M, DeJoseph MR, Wolfe A, Radovick S, Boehm U, et al. Positive, but not negative feedback actions of estradiol in adult female mice require estrogen receptor α in kisspeptin neurons. *Endocrinology*. (2015) 156:1111–20. doi: 10.1210/en.2014-1851

83. Mayer C, Acosta-Martinez M, Dubois SL, Wolfe A, Radovick S, Boehm U, et al. Timing and completion of puberty in female mice depend on estrogen receptor alpha-signaling in kisspeptin neurons. *Proc Natl Acad Sci USA*. (2010) 107:22693–8. doi: 10.1073/pnas.1012406108

84. McQuillan HJ, Clarkson J, Kauff A, Han SY, Yip SH, Cheong I, et al. Definition of the estrogen negative feedback pathway controlling the GnRH pulse generator in female mice. *Nat Commun*. (2022) 13:7433. doi: 10.1038/s41467-022-35243-z

85. Wang L, Burger LL, Greenwald-Yarnell ML, Myers MG, Moenter SM. Glutamatergic transmission to hypothalamic kisspeptin neurons is differentially regulated by estradiol through estrogen receptor α in adult female mice. *J Neurosci Off J Soc Neurosci*. (2018) 38:1061–72. doi: 10.1523/JNEUROSCI.2428-17.2017

86. Ghosh P, Saha SK, Bhattacharya S, Bhattacharya S, Mukherjee S, Roy SS. Tachykinin family genes and their receptors are differentially expressed in the hypothyroid ovary and pituitary. *Cell Physiol Biochem Int J Exp Cell Physiol Biochem Pharmacol*. (2007) 20:357–68. doi: 10.1159/000107521

87. Pintado CO, Pinto FM, Pennefather JN, Hidalgo A, Baamonde A, Sanchez T, et al. A role for tachykinins in female mouse and rat reproductive function. *Biol Reprod*. (2003) 69:940–6. doi: 10.1095/biolreprod.103.017111

88. Salehi S, Adeshina I, Chen H, Zirkin BR, Hussain MA, Wondisford F, et al. Developmental and endocrine regulation of kisspeptin expression in mouse Leydig cells. *Endocrinology*. (2015) 156:1514–22. doi: 10.1210/en.2014-1606

89. Cheong RY, Czieselsky K, Porteous R, Herbison AE. Expression of ESR1 in glutamatergic and GABAergic neurons is essential for normal puberty onset, estrogen feedback, and fertility in female mice. *J Neurosci Off J Soc Neurosci*. (2015) 35:14533–43. doi: 10.1523/JNEUROSCI.1776-15.2015

90. Wu MV, Tollkuhn J. Estrogen receptor alpha is required in GABAergic, but not glutamatergic, neurons to masculinize behavior. *Horm Behav*. (2017) 95:3–12. doi: 10.1016/j.yhbeh.2017.07.001

91. Yeo SH, Herbison AE. Estrogen-negative feedback and estrous cyclicity are critically dependent upon estrogen receptor-α expression in the arcuate nucleus of adult female mice. *Endocrinology*. (2014) 155:2986–95. doi: 10.1210/en.2014-1128

92. Wang L, Vanacker C, Burger LL, Barnes T, Shah YM, Myers MG, et al. Genetic dissection of the different roles of hypothalamic kisspeptin neurons in regulating female reproduction. *eLife*. (2019) 8:e43999. doi: 10.7554/eLife.43999

93. Krege JH, Hodgin JB, Couse JF, Enmark E, Warner M, Mahler JF, et al. Generation and reproductive phenotypes of mice lacking estrogen receptor beta. *Proc Natl Acad Sci USA*. (1998) 95:15677–82. doi: 10.1073/pnas.95.26.15677

94. Temple JL, Scordalakes EM, Bodo C, Gustafsson JA, Rissman EF. Lack of functional estrogen receptor beta gene disrupts pubertal male sexual behavior. *Horm Behav*. (2003) 44:427–34. doi: 10.1016/j.yhbeh.2003.09.002

95. Abrahám IM, Han SK, Todman MG, Korach KS, Herbison AE. Estrogen receptor beta mediates rapid estrogen actions on gonadotropin-releasing hormone neurons *in vivo*. *J Neurosci Off J Soc Neurosci*. (2003) 23:5771–7. doi: 10.1523/JNEUROSCI.23-13-05771.2003

96. Antal MC, Krust A, Chambon P, Mark M. Sterility and absence of histopathological defects in nonreproductive organs of a mouse ERbeta-null mutant. *Proc Natl Acad Sci USA*. (2008) 105:2433–8. doi: 10.1073/pnas.0712029105

97. Kuiper GG, Carlsson B, Grandien K, Enmark E, Häggblad J, Nilsson S, et al. Comparison of the ligand binding specificity and transcript tissue distribution of estrogen receptors alpha and beta. *Endocrinology*. (1997) 138:863–70. doi: 10.1210/endo.138.3.4979

98. Couse JF, Lindzey J, Grandien K, Gustafsson JA, Korach KS. Tissue distribution and quantitative analysis of estrogen receptor-alpha (ERalpha) and estrogen receptor-beta (ERbeta) messenger ribonucleic acid in the wild-type and ERalpha-knockout mouse. *Endocrinology*. (1997) 138:4613–21. doi: 10.1210/endo.138.11.5496

99. Naulé L, Robert V, Parmentier C, Martini M, Keller M, Cohen-Solal M, et al. Delayed pubertal onset and prepubertal Kiss1 expression in female mice lacking central oestrogen receptor beta. *Hum Mol Genet*. (2015) 24:7326–38. doi: 10.1093/hmg/ddv430

100. Naulé L, Marie-Luce C, Parmentier C, Martini M, Albac C, Trouillet AC, et al. Revisiting the neural role of estrogen receptor beta in male sexual behavior by conditional mutagenesis. *Horm Behav*. (2016) 80:1–9. doi: 10.1016/j.yhbeh.2016.01.014

101. Novaira HJ, Negron AL, Graceli JB, Capellino S, Schoeffield A, Hoffman GE, et al. Impairments in the reproductive axis of female mice lacking estrogen receptor β in GnRH neurons. *Am J Physiol Endocrinol Metab*. (2018) 315:E1019–33. doi: 10.1152/ajpendo.00173.2018

102. Cheong RY, Kwakowsky A, Barad Z, Porteous R, Herbison AE, Ábrahám IM. Estradiol acts directly and indirectly on multiple signaling pathways to phosphorylate cAMP-response element binding protein in GnRH neurons. *Endocrinology*. (2012) 153:3792–803. doi: 10.1210/en.2012-1232

103. Ogawa S, Lubahn DB, Korach KS, Pfaff DW. Behavioral effects of estrogen receptor gene disruption in male mice. *Proc Natl Acad Sci USA*. (1997) 94:1476–81. doi: 10.1073/pnas.94.4.1476

104. Ogawa S, Washburn TF, Taylor J, Lubahn DB, Korach KS, Pfaff DW. Modifications of testosterone-dependent behaviors by estrogen receptor-alpha gene disruption in male mice. *Endocrinology*. (1998) 139:5058–69. doi: 10.1210/endo.139.12.6358

105. Ogawa S, Chester AE, Hewitt SC, Walker VR, Gustafsson JA, Smithies O, et al. Abolition of male sexual behaviors in mice lacking estrogen receptors alpha and beta (alpha beta ERKO). *Proc Natl Acad Sci USA*. (2000) 97:14737–41. doi: 10.1073/pnas.250473597

106. Wersinger SR, Sannen K, Villalba C, Lubahn DB, Rissman EF, De Vries GJ. Masculine sexual behavior is disrupted in male and female mice lacking a functional estrogen receptor alpha gene. *Horm Behav*. (1997) 32:176–83. doi: 10.1006/hbeh.1997.1419

107. Sato T, Matsumoto T, Kawano H, Watanabe T, Uematsu Y, Sekine K, et al. Brain masculinization requires androgen receptor function. *Proc Natl Acad Sci USA*. (2004) 101:1673–8. doi: 10.1073/pnas.0305303101

108. Ogawa S, Gordan JD, Taylor J, Lubahn D, Korach K, Pfaff DW. Reproductive functions illustrating direct and indirect effects of genes on behavior. *Horm Behav*. (1996) 30:487–94. doi: 10.1006/hbeh.1996.0052

109. Wersinger SR, Rissman EF. Dopamine activates masculine sexual behavior independent of the estrogen receptor alpha. *J Neurosci Off J Soc Neurosci*. (2000) 20:4248–54. doi: 10.1523/JNEUROSCI.20-11-04248.2000

110. Gore AC, Wersinger SR, Rissman EF. Effects of female pheromones on gonadotropin-releasing hormone gene expression and luteinizing hormone release in male wild-type and oestrogen receptor-alpha knockout mice. *J Neuroendocrinol*. (2000) 12:1200–4. doi: 10.1046/j.1365-2826.2000.00578.x

111. Ogawa S, Taylor JA, Lubahn DB, Korach KS, Pfaff DW. Reversal of sex roles in genetic female mice by disruption of estrogen receptor gene. *Neuroendocrinology*. (1996) 64:467–70. doi: 10.1159/000127154

112. Ogawa S, Eng V, Taylor J, Lubahn DB, Korach KS, Pfaff DW. Roles of estrogen receptor-alpha gene expression in reproduction-related behaviors in female mice. *Endocrinology*. (1998) 139:5070–81. doi: 10.1210/endo.139.12.6357

113. Kudwa AE, Rissman EF. Double oestrogen receptor alpha and beta knockout mice reveal differences in neural oestrogen-mediated progestin receptor induction and female sexual behaviour. *J Neuroendocrinol*. (2003) 15:978–83. doi: 10.1046/j.1365-2826.2003.01089.x

114. Rissman EF, Early AH, Taylor JA, Korach KS, Lubahn DB. Estrogen receptors are essential for female sexual receptivity. *Endocrinology*. (1997) 138:507–10. doi: 10.1210/endo.138.1.4985

115. Couse JF, Curtis SW, Washburn TF, Lindzey J, Golding TS, Lubahn DB, et al. Analysis of transcription and estrogen insensitivity in the female mouse after targeted disruption of the estrogen receptor gene. *Mol Endocrinol Baltim Md*. (1995) 9:1441–54. doi: 10.1210/mend.9.11.8584021

116. Khbouz B, de Bournonville C, Court L, Taziaux M, Corona R, Arnal JF, et al. Role for the membrane estrogen receptor alpha in the sexual differentiation of the brain. *Eur J Neurosci*. (2020) 52:2627–45. doi: 10.1111/ejn.14646

117. Sano K, Tsuda MC, Musatov S, Sakamoto T, Ogawa S. Differential effects of site-specific knockdown of estrogen receptor α in the medial amygdala, medial pre-optic area, and ventromedial nucleus of the hypothalamus on sexual and aggressive behavior of male mice. *Eur J Neurosci*. (2013) 37:1308–19. doi: 10.1111/ejn.12131

118. Wei YC, Wang SR, Jiao ZL, Zhang W, Lin JK, Li XY, et al. Medial preoptic area in mice is capable of mediating sexually dimorphic behaviors regardless of gender. *Nat Commun*. (2018) 9:279. doi: 10.1038/s41467-017-02648-0

119. Karigo T, Kennedy A, Yang B, Liu M, Tai D, Wahle IA, et al. Distinct hypothalamic control of same- and opposite-sex mounting behaviour in mice. *Nature*. (2021) 589:258–63. doi: 10.1038/s41586-020-2995-0

120. Lee H, Kim DW, Remedios R, Anthony TE, Chang A, Madisen L, et al. Scalable control of mounting and attack by Esr1+ neurons in the ventromedial hypothalamus. *Nature*. (2014) 509:627–32. doi: 10.1038/nature13169

121. Lin D, Boyle MP, Dollar P, Lee H, Lein ES, Perona P, et al. Functional identification of an aggression locus in the mouse hypothalamus. *Nature*. (2011) 470:221–6. doi: 10.1038/nature09736

122. Yang B, Karigo T, Anderson DJ. Transformations of neural representations in a social behaviour network. *Nature*. (2022) 608:741–9. doi: 10.1038/s41586-022-05057-6

123. Bayless DW, Yang T, Mason MM, Susanto AAT, Lobdell A, Shah NM. Limbic neurons shape sex recognition and social behavior in sexually naive males. *Cell*. (2019) 176:1190–205.e20. doi: 10.1016/j.cell.2018.12.041

124. Musatov S, Chen W, Pfaff DW, Kaplitt MG, Ogawa S. RNAi-mediated silencing of estrogen receptor α in the ventromedial nucleus of hypothalamus abolishes female sexual behaviors. *Proc Natl Acad Sci USA*. (2006) 103:10456–60. doi: 10.1073/pnas.0603045103

125. Spiteri T, Musatov S, Ogawa S, Ribeiro A, Pfaff DW, Agmo A. Estrogen-induced sexual incentive motivation, proceptivity and receptivity depend on a functional estrogen receptor alpha in the ventromedial nucleus of the hypothalamus but not in the amygdala. *Neuroendocrinology*. (2010) 91:142–54. doi: 10.1159/000255766

126. Inoue S, Yang R, Tantry A, Davis CH, Yang T, Knoedler JR, et al. Periodic remodeling in a neural circuit governs timing of female sexual behavior. *Cell*. (2019) 179:1393–408. doi: 10.1016/j.cell.2019.10.025

127. Spiteri T, Ogawa S, Musatov S, Pfaff DW, Agmo A. The role of the estrogen receptor α in the medial preoptic area in sexual incentive motivation, proceptivity and receptivity, anxiety, and wheel running in female rats. *Behav Brain Res*. (2012) 230:11–20. doi: 10.1016/j.bbr.2012.01.048

128. Ribeiro AC, Musatov S, Shteyler A, Simanduyev S, Arrieta-Cruz I, Ogawa S, et al. siRNA silencing of estrogen receptor-α expression specifically in medial preoptic area neurons abolishes maternal care in female mice. *Proc Natl Acad Sci*. (2012) 109:16324–9. doi: 10.1073/pnas.1214094109

129. Ogawa S, Chan J, Chester AE, Gustafsson JA, Korach KS, Pfaff DW. Survival of reproductive behaviors in estrogen receptor beta gene-deficient (betaERKO) male and female mice. *Proc Natl Acad Sci USA*. (1999) 96:12887–92. doi: 10.1073/pnas.96.22.12887

130. Kudwa AE, Bodo C, Gustafsson JA, Rissman EF. A previously uncharacterized role for estrogen receptor beta: defeminization of male brain and behavior. *Proc Natl Acad Sci USA*. (2005) 102:4608–12. doi: 10.1073/pnas.0500752102

131. Nomura M, Durbak L, Chan J, Smithies O, Gustafsson JA, Korach KS, et al. Genotype/age interactions on aggressive behavior in gonadally intact estrogen receptor beta knockout (betaERKO) male mice. *Horm Behav*. (2002) 41:288–96. doi: 10.1006/hbeh.2002.1773

132. Antal MC, Petit-Demoulière B, Meziane H, Chambon P, Krust A. Estrogen dependent activation function of ERβ is essential for the sexual behavior of mouse females. *Proc Natl Acad Sci USA*. (2012) 109:19822–7. doi: 10.1073/pnas.1217668109

133. Walf AA, Ciriza I, Garcia-Segura LM, Frye CA. Antisense oligodeoxynucleotides for estrogen receptor-beta and alpha attenuate estradiol's modulation of affective and sexual behavior, respectively. *Neuropsychopharmacol Off Publ Am Coll Neuropsychopharmacol*. (2008) 33:431–40. doi: 10.1038/sj.npp.1301416

134. Nakata M, Sano K, Musatov S, Yamaguchi N, Sakamoto T, Ogawa S. Effects of prepubertal or adult site-specific knockdown of estrogen receptor β in the medial preoptic area and medial amygdala on social behaviors in male mice. *eNeuro*. (2016) 3 (2):ENEURO.0155-15.2016. doi: 10.1523/ENEURO.0155-15.2016

135. Takenawa S, Nagasawa Y, Go K, Chérasse Y, Mizuno S, Sano K, et al. Activity of estrogen receptor β expressing neurons in the medial amygdala regulates preference toward receptive females in male mice. *Proc Natl Acad Sci USA*. (2023) 120: e2305950120. doi: 10.1073/pnas.2305950120

136. Le Moëne O, Stavarache M, Ogawa S, Musatov S, Ågmo A. Estrogen receptors α and β in the central amygdala and the ventromedial nucleus of the hypothalamus: Sociosexual behaviors, fear and arousal in female rats during emotionally challenging events. *Behav Brain Res*. (2019) 367:128–42. doi: 10.1016/j.bbr.2019.03.045

137. Sano K, Morimoto C, Nataka M, Musatov S, Tsuda MC, Yamaguchi N, et al. The role of estrogen receptor β in the dorsal raphe nucleus on the expression of female sexual behavior in C57BL/6J mice. *Front Endocrinol*. (2018) 9:243. doi: 10.3389/fendo.2018.00243

138. Dombret C, Naulé L, Trouillet AC, Parmentier C, Hardin-Pouzet H, Mhaouty-Kodja S. Effects of neural estrogen receptor beta deletion on social and mood-related behaviors and underlying mechanisms in male mice. *Sci Rep*. (2020) 10:6242. doi: 10.1038/s41598-020-63427-4

139. Lonstein JS, Gréco B, De Vries GJ, Stern JM, Blaustein JD. Maternal Behavior Stimulates *c-fos* Activity within Estrogen Receptor Alpha-Containing Neurons in Lactating Rats. *Neuroendocrinology*. (2000) 72:91–101. doi: 10.1159/000054576

140. Champagne FA, Weaver ICG, Diorio J, Sharma S, Meaney MJ. Natural variations in maternal care are associated with estrogen receptor α Expression and estrogen sensitivity in the medial preoptic area. *Endocrinology*. (2003) 144:4720–4. doi: 10.1210/en.2003-0564

141. Moran CR, Gallagher JM, Bridges RS. The role of the estrogen receptor-α gene, Esr1, in maternal-like behavior in juvenile female and male rats. *Physiol Behav*. (2020) 216:112797. doi: 10.1016/j.physbeh.2020.112797

142. Gallagher JM, Nephew BC, Poirier G, King JA, Bridges RS. Estrogen receptor-alpha knockouts and maternal memory in nulliparous rats. *Horm Behav*. (2019) 110:40–5. doi: 10.1016/j.yhbeh.2019.02.002

143. Korach KS, Couse JF, Curtis SW, Washburn TF, Lindzey J, Kimbro KS, et al. Estrogen receptor gene disruption: molecular characterization and experimental and clinical phenotypes. *Recent Prog Horm Res*. (1996) 51:159–86

144. Rumi MAK, Dhakal P, Kubota K, Chakraborty D, Lei T, Larson MA, et al. Generation of Esr1-knockout rats using zinc finger nuclease-mediated genome editing. *Endocrinology*. (2014) 155:1991–9. doi: 10.1210/en.2013-2150

145. Fang YY, Yamaguchi T, Song SC, Tritsch NX, Lin D. A hypothalamic midbrain pathway essential for driving maternal behaviors. *Neuron*. (2018) 98:192–207.e10. doi: 10.1016/j.neuron.2018.02.019

146. Wu Z, Autry AE, Bergan JF, Watabe-Uchida M, Dulac CG. Galanin neurons in the medial preoptic area govern parental behaviour. *Nature*. (2014) 509:325–30. doi: 10.1038/nature13307

147. Kohl J, Babayan BM, Rubinstein ND, Autry AE, Marin-Rodriguez B, Kapoor V, et al. Functional circuit architecture underlying parental behaviour. *Nature*. (2018) 556:326–31. doi: 10.1038/s41586-018-0027-0

148. Ammari R, Monaca F, Cao M, Nassar E, Wai P, Del Grosso NA, et al. Hormone-mediated neural remodeling orchestrates parenting onset during pregnancy. *Science*. (2023) 382:76–81. doi: 10.1126/science.adi0576

149. Mei L, Yan R, Yin L, Sullivan RM, Lin D. Antagonistic circuits mediating infanticide and maternal care in female mice. *Nature*. (2023) 618:1006–16. doi: 10.1038/s41586-023-06147-9

150. Lonstein JS, Gammie SC. Sensory, hormonal, and neural control of maternal aggression in laboratory rodents. *Neurosci Biobehav Rev*. (2002) 26:869–88. doi: 10.1016/S0149-7634(02)00087-8

151. Mei L, Osakada T, Lin D. Hypothalamic control of innate social behaviors. *Science*. (2023) 382:399–404. doi: 10.1126/science.adh8489

152. Hashikawa K, Hashikawa Y, Tremblay R, Zhang J, Feng JE, Sabol A, et al. Esr1+ cells in the ventromedial hypothalamus control female aggression. *Nat Neurosci*. (2017) 20:1580–90. doi: 10.1038/nn.4644

153. Amico JA, Thomas A, Hollingshead DJ. The duration of estradiol and progesterone exposure prior to progesterone withdrawal regulates oxytocin Mrna levels in the paraventricular nucleus of the rat. *Endocr Res*. (1997) 23:141–56. doi: 10.3109/07435809709031849

154. Acevedo-Rodriguez A, Mani SK, Handa RJ. Oxytocin and estrogen receptor β in the brain: an overview. *Front Endocrinol*. (2015) 6:160/abstract. doi: 10.3389/fendo.2015.00160/abstract

155. Neumann ID. Brain oxytocin: a key regulator of emotional and social behaviours in both females and males. *J Neuroendocrinol*. (2008) 20:858–65. doi: 10.1111/j.1365-2826.2008.01726.x

156. Suzuki S, Handa RJ. Estrogen receptor-?, but not estrogen receptor-?, is expressed in prolactin neurons of the female rat paraventricular and supraoptic

nuclei: Comparison with other neuropeptides. *J Comp Neurol*. (2005) 484:28–42. doi: 10.1002/cne.20457

157. Patisaul HB, Scordalakes EM, Young LJ, Rissman EF. Oxytocin, but not oxytocin receptor, is regulated by oestrogen receptor β in the female mouse hypothalamus: regulatory role for ERβ. *J Neuroendocrinol*. (2003) 15:787–93. doi: 10.1046/j.1365-2826.2003.01061.x

158. Nomura M, McKenna E, Korach KS, Pfaff DW, Ogawa S. Estrogen receptor-β regulates transcript levels for oxytocin and arginine vasopressin in the hypothalamic paraventricular nucleus of male mice. *Mol Brain Res*. (2002) 109:84–94. doi: 10.1016/S0169-328X(02)00525-9

159. Moffitt JR, Bambah-Mukku D, Eichhorn SW, Vaughn E, Shekhar K, Perez JD, et al. Molecular, spatial, and functional single-cell profiling of the hypothalamic preoptic region. *Science*. (2018) 362:eaau5324. doi: 10.1126/science.aau5324

160. Yang CF, Chiang MC, Gray DC, Prabhakaran M, Alvarado M, Juntti SA, et al. Sexually dimorphic neurons in the ventromedial hypothalamus govern mating in both sexes and aggression in males. *Cell*. (2013) 153:896–909. doi: 10.1016/j.cell.2013.04.017

161. Yang T, Yang CF, Chizari MD, Maheswaranathan N, Burke KJ, Borius M, et al. Social control of hypothalamus-mediated male aggression. *Neuron*. (2017) 95:955–970.e4. doi: 10.1016/j.neuron.2017.06.046

162. Kim DW, Yao Z, Graybuck LT, Kim TK, Nguyen TN, Smith KA, et al. Multimodal analysis of cell types in a hypothalamic node controlling social behavior. *Cell*. (2019) 179:713–728.e17. doi: 10.1016/j.cell.2019.09.020

163. Remedios R, Kennedy A, Zelikowsky M, Grewe BF, Schnitzer MJ, Anderson DJ. Social behaviour shapes hypothalamic neural ensemble representations of conspecific sex. *Nature*. (2017) 550:388–92. doi: 10.1038/nature23885

164. Lo L, Yao S, Kim DW, Cetin A, Harris J, Zeng H, et al. Connectional architecture of a mouse hypothalamic circuit node controlling social behavior. *Proc Natl Acad Sci USA*. (2019) 116:7503–12. doi: 10.1073/pnas.1817503116

165. Liu M, Kim DW, Zeng H, Anderson DJ. Make war not love: The neural substrate underlying a state-dependent switch in female social behavior. *Neuron*. (2022) 110:841–56. doi: 10.1016/j.neuron.2021.12.002

166. Knoedler JR, Inoue S, Bayless DW, Yang T, Tantry A, Davis C, et al. A functional cellular framework for sex and estrous cycle-dependent gene expression and behavior. *Cell*. (2022) 185:654–71.e22. doi: 10.1016/j.cell.2021.12.031

167. Bayless DW, Davis CHO, Yang R, Wei Y, de Andrade Carvalho VM, Knoedler JR, et al. A neural circuit for male sexual behavior and reward. *Cell*. (2023) 186:3862–81.e28. doi: 10.1016/j.cell.2023.07.021

168. Smith EP, Boyd J, Frank GR, Takahashi H, Cohen RM, Specker B, et al. Estrogen resistance caused by a mutation in the estrogen-receptor gene in a man. *N Engl J Med*. (1994) 331:1056–61. doi: 10.1056/NEJM199410203311604

169. Paskulin DD, Cunha-Filho JS, Paskulin LD, Souza CAB, Ashton-Prolla P. ESR1 rs9340799 is associated with endometriosis-related infertility and *in vitro* fertilization failure. *Dis Markers*. (2013) 35:907–13. doi: 10.1155/2013/796290

170. Quaynor SD, Stradtman EW, Kim HG, Shen Y, Chorich LP, Schreihofer DA, et al. Delayed puberty and estrogen resistance in a woman with estrogen receptor α variant. *N Engl J Med*. (2013) 369:164–71. doi: 10.1056/NEJMoa1303611

171. Ge YZ, Xu LW, Jia RP, Xu Z, Li WC, Wu R, et al. Association of polymorphisms in estrogen receptors (ESR1 and ESR2) with male infertility: a meta-analysis and systematic review. *J Assist Reprod Genet*. (2014) 31:601–11. doi: 10.1007/s10815-014-0212-5

172. de Mattos CS, Trevisan CM, Peluso C, Adami F, Cordts EB, Christofolini DM, et al. ESR1 and ESR2 gene polymorphisms are associated with human reproduction outcomes in Brazilian women. *J Ovarian Res*. (2014) 7:114. doi: 10.1186/s13048-014-0114-2

173. Lang-Muritano M, Sproll P, Wyss S, Kolly A, Hürlimann R, Konrad D, et al. Early-onset complete ovarian failure and lack of puberty in a woman with mutated estrogen receptor β (ESR2). *J Clin Endocrinol Metab*. (2018) 103:3748–56. doi: 10.1210/jc.2018-00769

174. Bernard V, Kherra S, Francou B, Fagart J, Viengchareun S, Guéchot J, et al. Familial multiplicity of estrogen insensitivity associated with a loss-of-function ESR1 mutation. *J Clin Endocrinol Metab*. (2017) 102:93–9. doi: 10.1210/jc.2016-2749

175. Baetens D, Güran T, Mendonca BB, Gomes NL, De Cauwer L, Peelman F, et al. Biallelic and monoallelic ESR2 variants associated with 46,XY disorders of sex development. *Genet Med Off J Am Coll Med Genet*. (2018) 20:717–27. doi: 10.1038/gim.2017.163

Frontiers in Endocrinology

Explores the endocrine system to find new therapies for key health issues

The second most-cited endocrinology and metabolism journal, which advances our understanding of the endocrine system. It uncovers new therapies for prevalent health issues such as obesity, diabetes, reproduction, and aging.

Discover the latest Research Topics

See more →

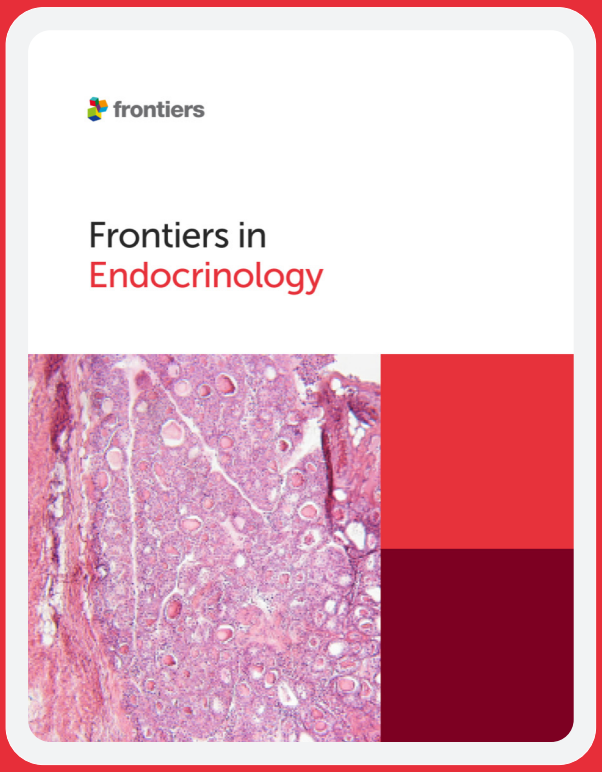

Frontiers

Avenue du Tribunal-Fédéral 34
1005 Lausanne, Switzerland
frontiersin.org

Contact us

+41 (0)21 510 17 00
frontiersin.org/about/contact